
NIGERIAN METALLURGICAL SOCIETY
37th ANNUAL CONFERENCE & ANNUAL GENERAL MEETING
ABUJA HYBRID 2022
THEME:
ROLE OF MATERIALS INDUSTRY IN ENERGY MIX
TRANSITION AND ENVIRONMENTAL SUSTAINABILITY
DATE:
26-29 OCTOBER 2022
TIME:
10:00AM GMT+1
VENUE:
CONFERENCE HALL, ASUU RESEARCHERS' CHALETS, UNIVERSITY OF ABUJA, FCT, NIGERIA
NMS PROCEEDINGS ABUJA 2022

PROCEEDINGS OF THE NIGERIAN METALLURGICAL SOCIETY

(Peer- reviewed)

The 37th Annual Conference and Annual General Meetings, Abuja 2022

Theme:

ROLE OF MATERIALS INDUSTRY IN ENEGRY MIX TRANSITION AND ENVIRONMENTAL SUSTAINABILITY

Published by the Nigerian Metallurgical Society, (NMS)

Nigerian Metallurgical Society (NMS)

Website: www.nigerianmetasociety.org

E-mail: nigmet_society@yahoo.com

ISSN: 2006-1919

Edited by:

Victor Sunday Aigbodion and Yusuf, Yakubu Ochejah

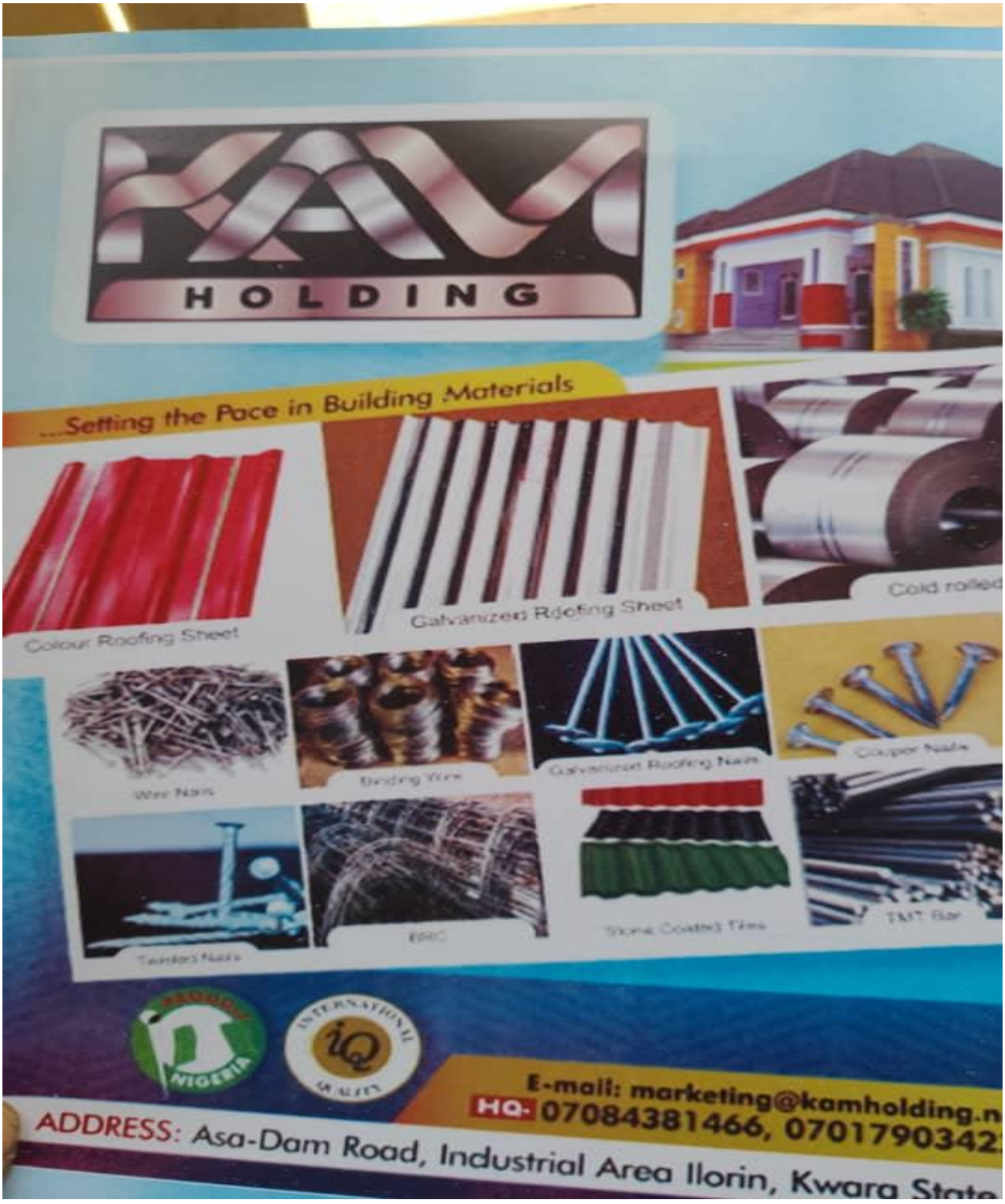
HOLDING
...Setting the Pace in Building Materials
Colour Roofing Sheet
Galvanized Roofing Sheet
Cold rolled
Wire Nails
Binding Wire
Galvanized Roofing Nails
Clipper Nails
Tumbler Nails
BMC
Stone Coated Tiles
TMT Bar
E-mail: marketing@kamholding.n
HQ: 07084381466, 0701790342
ADDRESS: Asa-Dam Road, Industrial Area Ilorin, Kwara State

Preface

This year's Conference theme **"ROLE OF MATERIALS INDUSTRY IN ENEGRY MIX TRANSITION AND ENVIRONMENTAL SUSTAINABILITY"** is very apt as it will give all stakeholders in the Engineering sector the ample opportunity to proffer solutions to this sector which is beneficial to our economic lives.

The plenary papers have been tailored to address those silent issues, institutional frameworks and situations why this sector is where and how it is today. The technical papers address specific issues in the Energy sectors with a view to bringing to focus the best possible way for transformation of Energy sectors for National development and sustainability through wealth creation, employment and revenue generation for the Nation.

We want to appreciate all our members and non – members alike whose received our "call for papers" and the impressive attendances during the conference even at very short notice. These responses indicate the love we all have for the advancement of the Country through the quality of papers presented at the Conference. The Technical committee received Fifty –nine (59) technical papers of which only twenty eight (28) were presented and published after peer reviewed by experts , professional and academic in these of specialization. All the papers presented covered all the areas of the sub-theme. The authors are appreciated for all the efforts put together to have produced quality papers. The papers presented during the conference were critically deliberated upon during the technical session of the conference. The technical committee was able to follow strictly the procedure for publishing quality paper which include, acceptance, presentation and with particular referencing to the theme cum the sub –theme of the conference. It must be noted by readers and users that the Society does not accept responsibility for the data, results and views published in the Society's proceedings, the author(s) are fully responsible for the content of their papers. This year's Conference proceedings can also be downloaded from the Society's website www.nigeranmetsociety.org

The Technical Committee wishes to appreciate all those who sent papers for the Conference and other that have contributed in one form or the other for the success of the conference and the successful production of these proceedings. Finally, on behalf of the Technical Committee of the Society, we wish to sincerely thank all our sponsors and wishing you all best in your professional and academic life.

Signed:

Engr. Prof. Victor Sunday Aigbodion FNMS
National Technical Secretary

Engr. *Yusuf, Yakubu Ochejah* MNMS
National Assistant Technical Secretary

Engr. Prof O.B.Oloche FNMS
President

Engr. Dr F. M Achiv FNMS
Vice President

Engr. Dr. O. O. Alabi MNMS
Secretary

Eng rOgbodo Joy N FNMS
Assist Secretary

Engr. S. M. Lanre MNMS
Treasurer

Engr. Dr. O O. .Ajani.MNMS
Financial Secretary

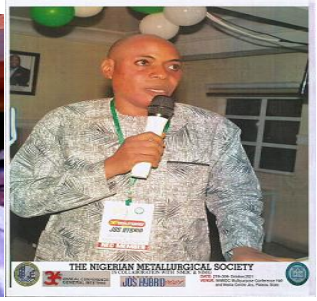

Engr.Ocheri.C MNMS
Publicity Secretary

Engr. Prof. A.S. Abdulrahman FNMS
Membership Secretary

Engr Prof. V.S. Aigbodion FNMs
Technical Secretary

Engr. Y. Y.Ochejah MNMS
Assist. Tech. Secretary

Engr M. D. Bwala FNMS
Internal Auditor

Prof. B.O Adewuyi
Professional development committee Chairman

Engr. Olasupo M.K FNMS
Ex-officio

Engr. Prof. B.A. Okorie FNMS
Ex-officio

Engr. Dr. Sanusi A. Mohammed FNMS
Ex-officio

Engr. Prof S.B. Hassan FNMS
Ex-officio

Conference Organising Committee (COC)

1.	Engr Olasupo M. kolawole	FNMS	Chairman
2.	Engr Prof Abdulrahman Salawu	FNMS	
3.	Engr Prof Victor S. Aigbodion	FNMS	
4.	Engr Ocheri Cyril	FNMS	
5.	Engr Ahmed Umar Danladi	FNMS	
6.	Engr Dr O. A Olasupo	FNMS	
7.	Engr Dr E. O Onche	MNMS	
8.	Engr O.L Oyelade	MNMS	
9.	Engr Sirajo Munir	FNMS	
10.	Engr Akinola Ayodeji	MNMS	
11.	Engr Dr. Ben Ugheoke	MNMS	Secretary

CONFERENCE ADVISERS

12.	Engr. Prof. O. B. Oloche	FNMS
13.	Engr. Prof. S. B. Hassan	FNMS
14.	Engr. Prof. B. O. Adewuyi	FNMS
15.	Engr. Dr.SanusiA. Mohammed	FNMS
16.	Engr. Prof. Linus Asuquo	FNMS
17.	Engr. Dr. E. Mudiare	FNMS
18.	Engr. Prof. B. A. Okorie	FNMS
19.	Engr. Dr. M. A. Adegbite	FNMS

WELCOME ADDRESS BY THE PRESIDENT OF THE NIGERIAN METALLURGICAL SOCIETY (NMS) ENGR. PROFESSOR O.B. OLOCHE, FNMS, MNSE, COREN Regd AT THE OPENING CEREMONY OF THE 37TH ANNUAL CONFERENCE AND ANNUAL GENERAL MEETING, HOLDING AT THE CONFERENCE HALL, ASUU RESEARCHERS' CHALETS, UNIVERSITY OF ABUJA, NIGERIA ON THURSDAY 27 OCTOBER 2022

It is with great delight that I warmly welcome you all, on behalf of the Executive Council and the entire members of the Nigerian Metallurgical Society (NMS) to the 37th Annual Conference and Annual General Meeting holding at Conference Hall ,ASUU Researchers' Chalets, University of Abuja ,FCT , Nigeria.

This year's theme of the Conference **"Role of Materials Industry in Energy Mix Transition and Environmental Sustainability"** was carefully chosen, considering the role of materials as an enabling resource to promote smart cities, help in the transition from fossil fuels to renewable energy and help in sustainable development.

Reliable and sustainable materials are fundamental to every country that needs to improve its social and economic well-being. We are now living in a time where the demand for natural resources exceeds its supply. While countries are competing for limited resources and industries are processing natural resources to finished goods, the environment is being destroyed through all the anthropogenic processes. One of the greatest challenges of the 21st century, is how politicians and scientists is to sustain the developmental needs of the world, while at the same time, the the protection of the environment.

Materials scientists are researchers who are more involved in doing researches to develop new ways to combine materials to improve their efficiency. Materials Engineers are more involved in using the invented materials from the researchers in the production processes.

THE HISTORY OF MATERIALS SCIENCE AND ENGINEERING

Man has benefited from different kinds of materials from the very beginning of this existence. For example, Among the first materials that man used for his day-to-day work were wood stone, animal skin and bones, fibres, clays, feathers, shells, and many others for different kinds of specific purposes. That is, man used these vital materials for making tools for farming, weapons for hunting, and utensils for cooking, shelter for accommodation, and for self-decorations for beauty enhancement.

Today's technology for smelting copper is known to have been originated from pottery making. This technology has been estimated to have been developed in about 9 or 10 thousand years back (Hummel, 2004).

The transformation of materials has led to its improvement from the ancient ceramics and metallurgy into modern sectors like ceramic superconductors, dielectric ceramics (which yield thinner dielectric layers for more compact electronics), intelligent or smart materials, structural composites, electronic polymers, biomimetic, complex fluids, "auxetic" materials (which grow fatter when stretched), organic composites, elastomers, biomedical materials (for implants).

The other medical applications are , artificial diamonds, fuel cell materials, biocompatible materials, ferroelectric films (for nonvolatile memories), self-assembling materials,

optoelectronics, improved sensors (based on metal oxides, or conducting polymers), improved battery technologies, ceramic coatings in air (by plasma de-position), artificial tissues, electrostrictive polymers, chemical-mechanical polishing, grated light valves, alkali luminescent silicon, planar optical displays without phosphors, metal thermoelectric converters, super-molecular materials

More efficient photovoltaic converters have improved the standard of living of many people today, and with continuous research, they will help further improve standard of living by ensuring safe and smart societies, the transition from fossil fuels to renewable energy, and ensuring the protection of the environment (Hummel, 2004).

THE GLOBAL MATERIALS CYCLE AND THE CIRCULAR ECONOMY.

The materials cycle simply involves the chain of extraction materials in their raw forms from the earth, processing them into useful finished goods, and the management of the waste products, which are produced after using the goods, to prevent environmental pollution.

Raw materials are divided mainly into two; Infinite (renewable) Raw materials are unlimited in supply, or its lost quantities can be restored in a very short time. A good example of an infinite raw material is Biomass, which is the green resources that are obtained from plants and trees.

We also have Finite (non-renewable) raw materials are resources that are limited in supply, like Gold. It has been estimated that, the amount of extraction of gold today exceeds its rate of formation by 17000 times (Derrick, 2020).

Extracted raw materials are normally useless, unless they are synthesised and processed to separate the useful materials from waste. For example, when miners extract gold ores from the earth, they further separate the pure gold from the gangue (useless part of the ore). Later, the materials can be engineered to be more useful for a particular task. For example, the pure gold can be shaped into sizes that are useful for some electronic devices.

The processed materials can be further designed in the manufacturing process before they are applied to the areas of benefits like in the defence sector for making weapons, the agricultural sector for making agricultural machines, the energy sector for making solar panels, or in the construction sector for building infrastructure. The end products of the materials are waste, which can easily pollute the earth if it is not properly managed. Most of the wastes are simply buried in the earth for them to rot and become raw materials again in the future.

The recent introduction of circular economy encourages waste products to be recycled instead of burying them. Circular economy is an economic system which has been developed to eliminate waste to ensure the continuous use of resources. The system encourages the refurbishment, re-use, sharing, repairing, recycling and re-manufacturing of always used finished products to help minimize waste environmental pollution and carbon emissions to protect the environment.

ENERGY, FOSSIL FUELS AND THE NEED FOR GLOBAL ENERGY TRANSITION

Energy is one of the most important factors for human civilization. Energy resources can be classified as primary energy resources, which are directly used without the need to convert them to another form, or secondary energy resources, where they are converted from a primary energy source.

The primary energy resources include wind power, wood fuel, solar power, and fossil fuels like natural gas, uranium, coal, and oil. The Secondary resources are hydrogen, electricity and other synthetic fuels. We can also separate energy resources into two; renewable resources are those energy resources that recover their quantity in a short time. Examples are solar power or

hydroelectric power. Those that are limited in supply, or they cannot recover in the shorter possible time are the non- renewable energy resources. Fossils fuels are non- renewable energy resources.

All renewable resources are also referred to as sustainable energy resources as their usage causes little to no harm on the environment. Their usually technologies are made to improve energy efficiency like carbon management and energy storage. Fossil fuels, which are the remains of the decomposition of animals and plants, make up the bulk of the world's current primary energy sources.

Fossil fuels are grouped into three main types: petroleum, coal, and natural gas. Liquefied petroleum gas (LPG) is a sub type of fossil fuel. LPG obtained from the production of natural gas.

Heat from burning fossil fuels is used either directly for heating or converted to electrical energy for power generation (Tong, 2019).

The benefits of materials science and engineering are clearly seen in all the stages of electrical production processes. Therefore, even though the question of the type of material to be used for a particular energy conversion system is only one criterion for energy conversion, it is one of the main backbones in energy production.

This transitioning will require a new generation of advanced materials like highly efficient solar cells, corrosion-resistant allows for energy conversion and turbine blades, super capacitor materials for greater electrical energy storage, high-efficiency and low-cost solar and many other functional materials for advanced electronics. Thus, there is a connection between efficient energy technologies and materials science research, where both combinations will ensure a future of safe and clean energy production.

ADVANCED MATERIALS IN THE GLOBAL ENERGY TRANSITION

Advanced materials are composite materials that are made to produce superior quality than conventional materials. These materials are needed for the successful transition from fossil fuels to renewable energy production. This is because, even though renewable resources are environmentally friendly, they are not efficient as fossil fuels.

Moreover, they are very expensive, as compared to energy produced from fossil fuels. Therefore, there are many ongoing researches in advanced materials science to invent materials for renewable energy production to correct the two problems. The future importance of advanced materials will direct global competition in materials science research towards it while at the same time there will be other benefits like the lower dependence on primary raw materials, low carbon footprint and higher quality of living.

THE APPLICATION OF MATERIALS FOR A GLOBAL ENVIRONMENTAL SUSTAINABILITY.

Sustainable environment is defined as the interaction of humans with the environment in the most efficient way, where the needs of humans are met, but humans do not destroy the environment in the process. Environmental sustainability is very important to ensure that the future needs of the next generations are protected. Global warming through fossil fuels is one main enemy to Environmental sustainability. We have seen that the main solution to the problem is the energy transition to renewable resources.

The earth is like a global environment, thus the activities of one country can affect all other countries. For example, even though the European Union has committed through its vision for 2050 to produce net zero greenhouse gas emissions through the use of renewable energy, global warming will still increase if the other countries continue to use fossil fuels. Man has used

different kinds of Materials for his existence on earth from the beginning. The importance of materials, and the need for efficient methods of harnessing benefits from the ecosystem has prompted man to composite materials.

As the world is ushering into a future of Smart Cities, Renewable energy production, and Environmental sustainability, Materials sciences researches are still needed to help increase the efficiency of today's materials and to invent new materials that allow for higher efficiency during product use.

Because the problem of Environmental Pollution affects everyone on Earth, there is the need for every country to take materials science research seriously, as it is a saviour to our problems. All countries must come together to support materials science research for environmental sustainability.

The good news is that all these materials are available in Nigeria's in a large commercial quantity which could be enhanced for energy mix and transition for environmental sustainability. The Nigeria nation should therefore take the advantages created by the availability of these materials for energy mix and transition.

Ladies and gentlemen, looking again at the theme of the conference and the city where this year's conference is taking place, you will definitely concur with me that we are in the right place the Federal Capital Territory (FCT) where we have the politicians, academics, policy makers, captains of industries. There are some strategic institutions and establishments located in Abuja such the University of Abuja, Energy Service Commission, Ministry of Mines and Steel Development and other very important government agencies and parastatals that should formulate policies that will affect the Nigerian economy and technology positively culminating to the Society benefiting from such formulated policies. With this strategy opportunities there is going to useful and robust discussion and purposeful interaction with the keynote speaker, plenary presenters, and all the stakeholders that are present today.

At the end of all the papers that will be presented during the conference, this is no doubt that the Society will come out with position papers, documents and a viable communique that will be sent to governments, policy makers, the law makers, the stakeholders and all the relevant media for implementation.

Once again, I sincerely welcome the Honorable Minister of Mines and Steel Development, the Vice Chancellor, Prof Abdul Rasheed Na'Allah, the Director General, Energy Service Commission, the Executive Secretary, NASENI, the Executive Council members of our great Society, all our invited guests, stakeholders, and the participants who had taken time to attend even in the midst of their crowded schedule.

I wish you a happy stay in the city of Abuja and assuring you that your stay within this period will be worthwhile. Abuja as we know is a city of very good clemency with natural weather. It is also the political and capital city of our great country Nigeria.

Thank you and God bless you all
Engr. Professor O.B. OLOCHE FNMS, MNSE, COREN Reg.
President, Nigerian Metallurgical Society.
+2348023784402
profoloche@yahoo.com

TABLE OF CONTENTS

NMS-PP 001

ELECTRIC VEHICLES AND ENERGY SOURCES FOR POWERING THEM

FIDELIS MFEWASE ACHIV
DIRECTOR, RESEARCH, DESIGN AND DEVELOPMENT
NATIONAL AUTOMOTIVE DESIGN AND DEVELOPMENT COUNCIL
ABUJA

ABSTRACT

At the beginning of the last century, vehicles had competing power sources: Steam, electricity and petrol/diesel. Petrol/diesel won as it was more convenient and cheaper, but it may lose in the future to electricity due to emerging trends. Governments in the developed economies are encouraging the production and sales of new energy vehicles for the fact that vehicles account for about 15%of the carbon dioxide that is responsible for global warming. Nations have committed themselves to reduce the emission of greenhouse gases like carbon dioxide and NOx. The use of Electric Vehicles is one of the methods to this end. Lithium-ion batteries so far have provided the required battery capacity to power electric vehicles. Other emerging batteries for powering electric vehicles are being developed. These include Aluminium-ion batteries, Solid state batteries, Lithium –Sulphur batteries, Metal - Air batteries amongst others. Other materials that make up the lithium-ion battery pack include Manganese, Mn, Nickel, Ni, carbon, C, (graphite) and Cobalt, Co.Lithium, the dominant material in Electric vehicle battery production is also available in Nigeriain very large reserves. We should therefore focus our efforts in mining and processing this materia lfor Nigeria to also tap into the Electric Vehicle battery supply chain. By so doing, ancillary activities will spring up in the sector with a positive multiplier effect on the GDP of Nigeria.

1. INTRODUCTION

At the beginning of the last century, vehicles had competing power sources: Steam, electricity and petrol/diesel. Petrol/diesel won as it was more convenient and cheaper, but it may lose in the future to electricity due to emerging trends.

The global acceptance rate of electric vehicles has increased by 43% in 2020, accounting for a total of more than 3million units sold. About 30% of all cars are expected to be electric by the year 2030 as stated by the International Energy Agency, IEA. As at today only 1% to 3% of total passenger cars are electric[1]. The success rate of electric vehicles can only be possible if customers prefer them over Internal Combustion Engines, ICE. To make electric cars appealing to customers, the major challenges concerning electric vehicles must be resolved. To address the issue of rocketing air pollution around the world, global warming and depleting fuel reserves, electric vehicles are a possible alternative to the current fuel-driven vehicles as they do no harm to the environment and require a clean and renewable source of energy to power them up. The current global energy consumption by different sources of energy is shown in figure 1.

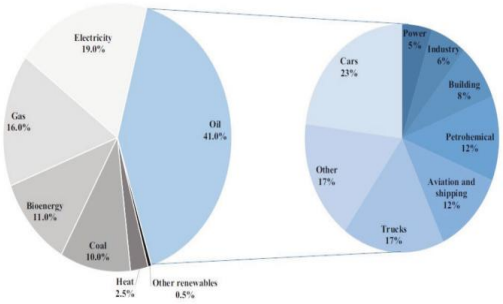

Fig1 :Global energy consumption by type (left) and global oil consumption by sector (right)

Battery power is the most essential element for a vehicle that runs on electricity. OEMs are constantly working towards increasing the driving range by increasing battery capacity that impacts the size, chemistry, and battery management system. A customer willing to use an electric vehicle needs the vehicle to have shorter charging durations, lesser maintenance, and a cheap cost of operation[2].

Governments in the developed economies are encouraging the production and sales of new energy vehicles for the following reasons:

a) In many large cities like Beijing, London, Paris and Los Angeles, vehicle exhausts emissions are the main contributors to air pollution that has adverse consequences on peoples' health, both the young and old.
b) Some countries that rely on imported petroleum resources - like Japan, Korea and China - want to reduce their imports.

2.0 VEHICLE CLASSIFICATION BY PROPULSION

EV – Electric Vehicle: Vehicle drives on electrical energy using at least one electric motor.

PEV – Plug-in-Electric Vehicle: Vehicle has a socket and can be propelled by electric power.

BEV – Battery Electric Vehicle: Vehicle drives on electrical energy stored in batteries.

HEV – Hybrid Electric Vehicle: Vehicle drives either with or without combustion engine. Does not have a socket for recharging battery.

PHEV – Plug-in Hybrid Electric Vehicle: Vehicle drives on stored electrical energy or with combustion engine depending on user preference.

ICE – Internal Combustion Engine: Vehicle drives on internal combustion engine.

FCEV – Fuel Cell Electric Vehicle: Vehicle drives on electrical energy generated by hydrogen fuel cell. Does not have a socket for recharging battery.

SEV – Solar Electric Vehicle: Vehicle largely drives on solar energy

wikipedia.org (source) evreporter.com last updated 16/1/2020

From above, electric vehicles can be classified into four main broad areas:

- Fuel Cell Vehicles (FCV)
- Hybrid Electric Vehicles (HEV)
- Plug in Hybrid Electric Vehicles (PHEV) and
- Battery Electric Vehicles (BEV).

2.1 Fuel Cell Vehicles (FCV)

Fuel Cells combine hydrogen and oxygen (from the atmosphere) to generate electricity and water. The electricity is used to run an electric motor that drives a vehicle. The fuel cell is over a hundred years old and vehicles using it for propulsion have been developed since the 1990s. Honda has been leasing fuel cell cars in California for more than a decade. Toyota and Hyundai are also experimenting with fuel cells encouraged by their governments. However, fuel cells remain experimental as the fuel cell need very expensive catalysts.

2.2 Hybrid Vehicles (HEV)

This have two power sources, an Internal Combustion Engine (ICE) and an electric motor/generator and is detailed in fig 2.1.The car is driven by the electric motor, powered by the battery. When the battery runs down, the ICE turns on and drives the generator, recharging the battery. For the same power, the ICE can be smaller than

the one in a normal car. This results in 10-15% fuel savings. Example is the Toyota Prius that was introduced in the 1990s.

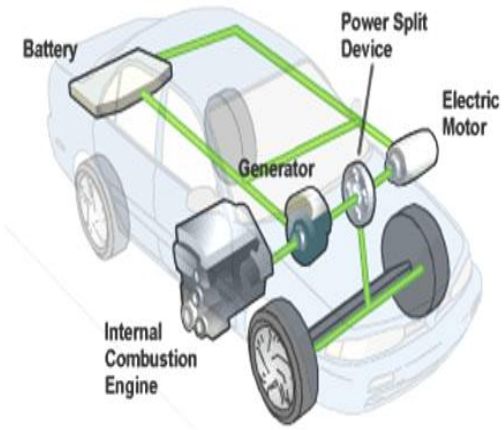

Figure 2.1: Hybrid Electric vehicle

2.3 Plug-In Hybrid Electric Vehicles (PHEV)

These are hybrid vehicles whose batteries can be charged with an external electricity source. They have bigger batteries than hybrid. If used for short distances, they may not need to be fuelled. However, for long distance the ICE comes on automatically when the battery charge becomes low. The ICE is sometimes called a range extender. The major vehicle manufactures (Toyota, Honda, GM, VW, BMW, etc.) have introduced PHEV of their models (Camry, Accord, etc.) about a decade ago.

2.4 Battery Electric Vehicles (BEV)

These have only an electric motor and batteries that needs to be charged from an external source. First generation BEVs, introduced about a decade ago have a range of only about 150km, while the current ones have a range of 700km on a single charge, Figure 2.2. Fast chargers have been deployed that can charge a battery to 80% of its capacity in 40 minutes. Examples include the Tesla Model 3 Long range, the All Electric Kia EV6, Tesla model S, Porsche Taycan 4S, Ford Mustang Mach-E CA Route 1 Edition, Etc.

Figure 2.2: Battery Electric Vehicle

Before electric vehicles take over from ICEVs, Battery cost and availability of charging stations has to be resolved. The main costly item of the Electric Vehicle is the battery, but every year, the battery cost has been coming down and it is expected that BEV will cost the same as equivalent ICEV by 2025. In 2017, Battery packs for EVs cost about $200/kWh, down from $1,000 in 2010. EVs will be price competitive with ICE vehicles when the battery packs price drop to about $100/kWh. The primary components of any battery are the positive (Cathode) and negative (Anode) electrodes, the electrolyte and separator. Lithium-ion (Li-ion) usually has graphite o silicon composite as the anode and Lithium alloys as the Cathode (e.g., Lithium Cobalt oxide, Lithium Iron Phosphate and Lithium Magnesium Oxide).The electrolytes are made of organic carbonates containing complexes of lithium-ions, e.g. Lithium hexafluorophosphate ($LiPF_6$). The Separator is made of Polyethylene/Polypropylene.

Batteries used in electric cars have a cylindrical shape and formed in a "swiss roll", i.e. a single a long sandwich of cathode, separator, anode and separator are rolled into a single spool. Tesla Model S models have 85-100 kWh battery, uses 7,104 of these cells.

Figure 2.3: Li-ion Battery and Pack

Figure 2.4: Nissan Leaf Li-ion Battery Pack

3.0 ENERGY SOURCES AND THEIR USE IN THE AUTOMOTIVE INDUSTRY:

Gasoline is used in cars, motorcycles, light trucks and boats. Aviation gasoline is used in many types of airplanes. Distillate fuels are used mainly by trucks, buses and trains and in boats and ships Jet fuel is used in jet airplanes and some types of helicopters.

Residual fuel is used in ships. Bio fuels are added to gasoline and diesel fuel.

Natural gas, a compressed natural gas and liquefied natural gas is used in cars, buses, trucks and ships. Most of the vehicles that use natural gas are in government and private fleet. Natural gas is also used to operate compressors to move natural gas in pipelines. Propane, (a hydrocarbon gas liquid) is used in cars, buses and trucks. Most of the vehicles that use propane are in government and private fleets.

Electricity is used by public mass transit systems and by EVs Source: US Energy Information Administration, monthly Energy Review, April 2022.

The oil being used produces harmful emissions when it is burnt in the engines of vehicles. These emissions mainly Carbon dioxide CO_2, Nitrous oxide NO_x and Carbon monoxide CO are the greatest contributing factors to global warming and pollution. www.researchgate.net>publication 5/7/2022.

4.0 MATERIALS FOR ELECTRIC VEHICLE BATTERIES

One of the main materials used to produce the batteries is Lithium, a light metal substance. Other necessary materials include the metallic elements of Cobalt, Manganese and Nickel. Prices of these materials have been rising as demand increases for Electric Vehicle (EV) batteries.

Lithium-ion batteries are expected to remain the most widely used technology for EVs in the future.

- Chinese companies currently produce the majority of materials to make EV batteries. The largest known supplier of cobalt is Democratic Republic of Congo, DRC. Chinese companies control most of the Cobalt mining there.

- Lithium is found in many parts of the world. Australia is the world biggest producer of lithium. Other major suppliers include China, Argentina and Chile. China also largely controls the Lithium supply chain.
- World demand for Lithium was about 317,200 metric tons in 2020. However, industry estimates predicted that the demand could rise to more than six (6) times that by 2030. This is because the production of EVs using Lithium-ion batteries is steadily increasing.
- The world's top Nickel supplier is Indonesia which produced about 1 million metric tons of the metal in 2021. Other nations with large Nickel operations include the Philippines, Russia, Australia, Canada and Brazil.
- One way to collect Lithium is through geothermal methods from underground water sources.
- Electric Vehicles continue to increase in popularity due to growing consumer awareness. The actions are taken to reduce pollution and address climate change, i.e. reducing Carbon pollution from the exhaust of the Internal Combustion Engines (ICE). With increasing demand for EV comes increasing demand for batteries.
- The five materials for EV battery production include: Lithium, Cobalt, Nickel, Manganese and Graphite
- The chemical elements form the basic building blocks of Lithium-ion battery cells and what gives them the power to store and release energy for propelling EVs

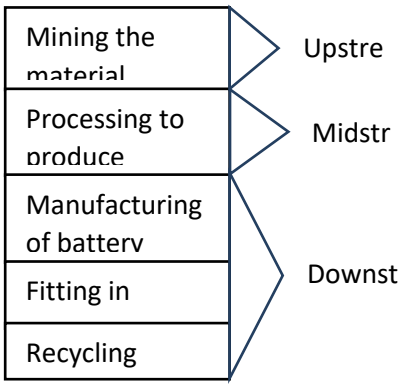

Figure 4.1: Processes of Lithium-ion battery
https://www.jessicaannarusso.com.
https://www.energy.gov/sitesdetantfiles

- Lithium is one of the key components in EV batteries, but, global supplies are under strain because of rising demand for EVs
- The world could face Lithium shortages by 2025, the International Energy Agency, (IEA) says while credit Suisse thinks demand could treble between 2022 and 2025, meaning supply would be stretched.
- About 2 billion EVs need to be on the road by 2050 for the world to hit net zero, the IEA says, but, sales stood at 6.6 million last year (2021) and some car makers are already selling out of EVs.
- Lithium supply faces challenges not only from surging demand, but because resources are concentrated in a few places and over half of today's production is in areas with high water stress.
- Future development with batteries or manufacturing methods could eventually alleviate some Lithium shortages.
- Scientist should begin to think of possible options to replace Lithium-ion for powering EVs and other devices.

Recycling of Lithium-ion Batteries

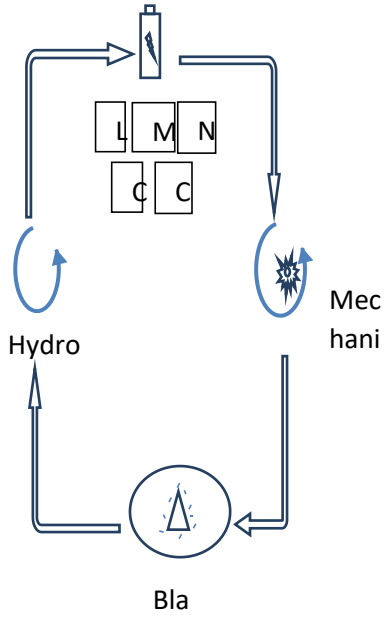

Figure 4.2: Recycling of Lithium-ion battery

4.1 Advances in Battery Technology

A lot of research is on-going in developing batteries for EVs other than Lithium-ion batteries. Other emerging batteries for powering electric vehicles are being developed. These include Aluminium-ion batteries, Solid state batteries, Lithium - Sulphur batteries, Metal - Air batteries amongst others.

5.0 EXTRACTION AND PROCESSING OF LITHIUM, COBALT, NICKEL, MANGANESE, GRAPHITE

Australia is the largest Lithium producer accounting for half of the world's production in 2020 followed by Bolivia, Chile and Argentina (the Lithium triangle) with estimated reserve of 50 million tons.

Lithium ore deposit is found in large quantities in Nigerian states such as Kogi, Nasarawa, Ekiti, Kwara, Cross River, Oyo, Plateau.

Nigeria: Lithium is of high grade. Commercial grades exposed elsewhere are in the region of 0.4% Lithium, but in Nigeria, it ranges from 1% to 13% which is classified as high grade compared to other regions. Another advantage is that the grade in Nigeria is hard rock grade which is what investors are looking for world wide.

5.1 Key Facts on Lithium

- Manufacturing of rechargeable batteries for electronics, electric vehicles and grid storage is the largest global use for Lithium representing 71% of world demand.
- Australia is the largest producer accounting for half of world's production, followed by Bolivia, Chile and Argentina with estimated reserve of about 50 million tons.

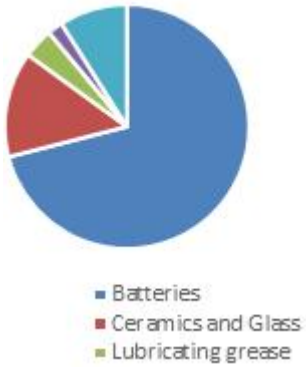

Figure 5: Uses of Lithium

World mine production of Lithium by Country 2020

Table 5.1: World production of Lithium

Ranking	Country	Tonnes
1	Australia	40,000
2	China	18,000
3	Chile	14,000
4	Argentina	6,200
5	Brazil	1,900
6	Zimbabwe	1,200
7	Other countries	900
	World Total	**82,000**

World reserve of Lithium by country 2020

Table 5.2: World reserve of Lithium

Ranking	Country	Lithium Content (Tonnes)	Percentage of Total (%)
1	Chile	9,200,000	43.7
2	Australia	4,700,000	22.3
3	Argentina	1,900,000	9.0
4	China	1,500,000	7.1
5	United States	750,000	3.6
6	Canada	530,000	2.5
7	Zimbabwe	220,000	1.0
8	Brazil	95,000	0.5
9	Portugal	60,000	0.3
10	Other countries	2,100,000	10.0
	Total	**21,055,000**	**100**

Source:www.nrean.gc.ca

From above scenario, there could be other large deposits of Lithium ore yet to be discovered across the globe and even in Nigeria. There is an unconfirmed report of large deposit of Lithium ore stretching from Kaduna state into the Federal Capital territory covering a stretch of over 18 km^2.

6.0 ELECTRIC VEHICLE CHARGING STATION INFRASTRUCTURE

6.1 Global EV Charging Stations

Consumers and fleets considering EVs and PHEVs need access to charging stations. For most drivers, this starts with charging at home or at fleet facilities. Charging stations at workplaces and public destinations may help bolster market acceptance by offering more flexible charging opportunities at commonly visited locations. As from 2015 to date, China is the global leader in number of publicly available chargers. It counts about 85% of the world's fast chargers and 55% of slow chargers. This reflects China's demonstrated leadership in the EV sector as well as its very densely populated urban characteristics.

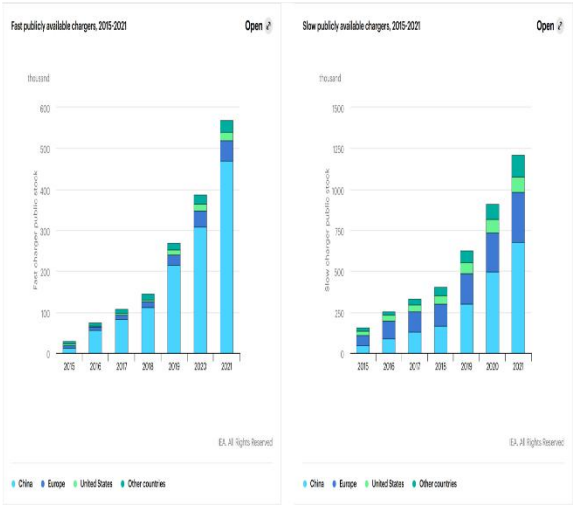

Figure 6.1: Global EV charging stations infrastructure development (for fast and slow charger)
Source:IEA, https://www.iea.org/reports/global-ev-outlook-2022/trends-in-charging-infrastructure

6.2. EV Charging Station By NADDC

The NADDC has started the building of charging station across the country. These charging stations are solar powered, therefore, there would be electricity for charging EV always (24/7). So far, there are four (4) existing and functional charging stations located at:

(i) Usman Danfodio University, Sokoto State,
(ii) University of Lagos, Lagos State,
(iii) University of Nigeria, Nsukka, Enugu State and
(iv) NADDC Abuja Office, FCT Abuja.

The Council has a proposal of building several other EV charging stations in all the six geo-political zones of the country. These charging stations would aid EV owners to have their vehicles charged at no cost and also encourage the patronage of EVs in Nigeria. Furthermore, this will allay the fear of EV owners to having their vehicles'

running out of power before getting to their destination. The access to public fast chargers would facilitate extended mileage, encourage consumers that lack access to private charging to purchase an EV, and therefore, tackle the barrier for EV adoption/acceptance in Nigeria.

Figure 6.2: EV Charging station at UDUS,

Figure 6.3: EV Charging station at Uni-Lag, Lagos.


Figure 6.4: EV Charging station at NADDC Office, FCT, Abuja

7.0 CONCLUSION

With the advent of EVs, It has become imperative for Scientist, engineers and the necessary government agencies responsible for exploration to step up efforts in the direction of looking for lithium and other EV battery material deposits across the country. EV development for now is largely hinged on availability of Lithium, more so that Lithium holds the key to a successful vehicle electrification programme in the world. The Lithium so found in Nigeria should be processed before export so that additional value can accrue to it before exportation. We should also be conscious of the fact that with the advent of electric vehicles, fossil fuels which Nigeria is a major producer and earns much of her foreign exchange will go into extinct thus, making Lithium-ion and other EV battery materials take the place of Petroleum product as a foreign exchange earner.

8.0 REFERENCES

1. Electric Cars Gain Traction, But Challenges Remain http://semiengineering.com/electric-cars-gain-traction-but-challenges-remain/ (accessed jun.16,2021).
2. Sankaran G. and Venkatesan S., 2021 J. Power Sources 502 p 230008
3. V.K. Bupesh Raja et al 2021 J. Phys.: Conf. Ser. 2129 012011
4F. M. Achiv & L. A. Isah, Review of Electric Vehicles Paper presented at the Technical Committee Meeting for the Development of National action plan on Electric Vehicles in Nigeria Ajuji Green which Hotel plot 1083, Joseph Gomwalk Street, off Abdulsalami Abubakar Road Gudu District Abuja.

NMS-PP-002

THE ROLE OF THE MATERIALS INDUSTRY IN ENERGY MIX TRANSITION AND ENVIRONMENTAL SUSTAINABILITY

S.O.O. OLUSUNLE *FNMS, FMSN, FNIMechE, FNSE, R.ENG, MNMGS, MASME, MNIM*
Engineering Materials Development Institute (EMDI-NASENI) Akure Ondo State

Abstract

The nation Nigeria is at the moment looking towards engineering materials as a key component for infrastructural and economic development thus foregrounding the importance of the theme of this year's conference titled *the role of the materials industry in energy mix transition and environmental sustainability*. Not only is the theme crucial but it is also very timely and multifaceted. It is a mix of the most challenging issues facing humanity and the planet.

I. INTRODUCTION

Globally, there is massive investment and research into efficient and affordable energy and energy hybridization that will be capable of meeting the increasing global population. Not a few experts are working assiduously to develop materials and technology that will harness the available scarce resources to meet the vast demand for energy. Many of these researches are looking away from the conventional fossil-based energy sources into renewable energy sources. However, some other researches are focused on the impact of these energy sources on the environment and their sustainability. Research into green energy has also generated great credence and interest from eco-friendly researchers. Nanotechnology has been tipped to play a crucial role in developing an appropriate energy composition and helping combat the sustainability challenges of climate change. There have been concerted efforts to develop and implement several policies positioned towards preserving the planet from greenhouse gases and other threats to the climate whilst providing adequate energy to power the planet. But in the midst of all these research and development lies the material and metallurgical scientist and engineers and the industry. These are crucial stakeholders saddled with innovation and the development of appropriate technology to help humanity preserve the planet.

McGill University in Canada describes sustainability as addressing our own needs without jeopardising the ability of future generations to meet their own needs. Social and economic resources is required in addition to natural resources.Sustainability is a three-dimensional societal aim that includes environmental, economic, and social aspects. These are collectively referred to as the pillars of sustainability and often equated to people, the planet and profits. This notion can be used to steer consumer decisions at the global, national, and individual levels. Sustainable development is similar to sustainability, and both names are frequently used interchangeably. The Mckinsey report, a global report index, stated that about nine technological innovations would shape the sustainability agenda of this decade[1]. These are public electric transport, electric trucks, cheap energy storage, long-term storage, plastic recycling, L.E.D. light efficiency, accessible solar power, hydrogen storage and carbon capture and storage. These nine innovations are aptly captured in the conference theme for this year. That shows the deep insight and calibre of professionals available in NMS. A big kudos to the local organizing committee for this foresight. Therefore, attempt will be made to

continue this keynote inline with some of the sub themes for the conference.

II. ENERGY MIX

Energy Mix

The energy mix is a collection of multiple primary energy sources combined to produce secondary energy for direct use, such as electricity. A diversified energy mix is widely regarded as an important aspect of energy security. Having several sources allows a country to continue operating without interruption if one of its energy sources fails.

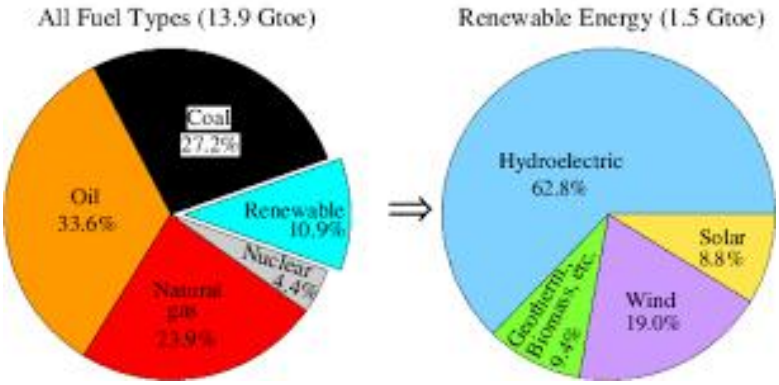

Fig 4. Total Global energy consumption by source (a) 2013 (b) 2018 (Source: Wikimedia Commons)

The Global Projected Energy Mix (2018 to 2040): The International Energy Agency (IEA) has published the World Energy Outlook every year since 1977, a highly anticipated yearly report that forecasts worldwide energy output and consumption. The most recent edition of the report delves into two different policy scenarios to demonstrate the choices and implications we face. The forecasts of the IEA are based on two policy scenarios: Scenario of Stated Policies and Scenario of Sustainable Development. This scenario is meant to reflect the impact of current public policy frameworks and proclaimed policy goals. However, the sustainable development scenario depicts a dramatic transformation of the global energy sector consistent with the U.N.'s Sustainable Development Goals (S.D.G.s), such as lowering carbon emissions. Figure 6 puts this in proper context

.

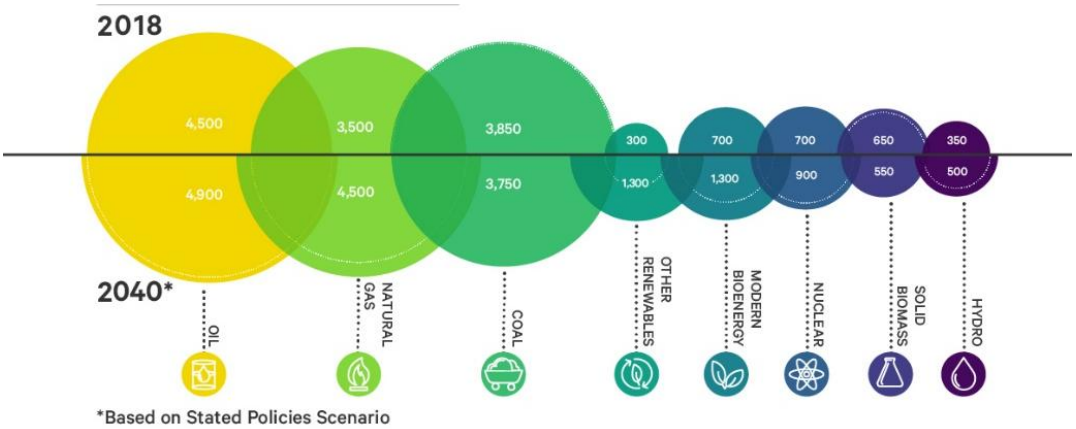

Fig 5. Changes in the global energy mix estimated in M.T.O.E. for 2018 versus stated policies 2040 [2]

Table 1. Stated Policies energy data scenario, as adjusted by C.A.P.P. in terms of Millions of Tonnes of Oil Equivalent (Mtoe) [2]:

	2018	2030	2040	Est. % of mix (2040)
Oil	4,500	4,750	4,900	28%
Natural Gas	3,500	3,900	4,500	25%
Coal	3,850	3,900	3,750	21%
Other Renewables	300	750	1,300	7%
Modern Bioenergy	700	1,050	1,300	7%
Nuclear	700	800	900	5%
Solid Biomass	650	600	550	3%
Hydro	350	450	500	3%
Global Total	**14,550**	**16,200**	**17,700**	**100%**

The interpretation of table 1 is that in the Stated Policies Scenario, the oil will be the greatest energy source in 2040, accounting for around 28% of global energy consumption, with natural gas coming in second at 25%. Because of rising demand in Asia, coal consumption, declining in Western markets, will remain stable at 2018 levels. Meanwhile, renewable energy (excluding hydro) will have a remarkable comeback. This category (which includes wind, solar, geothermal, and other renewables) will boost its share of the mix by more than 300 per cent over the next 22 years.

Table 2. Stated policies versus sustainable development for renewable energy generation for electricity [2]

Renewable Energy (Electricity Generation)	2018 (TWh)	2040 (TWh)	% Increase
Stated Policies	6,800	18,049	165
Sustainable Development	6,800	26,065	283

In the Stated Policies Scenario shown in table 2, oil will be the greatest energy source in 2040, accounting for around 28% of global energy consumption, with natural gas coming in second at 25%. Because of rising demand in Asia, coal consumption, declining in Western markets, will remain stable in 2018. Meanwhile, renewable energy (excluding hydro) will have a remarkable comeback, with this category (which includes wind, solar, geothermal, and other renewables) boosting its share of the mix by more than 300 per cent over the next 22 years. There are two scenarios but only one path. Both outcomes are possible, but we will most likely end up somewhere in the middle. This is useful to the NMS stakeholders in designing, implementing and policy formulation

.

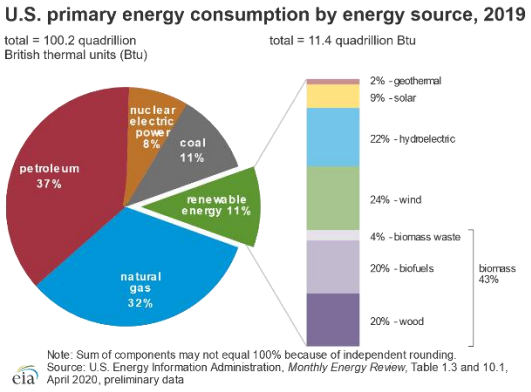

(a)

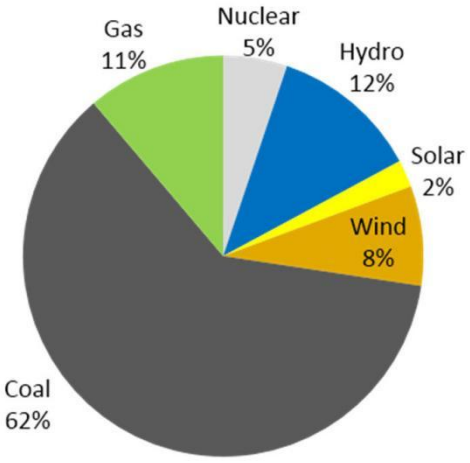

(b)

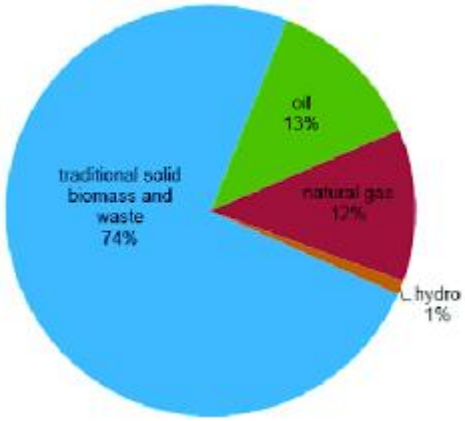

(c)

Fig 6. Primary energy mix consumption by energy source 2019 (a) U.S.A. (b) China (c)Nigeria [3]

The energy mix is different from electricity generation in Nigeria. Table 3 shows the gas-powered stations in Nigeria [3].

Table 3. Gas-powered stations in Nigeria [3]

Name	Design capacity	Status	Type	Construction/EPC Contractor
Afam VI	685 MWe	Operating fully	Combined cycle	Shell Petroleum Development Company of Nigeria Limited
Rusal Alscon	534 MWe	Operating fully	Open cycle	Rusal
Alaoji	504 MWe	Operating fully	Open cycle	Rockson Engineering Limited, Burns and McDonnell
Agip-Okpai	480 MWe	Operating fully	Combined cycle	Alstom, Sadelmi, Saipem
Geregu	438 MWe	Operating fully	Open cycle	Siemens. SDEM Erectors Nigeria
Egbema	338 MWe	Operating fully	Open cycle	Rockson Engineering Limited
Omoku	150 MWe	Operating fully	Open cycle	Rockson Engineering Limited
Delta-Ughelli Thermal Power Plant	942 MWe	Operating partially	Sub-critical thermal	-
Omotosho I and II	785 MWe	Operating partially	Open cycle	Chinese private investor &
Afam IV-V	724 MWe	Operating partially	Open cycle	Governemnt
Olorunsogo OCGT	500 MWe	Operating	Open cycle	Chinese private

Mineral for Energy Sustainability: Industries, People, processing and materials are the major contributors of climate change and threat to the environment. Climate-Smart Mining promotes the mining and processing of minerals and metals in a sustainable manner while reducing social, environmental, and climate impacts. Cobalt,

lithium, rare earths, and tellurium are included in the metals for which renewable energy accounts for a major portion of end-use. Lithium-ion batteries for electric vehicles and storage currently account for 4-8 percent of cobalt and lithium demand, with this figure rising to 43 percent by 2020.

Energy Audit: An energy audit is a survey and analysis of energy flows in a building with the purpose of energy conservation. It could involve a technique or system that reduces the amount of energy input while maintaining the system's output.

GREEN AND RENEWABLE ENERGY

Renewable energy is derived from renewable resources that are renewed naturally on a human timeline. Sunlight, wind, rain, tides, waves, and geothermal heat are all examples.Some renewable energy sources are not sustainable, despite the fact that the majority are. A major issue associated with renewable energy is reliability.The drawback with solar energy reliability is that it does not operate 24/7. It is best from 9am to 4pm. Although there are recent developments on a model of solar energy called organic solar cells that utilises infrared and UV as opposed to sunlight to generate electricity. Wind, hydro and others are seasonal and time based too. The problem of reliability in renewable energy is solved with a storage device such as batteries.

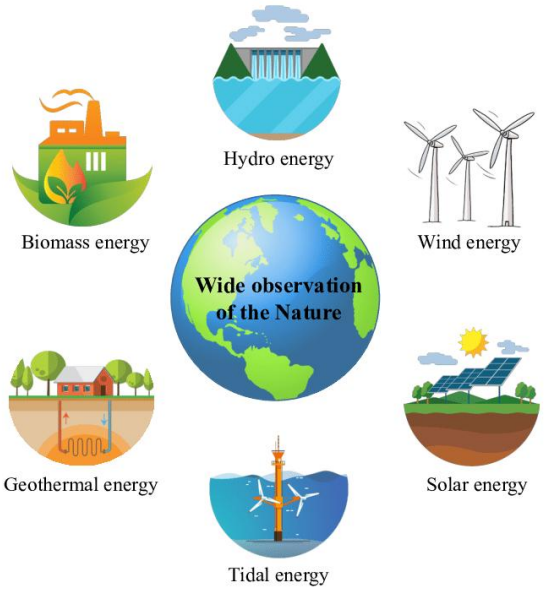

Fig1: Diagram showing the different forms of renewable energy

According to the European commission (EU), renewable energy usage is on the rise among the European nation states. The percentage usage of the key renewable energy is shown in the figure below. Renewable energy sources accounted for 34% of total electricity consumption in the EU in 2019, up from 32% in 2018. Over two-thirds of the total electricity generated from renewable sources came from wind and hydropower (35 percent each). Solar power (13%) was used to create the remaining electricity, followed by solid biofuels (8%), and other renewable sources (9 percent). Solar power is the fastest-growing source, accounting for 1% of all energy in 2008 as shown in Figure 2.

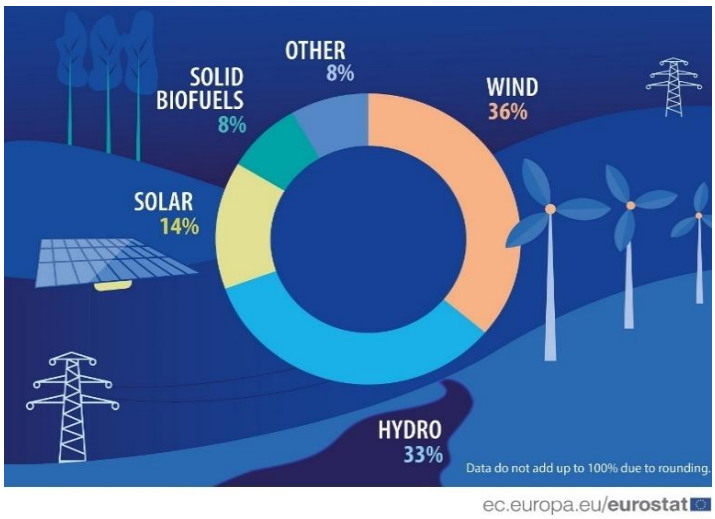

Fig2: Renewable sources generated electricity in the European Union (Source: EU)

In 2019, Austria (75%) and Sweden (70%) generated more than 70% of their electricity from renewable sources than the rest of the EU (71 percent). Denmark (65 percent), Portugal (54 percent), and Latvia (53 percent) also consumed a lot of renewable energy, accounting for more than half of the electricity consumed in these nations as shown in the Figure 3.

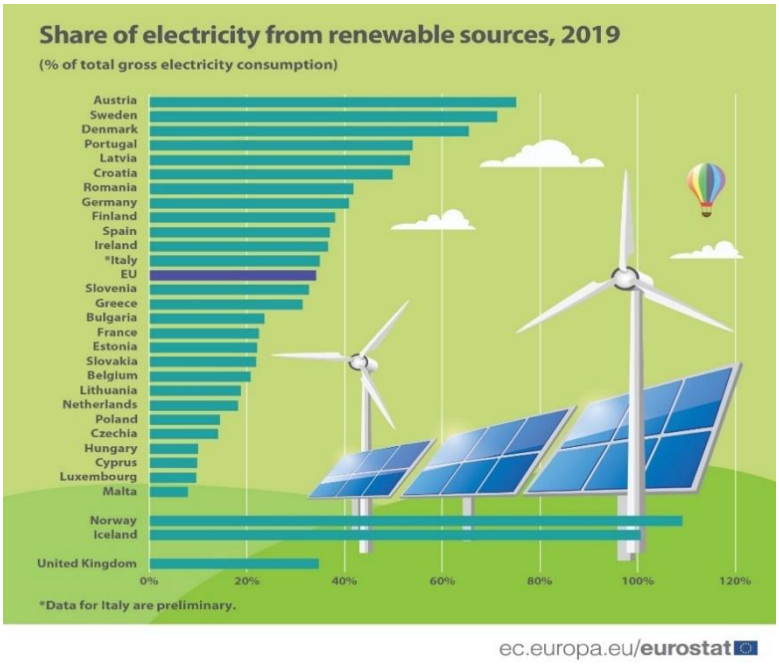

Fig3. Share of electricity from renewable resource, 2019. (source: https://ec.europa.eu/eurostat/web/products-eurostat-news/-/ddn-20210108-1)

Energy Savings Materials: They are materials that save and reduce the cost of electricity and energy in general while making the planet a better place. These include improved LED bulbs, home energy monitors, light control systems, smart thermostats. The United Kingdom government has approved a zero rate for

installations of such materials starting from 1 April 2022 to encourage their usage while helping to achieve net zero economy.

SUSTAINABLE ENERGY MATERIALS: It is imperative to have materials that are renewable, eco-friendly and sustainable for energy applications. Energy materials varies from region to region and so is their classification. However, they are key to development of all sectors of the economy. Energy materials are used in residential, industry, commercial and transportation. Energy is divided into heating and cooling, lighting, manufacturing and driving automobiles and transporting freight. Sustainable development necessitates highly efficient renewable energy production, storage, and management. Batteries and supercapacitors with a focus on sustainable materials, new chemistries, and design considerations for current and future applications in agriculture, mining, transportation, commercial, electronics, aerospace, biomedical, and other industries. Solar cells, photocatalytic water splitting, bioenergy, batteries, hydrogen storage, and fuel cells are among the applications. Scientists and engineers will be given a platform to present their most recent results connected to the Sustainable Energy Common Guideline.

III.ENVIRONMENTAL SUSTAINABILITY

Environmental sustainability is described as appropriate engagement with the environment to avoid natural environmental destruction or deterioration and ensure long-term environmental quality. The key components of environmental sustainability are air, water, management, and risk reduction. Maintain variety and redundancy, control connectedness, manage slow variables and feedback, create complex adaptive systems thinking, encourage learning, broaden involvement, and promote polycentric governance systems are the seven environmental principles.

The Global Risks Report 2022 presents the results of the latest Global Risks Perception Survey (G.R.P.S.), World Economic Forum Global Risks Perception Survey conducted between 2021-2022, followed by an analysis of key risks emanating from current economic, societal, environmental and technological tensions[4]. The report also shows that 23% are worried, 61.2% are concerned, 12.1% are positive, and 3.7% are optimistic when asked, “How do you feel about the outlook for the world? ”The report concludes with reflections on enhancing resilience, drawing from the lessons of the last two years of the COVID-19 pandemic. The key findings of the survey centred around:

Global risk perceptions highlight societal and environmental concerns. For the next five years, respondents again signal societal and environmental risks as the most concerning. However, over a 10-year horizon, the health of the planet dominates concerns: environmental risks are perceived to be the five most critical long-term threats to the world as well as the most potentially damaging to people and the planet, with “climate action failure”, “extreme weather”, and “biodiversity loss” ranking as the top three most severe risks. Respondents also signaled “debt crises” and “geoeconomics confrontations” as the most severe risks over the next ten years. Technological risks—such as “digital inequality” and “cybersecurity failure” are other critical short- and medium-term threats to the world, according to G.R.P.S. respondents

A disorderly climate transition will exacerbate inequalities. Respondents to the G.R.P.S. rank “climate action failure” as the number one long-term threat to the world and the risk with potentially the most severe impacts over the next decade. Climate change is already manifesting rapidly in

droughts, fires, floods, resource scarcity and species loss, among other impacts. In 2020, multiple cities around the world experienced extreme temperatures not seen for years—such as a record high of 42.7°C in Madrid and a 72-year low of -19°C in Dallas, and regions like the Arctic Circle have averaged summer temperatures of 10°C higher than prior years

Good examples of environmental sustainability include the following:

- Renewable energy, such as solar, wind, hydroelectric, and biomass.
- Recycling of metals, such as iron and steel, and minerals.
- Crop rotation and Cover crops.
- Selective logging.

Environmental sustainability, therefore, should be handled with top priority. It should reflect in our design, R & D and manufacturing process.

CLIMATE CHANGE: According to the United Nations, Long-term changes in temperature and weather patterns are called climate change. Although these changes are natural, human activities have been the primary driver of climate change since the 1800s, owing to burning fossil fuels (such as coal, oil, and gas) and producing heat-trapping gases. Rich countries, such as the United States, Canada, Japan, and much of western Europe, make up only 12% of the world population yet, they are responsible for 50% of all planet-warming greenhouse gas emissions from fossil fuels and industry over the last 170 years.

While the current consequences of human actions on earth's climate are irreversible on the timescale of humans alive now, every amount of prevented future temperature increases results in less warming that would otherwise remain indefinitely. During COP25 in Madrid, the German watch Institute announced the results of the Global Climate Risk Index 2020. Based on the impacts of extreme weather events and the socio-economic losses they create, the report identified Japan, the Philippines, and Germany as the most affected countries.

*How will NMS and her members be affected by Climate change??*Climate change can harm human health by deteriorating air and water quality, increasing the spread of some diseases, and changing the frequency and intensity of extreme weather events. Rising sea levels threaten coastal towns and ecosystems.

*Why the big fuss about climate change??*This rapid rise is an issue since it alters our climate too quickly for living things to adapt to. Climate change has a variety of consequences, including increased extreme weather events, increasing sea levels, altering species populations and habitats, and more.

*Why do we need to end climate change???*Warmer temperatures exacerbate public health issues such as heat-related illnesses, a rise in vector-borne infections, and reduced access to safe water and food. Short-lived climate pollutants can help halt global warming and reduce public health hazards.

CURRENT POLICY ON ENERGY: Globally, energy policy is shifting to decarbonisation in infrastructure and technologies. The overwhelming body of scientific evidence indicates that human-caused global climate change is occurring, with biophysical, social, and economic consequences at the local, national, regional, and global levels. It's simply going to get worse in the next decades.

Climate change has become a major threat to Nigeria's goal of sustainable human development, as it has in many other developing countries. The Federal Government of Nigeria has climate change adaptation and mitigation concerns properly integrated into its national development plan known as Vision 20:2020. The Federal Ministry of Environment, through the

special climate change unit, produced a 45 - page document titled "National Environmental, Economic And Development Study (Needs) For Climate Change In Nigeria" [5]. The report opined that responding to climate change from mitigation and adaptation angles requires strategic approaches from policy, regulatory and institutional frameworks and capacities.

Nigeria contributes minimally to greenhouse gas (GHG) emissions. The total GHG emissions (in CO2 equivalent) for the three main greenhouse gases (CO2, CH4 and N2O) and from the five main sectors (energy, industry, agriculture, land-use change and forestry - L.U.C.F. – and waste) were about 330,946 Gg CO2e in 2000. The GHG emissions were distributed unevenly among the three main gases, i.e. net CO2 was 214,523 Gg, representing 65% of the National GHG emissions, methane (CH4) was 109,319 Gg CO2e or 33%; and nitrous oxide (N2O) totaled 7,104 Gg (CO2e) or 2%. Energy: Total CO2 emissions in the energy sector amounted to about 108,000 Gg CO2 in 1995, and this is expected to rise to 186,000 Gg CO2 in 2020, 232,000 Gg CO2 by the year 2030 in the baseline scenario and 359,000 Gg CO2 in 2050, at an average annual growth rate of 2.2%. Cumulative reduction from baseline till 2030 is 887,000 Gg CO2.

The NEEDS report listed the following as the most promising mitigation options in Nigeria's energy system:

(i) introduction of compact fluorescent light (C.F.L.) bulbs at a negative incremental cost of $58/ton CO_2, with a 5.155m ton CO2 reduction capacity;

(ii) introduction of improved kerosene stoves in households, at the cost of $21/ton of CO_2 reduced (6.122 m ton CO2 reduction capacity) ;

(iii) fuel-oil to natural gas fuel substitution in the cement industry at $18/ton (7.49m ton CO_2 reduction capacity); (iv) improved electrical appliances ($16/ton) and wood-stoves ($3/ton) in the residential sector (9.566m ton CO2 reduction capacity); and introduction of efficient motors in the industry at $15/ton (10.738m ton CO2 reduction capacity).

These are lofty and will help curb the adverse effects of climate change. Implementing these policies however will be crucial in attaining a NetZero position.

RECYCLING THE GREEN ENVIRONMENT FOR THE CLEAN FUTURE:

If we are ready to go beyond short-term profits, recycling has the potential to be a significant tool for long-term sustainability. The CLEAN Future Act directs all federal agencies to use all existing authorities to put the country on a path toward a 50 percent reduction in greenhouse gas pollution from 2005 levels by no later than 2030, and to net zero no later than 2050. Nigeria needs to reduce the amount of scraps exported and use same to drive the foundry industry. A lot of money is lost to exportation of useful materials that can generate revenue to the country.

RESEARCH AND DEVELOPMENT FOR ENERGY SUSTAINABILITY

Research and development is an important factor in determining the effects of GDP and the development of financial markets and institutions. R&D enhancement reduces the impacts of market expansion on hydropower; however, such effects are incremental for solar, wind, bioenergy, and geothermal energy resources. Global R&D spending in the energy sector is anticipated to increase slightly to 22.5 billion U.S. dollars in 2019. As of 2018, less than half of this investment was for R&D in renewable energy. The sustainable development of the energy sector for countries with transitioning economies should be based on the energy trilemma (Energy security, Energy sustainability and Energy Affordability). Four principles are proposed: diversification of energy resources and energy generation sources, ensuring energy efficiency, ensuring energy affordability, and green

energy production. Reliable and affordable energy, particularly electricity, is essential for health care, education, and economic development. As of 2020, 790 million people in developing countries do not have access to electricity, and around 2.6 billion rely on burning polluting fuels for cooking.

WHAT ROLE CAN THE METALLURGICAL ENGINEER/SCIENTIST PLAY IN CLIMATE CHANGE AND SUSTAINABLE DEVELOPMENT:

According to a survey by the World Federation of Engineering Organisation ,engineers/scientists have a leading role to play in the decarbonisation and sustainability of the earth. Corporate organisations and professional bodies across the globe are already taking action and implementing technology and innovations to encourage a green and sustainable world. Chevron and Phillips 66 already bought into the Climate Transition. The royal academy of engineering (R.A.E.), United Kingdom, hasmobilised about450,000 engineers for U.K.'s 2050 decarbonisation strategy[6]. Also, the American Petroleum Institute (API) has a comprehensive policy on both near-term demands and long-term value for Oil & Gas for a greener economy. Engineers Australia, the equivalent of C.O.R.E.N. in Australia, engages and implements members to vote in the federal elections for candidates focusing on environmental sustainability and green energy. Here in Nigeria, the Nigerian Academy of Engineering has emphasized the need to deploy a multidisciplinary approach to mitigate the impact of climate change on the environment. The NAEng also recommended reducing or removing emissions, implementing a global climate change agreement and sensitizing the public on the effects of climate change. In 2010, the Nigerian Society of Engineers hosted Engineers here in Abuja for her A.G.M. The theme was "Engineering Response in Combating the Effects of Climate Change in Africa".

The metallurgical society has a huge role in developing the right energy mix that will contribute to the green economy and help in environmental sustainability. These roles may include:

- Research and development of materials for storing some of the green energy mixes such as hydrogen, small modular reactors, green nuclear energy
- Development of alloys capable of storing hydrogen, being used in the nuclear and small modular reactor
- Domestication and improvement in the use of 3D printing technology to meet the energy and other materials needs of the economy
- Lobbying and influencing policy at the grass roots while encouraging politicians to focus on and encourage environmental sustainability and a green economy.
- Society needs to encourage and engage the next generation of materials professionals, the young metallurgical professionals (students and emerging scholars), in the scheme of things for a green and environmentally sustainable Nigeria (world).
- Society needs to develop position paper(s) on these crucial areas and organise periodical webinars and other avenues for education and sensitisation of the populace.
- Organising programs and events where policymakers, experts, and stakeholders can come together to build on basic scientific data and quickly implement affordable, efficient, egalitarian, respectful, and inclusive solutions for everyone.
- Development of standards and codes for revenue generation and regulation of the sector

Current Trends and Opportunities for NMS

Most countries research hydrogen generation and storage. Namibia and South Africa have a ministry devoted to this technology. Other developed countries such as the U.S.A., U.K., and Germany already have hydrogen generation and storage machinery, small modulator reactor, and nuclear. Professionals' bodies in U.K. and U.S.A. (R.A.E. and A.S.M.E., respectively) are already meeting with government and government agencies for policy formulation

and other modalities to become leaders and key players in this sector. The Nigerian Metallurgical society can increase relevance and play an active role in the above technologies by developing key alloys, appropriate technology, and more education/awareness. A symposium or a relevant forum can be organised with key stakeholders, including government agencies, to demystify the technology with deep insight from the materials and metallurgical perspectives. Worthy of mention is nanotechnology and the fourth industrial revolution. Research should be increased on developing energy storage devices such as batteries to solve the reliability problem associated with renewable energy. Solar technology recently made a headway. There is solar that can generate electricity during the night or even when it is raining. This was hitherto a major drawback of solar energy. The technology utilises U.V. and infrared for charging solar panels instead of the traditional 9a.m. to 4.30p.m. sunray.

Energy Technology

- Solar
- Fossil Fuel
- Photovoltaics
- Power Generation
- Biomass
- Waste to Energy
- Hydrogen
- Renewable Energy
- Nanotechnologies for energy conversion, storage, and harvesting

Smart materials Nanomaterials in energy systems Materials for Energy Applications not limited to:-

- Materials for thermo electric energy conservation
- Inorganic and organic solar materials, including thin films and single crystal devices
- Materials for rechargeable battery applications
- Super Capacitors
- Materials and approaches for hydrogen generation and storage
- Materials and approaches for water splitting
- Fuel cells
- Photo catalysis
- Piezo electronics

Modern materials that might make energy transmission more efficient

- Advanced Composites
- Hybrid materials
- Engineered polymers and
- Low-density/high-strength metals or alloys

Energy materials encompass a broad class of materials that may have applications in energy conversion or transmission.

Contribution of Engineering Materials Development Institute (EMDI-NASENI) to the Sustainability of Nigeria:

E.M.D.I. is one of the Institutes under the National Agency for Science, and Engineering Infrastructure (N.A.S.E.N.I.) mandated to conduct research and development on engineering materials, processes, and systems to convert raw and semi-process materials into engineering materials of various types and prototypes.

Its mandates include the following:

To undertake research and development works into processes and systems for converting raw and semi-processed materials into engineering materials of various types, sections and sizes for application in machinery and equipment production.

To transfer engineering material production technologies to the private sector, industries and government agencies and render consultancy and extension services to such and other organisations

To establish and operate a physical and metallurgical laboratory for the testing of engineering materials of all types

To collaborate with cognate government ministries and agencies in the design of its research and development programmes and projects.

v. To accept on terms specified by it, trainees for practical work attachment in its works.

vi. Aggressive research into solar energy, hydro and other sustainable energy

Engineering materials development institute (E.M.D.I.) has developed some products that can be utilised in economic recovery and sustainability by individuals and organisations. E.M.D.I. leveraged science, engineering and technology to produce the following items and equipment.

- 3D printing machine
- s.
- Different categories of furnaces
- Different categories of hydro turbines and solar energy have been produced and can be tailored to help all categories of industries and individuals to meet their electricity needs
- Different categories of materials such as ductile iron (DI) and austempered ductile iron (A.D.I.)
- Different classes of C.N.C., NC and conventional machines can be used in manufacturing and producing varieties of products for the S.M.Es and other venture

NASENI INTERVENTION IN COVID-19

NASENI DISINFECTING TUNNEL-O

NASENI DISINFECTING TUNNEL-n

NASENI DISINFECTING CUBICLE

NASENI DISINFECTING SINK

(a)

(b)

(c)

(d)

Fig 9: Some selected E.M.D.I. products (a)Rotary furnace (b) ASTM grey cast iron grade 20 Manhole cover (c)Yam pounding machine (d)8-mould interlocking brick making machine

CONCLUSION

NMS and her stakeholders should consider sustainability, people and the environment in her day-to-day dealings, R & D, and production process. It took decades for the world to recognise the threat of climate change and take real action. The natural disaster cannot wait.It is an emergency that requires immediate intervention. Fortunately, many of the climatic standards, frameworks, and regulatory systems can be adapted to nature, which is now happening. Organisations that embrace the need to grasp the problem and act quickly and decisively will be best positioned to handle environmental risks and opportunities and reap the greatest benefits from the net-zero and nature-positive transformation.

As a professional body, the NMS is expected to be the driver, implementer and champion of policies and appropriate technology, especially in the areas of energy, climate change, and materials development (nanotechnology). It isdoing an excellent and lofty job, and I have no doubts that at the close of the A.G.M. and conference, more solutions and ideaswill be advanced in this regard.

We at E.M.D.I. and N.A.S.E.N.I. are open to collaborating and ceding technology. Our motto is “ASK US FIRST.”

REFERENCE

Rogers, M., *These 9 technological innovations will shape the sustainability agenda in 2019*. 2019, Mckinsey and Company.

2. Desjardins, J. *The World's Projected Energy Mix, 2018-2040*. 2020; Available from: https://www.visualcapitalist.com/the-worlds-projected-energy-mix-2018-2040/.
3. Occhiali, G. and G. Falchetta, *The changing role of natural gas in Nigeria.* 2018.
4. (WEF), W.E.F., *The Global Risks Report 2022 17th edition insight report*. 2022. p. 117.
5. FEDERAL MINISTRY OF ENVIRONMENT ABUJA, N.S.C.C.U., *NATIONAL ENVIRONMENTAL, ECONOMIC AND DEVELOPMENT STUDY (NEEDS) FOR CLIMATE CHANGE IN NIGERIA* 2010. p. 45.
Sutton, J. *Government Industrial Decarbonisation Strategy published*. 2021 [cited 2022 21 May 2022]; Available from: https://www.raeng.org.uk/news/news-releases/2021/march/government-industrial-decarbonisation-strategy-pub.

NMS-PP 003

Engr. Prof. Eli JidereBala, FNIMechE, FNSE, FAEng.

The Director General and Chief Executive Officer, Energy Commission of Nigeria At the Opening Ceremony of the 38thAnnual Metallurgical Conference of the Nigerian Metallurgical Society held at University of Abuja; 26th – 29th October 2022 On the Theme "Role of Materials Industry in Energy Mix Transition and Environmental Sustainability"

Protocols

I am highly honoured and delighted to be invited to deliver the keynote speech at this prestigious 38thAnnual Metallurgical Conference, a collaborative effort by the Nigerian Metallurgical Society, industries, and institutions, which are the key drivers of any nation to achieve sustainable development. The theme of this year's conference is apt and commendable at this time when Nigeria and indeed the whole world, are making efforts towards energy mix transition.

Though the figures vary significantly from one country to another, fossil fuels dominate the energy mix at the global level, accounting for over 80% of the total energy consumption, and 63% of electricity generation. Fossil fuels also account for about three quarters of the global greenhouse gas emissions responsible for global warming and climate change.

Consequently, countries are strategizing to achieve the ambitious targets establishedat the Paris Climate Agreement in 2015 to limit the increase in global temperatures to 1.5 degrees Celcius or 2 degrees Celcius at most. To achieve this goal, the world needs an energy mix transition currently dominated by fossil fuels.

Several recent studies, including the World Bank report on The Growing Role of Minerals and Metals for Low Carbon Future published in 2017,The Role of Critical Minerals in Clean Energy Transitions published by the International Energy Agency in 2021, and the Materials for the Energy Transition published by the International Renewable Energy Agencyin 2021,highlight the potential impacts that the transition from an energy mix dominated by fossil fuels to low-carbon energy technologies will have on demand for many minerals and metals.

According to the reports, minerals and metals expected to see heightened demand include: aluminum, copper, lead, lithium, manganese, nickel, silver, steel, and zinc, and rear earth minerals such as indium, molybdenum, and neodymium. The low carbon technologies that emerge as most applicable and beneficial will play a larger role in driving the demand for metals.The most significant is electric storage batteries, where the rise in relevant metals – aluminum, cobalt, iron, lead, lithium, manganese and nickel are expected to grow significantly depending on the degree to which countries commit to low carbon future and the intra-technology choices.

The types of mineral resources used vary by technology. Lithium, nickel, cobalt, manganese and graphite are crucial to battery performance, longevity and energy density. Rare earth elements are essential for permanent magnets that are vital for wind turbines and electric motors. Electricity networks need a huge amount of copper and aluminum, with copper being a cornerstone for all electricity-related technologies. The shift to a clean energy system is set to drive a

huge increase in the requirements for these minerals, meaning that the energy sector is emerging as a major force in mineral markets. Until the mid-2010s, the energy sector represented a small part of total demand for most minerals. However, as energy transitions gather pace, clean energy technologies are becoming the fastest-growing segment of demand.

A typical electric car requires six times the mineral inputs of a conventional fossil fuel car, and an onshore wind plant requires nine times more mineral resources than a similarly sized gas fired power plant. Demand outlooks and supply vulnerability vary widely by mineral, one of the studies projected that the energy sector's overall needs for critical minerals could increase by as much as six times by 2040, depending on how rapidly governments act to reduce emissions.

DistinguishedLadiesandGentlemen, the purpose of a keynote address is to set the basis for reflection and discussion. I therefore enjoin the conference participants to look in detail at the following aspects that are germane to the security of metals and minerals relevant to the ongoing energy mix transition.

1. Thorough analyses of the demand and supply outlooks in the short, medium and long-term horizons.
2. Promoting technology innovation at all points along the value chain by stepping up R&D efforts for technology innovation on both the demand and supply sides of the metals value chain.This can promote substitution, efficient utilization of the materials , and price reduction.
3. Ensuring adequate investments to diversify sources of supply so as to avoid scarcity and price escalation.

. Scaling up recyclingas in circular economy. Circular economy policies can play a pivotal role in preparing for rapid growth of waste volumes by incentivizing recycling for products reaching the end of their operating lives, supporting efficient collection and sorting activities and funding R&D into new recycling technologies.

. The waste that results from using the materials has the potential to pollute the environment if not properly managed. Mainstream higher environmental, social and economic governance (ESG) standards. Efforts to incentivize higher environmental and social performance can increase sustainably and responsibly produced volumes and lower the cost of sourcing them. If industry players with strong environmental and social standards are rewarded in the marketplace, this can also bring new suppliers to a more diversified market.

. Strengthening international collaboration between producers and consumers of the materials for energy mix transition.

Given the material intensity of low-carbon technologies, any potential demand -supply gaps or constraints could impact the speed and scale at which certain technologies are able to be deployed. As such, a broad range of industries will be exposed to the terrestrial, oceanic and economic risks associated with the production and use of these resources.

Conclusion

Nigeria is blessed with over 44 solid minerals deposits across the country which includes copper, lead, zinc, gold, iron ore, limestone, dolomite, kaolin, barites, tin, as well as gemstones and dimension stones. Some of the minerals are critical to the success of the energy mix transition goal. Nigeria should examine thoroughly how we can participate

effectively in the emerging materials for energy mix transition market.

In April this year, the Federal Executive Council approved the Revised National Energy Policy and its related National Energy Master Plan. The Policy and the Master Plan address climate change policies and how to achieve them. However, we should be thinking of how to mainstream energy mix transition materials into the documents in order to ensure the success of the transition programme. We look forward to the recommendations of the conference.

NMS-TP001

ENERGY AUDITING OF FURNACES AT THE FOUNDRY SHOP: TPERSPECTIVE OF THE AJAOKUTA STEEL COMPANY LIMITED

Ocheri C. , J. N. Ezeanyanwu, N.I. Amalu, A.C. Iyasara , Oyibo. A. O. & Adidi O. D.
Dept. of Metallurgical and Materials Engineering, University of Nigeria, Nsukka, Enugu State,
Dept. of Metallurgical and Materials Engineering Enugu State University of Science and Technology, Agbani
Projects Development Institute (PRODA), Enugu State, Nigeria
Department of Ceramic and Glass Technology , Akanu Ibiam Federal polytechnic , Unwana , Ebonyi State
Dept. of Welding and Fabrication Engineering ,
Department of Mechanical Engineering
Delta State Polytechnic , Ogwashi-Uku
Delta State
Email: cyril.ocheri@unn.edu.ng
Phone no: +2348051793922

ABSTRACT

The study's main objective is to evaluate the energy effectiveness of furnaces used in foundries. Two melting furnaces, the one tonne induction furnace and the six tonnes electric arc furnace (EAF), had been evaluated. There are various melting processes used in the production of some types of steel and cast iron elements in the furnaces. It was found that every melting procedure wasted more time, energy, and money rather than following the normal melting cycle of two and a half to three hours. Studies have been performed to determine how much time and energy were used when the furnaces were operated. The six tonnes capacity electric arc furnace's operational procedures were observed from 03/06/2005 to 01/08/2007 during a specified time period during which the experimental operations were conducted (5/10/2006 to 21/11/2007). The furnaces' meters were read before and after the manufacturing processes, which included the time required to complete a production melting cycle. The cost per kWh for the energy arrangement was set at = N9. The findings suggest that a total of 163.3 hr/min might have been saved by running the two furnaces at a typical melting rate of 2½ hr/min for each cycle. The procedures showed that a total of 19,400 kw/h of energy was spent, which could have been reduced by operating these furnaces, as well as a total cost reduction of (N133, 290). An energy audit becomes very useful in terms of reducing energy use, processing time, and equipment life.

Keywors: Energy, industry, metallurgical, money saved, interruptions, investment expenses, and auditing

1.0 INTRODUCTION

Optimizing the total amount of time, money, and energy spent on the production process is vital for groups, corporations, and private sector workers equally.

Any manufacturing organization would find it appealing to save money on energy bills. There is a way to implement an energy cost-effectiveness control program that is sustainable for homes with high electricity bills. [1] "Lower or a minimum expense of operations for improvements that minimize a customer's or manufacturing sector's utility bills between 15 to 25%." Investments with payback times of two

years or less should save 20-30% of their capital expenses on average[2].

In many instances, these energy cost mitigation techniques may also lead to decreased energy use and atmospheric pollution emissions. One of the initial steps in putting into place a good energy cost management program is to conduct an energy audit.[3] .An installation's consumption of energy, the cost of that energy, and a suggested initiative to improve working procedures are all thoroughly analyzed in an energy audit[4].

Implementing a framework to reduce energy consumption expenditures in order to increase cost-effectiveness. Because an audit is sometimes characterized as an energy survey or an energy review, its negative connotation is unaffected [4]. The energy audit is a fantastic event with tremendous benefits for the organization or entity. The Ajaokuta Foundry shop, with a nominal capacity of seven (7,000) tonnes, is a captive operation that produces ferrous and non-ferrous spare parts for the steel factory as well as clients outside the company.

Due to its remote position from urban areas, the Ajaokuta steel plant is planned to meet 78% of its internal spare parts demands in the types of machinery components and replacement parts with medium to heavy unit weights.

The steel plant's foundry shop is part of the interconnected network of ancillary service shops, with some shops located within a space parameter such as the Forge and Fabrication shop, Machine and Tool Shop, and Power Equip shop, in the same way that most integrated steel plants worldwide, particularly in third-world countries, have been built from the ground up to be self-sufficient in achieving their fundamental replacement component requirements in order to prevent prohibitively costly interruptions and losses.

A precision Die-Cast foundry would be able to produce large quantities of items or exact replicas, but the foundry shop is a jobbing business and cannot do either. It could only occasionally produce single unit commodities because the capacities of different vessels, furnaces, and other handling infrastructure vary substantially depending on the furnace[6].

The furnaces used in the production techniques were designed to achieve a melting period of between 212 and 3 hours for batch production, followed by a casting schedule of 35 to 50 minutes. Small component knocking-out and fettling takes between 1 and 1½ hours, and a further heat treatment takes between 2½ and 15 hours, depending on the composition of each item mixture.[7].

The production procedure, energy consumption, cycle time, and production cost were monitored for a period of two years. In two of the furnaces, research was conducted on the six tons electrical arc furnace and the one ton induction furnace from October 5, 2006, to November 21, 2007, and from June 3, 2005, to August 1, 2007, respectively.

It was noted that during these times, batches of melting cycles required a lot of time and energy to complete, which added up to high energy costs. As a result, the shop found it challenging to complete production processes in the allotted time due to the rising cost of energy and likely energy waste. The operating processes allow for the usage of card melting as a data collection method. As illustrated by tables (1) and (2), the gathered data were presented in tabular format. (2).

The variables were represented graphically to analyze the data that had been gathered. The discoveries led to the investigation process which becomes pertinent with significant connotations . Records indicated that there were several issues

associated with the production processes because heat cycles took an extended period of time to complete, an enormous amount of energy was consumed, and some revenue being wasted. These discoveries forced the shop to conduct energy audits on the furnaces in order to identify any potential causes for the anomalies that occurred and to suggest alternative solutions for reducing the issues caused by excessive energy use, energy waste, and the length of time required to complete a melting batch cycle.

2.0 Research Methodology

The first step in the audit procedure was to compile data on the equipment's functionality and bills for utilities history. When the data from the furnaces were analyzed, it became clear how the furnaces were likely to waste energy, cut energy expenses, and help the shop management identify the areas that needed to be looked into[8].

When it comes to the developments known as Energy Conservation Opportunities (ECOs) which have been discovered and evaluated, the processes provided the furnace operators with certain benefits and their cost-effectiveness. As part of an economic comparison, these ECOs were evaluated in terms of costs and benefits and ranked by the different ECOs. The actual processes of conserving resources and money got underway after an action plan was created [9].

2.1 Materials and Equipment

2.1.1 Materials

Approximately 16 steps constitute the operational processes for the foundry, including planning, pattern creation, sand preparation, core and mould production, drying the produced cores and moulds, melting and casting, quality and materials analyses, material selection, felting, and heat treatment processes, among others. Therefore, some basic raw materials were used to complete these procedures in order to accomplish these processes for the shop's operations. Figs. 1 to 4 display the different types of raw materials used in the manufacturing activities' production mix. Sand, binding materials such sodium silicate, bentonite, core oil, and industrial starch are used in the production of molds and cores. Patterns were made using materials like wax and wood. For melting and casting, various materials like ferroalloys, chamotte, crop ends, foundry returns, and pig iron are employed. Induction and electric arc furnaces were used to create a range of steel and cast iron materials. Cast iron is split among various kinds, including malleable, grey, nodular or spheroidal graphite iron (SGI), and white cast iron. Manganese, stainless, chromium, and other types of steel are among these

Fig 1: Pig iron

Fig 2: Crop end of steel scrap


Fig 3: Foundry Returns


Fig 4: Ferro Manganese

2.1.2 Equipment

In foundries, electric arc furnaces, induction furnaces, crucible furnaces, and centrifugal furnaces are the main equipment employed. One (1) low-frequency induction furnace and a six-ton electric arc furnace were the subjects of the study's inquiry. These furnaces were used to produce liquid metals through the melting and casting processes. The furnace types employed for this research project are depicted in the figures below

.


Fig 5: Electric Arc Furnace showing the charging view


Fig 6, the tapping spout

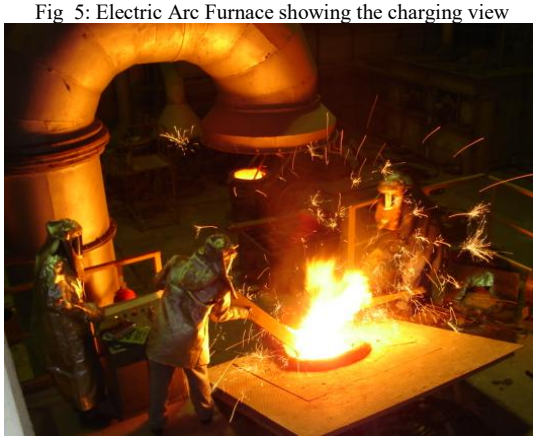
Fig 7 the de slagging process in the Induction furnace

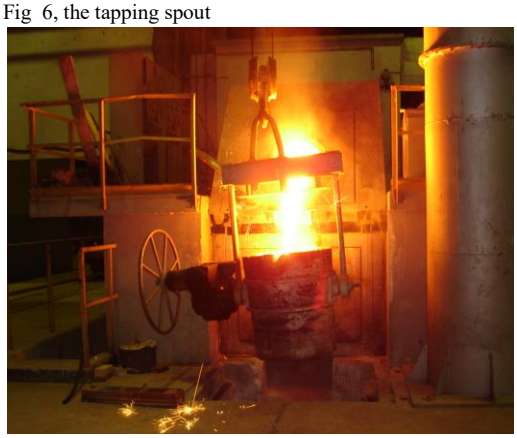
Fig 8: the teeming process from the induction furnace

These types of operational information provide an in-depth representation of the main processes or structures that utilize energy resources. The biggest energy and operational cost effects on this equipment should always be looked at while performing this offered a clear image of the energy, time, as well as manufacturing costs that had been conserved.[10].

2.2 Methods

The study methodologies used involved taking readings from meters mounted to the two furnaces before and after operational procedures in order to monitor the two furnaces' operational processes. Figure 9 displays an example of the melting card used to gather data.

The shop's electrical and electronic departments were required to keep an eye on the effectiveness and efficiency of the furnaces' operational processes. To check and verify the meter data, the workers in the melting and casting area worked along with those who worked in the area of quality control and materials analysis section.

APPENDIX D

ASCL — MELTING CARD

FURNACE: One Ton Indu · CAST NO. 37 · QUALITY S.G.IRON · DATE: 09/05/07

CHARGE	KG
PIG IRON	579.4
SCRAP I	
SCRAP II	
CAST-IRON SCRAP	
RETURN SCRAP(Foundry returns)	333
STEEL SCRAP	73.9
AMOUNT CHARGE	986.3

ADDITIVES	REMARKS	
Fe-Si	75%	12.5
Fe-Mn	75%	1.2
Fe-Cr		
Fe-Mo		
Fe-Ni		
Ca-Si		
Al		
AMOUNT ADDITIVE		13.7
TOTAL -FURNACE CHARGE		1000

POWER

	CURRENT CONSUMPTION	FREQUENCY
TIME		KWH
POWER ON	6.35 am	592
POWER OFF	7.30Pm	598

TOTAL CURRENT CONSUMPTION 4KW/ H

	FROM	TO	MIN./ HOURS
PATCH CHARGE	6.35 am	7.30pm	
MELTING DOWN	3.50 pm	7.25 pm	
TAP			

TOTAL DURATION OF MELTING TIME HOURS

DURABILITY: BOTTOM | SIDE WALLS | ROOF

LADLE SIZE

ADDITIONS 3Kg of Slag coagulant was added to the ladle as exothermic compound

ANALYSIS

	%C	%Si	%Mn	%P	%S	%Cr	%Mo	%Ni	%Mg	%Al	%Fe
TARGET	3.2	2.5	0.55	0.1	0.1				0.06		
ACTUAL	3.29	2.59	0.60	0.02	0.01	0.082	0.005	0.144	0.08	0.015	92.95

TIME	OPERATION	KG	C	Si	Mn	°C
6.35am	The furance was energized				Tempt readings	
10.45am-1.30pm	The system was stopped due to low current	low			1st	1389
1.30pm	The process of melting -re-started				2nd	1400
3.50 pm	Melt down was achieved				3rd	1419
7.05pm-7.06 pm	Deslagging took place				4th	1441
7.08 pm	1st sample was taken					
7.10 pm	Addition of Fe-alloys					
7.21 pm	2nd sample was taken					
7.22pm	0.06kg Mg was added into the Ladle					
7.24pm -7.25pm	Melt was teemed into the Ladle					
7.26pm - 7.35pm	Pouring / Casting took place					

FORMAN — MELTER — QUALITY CONTROL OFFICER

SOURCE: From Analysed Samples from Heat No:37 with the use of Spectro - Analytical Instrument; Quality Control and Materials Unit of Foundry & Pattern Making Shop

Fig 9: Sample of the melting card use for collecting data for the energy audit

3.0 RESULTS AND DISCUSSION

3.1 Operation Times: The facilities' period of operation were found. Two shifts and three brigades made up the shift organization under consideration [11]. A three-shift would be cost-effective from the perspective of energy costs because more kWh would be dispersed over the requested price. The sort of melting cards used to monitor the readings from the furnaces during operational activities are depicted in Fig. 9. The actions were imputed in the melting cards for accurate and effective tracking.

3.2 Energy Audit

There were some initial restrictions set. Prior to turning on the furnaces, the operations began by evaluating the last set of meter readings. When the process for operating was complete, comparable processes were performed accordingly. [11-12]. During these periods, data on the energy usage by facilities was gathered simply examining

utility bills, including metered invoices, melted cycle successful completion certain points, and the amount of energy utilized during each operational procedure. The approaches, which include a visual representation of the equipment and information on how it works, were created to provide people a better understanding of the energy audit processes. Analyzing the acquired data allowed for the determination of energy efficiency. [13-15].

3.3 Costs Associated with Electricity Consumption

The maximum kW/h capacity required for the shop at each melting cycle or heat was the main focus of the demand charge. Power is the term used to describe the varying amounts of energy used by the various institutions. The power readings were averaged over intervals of twenty-five (25) minutes to ninety (90) minutes by the electric utilities. Very slight modifications had no detrimental effects on how the furnaces worked. [16-18] . The shop might therefore be compensated for the heat demand based on the total value of an ideal melting cycle/heat average of the electricity consumed. [19] . The breakdown of energy bills into the parts that control the equipment produced the data. For a better graphical presentation, these cost components were first detailed separately in the tables before being plotted. The electricity cost per kWh into energy usage, length in hours and minutes (Hr./min), and cost per kW per heat were divided against the electricity bills.

The store produces liquid metal for steel and cast-iron items, which is based on consumer demand. Almost all of the country's energy requirements are met by the Thermal Turbo Plant and Thermal Power Station, a power plant housed inside a steel mill. (TPP& TPS). When the research studies were done (between 2005 and 2007), the energy structure rate was set at N9 per kWh.

3.4 Summary of Results

The six electric arc furnaces and the one induction furnace were anticipated to use an average of 3 kW/h of energy, take an average of 2½ to 3 hours to complete a melting cycle, and have appropriate manufacturing costs.

The data on the energy consumption in electric arc furnaces from March 6, 2005, to January 8, 2007, and from October 5, 2006, to November 21, 2007, was shown in Tables 1 and 2, respectively. The research studies took place for a total of 26 heats, or 182.78 hours and minutes. The furnace would have produced 122.98 hours per minute had it been run at the regular rate of 212 to 3 hours per minute, saving 59.8 hours per minute over the course of the 26 heats, as shown in figure 10.

As indicated in fig. 11, the energy consumption for 26 heats was calculated to be 20,600kW/h, as opposed to 10,200kW/h if the furnace had been run with a 3kw/hr energy input. These actions utilized a total of 10,400kW/h of energy, which might have been saved. The amount of resources/funds spent on the furnaces was calculated at N185,400 as cost-effectiveness for 26 heats at N9 per kW/h compared to what could have been spent at a minimal cost of N91,800, which could have saved at N93,600 as shown in fig. 12.Similar results were obtained for the one-ton induction furnace, as depicted in fig. 13. Calculated at 335.82 hours per minute, the total time needed for 45 heats the number of times the complete batch melted was fewer than the required time by at least 223.32 hours per minute, yielding a time savings of 103.5 hours per minute.

Fig. 14 showed a total energy consumption of 13,500 kW/h, which was more than the required minimum energy consumption of 4,500 kW/h. The loss of

9,000 kw/h may have been avoided thanks to these procedures.

According to Fig. 15, a total of N39, 690 might have been saved from these efforts. The 45 heats were found to have cost a total of N121,500 at a cost of N9 per kW/h as compared to a minimal cost of N81,810. In order to save time, energy, and money on the furnaces, the values of a six-ton electric arc furnace and a one-ton induction furnace may have been combined.

Table 1 shows the energy used by the electric arc furnace from October 5, 2006, to November 21, 2007.

Date	Time (HR/ MINS)	Duration (Hr/Mins)	Standard (Duration) Hr/Mins)	Duration Hr/Mins)	Max(EC) (Kw/h)	Standard (Kw/h)	Min(EC) (Kw/h)	Min Cost (N1)	Max Cost (N)2
1/9/2005	9.35 AM -6.35 PM	8. 1	2½ -.3	6.5	750	350	200	1800	6700
12/12/2005	9.48 AM-5.02 PM	7. 44	2½ -.3	4.67	1050	350	500	4500	9200
14/12/05	10.00 AM-7.32 PM	9.15	2½ -.3	7.92	1250	350	700	6300	8600
5/1/2006	7.44 AM-4.12 PM	8. 30	2½ -.3	6	1250	350	600	5400	3000
9/2/2006	8.21 AM-3.30 PM	7. 05	2½ -.3	5.25	1050	350	500	4500	8100
13/02/06	9.20.00 PM-6.21 PM	8.1	2½ -.3	6.7	10500	350	500	4500	9500
15/02/06	730 AM-3.09 PM	7. 36	2½ -.3	6.12	880	350	540	4860	7665
23/02/06	8.015M-5.15PM	9	2½ -.3	7.5	1050	350	570	5130	7856
1/3/2006	7.32 AM-5.15 PM	9.3	2½ -.3	8.2	895	350	390	3510	8656
13/03/06	9.30 AM- 7.22 PM	9.15	2½ -.3	8.12	1125	350	800	7200	12800
23/03/06	10 .25 AM-5.25 PM	7. 3	2½ -.3	6	1000	350	500	4500	9563
3/4/2006	8.24AM-3.52PM	5	2½ -.3	4.8	750	350	100	900	6500
1/9/2006	7.52AM-2.22 PM	7	2½ -.3	6.9	250	350	-100	-900	5499
3/11/2006	7.450 AM-6.23 PM	11.15	2½ -.3	7.65	2100	350	1200	10800	16660
17/11/06	7.56 AM-2.17 PM	5. 9	2½ -.3	4.76	650	350	100	900	6550
28/12/06	12.12 PM-4.34 PM	5.2	2½ -.3	3.6	1025	350	500	4500	7500
17/01/07	7.32 AM-1.24 PM	5.41	2½ -.3	4.22	550	350	438	231	5400
27/03/07	9.23 M-2.23 PM	3.03	2½ -.3	7.45	750	350	200	1800	4300
30/04/07	8.44 AM-3,15 PM	6.05	2½ -.3	4.52	550	350	679	346	3600
30/04/07	6.55 AM-3.13 PM	7. 59	2½ -.3	6.21	900	350	500	4500	8100

4/6/2007	6 .35AM-11. 45PM	4.1	2½ -.3	2.5	700	350	300	2700	6300
17/07/07	6.34 AM-4.15 PM	5. 40	2½ -.3	4.6	700	350	300	2700	6300
15/08/07	9.34 AM-6.12 PM	5.25	2½ -.3	3.54	700	350	300	2700	6300
17/08/07	7.24 AM-2.12 PM	5. 25	2½ -.3	6.45	700	350	300	2700	6300
4/10/2007	7.35 M-5.45PM	8.2	2½ -.3	9.3	600	350	200	1800	5400
21/11/07	6. 32 AM-4. 13 PM	8	2½ -.3	5.8	900	350	500	4500	8100
Total		**113.09**		**155.28**	**32625**	**9100**	**11317**	**92377**	**194449**

Date	Time (HR/ MINS)	Duration (Hr/Mins)	STD. (Duration) Hr/Mins)	Duration Hr/Mins)	Max Energy Consumption (Kw/h)	STD Energy Consumption (Kw/h)	Min Energy Consumption kW/h	Min Cost (₦1)	Max Cost (₦)2	Cost Benefit (₦)	Cost Benefit (₦)
3/4/2005	6.25 PM-5.40 AM	9.25	2½ -.3	9.23	300.00	155.00	145.00	2,175.00	27,000.00	1,800.00	26,100.00
5/5/2005	10.45AM-6.45PM	9	2½ -.3	6.40	500.00	155.00	345.00	5,175.00	81,000.00	1,800.00	78,300.00
16/ 5/05	11.45AM -7.45PM	9	2½ -.3	4.80	200.00	155.00	45.00	675.00	-	1,800.00	-
20/5/2005	8.30AM- 5.30 PM	10	2½ -.3	7.20	300.00	155.00	145.00	2,175.00	27,000.00	1,800.00	26,100.00
25/5/2005	12.00 PM -9.25 PM	10.42	2½ -.3	7.12	300.00	155.00	145.00	2,175.00	27,000.00	1,800.00	26,100.00
28/05/05	8.30AM- 5.30 PM	9	2½ -.3	6.30	200.00	155.00	45.00	675.00	-	1,800.00	-
2/6/2005	11.35AM -7.04 PM	9	2½ -.3	6.20	300.00	155.00	145.00	2,175.00	27,000.00	1,800.00	26,100.00
6/7/2005	10.30 AM- 6.55 PM	9.43	2½ -.3	6.12	400.00	155.00	245.00	3,675.00	29,700.00	2,610.00	28,710.00
12/9/2005	8.45AM -4.45 PM	9	2½ -.3	6.40	450.00	155.00	295.00	4,425.00	27,000.00	1,800.00	26,100.00
14/9/2005	8.45 AM -5.58 PM	10.33	2½ -.3	7.32	450.00	155.00	295.00	4,425.00	27,000.00	1,800.00	26,100.00
6/11/2005	8.10 AM - 4.40 PM	9.5	2½ -.3	7.00	450.00	155.00	295.00	4,425.00	27,000.00	1,800.00	26,100.00
8/2/2006	10.00AM - 6.00PM	9	2½ -.3	6.20	450.00	155.00	295.00	4,425.00	27,000.00	1,800.00	26,100.00
16/2/06	6.45 AM -2.30 PM	9.45	2½ -.3	7.22	450.00	155.00	295.00	4,425.00	27,000.00	1,800.00	26,100.00
19/2/06	2.40 PM -5.00 PM	4.4	2½ -.3	2,1	332.00	155.00	177.00	2,655.00	-	1,800.00	-
22/3/2006	10.15 AM-6.20 PM	9.12	2½ -.3	6,84	450.00	155.00	295.00	4,425.00	27,000.00	1,800.00	26,100.00
3/3/2006	9.43 AM -10.50 PM	14.12	2½ -.3	11,12	550.00	155.00	395.00	5,925.00	54,000.00	1,800.00	52,200.00
12/3/2006	9.15 AM -5.20 PM	9.12	2½ -.3	6.11	450.00	155.00	295.00	4,425.00	27,000.00	1,800.00	26,100.00
14/4/06	10.51AM-9.00PM	11,22	2½ -.3	6,67	450.00	155.00	295.00	4,425.00	27,000.00	1,800.00	26,100.00
16/.4/06	9.10 AM -4.30 PM	8.5	2½ -.3	3,5	450.00	155.00	295.00	4,425.00	27,000.00	1,800.00	26,100.00
17/5/06	5.00 PM -6.55 PM	2,66	2½ -.3	3,67	332.00	155.00	177.00	2,655.00	-	1,800.00	-
19/6/2006	8.00 AM - 4.15 PM	9.34	2½ -.3	4,34	450.00	155.00	295.00	4,425.00	27,000.00	1,800.00	26,100.00
20/6/2006	4.15 AM-7.50 PM	4.66	2½ -.3	2,22	450.00	155.00	295.00	4,425.00	27,000.00	1,800.00	26,100.00
26/6/2006	6.45 AM 5.55 PM	12,22	2½ -.3	6.40	450.00	155.00	295.00	4,425.00	27,000.00	1,800.00	26,100.00
1/7/2006	7.30 AM-4.50 PM	10.14	2½ -.3	7.30	450.00	155.00	295.00	4,425.00	27,000.00	1,800.00	26,100.00
4/7/2006	7.30 AM-4.20 PM	9.23	2½ -.3	5.30	550.00	155.00	395.00	5,925.00	54,000.00	1,800.00	52,200.00
6//07/06	4.35 AM-7.00 PM	3.36	2½ -.3	3.80	322.00	155.00	167.00	2,505.00	-	1,800.00	-
9/7/2006	7.20 AM- 5.07 PM	10.12	2½ -.3	6,22	450.00	155.00	295.00	4,425.00	27,000.00	1,800.00	26,100.00

12/7/2006	12.00PM-8.20PM	8	2½ -.3	5.20	450.00	155.00	295.00	4,425.00	27,000.00	1,800.00	26,100.00
18/07/06	8.15 AM-4.20 PM	9.17	2½ -.3	6.60	332.00	155.00	177.00	2,655.00	-	1,800.00	-
22/07/06	7.10 AM -2.10 PM	10.23	2½ -.3	3.60	450.00	155.00	295.00	4,425.00	27,000.00	1,800.00	26,100.00
12/8/2006	8.20 AM-9.25 PM	14.65	2½ -.3	11,11	550.00	155.00	395.00	5,925.00	54,000.00	1,800.00	52,200.00
13/09/06	10.00AM- 6.03PM	9.12	2½ -.3	6.84	459.00	155.00	304.00	4,560.00	27,000.00	1,800.00	26,100.00
16/09/06	6.15 AM -9.07 PM	4.32	2½ -.3	2.23	332.00	155.00	177.00	2,655.00	-	1,800.00	-
22/10/06	6.15 AM-3.00 PM	9.63	2½ -.3	7.22	550.00	155.00	395.00	5,925.00	54,000.00	1,800.00	52,200.00
12/1/2007	6.45AM2.00PM	6.34	2½ -.3	3.21	155.00	155.00	-	-	-27,000.00	1,800.00	-26,100.00
15/04/2007	9.20AM- .55PM	11.23	2½ -.3	9,12	550.00	155.00	395.00	5,925.00	54,000.00	1,800.00	52,200.00
19/05/2007	6.35AM- .30PM	13.34	2½ -.3	11,22	550.00	155.00	395.00	5,925.00	54,000.00	1,800.00	52,200.00
22/6/2007	6.15 AM -.40PM	14,55	2½ -.3	8,54	500.00	155.00	345.00	5,175.00	81,000.00	1,800.00	78,300.00
24/6/2007	8.30 AM -.50PM	7.54	2½ -.3	4,2	550.00	155.00	395.00	5,925.00	54,000.00	1,800.00	52,200.00
26/6/2007	3.00AM-.16PM	2,55	2½ -.3	3.,67	155.00	155.00	-	-	-27,000.00	1,800.00	-26,100.00
29/06/07	6.15 AM -.54PM	9.23	2½ -.3	5.78	450.00	155.00	295.00	4,425.00	27,000.00	1,800.00	26,100.00
1/7/2007	3.05 PM-6.20 PM	5.16	2½ -.3	4.12	300.00	155.00	145.00	2,175.00	27,000.00	1,800.00	26,100.00
9/7/2007	6.30 AM -.53PM	4,23	2½ -.3	3.40	300.00	155.00	145.00	2,175.00	27,000.00	1,800.00	26,100.00
10/8/2007	6.15 AM -.31PM	3.22	2½ -.3	1.40	300.00	155.00	145.00	2,175.00	27,000.00	1,800.00	26,100.00
18/8/2007	3.31 PM-5.30 PM	3.25	2½ -.3	3.50	200.00	155.00	45.00	675.00	-	1,800.00	-
		338.92		**169.52**	**18,019.00**	**6,975.00**	**11,044.00**	**165,660.00**	**1,190,700.00**	**81,810.00**	1,151,010.00

Table2: Energy Consumption for One Tonne Induction Furnace (03/06 2005 – 01/08/2007)

Table 3: Duration time taken(hr./min)

Furnace	Max	Min	Save
EAF	182.78	122.98	59.8
IND.	335.82	232.32	103.5
Total	518.6	355.3	163.3

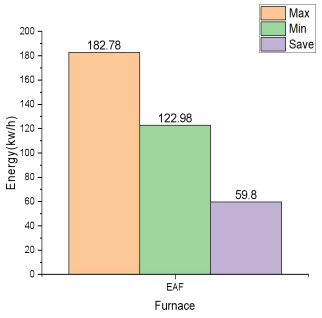

Fig 10: shows the max, saved & min time (hr/.min)

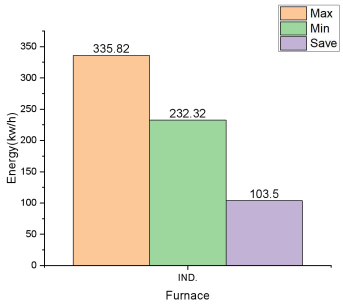

Fig 11: shows the max , saved & min energy consumed (kw/hr)

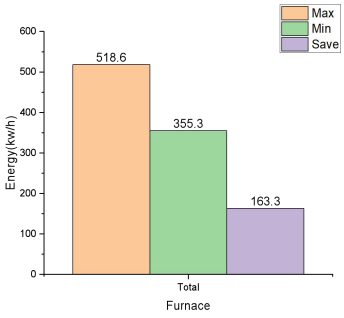

Fig 12 : shows the max, saved& min Cost(₦)

Table 4: Energy Consumed (kW/h)

Furnace	Max	Min	Save
EAF	20,600	10,200	10,400
IND.	13,500	4,500	9,000
Total	34100	14,700	19,400

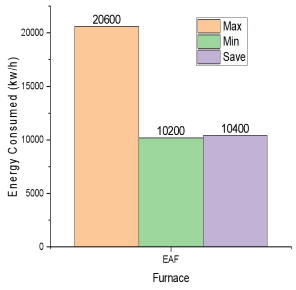

Fig 13 shows the max, saved & min time taken (hr/min)

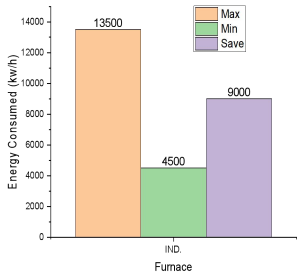

Fig 14: shows the max, saved & min time

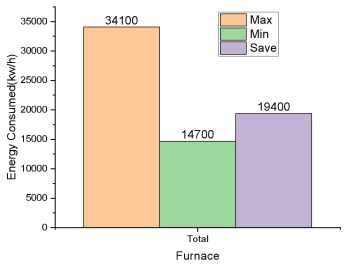

Fig 15 : shows the max , saved & min energy consumed (kw/hr)

Table 5: Cost Expended (₦)

Furnace	Max	Min	Save
EAF	185400	91800	93600
IND.	121500	81800	39690
Total	306,900	173600	133290

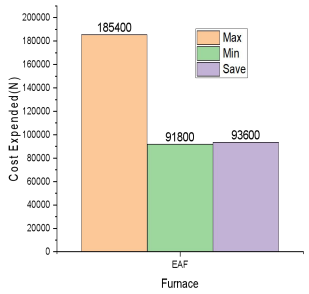

Fig 16 shows the time(163.3 hr/min)

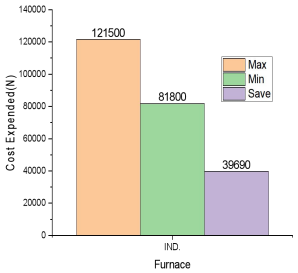

Fig 17 shows the level of energy(14700kw/hr

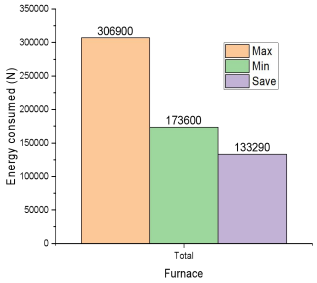

Fig 18 shows the time(₦133,290)

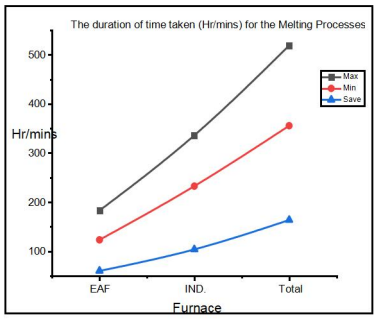

Fig 19: The duration of time Taken(hr/Mins)

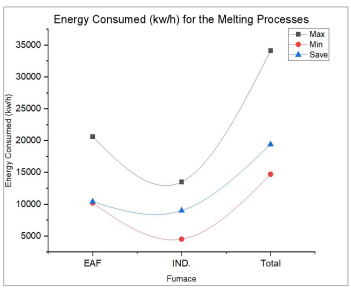

Fig 20: The Energy Consumed (kW/h)

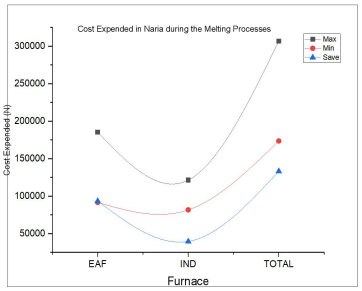

Fig 21: Cost Expended in Naria during

For the Melting Processes, the Melting Processes the Melting Processes

Tables (3), (4), and the values acquired from them were used to produce the graphs in figures 16, 17, 18, 19, 20, and 21. (5). As shown in fig. 16, running the two furnaces at a normal melting rate of 212 hr/min for each cycle may have resulted in a savings of up to 163.3 hr/min.

Figure 17 shows the total energy savings of 19,400 kW/h that might have been achieved by not using these furnaces. Fig. 18 illustrates how the use of these furnaces could have resulted in a N133,290 cost savings overall. Data analysis revealed that doing an energy audit was essential and necessary to avoid resource waste.

Only by reducing the time and energy required for the melting procedures, as well as the cost of operating these furnaces, could the operations be carried out. As illustrated in Fig. 20 as the energy consumed (kWh for the melting operations), Fig. 19 exhibited the amount of time taken (hr/min) for the melting procedures for the two furnaces taking into account the maximum time taken, the purported minimum, and the amount of time saved once the auditing was finished.

The highest, lowest, and amount of energy that was conserved during consumption are shown in the Energy Consumed (kW/h) for the melting processes in the two furnaces. The expenditures spent in Naira values throughout the melting operations for the two furnaces are displayed in Fig. 21 in accordance with the greatest amount, minimum amount, and amount saved when the energy audit investigation was carried out.

Fig 22: For the quarry industries, conical flake

Figure 23: A fixed jaw is often used in the quarry industry.

Fig 24: Utilized at the Delta Steel Plant are pallets.

Fig 25: brakes for railways used by the Railway Corporation

Energy audits are vital because of the nature of the operating processes and the types of furnaces used in foundries. The sorts of components produced also make it extremely important for carrying out such activities with a view to conserving energy,

time, and manufacturing costs. Various items from the shop are seen in Figs. 22 to 25, including a conical flask used in the quarry business, a fixed jaw crusher, 4.5-ton pallets used at the Delta Steel Company Limited Aladja, and railway brakes built for the Nigerian Railway Corporation.

Thus, in order to continue manufacturing an extensive range of goods for various industries at competitive prices, the leadership team of the workshop must conduct energy audits in accordance with recommendations for expense effectiveness and efficiency.

4.0 Conclusion

The information gathered showed that more resources/money were not utilized during the manufacturing of the various parts or items, more energy was used, and melting cycles for the two furnaces took longer to complete. According to the study, the energy audit undertaken identified the reasons for and shortcomings in the operation of the furnaces. The challenges found in the research investigations will be reduced or eliminated as a result of operating procedures being overloaded for more effective service delivery.

The workshop must therefore keep conducting regular energy audits on all the furnaces and vessels utilized in the manufacturing processes, not just the furnaces under inquiry but also other furnaces as well.

The goal is to decrease resource and energy waste as well as the amount of time it takes to complete the melting cycle. If the right analyses were then carried out, this may strengthen the shop management efforts, which could add up to increasing value for money for productivity improvements.

The data collected through the investigation's work could be utilized for coordinating the arranging and monitoring processes. As there are key actions that should be performed for reducing the amount of energy cost in any kind of production company, these procedures will decrease maintenance on the equipment as well as render it economical in succeeding operation. The current issues regarding the administrative processes in the shop will be determined through an extensive review.

The furnaces under study might be enhanced better in terms of performance expectancy, productivity, value for money, and customer service. Each of these modifications would reduce energy prices, the consumption of energy, and the amount of period needed to conclude the melting cycle for the castings portions.

REFERENCES

[1]. Instructions for Energy Auditors, Volumes II, U.S. Department of Energy, DOE/CS-0041/12&13, September 1978 and II, U.S. Department of Energy, DOE/CS-0041/12&13, September 1978. Available tHrough National Technical Information Service, Springfield, VA.

[2]. Energy Conservation Guide for Industry and Commerce, National Bureau of Standards Handbook 115, and Supplement, 1978. Available tHrough U.S. Government Printing Office, Washington, DC.

[3]Cape hart, B.L., Turner, W.C., and Kennedy, W.J Guide to Energy Management, Third Edition, The Fairmont Press, Atlanta, GA, 2000

. [4] Witte, Larry C., Schmidt, Philip S. and Brown, David R., Industrial Energy Management and

Utilization Hemisphere Publishing Corporation, Washington, DC, 1988.

[5] Ocheri C Daniel A & Theophilus OI "Financing for Plants, Equipment, and Operations for the establishment of a Plant for the manufacturing of Spheroidal Graphite Iron castings for Automobile Industry" Journal of Materials Science & Engineering. DOI 10-4172/2169-0022.1000316 vol6 issue 1 2017 pp 1-6

[6] Jones, J.A.T, Bowman, B. Lefrank P.A, Electric Furnace Steelmaking, in the Making, Shaping and Treating of Steel, R.J. Fruehan, Editor. 1998, the AISE Steel Foundation: Pittsburgh. p. 525-660.

[7] Preston, R., American Steel. Avon Books, New York, 1991

[8] Thurman, A., and Manta, D.P., Handbook of Energy Engineering, Fourth Edition,

[9] Albert Thurman and Eric A. Woodruff(2005) "Handbook of Financing Energy projects" The
Fairmont Press INC & Dekker CRC Press, 700 Indian Trail Lilburn GA 30047 pg 70-95

[10] J.A.T. Jones, B. Bowman, P.A. Lefrank, Electric Furnace Steelmaking, in the Making, Shaping and Treating of Steel, R.J. Fruehan, Editor. 1998, the AISE Steel Foundation: Pittsburgh. p. 525-660.

[11] Uger Atiko CEA Director of EMU Energy Research Centre "Energy Audit MENG 547 Energy Management &v Utilization 2016pp 1-30

[12] Thurman Albert, Terry Younger, William J. "Handbook of Energy Audit 9th Edition, the Fairmont Press Inc.: ISBN 10: 0-88173686-4 2013, pp 502

[13] Gupton G.W. HVAC Controls, Operation & Maintenance CRC Press, Marcel Dekker, the Fairmont ISBN10: 0521830168, 2013 pp 23- 45

[14] Anthony J. Pansini "Guide to Electrical Power Distribution System" 6th Edition. The Fairmont Press, Distributed by Marcel Dekker CRC Press ISBN 13: 9780881735062, 2005 pp 276

[15] Ocheri C, Onyeji Lawrence Ibe & Ojonimi Ile T' Statistical Quality Control of Chemical Compositions of Rolled Products: A Case study of the Light Section Mill of Ajaokuta Steel Company Limited' Industrial Engineering and Management 6 206 DOI 10: 4172/2169-0316. 10002062016 pp 1-6

[16] Alfa Firdaus Uly Amrina "Energy Audit Analysis by Business Intelligence Application, Faculty of Engineering, Mercu Buana University: ISSN: 1410-2331, Sergei Vol 19 N0 3 2015 pp 175-180

[17] Albert Thurman & Eric A Woodruff " Handbook of Financing Energy Project" The Fairmont Press, Inc. ISBN : 0-88173480-2 2005 pp 63-69

[18] Khagen Bora " Energy management in Pulp and Paper Industry: A case study of Cachar Paper Mill "The University of Ljubljana, Faculty of Economics and International Centre for Promotion of Enterprises (ICPE), Ljubljana, 2008 pp 8-30

[19] Albert Thurman. PE CEM and Eric Woodruff "Energy Project Financing Resources and Strategies for Success " The Fairmont Press, Inc., HD 9502-A2T51872998, 2009 pp 1-8

NNMS-TP002

A Comparative Study of the Physico-Chemical and Mineralogical Characterization of Bishe Cassiterite Ore and Dutsen Wai Cassiterite Ore for Economic Viability

Riko, K. S.[1]Nwokem, K.[1]Oyeladun O. A. W.[2] and Agbo A. N.[3]
[1]Department of Pure and Applied Chemistry, Kaduna State University
[2]Department of Mineral and Petroleum Resources Engineering, Kaduna Polytechnic, Kaduna.
[3]Defense Industries Corporation of Nigeria, Kaduna

Abstract

The research on a comparative study of the physio-chemical and mineralogical characterization of Bishe Cassiterite Ore and Dutsenwai cassiterite ore for economic viability was carried out. The physical observation revealed that the two ore processed are metallic lustre, dark bronze irregular or uneven breakages. For Bishe cassiterite the hardness was found to be 642HB, specific gravity of 4.974 and thermal conductivity was found to be 1.8897 W/mK, while Dutsenwai cassiterite's hardness was found to be 631HB, specific gravity of 4.797 and thermal conductivity was found to be 1.8897 W/mK. Dutsenwai cassiterite ore sample has more percentage tin mineral assay compare to that of Bishe cassiterite ore sample. The mineralogical analysis of Bishe cassiterite ore reveals only the presence of cassiterite as the major ore while that of Dutsenwai cassiterite ore reveals the presence of Cassiterite, Phlogopite, Loparite and Ferrocolumbite. Having carried out the physio-chemical and mineralogical characterization of Bishe Cassiterite Ore and Dutsenwai cassiterite ore, it was discovered that Dutsen Wai cassiterite Ore is more economically viable than Bishe Cassiterite ore. Furthermore, an engineering process route should be design for the beneficiation of Dutsen Wai cassiterite ore for economic and commercial purposes.

1.0 Introduction

Nigeria a nation adequately blessed with large deposit of non-ferrous metallic ores which are yet to be fully harnessed, characterized, and beneficiated due to lack of sufficient studies and technology. The non-ferrous metallic ores found in Nigeria include lead-zinc ore, tin ore (Cassiterite), niobium ore, uranium ore, and precious metals such as (Gold and Silver) (Abdulfattah et al, 2017)

Cassiterite is a tin oxide mineral (SnO_2) and is the principal source for tin metal (79.6% Sn). The color is shining black, brownish-black, reddish brown, gray, red, white, and rarely colorless. The crystal system is tetragonal with very common twinning. The fractures are subconchoidal to uneven and brittle. The luster is adamantine to metallic, greasy with white to brownish streak. The average specific gravity is ~7.0. The mineral hardness is between 6 and 7 in Mohs scale. The cassiterite is formed by hydrothermal process and occurs as veins, alluvial, and placer. The grains are resistant to weathering. Cassiterite contains 78.6% Sn and are the principle tin ore throughout ancient history and remains the primary source of tin metal, used as plates, cans, containers, solders, and polishing compounds and alloys (Haldar, 2020).

Cassiterite is the chief ore of tin (Sn), but it houses other associated minerals such as columbite, wolframite, ilmenite, monazite, and others. When this mineral deposit (cassiterite) is mined from the earth by artisanal miners, it is further processed either locally or industrially. The top tin producing countries in the world in 2014 are China

(125,000 tons), Indonesia (84,000 tons), Peru (23,700 tons), Bolivia (18,000 tons), Brazil (12,000 tons), Myanmar (11,000 tons), Australia (6100 tons), Vietnam (5400 tons), and Malaysia (3500 tons)(Haldar, 2020).

Tin occurs in Nigeria in the form of cassiterite with varying amounts of associated minerals. The major sources of ore bearing cassiterite in Nigeria are the alluvial and eluvial deposits from the biotite granites within the Jurassic alkaline ring complex of the Jos Plateau. More so, less than 5 % of the total production has been recovered from the pegmatites within the largely Precambrian basement complex consisting of magnesites, gneisses, but with the rapidly depleting reserves. Figure 1 shows the map of Kuru, a typical mining area, 20 Km away from Jos. Tin mining in Nigeria is over 100 years old. Prior to 1975, Nigeria was a major tin exporter of cassiterite concentrates which peaked at about 11,000 tons. There has been a dramatic decline to about 2000 tons. Among the factors accounting for the collapse of this tin industry include the inaccessibility of placer deposits and the current prohibitive cost of mining the ores beneath the basalt flows of Jos (Ogwuegbu, 2011).

Also, the need to carry out a comparative study of the physio-chemical and mineralogical characterization of Bishe cassiterite ore and Dutsenwai cassiterite ore in order to find out the deposit meetup with the cutoff grade is essential in the mining and mineral industries. Therefore, there is need to characterize Bishe Cassiterite Ore and Dutsen Wai Cassiterite Ore for economic viability. To achieve this, determination of the physical properties (colour, hardness, relative density, electrical and thermal conductivities) of the ore samples, chemical compositions of the ores sample using XRF analytical equipment and mineralogical compositions of the ores sample using XRD/SEM-EDS analytical equipment.

2.0. MATERIALS AND METHODS

2.1. Equipment and Materials

The equipment that was used in the course of this work were: pulverizing machine, gravity bottle (pycnometer), ball milling machine, weighing machine, X-ray fluorescence spectroscopy (XRF) and X-ray diffractometer (XRD). The materials used include: cassiterite ore and water.

2.2 **Methods**

2.2.1 Sample collection and preparation of the Cassiterite

50kg was collected from various location of the Bishe Cassiterite Ore and Dutsenwai Cassiterite Ore deposit at Bassa Local Government Area and Lere Local Government Area of Plateau State and Kaduna State respectively, Nigeria and these samples collected were the true representation of the entered ores deposit. In the laboratory, the samples underwent re-sampling using Jones riffle. The samples were pulverized and blended thoroughly so as to achieve homogeneity. The two homogenous samples were used for both chemical analysis and mineralogical analysis.

2.2 Physical Observation

Method

. The sample colour was determined using colour chart.

i. The sample was examined by looking at the geometric shape of the mineral

ii. The sample was checked to determine wherever the breakage was as either irregular or conchoidal.

2.3 Determination of the Hardness of the Ores

Hardness measurements on all the specimens will be carried out using Mohr's scale.

2.4 Determination of Specific Gravity (Relative Density)

Procedure

. The sample was washed thoroughly in order to remove dust and weighed

ii. Empty specific gravity bottle (pycnometer) was weighed and the weight was recorded
iii. The ground sample was filled into the specific gravity bottle to about 1/3 of the bottle and weighed the sample and bottle and the weight recorded
iv. The remaining space in the bottle was filled with water and weighed
v. The content of the bottle was discarded and filled afresh with water and the weight of bottle filled up with water was determined.

$$\text{Mass of empty bottle, } M_1$$
$$\text{Mass of empty bottle + ore, } M_2$$
$$\text{Mass of empty bottle + ore + water } M_3$$
$$\text{Mass of empty bottle + water, } M_4$$
$$\text{Mass of water filling the bottle, } M_4 - M_1$$

2.2.5 Determination of Thermal conductivity
Thermal Conductivity (TC) of the samples with specific heat capacity were measured using radial heat conduction apparatus (Armfield equipment model HT12) with heat transfer service unit (Armfield equipment model HT 10XC). The probe consists of single heater and thermocouple. Constant electrical power was supplied to the heater, the temperature of wire rose in exponential progression. Temperature rose with time line increased given to TC.

2.2.6. **Chemical characterization of the Cassiterite**

$$\text{Mass of water having equal volume as ore} = (M_4 - M_1) - (M_3 - M_2)$$
$$\text{Relative Density of the Ore (S. G.)} = \frac{(M_2 - M_1)}{(M_4 - M_1) - (M_3 - M_2)} \ldots \text{Equation 1}$$

Figure 2: Pycnometer

The head sample collected from the various locations and depths of the Cassiterite was subject to chemical analysis using XRF. The Cassiterite sample was analyzed by determining the percentage of composition of each element in the sample.

2.2.7. Mineralogical characterization of the Cassiterite

The head sample collected from the various locations and depths of the Cassiterite was subject to mineralogical analysis using XRD (X – Ray Diffractometer) Empyrean BV of Netherland Model.

3.0. RESULTS AND DISCUSSIONS

3.1. Physical Properties of Bishe Cassiterite Ore and Dutsenwai cassiterite

Table 4.1: Physical Properties of Bishe Cassiterite Ore and Dutsenwai cassiterite

Property	Value	
	Bishe Cassiterite	**Dutsenwai cassiterite**
Physical observation	Dark bronze	Light Dark
Hardness	642	631
Specific Gravity	6.67	5.53
Thermal Conductivity	0.7874W/mK	1.8897 W/mK
Heat Transfer	78.7383	188.9720
Specific Heat	2.0×10^{-3}	5.0×10^{-3}
Diffusivity	79.5671	79.5713

Table 1 shows that the physical properties of the Bishe cassiterite ore and Dutsen Wai cassiterite; where the physical observation reveal that the ore processes metallic lustre, dark bronze irregular or uneven breakages, for Bishe cassiterite the hardness was found to be 642HB, specific gravity of 6.67 and thermal conductivity was found to be 1.8897 W/mK. Also, for Dutsenwai cassiterite the hardness was found to be 631HB, specific gravity of 5.53 and thermal conductivity was found to be 1.8897 W/mK which can be influenced by the present of order element in the ore (Anthony et al, 1995; Wills, 2006; Weiss, 1985).

3.2 Determination of Chemical Property

3.2.1 Chemical Analysis

Table 2: The Result of Chemical Analysis of Head Sample of the of Bishe Cassiterite Ore

Element	O	Al	Si	P	S	Cl	Ti	K
%	30.870	1.930	6.501	0.053	0.124	0.331	9.031	0.126
Element	Ca	Fe	Sn	Zr	Nb	Ta	Mn	W
%	1.305	8.013	29.980	3.297	5.370	1.247	0.766	0.459

Table 2 shows the result of chemical analysis of Bishe cassiterite ore contains 8.013% Fe, 29.980%Sn, 0.071%Cu, 0.766%Mn, 1.305%Ca, 3.297%Zr, 9.031%Ti and 5.370%Nb, with silica, tin, iron, niobium and titanium minerals predominant in the matrix of the ore, while other minerals associated with the ore in minor percentage making the ore deposit another potential source for tin mineral; with 29.980% tin having meeting up with industrial standard and cut-off grade (Weiss, 1985).

Table 3: The Result of Chemical Analysis of Head Sample of Dutsenwai Cassiterite Ore

Element	O	Al	Si	P	S	Cl	Ti	K
%	23.381	1.327	0.968	0.000	0.039	0.240	1.171	0.080
Element	Ca	Fe	Sn	Zr	Nb	Ta	Mn	W
%	1.305	1.458	66.232	0.068	0.953	0.510	0.000	0.145

Table 3 shows the result of chemical analysis of Dutsenwai cassiterite ore contains 1.458%Fe, , 3.007%Ca, 66.232%Sn, and 1.171%Ti with tin mineral predominant in the matrix of the ore, while other minerals associated with the ore in minor percentage making the ore deposit another potential source for tin mineral; with 66.232% tin having meeting up with industrial standard and cut-off grade. The Dutsenwai cassiterite ore is high grade of tin ore (Weiss, 1985).

3.2.2 Determination of Mineralogical Property

Table 4: XRD Analysis Result for the Head Sample of Bishe Ore

Card Number	**Score**	**Mineral Name**	**Chemical Formula**
96-900-7434	70	Cassiterite	Sn2.00 O4.00

Table 5: XRD Analysis Result for the Head Sample of Dutsenwai Cassiterite Ore

Card Number	**Score**	**Mineral Name**	**Chemical Formula**
96-900-7434	66	Cassiterite	Sn2.00 O4.00
96-900-4660	11	Phlogopite	O22.16 F1.84 Si5.9
96-900-4549	22	Loparite-Ce	Na1.84 La0.36 Ce0
96-900-3735	6	Ferrocolumbite	Fe3.16 Nb7.60 Mn0

From Table 4, the mineral present is cassiterite. The mineral composition of the ore revealed that the tin is a cassiterite ore deposit (Weiss, 1985). From Table 5, the mineral present are as follows: cassiterite, phlogopite, loparite and ferrocolumbite. The mineral composition of the ore revealed that the tin is a cassiterite ore deposit with other associate mineral (Weiss, 1985).

This reveals that both deposits meet up the cut-off grade for mining, hereby, making the two deposits variable for economy. However, Dutsenwai cassiterite ore sample has more percentage tin mineral assay compare to that of Bishe cassiterite ore sample

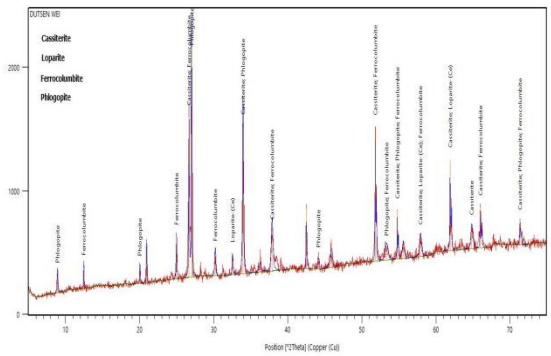

Figure 1: XRD Pattern for Head Sample of Bishe Ore

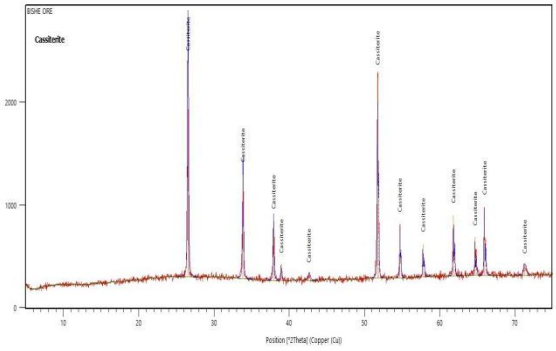

Figure 4.2: XRD pattern the Head Sample of Dutsenwai Cassiterite Ore

Plate 4.1: SEM Result of Bishe Cassiterite Sample (× 500)

Plate 4.2: SEM Result of Dutshen Wei Cassiterite Sample (× 500)

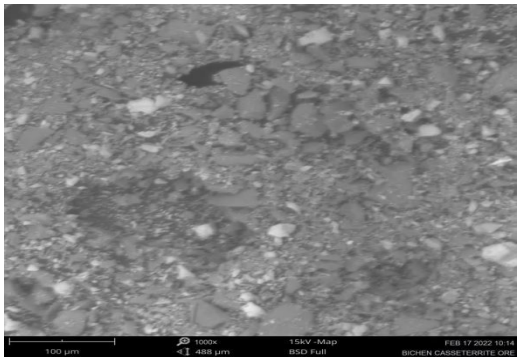

Plate 4.3: SEM Result of Bishe Cassiterite Sample (× 1000)

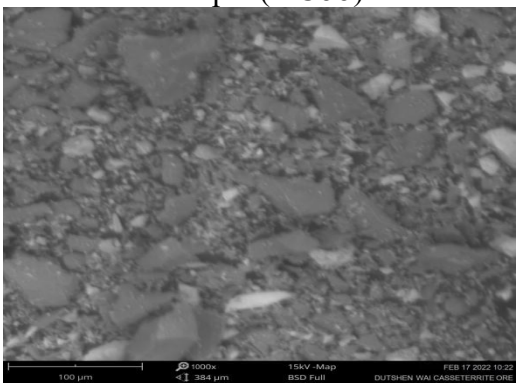

Plate 4.4: SEM Result of Dutshen Wei Cassiterite Sample (× 1000)

Plates 4.1 to 4.4 shows the SEM micrographs of the cassiterite ore sample. From the results can be observed that five phases can be recognized: the embedding resin (black background), cassiterite, phlogopite (light grey), loparite (white) and ferrocolumbite (grey particle). Furthermore, it could also be observed that the minerals are separated by grains boundaries, no interlocking of minerals and the mineral particles vary in seizes ranging from 80 to 320μm. This phenomenon indicates that the minerals can be easily freed from each other during comminution, hence the low requirement in the energy required for the liberation of the tin mineral (Haldar, 2020).

4.2.3. Petrological Analysis of the Head Samples

Plate 4.5: Micrograph of Bishe Cassiterite ore Sample under plane polarized light (X 1000)

Plate 4.6: Micrograph of Dustenwei Cassiterite ore Sample under plane polarized light (X 1000)

4.1. Conclusion

The research on a comparative study of the physio-chemical and mineralogical characterization of Bishe Cassiterite Ore and Dutsenwai cassiterite ore for economic viability was carried out and following conclusions were drawn:

i. The physical observation reveals that the ore processes metallic luster, dark bronze irregular or uneven breakages, for Bishe cassiterite the hardness was found to be 642HB, specific gravity of 6.67 and thermal conductivity was found to be 1.8897 W/mK. Also, for Dutsenwai cassiterite the hardness was found to be 631HB, specific gravity of 5.53 and thermal conductivity was found to be 1.8897 W/mK

4.0. CONCLUSION AND RECOMMENDATION

Dutsenwai cassiterite ore sample has more ercentage tin mineral assay compare to that of Bishe cassiterite ore sample

The mineralogical analyses of Bishe cassiterite ore reveals only the presence of cassiterite as the major ore while that of Dutsenwai cassiterite ore reveals the presence of cassiterite, phlogopite, loparite and ferrocolumbite

4.2. Recommendation

Having carried out the physio-chemical and mineralogical characterization of Bishe Cassiterite Ore and Dutsenwai cassiterite ore, it was discovered that Dutsen Wai cassiterite Ore is more economically viable than Bishe Cassiterite ore. Furthermore, an engineering process route should be designed for the beneficiation of Dutsen Wai cassiterite ore for economic and commercial purposes.

References

Abdulfattah, F. Rafukka, I. A. and Manladan S. (2017) Trends in Characterization and

Beneficiation of Non-ferrous Metallic Ores in Nigeria Materials Science, Geolog, C. E. (2020) Benefits of cassiterite mining by artisanal miners in Jos Plateau, Nigeria, Bulletin of the National Research Centre 44:113.

Haldar, S. K. (2020) Minerals and rocks in Introduction to Mineralogy and Petrology (Second Edition), Elsevier Inc. pp 1-51

Ogwuegbu M., Onyedika G., Hwang J., Ayuk A., Peng Z., Li B., Ejike, E.N.O. and Andriese M. (2011): Mineralogical Characterization of Kuru Cassiterite Ore by SEM-EDS, XRD and ICP Techniques, Journal of Minerals & Materials Characterization & Engineering, Vol. 10, No.9, pp.855-863,

Oyeladun, O. A. W. (2015): Characterization of Azara Copper Ore Deposit, Nasarawa State

(M. Sc. Thesis) A. B. U., Zaria, (Unpublished)

A STUDY OF THE APPLICATION OF COMPUTER NUMERICAL CONTROL (CNC) ON PRODUCTION OF FOAM PATTERN FOR FOUNDRY.

MUKORO, EJOVWOKODE EDWARD
DEPT OF FOUNDRY
FED. POLY. IDAH
08077130235 mukoroedward@gmail.com

ABSTRACT

Computer Numerical Control (CNC) brings automation to the foundry industry. By shaping foam patterns with speed, accuracy and repeatability; it adds value to the casting process in terms of quality and low cost. Designs of chain motor saw connecting rod and farm tractor gear selector bracket were made; their polar coordinates and programming codes were determined and simulation conducted. Computer Numerical Control milling machining successfully shaped blank polystyrene foam into desirable foundry patterns.

Keywords: CNC, polystyrene foam, pattern, coordinates, simulation.

INTRODUCTION

The foundry process route begins with pattern making. The pattern is the form around which moulding sand is rammed. Patterns are the "tooling" that brings repeatability and replicability to all metal casting process. The pattern creates the mould cavity in sand, plaster or other media that will yield the casting exterior. It is the model or replica of the component we intend to produce (Jain, 2004 p5, 6). Patterns can be made from soft wood (pines), hardwood (mahogany), metal (brass, bronze, grayiron, aluminium, steel), plaster, plastics and low-melting-point alloys (such as lead-bismuth alloys). For use in precision casting, evaporative pattern casting also called Full Mould or expendable patterns are made of wax, tin, frozen mercury and polystyrene plastic (foam). (Adikwanduaba 2005 pp171)

CNC is the process of "feeding" a set of sequenced instructions into a specially designed, programmable controller and then using it to direct the movements of a machine tool such as a milling machine, lathe or flame cutter. The program directs the cutter to follow a predetermined path at a specific spindle speed and feed rate, so resulting in the production of the desired geometric shape in a workpiece (Pengzhang, 2010;Ogbonna,etal2020). One of the modes CNC controllers can operate is the polar coordinate command. Polar coordinate command is a **numerical** control system in which all the coordinates are referred to a certain pole. Position is defined by the polar radius and polar angle with respect to this pole (Kuang-Itua chang, 2013). A special universal language was created for CNC machines called G&M- code (Mike Lynch, 1997). CNC is considered to provide more precision, complexity and repeatability than is possible with manual machining. Other benefits include greater accuracy, speed and flexibility as well as capabilities such as contour machining which allows milling of contoured shapes (Grace-Flood, 2017).

Conventional metal casting processes have dominated foundry operations over the years- requiring wood/metal pattern making; elaborate bonded sand conditioning and cavity moulding ; core-box and core making and extensive fettling (Atanda, et al 2012 pp72-76). Foam pattern casting defies all these conventions- no draft, no core, no flash while allowing undercuts and offering attractive polystyrene pattern costs, are its unique advantages.

Most binder-associated problems (such as sand handling, moisture control, binder control and sand conditioning are greatly reduced or by-passed. Even the semi-skilled moulder is eliminated and the cost of cleaning drastically reduced. Unbounded sand is mostly used in this casting process. The cavityless mould is always full, initially with a coated expanded polystyrene pattern embedded in moulding sand and progressively and simultaneously replaced by the inflow of molten metal whose heat destroys the plastic pattern by vapourization and forces

the vapour from the mould through the mould wall permeability and/or by venting and the final casting results (Omidiji, et al 2012, pp186-193).

STATEMENT OF THE PROBLEM

1. Polystyrene foam is commonly used as a packaging material for fragile items like radio, television, video, refrigerator etc. After the purchase of the devices , the foam is discarded in the environment. Apart from polluting the surrounding, it is not easily degradable (Olawale, 2011; Enwelu, 2014).
2. Conventional patternmaking materials like wood and metal require a great deal of consideration for allowances and dexterity and additives for mould, to facilitate its removal from cavity.
3. For one-off and short-production runs the use of wood and metal for pattern making is costly.

RATIONALE/JUSTIFICATION FOR THE STUDY

The purposes of this study are:

1. To increase the use of polystyrene foam as pattern material.
2. To deploy the use of computer numerical control (CNC) machining to shape the foam.
3. To make foam pattern casting competitive even in mass production.

METHODOLOGY

The study of the application of computer numerical control (CNC) for the production of foam pattern in foundry will be undertaken with the utilization of two components:

1. Chain motor saw connecting rod
2. Farm tractor gear selector bracket

Picture of Chain motor saw connecting rod and Picture of Farm Tractor Gear Selector Bracket

The orthographic projections of the components are here under shown with measurements in millimeters(mm)

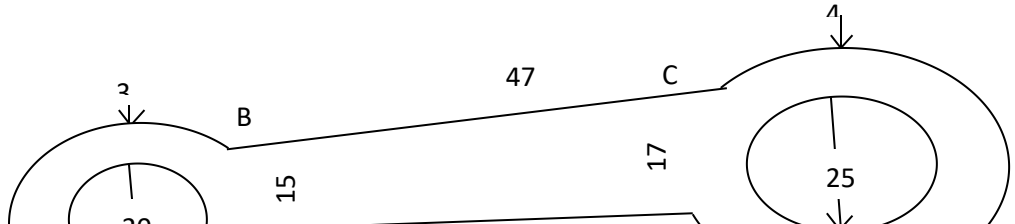

Points	Coordinates	
	X	**Y**
A	0	20
B	0	35
C	51	36
D	51	19
A	0	20

G & M CODE for Computer Numerical Control Milling

M4	S2000
G0	X0 Y0 Z3
G0	X0 Y20 Z3
G1	X0 Y20 Z-20 F150
G02	i-13 J27.5 R13 C334 E16
G1	X0 Y35
G1	X51 Y36
G02	i67.5 J27.5 R16.5 C158 E209
G1	X51 Y19 Z-2
G1	X0 Y20
G0	X0 Y20 Z3
G0	X-13 Y27.5
G1	X-13 Y27.5 Z-2 F150
G02	i-13 J27.5 R10 C0 E0
G0	X67.5 Y27.5 Z3 F150
G1	X67.5 Y27.5 Z-2
G02	i 67.5 J27.5 R12.5 C0 E0
G0	X0 Y0 Z3
M5	

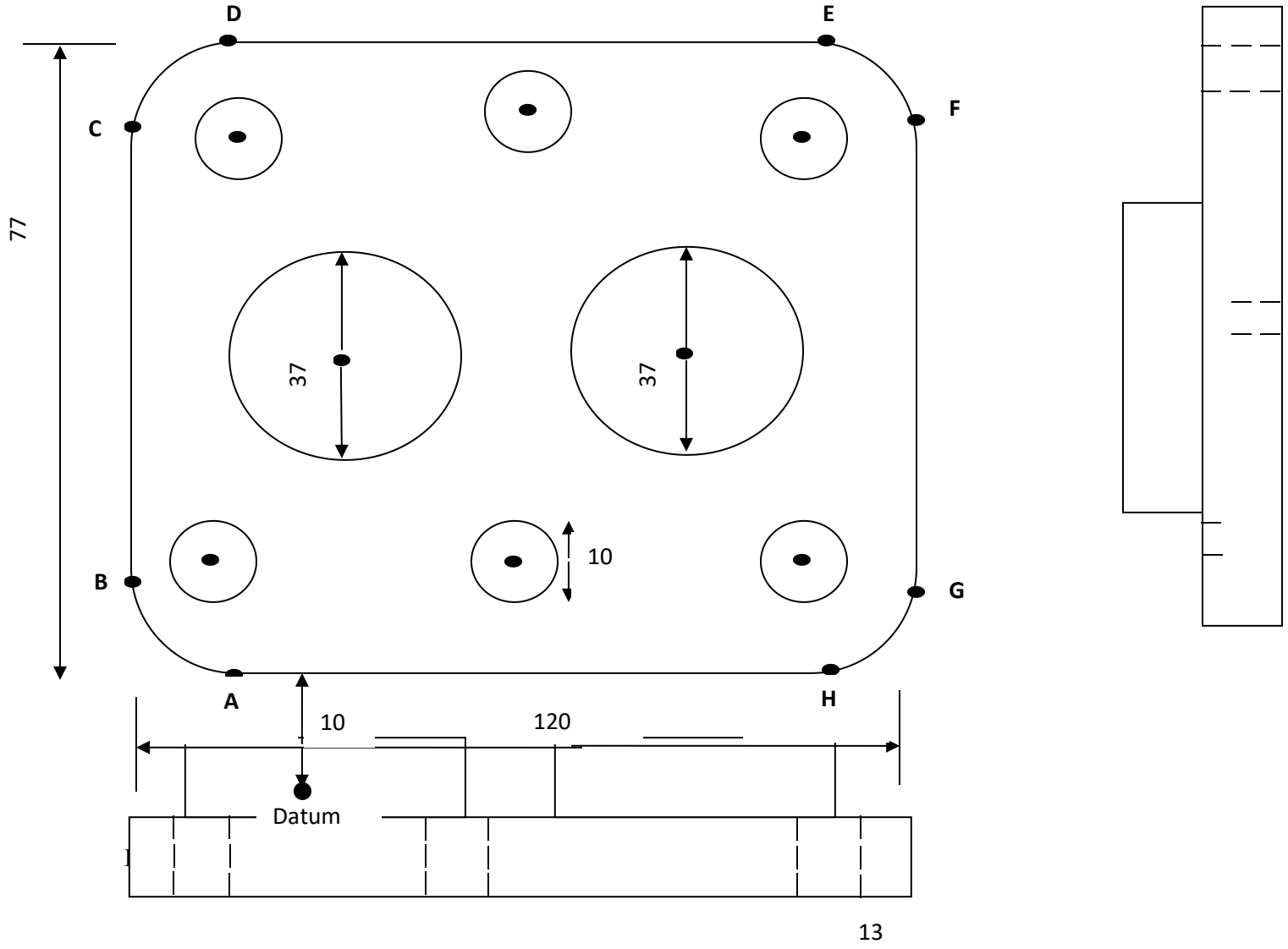

10

A	-10	10
B	-20	20
C	-20	77
D	10	87
E	90	87
F	100	77
G	100	20
H	90	10
A	-10	10

G & M CODE for Computer Numerical Control Milling

M4	S2000
G0	X0 Y0 Z3
G0	X0 Y10 Z3
G1	X0 Y10 Z-10 F150
G1	X-10 Y10
G02	i-10 j20 R10 C270 E180
G0	X-10 Y20 Z3

```
G1      X-10   Y20    Z-10
G02     i-10 j20 R5 C270 E270
G0      X-20 Y20 Z3
G1      X-20 Y20 Z-10
G1      X-20 Y77
G02     i-10 j77 R10 C180 E90
G0      X-10   Y77    Z3
G1      X-10   Y77    Z-10
G02     i-10 j77 R5 C270 E270
G0      X-10 Y 87 Z3
G1      X-10 Y87 Z-10
G1      X90 Y88
G02     i90 j77 R10 C90 E0
G0      X90    Y77    Z3
G1      X90    Y77    Z-10
G02     i90 j77 R5 C0 E0
G0      X100 Y77 Z3
G1      X100 Y77 Z-10
G1      X100 Y20
G02     i90 j20 R10 C0 E270
G0      X90    Y20    Z3
G1      X90    Y20    Z-10
G02     i90 j20 R5 C0 E0
G0      X90 Y10 Z3
G1      X90 Y10 Z-10
G1      X-10 Y10
G0      X0     Y10    Z3
G0      X10    Y50    Z3
G1      X10    Y50    Z-10
G02     i10 j50 R18.5 C0 EO
G0      X70    Y50    Z3
G1      X70    Y50    Z-10
G02     i70 j50 R18.5 C0 E0
G0      X27    Y20    Z3
G1      X27    Y20    Z-10
G02     i27 j20 R5 C0 E0
G0      X47    Y77    Z3
G1      X47    Y77    Z-10
G02     i47 j77 R5 C0 E0
G0      X0 Y0 Z3
M5
```

SIMULATION:

a. Click with the mouse over the SES-MILL icon on the desktop.
b. Select the FILE function and the NEW sub-function. The editor window appears with the added menu functions.
c. Type the above G&M-code milling program.
d. Compare the program with the drawing, check each instruction.
e. Select the function FILE and the SAVE AS sub-function. A dialog window is opened requesting the file name.
f. Type the name ARCI and click OK. The program is saved under the name ARCI.TAP

g. Select the OPTIONS function again. Select the SIMULATION sub-function in simulation mode, the software simulates the machine behavior on the screen, without processing the material. This option enables us to check our program before milling the material.
h. Select the function RUN and the RUN sub-function. A graph window appears. The program is executed step by step graphically on the window, observe the drawing. The colours of the lines describe the z-dimension of the lines.
i. If the graph is not correct according to the program, correct the program and run it again. (Zelinsky, 2014)

MACHINING

a. Locate the material (polystyrene foam) on the table of the machine (TPS-3910) and tighten it with the handy screws. Check that the material lies horizontally on the table.
b. Select the function MONITOR and the sub-function SES MONITOR. The CNC monitor appears. Make sure that all the check boxes of 'HOME X', 'HOME Y', and 'HOME Z' are checked and press the "GO TO MACHINE HOME" button. The machine should move to the absolute home position.
c. Select the OPTIONS function and the MACHINE sub-function in other to operate the system.
d. Select the function MONITOR and the sub-function CNC MONITOR. The CNC monitor appears. Make sure that all the check boxes of HOME X, HOME Y and HOME Z are checked, and press the 'GO TO MACHINE HOME' button. The machine should move to the absolute home position.
e. Move the cutter center to the relative project home with the STEPS (mm) and the MOVE buttons
f. Turn ON the milling motor by clicking over the "start spindle motor" button.
g. Lower the cutter slowly and the cutter almost touches the material surface.
h. Press the "DEFINE PROJECT HOME" button.
i. Select the RUN function and the RUN sub-function.

The system milled the materials according to the programs.

CNC Milling Machine

RESULTS

The simulation drawings of the two components are shown here under

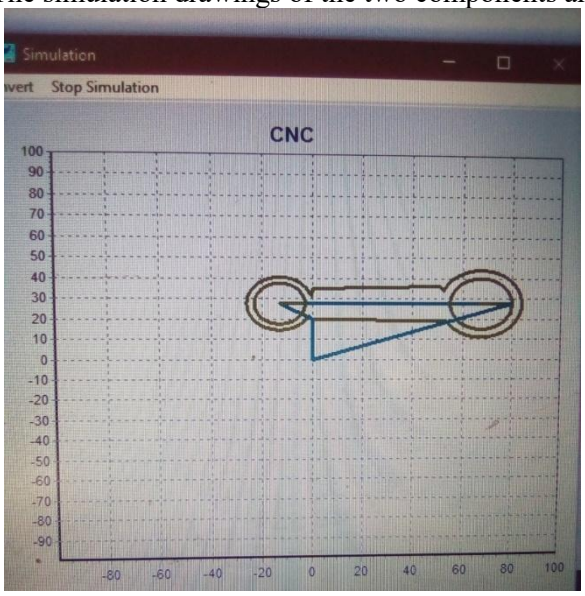

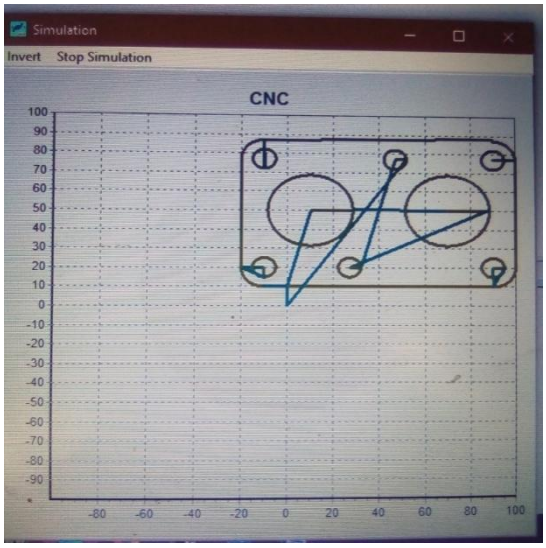

In the simulation, the software draws the mill's movement on the screen and drag lines accordingly. Each line receives a colour according to the milling depth. In this simulation, the software simulates the machine behavior on the screen without processing the material. This stage enables us to check the program before milling the material.

Picture of typical foam patterns are shown below:

In the machine operation, the computer sends movement commands to the systems control unit and the control unit executes the processing.

FINDINGS

1. Speed and quality of foam pattern production were improved with CNC deployment.
2. Foam pattern use in the foundry is environmentally friendly. It met the Waste to Wealth campaign and recycling strategy. (Note: Polyurethane foam is unsuitable for cavityless casting because it produces unacceptable residue and poor surface).

DISCUSSION

The evaporative foam pattern casting uses disposable polystyrene pattern. It is very strategic if foundries in Nigeria incorporate this casting innovation as it makes use of waste plastics and offers attractive value added features. The vertical mill is ideal for shaping polystyrene. Carved fillets, best generated with a

ball-end cutter using the vertical mill or router are the only practical solution for a radiused inside corner. If a run of duplicate patterns is For some complex shapes, patterns may require two or more parts that are assembled and glued into place; polystyrene patterns can be joined by moistening the surface with carbon tetrachloride. Gating, runners and risers may or may not be integral with the pattern. The parts that result may be assembled accurately by using male and female grooves, dowels, mechanical lock,etc. Top gating is usually more efficient and more likely to produce a defect free casting. After shaping, the patterns and other assemblies are coated with permeable refractory slurry such as bonded zircon flour before moulding.

CONCLUSION

Patterns of chain motor saw connecting rod and farm tractor gear selector bracket were milled from waste polystyrene foam using computer numerical control (CNC). While such shaping by hand took two hours; conventional milling took 45 minutes; CNC took 5 minutes. Surface finish and dimensional accuracy was excellent.

RECOMMENDATIONS

While a foundry can practice foam pattern casting by generating its patterns from pre-expanded polystyrene beads foamed physically in metal mould placed in autoclave (Adikwanduaba, 2005); it is hereby recommended that CNC milling of discarded polystyrene foam packaging be adopted in foundry practice. This practice has the double advantage of making patterns available for foundry practice as well as ridding the environment of waste.

ACKNOWLEDGEMENT

The author is indebted to the department of mechanical engineering Federal Polytechnic Idah for availing the CNC unit for demonstration.

REFERENCES

1. Adikwanduaba, S (2005): "Technology of Foundry Practice". BillFred Printing and Publishing, Owerri pp153-154
2. Atanda, P.O; Olawale, J.O; Shittu, M.D;Adewoye, O.O; Afonja, A.A (2012): "Current Status of Irons Foundry in Nigeria". required, the tape-controlled or tracer milling machine (now CNC) is often justified (Richard Crowder, 2020).
   Proceedings of the OAU Faculty of Technology Conference 2012 pp72-76
3. Enwelu, C; Okeke, O.C; Chukwu, E.O(2014): "Solid Waste Management Challenges in Nigeria". "Journal of Management and Technology" Federal Polytechnic Idah pp45, 46
4. Grace-Flood, Liam (2017): "Goliath Represents a New Breed of CNC machine" –internet-
5. Jain, P.L (2004): "Principles of Foundry Technology" 4th Ed. Tata McGrawHill Publishing Company Ltd. New Delhi p14, 146, 350, 373
6. Kuang-Hua Chang (2013): Product Manufacturing and Cost Estimating using CAD/CAE. –internet-
7. Mike Lynch (1997): "Key CNC concept. The fundamentals of CNC" Modern Machine Shop
8. Olawale, J.O; Adeoye, M.D; Shittu, M.D (2010) "Recycling of Plastic Materials" Proceedings of the OAU Faculty of Technology Conference 2011 pp127-132
9. Omidiji, B.V; Khan, R.H; Abolarin, M.S (2012): "Effects of process parameters on the tensile properties of aluminium alloys components obtained by evaporative pattern casting (EPC) process". Proceedings of the OAU Faculty of Technology Conference 2012 pp186-193
10. Ogbonna,G.N;Suleiman,I;Nuhu,S.K(2020):Optimizing interpersonal and attitudinal skills of metalwork industrial workers in computer numerical control machining in northern Nigeria. INDUSTRIAL TECHNICAL EDUCATION JOURNAL pp266-275 vol.2, no 1 May2020. An official publication of the Department of Industrial Technical Education, University of Nigeria Nsukka
11. Peng Zhang (2010): Advanced Industrial Control Technology.-internet-
12. Richard Crowder (2020): Electric Drives and Electromechanical systems 2nd Ed. –internet-
13. Zelinsky, Peter (2014): "New users are adopting simulation software" Modern machine shop.

NMS-TP004

Effect of Two-Step Austempering Heat Treatment on the Dry Sliding Wear Behavior of Austempered Ductile Cast Iron

Kamilu Adeyemi Bello[1], Rayyan Mamuda. Dodo*[1], Muhammad Sani Babaswasun[1], Abdullahi Umma[2], Abdulmumin Adetayo Adebisi[1], Md Abdul Maleque[3]

[1]Department of Metallurgical and Materials Engineering
Ahmadu Bello University Zaria. Nigeria.
[2]Department of Mechanical Engineering, Bayero University Kano, Nigeria,
[3]Department of Manufacturing and Materials Engineering,
International Islamic University Malaysia, Kuala Lumpur, Malaysia

*Email: rdmamuda@abu.edu.ng**

Abstract

The study targeted the impact of two-step austempering heat treatment on the tribological (wear and friction) properties of austempered ductile cast iron (ADI). Wear samples were prepared from ductile cast iron in accordance with ASTM standards. Afterwards, samples treated with two different austempering heat treatments; conventional and two-step austempering treatments (step-up and step-down schemes). The conventional austempering treatment was conducted by austenitizing as-cast samples at 927 ^{o}C and then austempered at 400 ^{o}C. In the event of step-up austempering treatment, the as-cast samples were austenized at 927 ^{o}C, initially austempered at 250, 300 and 350 ^{o}C followed by second austempering at 400 ^{o}C for each sample. However, samples were austenized at 927 ^{o}C, first austempered at 400 ^{o}C and then austempered again between 250 and 350 ^{o}C for step-down treatment scheme. Wear and co-efficient of friction for as-cast and ADI samples were evaluated using ball-on-disc tribometer machine. Additionally, microstructures of the as-cast and ADI samples as well as the worn surface morphologies of the samples were also examined using optical microscopy. The result indicated that the latter austempering heat treatment demonstrated lesser wear rate and co-efficient of friction as compared to the as-cast and conventional ADI samples. Furthermore, two-step austempering treatment conducted at 300 ^{o}C for both step-up and step-down exhibited optimum wear resistance and low friction, which could be attributed to the finer ausferritic structure obtained in this condition. Thus, the results of this finding indicate that two-step austempering treatment successfully enhanced wear and friction properties of as-cast ductile cast iron.

Keywords: Austempered ductile cast iron (ADI); Two-step austempering treatment; Step-down scheme; Step-up scheme; Microstructure; Tribological properties;

1. INTRODUCTION

Austempered ductile cast iron (ADI) is viewed to be an essential engineering material as a result of its promising properties such as minimal wear rate, excellent ductility with outstanding strengths and fracture toughness [1] and fatigue properties [2]. Accordingly, the outstanding properties led to its extensive application in many load bearing applications in automotive industry (such as crankshafts, transmission gear, connecting rods), defense industry (Cannon shells, aircraft landing gears etc.), earth moving machineries and railroads.

Due to its distinctive microstructure, which is made up of ferrite (α) and high carbon austenite (γ_{HC}), ADI has a number of appealing properties. This contrasts with austempered steels, which have ferrite and carbide as their microstructure. Because of this distinction, the austempering reaction's byproduct in ductile iron is frequently called ausferrite rather than bainite

[2,3]. Ductile iron has a significant quantity of silicon, which prevents carbide from precipitating during the austempering reaction and preserves a significant proportion of stable high carbon austenite (γ_{HC}). To ensure that ADI has enough hardenability to be quenched to the austempering temperature without producing pearlite, minimal amounts of alloying elements like nickel, molybdenum and copper are often added.

Nodular cast iron that has been alloyed and heat treated is designated as ADI. High-quality ductile or nodular cast iron served as the foundation for the development of ADI. The next step is an isothermal heat treatment procedure called "austempering." The commonly utilized austempering procedure, also known as single-step austempering, involves first quenching the casting at an intermediate temperature of 260–400 °C after austenitizing it at a temperature between 871 and 982 °C for long enough to form a complete austenite (γ) matrix. For 2-4 hours, the casting is kept at this temperature. In contrast to the two-step austempering procedure, ADI has an a dual-stage phase change reaction during this austempering. Austenite (γ) breaks down into ferrite (α) and high carbon or transformed austenite in the first reaction as depicted in equation (1):

$$\gamma \longrightarrow \alpha + \gamma_{HC} \qquad (1)$$

However, if ductile cast iron is maintained at the austempering temperature for an extended period of time, a second reaction takes place, which even more transforms the high carbon austenite into ferrite and ε- carbide as illustrated in the following equation (eqn 2).

$$\gamma_{HC} \longrightarrow \alpha+\varepsilon \qquad (2)$$

The material will be brittle in such a situation owing to the microstructure which consists of ε-carbide [15]. The austempering procedure must avoid this reaction since the carbide is a harmful phase component. The optimal mechanical property (friction and wear) combination is achieved in ADI after the first reaction is finished but before the start of the second reaction, as has been well proven [16,17]. The "process window" is the window of time that exists between the end of the first reaction and the beginning of the second reaction. To increase the size of this process window, alloying components are added to ADI [1-3].

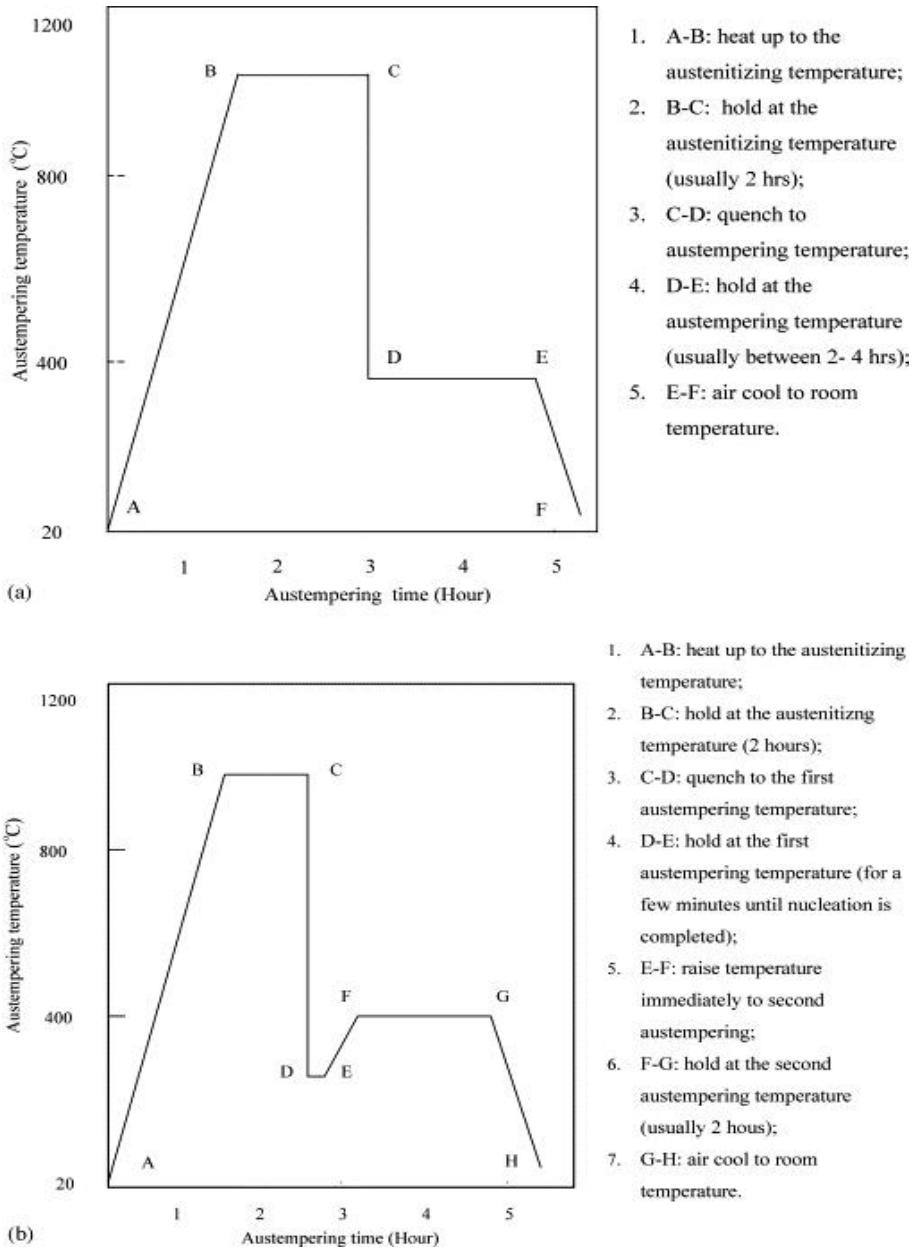

Figure 1: Schematic diagram of the conventional and conceived two-step austempering treatments

In order to circumvent the aforementioned restrictions and to achieve a better balance of tensile strength and toughness, several researchers have suggested a two-step austempering heat treatment [4-8, 14].

Two categories can be used to group the two-step austempering processes:

1. Step-down austempering: In this procedure (also known as high-low austempering), after austenitizing, the ductile iron castings are first quenched at a higher temperature. The alloy is then transferred to a second salt bath, whose temperature is maintained at a lower temperature than the first salt bath, after a predetermined amount of time in the first salt bath. The alloy is austempered for a sufficient length of time in the

second salt bath, and then the samples are air cooled.

2. Step-up austempering: This procedure, also known as low-high austempering, involves quenching nodular cast iron to a lower austempering temperature after austenitizing and holding it there for a predetermined amount of time. Then, a second step of austempering is performed at a higher temperature by either raising the temperature of the first salt bath or moving the casting to another salt bath that is kept at a higher temperature than the first salt bath. The samples are austempered for an appropriate length of time at this second temperature before being air cooled.

In the face of ADI, step-down and step-up austempering techniques have both been used. It has already been demonstrated that step-up austempering improves the mechanical characteristics of ADI significantly [6–11] by virtue of ADI's finer ferrite and increased austenitic carbon content. But there is a bit of discussion surrounding the step-down austempering procedure. Even though some researchers [12] have claimed to some extent that step-down austempering process has improved mechanical properties, other researchers [13] have maintained that there are no appreciable differences between the mechanical properties of ADI processed using conventional and step-down austempering processes. The impact of these austempering processes on the microstructure and the tribological properties of ADI was investigated in this study to determine the effectiveness of this step austempering process as compared to the conventional austempering process, and a ductile cast iron was processed by both the processes in the upper bainitic temperature range.

2.0 EXPERIMENTAL PROCEDURE

The Ductile cast iron used in the study had been produced through the conventional sand casting method. The chemical composition of the as-cast sample is represented in Table 1. The as-cast rods with dimension of 600mm length and 16mm diameter were machined to standard dimension required for the wear and friction test sample using the lathe machine. In this investigation ball-on-disc tribometer was employed to obtain the friction and wear data. A spherical stainless steel ball of 6.35 mm diameter long operating with a load of 8N, linear speed of 15 cm/s and a length of 100 m was slid over a ductile cast iron disc. The disc's wear track is a circular ring with a 5 mm average radius. The top sample is linked to the revolving ball, while the bottom sample is held in place by a sample holder. Wear studies were performed using ball-on-disc (Anton Paar-Strasse) tribometer machine, attached with information acquirement system in which the results of the experiment are displayed on the screen of the monitor attached to the machine. For every sample two tests were performed and average value is reported. The results of coefficient of friction (COF) and the wear rate were displayed as well by the machine. Optical microscope (OM) was used for characterization of the worn samples before and after the test.

Table 1: Chemical composition of the as-cast ductile iron (wt. %)

Element	Percentage (wt. %)
Fe	93.79
C	3.40
Si	2.32
Mn	0.208
P	0.042
S	0.004
Cr	1.0
Mo	0.005
Ni	5.0
Al	<0.001
Cu	0.054
Ti	0.023
V	<0.002
Mg	0.026
Nb	0.01

2.1 Heat Treatment Operations

A two-step austempering treatment (step-up and step-down schemes) was used on the second batch of samples after they had been prepared for two separate heat treatment operations: the conventional single-step austempering technique (second treatments). All the conventional and

two-step treatments were done for comparison purposes.

2.2 Conventional Single-Step Austempering Heat Treatment

The conventional single-step austempering heat treatment was carried out by heating two as-cast ductile iron samples to the austenitizing temperature of 927 °C for 60 minutes and then quenched in a salt bath (50% $NaNO_3$ + 50% KNO_3) maintained at 400 °C for 60 minutes. Afterwards, the samples air cooled. The schematic diagram of this process is illustrated in Figure 2.

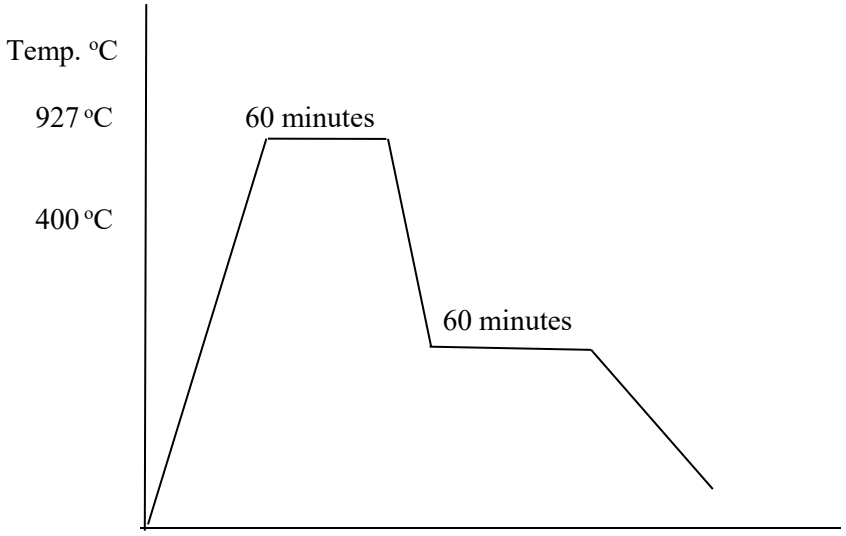

Figure 2. Schematic diagram for conventional austempering heat treatment

2.3 Step-Up Austempering Heat Treatment

The step-up austempering heat treatment took place by heating six as-cast ductile iron samples to 927 °C for 60 minutes and then quenching in a first salt bath (50% $NaNO_3$ + 50% KNO_3) maintained at some lower predetermined austempering temperatures of 250°C, 300 °C and 350 °C for 10 minutes. Subsequently, these samples were then quickly moved to a second salt bath that was kept at 400 °C for 60 minutes. This was followed by cooling in air. The schematic diagram of the process is illustrated in Figure 3.

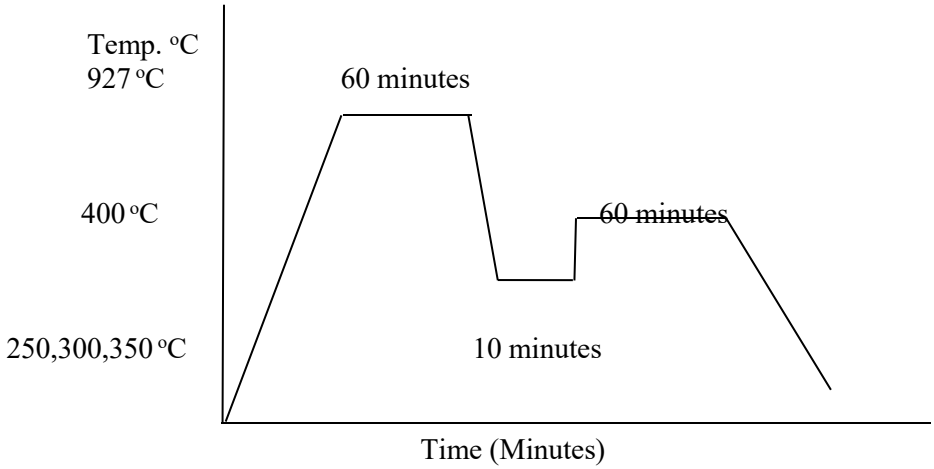

Figure 3. Schematic diagram for step-up austempering heat treatment

2.4 Step-Down Austempering Heat Treatment

The step-down austempering heat treatment involved heating six as-cast ductile iron samples to 927 °C and holding for 60 minutes and then quenched in a first salt bath (50% $NaNO_3$ + 50% KNO_3) maintained at a high temperature of 400 °C for 10 minutes. Next, these samples were swiftly transferred to a second salt bath kept at a lower range of predefined austempering temperatures for 60 minutes: 250 °C, 300 °C and 350 °C. This was followed by cooling in air. The schematic diagram of the process is presented in Figure 4

.

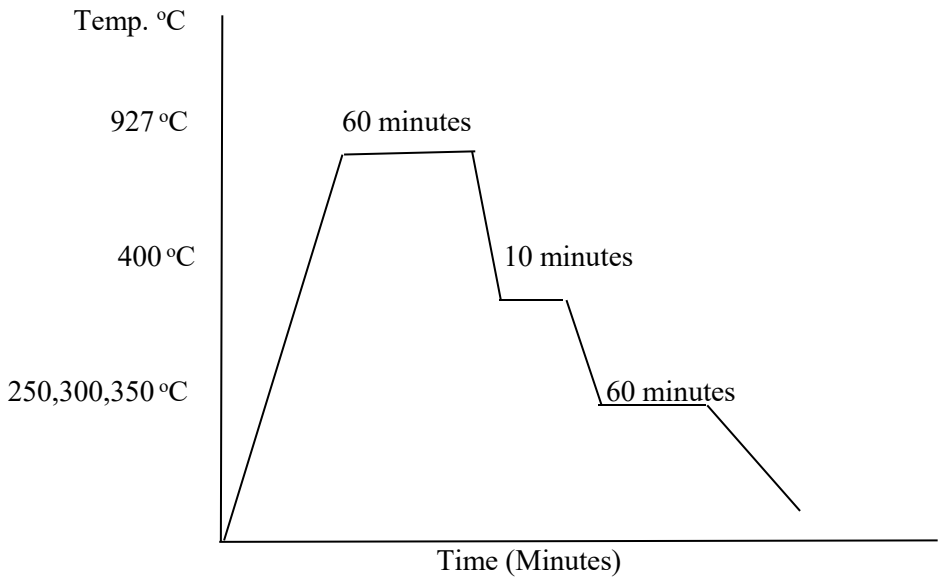

Figure 4. Schematic diagram for step-down austempering heat treatment

2.5 Microstructural Analysis

The samples for microstructural analysis were ground using abrasive grinding papers with grades 60, 120, 180, 240, 360, and 600 grits to obtain a smooth shiny mirror-like surface. During the grinding, water was added to cool off the surface of the samples in order to prevent change in microstructure of the samples. Water was used to wash away all the ground particles on the surface of the samples. Polishing of the sample was done on a rotary polishing table with the help of a fine polishing cloth. During the polishing process, an alumina powder was being applied to the surface of the polishing cloth in order to give a smoother shiny and glossy surface that was free from final traces of grinding scratches. The samples were then etched by dipping a cotton wool into a 2% nital solution. It was then removed and applied to the polished surface of the samples; a smooth dull surface was obtained which was ready for microstructure viewing. Lastly, the micrographs snaped with the aid of an optical microscope (OM).

3.0 RESULTS AND DISCUSION

The results obtained for wear rate and co-efficient of friction (COF) for as-cast and austempered ductile iron (ADI) samples are presented in Table 2, 3, 4 and 5 respectively.

Table 2: Result of wear and co-efficient of friction (COF) for as-cast ductile iron sample

As-cast samples		Responses	
Exp. No.	**Type**	**Wear rate (mm^3/Nm)**	**Co-efficient of friction**

1.	A	0.0196	0.247

Table 3: Results of wear and co-efficient of friction (COF) for conventional single-step ADI samples

Conventional single-step austempering process						Responses	
Exp. No.	Type	Austenitising		Austempering		Wear rate(mm^3/Nm)	COF
		Temp. (°C)	Time (Min)	Temp. (°C)	Time (Min)	Mean	Mean
2.	B	927	60	400	60	0.0166	0.182

Table 4: Results of wear and co-efficient of friction (COF) for two-step ADI (stepped-down scheme) samples

Two-step austempering process (Step-down austempering)								Responses	
Exp. No.	Type	Austenitising		First stage austempering		Second stage austempering		Wear rate (mm^3/Nm)	COF
		Temp. (°C)	Time (Min)	Temp. (°C)	Time (Min)	Temp. (°C)	Time (Min)	Mean	Mean
3.	C	927	60	400	10	250	60	0.0189	0.208
4.	D	927	60	400	10	300	60	0.0105	0.144
5.	E	927	60	400	10	350	60	0.0162	0.182

Table 5: Results of wear and co-efficient of friction (COF) of two-step austempered (step-up scheme) samples

Two-step austempering process (Step-up austempering)								Responses	
Exp. No.	Type	Austenitising		First stage austempering		Second stage austempering		Wear rate (mm^3/Nm)	COF
		Temp. (°C)	Time (Min)	Temp. (°C)	Time (Min)	Temp. (°C)	Time (Min)	Mean	Mean
6.	C	927	60	250	10	400	60	0.0189	0.266
7.	D	927	60	300	10	400	60	0.0152	0.162
8.	E	927	60	350	10	400	60	0.0179	0.189

The wear rates and co-efficient of frictions are graphically depicted in Figures 5 and 6 respectively for as-cast and ADI samples. The wear rate and co-efficient of friction values varies with austempering treatment temperature for all the ADI samples. The as-cast sample showed higher wear rate and friction values compared to ADI samples. The wear rate and friction values obtained for samples processed by both step-up and step-down austempered at 300 °C appears to be lower compared to conventionally processed ADI and other two-step ADI samples, indicating high wear resistance is achieved under this condition.

From the graphical representation below, it shown that two-step austempering at 300 °C for both step-up and step -down are preferable to conventional single-step austempering. This may have justified by the finer ausferritic structure obtained in this samples (Plate 2b and 3b). Hence, ADI processed by two-step treatment (step-down and step-up schemes) showed high wear resistance as compared to the conventional ADI and as-cast samples. This observation is similar to investigation carried out by Perloma and Anderson [13]. In order to achieve the ideal balance of strength and ductility, the authors employed both step-down and step-up austempering on ductile cast iron. With a two-step austempering process rather than the conventional one-step austempering treatment process, they were able to achieve the most effective balance of strength and ductility.

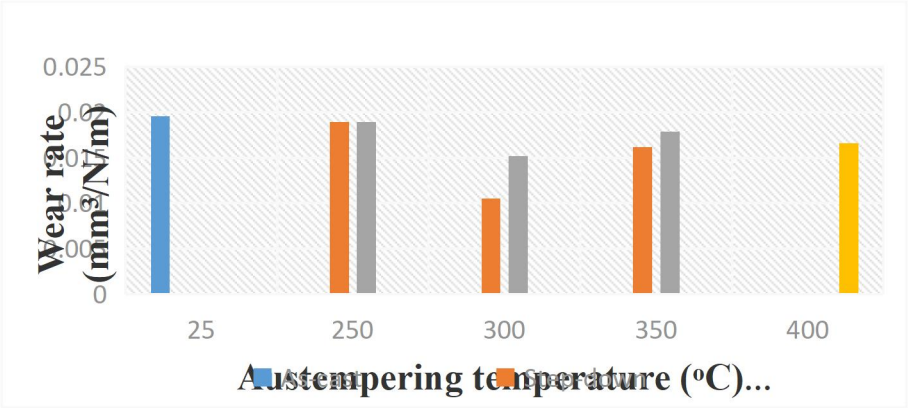

Figure 5: Comparison of wear rate for as-cast and ADI samples at different austempering temperatures

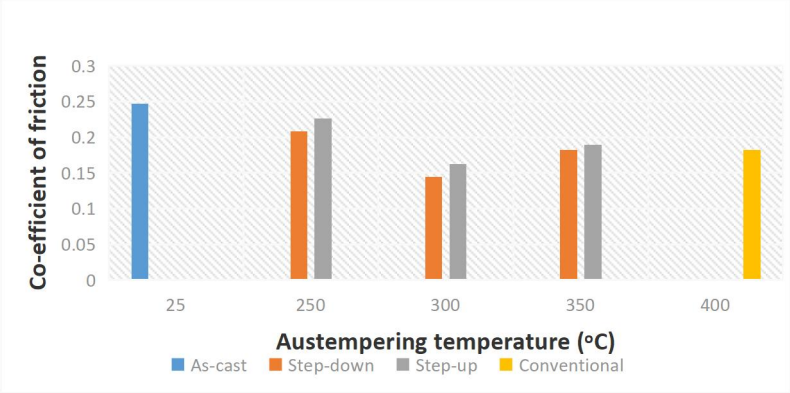

Figure 6: Comparison of co-efficient of friction for as-cast and ADI samples at different austempering temperatures.

Microstructural Analysis of the As-cast and ADI Samples

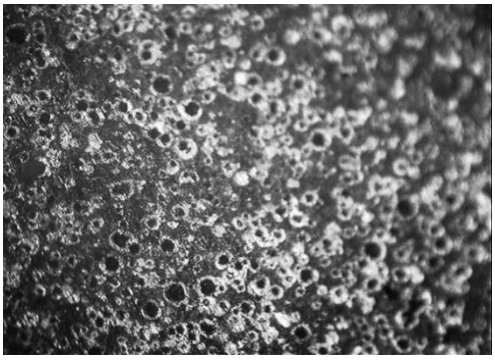

(a)

Plate 1a: Microstructures of as-cast ductile iron, ×100.

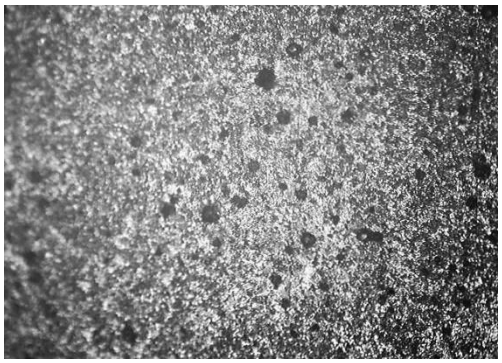

(b)

Plate 1b: ADI microstructures that have undergone the conventional austempering procedure. All samples were austempered in a salt bath maintained at 400 oC for 60 minutes, after being austenitized at 927 ºC for 60 minutes ×100.

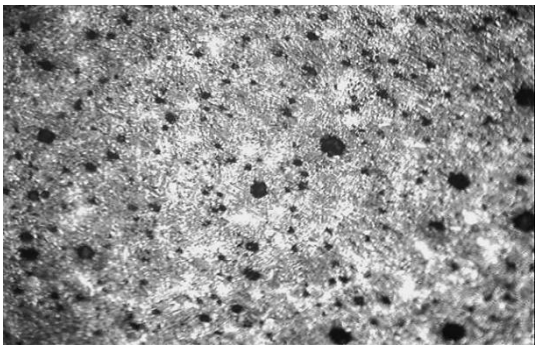

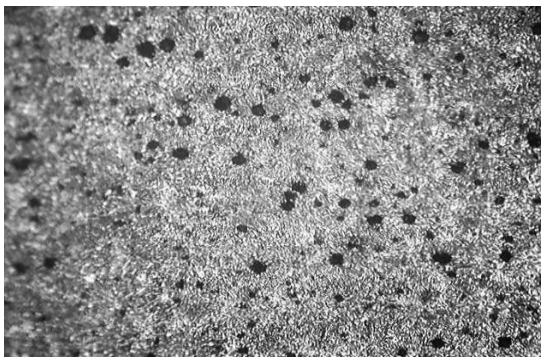

(b) **(c)**

Plate 2: A step-down austempering procedure was used to treat the ADI microstructures. All samples were austenitized for 60 minutes at 927 oC, quenched for 10 minutes in a 400 oC salt bath (first austempering temperature), and then swiftly transferred to lower temperature salt baths (second austempering temperatures) kept at, respectively (a) 350 ºC, (b) 300 ºC and (c) 250 ºC for 60 minutes, ×100.

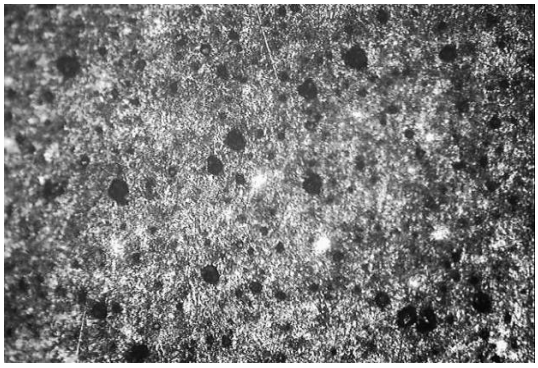

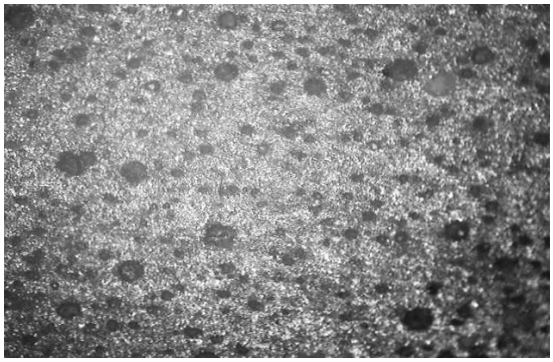

(a)

(b)

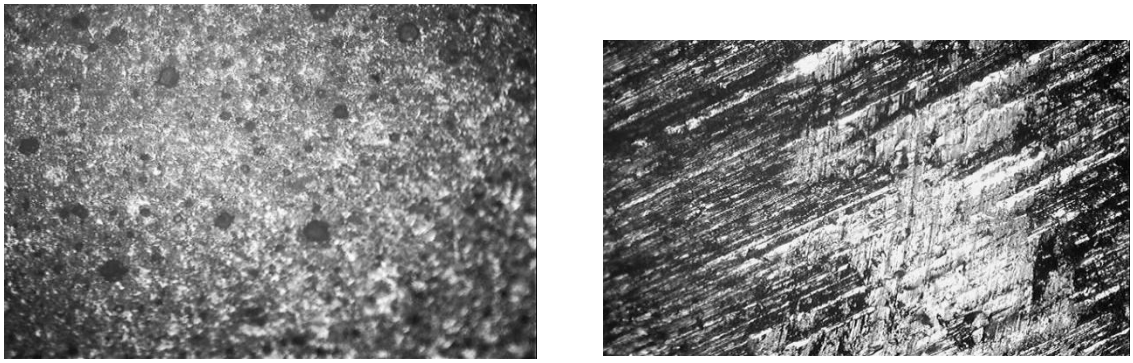

(c)

Plate 3: Microstructures of ADI processed by a step-up austempering process. All samples were austenitized at 927 °C for 60 minutes and quenched to the (a) 250 °C, (b) 300 °C and (c) 350 °C salt bath (first austempering temperatures) for 10 minutes, and then promptly transferred to the higher temperature salt bath (second austempering temperature) held at 400 °C for 60 minutes, ×100.

The as-cast microstructure is depicted in Plate 1a. The structure obviously consists ferrite and graphite in a pearlite matrix. The structure bears the predicted "bull's eye" appearance because the white ferrite phase enhanced the bark graphite nodules. The microstructures of the samples processed by conventional, step-down and step-up austempering processes are reported in Plate 1b, 2a–c and 3a–c respectively. As seen in Fig. 1b, the microstructures of samples austempered by conventional process at temperature of 400 °C appears to have a fine ausferritic structure (mixture of ferrite and austenite) with nodular graphite with nodular graphite distributed throughout the matrix. The microstructures of the samples subjected to the step-down austempering procedure can be seen in Fig. 2a–c which contain combination of ferrite and austenite.

The microstructure of the samples austempered at higher temperature of 350 °C had a much coarser ausferritic structure (Plate 2c) and the samples austempered at 250 °C showed a fairly coarsed structure (Plate 2a). However, for step-down austempered samples at 300°C had a finer structure (Plate 2b). This similar trend was also observed by Putatunda [4] that the samples austempered at higher temperature during step-down austempering treatment had a much coarser bainitic (ausferritic) structure while that of the samples treated at lower temperature had a finer bainitic structure. The microstructures of the samples processed by the step-up austempering process showed similar trend comparable to the step-down austempered samples (Fig.3a-c). It is therefore evident that the two-step austempering conducted at 300 °C for step-down and step-up show finer ausferritic structure as compared to the as-cast, conventionally austempered and other two-step austempered conditions.

WORN SURFACE MORPHOLOGIES

Plates 4-7 show the optical micrographs of the worn surfaces of the as-cast and austempered samples when slided through 100m under the normal load of 8N, and velocity of 15cm/s using ball-on-disk tribometer.

Plate 4: Worn surface morphology of as-cast sample after ball-on-disc wear test, x100.

a

Plate 5: Worn surface morphology of conventional austempered sample (austenitised at 927 °C for 60 minutes & austempered at 400 °C for 60 minutes.), x100.

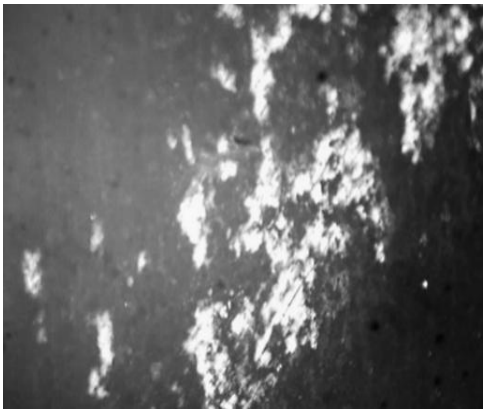

(b)

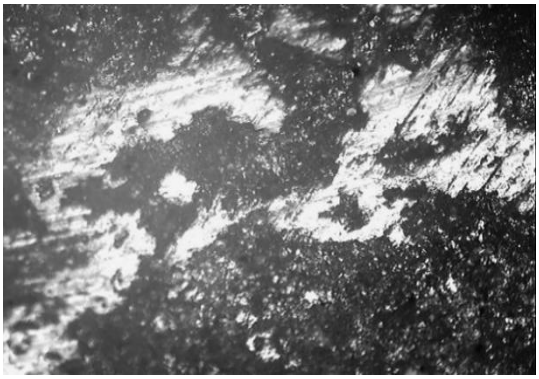

(c)

Plate 6: Worn surface morphology of set-down austempered sample (austenitised at 927°C for 60 minutes & austempered at 400 °C for 10 minutes. Then the sample was immediately transferred to a second salt bath medium & austempered at; (a) 250 °C (b) 300 °C and (c) 350 °C for 60 minutes), x100.

(a)

(b)

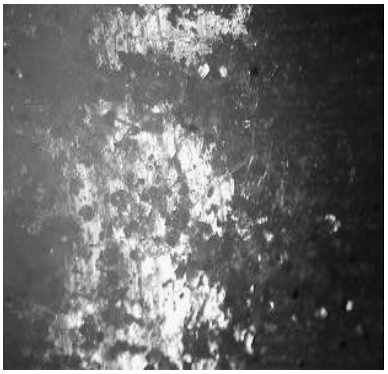

(c)

Plate 7: Worn surface morphology of set-up austempered sample (austenitised at 927 °C for 60 minutes & austempered at; (a) 250 °C (b) 350 °C (c) 350 °C for 10 minutes. Then the sample was promptly transferred to a second salt bath medium & austempered at 400°C for 60 Minutes.), x100.

Plate 4 shows the worn surface morphology of as-cast ductile iron sample. The sample exhibited significant adhesive wear with presence of tears, deep plough and rough grooves. This is an indication of the high wear rate and friction obtained in the sample. Plate 5 shows the worn surface of the conventionally ADI sample. As seen in Plate 5, the optical microscopy showed that the surface topography of the ADI worn surface bore typically of shallow wear scars and grooves studded with small pits. It displayed moderate wear rate and co-efficient of friction with mild significant adhesive wear which displays shallow grooves, plough and scratches. Plate 6 shows the surface morphology of worn sample processed by step-down treatment. It can be seen from Plate 6 that Plate 6a and 6c showed transferred phenomena without any significant adhesive wear but with the presence of voids and pits scattered on the surface, whereas Plate 6b exhibited abrasive wear with smooth surface. The worn surface morphologies of the samples subjected to the step-up austempering process showed similar trend comparable to the step-down austempered samples (Plate 7a-c).

4.0 CONCLUSION

Conventional and two-step (step-down and step-up schemes) austempering heat treatments employed to ductile cast iron samples. The following conclusions were drawn from the experimental results:

i. The as-cast structure of nodular iron obviously encompasses of “bull’s eye” dark graphite nodules surrounded by white ferrite shell.
ii. The microstructures of the ductile treated with both conventional and two-step (step-down and step-up) austempering process schemes contained dual structure of ferrite and austenite (ausferrite).-
iii. The two-step austempering heat treatment schedules resulted in lesser wear rate and friction in the treated ADI samples as compared to the as-cast sample and conventional ADI samples.
iv. Two-step austempering treatment conducted at 300 ^{o}C for both step-up and step-down schemes showed optimum wear resistance and low friction, which could be attributed to the finer ausferritic structure obtained in this condition. However, the results indicated that the best combination of wear rate and co-efficient of friction was displayed by the step-down austempered samples.

5.0 REFRENCES

Yang, J.; Putatunda, S.K. Improvement in strength and toughness of austempered ductile cast iron by a novel two-step austempering process. Materials & Design, 25 (2004) 219–230.

Cakir, M.C, Bayram, A., Isik, Y., Salar, B. The effects of austempering temperature and time onto the machinability of austempered ductile iron. Materials science and Engineering A 407 (2005) 147-153.

Ayman, H.E., Megahed, M.M., Sadek, A.A., Abouelela, K.M. Fracture toughness characterization of austempered ductile cast iron produced using both conventional and two-step austempering process. Materials & Design, 30 (2009) 1866-1877.

Putatunda, S.K., "Comparison of the mechanical properties of austempered ductile cast iron (ADI) processed by conventional and step-down austempering process. 25:8, (2010) 749-757.

Hsu, C.H.; Chuang, T.L. (2001) Influence of stepped austempering process on the fracture toughness of austempered ductile iron. Metallurgical and Materials Transaction A, 32, 2509–2513. G

Hafiz, M. Mechanical properties of SG iron subjected to variable and isothermal austempering temperatures heat treatment. Materials Science and Engineering A. 2003, 340, 1–7.

Yang, J.; Putatunda, S.K. A novel processing of austempered ductile cast iron. Materials Science Forum, (2003) 426–432, 913–918.

Putatunda, S.K. Development of austempered ductile cast iron with simultaneous high yield strength and fracture toughness by a novel two-step austempering process. Materials Science and Engineering A 2001, 315, 70–80.

Yang, J.; Putatunda, S.K. Influence of a novel two-step austempering process on the strain hardening behavior of austempered ductile iron. Materials Science and Engineering A 2004, 382, 265–279.

9. Yang, J., Putatunda, S.K. Near threshold fatigue crack growth behavior of austempered ductile cast iron processed by a novel two-step austempering process. Materials Science and Engineering A 2005, 393, 254–268.
10. Yang, J.; Putatunda, S.K. Effect of microstructure on abrasion wear behavior of austempered ductile cast iron processed by a novel two-step austempering. Materials Science and Engineering A 2005, 406, 217–228.
11. Francucci, G.; Sikora, J.; Dommarco, R. Abrasion resistance of ductile iron austempered
14. M. R. Dodo, K. A. Bello, U. Shehu, M. Abdulwahab, G.A. Ibrahim Effect of Novel Austempering Parameters on the Microstructures and Mechanical Properties of Nodular Cast Iron' Nigerian Journal of Engineering, Faculty of Engineering, Ahmadu Bello University, Zaria. (2015) 22(1):15-25.

by the two-step process. Materials Science and Engineering A 2008, 485, 46–54.
2. Hsu, C.H.; Chuang, T.L. Influence of stepped austempering process on the fracture toughness of austempered ductile iron. Metallurgical and Materials Transaction A 2001, 32, 2509–2513.
3. Pereloma, E.V.; Anderson, C.S. Microstructure and properties of austempered ductile iron subjected to single and two-step processing. Materials Science and Technology, 22, (2006) 1112–1118.

NMS-TP05

IMPLICATIONS ON THE CONTINUOUS DELAY IN THE REVITALIZATION RESUSCITATION COMPLETION AND OPERATIONALIZATION OF THE AJAOKUTA STEEL PLANT: A GROWING CONCERN

Ocheri C[1]. R.E. Njoku[1], N.I. Amalu[2,] J. N. Ezeanyanwu[2] A.C. Iyasara[2], Oyibo A.O.[3]& Adidi O. D[3].
[1]Department of Metallurgical and Materials Engineering, University of Nigeria, Nsukka
[2]Projects Development Institute (PRODA), Enugu State, Nigeria
[2]Department of Metallurgical and Materials Engineering, Enugu State University of Science and Technology, (ESUT)
Department of Ceramic and Glass Technology , Akanu Ibiam Federal polytechnic , Unwana , Ebonyi State
Dept. of Welding and Fabrication Engineering ,
Department of Mechanical Engineering
Delta State Polytechnic , Ogwashi-Uku
Delta State
Corresponding author: Ocheri C
cyril.ocheri@unn.edu.ng
+2348068433419

ABSTRACT

The design, construction, erection and operationalization of the Ajaokuta Steel plant was awarded to the then the Soviet Union. This agreement was based on the importance and significant of steel development in a nation such as Nigeria. The establishment of the plant was first conceptualized as far back as 1967. As a result of a technical/economic agreement enter into between the governments of Nigeria and the Soviet Union, a team of the Soviet Union experts arrived in Nigeria and carried out a feasibility study on the construction of an iron and steel plant. Its projected steel plant was suggested to adopt the blast furnace technology. The report additionally acknowledged the poor quality of the nation's iron ore resources and suggested geological studies to evaluate how much richer ores could potentially be identified. As consequently, the Soviet geological specialists stated in 1968 that there were excellent chances of discovering rich iron ores and coal resources in Nigeria after conducting a general geological survey of the country's mineral deposits. A contract was signed in 1970 between Nigeria and Technoexport of the former Union of Soviet Socialists Republic (USSR) to assess the amount of iron ore reserves and other essential resources that may be utilized in the anticipated establishment of an integrated steel plant at the Ajaokuta steel City. According to the provisions of the agreement, Technoexport agreed to provide the technical expertise and equipment required for conducting additional geological research..The significant succeeds of the survey that followed included the location of the Itakpe ore resources in what was once a part of Kwara State but is now Kogi State. The government established the Nigeria Steel Development Authority (NSDA) as a relevant body to interface with the team. The integrated steel plant adopted the blast furnace-basic oxygen furnace (BF-BOF) technique for the production of iron and steel products. From the installed capacity of 1.3 million tonnes per year, the design contains a mechanism for increasing the capacity to 2.6 million tonnes and ultimately to 5.2 million tonnes

per year. Early 1980s witnessed the start of rolling, and production stopped in 1988.. After the last production process was abruptly stopped in 1988, the rolling process was restarted from November 2004 to 2007. It is sad to report that since 2007 to date the mills have not been operational leading to total disuse since it was lastly operated in 2007. One concern that immediately comes to mind is if the country has leaders who have the long-term interest of the country at heart after the steel plant experienced such a great deal of negligence at the hands of the government officials. Selfish implementations of whatever policies and inconsistent policies had haphazard on the operationalization of the plant; these processes have therefore contributed majorly as setback. One can question the sincerity of the leaders in the revival, resuscitation completion, and operationalization of the moribund steel plant located at the Ajaokuta Steel City due to concerns raised by numerous Nigerians in various sectors.

Key words: Implication, resuscitation, growing colossal, humongous and Concern

1.0 Introduction

The idea for the production of steel first emerged in 1958, when the ideal of creating a domestic steel industry originally developed. This national endeavour did not come to fruition until the late 1970s, however, following a number of feasibility studies. Similar to how original studies focused on building rolling mills, greater knowledge of the country's vast iron ore and coal deposits sparked the ambition to build Nigeria's first totally integrated iron and steel plant.

The Federal Government adopted the decision to build more steel plants in the nation as a result of the domestic demand for steel, particularly the long goods used in the building industry, growing at an increasingly rapid rate. The 1975/80 growth plan, in which the Federal Government announced its aim to establish additional steel plants based on the Direct Reduction Iron (DRI) technologies, was a bravely diving and significant step in the steel industry. This action was taken to utilize use of the abundant natural gas resources that were being wasted in some of the nation's oil fields. (Niger Delta region). Studies in this area were strengthened, and several multinational businesses were invited to submit bids based on guidelines provided by the previous National Steel Development Authority. (NSDA).

Following careful deliberation, the partnership of Germans and Austrians suggested building the plant in Ovwian-Aladja, in the former Bendel State (now known as Delta State), using the Midrex Direct Reduction technique. In addition to establishing the Delta Steel Plant, the federal government also built rolling mills in three significant market hubs around the nation. As a result, Kastina, Jos, and Oshogbo each have a capacity of 210,000 tonnes per year for their respective inland rolling mills. This steel policies were being carried out by the now-defunct NSDA, whose final significant task was the signing of the Global contract with TPE to construct and erect an integrated steel on July 13, 1979.

General Olusegun Obasanjo, the head of state at the time, signed a global agreement with TPE for the construction and erection of Nigerian steel in 1979, which marked the beginning of the construction of the steel plant, underlined a vision fundamental to the growth and development of the Nigerian economy. This concept was advocated and a strong infrastructure foundation was established by President Alhaji Shehu Shagari in 1979, basically creating what is now known as Nigeria's steel sector. Nigeria's steel industry had been practically in a coma since 1988. Providentially, forty –three (43) years after the signing of the global contract in 1979, there has not been concert efforts in reviving, resuscitation, completion and operationalization of this edifice, which is capable in turning around the fortune of the nation in a positive direction for industrial, technological and economic growth and development. It should be a statement

demonstrating that we as a people have overcome all international conspiracies and fears about, not only of Nigerian steel, but also about its benefits as an alternative economic factor to petroleum and agriculture, the catalyst for technological advancement and relative industrial self-sufficiency.

The steel plant, like our other steel plants and those who initially dreamt of the steel dreams, are convinced beyond all reasonable doubts either in technology, engineering or techno-economics that the infrastructure will jump start global development and economic transformation. Ajaokuta, in comparison with emerging and unproven new technologies for iron and steel production represents the best option for commercial production of steel for the Nigerian, continental and world market. The plan is to target all markets.

The installed capacity of the integrated steel plant is 1.3 million tonnes annually, with design provisions for expanding that capacity to 2.6 million tonnes and subsequently to 5.2 million tonnes annually for the production of iron and steel. After the final production phase was abruptly stopped in 1988, the rolling process started up again in November 2004. 5.5 mm to 12 mm wire rod and 8 mm to 30 mm rebars are both used in the rolling procedures. The 0.88 metric tonne per annum (MTPA) capacity of the coke batteries, the 2.6 MTPA capacity of the sinter plant to produce fluxed sinter, and the 1.3 MTPA capacity of the blast furnace to produce hot metal were all revived and modified.

Three continuous bloom casters with four strands each comprise the rolling mill, The plant was designed in addition to utilize two basic oxygen furnaces that can each produce 130 tonnes of liquid steel annually. 400,000 TPA for the light section mill, 795,000 TPA for the billet mill, and 130,000 TPA for the wire rod mill. Structural and Medium Section Mills, 560,000 TPA (MSSM). The Thermal Power Plant, which utilized two generators of 55 MW each to produce 110 MW throughout the period of the concessions. One of the supporting units that was adequately furnished with equipment for producing components and spare parts in line with various standards was the Engineering Complex.

2.0 Challenges /reasons attributed to the delay in the completion of the plant

Several challenges/ reasons have been adduced for the inability of the plant to take-off fully such as lack of government political will and lack of patriotism and lack of focus.

The steel plant was designed primarily to accomplish a number of goals, including:

(1) To serve as the foundation for processing the country's mineral resources and to open up new export markets for increased foreign exchange revenues.

(2) To give the nation the technological foundation it needs to industrialize.

(3) To promote local industrial development through import substitution and currency preservation.

(4) To increase the number of jobs available to qualified Nigerians.

Initially, it was during the cold war when the then USSR agreed to build the plant. There was a cold war between the Eastern bloc and the Western bloc. It should be known that the western bloc including America initially resisted Nigeria from developing her own steel plant. The western bloc has been telling Nigeria that she does not have the capacity and capability to build and maintain a steel plant. According to Sanusi (2003:23), the USSR came to help us out, and here we have the steel company, so unfortunately the first mistake was when the USSR were holding discussions to build Ajaokuta, they also went to sign to develop the entire steel sector together, to help the plant in getting finished products. Unfortunately, the Government allowed the western bloc to be brought into the contract - the Germans and French- by giving them the civil works. This was a deliberate act, which further posed some challenges to the then USSR.

Sometimes the western world contractors would say they do not understand the Soviet design, so that's how the country has been tossed here and there. This they did to bring delays, which eventually worked because Nigeria relied heavily on western financiers.

Nigeria went to the World Bank, a western institution to borrow money to execute the project. This singular act gave them the opportunity to discourage Nigeria from having the money, and this delayed payment of contactors handling the job expectedly left the country. After a few years, another government would say no, we must complete the plant; they would pay all the bills to those contractors before they came back to start working again.

When they came back, they would continue, after about two years the same scenario happens again. Therefore, monies were spent and nothing was achieved. It was the plan of the west, but today it is Nigeria versus the west.

The former USSR has been disappointed. The West has always silently acted against Nigeria's development because they know the potential of Nigeria in terms of the human population, capacities, natural resources, and all the well-being God has endowed Nigeria with. Nigeria as a country has the greatest market in the west. If it has well set out industries, that means that Nigerian will not go to the west to buy steel products. Even some leaders who are sincere, honest, and willing to complete the plant are frustrated because the avenues are created to demobilize such interests.

Imagine a Canadian company that was brought in some time ago to access the real problem of the steel plant. They came with already completed reports to hand over to the Nigerian government and the report was that the plant was not viable, that steel production in Nigeria was not viable, and we should forget it. In the end, they said that the plant should be converted into an electricity generating company. After the objection to it, they mellowed it down, but still mentioned it in the final report they submitted. After the episode the then Vice President of the World Bank visited Nigeria and made the same careless remarks forget about the steel plant that it was not viable; it should be converted into an electricity-generating company. The Hatch Association also did an earlier report and their verdict was to scrap the steel plant.

Another Company, Kobe steel with Japanese technology, came with a view to changing the concept of the established steel plant. They introduced a technology called fast melt, making claims that the blast furnace technology was obsolete and should be scrapped. But when they were told to follow the principle of Build Own and Transfer (BOT) they disappeared into thin air and never surfaced again.

An American-based corporation known as SOLGAS Energy operated the plant as if it were an electrical provider, but they also were unsuccessful as they were confused and unsure of what to do. Finally, the straw that broke the camel's back was when Global Infrastructure Holding Limited, an Indian corporation, took over operation of the plant from October 2004 to June 2007. They changed the aim and objectives for the establishment of the steel plant by not complying with basic concepts. Their motive was to set Nigeria back by cannibalizing the existing equipment and looting already stockpiled raw materials and spares from the steel plant.

From these analyses, it could be seen that our problem started from the fundamental level and it is the machination of the western bloc. They tried all the means and ways to deprive the nation of developed and viable steel plant for the production of liquid steel.

The advantages that result from the construction of a profitable steel plant are numerous; they include the creation of jobs, social services (such as healthcare, housing, and education), the growth of upstream and downstream industries, as well as industrial and economic development.

Reviewing the steel sector, which has been considered to as the cornerstone of Nigeria's industrialization. The plant has a multiplicative effect on the economy as a whole. If Phase 1, which was designed to produced 1.3 million tonnes of liquid steel, had been finished and put to use commercially, the nation would have immediately benefited from its proceeds . Employing more than 10,000 people at the plant; employing at least 80,000 Nigerians in the raw material industries that supply the plant's feedstock; employing at least another 100,000 Nigerians in the industries that use the plant's products; conserving foreign exchange used to import steel products annually; and contributing at least 30% of the inputs to Nigeria's automotive industry in the first year.

Export potential to the ECOWAS sub-region; the majority of Nigerian firms have trouble finding suppliers for their machinery and replacement parts. A facility with a sophisticated Engineering Works Complex can help significantly.

Effects of multiplication on the industries for economic growth in both the upward and downward streams. There are some implications and consequences attached to the delay and un-operationalization of the plant such as the nation stand the risk of losing all the critical hydraulic sub- assemblies:

Instrumentation network, electrical installations & refractories brick work (BF, SMS, 49 Coke Oven Batteries);

Rotary kilns for Lime Plant, Aluminium Silicate, Tar Bonded, Foundry, etc) that form the main fabric of the 420 process units of the steel plant which replacement would be running into hundreds of millions of dollars if the total rehabilitation does NOT start this year;

The above facilities were laid in 1982- 1993, most of refractories, have 7years, special refractories 20-26 years. Refractoriness is kept under mobile conservation.

The government has a lot to do in making sure that the plant is revived, resuscitated, completed and operationalized for the well-being of the corporate existence of Nigeria and Nigerians. The continuous delay in the operationalization of this plant will continue to translate to doom to our national structure and economy emancipation.

3.0 SERIES OF CONTRADICTORY DECLARATIONS ON AJAOKUTA STEEL & ITAKPE IRON MINING PROJECTS IN THE RECENT TIMES

(i)The Minister of Mines and Steel Development told the world in October 2019 that the Nigeria's President and Russian's President had a memorandum of understanding in Sochi, Russia whereby, the Russian's President agreed to assist the Nigerian government towards the rehabilitation, reactivation, completion, and commissioning of the steel project by offering both technical and financial assistance to the tune of $500million and mobilizing other financial resources from the Russian investors towards the implementation of that agreement What happened?

(ii)As a follow-up to this MOU, the Minister also informed the world that another meeting was held in Cairo, Egypt, whereby, AfriEXIM Bank agreed on March 2020 to provide some counterpart funding towards the execution of the Sochi agreement. What happened?

(iii)In the same year 2020, in the month of June/July, the Minister said that about 60 Russians have been earmarked to come to commence another technical audit towards the execution of the Sochi agreement and that the COVID-19 epidemic was delaying them.

(iv)By October 2020, the Minister reiterated that the both the plants at Ajaokuta and Itakpe would be commissioned before the expiration of the Bihari's administration and that the Russians were then ready to commence activities. What happened?

(v)By March/April 2021 the Minister still reminded the world that Ajaokuta & Itakpe would soon undergo rehabilitation and that Presidential Implementation Committee, comprising (13members) with Mr. Boss Mustapha as the Chairman, had been inaugurated for that purpose. What happened?
(vi)By June/July 2021, the Minister announced through the print/electronic media that the Presidential Implementation Committee was considering a STEEL SUMMIT (which he described as the first of its kind) to determine the way forward for the plant. What happened?
(vii)By November 2021, the Minister informed the world through the interview he granted, Mr. Ajuri (Presidential Assistant on Media) that at last, the Russian-Ukrainian Consortium would be arriving in January 2022 (1st or 2nd week) to do their comprehensive presentations on the two projects and that the technical audit would commence in March 2022, all to no avail. What happened?
In March 2022, the Minister shocked the whole of Nigeria through the interview he granted. Mr. Ajuri where he declared that a local Nigerian Company would now work with a British firm since the Russian-Ukrainian is at war (whereas the Consortium of the Russian companies had twice in May 2021. Also on April 7, 2022, he said that a list of experts has been sent and awaiting to be officially invited to Abuja. He further declared that the ongoing war could not deter them, as they already have their representatives in Algeria, UAE waiting for the Nigerian invitation). What happened?
(viii)Nigerians are shocked that in spite of all these preparations made by the Consortium of companies (Original Builders) to come to Abuja to start urgent rehabilitation of the two projects with their technical and financial resources. The hon. minister requested N853million to engage what he called transactional advisors on the Ajaokuta & Itakpe projects, which have been left abandoned and idled for over 28years.How did we get here?
(ix)Looking at these scenarios that has been playout in the handling of the two plants located at Ajaokuta and Itakpe, it could suffice to state that the Ajaokuta steel plant as of 1995 had gulped $8 billion (conservative administrations). Nigerians are not overly surprised by the ministry's actions given the recent events, especially considering the fact that the steel plant's original builders already sent the Minister and the Presidency a detailed work scope for the complete rehabilitation, completion, and commissioning of the two projects in May 2021.
For the Ministry of Mines and Steel Development to be requesting N853M at this time when a consortium of original builders is waiting to be invited after sending their list of experts to the presidency repeatedly. It is should be noted that some African countries like Egypt, South Africa, and Algeria have expanded their steel production capacities three folds within the last 35 years while Nigeria is still struggling to complete 1.3 million metric tonnes/year. South Africa is now at 14 million metric tonnes/year, Egypt at 6.5 million tonnes/year, and Algeria at 2.5 million tonnes/year. Yet Nigeria calls itself the giant of Africa. What is responsible for Nigeria's situation is that Nigerians are heavily engrossed in mind blogging corruption, which led to the collapse of 56, 000 projects in Nigeria.
Since, independence, the introduction of the Structural Adjustments Programme (SAP) in 1986, opened the floodgates to massive importation of everything under the sun, which progressively weakened the Naira over the years compounded with a non-diversified economy. The Minister and the ministry failed to inform Nigerian about the true position of the steel plant. The following was reported by Felix Onuah and stated in part, "Abuja, Sept. 3(Reuters) - The Nigerian government has made arrangements to pay $496 million to resolve claims over the steel facility. Nigeria has agreed to pay $496 million to resolve a multi-billion dollar claim from

Global Steel Holding Ltd following the termination of a contract. The decision was taken to revival and resuscitate and operationalization of the steel plant that has been in limb for a long period with a view to improving the the nation's steel plant , as was stated by presidency. "It was expected the ministry to have correct and the right information on the litigation issue as it concerned the steel plant rather making some statements that were at variance with the reality on the subject matter," .

4.0 BENEFITS FROM THE STEEL INDUSTRIES

Today, billions of dollars are spent on the importation of steel; this enormous sum of money is an intolerable waste of our limited resources and could have been allocated to other crucial areas of the economy. On the contrary side, it is anticipated that the steel plant , once completed, will produce a significant amount of foreign currency through exports. The goods of the facility are also expected to be shipped to other African nations and the West African sub-region, as was the case when the plant was operated by Global Steel Holding Ltd (GSHL), as they made enormous sums of money. An assertion that the plant generated $74 million in foreign currency for the sales of 128,000 metric tonnes of rolled products during the relatively short period that Global Steel Holding Ltd (GSHL) existed was credited to the then management (Ajasteel 2006:6).

The study states that ribbed bars were sold to four countries in West Africa, namely: Mauritania (3,800 metric tonnes), Cote d'Ivoire (3,400 metric tonnes), the Benin Republic (1,050 metric tonnes), and Mail (600 metric tonnes). a lack of output from the rolling mills in comparison to their potential. Therefore, it is imperative that the government take action; otherwise, despite the enormous sums paid to this industry and even the corporation each year, we will continue to import steel products into the country. Without a doubt, the establishment of the plants will lead to the transfer of technology to the nation. This will create fresh opportunities for technical advancement. It was anticipated that foreign investors would be drawn to the steel development once the steel plant was operational. In fact, nothing can be accelerated or made to happen in the much-discussed technology transfer to emerging nations, particularly with regard to the country's industrial start-up of the steel plant.

Since steel has provided an important contribution to national development, it has attracted the aforementioned sectors that process raw materials, including mining, beneficiation, coking, calcining, refractory production, and spare parts manufacturing. Steel is a crucial input raw material for a wide range of other industrial operations or works in all of its different crude or primary forms, as well as its byproducts. The manufacturing of raw steel would stimulate or activate numerous related sectors. A sizable population of unemployed persons would be removed from the unemployment situation with respect to the high number of personnel trained. The integrated steel plant was built for steel plants and is labour- and capital-intensive.

Efobi (2002) estimates that the steel plant needs 10,000 workers. Each Nigerian employee in the steel communities is likely caring for 10 other Nigerians, so when you plan for 10,000 employees, you should actually be providing amenities for more than 100,000 people. When considering into account the steel plants' upstream and downstream multiplier effects as well as the welfare amenities like schools, hospitals, markets, shopping centers, filling stations, maintenance garages, and security personnel, it could be observed that plans indicate for a township that can accommodate about 300,000 people. What additional or more comprehensive approach for reducing unemployment is needed when the steel plant provides care for 300,000 people?Those that witnessed the condition of the villages close to the steel plant will bear witness to the tremendous amount of transformation that took place in Steel Township.

The good news therefore is that the government has finally settled the litigation between the Nigeria government and Global Steel Holding Ltd having agreed to pay the sum of $496m in order to allow the Nigerian government to regain the ownership of the steel plant. This development will also pave way for the nation to begin to plant on how to commence the resuscitation, rehabilitation and operationalization of the steel plant for the betterment of the nation.

5.0 CONCLUSION

In conclusion, the government should put more efforts into achieving the following;

That all the completed units of the steel plant should be made functional, which are the secondary units of the plant, consisting of four rolling mills, the engineering workshops, and their support services, which have since been completed and taken over by Nigerian management immediately the exit of the Global Infrastructure Nigeria Limited (GINL) .

Nevertheless, unfortunately, these units have not enjoyed sustained operations due to inadequate funding. Some industries in the country turned their attention to Ajaokuta as a source of spare parts, replacement components, and consumables, thereby creating and preserving jobs at Ajaokuta and the associated industries. The steel plant's completion and commissioning have been subject to controversy for a very long time. The time has come to take an additional look at the plant and to reconsider whether producing iron and steel in the format that was first intended is both desirable and feasible. Given the already made investment, it should be investigated to determine if it would not be worthwhile to operate the manufacturing plant into a bustling complex of other industrial endeavours. The final 2% of the plant's technical preparedness ought to be completed using funding from the federal government. The good news is that the Nigerian government has released to the Indian company the first instalment of $ 250 million for the settlement of the plant as reported by Eniola Akinkuotu' . "As part of the first payment of the $496 million agreed upon by all parties over the dispute stemming from the plant . The payment of the said amount was reported on Thursday, September 15, 2022, that Global Steel received the first $250 million settlement, according to Gwandu.

6.0 Growing Concern and Recommendations

The Ajaokuta and Itakpe projects have been abandoned for the past 28 years

The Ajaokuta steel plant has gulped $8Billion (conservative estimate)

Non- completion and operationalization of these projects will continue to deteriorate due to idleness and disuse with colossal amounts been wasted.

The original builders / experts should be invited to take another assessment of the plants in order to determine the state of decay and to proffer solution on how bring back the plant to life again by providing comprehensive work scope for the rehabilitation, reactivations and operations of the Ajaokuta and Itakpe projects.

Looking at the scenarios of the rate of crimes and criminalities in Nigeria, which have snow ball to insecurities, life threaten, hunger and lack of operationalization of some moribund steel plants, the government should therefore take the advantage that have been created make sure that these moribund plants are revived and operationalized .

References

[1] Abubakar Sadiqi – “Under the Auspices of steel Week in Nigeria at Ajaokuta Steel Company Limited “A paper presented at Steel week on 9- 13 the April 2002

[2] Ajaokuta Steel Company Limited: Diary 1987

[3] Alhaji Magaji Inuwa: A welcome address delivered by the General Manager/Chief Executive, Ajaokuta steel company at 1986 Annual Conference of Nigerian Metallurgical Society.

[4] Chukukere E.U. Steel Industries- Strategies for Rational Development, A paper delivered at 1986 Annual Conference of Nigerian Metallurgical Society.
[5] Company Report: Ajaokuta steel company limited detailed Project Report (DPR) Vol. I part II Explanatory Note.
[6] Evaluation Report of Ajaokuta steel company limited by Voest-Alhine Industrial Service GmbH Linz / Austria 1997
[7] Gr Singh " Use of Steel Products in a Developing Country " .The India experience A Paper Presented at Ajaokuta Steel Company Limited At a steel week held on 9-13th 2002
[8] Marietu Tenuche: Ajaokuta. The Prospects and problems of Steel Development in Nigeria, A paper presented to Confluence Journal of Management, Kogi state University Anyigba, Vol. 1 No.1 January –June 2001
[8] Nwachukwu C.C. ''Management theory and Practice'' published by Africana –FEP Publisher Limited.
[9] Ocheri Cyril: Commercialization Opportunities of the Completed Units of the Ajaokuta Steel Company Limited. An MBA Thesis submitted to Michael Ajasin University Akungba Akoko, Ondo State -July 2002.
[10] Priorities and Aspects of the Ajaokuta Iron and steel Company Development" A Paper Presented at Ajaokuta Steel Company Limited at a steel week held on 9-13th 2002
[11] Project Report: Ajaokuta steel company limited detailed Project Report (DPR) Vol. IV on Personnel
[12] Project Report: Ajaokuta steel company limited Detailed Project Report (DPR) Vol. V Repair shop, List of Equipment.
[13] Project Report: Investment Profile of Ajaokuta steel company limited, March 1990
[14] Revamping the Voest – Alphine Steeling company LD III K Linz 12.Alhaji Bunu Sherif Musa-"Speech Delivered by the Honorable Minister for Mine, Power and Steel": A proceedings 1986 Annual Conference of Nigerian Metallurgical Society.
[15] Speak out – ISSSAN Labor Journal Vol.2 No.2 second Quarter Edition (April – June 2003)
[16] Status Report and Business Plan for Ajaokuta steel company limited April 1999
[17] The effect of the various steel making process on the energy balances of Integrated Iron and steel work special report 71, The Iron and Steel institute of London.

[18] "The Role of Metallurgical Industry in the Nigerian Economic Development " A proceeding of Nigerian Metallurgical Society (NMS) 4th Annual Conference held at ASCL 29 – 31 October 1986.
[19] Tim Chi Efobi "The Impact of the Steel Industry on the Development on Human Resources and Poverty Alleviation " A paper presented at Steel week on 9-13th 2002 at Ajaokuta Steel Company Limited.
[20] Wakawa M.B. Strategies for the sustaining of optimal Capacity Utilization of the Ajaokuta Steel Company Limited, Processing of the Nigerian metallurgical Society (NMS) November 30th - December 3rd 1994.
[21] Werner W. Paulukuhn "Reflections on the Importance of a Steel industry to national Development" A Paper Presented at Ajaokuta Steel Company Limited At a steel week held on 9-13th 2002

NMS-TP06

ZINC NANOCOMPOSITES WITH CALCIUM OXIDE NANOPARTICLES SYNTHESIZED FROM OYSTER SHELL NANOCOMPOSITES

S.M. Adams[1, 2], F.O. Anianwu[1] V.S.Aigbodion[1]
[1]Department of Metallurgical and Materials Engineering, University of Nigeria, Nsukka
[2] *Department of Metallurgical and Materials Engineering, Airforce Institute of Technology (AFIT) Kaduna
[2*]Corresponding author: E-mail address ademu.sani@ yahoo.com

ABSTRACT

The electrochemical oxidation and wear performance and as well as the surface morphological features of novel zinc reinforced with calcium oxide nanoparticles (10 g/1 CaOnp) coating formulations from oyster shell were investigated. The electro-deposition was done with a current density of 1.5 to 2.0 A/cm^2. We looked at wear, oxidation, hardness, corrosion rate and morphological features. These composite coatings were characterized as having reduced wear rates, as well as enhanced corrosion and oxidation resistance. The hardness values were found to increase by 65.53% and the oxidation protection was increased by 57.14% at 1.5A/cm^2 current density. The lower corrosion and wear resistance and greater hardness values achieved are due to the smaller crystallite size of the deposited sample. It was discovered that discarded oyster may be utilized to improve the corrosion resistance and hardness properties of mild steel by electro-deposition. Mild steel has been demonstrated to be more resistance to corrosion, wear, and oxidation when coated with CaOnp produced from oyster shells.

Keywords: Oyster shell, agro-waste, wear, corrosion, mild steel, electro-deposition.

1.0 Introduction

Zinc plating is often used to provide a protective layer against water and other elements in the air that cause corrosion. A very common zinc coating technology is the electrolytic deposition of a zinc coating from an electrolyte [1]. Galvanizing is the process of applying a protective zinc coating to iron or steel, to prevent rusting. The most common method is hot dip galvanizing, in which steel sections are submerged in a bath of molten zinc. Mild steel is the steel that is used widely in the manufacturing and construction industries. Steel is an alloy of iron with a low carbon in the range of 0.5–0.26%. Among the areas that use mild steel are cleaning industrial, oil field, petrochemical processing, heat exchangers, tanks and others. However, corrosion, oxidation, and friction-wear applications are the main problems of this material due to its poor hardness and severe corrosion, oxidation, and wear transition [2]. Electro-deposition or electroplating is a process for metallic coating over a base material. Zinc metal has a number of characteristics that make it a well-suited corrosion protective coating for iron and steel products. Zinc excellent corrosion resistance in most environments' accounts for its successful use as a protective coating on a variety of products and in many exposure conditions [3, 4].Recently, the researchers' attention was towards the electroplating of zinc because of its wide usage in the protection of ferrous metals for industrial applications such as pipes, strips, sheets, steel wires, fabricated ferrous metal parts and tubes [5]. Punith et al. [6], and Rekha et al. [7] studied the corrosion behavior of Zn composites using

nano-sized carbon particles. A 3.5 wt% NaCl electrolyte solution was used as the corrosive medium. They observed that the composites had higher anodic potentials. Vathsala et al. [8] reported on the corrosion behavior of Zn/ZrO_2 nanoparticles. They observed that the addition of ZrO_2 nanoparticles improved corrosion protection, formed stable passivation, and affected the electrode reaction kinetics. Aigbodion et al. [9] reported the co-deposition of Zn–ZnO-Ant hill powder composite coating on mild steel. They observed that for Zn–ZnO-25gAnt hill and Zn–ZnO-25gAnt hill + orange juice, maximum corrosion protection efficacy was 92.86% and 94.41%. Shourgeshty et al. [10] described the corrosion, friction, and wear of Zn–Ni and Zn–Ni–Al_2O_3 multilayer coatings with 32, 128, and 512 layers on a low carbon steel substrate using pulse electro-deposition. They revealed that increasing the number of layers (thinner layer thickness) and the inclusion of alumina nanoparticles increased the corrosion and wear resistance of coatings. Hammami [11] reported on the good corrosion resistance of Zn–Ni/SiO_2 nano-sized particle composite coating in 3 wt% NaCl solution. Aigbodion and Akinlabi [12] obtained high corrosion resistance when zinc/eggshell particles were used to coat mild steel. Popoola and Fayomi [13] reported the effects of depth of immersion, distance between the cathode and anode, voltage (0.5–1.0 V), and coating time on the properties of the zinc coating of mild steel. The best property at a coating voltage of 0.8 V for 20 min was obtained [14]. And it showed an increment in current efficiency using an acidic sulfate-based electrolyte and a deposition temperature of 40–45 ◦C. It was concluded that rises in temperature affect the crystal size and rate of deposition. Adams et al. [15] described the use of eggshells as a source of $CaCO_3$ for enhancing the hardness values and wear behavior of composite coatings on mild steel. $CaCO_3$-derived eggshell particles weighing 0, 5, 10, 15, and 20 g were used to make the composite covering. The anti-wear behavior of Zn-20 g $CaCO_3$-derived eggshell particles composite mild steel was found to be the best. From the literature, it was observed that the development of zinc composite coating for the enhancement of corrosion rate, oxidation behavior, wear and friction is promising and has attracted the attention of the research community. The co-deposition of zinc on mild steel using CaO nanoparticles derived from oyster shell waste was considered in this work to replace the high-cost, toxic, carcinogenic metallic oxide nanoparticles currently used in electrodeposition. Oysters were chosen to produce the CaO nanoparticles for this work since Suree et al. [16] found out that oyster shells contain 96% calcium carbonate ($CaCO_3$) and that the calcium carbonate structure in oyster shells can transform to calcium oxide (CaO) when heated at a temperature above 700 ◦C. Oysters coming under the genus crassostrea and saccostrea are observed along the Indian coasts [17]. Oyster shell is composed of protein, polysaccharides, and minerals including calcium, magnesium, sodium, copper, iron, nickel, strontium and some microelements. Chemical and microstructure analysis showed that oyster shells are predominantly composed of calcium carbonate with rare impurities [18]. The oyster species found in Nigeria is Crossostrea gasar, which is also known as the mangrove oyster. It has been reported that oysters are tolerant organisms capable of withstanding wide variations in temperature, salinity and dissolved oxygen which makes them a worldwide cultivated species.

2. Materials and method

2.1. Materials

The oyster shells were collected from the seaside in Rivers State, Nigeria. Mild steel

with a chemical composition of 98%Fe, 0.25%C, 1.03%Mn, 0.20%, 0.28%S, and 0.04%P was used in this work was sourced from Ajaokuta Steel Company Limited, Kogi State, Nigeria. All the reagent used in this work were sourced from Joel Chem University of Nigeria, Nsukka
Nigeria.

2.2.Method

2.2.1. Preparation of CaO nanoparticles (CaOnp)

The production of the nanoparticles was similar to the method used elsewher [15]. The oyster shells were initially washed to remove the fresh remnants with deionized water and dried at 80 ◦C. The oyster shells were cleaned, dried, and ground into powder form using a ball milling
machine. The calcined oyster powder was dissolved in 500 ml of 1MHCl. The mixture was stirred for 5 h and filtered to obtain a $CaCl_2$ solution. The 250 ml of 1 M NaOH solution was added to the $CaCl_2$ solution and stirred for a period of 3 h. The mixture was centrifuged and cleaned with deionized water to obtain a pH of 7. The gel $Ca(OH)_2$ was then aged for 24 h at 100◦ Celsius before being filtered, and the filtrate was then heated for 24 h in a muffle furnace at 900◦ Celsius to produce calcium oxide nanoparticles. Equations (1) - (3) gives the reaction mechanism (1) [15]:

(Oyster shell) $CaCO_3$ (s) + 2HCl (aq)) $\rightarrow CaCl_2$ (aq) + H_2O (l) +CO_2 (g) (1)

$CaCl_2$ (aq) + 2NaOH (aq)$\rightarrow Ca(OH)_2$ (s) + 2NaCl (aq) (2)

$Ca(OH)_2$ (s) + Heat)$\rightarrow$CaO (s) + H_2O (3)

2.2.2. Manufacturing of the composite coating.

Before the electro=deposition, the mild steel substrates were cleaned mechanically using a set of emery papers of 400–1200 PC and degreased using acetone. An alkaline electroclean treatment of the degreased substrate was done with 20gL-1 Na2CO3 and 35gL-1 NaOH for 2 h. The samples were activated in a 30% HCl solution for a period of 60 s, rinsed with distilled water and dried. The development of the novel composites was done using the electrodeposition method. In addition, 100 g/l $ZnCl_2$, 5 g/l Thiourea, 15 g/l Boric acid, and 100 g/l KCl were used in the
preparation of the electro=deposition bath. In the formulation of the composite coating, 10 g/l CaOnp, current densities of 1.5 and 2.0A/cm^2, a deposition temperature of 80 ◦C, and a deposition time of 15 min were used. This was made possible after several preliminary experiments. The bath mixture was stirred for 24 h using an aquarium pump and a magnetic stirrer. The substrate was used as the cathode and zinc metal as the anode, and was placed in a vertical position of 12 mm inside the bath while direct current from the rectifier was connected to the electrodes. Figure 1 displays the photograph of the electro-deposition process.

2.3 Characterization of the samples deposited

The Joel JEM- 2100F model was used for transmission electron microscopy (TEM) in order to evaluate the particle size of the CaOnp. The powder of CaOnp was dissolved in ethanol and placed on a carbonized copper mesh sheet, and was allowed to dry before the TEM analysis. A VEGA 3 TES- CAN model scanning electron microscope (SEM) was used to evaluate the microstructure of the composite coating. An X'Pert Pro model diffractometer (XRD) was used to evaluate the phases. The dry sliding conditions of the developed composites were conducted against a hardened En 31 counter face using a tirbometer (ANTON PAAR, TRB3, version 8.1.8). The wear test was done as per ASTM standard G99 at a speed of 350 rpm, sliding time of 1000sec, and 20 N applied load. The worn out surface was created using a scanning electron microscope. An electrochemical analyzer model CHI660D

was used to conduct the electrochemical corrosion behavior of the coated samples. The reference electrode was Ag/AgCl, the sample working electrode was graphite rod, and the counter electrode was graphite rod. A working electrode surface area of 1.0 cm^2 was used for the analysis and was immersed in simulated seawater prepared with 3.5% NaCl. In accordance with ISO 9227:2017, 0.5 to 0.5 V, 30 ◦C, 0.5 mV/s scanning rate, and 100% relative humidity (RH) were used. The oxidation behavior of the substrate and coated samples was determined using heating process, three readings were taken in each of the tests, and the average was used for the analysis.

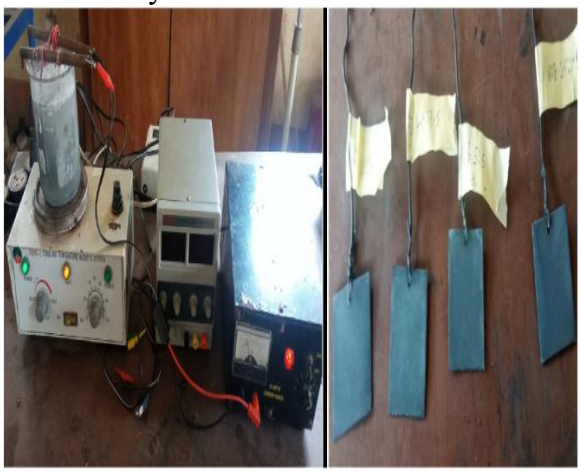

Figure 1: Photograph of electrodeposition process and the coated samples

thermal gravimetric analysis (TGA) (TA Instruments TGA Q50). A test piece area of 2 mm2 was used for the analysis. The TGA experiment was conducted by heating the samples from the room. The panel was heated to 900 ◦C with a jumping heating mode under flowing air injection. The panel was held at 900 ◦C isothermally for 15 min to record the oxidation weight change. The mass change was determined simultaneously using a high- sensitivity electronic balance. During the

3. Results and discussion

3.1 CaOnp TEM image

The results obtained show that the morphologies of CaOnp has a particle size of 48.5 nm in diameter, and was found to be round and spherical in random distribution. There is no segregation and agglomeration of particles as presented in Figure 2. Calcium, silicon, oxygen and carbon were seen present in the EDS of the CaOnp. The high peak of Calcium confirmed that the produced CaO from oyster shells contains CaO. This is consistent with the findings of Suree et al. [16] that reported that oyster shells contain 96% calcium carbonate ($CaCO_3$).

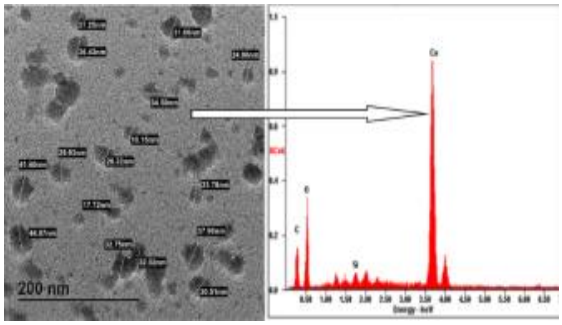

Figure 2: TEM/EDS OF THE CaOnp

3.2 XRD Examination

In Figure 3 the XRD spectrum of the developed composite coatings on mild steel was shown. The Zn-CaOnp coating had a stable phase and microcrystalline structure with different peaks, while the substrate only showed two main phases of crystallographic plane of (111) and (101), which corresponded to Fe (cubic) and C (hexagona) respectively. There was the presence of (104), (102) phases of CaO (rhombohedral) and ZnO (cubic) structures in addition to the Fe (cubic) and C (hexagonal) phases in the coated samples. This evidence of more diffraction peaks was sparingly observed in the coated sample at 1.5A/cm^2. This was used to support the earlier conclusion that there were more transfers of CaOnp to the cathode during the electro-deposition. When eggshell was used as a deposition material for the electro-deposition of mild steel, Aigbodion and Akinlabi [12] found the same thing. The d-spacing values were calculated using equation (4) [11]:

$2d \sin \theta = n\lambda$ (4)

Where: $\lambda = 1.5406$ Å for CuKα, n = 1, target and θ = Bragg's angle.

The grain size (G) of the samples was calculated using equation 5 [19]

$G = k\lambda / \beta \cos \theta$ (5)

Where: k = constant (0.9 approximately), β = Full width at half maximum intensity (FWHM). The dislocation density (δ) was computed using equation (6) [20]:

$\delta = 1/ G^2$ (6)

Equation (7) was used to compute microstrain (ε) [19]:

$\varepsilon = \beta \cos \theta / 4$ (7)

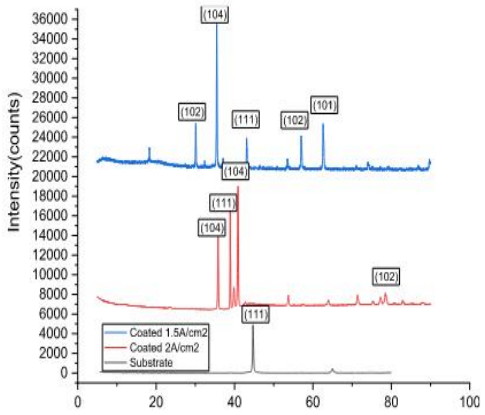

Figure 3: XRD spectrum of the samples

3.3 Microstructure of the samples deposited

Microstructure is an instrument used to evaluate the integrity of coated samples. The SEM image and the EDS of the samples are displayed in Figures 4 and 5. There was evidence in Figure 8 that the presence of CaOnp on the surface of the samples was visible. The coated samples differ from the uncoated samples (compare Figure 4a with Figures 4b and 4c). The uncoated sample has a clear surface with no deposited material, whereas the presence of small nanocrystalline nodules CaOnp uniformly and completely covered the entire surface of the sample coated at 1.5A/cm^2. The higher content of CaOnp obtained at a current density of 1.5A/cm^2 was attributed to proper dissolution of CaOnp, which results in the formation of Zn-CaOnp globules. The microstructure revealed Zn-CaOnp. In the microstructure, CaOnp second phase bonding strength was seen in the microstructure due to the increased dissolution of CaOnp. Pores, cracks, and defects were not observed in the SEM image, which shows effective coating. As shown in Figure 4c, increasing the current density to 2.0A/cm^2, results in a partial coating of the sample. The non-uniform coating obtained at current density was attributed to the reduction of nucleation density, cathodic

current efficiency, and grain refinement. Roventi [21] found that adding Al_2O_3 to the Zn–Ni matrix leads to a more even distribution of Al_2O_3 in the zinc matrix, smaller crystallites, fewer surface flaws, and a more dense and compact deposit. This effect is in line with those findings. An energy dispersive spectrometer (EDS) was used to analyze the SEM images, and Figure 5 presented the EDS spectrum. It was observed that a high peak of Fe and the absence of Zn and Ca were observed in the EDS of the substrate as displayed in Figure 3a. However, there was a high peak of Zn and Ca in the EDS of the coated samples. This shows that the coated materials were obtained in the coated samples as displayed in Figures 4b and 4c. The sample coated at 1.5A/cm^2 had a higher Ca percentage of 2.8% as compared to coating at a current density of up to 2.0A/cm^2 with a Ca percentage of 1.8%. The observation is consistent with the work of [15].

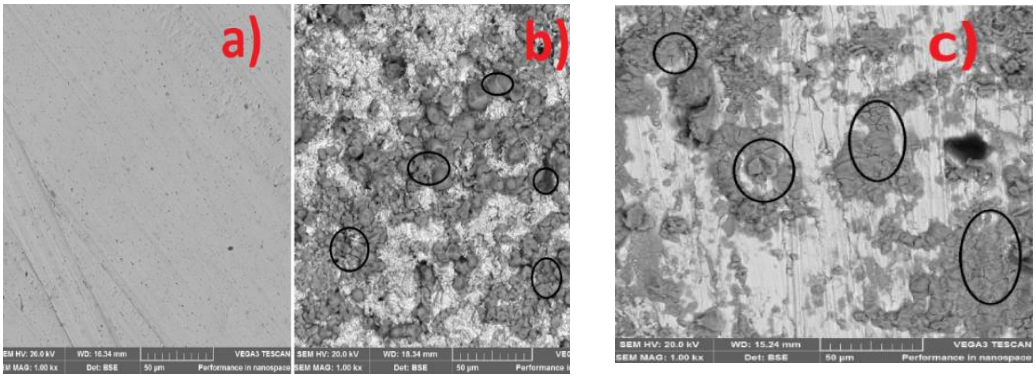

Figure 4: SEM surface images of (a) substrate (b) coated sample at 1.5A/cm^2 current density (c) coated sample at 2A/cm^2 current density

3.4 Surface AFM analysis.

An atomic force microscope was further used to discuss the surface roughness of the samples. Figure 6 presents the AFM spectrum of the coated samples at current densities of 1.5 and 2.0 A/cm^2 respectively. It was observed that the sample coated at a current density of 1.5 A/cm^2 had lower surface roughness than the sample coated at a current density of 2 A/cm^2. For example, the surface roughness rises from 0.7 nm to 2.4 nm at a current density of 1.5 and 2.0A/cm^2 respectively.

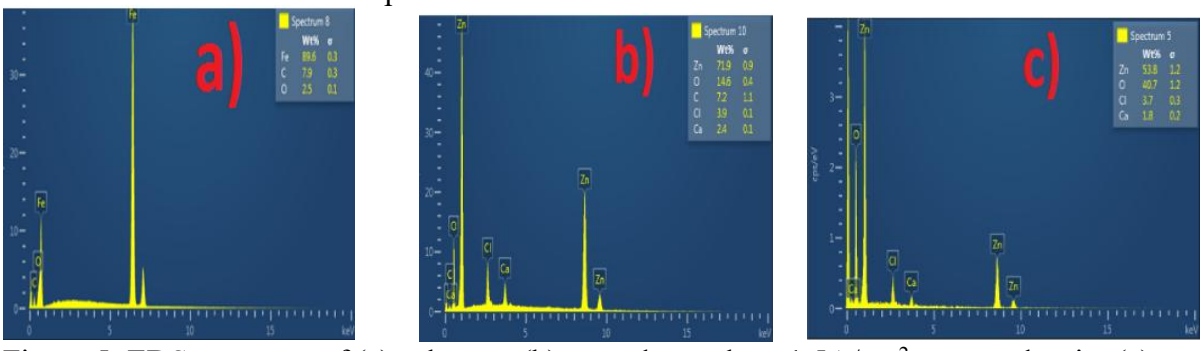

Figure 5: EDS spectrum of (a) substrate (b) coated sample at 1.5A/cm^2 current density (c) coated sample at 2A/cm^2 current density

. This corresponded to a 70.83% enhancement in surface roughness.

The CaOnp sticking and segregation on the Ca-rich Zn matrix result in high surface roughness at a higher current density of 2.0A/cm^2. Also, both samples showed a lot of peaks with different heights.

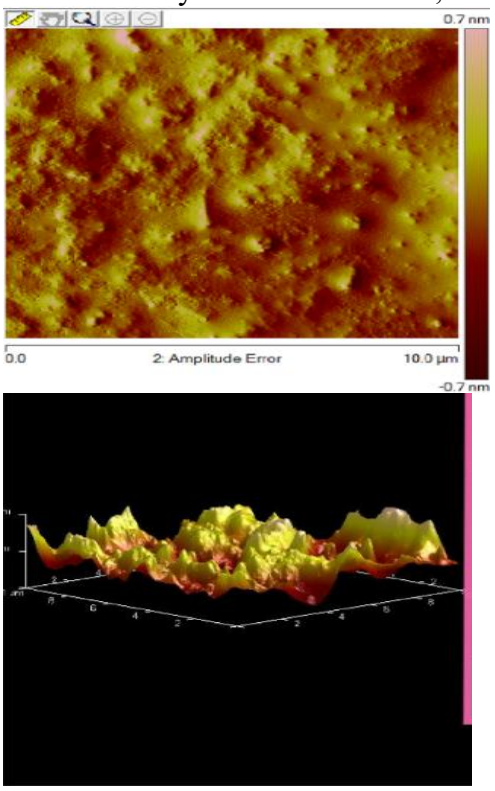

Figure 6a: AFM surface images of coated sample at 1.5A/cm^2

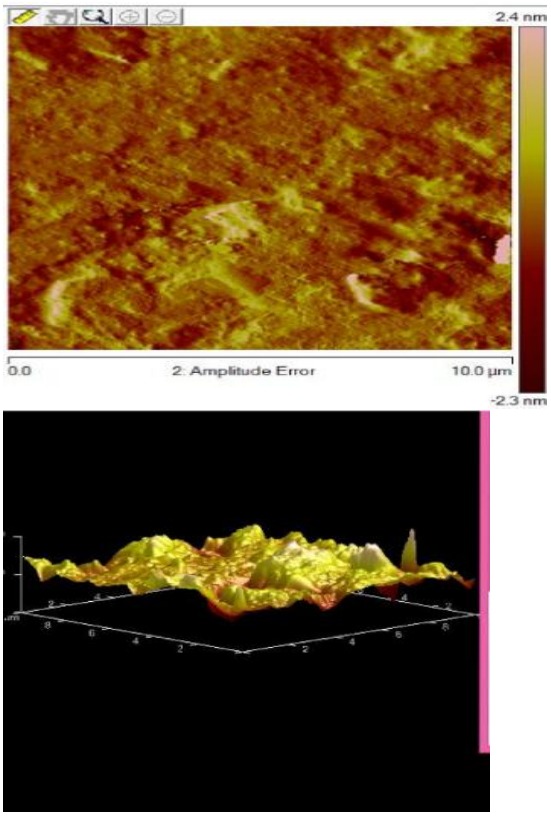

Figure 6b: AFM surface images of coated sample at 2A/cm^2 current density

3.5 Coating thickness and hardness values

Results of the coating thickness and hardness tests are presented in Figure 7. It was observed that there was a direct relationship between the coating thickness, surface roughness and the hardness values, and that a mean rise in the coating thickness of the samples led to an increment in the hardness values. However, the sample has optimal hardness values and coating thickness at 1.5A/cm^2. The higher amount of CaOnp that covered the entire surface, as can be seen in the SEM images, increases the coating thickness of the sample deposited at 1.5A/cm^2. The high hardness values of the coating were attributed to the higher dislocation density of the samples and strain hardening of the samples, which resulted in an increment in hardness values [22, 23]. Hardness values of 235, 389, and 345HB were obtained for the substrate and coated samples at 1.5 and 2A/cm^2 current densities, respectively. This corresponded to a 65.53% enhancement in the hardness values at 1.5A/cm^2 current density. Liu et al. [24] previously reported an increase in hardness values as a result of an increase in dislocation density, which was attributed to dispersive strengthening and grain refinement of the particles that strengthened and hardened the composite coating.

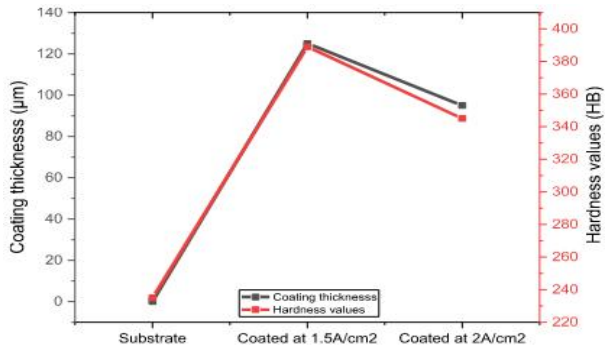

Figure 7: Variation of hardness values and coating thickness with sample condition.

3.6 Electrochemical analysis

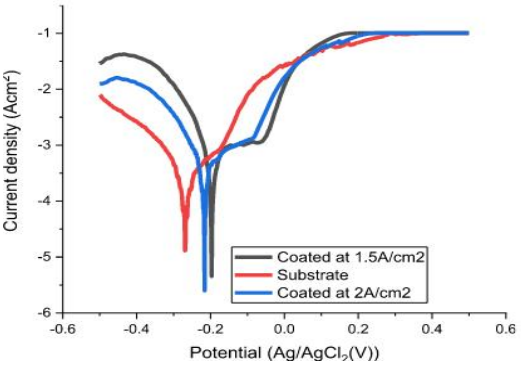

Figure 8: Tafel plots of the electrochemical process.

$Fe + H_2O + Cl^- = [FeClOH] + H^+ + e^-$ (8)

$[FeClOH] + H^+ = Fe^{2+} + Cl^- + H_2O$ (9)

The ferrous ions react with hydroxide ions, to formed iron hydroxide and dissolved in the water medium and results to light green solution as shows in equation 10

$Fe^{2+}+2OH^-=6Fe(OH)_2$ (10)

The oxide formed does not firmly adhere to the surface of the steel and flakes off, causing great corrosion attack. These findings are consistent with previous research [26]. However, in the coated samples, a stable oxide that covered the entire surface of the mild steel reduced severe corrosion attack, making the sample noble and decreasing the chloride ions. In Fig. 8, it was demonstrated that potential and polarization resistance rose for the coated

Figure 8 presents the Tafel plots, while Figure 9 displays the corrosion results. There was evidence that the coated samples shifted the cathodic

branch to the right. That means that the coating has a higher anodic potential than mild steel. The higher corrosion rate of the mild steel is attributed to higher dissolution due to the presence of chloride ions; this involves electron discharge of the mild steel in the chloride environment, which results in an unstable oxide film, as can be used in Equations (8)(9) [25].

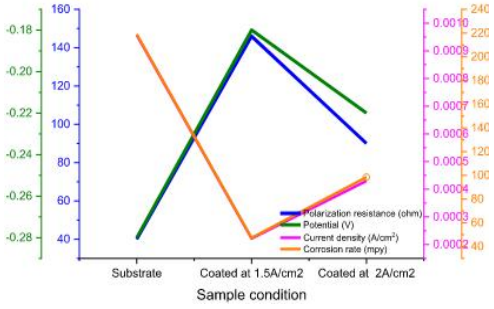

Figure 9: Corrosion results of the electrochemical process.

samples as compared with the substrate. There was also a reduction in the corrosion rate and current density for the coated samples. For example, at 1.5 and 2A/cm2 current density, the substrate and coated samples had corrosion rates of 219, 98.5, and 47.3 mpy, respectively, corresponding to a 79.49 enhancement in corrosion protection at 1.5A/cm2. This was attributed to the nanocrystalline nodule structure of CaOnp that formed a stable film, as seen on the corroded surface in Figure 10.

The substrate has more corrosion damage, as seen in Fig. 10a, with evidence of great cracks and pits as a result of great corrosion damage. Based on Figure 10a, it can be concluded that the high corrosion damage of the substrate is caused by a local corrosion attack mechanism (Figure 10b).

Slight corrosion attack was obtained in a

sample coated at 2A/cm^2 current density, as can be seen in Figure 10c. This was attributed to improper coating of the surface of the mild steel, which exposed the uncoated section to corrosion attack. This is in accordance with the findings of [27, 28]. The coated samples' Tafel curves changed so that the current density was lower, the potential was higher, and the polarization resistance was higher. This happened because a passive film formed over the sample, which stopped corrosion attacks.

3.7 Friction-wear analysis

The friction and wear results of this work are displayed in Figures 11 and 12. It was seen clearly that the substrate has a higher friction and wear rate as compared with the Zn-CaOnp coated samples. The low friction coefficient and wear rate of the coated samples were attributed to the self-lubrication effect and hardness values provided by the CaOnp during sliding. This self-lubrication effect of Ca-rich compounds has been previously reported by Ref. [15]. The friction and wear loss increase with each increment in sliding time. The coated sample at 1.5A/cm^2 has a lower wear rate as compared with the sample coated at 2.0A/cm^2. This was attributed to the low friction coefficient as a result of higher lubrication due to the higher dispersion of CaOnp as obtained in the SEM image.

The worn out surface of the substrate (Figure 13a) shows high craters and grooves as compared with the coated samples (Figures 13b and 13c). These delaminations, grooves, and craters show the presence of adhesive and abrasive wear. The third body removing of counterface material due to the effect of En-31 counterface material was referred to as abrasive wear, while the transfer of material to the counterface was referred to as adhesive. The sample coated at 1.5A/cm^2 had the highest reduction in wear track as compared with other samples under investigation. This was used to support the lower wear rate and friction coefficient recorded. The low friction coefficient,

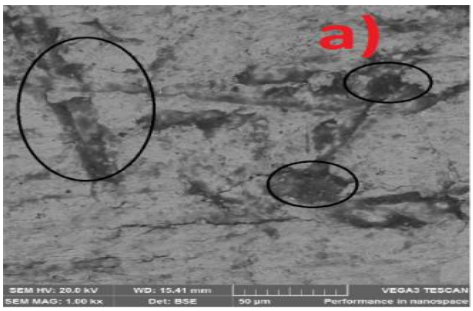

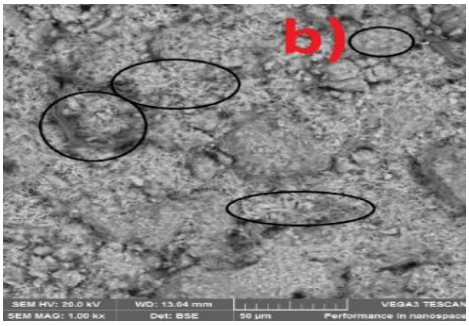

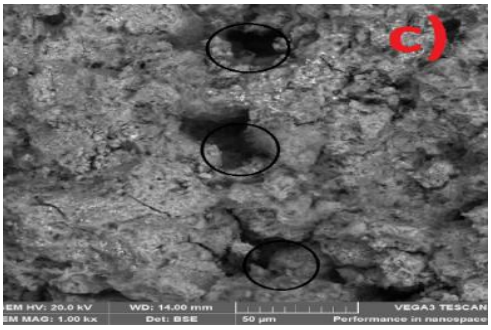

Figure 10: SEM corroded surface (a) Substrate (b) Coated sample at 1.5A/cm^2 current density (c) Coated sample at 2A/cm^2 current density

.which results in high dissolution of Ca atoms that created more self-lubrication action during the sliding operation was responsible, since observation has been reported by Premkumar et al. [29]. The low stable phases and weak coverage of the entire surface of the mild steel by the CaOnp result in high wear debris and material removal of the composite coating at 2.0A/cm^2 as compared with that of 1.5A/cm^2. When comparing the coated sample at 2.0A/cm^2 to the coated sample at 1.5A/cm^2, we found that the coated sample at 2.0A/cm^2 had more craters. This shows that the coated sample at 2.0A/cm^2 has more adhesive wear.

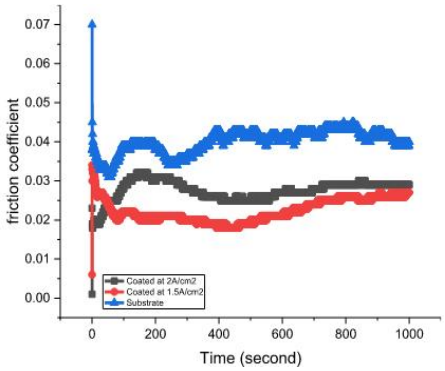

Figure 11: Variation of Friction

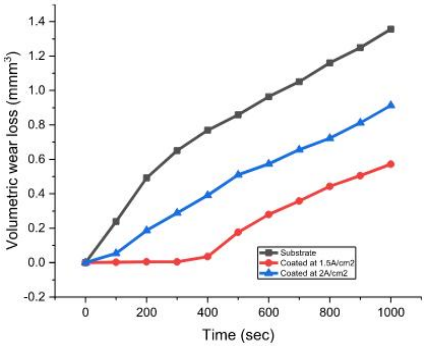

Figure 12: Variation of volumetric coefficient with sliding time wear loss with sliding time.

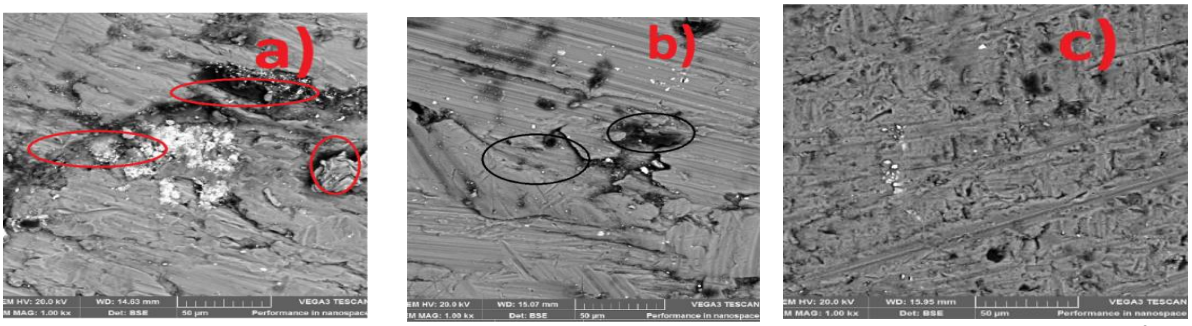

Figure 13: SEM worn out surface images of (a) Substrate (b) coated sample at 1.5A/cm^2 current density (c) coated sample at 2A/cm^2 current density

4Conclusions

A high performance zinc composite coating generated from discarded oyster shell were studied for the improvement of mild steel corrosion, and wear resistance. The following conclusions may be drawn from the work:

1. CaOnp dissolving in the Zn matrix has a big effect on the structure of nodules and the formation of grain boundaries in the Zn-CaOnp coatings that have been made.
2. The Zn-CaOnp composite coatings had a low rate of wear and a low friction coefficient. This was because the coated sample lubricated itself when it moved and the hardness values were high.
3. A 65.53% enhancement in the hardness values was obtained at 1.5A/cm^2 current density. This increase in hardness was caused by an increase in the number of dislocations.
4. According to Tafel measurements, the composite coatings have better anti-corrosive characteristics.
5. CaOnp made from oyster shells has been shown to make mild steel more resistant to corrosion, wear.

Acknowledgement

The authors hereby appreciates and acknowledges the Africa Centre of Excellence for Sustainable Power and Energy Development (ACE- SPED), University of Nigeria, Nsukka; Airforce Institute of Technology (AFIT), Kaduna; Energy materials research group, University of Nigeria, Nsukka, Nigeria; and Faculty of Engineering and Built Environment, University of Johannesburg, Auckland Park, South

Africa for their supports.

References

1. Vlastimil Kuklik, Jan Kudlacek (2016). Dip galvanizing of Steel Structures. Science Direct, pp7-16. Doi.org/10.1016/B978-0-08-100753-2.00002-1
2. R. Winand (2011). Electrodeposition of zinc and zinc alloys, in: Modern Electroplating, 5th edition. JohnWiley & Sons, Inc., Hoboken, NJ, USA, pp. 285–307.
3. V.S. Aigbodion, S.I. Neife, I.Y. Suleiman (2019). Surface modification of mild steel by co-deposition using Zn-ZnO-Ant hill particulate composite coating in simulated seawater, Proceed. of the Instit. of Mech. Eng., Part M, J. of Eng. for the Marit. Envir. 233 (1) 245–256, https://doi.org/10.1177/1475090218792382.
4. L.M. Muresan (2016).Electrodeposited Zn-nanoparticles composite coatings for corrosion protection of steel, in: Handbook of Nanoelectrochemistry, Springer International Publishing, Cham, Switzerland, pp.333-353.
5. Murakami, FS, Rodrigues, PO, De Campos, CMT, Silva, MAS (2007). Physicochemical study of CaCO3 from egg shells. Cience Tecnol Aliment 27:658-662. https://doi.org/10.1590/S0101-20612007000300035
6. M.K. Punith Kumar, M.P. Singh, C. Srivastava (2015). Electrochemical behavior of Zn–graphene composite coatings, RSC Adv. 5, pp. 25603–25608.
7. M.Y. Rekha, C. Srivastava (2019). Microstructure and corrosion properties of zinc grapheme oxide composite coatings. Corrosion sci. 152, pp. 234 - 248
8. K. Vathsala, T.V. Venkatesha (2011). Zn–ZrO2 nanocomposite coatings: elecrodeposition and evaluation of corrosion resistance, Appl. Surf. Sci. 257, pp. 8929 – 8936.
9. V.S. Aigbodion, S.I. Neife, I.Y. Suleiman (2019). Surface modification of mild steel by co-deposition using Zn-ZnO-Ant hill particulate composite coating in simulated seawater, Proceed of the Institute of Mech. Eng., Part M, J. of Eng. for the Marit.

Envir. 233 (1) (2019) 245–256, https://doi.org/10.1177/1475090218792382.

10. M. Shourgeshty, M. Aliofkhazraei, A. Karimzadeh, R. Poursalehi (2017). Corrosion and wear properties of Zn–Ni and Zn–Ni–Al2O3 multilayer electrodeposited coatings, Mater. Res. Express 4 (9) (2017), 096406, https://doi.org/10.1088/2053-1591/aa87d5.
11. O. Hammami, L. Dhouibi, P. Berçot, E.M. Rezrazi, E. Triki (2012). Study of Zn-Ni alloy coatings modified by nano-SiO2 particles incorporation, Int. J. Corros. 2012 (2012), 301392.
12. V.S. Aigbodion, E.T. Akinlabi (2019). Explicit microstructural evolution and electrochemical performance of zinc eggshell particles composite coating on mild steel, Surface. Interfac. 17 (2019), 100387, https://doi.org/10.1016/j.surfin.2019.100387.
13. A.P.I. Popoola, O.S.I. Fayomi (2011). Effect of some process variables on zinc coated low carbon steel substrates, Sci. Res. Essays 6 (20) (19 September, 2011) 4264–4272.
14. T.J. Tuaweri, E.M. Adigio, P.P. Jombo (2013). A study of process parameters for zinc electrodeposition from a sulphate bath, Int. J. Eng. Sci. 2 (2013) 2319–6734.
15. S.M. Adams, E. Atikpo, V.S. Aigbodion (2022). CaCO3 derived from eggshell waste for improving the hardness values and wear behavior of composite coating on mild steel via co-deposition, Int. J. Adv. Manuf. Technol. 119 (2022) 5483–5496.
16. Suree Tongwanichniyom, Thanit Pattamapitoon, Napimporn Sangvichien and Somkiat Phornphisutthimas (2021). Production of calcium oxide from waste oyster shells for a value-added application of antibacterial, Ecol. Environ. Conserv. 27 (2) (2021) 539–547.
17. Ajith Thomas John (2016). Chemical composition of the edible oyster shell Crassostrea madrasensis. J. of marine Bio and Aquaculture. Doi.org/10.15436/2381-0750.16.972
18. Yoon, G.I., Kim, B.T., Kim, B.O. (2003). Chemical-mechanical characteristics of crushed oyster Shell. Waste management, 23(9):825-834.
19. L.M. Tavares, E.M. da Costa, J.J. de Oliveira Andrade, R. Hubler, Bruno Huet (2015). Effect of calcium carbonate on low carbon steel corrosion behavior in saline CO_2 high pressure environments, Appl. Surf. Sci. 359 (2015) 143–152.
20. B.M. Praveen, T.V. Venkatesha (2009). Generation and corrosion behavior of Zn-nano sized carbon black composite coating, Int. J. Electrochem. Sci. 4, pp. 258–266.
21. G. Roventi (2017). Electrodeposition of Zn-Ni-ZrO2, Zn-Ni-Al2O3 and Zn-Ni-SiC nanocomposite coatings from an alkaline bath, Int. J. Electrochem. Sci. 663–678.
22. S. Anwar, F. Khan, Y. Zhang, S. Caines (2021). Zn composite corrosion resistance coatings: what works and what does not work? J. Loss Prev. Process. Ind. (2021) 69.
23. S. Anwar, F. Khan, Y. Zhang (2020). Corrosion behaviour of Zn-Ni alloy and Zn-Ni-nano-TiO_2 composite coatings electrodeposited from ammonium citrate baths, Process Saf. Environ. Protect. 141 (2020) 366–379
24. J.H. Liu, J.X. Yan, Z.L. Pei, J. Gong, C. Sun (2020). Effects of Mo content on the grain size, hardness and anti–wear performance of electrodeposited nanocrystalline and amorphous Ni–Mo alloys, Surf. Coating. Technol. (2020), 126476, https://doi.org/10.1016/j.surfcoat.2020.1264.
25. C.C. Daniel-Mkpume, V.S. Aigbodion, D.O.N. Obikwelu (2021). Electrochemical analysis and microstructure of value-added functional Zn-ZnO-rice husk ash composite coating of mild steel, Chem. Data Collect.

35 (2021), 100767, https://doi.org/ 10.1016/j.cdc.2021.100767.
26. K.K. Maniam, S. Paul (2021). Corrosion performance of electrodeposited zinc and zinc-
alloy coatings in marine environment, Corros. Mater. Degrad. 2 (2021) 163–189, https://doi.org/10.3390/cmd2020010.
27. Mehmet Kul1, Kürs ad O guz Oskay, Fuat Erden, Erdem Akça, Ramazan Katırcı, Erkan K oksal, Evindar akıncı (2020). Effect of process parameters on the electrodeposition of zinc on 1010 steel: central composite design optimization, Int. J. Electrochem. Sci. 15 (2020) 9779–9795, https://doi.org/10.20964/2020.10.19.
28. H.M. Muzamma, H. Ma, H.M. Liang, Z. Gao, J. Cao, C. Wang, A. Kunwar (2020). Fabrication of cerium myristate coating for a mechanochemically robust modifier-free superwettability system to enhance the corrosion resistance on 316L steel by one-step electrodeposition, Surf. Coating. Technol., 125970, https://doi. org/10.1016/j.surfcoat.2020.1259.
29. A. Premkumar, A. Elayaperumal, S. Arulvel, M.S. Jagatheeshwaran (2019). Partial dissolution of precipitated-calcium carbonate (P-CaCO3) in electroless nickel-phosphorus (Ni-P) coating and its surface characterization, Mater. Res. Express 6(6), 066409, https://doi.org/10.1088/2053 1591/ab0934.

NMS-TP07

PERFORMANCE OF HYBRID FLAME RETARDANTS ON THE FLAMMABILITY OF WOOD SAWDUST REINFORCED POLYESTER COMPOSITE

I.C Ike-Eze[1,2],V.S Aigbodion[1,2], A.D Omah[1,2], E.O Oji[1]

1.Department of Metallurgical & Materials Engineering, University of Nigeria Nsukka
2. African Centre of Excellence for Sustainable Power & Energy Development
** Corresponding author:* ikechukwu.ezema@unn.edu.ng;

Abstract

The performance of hybrid flame retardants - aluminum hydroxide Al $(OH)_3$ also known and called aluminum trihydrate (ATH) and snail shell powder (SSP) on the flammability of wood sawdust filled polyester composites has been studied. Hand lay-up method was used in producing the formulated composites. The flammability test was carried out using a Cone Calorimeter apparatus according to ASTM E1354 for ATH/SSP content of 5g, 10g 15g and 20g in 30% wood sawdust volume fraction reinforced polyester composite. Sample F containing 20% ATH/SSP gave the optimum performance, in which the total heat released (THR) decreased from 93.8 MJ/m^2 for the pure polyester to 74.3 MJ/m^2. The maximum average heat rate emission (MAHRE) was also reduced from 172.1kW/m^{2}to 158.3 kW/m^2 and the peak heat release rate (pHRR) was also reduced from 4.632kW/m^2 to 4.458kW/m^2. The indication is that a combination of ATH and SSP is effective in retarding the flammability of wood sawdust reinforced polyester composite panels. The total smoke released did not follow a particular order while the total oxygen consumed decreased as the content of the retardant increased. Although, the addition of the flame retardants increased the propensity of the material to ignite at lower times (lower ignition times), other factors analyzed indicated that ATH/SSP hybrid is an effective flame retardant formulation.

Keywords: *Polymer composite, Snail shell, Flame retardants, Flammability tests*

1.0 INTRODUCTION

A composite is a material made with several different constituents intimately bonded together. Composite consists of a discontinuous phase (reinforcement) embedded in a continuous phase (matrix). The structure of a composite is such that the matrix is weaker and needed to be reinforced with fibers or particles for better performance. This has brought about the increase in choice of natural fibre /wood particle reinforced polymer composites in various applications such as automotive components, building materials, and the aerospace industry due to their biodegradability and economic advantages over conventional synthetic fiber composites [1-3]

As organic materials, the polymers and the wood fibers are very sensitive to flame. Improvement on how to reduce the flaming tendencies of these classes of composite materials has become more and more important in order to comply with the safety requirements of the naturalfiber/wood particles composite products, hence research on this area is gaining attention [4-10]

The burning process is comprised of five fundamental steps, which are, heating, decomposition, ignition, combustion and propagation. Flame retardancy can be achieved by the disruption of the burning process at any of these stages that can lead to the termination of the process. The most expeditious method used to acquire flame retardancy is the incorporation of flame-retardants that can interfere with the

combustion during a particular stage of the process so that the resulting system can be quenched or its propagation rate reduced. Hydrated minerals such as aluminum hydroxide, magnesium hydroxide and magnesium carbonate have a high-water content and function as flame retardants by liberating their chemically combined water, thus cooling the polymer and delaying ignition. The decomposition of these hydrated minerals is endothermic reaction such as:

$Al(OH)_3$+ Energy$\rightarrow Al_2O_3 + H_2O$

$Mg(OH)_2$+ Energy$\rightarrow MgO + H_2O$

The release of water starts at temperatures as low as 205°C and 230°C respectively for aluminum hydroxide and magnesium hydroxide. This leads to reduced heat release and smoke evolution[11].

Ali[12] defined fire retardants (FR) "as group of chemicals which are widely used at selected concentrations in many applications, including the manufacture of industrial and domestic products such as electronic equipment, textiles, plastic polymers and car body parts primarily to protect materials against ignition and to prevent fire-related damages". Bruce[13]also stated that "originally fire retardant polyester resins were made with halogenated raw materials such as tetrabro-mophthalic anhydride, tetrachlorophthalic an-hydydide or chlorendic acid or anhydride. These products performed well until toxicity issues became important". In the past decade, various researchers have adopted numerous flame retardants while considering the environmental and health safety implications of these retardants, [14] reported that metallic hydroxides are considered most neutral and effective flame retardants in which magnesium hydroxide [$Mg(OH)_2$] and aluminum hydroxide [$Al(OH)_3$] are the most widely used metal hydroxide flame retardant additives for polymers.

Sain*et-al*[14] studied flame retardant and mechanical properties of natural fiber polypropylene composites containing magnesium hydroxide and reported that about 25wt% of magnesium hydroxide can effectively reduce the flammability of the filled composite to 50%. However, the mechanical properties of the flame retardant filled composites show a marginal decrease compared to the composites without a flame retardant but all the same gave better mechanical properties compared to virgin polypropylene.

Kruger *et-al*[15] studied the flame retarding ability of polyethylene composite reinforced with graphite and intumescent fire retardant additives using cone calorimeter. All the flame retarded compounds significantly decreased the peak heat release rate. The lowest value of 187±1 $kWm^{-2}$was obtained with a compound containing 10wt % expandable graphite and 20wt.% ethylenediamine phosphate.

The main objective of this work is to study the synergetic effects of aluminum hydroxide ($Al(OH)_3$and egg shell powder on the flammability of wood sawdust reinforced polyester composites.

2.0 MATERIALS AND METHODS

2.1 Materials

The polyester resin and its catalyst and accelerator were purchased from Ndidiamaka Chemicals Enugu Nigeria. The powder form of aluminum hydroxide $Al(OH)_3$ whitish in color was supplied by a vendor.The wood sawdust and sieved egg shell powder were used as supplied by ICE-JEB Technical Services Ltd.

2.2 Production of Test Specimen

A control sample of 100% polyester was properly prepared by mixing the resin with a corresponding ratio of the accelerator and the catalyst. It was thoroughly stirred and cast into moulds A. Another sample of 30% sawdust in polyester resin was prepared,

thoroughly stirred and cast into mould B. Different sample each with same composition of 30% saw dust were prepared with 5g, 10g, 15g and 20g of ATH/ESP in 1:1 ratio and moulded into various composites panelslabelled C, D, E and F respectively. The samples were allowed to cure for two days at room temperature and then carefully demoulded and trimmed.

2.3 Flammability Test.

The flammability test was done by a horizontal burning test as per ISO 5660-1 standard using a Cone Calorimeter. This instrument determines the rate of heat released of a material or product exposed to a controlled level of radiation heat. The method also determines the ignition, loss of mass, smoke release rate among others.The specimen (100x100x10) mm was placed on a sample holder fixed onto a weighing cell. A conical heating element provides a constant radiation heat onto the specimen's surface. The radiation heat was set before hand to 35kw/m^2. This radiation approximates to real life fire situations.

The determination of the rate of heat released is based on the fact that the heat liberated during combustion is in proportion with the amount of oxygen used,per Kg of oxygen consumed, an average of 13.1 MJ of energy is released. The smoke and combustion gases of the specimen are aspirated to measure the amount of oxygen. On this basis, it is possible to calculate the amount of heat liberated during the burning of the specimen. It is also possible to measure the amount of smoke produced, as well as the amount of CO and CO_2 in the fumes. Finally, the mass loss and the ignition time are registered. Therefore, the Heat Release Rate (HRR), Total Heat Released (THR), Smoke Release Rate (SRR) and some other parameters were obtained in the course of the test.

Plate 1: The cone calorimeter and burning panel inside the calorimeter.

3.0 RESULTS AND DISCUSSIONS

Table 1 indicates the ratio of the retardant, the reinforcement and the polyester matrix as used in this work. The results obtained from the cone calorimeter are summarized in Table

2 and the detail outcomes are presented in Figures 1 to Figure 5.

Table 1: *Wt% of wood sawdust, ATH/ESPretardant and polyester resin*

Sample code	Volume fraction of sawdust	Volume fraction of Polyester resin	Mass of retardant (g) ATH/SSP	Volume of sawdust (cm^3)	Volume of resin(cm^3)	Volume of composite (cm^3)	Total mass of composite (g)
A	0	100	0	0	55.44	55.44	73.02
B	30	70	0	16.63	38.81	55.44	73.02
C	30	70	5	16.63	38.81	55.44	78.02
D	30	70	10	16.63	38.81	55.44	83.02
E	30	70	15	16.63	38.81	55.44	88.02
F	30	70	20	16.63	38.81	55.44	93.02

Table 2:*Summary of Cone Calorimeter flammability data*

Sample Code	TOI (sec)	TFO (sec)	Mass lost (g/m^2)	FIGRA
A	78	995	5132.3	1.606
B	72	-	4779.0	1.33
C	62	-	5196.1	1.858
D	70	1219	5227.6	1.786
E	60	915	5234.6	2.038
F	58	1490	4679.3	1.739

Table 2 presents some results of the cone calorimeter flammability test indicating the variation of the flame retardant content against the time if ignition (*TOI*), time to flame out (TFO), Carbon dioxide yield (CDY), Carbon monoxide yield (CMY), peak heat release rate pHRR, time to reach the pHRR (T), the fire growth rate (FIGRA) and mean effective heat of combustion (MEHOC) among others. The details of the variation of the important parameters from the test are outlined as follows:

(i) ***Ignition and Flame Out Times***

Table 2 lists the ignition and flame out times for the various samples. The time to ignition (TOI) was 78 seconds for the unreinforced polyester and 72 seconds for the composite containing 30% volume fraction of saw dust. The addition of the flame retardants increased the propensity of the material to ignite at lower times such that the ignition time reduces as the flame retardant content increases. This phenomenon is attributed to the lower thermal stability of the additives relative to the neat polymer and the destabilization of the polymer bond chains by the presence of the additives. Addition of the flame retardants resulted in the initiation of mass loss at lower temperatures. This implies that flammable volatiles could have been released at an earlier stage in the fire tests. The time to flame out (TFO) showed considerable variability. It was 995 seconds for the neat polyester. It was longer for all flame retardant added composite except for sample E which had 915 while that of Sample B and C were not shown by the cone calorimeter.

From Table 1, other important parameters such as carbon dioxide yield (CDY) and

carbon monoxide yield (CMY) are indicators of complete and incomplete combustions respectively. While the CDY did not follow a particular pattern, the CMY increased with increase in the retardant content. This is an indication that the flame was not very successful in its propagation due to the presence of the flame retardants.

(ii) ***Total Heat Release (THR)***

Figure 1 compares the results of the total heat release of samples. It was observed that the total heat released decreases with increase in flame retardant content which is an indication of effective retardancy of the retardant. The increase in the total heat release by sample D being higher than sample C may be as result of more oxygen consumed by it.The most important parameters is the fire load which is the total amount of heat that can be generated by a flammable material if it is ignited. In the cone calorimeter this index is quantified by the total heat released (*THR*). In the Figure1, it is shown that the total heat released was decreased from 93.8 MJ/m^2 for the pure polyester as the content of retardants increased down to 74.3 MJ/m^2 for the sample F containing 20% ATH.

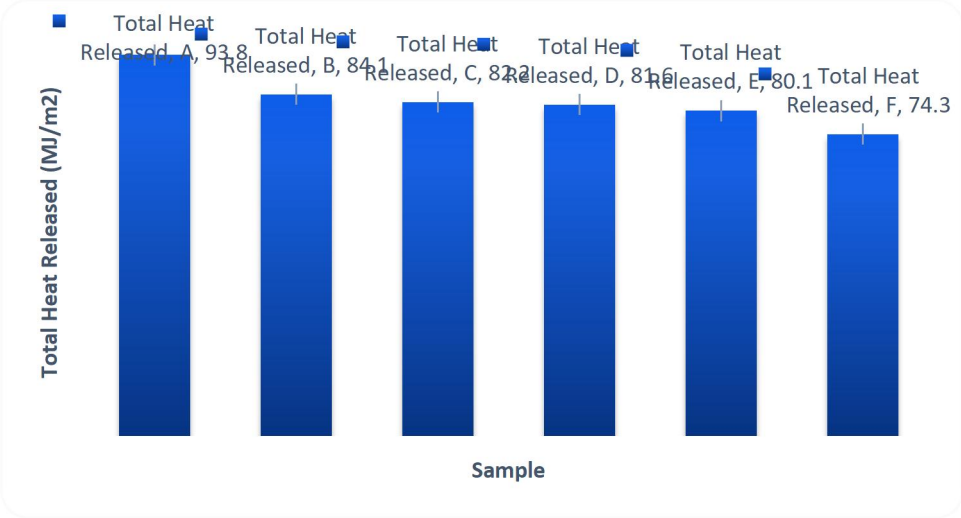

Figure 1:*Effect of ATH/SSP Retardant on Total Heat Release(THR) of wood sawdustpolyester composite*

(iii) Peak Heat Release Rate (PHRR)

Figure 2 denotes the effect of increase of the retardant content on the mean heat release rate. It was observed that the mean heat release rate (pHRR) decreased as the content of the ATH retardant increased. For a material to be effectively flame retarded, this index should assume low values. This is been achieved in this study and it is an indication of formation of heat-insulating protective barriers at the solid surface exposed to the radiant heat. These layers limited heat transfer to the substrate and this slowed down the rate of thermal degradation of the polymer /composites. This, in turn, reduced the rate at which volatile fuel was released which means that less material was consumed within a given time.

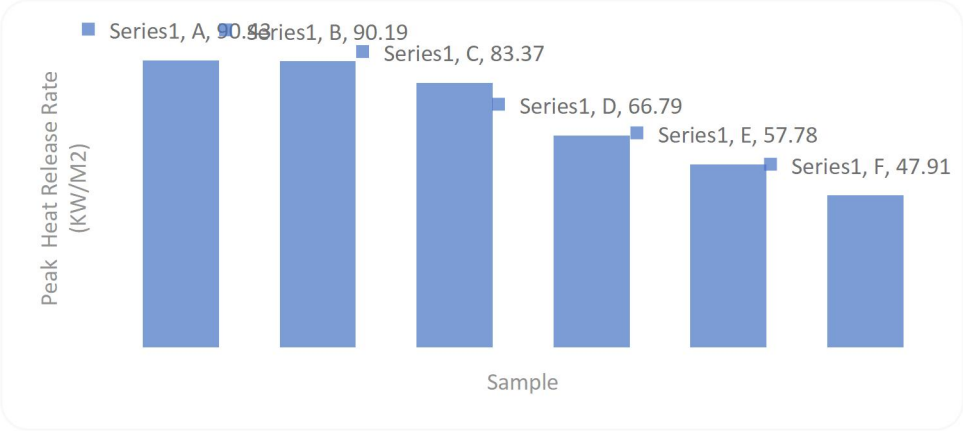

Figure 2:*Effect of ATH/SSP retardant on peak heat release rate (PHRR) of wood sawdust polyester composite*

(iv) *Fire Growth Rate (FIGRA)*

The Fire Growth Rate (*FIGRA*) proposed by Petrella (Petrella (1994), can be used as proxy estimators for the flame spread. The *FIGRA* can usually be determined from the expression.

$$FIGRA = \frac{pHRR}{T} \quad \ldots\ldots\ldots\ldots (1)$$

Where pHRR = peak heat release rate and T = time to reach the pHRR

From Table 1, it was observed that the FIGRA did not follow any definite pattern and hence the fire growth rate is not necessarily a function of flame retardant but many be sensitive to other factors such as oxygen limiting index which was not considered in this report

(v) *Maximum Average Rate of Heat Emission (MARHE).*

The MARHE parameter is defined as the peak value of the cumulative heat emission divided by time. It provides a measure of the propensity for fire development under full scale conditions. From Figure3, it was observed that the maximum average rate of heat emission increase with increase in the flame retardant content until when a higher value of about 20g was added. This is an indication that the lower values (5g-15g) did not contribute effectively in retardancy of the flame. It can be argued that, in attempts to quench flame a certain minimum of the quenching agent must be in place otherwise they will act as further boast to the flame. It was observed that at 20g addition of the ATH, the rate of MARHE was drastically reduced from 172.9 KW/m^2.to 158.3 KW/m^2

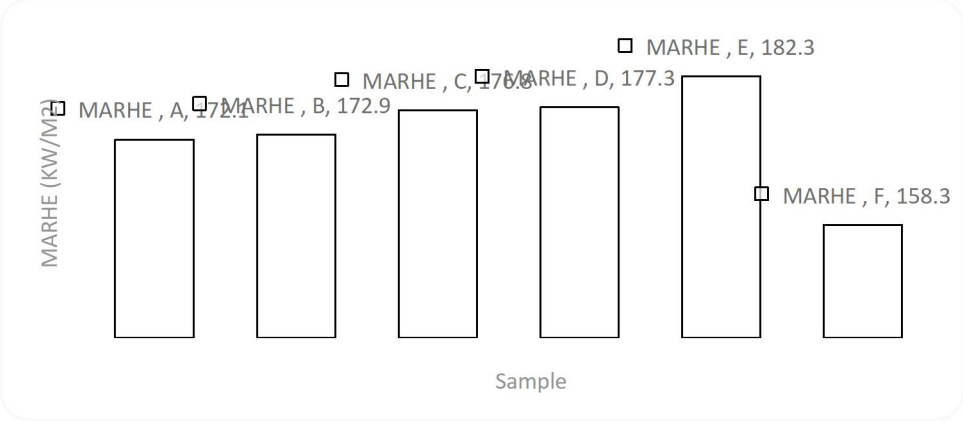

Figure 3:*Effect of ATH/SSP retardant on Maximum Average Rate of Heat Emission (MARHE)of wood sawdust polyester composite*

(vi) ***The Smoke Release***

The smoke release rate is also an important parameter in analyzing the flammability of a material. Figure 4compares the total smoke release (*TSR*) of all the samples during the flaming phase in the cone calorimeter tests apparatus

.

Figure4: *Effect of ATH/SSP retardant on Total Smoke Release (TSR) of wood sawdust polyester composite*

From Figure 4, it can be seen that the total smoke released did not follow a particular order. The addition of the flame retardant increased the total amount of smoke released significantly. This however is an indication of incomplete combustion. This is supported from Table 2 where it can be seen that the carbon monoxide yield (CMY) continues to increase as the retardant content increased. Again, the overall increase may be attributed to the lower molar mass and consequently higher volatility of the intumescent flame retardants. Although the smoke generated by fires reduces visibility and this can significantly affect life safety in underground mining applications, its implication is an indication of difficulty for the materials to burn freely.

(vii) *Total Oxygen Consumed*

Figure 5 presents the result of the total oxygen consumed by each sample during the cone calorimeter test. It was observed that the total oxygen consumed decreases with increase in the flame retardant content. This is an indication that the flame had it difficult to propagate effectively.

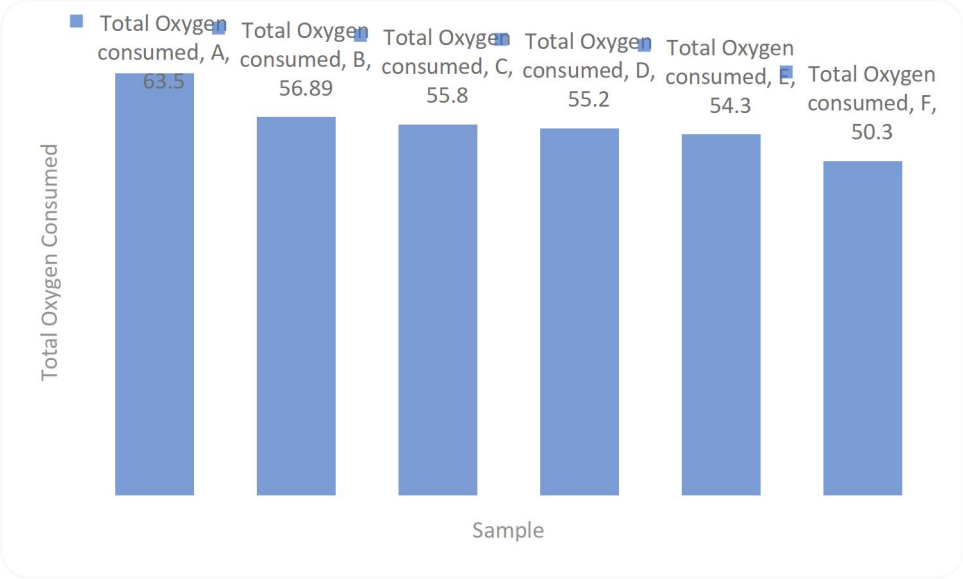

Figure5: *Effect of ATH/SSP retardant on Total Oxygen Consumed (TOC) of wood sawdust polyester composite*

This is a further confirmation that the layers limited heat transfer to the substrate and this slowed down the rate of thermal degradation of the polymer /composites. This, in turn, reduced the rate at which volatile fuel was released which means that less material was consumed within a given time. Less oxygen was been utilized as the flame retardant content increased. This indicates the even though the ignition time reduces with increase in the retardant content the propensity of the flame as it propagates was reduced.

CONCLUSION

The combined effect of aluminum hydroxide and snail shell powder as a flame retardant, on the flammability of saw dust reinforced polyester composite was studied. It was found that the formulated retardanteffectively reduced the flammability of saw dust filled polyester composites, this is because increase in the weight percent of the hybrid retardant led to a decrease in total heat released and other flammability indices studied. It can be argued that, in attempts to quench flame a certain minimum of the quenching agent must be in place otherwise they will act as further boast to the flame. It was observed that at 20g addition of the ATH/SSP, the rate of Maximum Average Rate of Heat Emission– which is a measure of the propensity for fire development under full scale conditions was drastically reduced from 172.9 KW/m^2.to 158.3 KW/m^2. The smoke released was observed not to follow any pattern while the oxygen consumed decreased with increase in volume of the retardants.

Acknowledgment:

The authors would like to appreciate Tertiary Educational Trust fund (TETFund), Nigeria and University of Nigeria Nsukka for sponsoring this research under her IBR intervention 2020 and Conference Intervention 2022.

REFERENCES

.Marwan Mostafa and Nasim Uddin, (2015): Effect of Banana Fibers on the Compressive and Flexural Strength of Compressed Earth Blocks. *Buildings*, *5*, 282-296 doi:10.3390/buildings5010282.

2. Alcides L. Leao1; Roger Rowell; and Nilton Tavares (1998): Applications of Natural Fibers in Automotive Industry In Brazil -

Thermoforming Process. *Science and Technology of Polymers and Advanced Materials.* Edited by P. N. Prasad *et al.,* Plenum Press, New York, **1998**, pg 755-761.

3 Muhammad Yasir Khalid, Ans Al Rashid, Zia Ullah Arif, Waqas Ahmed, Hassan Arshad, Asad Ali Zaidi,(**2021**): Natural fiber reinforced composites: Sustainable materials for emerging applications. Results in Engineering 11 100263

4.Aruna Subasinghe, Raj Das & Debes Bhattacharyya **(2016)**: Study of thermal, flammability and mechanical properties of intumescent flame retardant PP/kenaf nanocomposites, International Journal of Smart and Nano Materials, 7:3, 202-220, http://doi:10.1080/19475411.2016.1239315

5.Ertugrul Altuntas, Nasir Narlioglu and Mehmet Hakki Alma: Investigation of the Fire, Thermal and Mechanical properties of Zinc Borate and Synergic Fire Retardants on Composites Produced with PP-MDF Waste. BioResources 12(4) 6971-6983.

6. Mustafa E. Üreyen and Elif Kaynak (**2019**): Effect of Zinc Borate on Flammability of PET Woven Fabrics. Hindawi, Advances in Polymer Technology, Article ID 7150736, 13 pages. https://doi.org/10.1155/2019/7150736

7. Atika h Isma il, Azman Hassan *, Aznizam Abu Bakar & M. Jawaid,**(2013)**"Flame Retardancy and Mechanical Properties of Kenaf Filled Polypropylene (PP) Containing Ammonium Polyphosphate (APP)". *Sains Malaysiana 42(4) 429–434.*

8. Huang H, M. Tian, L. Liu, W. Liang, and L. Zhang,**(2006)**: Effect of particle size on flame retardancy of Mg(OH)2-filled ethylene vinyl acetate copolymer composites,*Journal of Applied Polymer Science*, vol. 100, pp. 4461-4469.

9.Obidiegwu M. U**, (2012**): Flammability properties of low-density polyethylene/wood fibre composites". *IOSR Journal of Engineering*, Vol. 2(4) pp: 777-780. *Available at* www.iosrjen.org

10. Ali I. Al-Mosawi Ali I. Al-Mosawi, Abbas A. Sakhir, Mushtaq T. Albdiry, and Tareq Majeed, **(2012):**Experimental Investigation in Zinc Borate Effect on Flammability Characteristics of Polymeric Composite Material". *Academic Research International. ISSN-L: 2223-9553, ISSN: 2223-9944 Vol. 3, No. 2.*

11. Green, J., **(2001)**: Flame Retardants and Smoke Suppressants," in Lutz, J. T., and Grossman, R. F., eds., *Polymer Modifiers and Additives,* Marcel Dekker.

12. Ali I. Al-Mosawi **(2011)**: Hybrid fire retardants to increasing combusting resistance for fibers-reinforced composites. National Journal of Chemistry, Vol. 41 pp48-54

13.Bruce Curry, (**2003**):Fire Retardant Polyester Resin Formulations. http://:www.AOC.RESINS.com>tech-fr-formular; PDF download 08/06/2016

14. Sain e*t al,* M. Sain, S.H. Park, F. Suhara, S. Law **(2004):** Flame retardant and mechanical properties of nature fiber-PP composites containing magnesium hydroxide". *Polymer Degradation and Stability* 83 pp 363–367

15Kruger Herman , Walter W. Focke, Washington Mhike, Albertus Taute, Albert Roberson and Osei Ofosu. **(2014):** Cone calorimeter study of polyethylene flame retarded with expandable graphite and intumescent fire retardant additives. *Journal of Fire Sciences*Vol. 32(6) 498–517 http://jfs.sagepub.com/content/32/6/498

NMS-TP008

INVESTIGATION OF CORROSION INHIBITION ON ALUMINUM USING *JATROPHA CURCAS* LEAF EXTRACT

Gerald Ezema[1] and Macdenis Egbuhuzor[1]*

1. **Department of Materials & Metallurgical Engineering, University of Nigeria, Nsukka**

*** Onyekachi.egbuhuzor@unn.edu.ng; 08066348763**

ABSTRACT

The inhibitive effect of *Jatropha curcas* leaves extract on aluminium corrosion in 2M H_2SO_4 solution was investigated using potentiodynamic polarization and weight loss methods to monitor the corrosion rate. The obtained leaves were air-dried and crushed into smaller particles before the extract was gotten by the Soxhlet solvent extraction method. The extract concentration used was 0.5g/L, 1.0g/L, 1.5g/L, and 2.0g/L for potentiodynamic polarization and weight loss methods in 2M H_2SO_4 solutions, respectively. The inhibition efficiency of 71.2% was obtained from 2.0g/L extract in an H_2SO_4 solution. The overall results obtained from both potentiodynamic polarization and weight loss methods indicated that *Jatropha Curcas* leaves extract can slow down the corrosion rate of aluminium in an acidic environment.

KEYWORDS: ALUMINIUM, CORROSION RATE, INHIBITION EFFICIENCY, JATROPHA, LEAF EXTRACTS

1.0 Introduction

Corrosion is a natural phenomenon which degrades the properties of metal and alloys through electrochemical means and consequently makes them unfit for the specific role. Several techniques have been applied[1] to reduce the corrosion of metals,which include use of inhibitors, barrier coatings, anodic and cathodic protection, alloying, electroplating etc. The inhibitors are used during the acid pickling procedure and this has proven to be a more practical method for metal protection against corrosion in acidic media. Organic inhibitors are preferred and used now because most of the effective and efficient organic inhibitors are compounds containing hetero-atoms such as oxygen, nitrogen, sulphur, and phosphorus which are easily adsorbed on the metal surface to give effective protection to the metals. One of the major functions of an inhibitor is to displace water from the metal surface it is applied to, interact with anodic or cathodic reaction sites of the metal sample to retard the oxidation and reduction of corrosion reaction, and prevent the transportation of water and corrosion active species on the surface[1][2].

Aluminium forms a passive protective layer on its surface as its corrosion product and this makes it to be less corrosive. This passivation is worsened in an aqueous acidic environment. There have been extensive investigations and reports on the acidic corrosion of aluminium and its alloys and its inhibition[3][4][5]. Industrial effluents and other activities such as pickling, anodizing and metal cleanings cause corrosion in aluminium and its alloys used in different applications[6]. Plant extracts have proved to be more eco-friendly, cheap, non-toxic readily available and biodegradable corrosion inhibitors. This has changed the research focus from some of the harmful inorganic inhibitors to this cheap, biodegradable and readily available organic inhibitors from plant extracts [7][8][9][10][11].

These plant extracts contain heteroatoms such as Sulpher (S), Oxygen (O), Nitrogen (N), and Phosphorus (P) in their phytochemical composition and these atoms

are the major inhibitive properties of these extracts[6][10][12][13].

This research work investigated the corrosion inhibition of Jatropha leaves extracts on aluminium in a sulphuric acid medium.

2.0MATERIALS AND METHODS

2.1 Materials and equipment

Materials used include Jatropha leaves sourced within Ajuona Obukpa near the University of Nigeria Nsukka. The leaves were taken to the herbarium of the Department of Botany for identification, deposition and numbering. Other materials used include analytical grades of 2M solutions of H_2SO_4, Methanol, distilled water, acetone, ethanol, hardener, masking tape, and emery paper. Also used for this experiment include 2024 type aluminium cable obtained from Cutix PLC Nnewi in Anambra state, beakers, conical flask, water bath, soxhlet extractor, Rotary evaporator, Tafel machine, Electronic Scale or weighing balance, desiccator etc.

2.2. Material Preparation

2.2. 1. Metal Specimen Preparation

The aluminium cable of the 2024 type was obtained from Cutix PLC and the elemental composition of the aluminium was confirmed using the elemental analyzer and the composition was recorded in table 1.0. The cable was mechanically press-cut into coupons. To remove oils and impurities from the surface of the coupon, they were washed in ethanol and polished with fine abrasive, then rewashed, rinsed in acetone to dry and stored in a desiccator before use[14].

Table 1.0 Elemental composition of Aluminium

Si%	Fe%	Cu%	Mg%	Mn%	Zn%	Cr%	Ti%	V%	B%	Ga%	Al
0.100	0.400	0.050	0.030	0.010	0.050	0.010	0.020	0.020	0.050	0.030	99.23

2.2.2 Jatropha leave Extract Preparation.

Jatropha leaves were sourced within Ajuona Obukpa near the University of Nigeria Nsukka. The leaves were taken to the herbarium of the Department of Botany for identification, deposition and numbering. The obtained jatropha leaves were air dried by exposure to the atmosphere. After drying, the leaves were crushed to powder and placed Soxhlet apparatus ready for extraction. The required extraction solvent (methanol) is heated using a heating mantle to a reflux. The heated methanol evaporates, travels up a distillation arm, passes through a condenser, and the cools. The cooled solvent vapour s drips down into the chamber with the solid material. The dissolution of some of the compounds in the dry powdered leaves will occur as the warm solvent drips down it and this forms a combination of extract and the solvent. The cycle is repeated until the desired quantity is obtained.. After many such cycles, the desired extract was concentrated in the distillation flask[15]. After extraction methanol was removed with a Rotary evaporator, yielding the extracted compound. The extract is then put in a sealed container, and stored in a refrigerator before use. Phyto-chemical analysis was conducted on the extract using FT-IR and GC-MS to determine the composition of the extracts and the active ingredients

Phyto-constituents	Extract
Saponins	++
Flavonoids	+++
Tannins	+++
Alkaloids	+++
Glycosides	-
Terpenoids	++

Steroids	-

Footnote: +++ = high in abundance; ++ = moderate in abundance; - = absent

2.3 Experimental Setup

The aluminium cable with a diameter of 3cm and a length (height) of 3cm was measured and cut into the required numbers of the specimen. Table 2.0 below shows the initial weights and areas of various specimens

Table 2.0 Initial weights and areas of various coupons

Specimen notation	Initial weight (g)	Total surface area (mm^2) Using, $A= 2\pi r^2+2\pi rh$
A	1.48	42.411
B	1.48	42.411
C	1.48	42.411
D	1.48	42.411
E	1.48	42.411

2.4 WEIGHT LOSS MEASUREMENT

The specimens were weighed before and after immersion in 2M of H_2SO_4 every 72 hours for 15 days in the absence and presence of various concentrations of jatropha curcas extract. Weight loss is measured as the difference between the weight (W_i) of the coupon before immersion and W_f final weight of the coupon after immersion at a specified time interval as shown in equation 1.

Weight loss (W) = $W_i - W_f$ 1

Where W = weight loss, W_i =initial weight and W_f = final weight of the individual specimen.

$$Corrosion\ Rate \quad (R) = \left(\frac{87600\Delta W}{\rho At}\right) \quad 2$$

Where, ΔW = weight loss in gram, ρ = density of the metal sample (g/cm^3), A = surface area of exposed metal sample (cm^2) and t = time of exposure (in hrs).

2.6 Inhibition Efficiency (% IE): This is a parameter used to measure the effectiveness or performance of a corrosion inhibitor in percentage as expressed in equation 3.0. It is regarded as the measure by which the corrosion rate is regulated in the inhibited solution compared to the corrosion rate in the blank solution[16].

$$\%IE = (R_b - R_i)/\ R_b\ x\ 100 \quad 3$$

Where, Rb = corrosion rates of the blank solution, Ri = corrosion rates of inhibited solution.

2.5 MEASUREMENT OF CORROSION RATE

Corrosion Rate (R): Corrosion rate gives information on the depth of penetration of the corrodent into the metal surface and the extent of damage of the metal surface with time. It is expressed in millimetre per year (mm/yr) or milligrams/square mm per year. This is expressed mathematically as in equation(2)

2.7 Potentiodynamic polarization (PDP) Standard electrochemical experiments were carried out in a three-electrode type

cells-working electrode, reference electrode and counter electrode with different compartments for the reference electrode (Ag/AgCl)[17]. The counter electrode was made of a platinum plate and working electrode (aluminium cable) at a known surface area which was embedded in a tube of polytetrafluoroethylene, fixed by masking tape to hold them together. Before electrochemical measurements, the prepared specimen electrode was immersed in the test solution at open circuit potential (OCP) until it reached a steady state.

The electrochemical measurements were performed on the aluminium specimen for the control and various concentrations of inhibitor using an electrochemical analyzer. The potentiodynamic polarization study was carried out at a constant scan rate of 0.01V/s at -1.5 to 1.5V intervals with respect to

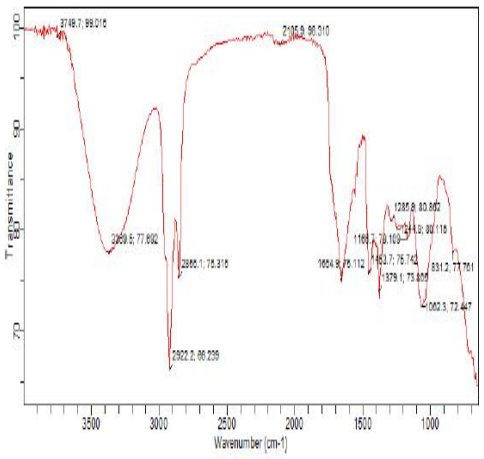

Fig.1 for jatropha extract, the infrared absorption bands identify the various functional groups of the molecule.

4.2 GC-MS ANALYSIS.

The GC-MS results showed the presence of the following major compounds; Oleic acids, octadecadienol,Di-tert-butylphenol, Octadecadienoic acids, dihydroxypropylester, Octadecadienoic acid, dimethyl tetradecahydro phenanthrene, Hexa

corrosion potential (Ecorr). Corrosion current density (Icorr) values were calculated using Tafel extrapolation method and by taking an extrapolation interval of 0.1V around Ecorr value once stable. The inhibition efficiency (IE%) was calculated [18]by

$$IE\% = \frac{icorr - i'corr}{icorr} x\,100 \quad --\ 4$$

Where i_{corr} and i'_{corr} are the corrosion current densities of aluminium in the absence and presence of the inhibitor respectively[19].

3.0 RESULTS AND DISCUSSION

3.1 The Fourier Transform Infrared and Gas Chromatography-Mass Spectroscopy (FTIR-GCMS) Analysis.

The FTIR and GC-MS analysis were undertaken to detect the functional groups/organic compounds present in the jatropha curcas leaves extracts.

and Octadecenal, Cetene, Cycloeicosane, Linoelaidic acids, Hexadecanoic acid methyl esters, Dibutyl phthalate, cis-Vaccenic acids, and other compounds that supply the heteroatoms. These organic compounds contain heteroatoms which attach themselves to the metal atoms and are responsible for the corrosion inhibition of these plant extracts inhibition are responsible for the

4.3 Potentiodynamic Polarization Plots For Tafel and OCPT

Diffenrent concentrations of the plant extract was used to study the polarization behavior of aluminium coupon in 2M solution of sulfuric acid (H_2SO_4) after 24h immersion. Figures 7-11 shows the polarization behaviou of the aluminium coupon using a control specimen and different concentrations of the extracts immerses in the acidic medium for 24h. On addition of the extract, it is observed that there is significant decrease in the current as shown in the cathodic curve. This is because the

phytochemical constituents in the extract blocked the external surfaces of the coupon from the corrosive effects of the acidic medium. The suppression of corrosion of the exposed aluminium coupon with elongation of time of immersion shows that sufficient time should be allowed for better adsorption of the inhibitor molecules on the metal specimen[20][21].

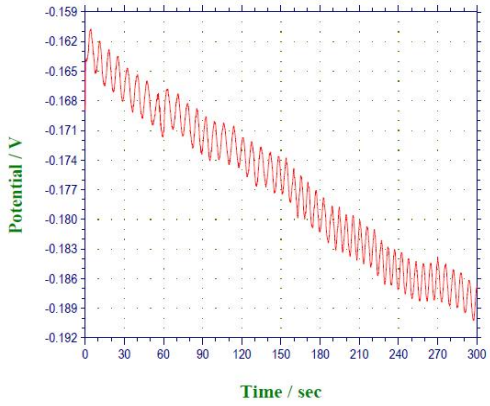

Fig.2 Open circuit potential graph of control specimen

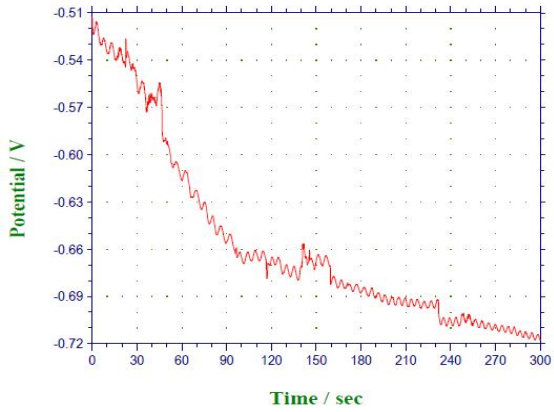

Fig. 3 Open circuit potential graph of 0.5mL concentration of extract

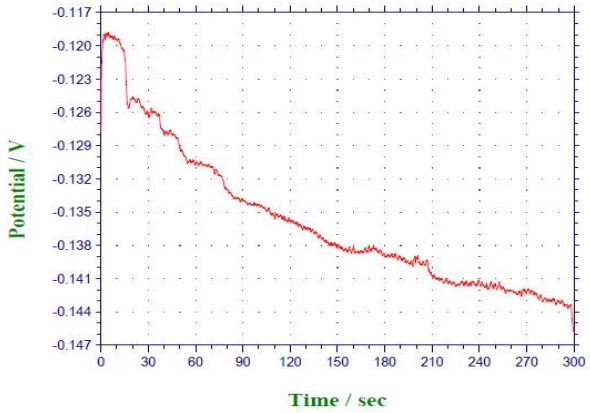

Fig .4 Open circuit potential graph of 1.0mL concentration of extract

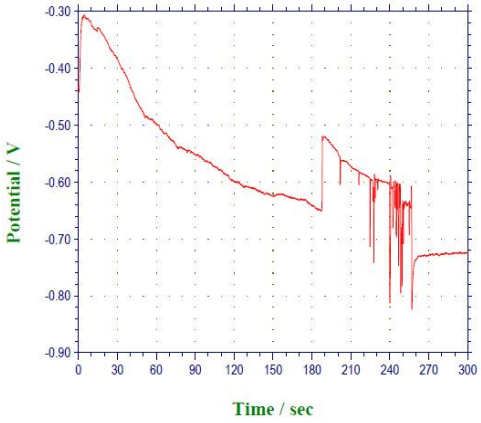

Fig 5 Open circuit potential graph of 1.5mL concentration of extract

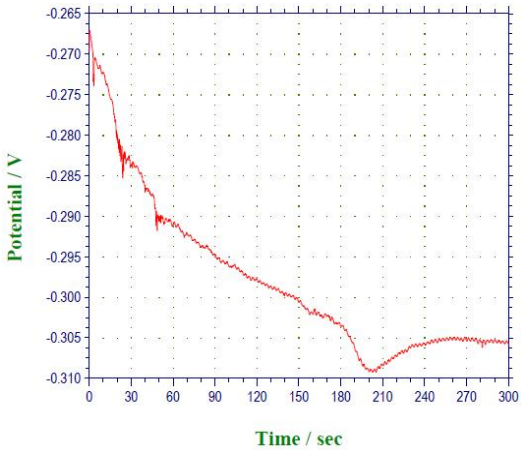

Fig. 6 Open circuit potential graph of 2.0mL concentration of extract

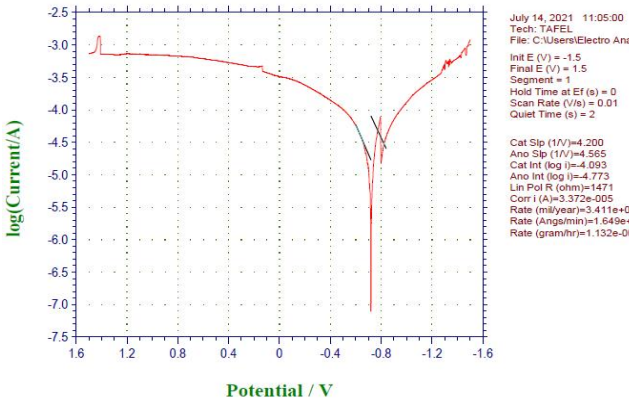

Fig. 7 Tafel graph of control specimen

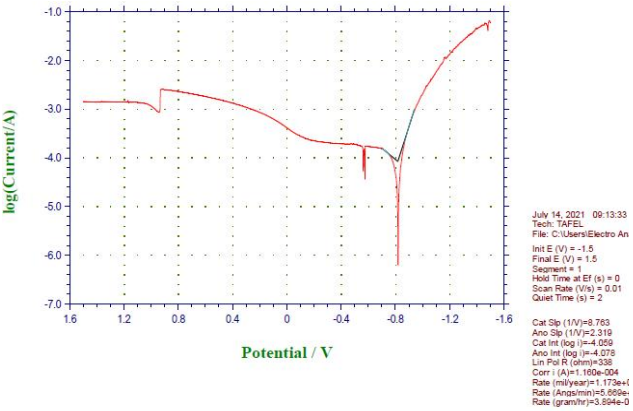

Fig. 8 Tafel graph of 0.5mL concentrate of extract

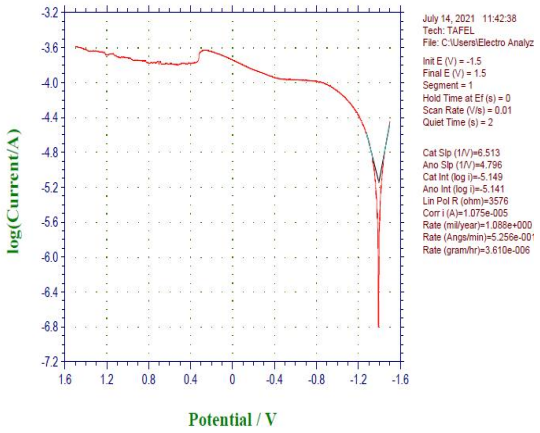

Fig. 9 Tafel graph of 1.0mL concentration of extract

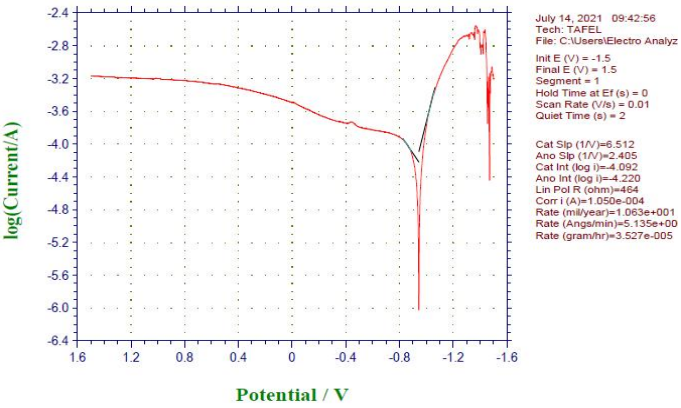

Fig. 10 Tafel graph of 1.5mL concentration of extract

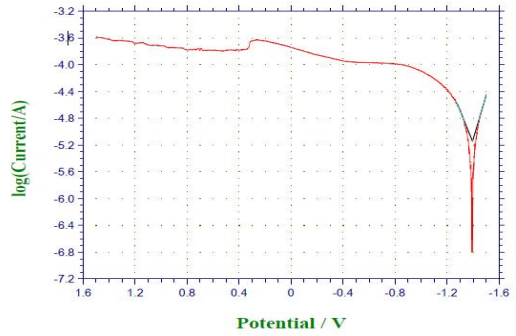

Fig. 11 Tafel graph of 2.0mL concentration of extract

Table.3: Summary of Tafel's result

Sample code	1	2	3	4
composition	Control	0.5mL	1.0mL	1.5mL
Linear polarization (ohms)	1471	338	3586	464
Anodic slope (1/V)	4.565	2.319	4.796	2.405
Cathodic slope (1/V)	4.200	8.763	6.513	6.512
Corrosion rate (mil/yr)	3.411	1.173	1.088	1.063
Corrosion current (A)	3.372	1.160	1.075	1.050
Scan rate (V/s)	0.01	0.01	0.01	0.01

From table 4, we can see that the corrosion rate reduces with an increase in inhibitor concentration. The table shows so many parameters used and obtained during the potentiodynamic experiment

4.4 Weight Loss Studies

Table 4 Weight loss and inhibition efficiency values for aluminium in 2M H_2SO_4 at room temperature, with and without jatropha extract after 24hours.

Conc. (mL)	Initial weight (g)	Final weight (g)	Weight loss (g)	Cor. Rate (mm/yr)	IE%
Blank	1.48	1.37	0.11	3.54	0
0.5	1.48	1.44	0.04	1.18	66.7
1.0	1.48	1.45	0.03	1.08	69.4
1.5	1.48	1.45	0.03	1.05	70.3
2.0	1.48	1.45	0.03	1.02	71.2

Table. 6 Weight loss and inhibition efficiency for values for aluminium in 2M H_2SO_4 at room temperature, with and without jatropha extract after 48hours.

Conc. (mL)	Initial weight (g)	Final weight (g)	Weight loss (g)	Cor. Rate (mm/yr)	I.E%
Blank	1.48	1.26	0.22	3.54	
0.5	1.48	1.41	0.07	1.16	67.1
1.0	1.48	1.41	0.07	1.08	69.4
1.5	1.48	1.41	0.07	1.07	70.0
2.0	1.48	1.42	0.07	1.04	70.7

Table 7: Weight loss and inhibition efficiency for values for aluminium in 2M H_2SO_4 at room temperature, with and without jatropha extract after 72hours.

Conc. (mL)	Initial weight (g)	Final weight (g)	Weight loss (g)	Cor. Rate (mm/yr)	I.E%

Blank	1.48	1.15	0.33	3.53	
0.5	1.48	1.37	0.11	1.18	66.6
1.0	1.48	1.37	0.10	1.08	69.4
1.5	1.48	1.38	0.10	1.05	70.2
2.0	1.48	1.38	0.10	1.02	71.1

Table 8: Weight loss and inhibition efficiency for values for aluminium in 2M H_2SO_4 at room temperature, with and without jatropha extract after 96 hours.

Conc. (mL)	Initial weight (g)	Final weight (g)	Weight loss (g)	Cor. Rate (mm/yr)	I.E%
Blank	1.48	1.04	0.44	3.538	
0.5	1.48	1.33	0.16	1.16	66.4
1.0	1.48	1.34	0.14	1.08	69.4
1.5	1.48	1.35	0.13	1.06	70.0
2.0	1.48	1.35	0.13	1.023	70.9

Table 9: Weight loss and inhibition efficiency for values for aluminium in 2M H_2SO_4 at room temperature, with and without jatropha extract after 120hours.

Conc. (mL)	Initial weight (g)	Final weight (g)	Weight loss (g)	Cor. Rate (mm/yr)	I.E%
Blank	1.48	0.92	0.56	3.55	
0.5	1.48	1.30	0.18	1.17	66.7
1.0	1.48	1.31	0.17	1.08	69.4
1.5	1.48	1.31	0.17	1.06	70.2
2.0	1.48	1.32	0.16	1.02	71.2

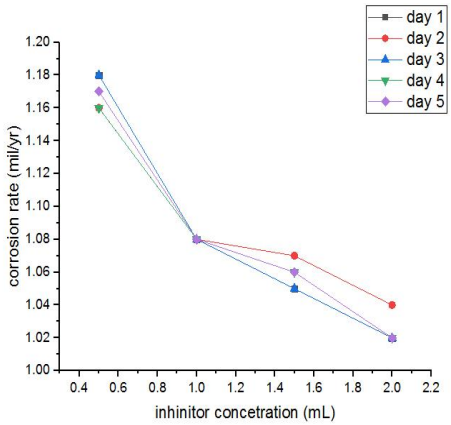

Fig. 17 Variation of inhibitor concentration against corrosion rate

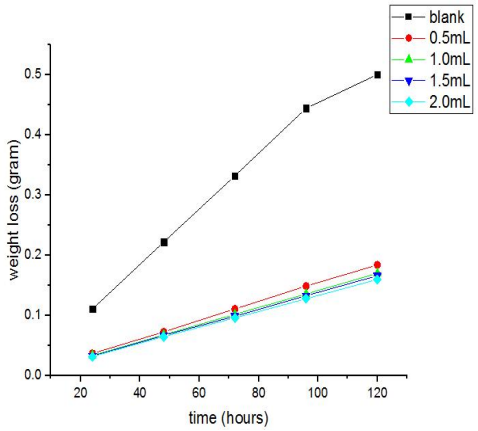

Fig. 18 Variation in time against weight loss

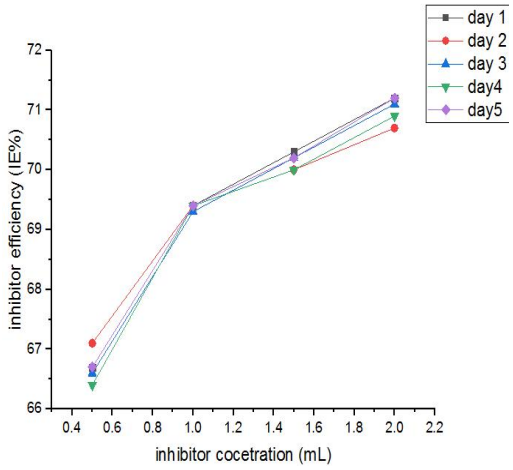

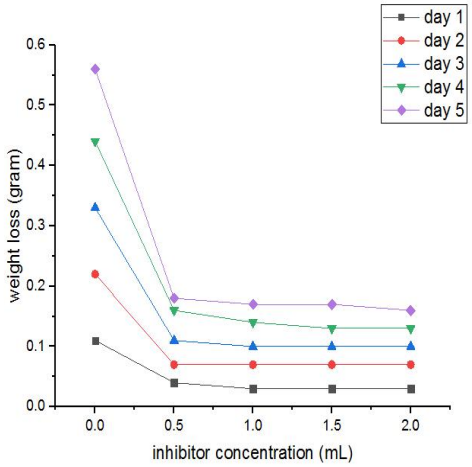

Fig. 20 Variation of inhibitor concentration against inhibitor efficiency

Fig. 21 Variation in inhibitor concentration against weight loss

From fig.17, 19 and 21, it can be deduced that an increase in inhibitor concentration reduces both the corrosion rate and weight loss of aluminium cable in H_2SO_4 SO solutions with varying concentrations of jatropha curcas leaves extract[22]. Fig. 18, illustrates that the magnitude of weight loss of aluminium cable is time-dependent. An increase in immersion time increases the weight loss of aluminium. And also fig. 20, proves that the increase in inhibitor efficiency was a result of the increase in the concentration of the jatropha leave extract[23].

CONCLUSION

The results gotten from both potentiodynamic polarization and weight loss methods have proven that Jatropha curcas extracts is an excellent eco-friendly corrosion inhibitor of mild steel (MS) in 2M H_2SO_4. In both methods of the study, the addition of more of the leave extracts that is increase in the concentration of the extracts, decreased its corrosion rate and weight loss and increased the inhibition efficiency because of the adsorption of the more phytochemicals on the surface of the coupon.

ACKNOLWDGEMENT

The authors would like to thank TEDFUND for their sponsorship of this paper presentation at the 37th Annual general Meeting and Conference of Nigerian Metallurgical Society at University of Abuja between 26th -29th October 2022.

References

[1]S. I. Durowaye, G. I. Lawal, I. A. Raheem, and V. O. Durowaye, "Corrosion Response of Cast Aluminium Alloy for Extension Clamp Fabrication," *Am. J. Mater. Sci.*, vol. 4, no. 4, pp. 159–164, 2014.

[2] I. B. Obot, S. A. Umoren, and N. O. Obi-egbedi, "Corrosion inhibition and adsorption behaviour for aluminuim by extract of Aningeria robusta in HCl solution : Synergistic effect of iodide ions," *J. Mater. Environ. Sci*, vol. 2, no. 1, pp. 60–71, 2011.

[3] A. Ennouri, A. Lamiri, and M. Essahli, "Corrosion inhibition of aluminium in acidic media by different extracts of Trigonellafoenum-graecum L seeds," *Port. Electrochim. Acta*, vol. 35, no. 5, pp. 279–295, 2017.

[4] R. M. Hassan and I. A. Zaafarany, "Kinetics of corrosion inhibition of aluminum in acidic media by water-

soluble natural polymeric pectates as anionic polyelectrolyte inhibitors," *Materials (Basel).*, vol. 6, no. 6, pp. 2436–2451, 2013.

[5] P. M. Ejikeme, S. G. Umana, and O. D. Onukwuli, "Corrosion inhibition of aluminium by Treculia Africana leaves extract in acid medium," *Port. Electrochim. Acta*, vol. 30, no. 5, pp. 317–328, 2013.

[6] B. Kasuga, E. Park, and R. L. Machunda, "Inhibition of Aluminium Corrosion Using <i>Carica papaya</i> Leaves Extract in Sulphuric Acid," *J. Miner. Mater. Charact. Eng.*, vol. 06, no. 01, pp. 1–14, 2018.

[7] E. I. Ating, S. A. Umoren, I. I. Udousoro, E. E. Ebenso, and A. P. Udoh, "Leaves extract of ananas sativum as green corrosion inhibitor for aluminium in hydrochloric acid solutions," *Green Chem. Lett. Rev.*, vol. 3, no. 2, pp. 61–68, 2010.

[8] L. A. Nnanna, I. U. Anozie, A. G. I. Avoaja, C. S. Akoma, and E. P. Eti, "Comparative study of corrosion inhibition of aluminium alloy of type AA3003 in acidic and alkaline media by Euphorbia hirta extract," *African J. Pure Appl. Chem.*, vol. 5, no. 8, pp. 265–271, 2011.

[9] I. Alinnor and P. M. Ejikeme, "Corrosion Inhibition of Aluminium in Acidic Medium by Different Extracts of Ocimum gratissimum," *Am. Chem. Sci. J.*, vol. 2, no. 4, pp. 122–135, 2012.

[10] E. E. El-Katori and S. Al-Mhyawi, "Assessment of the Bassia muricata extract as a green corrosion inhibitor for aluminum in acidic solution," *Green Chem. Lett. Rev.*, vol. 12, no. 1, pp. 31–48, 2019.

[11] M. Prabakaran, S. H. Kim, A. Sasireka, K. Kalaiselvi, and I. M. Chung, "Polygonatum odaratum extract as an eco-friendly inhibitor for aluminum corrosion in acidic medium," *J. Adhes. Sci. Technol.*, vol. 32, no. 18, pp. 2054–2069, 2018.

[12] P. Kumari and L. M, "PLANT EXTRACTS AS CORROSION INHIBITORS FOR ALUMINUM ALLOY IN NaCL ENVIRONMENT - RECENT REVIEW," *J. Chil. Chem. Soc.*, vol. 67, no. 2, pp. 5490–5495, 2022.

[13] N. Nnaji, N. Nwaji, J. Mack, and T. Nyokong, "Corrosion resistance of aluminum against acid activation: Impact of benzothiazole-substituted gallium phthalocyanine," *Molecules*, vol. 24, no. 1, pp. 1–22, 2019.

[14] O. M. Egbuhuzor, I. C. Madufor, S. C. Nwanonenyi, and J. O. Bokolo, "ADSORPTION BEHAVIOR AND CORROSION RATE MODEL OF SODIUM CARBOXYMETHYL CELLULOSE (NA-CMC) POLYMER ON ALUMINIUM IN HCL SOLUTION," *Niger. J. Technol. Vol.*, vol. 39, no. 2, pp. 369–378, 2020.

[15] P. K. Halder, M. U. H. Joardder, M. R. A. Beg, N. Paul, and I. Ullah, "Utilization of Bio-Oil for cooking and lighting," *Adv. Mech. Eng.*, vol. 2012, no. 190518, pp. 1–5, 2012.

[16] T. Ramde, S. Rossi, and C. Zanella, "Inhibition of the Cu65/Zn35 brass corrosion by natural extract of Camellia sinensis," *Appl. Surf. Sci.*, vol. 307, pp. 209–216, Jul. 2014.

[17] H. Gerengi, I. Uygur, M. Solomon, M. Yildiz, and H. Goksu, "Evaluation of the inhibitive effect of Diospyros kaki (Persimmon) leaves extract on St37 steel corrosion in acid medium," *Sustain. Chem. Pharm.*, vol. 4, pp.

57–66, Dec. 2016.

[18] S. Javadian, A. Yousefi, and J. Neshati, "Synergistic effect of mixed cationic and anionic surfactants on the corrosion inhibitor behavior of mild steel in 3.5% NaCl," *Appl. Surf. Sci.*, vol. 285, pp. 674–681, Nov. 2013.

[19] L. Tang *et al.*, "The synergistic inhibition between hexadecyl trimethyl ammonium bromide (HTAB) and NaBr for the corrosion of cold rolled steel in 0.5 M sulfuric acid," *J. Mater. Sci.*, vol. 41, no. 10, pp. 3063–3069, May 2006.

[20] V. Saraswathy and H.-W. Song, "Electrochemical studies on the corrosion performance of steel embedded in activated fly ash blended concrete," *Electrochim. Acta*, vol. 51, no. 22, pp. 4601–4611, Jun. 2006.

[21] L. R. Chauhan and G. Gunasekaran, "Corrosion inhibition of mild steel by plant extract in dilute HCl medium," *Corros. Sci.*, vol. 49, no. 3, pp. 1143–1161, Mar. 2007.

[22] B. M. Prasanna, B. M. Praveen, N. Hebbar, M. K. Pavithra, T. S. Manjunatha, and R. S. Malladi, "Theoretical and experimental approach of inhibition effect by sulfamethoxazole on mild steel corrosion in 1-M HCl," *Surf. Interface Anal.*, vol. 50, no. 8, pp. 779–789, Aug. 2018.

[23] D. K. Gupta *et al.*, "Study of Jatropha Curcas Extract as a Corrosion Inhibitor in Acidic Medium on Mild Steel by Weight Loss and Potentiodynamic Methods," *J. Nepal Chem. Soc.*, vol. 41, no. 1, pp. 87–93, 2020.

NMS-TP09

Thermo-Physical Properties and Compressive Strength of Polypropylene(PP)/Sugarcane Bagasse Ash Particulate (SBAP)Compositesfor Dental Implant application

I.A. Hayatudeen**2R.M. Dodo*1, K.A. Bello[1], U. Abdullahi[3], Y. Abdullahi[1]
[1]Department of Metallurgical and Materials Engineering, Ahmadu Bello University, Zaria, Nigeria
[2]Department of Mechanical Engineering, Kaduna Polytechnic, Kaduna State, Nigeria
[3]Center for Energy Research and Training (Nigeria Atomic Energy Commission), Ahmadu Bello University, Zaria – Nigeria,
Corresponding authors' emails: rdmamuda@abu.edu.ng*,babesalaahaa@yahoo.com**

Abstract

The study report thermo-physical properties and compressive strength of polypropylene (PP)/sugarcane bagasse ash particulate (SBAP) composites for dental implant application. PP/SBAP composites were produced by melt mixing using a two-roll mill and compression molding techniques. The influence of the SBAP content on composites were studied. Five composites' samples of dimension 120x120x3 mm were fabricated by adding 10 – 50 wt% of SBAP. In the event of the SBAP loading, 10 wt% regular interval was maintained. The thermo-physical properties of the composites were experimentally determined. Compression test and the microstructural examination on the composites were carried out to know the compressive strength and the morphology of the composites respectively. There was no appreciable water absorption of the composite and the density of the composites were significantly low. However, the increase in SBAP was found to increase the thermal conductivity, specific heat capacity and compressive strength of the composites. Further, the SEM images of the composites shows that both the PP and SBAP were unevenly distributed. Thus, based on the results obtained 50 wt% PP/SBAP is hereby recommended to be used as dental implant material.

Keywords:thermo-physical properties, compressive strength, SEM images, polypropylene, sugarcane bagasse ash particulates, dental implant

Introduction

It's no doubt that virtually every segment of our everyday lives' activities namely transportation, housing, clothing, communication, recreation, dentistry and food production is influenced by materials(Onuoha et al., 2017).In dentistry, appropriate materials are utilized in the design and fabrication of dental implant. Laterally, dentalim plant is a surgical part that interfaces with the bone of the jaw or skull to support a dental prosthesis such as a crown, bridge, denture, facial prosthesis or to act as an orthodontic anchor(Wedad et al., 2018).Again, in the past decadesthe implant has been the first choice by patients for replacing their missed teeth because of their many advantages(Wedad et al., 2018).Bronze teeth, amalgam, titanium teeth and so on reflect the properties of natural teeth to a certain degree. Like tough alloy, the properties of natural teeth vary from the outside to inside. These attributes give human teeth effective mastication ability (He and Swain, 2007). The splendid properties of natural teeth enable them to

carry out the functions of incision, laceration and grinding of food during mastication (Kishen et al., 2000). Development of materials for dental implant have received international attention. However, a material that can completely substitute human teeth with regard to biocompatibility and properties has not yet been obtained(Ya-Rong et al., 2014). Further, human teeth have a more complicated structure, better properties and better biocompatibility than all oral restorative materials, including synthetic resin materials, ceramic and dental alloys(Ya-Rong et al., 2014).Determination of the various physical properties of newly developed material intended for dental implant applications is quite essential. Aunique implant material must have properties similar to human tooth. In the fabrication of endosseous implants, materials are divided based on their chemical composition and biological responses. The design principles of the implant should be compatible with physical properties of the oral implant material(Velmurugan, 2017).The materials commonly in used are metals, ceramics orpolymers. Among metals, titanium is the promising material for intraosseous applications because it has typical properties close to that of the human teeth. Again, it has ability to repair itself if damaged. However, titanium has limitation in that it's unaesthetic in the frontal area. Ceramic implants are being developed to overcome the said disadvantage of titanium(Kohal and Klaus, 2004). Zirconiais the most commonly found ceramic for dental implant fabrication. Compared with titanium implants, zirconia displays least particle discharge and they are thought to be dormant in the body(Velmurugan, 2017). Notwithstanding, the lower toughness of zirconia most likely affect the required performance during mastication. On the other hand, a variety of polymers have been utilized as dental implant materials namely polymethylmethacrylate, polytetrafluoroethylene, polyethylene and polypropylene (Glantz, 1998).This is because they are thermally insulating and tend to be more translucent. However, the inferior mechanical properties are eliminated by reinforcing the polymer with ceramic. Accordingly, an attempt has been made in the present study to evaluate thermo-physical properties and compressive strength of the newly developed polypropylene composites for dental implant application.

Materials & Methods

2.0 Materials & Methods

2.1 Production of PP/SBAP composites

The methods used in the preparation of SBAP and compression molding techniquesfor the composites' samples production are similar to that used by Dodo et al, (2021).

2.2 Thermal Conductivity

Samples of dimension 20x20x3 mm were prepared from each sample (ASTM CI77). The test is carried out by guarded plate method by placing a sample between two plates heated to different temperatures that's T_h and T_C. when a steady state is reached, the temperature at the end of the sample is equal and this is detected by temperature sensors in contact with the sample. The thermal conductivity is calculated from the given relation;

$$K=\frac{\rho \times L}{A(T_h-T_c)}$$

2.3 Specific heat capacity

Samples with dimensions 20x20x3 mm were prepared from each composition. The test was conducted using method of mixtures. A copper calorimeter of specific heat capacity S_c (0.093cal/g.℃) and a measured mass Mc is partially filled with mass Mw of water at

temperature T_1. The sample with mass Ms heated to a temperature T_b(ina boiling water separately), then quickly immersed into the calorimeter. The temperature of the calorimeter and the water contained quickly rises to a value T_2. It then slowly begins to fall as heat is lost to the atmosphere.

Therefore if no heat loses occur, heat lost by the sample(s) given by $M_sS_s(T_b-T_2)$ calories must be equal to the heat gained bythe calorimeter and the contained water($M_CS_C+M_wSw)(T_2-T_1)$.

Hence, Specific heat capacity of the sample(s) S_s can be calculated as follows:

$$S_s = \frac{(MCSC+ MwSw)(T2-T1)}{Ms(Tb-T2)}$$

2.4 Melting temperature

Samples of this test were dimensioned 20x20x3 mm and placed on a heating stand inside a small metallic furnace (in accordance to ASTM D3418). The samples were first heated rapidly to a temperature of about 137 ℃, which is called the starting temperature, and then heating is done at the rate of 0.5 ℃ per min with careful observation of the temperatures' rise. On reaching melting temperature,samples begin to soften. Those temperatures were recorded.

2.5 Density

Samples with dimension 20x20x3mm were prepared from each composition. The test was conducted using a weighing balance, the initial mass of each sample was determined, while the volume of each sample was calculated. The density determined using following relation;

$$\rho = \frac{m}{v}$$

2.6 Compression test

Three samples from each composition of 10x10x3mm dimension were sectioned and mounted on an Enerpac compression testing machine. One sample, at a time, was compressed (ASTM D695). Average of the results was taking in kN/mm^2

2.7 Water Absorption Test

The weights of dried samples measured and recorded as W_o. Subsequently, samples then immersed in distilled water at ambient temperature. After 2 hours (3 days), the samples were removed from the bath and carefully dried with absorbent paper before weighing. The weight of the samples following the immersion was recorded as W_t. The weight gain, W_g, due to water absorption was calculated as follows:

$$W_g = \frac{Wt-Wo}{Wo} \times 100\%$$

3.0 Results and Discussion

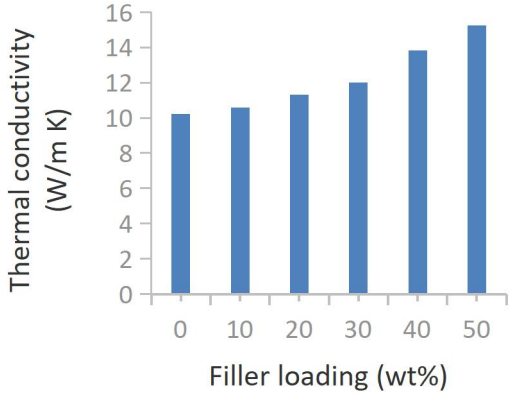

Figure 1: Thermal conductivity versus SBAP loading

From Figure 1, it can be observed that the thermal conductivity of the composite increases evenly upon the addition of sugarcane bagasse ash particulate reinforcement. However, a maximum and minimum thermal conductivity were noted at 0 and 50% addition respectively. With this behaviour it showed that a higher filler loading results in higher thermal conductivity values (Karthik, *et al.,* 2015).

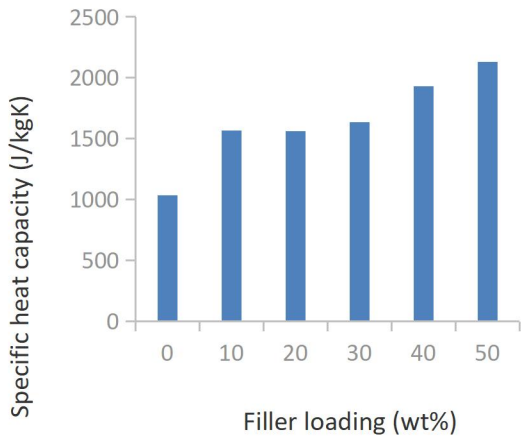

Figure 2: Impact of filler loading on the specific heat capacity of the PP/SBAP composites

Figure 2 indicate that the specific heat capacity of the composite increases continuously with the filler loading. Obviously, the 50% addition led to the highest rise in specific heat capacity. Therefore, bagasse ash particulate has considerable impact on specific heat capacity. Similarly, an improvement in specific heat capacity in polylactic acid reinforced with hemp and lyocell fibers was reported (Baghaei, *et al.,* 2014).

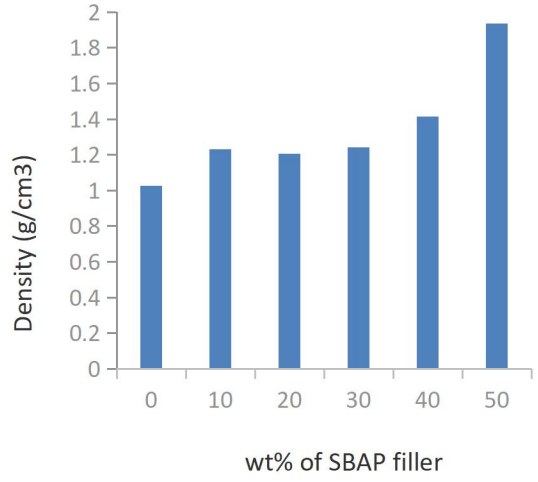

Figure 3: Density of the composites with weight fraction of the SBAP

Itis illustratedin Figure 3 that density of 0 and 20 wt% compositions were lower than that of the other composites. It is interesting to note that, an increase in the loading of SBAP causes a mild rise in the density of the composites. Likewise, a modest rise in density took place in poly (vinyl chloride) reinforced with sugarcane bagasse(Wirawan, *et al.,* 2011).

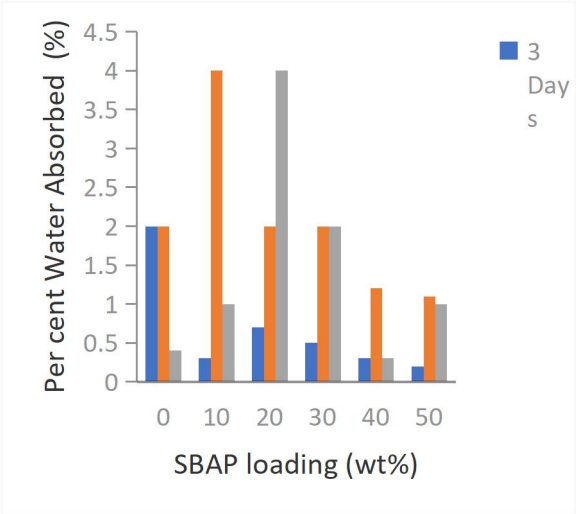

Figure 3: Water absorption charts of PP/SBAP compositesfor days at various filler content

From Figure 4, it is noteworthy that water absorption rate occurs more significantly to composites with 10 and 20 wt%filler additions. Notwithstanding, no appreciable water absorption was noticed at higher filler loading. At lower per cent filler loading, the cell wall of lignocellulosic SBAP swells until saturation took place. Then, the swelled particulates start to occupy the free spaces between the particulate bundles. Thus absorbed much higher moisture. However, at higher reinforcement content such free spaces are absent and consequently water absorption rate is not pronounced. According to Paula et al. (2014), lignocellulosic materials have strong affinity for water absorption.

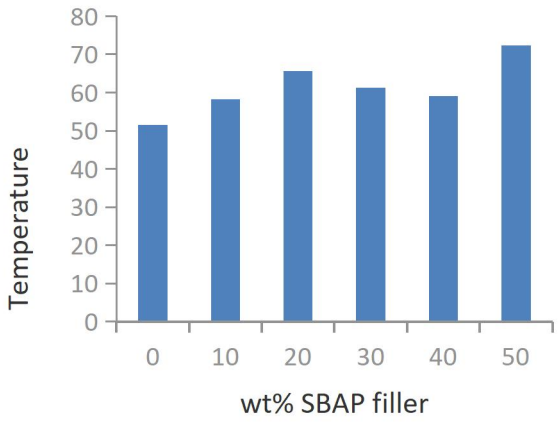

Figure 5: Melting temperature against SBAP additions

In a similar manner, it can be observed from Figure 5 that the presence of SBAP in PP makes melting temperature of the thermoplastic to mildly fluctuates. Nonetheless, a considerable rise in the melting temperature on 50 %wt filler addition occurred. However, the melting temperature of α- and β-phase of PP were reported to be 165 and 150°C respectively (Tordjeman et al., 2001). Since the environmental working condition of the human teeth at most does not exceeds 100°C, any of the composition of the developed composites could be considered as regard to the melting temperature.

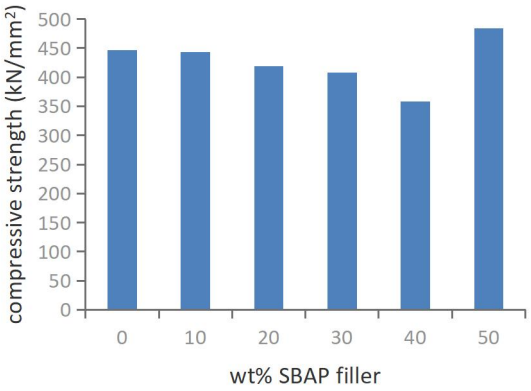

Figure 6: compressive strength versus wt% compositions

From Figure 6, it clear that compressive strength declines mildly with increased bagasse content. The behaviour, however, could be linked to a near soft nature of SBAP at lower proportion. Nonetheless less pores and more compact mixture is achieved on 50 %wt SBAP addition. Thus, the composite at this composition has the highest compression strength. It is in literatures that the compressive strength of the enamel and dentin parts of the human teeth are 10 and 100 MPa respectively (Manila *et al*., 2016). Therefore, 50 %wt PP/SBAP composite with about 480kN/mm^2 is likely to perform efficiently as dental implant material

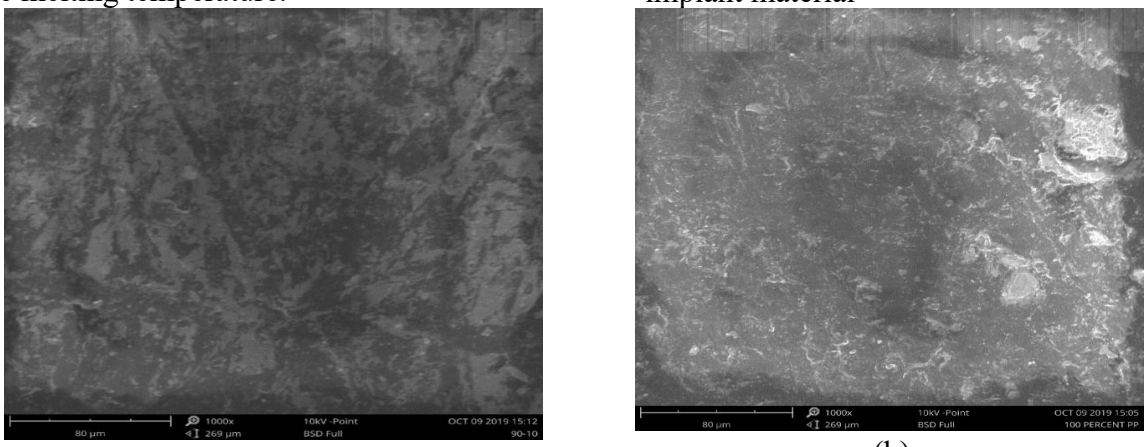

(a) (b)

Plate 1: SEM image of (a) neat PP (b) 10 wt% PP/SBAP composite

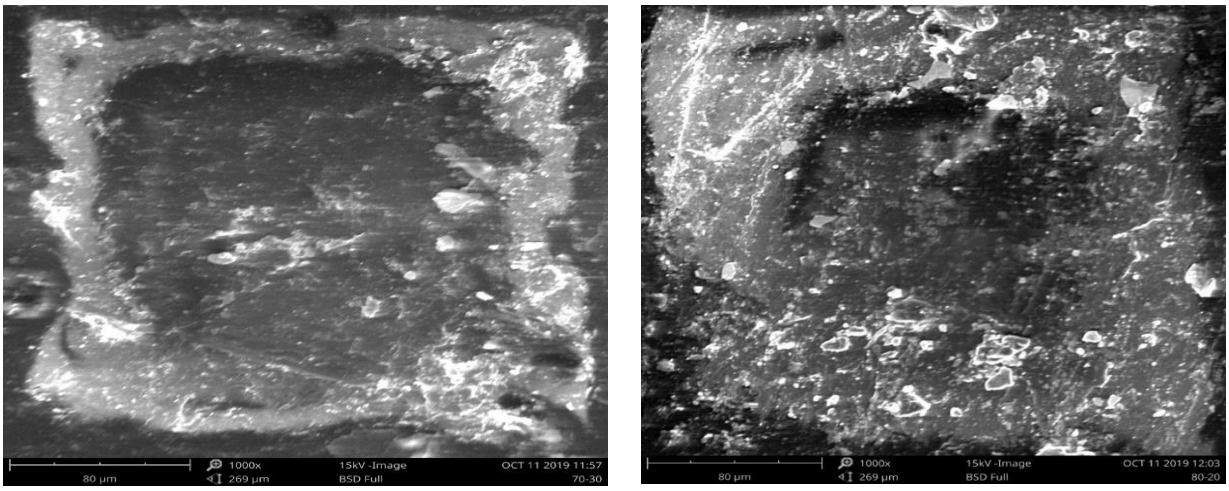

(a) (b)

Plate 2: SEM image of (a) 20 wt% PP/SBAP composites (b) 30 wt% PP/SBAP composites

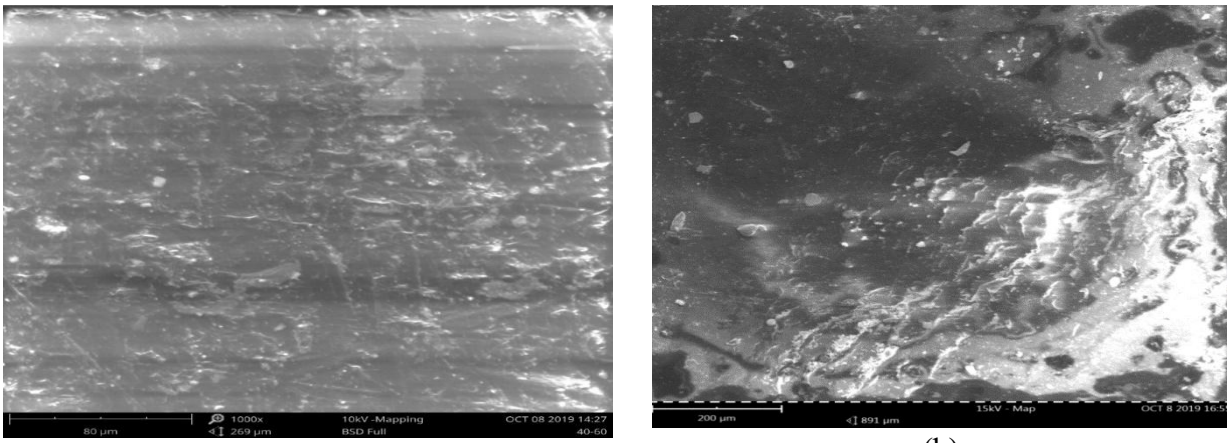

(a) (b)

Plate 3: SEM image of (a) 40 wt% PP/SBAP composite (b) 50 wt% PP/SBAP composites

The SEM images in Plates1- 3 provide information on the morphology of the composites. From Plate 1(a), it could be observed that neat PP matrix structure consists of amorphous(white) and crystalline (dark) phase. Likewise, Plates 1 (b), 2 and 3, show clusters of SBAP in the PP-matrix. Accordingly, the uneven distribution of the reinforcement in matrix causes fluctuations in the composites' properties across all the compositions (Figures 1-6). Similarly, site agglomeration of SBAP is observed as well. Thus, in the crystallization process, ordered chain arrangement in the PP-matrix was prevented. These agree with the observations of Chan *et al.* (2015).

Conclusions

Based on the results of the thermal properties, the developed composites conduct heatat a relatively higher rate than the PP. However, the thermal insulation of all the composites is within the acceptable range and so the effects of thermal the implant from the composites caused by abrupt temperature change due to

drinking or eating hot or cold substances would not be severe. A mild water absorption resulted in composites with higher filler content. Even though, density of the developed composites rises to about 2 g/cm^3; the composites are lighter compare to human tooth (average density of 2.9g/cm^3). Furthermore, additions of SBAP led to a significant improvement in the compressive strength of the composites. Based on the results, therefore, 50 wt% PP/SBAP composite proved itself worthy of the dental implant application.

References

Baghaei, B., Skrifvars, M., Rissanen, M., & Ramamoorthy, S. K. (2014). Mechanical and thermal characterization of compression moulded polylactic acid natural fiber composites reinforced with hemp and lyocell fibers. *Journal of applied polymer science*, *131*(15).

Chan K. W., Wong H. M., Yeung K. W. K., and Tjong S. C., (2015). *Materials,* **8,** 992.

Dodo R. M., Abubakar I. I., Bello K. A., Asuke F., Abdullahi I. and Shamsu M. Evaluation of Abrasion, Biocompatibility and Degradation Behaviour of Polypropylene/Sugarcane Bagasse Ash Particulate Composites for Dental Application, Nigerian Journal of Materials Science and Engineering(2021) 11(2): 70– 74.

Glantz P.O. The choice of alloplastic materials for oral implants: does it really matter? Int J Prosthodont, 1998;11(5):402-7.

He LH, Swain MV. (2007). Enamel - a ‘‘metallic-like’’ deformable biocomposite. *J Dent* 2007; 35(5): 431–437.

Karthik, M., Faik, A., Blanco-Rodríguez, P., Rodríguez-Aseguinolaza, J., & D’Aguanno, B. (2015). Preparation of erythritol–graphite foam phase change composite with enhanced thermal conductivity for thermal energy storage applications. *Carbon*, *94*, 266-276.

Kishen A, Ramamurty U, Asundi A. Experimental studies on the nature of property gradients in the human dentine. Biomed Mater Res 2000; 51(4): 650–659.

Kohal R.J, Klaus G. A zirconia implant-crown system: a case report. Int J Periodontics Restorative Dent 2004;24(2):147-53.

Manila C., Stefano P., Silvia M., Roberto P., Eagle M., Luigi T., and Stefano S., (2016). *Nanomaterials,* **6**, 134.

Paula, G.P., Rodríguez, R. J. S., Rangel Duarte, L. P., *et al*, “Formulation and characterization of polypropylene composites alkali treated bagasse fiber”, *Materials Science Forum*, 775, 319-324, 2014.

Onuoha C., Onyemaobi O.O., Anyakwo C.N., Onuegbu G.C. (2017). Physical and morphological Properties of Periwinkle Shell-Filled Recycled Polypropylene Composites. *International Journal of Innovative Science, Engineering & Technology, 4(5), May 2017,* 186-196.

Velmurugan D, Santha A.M, Sarate S. G.Dental implant materials, implant design, and role of FEA- A brief review. J. Evolution Med. Dent. Sci. 2017;6(44):3487-3492, DOI: 10.14260/Jemds/2017/753.

Wedad Q., Tahani A., Amani A., Kholud A., Ibtihal A. (2018). Review on Dental Implantology, *The Egyptian Journal of Hospital Medicine (April 2018) 71(1),* 2217-2225.

Wirawan, R., Sapuan, S. M., Yunus, R., & Abdan, K. (2011). Properties of sugarcane bagasse/poly (vinyl chloride) composites after various treatments. *Journal of Composite Materials*, *45*(16), 1667-1674.

Ya-Rong Z., Wen D., Xue-Dong Z. and Hai-Yang Y. (2014). Review of research on the mechanical properties of the human tooth, *International Journal of Oral Science* (2014) 6, 61–69.

NMS-TP010

THE EFFECT OF ERBIUM SOLUTION QUANTITY ON PROPERTIES OF SPRAY-GENERATED ZINC SULPHIDE THIN FILMS

P. O. Offor[1], G.M. Whyte[2], P. S. Nnamchi[1], C. C. Daniel-Mkpume[1], A. D. Omah[1], C. S. Obayi[1], C. Ocheri[1], F. U. Whyte[1], O. C. Nwoko[1], V. S. Aigbodion[1], I. C. Ezema Ike-Eze[1], B. A. Okorie[1], and F. I. Ezema[2]

1. Metallurgical and Materials Engineering Department, University of Nigeria, Nsukka, Nigeria.
2. Crystal Growth Laboratory, Physics Department, University of Nigeria, Nsukka, Nigeria.
3. Africa Centre of Excellence for Sustainable Power and Energy Development (ACE-SPED) University of Nigeria,

peter.offor@unn.edu.ng, peterjoyoffor@yahoo.com

Abstract

This work focused on the study of the effects of Erbium solution quantity on properties of Erbium-doped zinc sulphide thin films. These films were deposited on non – conducting glass substrates at 200°C by the method of spray pyrolysis. The chemicals used were Zinc acetate dehydrate [$Zn(CH_3COO)_2.2H_2O$] as source of zinc, thioacetamide [$CH_3CS.NH_2$] as source of Sulphur, Erbium nitrate hexahydrate [$ErH_{12}N_3O_{15}$] which were all diluted in deionized water to form the precursor solution. The precursor solution was made of 10 ml of the $Zn(CH_3COO)_2.2H_2O$ and $CH_3CS.NH_2$ solutions each with varying volumes of $ErH_{12}N_3O_{15}$ solution of 0, 5, 10, 15, and 20 ml, with ammonia as chelating agent. The structural, morphological, optical and photoluminescence studied by X-ray diffractometry (XRD), scanning electron microscopy (SEM), UV-spectrophotometry and photoluminescence spectrometry. The films are amorphous in nature. The surface morphology showed nano-dot like particles. The transmittance lies between 44.04 and 82.53% at 600 nm while the refractive index is betwixt 1.57 – 3.97. The band gap is between 3.05 and 3.42 eV. The photoluminescence of the films showed near band edge emissions. The films may be used in production of photovoltaic cells.

Key words: Erbium-doped, band gap, photoluminescence

1. Introduction

There has been an ever-increasing need for the use of power in various sectors of life due to increase in world population as in industrial, agricultural, health and even domestic use, in this regard generation of power has been one of the major problems in contemporary countries [1].

Global warming and climate change have been a major concern to not just the 'green thumbed community' but to the world at large due to its destructive effect and endangering concerns; not just on animals especially wildlife and humans but also mostly on our environment [2, 3]. In recent years, the need to save the planet has brought about new and innovative solutions to not only reduce the use of fossil fuels but to ultimately stop its use in years to come. Hence the emergence of the term "renewable energy" also known as sustainable power [4].

A major example of renewable energy is solar energy which is energy gotten from the sun which can be stored and transformed to other forms of energy and this can be done using solar cells [4]. Solar cells or photovoltaic cells are devices that convert light energy to heat energy by electrochemical reaction which was discovered and demonstrated in 1839 by Edmond Becquerel a French scientist [5]. This cell has three main types; crystalline silicon cells, organic cells and thin film cells

[6] of which the latter is the area of interest of this research. The mean cost for manufacturing of thin-film module is reduced by 64% in contrast to 51% for non-thin-film modules. This makes it to have greater possibility for large scale production of less costly modules [7]. It was suitable due to its low cost, light weight and efficiency in electricity. The main types of thin films are Zinc sulphide, Cadmium telluride, Copper-Indium-Gallium Selenide and amorphous Silicon.

There has been a lot of research on Zinc sulphide because of its numerous applications especially in nano-electronics and optoelectronics [8] Most of these properties has been added or improved due to doping with numerous elements such as Cu, Co, Mn, Co, Cd, Eu, Sm and so on and have been studied by many researchers because of their extensive photoluminescence and also electroluminescence properties an example is the manganese doped Zinc Sulphide producing a yellow-orange emission and also rare earth elements such as Samarium (Sm), Thulium (Tm) or Terbium (Tb) which produce red, blue or green emissions respectively [9, 10]. There are various studies of Zinc sulfide both as in bulk and in thin films. ZnS has been deposited over the years with various techniques; reactive evaporation, sputtering, chemical vapour deposition, atomic layer epitaxy, sol-gel processing [11] and chemical spray pyrolysis [12]. From previous research, ZnS with concentration 0.1M/L at 400^0C using the UV-VIS spectrophotometer showed good optical transparency with wavelength range (300-900) nm [13]. There are also works on ZnS and erbium by expensive and inexpensive methods such as ion plantation and chemical capping, but none using the spray pyrolysis technique [14, 15]. ZnS nanophosphor was synthesized with 0 – 15% Erbium concentration by co-precipitation means [14]. It was observed at relative cell efficiency that current density was relatively enhanced in the solar cell. ZnS doped with rare earths as erbium, neodymium and thulium emit green, orange and blue visible (VIS) photons. ZnS doped with rare earths also emit near infrared (NIR) photons which have potential applications in communication gadgets [16]. Doped and undoped ZnS thin films were fabricated by means of rf magnetron cosputtering with 1.5 mol % each one of NdF_3, TmF_3 or ErF_3. EL peaks were exhibited in the VIS and NIR regions [16]. Rare-earth-doped films are convenient for photoelectronic materials. It has been noticed that Er-doped Arsenic Selenide thin films displayed superior luminescence properties [17]. In a study, Er-doped ZnS quantum dots produced by hydrothermal process were observe to exhibit excellent luminescence properties [18].

2. Experimental procedure

Erbium-doped and undoped ZnS films were spray-created on soda lime glass (slg) substrates at 200 °C. The substrates were cleaned according to the procedure presented in the literature [17]. The materials used for this experiment includes Zinc acetate dehydrate, Thioacetamide, Erbium nitrate hexahydrate, Ammonia and Deionized water (DW). Zinc acetate dehydrate [$Zn(CH_3COO)_2.2H_2O$] as source of zinc, thioacetamide [$CH_3CS.NH_2$] as source of Sulphur, Erbium nitrate hexahydrate [$ErH_{12}N_3O_{15}$] as the source of erbium and deionized water as the solvent in the solution. 0.03 M solution each one of $Zn(CH_3COO)_2.2H_2O$ and 0.011 M of $ErH_{12}N_3O_{15}$ was made in DW. The precursor solution was made of 10 ml of the zinc and thioacetamide solutions each with varying volumes of $ErH_{12}N_3O_{15}$ solution of 0, 5, 10, 15, and 20 ml, with ammonia chelating

agent. The solutions were sprayed on the preheated slg substrates at nozzle to substrate distance of 20 cm, using air as carrier gas and substrate temperature of 200 ^{0}C to form Erbium-doped ZnS films with the samples labelled 0, 5, 10, 15 and 20 ml. The 0 ml solution means absence of Erbium in the solution, the undoped control sample.

The structural, morphological, optical and photoluminescence studies were carried out using X'Pert High HighScore PANalytical B. V X-ray diffractometer (XRD), scanning electron microscope (SEM) by VEGA3 TESCAN, photoluminescence spectrometer and UV-spectrophotometer. X-ray diffraction was used to determine the crystallinity of the film (XRD). Scanning electron microscopy was used to examine the surface morphology of the films. UV–visible spectroscopy (HP 8453, Agilent) was used to determine the absorption, transmission, and reflectance of light throughout the wavelength range of 200 – 1100 nm. SEM analysis was conducted on the thin film to determine the morphology of the doped thin films. Furthermore, we studied how light passed through the thin films using Photoluminescence.

3. Results and discussions

3.1 Structural analysis

Figure 1 depicts XRD pattern of the films prepared at 200 ^{o}C with 0, 10 and 20 ml Erbium concentrations. It shows that the films are amorphous structure in nature

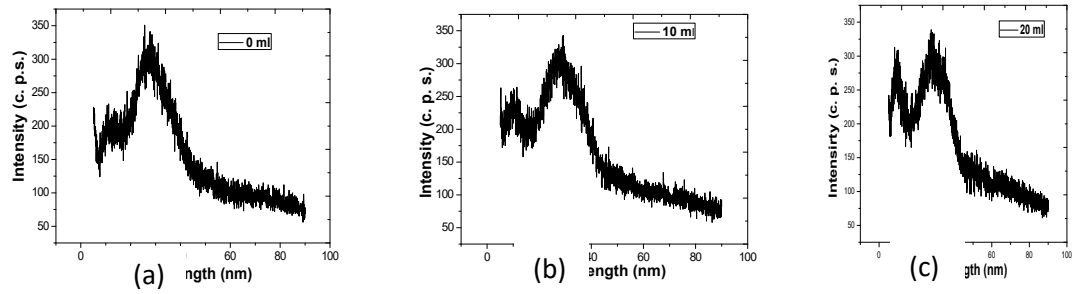

Figure 1. X-ray diffraction of ZnS thin films (a) 0 ml (b) 10 ml (c) 20 ml

Figure 1 shows the XRD pattern of ZnS produced with 0, 10 and 20 ml Erbium concentrations are amorphous in nature and contain remnants from undecomposed precursor as reported in Ref. [19].

3.2 Surface morphology

Figure 2 shows the surface morphology of Erbium-doped Zinc sulphide films.

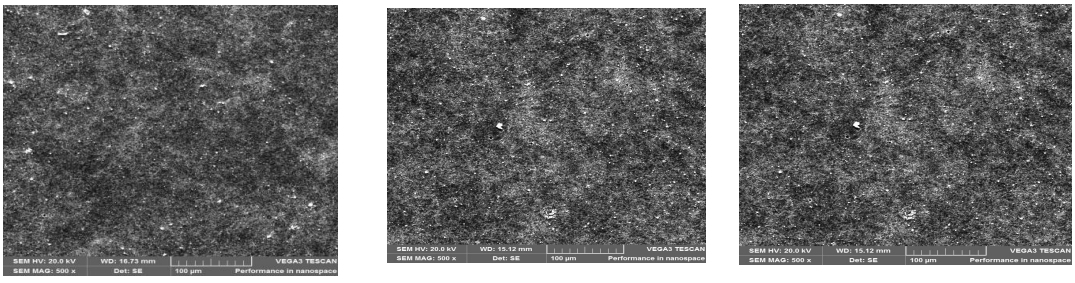

(a) (b) (c)

Figure 2. SEM micrograph of ZnS thin films (a) 0 ml (b) 10 ml (c) 20 ml

The surface morphology of the thin films was assessed by scanning electron microscope (SEM). Figure 2 (a) which contains 0 ml Erbium solution displayed a smooth surface with nanodot-like particles. Figure 2 (b) contains 10 ml of the erbium solution, shows a fibrous nano-sized structure with tiny blank spots dispersed randomly around the surface. While Figure 2 (c) has a fibrous-like clusters but it's less defined and it also has blank spots but are more visible than in Figure 2 (b). Moreover, it contains some voids or pores.

3.3 Optical properties

The study of the ZnS films by means of optical absorbance, reflection, refraction, transmission and band gap energy was evaluated and analyzed as shown below. These analyses provide information on the quality of the thin film and some optical constant. All Figures show a series of ZnS thin films prepared with variations of Erbium solution.

3.3.1 Absorbance

Figure 3 shows the absorbance plot of Erbium-doped Zinc sulphide films.

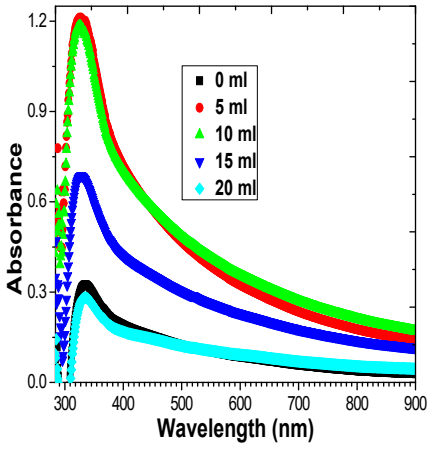

Figure 3. Absorption spectra of ZnS thin films.

The graph above shows a plot of absorbance against wavelength of zinc sulphide thin films deposited with different volumes of Erbium solution. Figure 3 shows a pronounced increase in absorption near the absorption edge which signifies high absorbance at the shortwave region of the electromagnetic spectrum and this decreases with wavelength which is in accord with Ref. [20]. At 600 nm, the absorbance for 0 ml and 20 ml of Erbium have the same value of 0.15 and this is followed by 15 ml, 10 ml and finally 5 ml. this evaluation shows it can be used as optoelectronic device and solar cells.

3.4.2 Transmittance

Figure 4 shows the transmittance plot of Erbium-doped Zinc sulphide films.

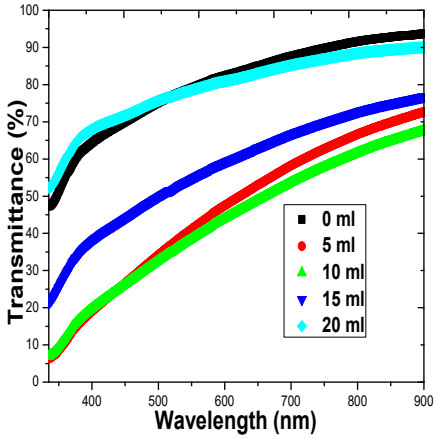

Figure 4. Transmittance spectra of ZnS thin films

Figure 4 shows transmittance spectra as a function of wavelength of zinc Sulphide thin films. The graph shows that at 600 nm, the transmittance of all the thin films are above 40%. As shown from the graph the films are a bit curved indicating homogeneity in the shape and size. Figure 4 shows the following values for 0 ml, 5 ml, 10 ml, 15 ml and 20 ml as 82.53%, 46.85%, 44.04%, 59.10% and 81.15% respectively all at 600 nm. This is in accord with Ref. [21]. 0 ml and 20 ml having the highest transmittance is suitable

for window layers while the others with low transmittance can be used for anti-reflective coatings.

3.4.3 Reflectance

Figure 5 shows the reflectance plot of Erbium-doped Zinc sulphide films.

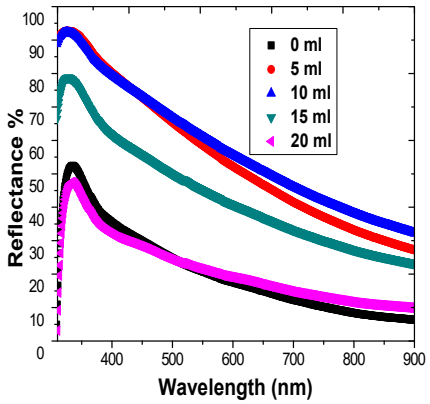

Figure 5. The reflectance spectra of ZnS thin films.

Figure 5 displays that the films' reflectance reduced with increase in wavelength as seen in the literature [22]. The reflectance of the films altered with solution quantity. The film made with 10 ml Er solution has highest reflectance followed by the ones deposited at 5, 15, 20 and 0 ml solution in reducing order.

3.4.4 Refractive Index

Figure 6 shows the refractive index plot of Erbium-doped Zinc sulphide films.

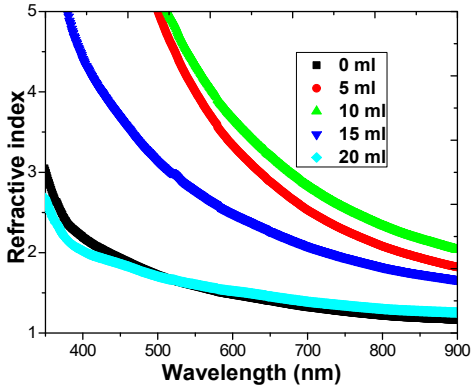

Figure 6. Refractive index for ZnS thin films

Figure 6 shows a plot of refractive index of the erbium-doped zinc sulphide thin films. The refractive index, at 550 nm of the films have the following values of 1.57, 3.97, 4.35, 2.75, 1.63 for 0, 5, 10, 15 and 20 ml films respectively. The low refractive index films are good for antireflection coatings whereas the high refractive index films can be used in anti-dazzling coatings and poultry production as reported in [23].

3.4.5 Energy band gap

Figure 7 shows the energy band gap plot of Erbium-doped Zinc sulphide films.

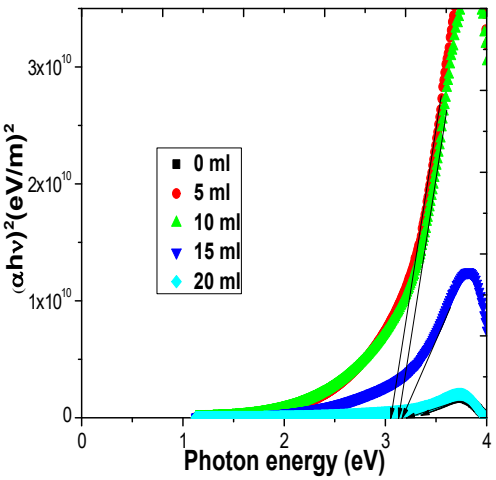

Figure 7. Optical band gap of ZnS:Er with photon energy as its function.

The estimated band gaps for the film deposited with 0 ml, 5 ml, 10 ml, 15 ml and 20 ml volume concentration are 3.42, 3.23, 3.17, 3.13 and 3.05 eV respectively. The band gap of the films are in agreement with the values reported in the literature [13].

3.4.6 Photoluminescence

Figure 8 shows the photoluminescene spectra of Erbium-doped Zinc sulphide films.

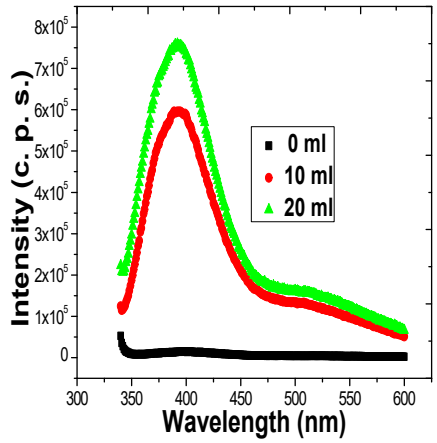

(a)

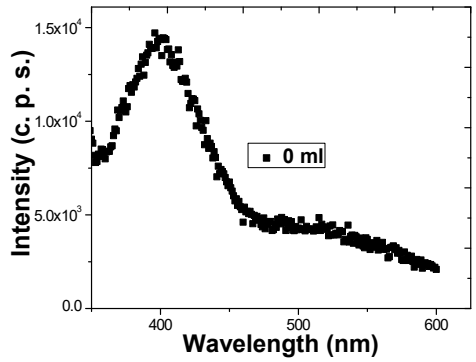

(b)

Figure 8. Photoluminescence spectra of ZnS thin films (a) 0 ml, 10 ml, 20 ml, (b) 0 ml

Figure 8 shows PL excitonic near band edge and trapped emissions in the films as in [20]. The excitonic near band emissions appeared at emission wavelengths of 392.08, 393.94 and 399.78 nm nm for the films made with 20, 10 and 0 ml solutions respectively. This reflects that the peaks originated from the impurity states associated with Erbium as stated in [24]. The peak intensity increased with solution quantity due to increase in defect states in the mid band region of the film. The PL indicates trapped emissons at at emission wavelengths of 508.29, 507.39 and 518.62 nm for the films made with 20, 10 and 0 ml solutions respectively. This may be attributed to emission of trapped states of ZnS connected with zinc and sulfur vacancies reported in [24].

Conclusion

Erbium-doped zinc sulphide thin films have successfully been synthesized using the chemical spray pyrolysis method. This was done using a triple source precursor of zinc acetate dehydrate, thioacetamide of 10 ml each and variations of volume of erbium nitrate hexahydrate of 0, 5, 10, 15 and 20 ml, in the presence of a complexing agent which was ammonia at a temperature of 230^{0}C. Studies on its structural, morphological, optical and photoluminescence were carried out using X-ray diffractometer (XRD), scanning electron microscope (SEM), UV-spectrophotometer and photoluminescence spectrometer. The films have a wide range of transmittance values between 35% and 85% at 550nm and relatively high refractive index of above 1.50 at 550nm, due to this property, it can be used for anti-reflective coatings. The band gap is between 3 and 3.3eV. The XRD analysis displayed an amorphous structure and nano-sized, the surface morphology shows a fibrous structure and presence of some nano blank spots being dispersed. The photoluminescence of the films shows near band edge emissions. This can be used in production of photovoltaic cells and optoelectronic devices.

Acknowledgement - The authors hereby appreciate and acknowledge the Africa Centre of Excellence for Sustainable Power and Energy Development, ACE-SPED, University of Nigeria, Nsukka for their support.

References

1. C. K. Amuzuvi and E. Effah (2014), Design of a Photovoltaic System as an Alternative Source of Electrical Energy for Powering the Lighting Circuits for Premises in Ghana, Journal of Electrical and Electronic Engineering, 2(1), pp. 9-16
2. C. C. Julian (2011), Physics of Solar Energy, John, W. & Sons, Inc., Hoboken, New Jersey.
3. K. Bhaskar (2007), Zinc Cadmium Sulphide And Zinc Sulphide As Alternative Heterojunction Partners for $CIGS_2$ Solar Cells, MSc. Degree, University of Central Florida Orlando, Florida
4. P. Kusterle (2014), Intermediate Band Solar Cells Based on Cr:ZnS Device Characterization and Simulation, MSc. Degree Thesis, Norwegian University of Science and Technology (NTNU), Trondheim, Norway.
5. R. Williams (1960), "Becquerel Photovoltaic Effect in Binary Compounds'. The Journal of Chemical Physic. 32 (5): 1505-1514. Doi:10.1063/1.1730950.
6. A. B. Waheed (2015), A Review on Solar Cells from Si-Single Crystals to Porous Materials and Quantum Dots, Journal of Advanced Research, 6, 123–132
7. K. L. Chopra, P. D. Paulson and V. Dutta (2014), Progress In Photovoltaics: Research And Applications, Prog. Photovolt: Res. Appl. 2004; 12:69–92 (DOI: 10.1002/pip.541)
8. M. A. Shakil, S. Das, M. A. Rahman, U. S. Akther, M. K. Hassan, and M. K. Rahman, A Review on Zinc Sulphide Thin Film Fabrication for Various Applications Based on Doping Elements, Materials Sciences and Applications, vol. 9, no. 9, pp. 751–778, 2018, doi: 10.4236/msa.2018.99055.
9. H. Kobayashi, S. Tanaka, V. Shanker, M. Shiiki, T. Kunou, J. Mita, and H. Sasakura (1985), Multicolor Electroluminescent Zns Thin Films Doped with Rare Earth Fluorides, Physica Status Solidi (a), Vol. 88, no. 2, pp. 713–720, 1985, doi: 10.1002/pssa.2210880239.
10. T. T. Nguyen, X. A. Trinh, L. H. Nguyen, and T. H. Pham (2011), Photoluminescence Characteristics Of As-Synthesized And Annealed ZnS:Cu,Al Nanocrystals, Advances in Natural Sciences: Nanoscience and Nanotechnology, Vol. 2, No. 3, doi: 10.1088/2043-6262/2/3/035008.
11. W. Tang and D. C. Cameron (1996), Electroluminescent Zinc Sulphide Devices Produced by Sol-Gel Processing, Thin Solid Films, Vol. 280, no. 1–2, pp. 221–226, 1996, doi: 10.1016/0040-6090(95)08198-4.
12. P. O. Offor, G. M. Whyte, V. A. Ezekoye, A. D. Omah, S. N. Ude, C. Ocheri, N. Ezukwoke, I. C. Ezema, I. G. Madiba, B. A. Okorie, M. Maaza and F. I. Ezema (2019), Structural, Morphological and Optical Properties of Spray-Formed Silver-Doped Zinc Sulphide Thin Films, Optik, https://doi.org/10.1016/j.ijleo.2019.03.063
13. N. M. Saeed (2011), Structural and Optical Properties of ZnS Thin Films Prepared by Spray Pyrolysis Technique, Thin Solid Films, Vol. 14, No. 2, pp. 86–92, 2011, doi: 10.1016/S0040-6090(00)01404-8.
14. A Pattnaik, S Jha, M Tomar, V Gupta, B Prasad and S Mondal (2018), Improving the Quantum Efficiency of the Monocrystalline Silicon Solar Cell Using Erbium-Doped Zinc Sulphide Nanophosphor in Downshift Layer, *Mater. Res. Express* 5 095014,
15. Li Lihua, Zhang Xiang, Li Xinli, Huang Jinliang, Alex A. Volinsky C (2018),

Synthesis and Photoluminescence of Er^{3+} and Yb^{3+} Doped ZnS Nanocrystals, Rare Metal Materials and Engineering Vol. 47, Issue 6, pp. 1744 – 1748

16. W. Glass, A. Kale, N. Shepherd, M. Davidson, D. DeVito, and P. H. Hollowaya (2007), Sputter deposited electroluminescent zinc sulfide thin films doped with rare earths, Journal of Vacuum Science and Technology A 25, 492, pp. 492 – 499, doi: 10.1116/1.2718956
17. G. M. Whyte, Chawki Awada, P. O. Offor, F. U. Otung, Adil Alshoaibi, Abdullah Aljaafari, A. B. C. Ekwealor, M. Maaza and Fabian I. Ezema (2020), Optical and Photoluminescence Performance of Electrodeposited Arsenic Selenide Thin Film Doped with Erbium Ion, Optical Materials 99, 109556, pp. 1 – 7, https://doi.org/10.1016/j.optmat.2019.109556
18. G. Li, L. Li, L. Yang and J. Huang (2013), Optical Properties of Water-Soluble Er-Doped ZnS Quantum Dots Synthesized by a Hydrothermal Process, Advanced Material Research, Vol. 800, pp. 402 – 405
19. T. Dedova, M. Krunks, I. Gromyko, V. Mikli, I. Sildos, K. Utt, and T. Unt (2014), Effect of Zn:S molar ratio in solution on the properties of ZnS thin *fi*lms and the formation of ZnS nanorods by spray pyrolysis, Phys. Status Solidi A 211, No. 2, 514–521, DOI 10.1002/pssa.201300215
20. P. O. Offor, A. C. Nwanya, A. D. Omah, M. Maaza, B. A. Okorie, and F. I. Ezema (2017), Chemical spray pyrolysis deposition of zinc sulphide thin films using ethylenediaminetetraacetic acid disodium salt complexant, 2017, doi: 10.1007/s10008-017-3668-2.
21. P. O. Offor, S. N. Ude, G. M. Whyte, C. S. Obayi, P. S. Nnamchi, A. D. Omah, F. U. Whyte, S. Madu, U. C. Ogbuefi, C. C. Daniel-Mkpume, B.O. Anyaka, B. A. Okorie and F. I. Ezema (2020), The Influence of Substrate Temperature on Properties of Zinc Sulphide Thin Films Synthesized by Chemical Spray Pyrolysis, Asian Journal of Basic Science and Research, Volume 2, Issue 1, pp. 01-15,
22. P. O. Offor, B. A. Okorie, F. I. Ezema, V. S. Aigbodion, C. C. Daniel-Mkpume and A. D.
23.
24. Omah (2015), Synthesis and Characterization of Nanocrystalline Zinc Sulphide Thin Films by Chemical Spray Pyrolysis, Journal of Alloys and Compounds, 650, pp. 381 – 385, DOI: 10.1016/j.jallcom.2015.07.169
25. P. A. Ilenikhena (2008), Comparative Studies of Improved Chemical Bath Deposited Copper Sulphide (CuS) and Zinc Sulphide (ZnS) Thin Films at 320k and Possible Applications, African Physical Review, 2: 0007, pp. 59 – 67.
26. E. Shahriari, Z. M. Farsani, M. G. Varnamkhasti and R. Zamiri (2017), Linear and non-linear optical properties of Ag doped ZnS thin film, Opt. Quant. Electron, pp. 49:151 DOI 10.1007/s11082-017-0991-x

NMS-TP011

Evaluation of Flexural Strength and Water Absorption Behaviour of Glass Fiber Reinforced High-Density Polyethylene Matrix Composite

A. A. Musa*, U. Muhammad and I. Abdullahi
Department of Metallurgical and Materials Engineering, Ahmadu Bello University, Zaria, Nigeria.
*Corresponding author: E-mail: **abdulrahman@abu.edu.ng**; Tel: +2348039162744

Abstract

The current study investigates the effect of fiber variation on the flexural strength and water absorption behaviour of glass fiber reinforced high-density polyethylene (HDPE) composite. The glass fiber was varied from 5%, 10%, 15%, 20% to 25%. The measured weight of the fiber was added to the molten HDPE in a compression mold and then compressed using a standard compression machine. The results obtained showed that the water absorption of the produced composite increase as the percentage of glass fiber increases. However, the highest water absorption value was recorded as 16.01% at 25wt.% of the glass fiber. The flexural strength increased from 22.9N/mm^2 at 5% to 26.4N/mm^2 at 20% fiber content which decreased to 18.2N/mm^2 as the percentage fiber content further increase to 25%. Hence, the optimum flexural strength of the composite was observed at 20wt.% of the reinforcement, while the water absorption results indicate that the higher the glass fiber volume, the higher the water absorption of the composite.

Keywords: Flexural strength, HDPE, water absorption, glass fiber, composite

1. Introduction

Composite materials are becoming very popular in most industries for different applications due to their unique and combined qualities such as high specific properties, lightweight, excellent resistance to corrosion, and less expensive (Morampudi, *et al*., 2021; Clyne and Hull, 2019). Fiber-reinforced composite material has been reported to have attracted many applications due to its lower weight and superior properties when compared to metal and ceramic reinforcements (Zhu, *et al*., 2021; Yang, *et al*., 2019).

Composite materials generally exhibit a desirable combination of properties that is superior and better than their respective building blocks (Bhimasankaram, *et al.,* 1998).

Key factors that influence the properties of these composite materials include the fiber types, fiber loading, fiber orientation, fiber size, and the type of matrix materials (Ramesh, 2019). Fiber loading influences the properties of fiber-reinforced polymer matrix composites (Andrew *et al*., 2019). Studies have also shown that the tensile strength, stiffness, and impact toughness of fiber-reinforced polymer matrix composite depend largely on the fiber volume (Alam, *et al*., 2010). Improving the properties of fiber-reinforced polymeric composite through optimum fiber content has made it a suitable and alternative material for many critical applications (Al-Oqla, 2021).

Glass fiber reinforced polymer (GFRP) composite plays a major role in the composite industry and has been utilized to manufacture many engineering materials for industrial usage (Sanjay and Yogesha, 2017). It is very light, strong, and economical and accounted for about 70% of the total reinforcements used in composite production globally. Most of the GFRP Composites are used in the construction,

building, and transportation sectors (Gonçalves, *et al*., 2022). However, one of the problems normally encountered during the application of glass fiber reinforced composites is their brittle failure due to their lower ductility (Khalid, *et al*., 2021). The tensile and flexural strengths have also been reported to be lower when compared to that of carbon fiber reinforced composites and other composite materials (Van de Werken, *et al*., 2021). The demand for lightweight materials and fuel efficiencies in aerospace and automobile sectors as well as the production of more corrosion-resistant equipment for critical applications are the major drivers of the increasing demand for GFRP in recent years. Polyethylene has been widely recognized as one of the commonly used polymers for the synthesis of GFRP (Mangoush, *et al*., 2021). Therefore, this study investigates the effect of glass fiber volume on the flexural strength and water absorption behaviour using high-density polyethylene (HDPE) as the matrix material.

2. Materials and Method

2.1 Materials

The materials used in this research are high-density polyethylene as the matrix and glass fiber as the reinforcement which were both obtained from the Nigeria institute of leather and science technology (NILEST), Zaria, Kaduna State.

2.2 Sample Preparation

The glass fiber was prepared in a different form to the desired fiber length. The length of the glass fiber used in this study is 27.67mm and the diameter was measured to be 0.48mm using dinoliite microscope, attached to a tribometer machine. A metallic mold of dimension 150 x 160 x 5 mm was used to prepare the composite. The mold was thoroughly cleaned to remove dirt and dust to produce a better composite. A lubricant was added to the mold for easy removal of the hot sample after production. The required mass of the mixture to fill up the mold was 114g. The mass of the reinforcement based on the different weight percentages of 5%, 10%, 15%, 20%, and 25% was then calculated and added to the matrix (HDPE) material to make up 100% for each of the samples, and then compressed through the application of external pressure.

2.3 Composite production

The composites were produced using a standard compression molding machine. The high-density polyethylene and the glass fiber were intimately mixed at a temperature of 170^0C which is the temperature at which the matrix becomes flowable to mix up with the glass fiber. The hot compressed sample was collected from the two-roll mill machine and immediately placed in the mold and compressed at a pressure of 3Pa and a temperature of 150^0C for 5 minutes. The sample was then removed, and allowed to cool and cured at room temperature. After the composite has been cured some of the excess resin splashed around the edges of the part was then carefully removed using scissors. The process was repeated for all the compositions of the reinforcement.

2.5 Water absorption test

Water absorption is a physical test that gives a detail of the level at which the composite materials absorb solvents when placed in a moist environment. The sample for the water absorption test was cut, dried, and taken the initial weight as (w_1) using a digital weighing balance. It was then immersed in an enclosed water container at room temperature for 5 days (120 hrs.), after which the final weight was taken and recorded as (w_2) for each sample. The percentage weight gained was calculated and recorded for each sample using equation 1.

$$\%\text{Moisture Absorbed} = \frac{w_2 - w_1}{w_1} \quad 1$$

2.6 Flexural Test

The flexural test was carried out using the Hounsfield tonometer with a crosshead speed of 1.3mm/min. The samples were cut to a specified dimension of 30mm in width, 100mm in length, and 3mm in thickness. The three-point flexural strength test method was used in which each sample was bent and tested using improvised support at both ends and a center point load is applied, gradually increasing the amount of the force until it breaks. If a load (P) is applied over the entire span (L), acting on a cross-sectional area (A), then flexural strength could be calculated using the relationship in equation 2.

Flexural strength $(\sigma_f) = \frac{3\ x\ load\ span\ (P) x\ length\ span\ (L)}{2\ x\ width\ (b) x\ thickness\ (d)^2} = 3PL\ /2bd^2$ 2

3. Results and Discussion

3.1 Flexural strength result

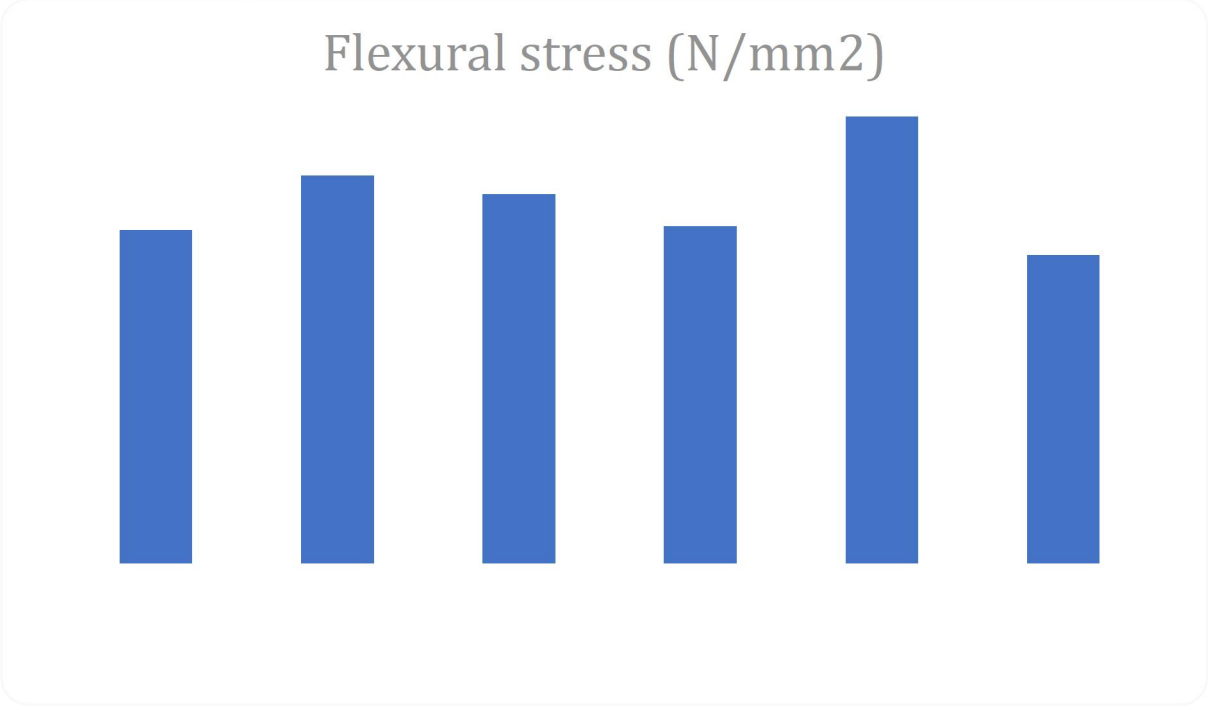

Figure 4.2: Flexural strengths against weight precent reinforcement

The flexural strength result is presented in Figure 1. It can be observed from the Figure that the flexural strength of the composite material increased gradually as the weight percent reinforcement increases up to 20% and slightly decreases as the weight percent reinforcement further increased to 25%. The optimum flexural strength obtained at 20% reinforcement was 26.42N/mm^2 which decreases to 18.2N/mm^2 at 25% reinforcement. This further decrease in the flexural strength at higher percentage reinforcement may be due to an increase in brittleness of the composite material caused by the excess glass fiber. The fluctuation of flexural strength at 5 to 15% reinforcement can be attributed to the nonuniformity and defect during mixing, compounding, and compressing of the composite materials, which may result in creating voids within the composite structure. However, it can be seen that the flexural strength of the composite without reinforcement (control) is lower compared to the reinforced composites except at 25% reinforcement which appears to be the least.

3.2 Water absorption result

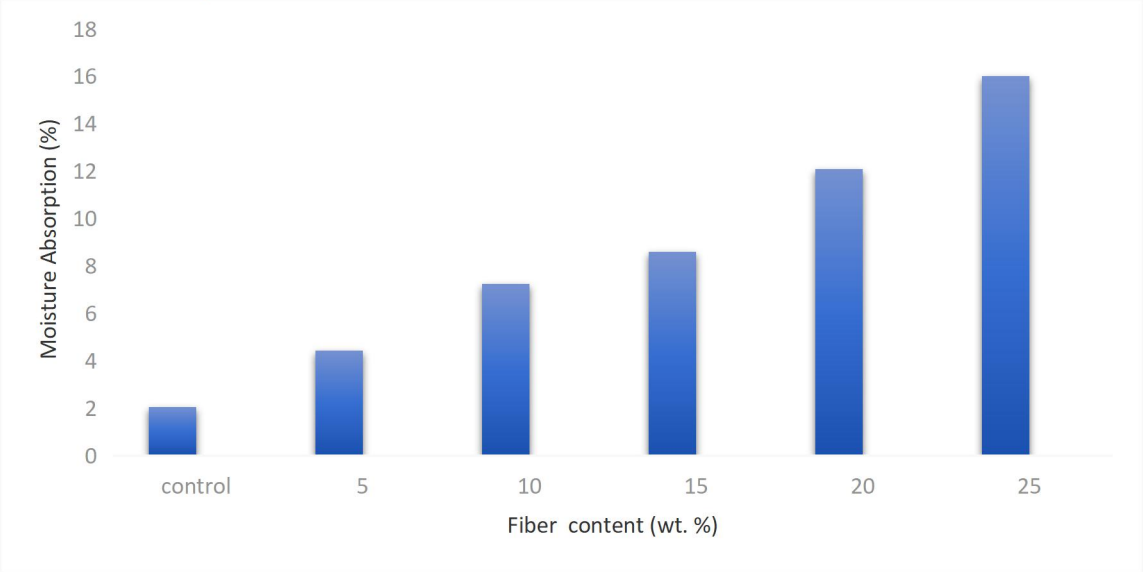

Figure 2: Percentage of water absorption at different weight percent reinforcement

Figure 2 shows the result of water absorption of the glass fiber reinforced high-density polyethylene composites for 5 days of immersion time at room temperature. The water absorption value was observed to increase continuously with increasing percentage reinforcement. The unreinforced sample shows the least water absorption, followed by 5% reinforcement and the highest water absorption was at 25% reinforcement. This water absorption result indicates that an increase in the amount of glass fiber in high-density polyethylene makes it more susceptible to moisture.

Conclusion

Based on the results obtained from the present study, the following conclusions were made.

i. Both the flexural strength and water absorption of the composite depend on the glass fiber content

ii. The maximum flexural strength of 26.4 N/mm^2 was achieved at 20% fiber loading. The water absorption increases gradually with an increase in the percentage of the glass fiber.

References

Alam, S., Habib, F., Irfan, M., Iqbal, W., & Khalid, K. (2010). Effect of orientation of glass fiber on mechanical properties of GRP composites. *Journal of the Chemical Society of Pakistan*, *32*(3), 265-269.

Al-Oqla, F. M. (2021). Flexural characteristics and impact rupture stress investigations of sustainable green olive leave bio-composite materials. *Journal of Polymers and the Environment*, *29*(3), 892-899.

Andrew, J. J., Srinivasan, S. M., Arockiarajan, A., & Dhakal, H. N. (2019). Parameters influencing the impact response of fiber-reinforced polymer matrix composite materials: A critical review. *Composite Structures*, *224*, 111007.

Bhimasankaram, T., Suryanarayana, S. V., & Prasad, G. (1998). Piezoelectric polymer composite materials. *Current Science*, 967-976.

Clyne, T. W., & Hull, D. (2019). *An introduction to composite materials*. Cambridge university press.

Gonçalves, R. M., Martinho, A., & Oliveira, J. P. (2022). Recycling of reinforced glass fibers waste: Current status. *Materials*, *15*(4), 1596.

Khalid, M. Y., Rashid, A. A., Arif, Z. U., Akram, N., Arshad, H., & García Márquez, F. P. (2021). Characterization of failure strain in fiber-reinforced composites: Under on-axis and off-axis loading. *Crystals*, *11*(2), 216.

Mangoush, E., Garoushi, S., Lassila, L., Vallittu, P. K., & Säilynoja, E. (2021). Effect of Fiber Reinforcement Type on the Performance of Large Posterior Restorations: A Review of In Vitro Studies. *Polymers*, *13*(21), 3682.

Morampudi, P., Namala, K. K., Gajjela, Y. K., Barath, M., & Prudhvi, G. (2021). Review on glass fiber reinforced polymer composites. *Materials Today: Proceedings*, *43*, 314-319.

Ramesh, M. (2019). Flax (Linum usitatissimum L.) fiber-reinforced polymer composite materials: A review on preparation, properties, and prospects. *Progress in Materials Science*, *102*, 109-166.

Sanjay, M. R., & Yogesha, B. (2017). Studies on natural/glass fiber reinforced polymer hybrid composites: an evolution. *Materials today: proceedings*, *4*(2), 2739-2747.

Van de Werken, N., Koirala, P., Ghorbani, J., Doyle, D., & Tehrani, M. (2021). Investigating the hot isostatic pressing of an additively manufactured continuous carbon fiber reinforced PEEK composite. *Additive Manufacturing*, *37*, 101634.

Yang, G., Park, M., & Park, S. J. (2019). Recent progress of fabrication and characterization of fiber-reinforced composites: A review. *Composites Communications*, *14*, 34-42.

Zhu, C. Y., Gu, Z. K., Xu, H. B., Ding, B., Gong, L., & Li, Z. Y. (2021). The effective thermal conductivity of coated/uncoated fiber-reinforced composites with different fiber arrangements. *Energy*, *230*, 120756

.

NMS-TP012

Effect of Current Variation on Some Mechanical Properties of Medium Carbon Steel Weldment Using Shielded Metal Arc Welding Process

A. A. Musa*, H. T. Danladi and A. K. Oyinlola
Department of Metallurgical and Materials Engineering, Ahmadu Bello University, Zaria, Nigeria
*Corresponding Email address: abdulrahman@abu.edu.ng; Tel: 08039162744

Abstract
The present study investigates the effects of current variations on hardness, impact, and tensile strength as well as the microstructural features of medium carbon steel weldment using the shielded metal-arc welding (SMAW) process. The as-received (unwelded) medium carbon steel was prepared following the American Society for Testing and Materials (ASTM) standard for tensile and impact testing and then welded using the SMAW process. The tensile, impact and hardness tests were carried out on the unwelded as well as the welded samples using Denison universal tensile testing machine, Izod impact testing, and Rockwell hardness testing machine respectively. The microstructural characterization of all the samples (welded and unwelded) was also examined using optical microscopy. From the results of the mechanical properties conducted, it was observed that there were some changes in the properties of the welded samples at the different current conditions when compared with that of unwelded parent metal. The welding current of 120 amps gave the highest tensile strength of 651.17 MPa, while the maximum hardness of 50.7 HRA was achieved at a welding current of 110 amps. For the impact energy, the unwelded metal gave the highest impact energy as compared to the welded metal at the different welding current conditions. Based on this investigation, the welding current has a great influence on the mechanical properties and microstructural transformation of medium carbon steel weldment.

Keywords: SMAW welding, Tensile strength, Hardness, Impact energy, Microstructure

1. Introduction

Welding is a fabrication process that joins materials, usually metals or thermoplastics, by causing fusion between the parent metal and the filler material, which is distinct from lower temperature metal-joining techniques such as brazing and soldering, that do not melt the base metal (Syambabu, *et al*., 2016; Nutalapati, *et al*., 2016; Dwivedi, 2022).

The earliest evidence of welding practice dated back to the Middle Ages (Bronze Age). Welded gold boxes are evidence to support the existence of welding practice during this period (Mohammed, *et al.,* 2013). Welded iron tools by the Egyptians during this period attest to the historical existence of welding practice and most of their iron tools were made through the welding process. During this period a set of specialized workmen called the blacksmiths came to the fore. Blacksmiths of the middle ages welded various types of iron tools by hammering, popularly known as forge welding. The welding methods remained unchanged until the dawn of the 19th century following the development of special welding techniques such as arc welding, oxy-fuel welding, and resistance welding (Mohammed, *et al.,* 2013; William *et al.,*1991). After the end of World War 1, the American Welding Society (AWS) was established to project the merit of welding processes (Guiraldenq and Duparc, 2017)).

However, within the past fifty years, there has been a great improvement in the

technical and scientific knowledge and equipment in welding and power demand (Weman, 2003). For manual welding methods, labour cost generally makes up the vast majority of the total cost. As a result, many cost-saving measures are focused on minimizing operation time. To achieve this, welding procedures, with high deposition rates can be selected, and weld parameters can be correctly chosen to increase the overall welding process. One of the most important welding parameters normally considered during welding operation is the welding current as it directly determines the total amount of heat energy input into the weld joint (Tomaz, *et a*l., 2021).

Welding is more economical, convenient, and less susceptible to failure or corrosion as compared to other joining processes (Khanna, 1999). Owing to the advantages of welding over other joining processes, numerous welding processes have been developed which include arc welding, Oxy-fuel welding, friction welding, resistance welding, cold welding, diffusion welding, etc. Among these aforementioned welding processes, the arc welding process is the most popular and frequently used in most industries for both fabrication and maintenance purposes. (Khanna, 1999; Chen, *et al*., 2020).

Medium carbon steel is the most common form of steel because it is less expensive and provides material properties that are acceptable for many applications (Tewari, *et al.,* 2010). These steels are used for making connecting rods, gear shafts, axles, spring clips, wires and rods, automobile parts, and constructions (Khanna,1999). For various engineering applications, these materials are often subjected to the welding process, and one of the important welding parameters that greatly affected most welding processes as well as the resulting weld quality is the welding current (Musa *et al.,* 2020). Therefore, this study investigates the effect of welding current variations on the tensile strength, hardness, impact energy, and the microstructural changes of medium carbon steel weld for industrial applications.

2. Materials and Method

The materials used in this study are mild steel electrodes (E6013), medium carbon steel rod, grit papers, and etchant. The chemical analysis of the medium carbon steel was carried out using a computerized mass spectrometer at Nigeria Machine Tools Industry, Oshogbo, Osun State-Nigeria. The chemical composition is presented in Table 1.

Table 1: Chemical composition of medium carbon steel

Chemical Analysis (%)										
C	Si	Mn	P	S	Cr	Mo	Ni	Cu	Co	Fe
0.332	0.132	0.453	<0.005	<0.003	0.081	<0.005	0.112	0.256	<0.002	98.619

2.1. Sample Preparation

The sample preparation was done based on the American Society for Testing and Materials (ASTM) standard to assess the effect of the current variation of medium carbon steel weldment using the shielded metal-arc welding process. The samples were first cut based on the standard test sample for tensile testing, impact, and hardness testing. The faces of each of the samples were cleaned properly and

smoothened before the welding to ensure a sound weld joint.

2.2 Experimental Method

2.2.1 Tensile test

Tensile test of the prepared welded steel rod and the unwelded samples was carried out using a 500KN Denison universal tensile testing machine, model number T4282, at the Department of Mechanical Engineering, Ahmadu Bello University, Zaria. The specimens have a cylindrical cross-section with a 20mm diameter. The tests were performed by first marking the gauge length of 80mm with the aid of a marking punch. The two ends of the specimens were then clamped into the upper jaw and the lower cross head which is static and the applied load is recorded by the load cell. During the test, the load was increased gradually until a fracture occurred. The maximum loads and extension were recorded at failure by the load cell and the extensometer respectively.

2.2.2 Impact Test

The impact test was performed using the Izod impact testing method. The test specimen was prepared by making a V-notch at the center of the specimen to serve as a stress concentrator. The specimen was then clamped to the vice on the machine with the V-notch facing the pendulum hammer. The pendulum was raised to a certain height and the gauge was set at zero before it was released. The energy absorbed in breaking the specimen was then taken and recorded. The dimensions of the test specimens were 70mm in length and l3.2mm in diameter.

2.2.3 Hardness Test

Hardness testing of welded joints and HAZ was performed using Rockwell Hardness Testing Machine. The specimens were first properly cleaned to remove any forms of dirt or oxides from the surface, and then placed on the anvil of the machine, and slowly turned the handwheel until the specimen was raised to touch the diamond indenter and the digital dial reads zero. A hardness test was conducted along the weld zone axis, at 2mm intervals from the fusion line to ensure that the parent material, heat-affected zones, and weld zone were captured. Rockwell hardness scale A was used with a minor load of 10kgf and the major load of 60kgf. The Rockwell hardness numbers were then read directly from the dial and the same process was repeated for the rest of the samples.

2.2.4 Microstructural Examination

The sample from the individual specimen was subjected to metallographic sample preparation processes starting from grinding, polishing, and etching. The grinding process was performed to obtain smooth surfaces of the specimen, using grit papers of different grit sizes. The rough grinding was done using grit papers of 150, 400, and 600 sizes while the fine grinding was achieved using grit paper of 800 and 1200 sizes. After grinding, polishing was carried out to further smoothen the surface to achieve a perfect mirror-like surface. This was accomplished using an electrically rotating polishing cloth on a polishing machine. To control heat generation during polishing and to avoid change in microstructure due to the generation of heat, alumina (Al_2O_3) was used as a polishing compound. The specimens were moved on the polishing machine in a direction opposite to the direction of the rotating disc until a mirror-like surface is achieved. The polished specimen was then etched using 2% Nital. This operation was done by dipping cotton wool into the etchant and swabbing the damp cotton wool across the specimen surface. The etched specimens were immediately put into water to control the action of the etchants and prevent the specimen from over-etching or damaging.

The etched specimens were then placed under the metallurgical microscope at a

magnification of x100 and the microstructures were observed, viewed, and captured.

3. Results and Discussion

3.1 Tensile strength result

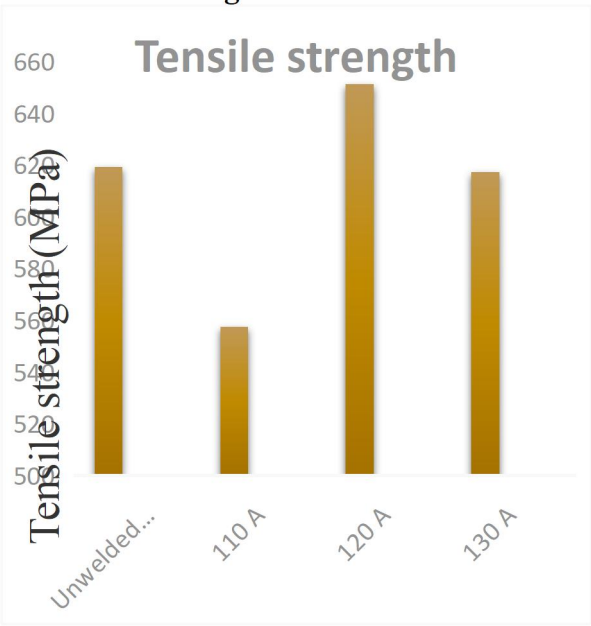

Figure 1: Tensile strength of unwelded and welded metal at different welding currents

The result of the tensile strengths of the weld and unwelded metal at different welding currents is presented in Figure 1. It can be seen that the tensile strength of the base metal (unwelded) is 619.25 MPa. At the welding current of 110 amps, the tensile strength of the weld metal is 557.36 MPa. The lower tensile strength observed at the welding current of 110 amps can be attributed to the lack of proper weld penetration due to low heat energy input, thereby making the weld to be very brittle and failing without any appreciable plastic deformation during tensile testing. At the welding current of 120 amps, the tensile strength increased to a maximum value of 651.17 MPa, indicating that the heat energy is enough to produce full weld penetration and sound weld joint. As the welding current increased further to 130 amps, the cooling rate becomes slower due to the increase in heat energy input into the weld joint, leading to the formation of coarse ferrite and pearlite structures, hence, reducing the tensile strength to 617.36 Mpa.

3.2 Impact energy results

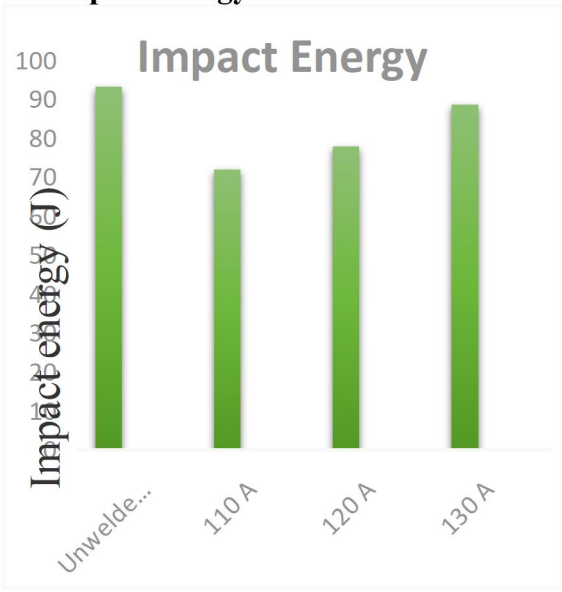

Figure 2: Impact energy of unwelded and welded metal at different welding currents

The impact energy results shown in Figure 2 indicate that the welds have lower impact energy as compared to that of the unwelded metal. The decrease in the impact energies of the weldment is due to the formation of brittle structures at the weld joint after welding, particularly at a low welding current. As the welding current increase from 110 to 130 amps, the impact energy increases from 71.96 to 88.5 J. This is due to an increase in the ductility of the welds as the structures become coarser.

3.3 Hardness results

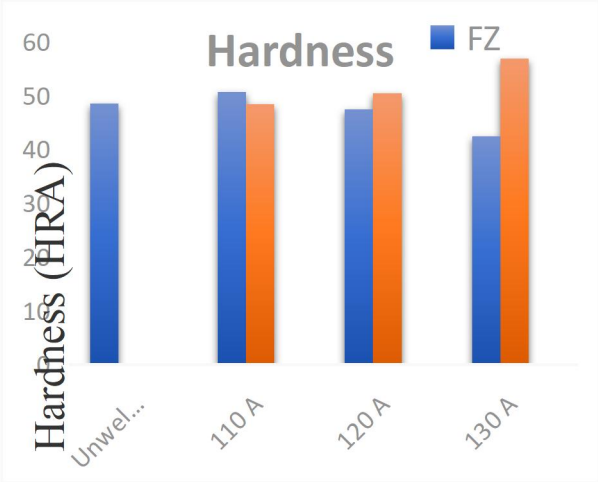

Figure 3: Hardness values of the weldment at the fusion and heat-affected zones at different welding currents

Figure 3 shows the hardness values of the weldment at the fusion and heat-affected zones with different welding currents The hardness values at the fusion zone of the weldment decrease gradually as the welding current increases from 110 A to 130 amps. The highest hardness value of 50.7 HRA was obtained at a welding current of 110 amps which is slightly above the hardness of the unwelded metal of 48.5 HRA. The hardness values at the welding currents of 120 and 130 amps are 47.4 and 42.43 HRA respectively. This decrease in the hardness as the welding current increases is because the weld structures become coarser and soft as the heat energy input is higher due to the high welding current. At the heat-affected (HAZ), the hardness appears to take the opposite trend to that of the fusion zone. As can be observed from Figure 3, the hardness at the HAZ increases gradually as the welding current increases. This is because as the welding current increases, the heat energy input into the fusion zone increase, and the cooling rate decreases. Hence, the adjacent heat-affected zone cools relatively faster, leading to the transformation of more austenite into martensite structures within the zone, making it more brittle and harder. The microstructural examinations further explained the structural transformation that occurs during the heating and cooling processes in this zone as the grain sizes are more refined than that of the fusion zones.

3.4 Microstructural examination result

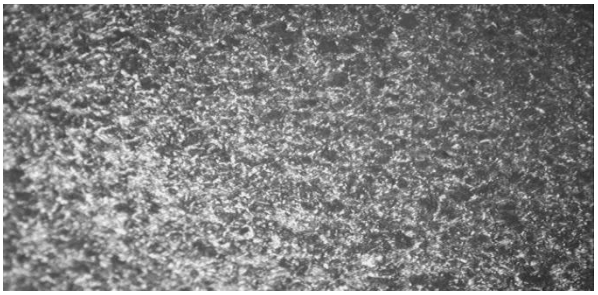

Plate 1 Microstructure of the parent metal specimen (x100)

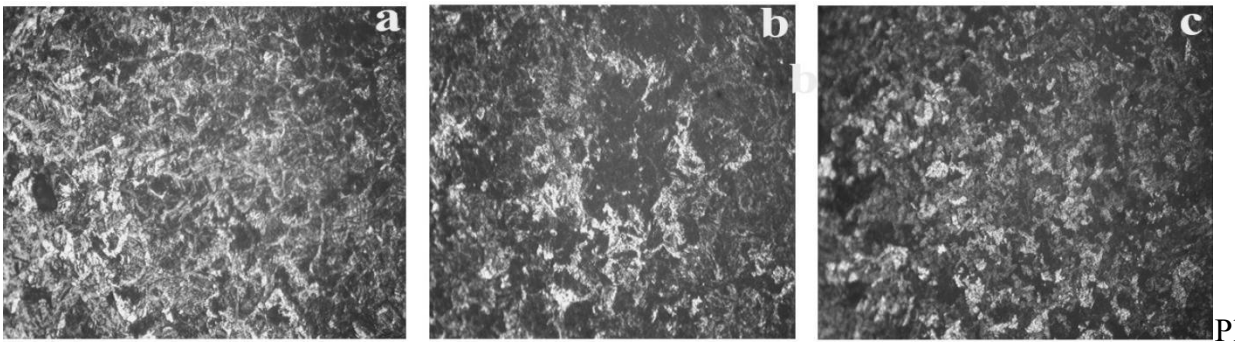

Plate 2: The microstructure of the welded metal samples at (a)110A (b)120A (c)130A (x100)

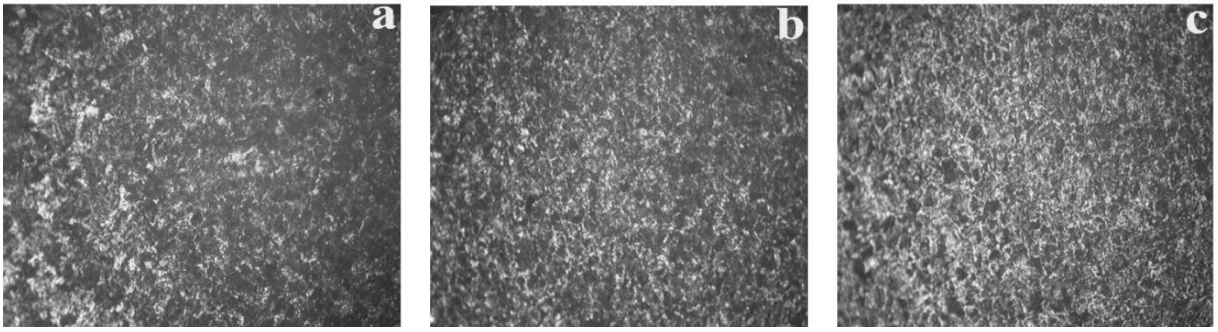

Plate 3: The microstructure of the heat-affected zone at (a)110A (b) 120A (c) 130A (x100)

Plate 1 shows the micrograph of the as-received sample (unwelded) which reveals predominantly fine pearlite grains (black portion) distributed in a ferrite matrix (white portion) which indicates the original microstructure of the base metal before welding.

Plates 2(a-c) show the microstructures of the weldment zone. As can be seen in the micrographs, the microstructures revealed coarse pearlite grains (black portion) distributed in a ferrite matrix (white). The pearlite becomes more pronounced as the current increases indicating a slow rate of cooling. At 130A, the pearlite structures tend to fragment and become saturated within the ferrite structures. Plates 3 (a-c) show the microstructures of the heat-affected zones, from the Plate, the microstructures revealed fine pearlite structures distributed within the ferrite matrix at all the welding conditions. The refined structures at the heat-affected zones of the weld were due to the increase in the cooling rate at those points.

4. Conclusion

From the results of mechanical and microstructural study obtained in this work, the following conclusions were made;

1. The quality of the weld joint produced is greatly affected by the welding current used to perform the welding.
2. The maximum tensile strength of 651.17 MPa is obtained at a welding current of 120 amps, and the maximum hardness of 50.7 HRA was achieved at a welding current of 110 amps. While for the impact energy, the unwelded metal gave the highest impact energy as compared to the welded metal at the different welding current conditions.
3. The microstructural examination shows coarsening of grains as the welding current increases from 110 to 130 amps with more pearlite structures.

References

Chen, F. F., Xiang, J., Thomas, D. G., & Murphy, A. B. (2020). Model-based parameter optimization for arc welding process simulation. *Applied Mathematical Modelling*, *81*, 386-400.

Dwivedi, D. K. (2022). Brazing, Soldering, and Friction Stir Welding. In *Fundamentals of Metal Joining* (pp. 223-232). Springer, Singapore.

Guiraldenq, P., & Duparc, O. H. (2017). The genesis of the Schaeffler diagram in the history of stainless steel. *Metallurgical Research & Technology*, *114*(6), 613.

Khana, O.P. DRT (1999). "Material Science and Metallurgy" Dhanpat Real Publication (P) Ltd, New Delhi.

Mohammed, R.A., Abdulwahab, M., and Dauda, E.T. (2013)." Properties Evaluation of Shielded Metal Arc Welded Medium Carbon Steel Material"*, International Journal of Innovative Research in Science, Engineering and Technology, 2*(8), pp. 3351 - 3357

Musa, A. A., Dauda, E. T., Bello, K. A. (2020). Influence of TIG Process Parameters on the Microstructure and Hardness Property of AISI 430 Ferritic Stainless Steel Welds using Response Surface Methodology Approach. *Nigerian Research Journal of Engineering and Environmental Sciences* 5(1), pp. 239-252

Nutalapati, S., Azad, D., & Naidu, G. S. (2016). Effect of Welding Current on Welding Speed and Ultimate Tensile Strength (UTS) of Mild Steel. In *IOP Conf. Series: International Journal of Mechanical Engineering and Technology (IJMET) Volume* (Vol. 7, pp. 156-176).

Syambabu N., Azad, D. and Swami, G. N. (2016). Effect of Welding Current on Welding Speed and Ultimate Tensile Strength (UTS) of Mild Steel. *International Journal of Mechanical Engineering and Technology (IJMET),* 7(5), pp.156 –176.

Tewari, S., P., Ankur, G., and Jyoti, P. (2010*). "*Effect of welding parameters on the weldability of material", *International Journal of Engineering Science and Technology:* Varanasi-221005, U.P., INDIA 2(4), Pp512

Tomaz, I. D. V., Colaço, F. H. G., Sarfraz, S., Pimenov, D. Y., Gupta, M. K., & Pintaude, G. (2021). Investigations on quality characteristics in gas tungsten arc welding process using artificial neural network-integrated with genetic algorithm. *The International Journal of Advanced Manufacturing Technology*, *113*(11), 3569-3583.

Weman, K. (2003). Welding processes handbook. New York, NY: CRC Press LLC, ISBN 08493-1773-8.

William, A., Bowditch., and Kevin., E., B. (1991). "Welding Technology Fundamental", Good heart-Wilcox Company Inc., USA,

NMS-TP013

Reduction of the Size of an Integrated Steel Plant by Using a Designed Simulated Tool

OCHERI Cyril,[1]TCHOTANG Théodore[1] , KANMOGNE Abraham[1] , TAPAMO Hippolyte M[1]NJOKU R.E[1] and A.D **OMAH[1]**

[1]Department of Metallurgical and Materials Engineering, University of Nigeria, Nsukka, Nigeria

[1]Department of Industrial and Mechanical Engineering, National Advanced School of Engineering of Yaounde (NASEY), Cameroon

[1]Department of Computer Science, University of Yaounde 1, Yaounde, Cameroon

cyril.ocheri@unn.edu.ng, tchotang@yahoo.com, abraham_kanmogne@yahoo.fr,htapamo@gmail.com

Corresponding Author : **OCHERI Cyril**

Email: cyril.ocheri@unn.edu.ng

Phone no: +2348051793922

ABSTRACT

The investigation on the reduction of an integrated steel plant using a generated simulated tool of MATLAB software developed using the graphical user interface development environment. (GUIDE). Three components—input, store selection, and outcome made up the model. The cost to set up shops in US dollars, the plant's capacity in tons, the amount of raw materials needed, the cost of hiring staff, the amount of net sales, and the net profits are all included in the result pane. (USD). Three factors the number of employees, the Net Profit Margin that could also be accrued from the Net Sale, and the Net Profit Margin that could also be accrued from the Net Income were used to conduct the financial analysis of the plant. The created data and parameters were utilized to generate several graphs for each of the selected inputs after the planned model was run. A reduction of 5% was applied as an interval variation, ranging from 100% to 5%. The output from the graphs demonstrates the facility's capacities for shrinking the size of the shops for an integrated steel mill based on additional characteristics. Based on the requirement to reduce shop sizes for efficient steel plant establishment and operations, conclusions and recommendations were drawn. The sinter plant, blast plant furnace, and basic oxygen furnace are the shops that were modeled. The percentages of 100%, 50%, and 5% in the research findings for the reduction processes show that the outcomes decreased gradually as the choice of input parameters was imputed. The total cost of establishing each of these three companies in USD was calculated as follows: 5% = 100% = 4, 223, 769, 753,20; 50% = 2,111, 884,876.60; and 5% = 211,188,487.66; plant capacity for 100% = 221,819,070 tonnes. The raw materials in tonnage for 100% are 3,868, 640,358.00, 50% are 1,934, 320, 179, and 5% are 193, 432,017.90. The remuneration of staff in USD for 100% is 14, 218, 042.40, 50% are 7,109, 021.20, and 5% are 710, 902.12. The total net sales in USD are 5,841, 242 657.00, 2,920, 621, 329, and 292,062,132.90, respectively, at 100%, 50%, and 5%.The net profit at 100% is 72.12%, at 50% it is 34.4%, and at 5% it is 3.44%. The rate of investment at 100% is 60.91%, at 50% it is 30.45, and at 5% it is 3.05%. The breakeven point at 100% is 64.63%, at 50% it is 32.32, and at 5% it is 3.23. The number of employees per shop at 100% is 3468, at 50% it is 1734, and at 5% it is 173.

Keywords: Reduction , Size, Modeling steel plant and Simulation

1.0 INTRODUCTION

The primary objective of the research was to use a design simulation tool to reduce the size of down an integrated steel production. The methods permit the reduction of the size of an existing steel plant. The construction of a new plant depends on the preferences of the stakeholders using the following factors and criteria, which include among others ; the installation cost (USD), plant capacity (tonnes/annum), necessary raw materials (tonnes/annum), and the remuneration of the workers to be hired (USD) [1]. The things that could be sold are known as Net Sale (USD), while profits are expected to be created, which is known as Net Profit Margin (Percent), rate of returns on investment (percent), break-even (percent), and the number of staff. Simply by imputing the percentage choice for the processes can the required capacity be calculated. In order to create a manageable steel factory, this research focused on shrinking the size of an integrated steel plant. The process was modeled, and a virtual tool was used to construct a plant that can produce liquid steel. The money made from this facility could then be reinvested in the economy to stimulate growth, create jobs for the teeming youth population, and create riches. The nineteen (19) shops/units that make up the modeled and simulated steel plant . [2] . The model was designed to provide for the essential impute by adjusting the fraction of option and then delivering all appropriate possibilities.

2.0 MATERIALS

2.2 Designed Simulated Tools for the Reduction of an Integrated Steel Plant

MATLAB software and a Graphical User Interface Development Environment will be used as the research's primary tool. The approach is based on a tool that is meant to mimic and reduce an integrated steel mill. For the simulation of the model, the source code was created. The integrated steel plant depicted in the planned model is made up of several shops and modules. The following elements make up the model:

Sinter plants, coke oven batteries, power plants, wire rod mills, billet mills, medium section and structural mills, oxygen plants, lime calcination plants, blast furnaces, etc. Shop for Forging and Fabrication, Foundry Shop m) Pattern Making Shop , Tool and Machine Repair Shop Rubberizing Shop, Carbonic Acid Plant, Aluminum Silicate Refractory Plant, Tar Bonded Dolomite Plant, Basic Oxygen Furnace Plant, and (o) Rubberizing Shop.[3]. A model of an integrated steel plant can be shown in Figure 1. Utilizing MATLAB's Graphical User Interface Development Environment, the created model was further improved and used as a simulation tool for reducing the capacity of steel factories that were either already in existence or were being developed.

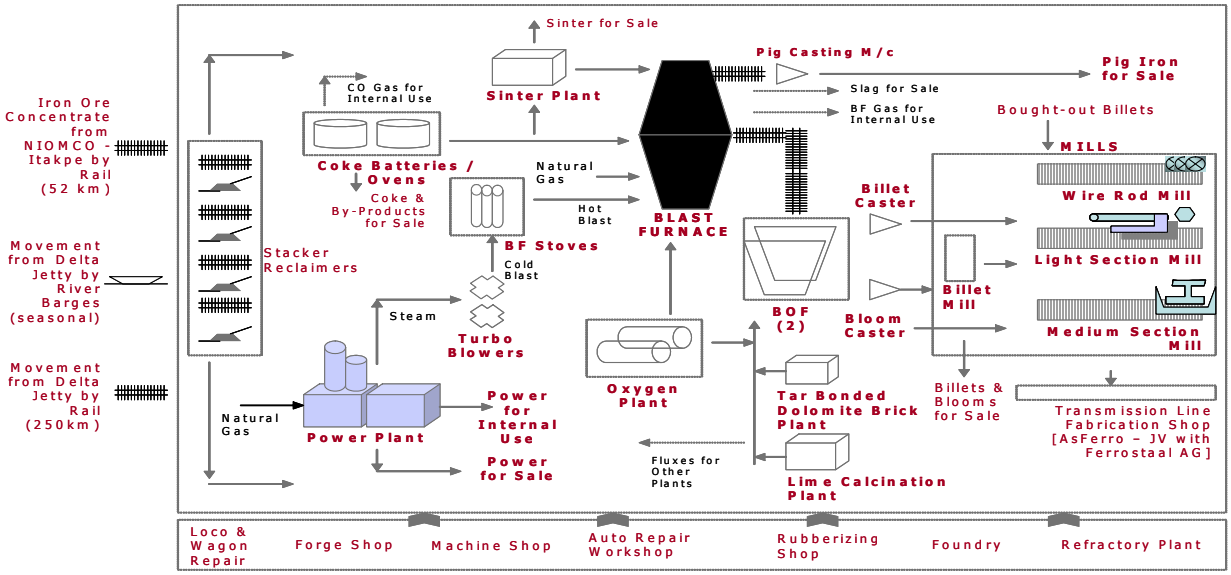

Figure 1: Design of a graphic Model for an Integrated Steel Plant

2.2 SOFTWARE: MATLAB

The numerical computing environment and programming platform MATLAB has a number of models. It combines compute, visualization, and programming to create a user-friendly platform to handle numerous technical computing concerns. MATLAB is the most straightforward and well-liked programming environment for engineers and scientists thanks to certain exceptional features. The decision to use the MATLAB program for the modeling and simulation of the Metallurgical and Materials Process Engineering Application was taken with a focus on its particular features and qualities with specific references to the design of an integrated steel plant.

Vector and matrix calculations are handled by the software MATLAB. The ability to deal with vectors and matrices is implied by the name of the website, matrix laboratory. Although this variable can alternatively be a matrix or a vector, MATLAB enables you to work with complex variable functions. High-performance numerical computing and visualization are both capabilities of the software program MATLAB. It offers an interactive setting with a vast array of integrated functions for technical computation, graphics, and animation. The best part is that its high-level programming language also offers simple extensibility. Matrix Laboratory is the name of the program [4]; The built-in functions of MATLAB are helpful tools for computing in linear algebra, data analysis, signal processing, optimization, solving ordinary differential equations (ODEs) numerically, quadrature, and many other types of scientific computation. Most of these functions are based on modern algorithms. For 2-D and 3-D graphics, as well as for animation, there are numerical functions. MATLAB now offers an external GUI to execute these programs inside MATLAB for individuals who can't live without their FORTRAN or C functions.

However, the user is not limited to the built-in functionalities; he can develop his own functions in the MATLAB language. Once defined, these functions behave exactly like built-in functions. The MATLAB language is incredibly simple to use and learn.

2.2.1 Graphical User Interface Development Environment (GUIDE)

:Applications for the main graphical user interface include MATLAB core functions may be used much more quickly and simply than Borland C previously. It's crucial to emphasize the adaptability of its toolboxes as well. It seems simple to use the instrument control toolbox, which is operated through the machine's serial port and handles all acquisition and control functions. [5] .

2.3 Algorithm of an Integrated Steel Plant

The modeling processes, the Start program, and the input Percentage of the System Designed start. enter the per-tonne cost of the basic ingredients.. Put the proportion in decimal form, Calculate the establishment cost in USD, determine the plant's capacity. (in tonnes per annum), Determine the necessary raw materials, Calculate the staff's annual salary in accordance with the percentage. Calculate the annual volume of sellable goods, Determine the Revenue Generating, Determine the Profit, Do the Net Profit Ratio calculation. Calculate the break-even point and the rate of return on investment.[6].

Lastly, output Establishment Cost, discharge the new capacity, Output the New Raw Materials, Output the Staff, Output the Tonnes of Saleable Goods, Output the Revenue Generated, Output the Expected Profit, Output the Net Profit Ratio, Output the Rate of Return on Investment, Output the Break-Even Point, and the Program is Stopped Through the End Program. Figure 2 shows a flow chart that illustrates the method. demonstrates the model built for the simulation generated for this research effort. .The model was created for all 19 of the modeled shops, but for the purposes of this research, only three shops—the sinter plant, the blast furnace plant, and the basic oxygen furnace (BOF)—will be discussed because they are all modelled and simulated using the same methodology as the other shops.

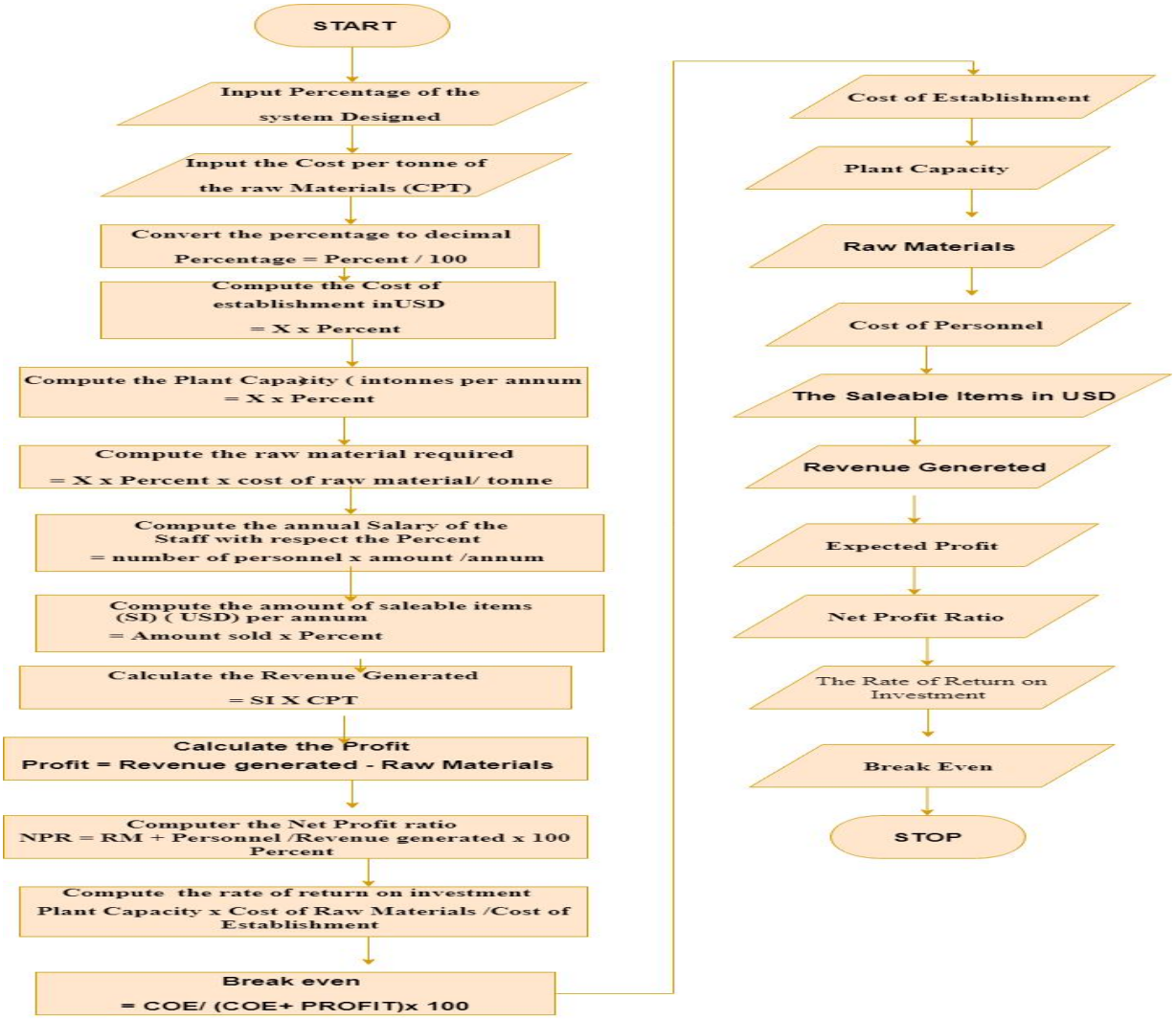

Figure 0: Algorithm of an Integrated Steel

3.0 METHODS

The planned model, which in this study's endeavor is an integrated steel mill, is made up of 19 shops. The model was divided into three parts: the input pane, shop selection pane, and result pane. The sinter plant, coke battery oven plant, power plant, billet mill, wire rod mill, light section mill, medium section mill, and structural mill are all included in the shop section pane. There are also oxygen plant, lime calcination plant, blast furnace, forge and fabrication shop, foundry shop, pattern making shop, machine and repair tool shop, carbonic acid plant, and aluminum silicate refractive plant. The staff per shop number, current cost per tonne, and percentage choice are all included in the entry window.

The Ajaokuta Steel Plant in Kogi State and the Delta Steel Plant in Aladja, Delta State, both have the capacity to produce 1.3 million metric tonnes of liquid steel yearly. The two integrated steel plants that are currently in operation in Nigeria are the Ajaokuta Steel Plant and the Delta Steel Company Limited. 1.3 metric tonnes of liquid metal can be produced annually by

both steel plants. MATLAB software application was used to create, model, and simulate the process model. GUIDE stands for Graphical User Interface Development Environment. (GUIDE).

Data from the Ajaokuata Steel Plant's current integrated system was gathered for the research project. All of the entered values and parameters were modelled with percentage options ranging from 100% to 5% with a 5% interval. The research work's graphs clearly show how the reduction operations were carried out to create or construct a manageable integrated steel factory. Figure 2 shows a demonstration of the designed model, which consists of three panes. The parameters are imputed differently depending on how the plant to be floated reduced or established. [7]

Figure 3: A demonstration of the three-pane model

3.1 Establishment of a Sinter Plant and the process of Sinter production

During the sintering process, which is facilitated by heat created within the aggregate itself as a result of solid fuel combustion, fine mineral particles are agglomerated into a porous, lumpy mass. Sintering, a pre-treatment step in the iron-processing process, involves combining fluxes, fine iron ore particles, and secondary iron oxide waste through fire. (collected dust, mill scale, etc.). (lime, limestone, and dolomite). To allow the flow of hot gases while the blast furnace is in operation, the particles must aggregate[8].[8]. The generated model is shown in Figure 4, along with the results obtained after executing 5% of the choice percent imputation on the input pane, showing the modeled stores on the shop selection pane and the imputation results on the result pane. Six values were also displayed in the input pane as the number of workers required to operate the shop at a 5% imputation.

Figure 4: The model of the Sinter Plant with 5% inputted

3.2 Blast Furnace Plant

In a blast furnace, iron oxides are reduced and converted into liquid iron, or "hot metal." The interior of the blast furnace is lined with refractory bricks and is a massive steel stack. Hot air is pushed into the bottom while iron ore, coke, and limestone are placed at the top [9]. Blast furnace: a device used to remove iron The blast furnace can extract iron because carbon can displace iron. Because it is more affordable, this approach is more effective than electrolysis. [9]. For iron to be extracted from its ore, three things are required.Iron ore, haematite, limestone (calcium carbonate), coke, that is primarily composed of carbon, and haematite, which frequently contains sand with iron oxide, Fe_2O_3, constitute the charge. blast furnace, a huge chimney, is where the charge is put. The blast furnace has a masonry interior that is fireproof and around 30 meters high. The bottom is blasted with hot air. There are numerous reactions that happen before iron is finally formed. Liquid Molten Metals, Pig Iron Casting, and Blast Furnace Slag are some examples of blast furnace products [10].

The generated model is shown in Figure 3 together with the outcomes obtained after executing 5% of the choice percent imputation on the input pane, showing the modeled stores on the shop selection pane and the imputation results on the result pane. The input pane also showed three numbers representing the number of employees needed to run the shop at a 5% imputation.

Figure 5: The model of the Blast Furnace Plant with 5% inputted

3.3 Basic Oxygen Furnace Plant

The interesting process of making the magic alloy involves complex metallurgical reactions and processes, starts in the earth's crust, and demands a high level of technological proficiency. Iron ore is the raw material, while steel is the finished product, which is hard and shiny. With a capacity of 10 million tonnes per year, Tata Steel's Jamshedpur factory, which started making steel in India in 1912, is today one of the biggest integrated steel-making facilities in the entire nation. [11]. The production of red-hot molten steel in all of its different forms and the steel's transformation into the glittering symbol of industrial progress by looking inside the modern Tata Steel complex, which has undergone substantial revisions from its original design. Iron has been used by humans to make tools, swords, and ornaments for more than 3,000 years. Iron is a part of contemporary society and is known as the metal of antiquity. Iron was once more expensive than gold, that much is true.

Figure 6: The model of the Basic Oxygen Plant with 5% inputted

4.0 RESULTS AND DISCUSSION

4.1 Establishment of a Sinter Plant

Table 1 displays the results of the modeling and simulation of the sinter plant. This processing facility handles the chosen percentage of 100% to 50% and 5% imputation was carried out with 5% interval changes. It is intended by implications that the parameters for the cost of establishment, plant capacity, raw materials, labor costs, net sales, net income generated, net profit margin, rate of returns, break-even, and the number of employees per shop have been reduced from their original imputations. The graphs in figure 7 below were made using the calculated numbers. (a-g). All of the characteristics and results of the created modeling's successful testing indicated that the model was capable of performing crucial jobs. The calculated results gave the sinter plant the variable it needed to operate, and the cumulative results gave the integrated steel plant the variable it needed to operate.

Table 1 The information received by varying the parameters that were imputed for the sinter plant

S/NO	ITEMS	UNIT	100%	50%	5%
1	Cost of Establishment	USD	300,000,000.00	150,000,000.00	15,000,000.00
2	Plant Capacity	Tonnes	88,000.00	44,000.00	4,400.00
3	Raw Materials	Tonnes	378,767,150.00	189,383,575.00	18,938,357.50
4	Salary of Personnel	USD	99,976.80	49,988.40	4,998.84
5	Net Sale	USD	491,799,263.40	245,899,631.70	24,589,963.17
6	Net Income	USD	113,132,090.00	56,566,045.00	5,656,604.50
7	Net Profit Margin	%	23	11.5	1.15
8	Rate of Return	%	37.6	18.8	1.88
9	Break-Even	%	72.6	36.3	3.63
10	Personnel Per Shop	Number	120	60	6

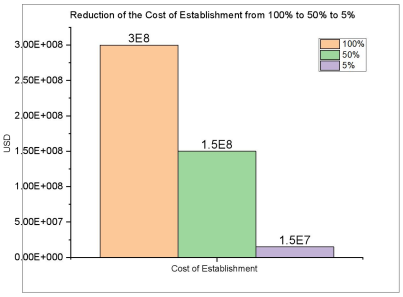

(a) Cost of Establishment

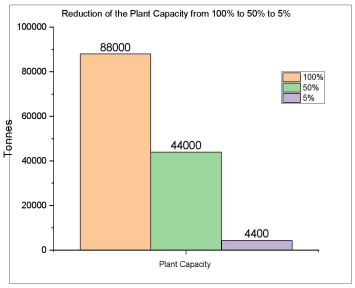

(b): Plant Capacity

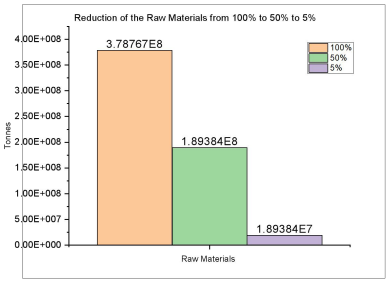

(c) Raw Materials

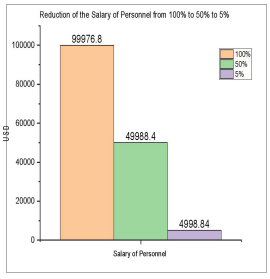

(d) Salary of personnel

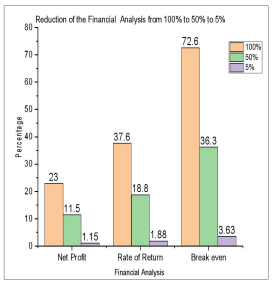

(e) Net sale & Net income

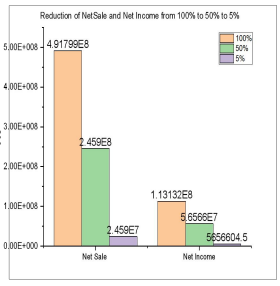

(f) Financial Analysis

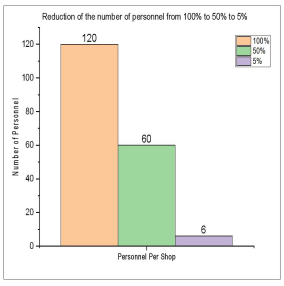

(g) Personnel of the Shop

4.2 Blast Furnace Plant

Table 2 lists the results of the modeling and simulation of the blast furnace plant, including the values obtained after choosing an imputation range of 100% to 5% and applying 5% interval variations. This phrase describes how the results for all the modeled parameters including the cost of establishment, plant capacity, raw materials, labor costs, net sales, net income generated, net profit margin, rate of returns, break-even point, and the number of employees per shop increase as the number of imputations increases. After imputed values of 100% to 50% and 5% of the values on the basis of percentage option, the outcomes of the modelled and simulated values were generated. Figure 8's bar charts were created using the values that were generated.(a-g). The assessments of the numerous bar charts revealed that, depending on the selected percentage imputations, the annual capacity of the selected parameters decreases. The developed modeling was successfully tested, and all of the parameters and outcomes showed that the model could carry out essential tasks. The obtained results added up for the operation of a combination steel plant and gave the necessary variable for the operation of a blast furnace plant.

Table 2: Data from the variation of parameters estimated for the blast furnace plant

S/NO	ITEMS	UNIT	100%	50%	5%
1	Cost of Establishment	USD	333,000,000.00	166,500,000.00	16,650,000.00
2	Plant Capacity	Tonnes	1,350,000.00	675,000.00	67,500.00
3	Raw Materials	Tonnes	378,767,140.00	189,383,570.00	18,938,357.00
4	Salary of Personnel	USD	9,997.80	4,998.90	499.89
5	Net Sale	USD	491,799,260.00	245,899,630.00	24,589,963.00
6	Net Income	USD	113,032,160.00	56,516,080.00	5,651,608.00
7	Net Profit	%	23	11.5	1.15
8	Rate of Return	%	17.4	8.7	0.87
9	Break-even	%	85.2	42.6	4.26
10	Personnel Per Shop	Number	60	30	3

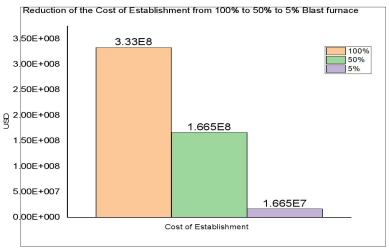

(a)Cost of Establishment

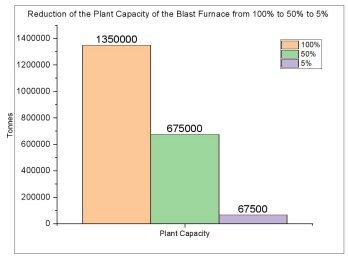

(b) Plant Capacity

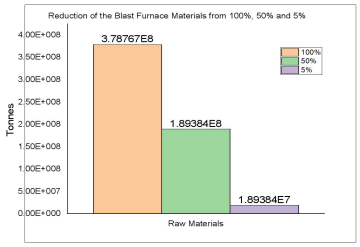

(c) Raw Materials

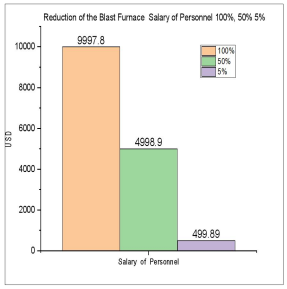

(d) : Salary of personnel

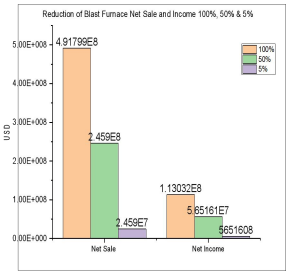

(e) Net sale & Net income

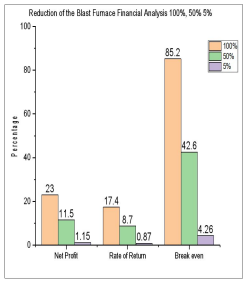

(f) Financial Analysis

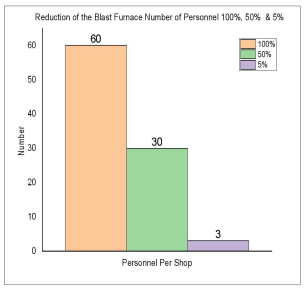

(g) Personnel per Shop

4.3 Basic Oxygen Furnace Plant

The results of the modeling and simulation of the basic oxygen furnace plant are shown in Table 3. The results obtained in this approach were calculated using a 100-5% imputation choice percentage with 5% interval fluctuations. By implications, it is meant that as the imputations are reduced, the results for all the modeled parameters such as the cost of establishment, plant capacity, raw materials, labour costs, net sales, net income generated, net profit margin, rate of returns, break-even point, and the number of employees per shop are also reduced. In Figure 9, the input pane shows the generated model, the results of the 5% choice percent imputation, the shop selection pane shows the modeled stores, and the result pane shows the imputation's outcomes.(a-g). Six values were also displayed in the input pane as the number of workers required to operate the shop at a 5% imputation. The generated modeling was successfully tested, and all the results and parameters indicated that the model was capable of performing crucial functions. A basic oxygen furnace plant's operating variable was provided by the determined outcomes, and an integrated steel plant's operating variable was provided by the accumulated results. After imputed values of 100% to 50% and 5% of the values on the basis of percentage option, the outcomes of the modelled and simulated values were generated. The results obtained were utilized to create bar charts, which showed how the annual capacity of the selected metrics decreased as the percentage imputations were reduced.

Table 3: Data from variations in the parameters that were imputed for the blast furnace plant

S/NO	ITEMS	UNIT	100%	50%	5%
1	Cost of Establishment	USD	476,666,660.00	238,333,330.00	23,833,333.00
2	Plant Capacity	Tonnes	1,300,000.00	650,000.00	65,000.00
3	Raw Materials	Tonnes	547,425,000.00	273,712,500.00	27,371,250.00
4	Salary of Personnel	USD	49,989.00	24,994.50	2,499.45
5	Net Sale	USD	999,861,215.40	499,930,607.70	49,993,060.77
6	Net Income	USD	452,486,204.40	226,243,102.20	22,624,310.22
7	Net Profit	%	45.2	22.6	2.26
8	Rate of Return	%	95	47.5	4.75
9	Break-even	%	51.4	25.7	2.57
10	Personnel Per Shop	Number	120	60	6

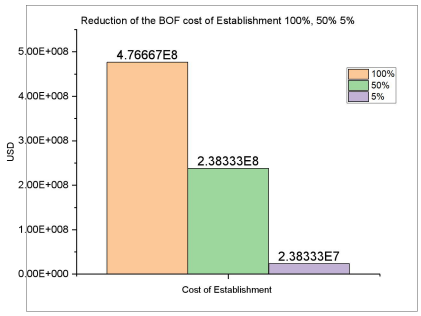

(a): Cost of Establishment

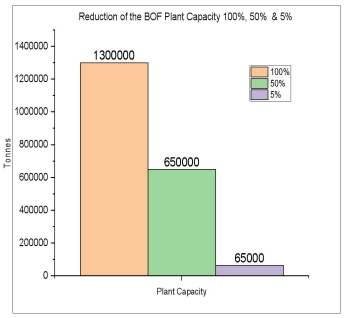

(b) Plant Capacity

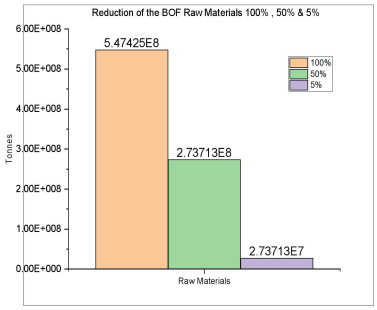

(c) Raw Materials

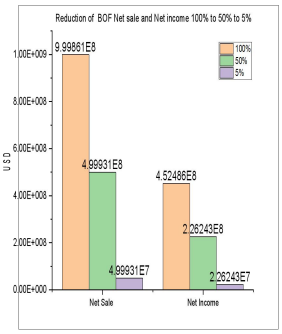

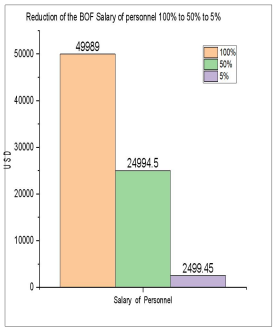

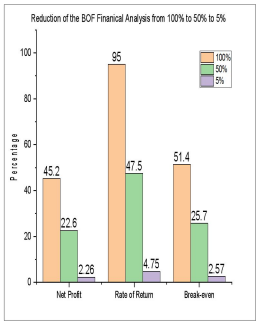

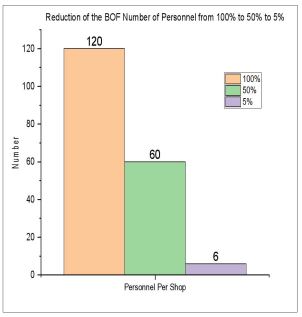

(d) Salary of personnel (e) Net sale & Net income (f) Financial Analysis (g) Personnel per Shop

5.0 Conclusion

An integrated steel plant's size was reduced using customized simulation tools and the MATLAB software with Graphical User Interface Development Environment (GUIDE). By adjusting the selected percentages of the imputations, the design allows for a reduction in the capacity of the various shops and units. The purpose of the research was to create a model for an integrated steel plant that could be operated based on the capabilities of the stakeholders and other people involved in the manufacturing of liquid steel. The model tools were created to give scientists, experts, and engineers very good opportunities and convenience for designing and establishing an integrated steel plant that could be managed with a view to determining the financial analysis in these three financial aspects: Rate of Return, Net Profit Ratio, and Break-Even. The capacity of the numerous shops/units, the requirements for raw materials, and the cost of setting up each shop/unit were all captured by the modeling. During this design, the demands and requirements of the personnel were also taken into consideration. In general, the stores and units are able to make money by selling created goods, which means that profits will be made from the sale of commodities that can be sold. Further research revealed that as long as the integrated steel factory is in operation, the Shops/Units will be able to provide a good rate of returns, Net profit margin, and break-even.

This translates to the fact that money will be made, jobs will be made, wealth will be created, and technology will be transferred based on the abilities of the people hired to carry out the manufacturing operations. In conclusion, the research was also done to introduce the main modeling and simulation procedures that are now used in the design and construction of a controllable steel plant. A proposal for the construction of an integrated steel plant to produce liquid steel was made. For the metallurgical and material processes, the modeling and simulation software application statuses were carried out.

Depending on the entered parameters into the constructed model, subsequently , this was intended to run at an operational steel plant with a liquid steel production capacity of tonnes per year. To achieve this production, all additional facilities and materials were constructed according to precise criteria known as choice imputation. The backdrop of the design and the research's goals are revealed through this study. An integrated steel plant's capacity, cost of construction, cost of raw materials, cost of labor, cost of saleable goods, revenue

generation, profitability, and financial analysis are summed up here.

REFERENCES

[1]llma,"Production Processes,"International Iron Materials Association, vol. 4, no. 3, pp. 12-23, 2016

[2] R. R. D. Klein, "Simulation Modelling and Health -Care Decision Making ","Medical Decision Making, p. 13; 347, 1993.

[3] C. P. Lopez, "MATLAB Graphical Programming Practical Hands-on MATLAB Solution", Springer Apress, pp 167, 2010.

[4] X. Youlin Yang Shuguang, "Simulation and Optimization of Chemical Process.","Beijing Chemical Industry, pp. 37(8): 35-38, 2008.

[5] Z. Chenchen, "Introduction of the useful industrial flowsheet simulation program, AspenPlus,"Power System Engineering, pp. 19(2): 56-58, 2003.

[6] M. L. B. Cai, "A software of Design and Simulation of the Chemical Engineering Process,"ChemCAD, Guangdong Chemical Industry, pp. (8) : 47-48, 2005.

[7] U.EPA, "Coke Oven Emission from Wet-Coal Charged By - Product Coke Oven Batteries," U.S. Environmental Protection Agency, and Research Triangle Park, North Carolina, 1985b.

[8] V. O. D. et.al, "Environmental Assessment of Coke By-Product Recovery Plant," EPA Report No. 600/2-79. Ind. Environm. Research Lab, U.S. EPA, Research Triangle Park, North Carolina, 1979.

[9] B. S. A. &. Linchevsky, " Iron and Steel Making,"Moscow Russian Federation, p. Mir Publication, 1983.

[10] J. Adigwe, "Raw Materials for Nigerian Iron and Steel Industry","Adigwe, J.F.C." Raw Materials for Nigerian Paper delivered at Delta Steel Aladja's 1st National Conference of NMS, pp. 18-20, 1983 [11] Isah, J.O. "Ajaokuta Steel Company Limited" Timely Completion of Nigeria Iron and Steel Projects the Key to Rapid Industrialization Ajaokuta Steel Project As A Case Study "," in 29th Annual Conference of the Nigerian Metallurgical Society (NMS), Ajaokuta, 2013.

NMS-TP014

DEVELOPMENT AND CHARACTERIZATION OF A HYBBRID BIO-COMPOSITE INSULATOR FOR ELECTRICAL/ELECTRONIC INSULATION APPLICATIONS.

A. D. Omah[1,3], F.C. Okeke[3], S. Edelugo[2,3],V.S. Aigbodion[1,3], E.O. Oji[1], C. Ocheri[1], P.O. Offor[1], C. C. Daniel - Mkpume[1], S.N, Ude[1], I.C. Ezema Ike-Eze[1] and B.A. Okorie[1].

[1]Department of Metallurgical & Materials Engineering, University of Nigeria, Nsukka, Nigeria.
[2]Department of Mechanical Engineering, University of Nigeria, Nsukka, Nigeria.
[3]African Centre of Excellence, ACE-SPED, University of Nigeria, Nsukka, Nigeria.
Corresponding Author: Dr. A.D. Omah
Email: augustine.omah@unn.edu.ng
Phone no: +2348033863639

Abstract
There is dearth of information in literature on the materials combination of agro-waste particulate and flakes in hybrid composite development for polymer composite insulator applications. Thus, this work examined the dielectric properties of hybrid composites using Breadfruit shell (BFS) and Palm Kernel Shell (PKS) as reinforcements. The reinforcing materials were milled into particulates/flakes and sieved into sieve grades of 500 µm for PKS and 2 mm flakes size for BFS. The BFS flakes used varied from 50wt% to 90wt% in increasing order, while the PKS particulates varied from 50wt% to 10wt% in decreasing order. The morphologies and microstructures of the composites developed were investigated using SEM/EDS. The polymer composites were subjected to dielectric test such as breakdown voltage, dielectric loss and dielectric constant. The effect of wt.% variation of the BFS flakes on the above mentioned properties was used as criteria for the evaluation of the composites. Optimal values for breakdown voltage and dielectric constant were obtained at 70 wt.% BFS flakes. Dielectric Loss had its optimum value at 50 wt.% The dielectric properties investigated increased with increase in BFS flakes; this implies that flakes addition enhanced the dielectric properties of the composites. All the composite samples showed minimal moisture content and water absorption capacity thereby making the produced insulators to be candidate materials for good electrical insulation both in outdoor and indoor applications. The results established that this hybrid polymeric based insulative materials developed, will find applications as electrical transmission insulator, circuit boards and other related engineering applications.

KEY WORDS: Composite, Hybrid, Insulator,

Introduction

Energy and electrical power are eventually used in all humans' day to day activities. The significant increase in the world population has resulted in high demand for electrical power. Although fossil fuel is one of the major sources of energy, it is fast depleting due to high consumption and fast increasing population [1]. Moreso, due to the production of greenhouse effects by fossil fuel, it places danger on global warming [2]. This can lead to the complete destruction of the ozone layer if nothing is done in the future as predicted by scientists. This has led to the innovation of clean, affordable and sustainable energy such as renewable energy resources [3]. Notwithstanding how electrical power is generated and transmitted to the final consumer is very vital. It is worth noting that as energy generation is important, appropriate energy distribution have great roles to play in the sector, which can be achieved with advanced materials. The transmission system consists of electric pole, electric wire and an insulator separating the pole and the wire. One of the reasons for the poor electrical power supply to final consumers in Africa especially Nigeria is due to poor distribution system. For instance, fall of electric poles, wires and insulators as well, along our roads.

Studies have also shown that major challenges in the energy sector especially in electricity transmission is the overloading of power grid due to higher demand for electricity than the delivery. A recent survey has it that over 70% of the Sub-Saharan population lack access to electricity; over 1.6 million women and children die from fumes released by indoor biomass stoves, and over 3.2% of sales are lost from power outages annually Lemma *et al*[4]. All these are indications that supply is far much lower than the demand for electricity, which calls for increase of power in the grid through the development of advanced materials for such purpose. Moreover, since the invention of electric light and transmission of power in the grid in the 19th Century by Thomas Edison, electricity has been transmitted via high tension poles, wires and insulators. The insulator separated the electrical poles from the electrical conductors (wires).

Insulators are device used on electricity supply network in order to support, separate or contain conductors at high voltages. Insulators been employed for power transmission have two main functions such as mechanical load - bearing for structure and at the same time provides sufficient electrical insulation between the energized conductor and the supply pole or circuit board. [5].

There is an increased demand for insulators in electrical industries, and the availability of agro waste materials (plant and animal waste) are at high rate which if not properly disposed affect the environment and human health. Since the classes of reinforcing materials previously used are non-sustainable materials as they are not environmentally friendly; in addition, sourcing and production of such synthetic materials are costly, difficult, and required sophisticated equipment to prepared them. Therefore, with such reinforcing synthetic materials, the global aim of sustainable engineering at low cost cannot be achieved. Thus, this increased demand for new insulating materials with higher specification led to the idea of combining the disposable component of harvested agricultural products, referred as agro-waste materials to form a hybrid bio-composite. The use of agricultural residues to manufacture composite appears to have environmental and economic advantages [6].

Ceramic materials like porcelain are mostly used for the electrical transmission insulators due to their high thermal resistance, high operational temperature, corrosion resistance and good hardness; however, they are difficult to process. The use of polymer insulative materials for electrical transmission insulator can avert the challenges faced by ceramic materials due to their excellent properties which include: light weight, chemical resistance, flexibility, easy processibility, low cost, high breakdown strength etc. [7].

However, polymer insulators for electrical power transmission also have some shortcomings. Thus, one of the common ways to overcome such polymers' shortcomings is by incorporation of foreign bodies into the polymer matrix which helps to modify the polymer matrix and tailor their properties to desired properties [8]. El – Wazery *et al* [9] achieved high mechanical properties by introduction of glass fibre into polyimide. Also, much effort has been made to develop the composite materials such as polymer - ceramic composites in order to merge both properties of the materials for properties improvement [10].

One of the polymers used for electrical power transmission insulator for both insulation sheath and insulation core rod is epoxy resin [11]. But the drawbacks observed in epoxy resin as based material in the design of polymer composite insulator often led to loss in dielectric strength and leakage current. Moreso, using glass fibre as a reinforcing phase might result to low interfacial bond and low mechanical strength[12]. These classes of reinforcing materials are non-sustainable materials since they are not environmentally friendly. In addition, sourcing and production of such synthetic materials are costly, difficult, and required sophisticated equipment to prepared them. Therefore, with such reinforcing synthetic materials, the global aim of sustainable engineering at low cost cannot be achieved. Therefore, the motivation that led to this study are in three categories:

i. To develop polymeric based insulative materials to replace currently used ceramic based insulative materials for electrical power transmission insulator
ii. To address the challenges associated with polymeric materials as outlined above
iii. To use sustainable materials in achieving i and ii above to ensure development of sustainable engineering materials

The above three-point objectives are aimed to be achieved in this study by adding different bio particles to a polymer. This method leads to the production of **HYBRID BIOCOMPOSITES.** This method synergistically integrates the advantages of polymers and the bio particles; and thus, dielectric properties of the composites can be improved by properly selecting the fillers, their shape, size and concentration. The fillers for the biocomposites include: palm kernel shell particles (PKS) and bread fruit shell flakes as sustainable materials to replace glass fibre in the epoxy materials currently in use.

PKS is an agro-waste product obtainable in the production of palm oil. It has been used toimprove various mechanical and thermal properties of polypropylene [13], recycled polyethylene[14],aggregate in concrete [15] etc. Bread fruit is a local food consumed in Africa and its shells litter the whole environment thereby constituting environmental pollution. Both BFS and PKS are readily accessible within our locality in abundance. Therefore, they are aimed to be used to address the shortcomings associated with epoxy and develop advanced electrical transmission insulator[16]. This study therefore was to determine the dielectric properties of hybrid composites developed from sustainable agro waste materials (bread fruit shell flakes and palm kernel shell particles).

The main aim of this study is to develop a polymer composites insulator using breadfruit flakes and PKS for high voltage transmission insulator. This is to be achieved through the following objectives:

- Characterization of the developed polymer composites using SEM, XRD, etc.
- Evaluation of the insulative properties of the developed composites insulator
- Development of a prototype of the high voltage transmission insulator using epoxy and BFS/PKS.

Materials

The following materials were used in this study for the development of the polymer composites insulators: Epoxy resin as the matrix, Hardener (HY951), and Breadfruit Shell (Flakes) and Palm kernel shell (Particulates) as the reinforcement

Method

These agro-waste: the palm kernel shell (PKS) and the breadfruit shell (BFS) were sourced from Nsukka locality in Enugu State.They were washed and sun dried for seven days to remove water, residual oil in PKS and other dirt in BFS so as to ensure proper bonding with the polymer matrix. Large quantity of BFS was collected and taken to a local milling machine, where it was milled into smaller flakes. The breadfruit flakes were then taken to University of Nigeria, Nsukka Civil Engineering Laboratory where a Vibrating Sieving Machine was used to sieve the flakes to 2.00 mm. See figure 1.

Fig.1: (a) Palm kernel shells (b) Powdered PKS (c) Breadfruit shell (Ukwa shell)

The PKS was equally milled to get the required granules after which it was taken to University of Nigeria Civil Engineering Laboratory where a Vibrating Sieving Machine was used to sieve the particles to 500 µmparticle size.The PKS particles and the BFS flakes were thoroughly mixed with the epoxy at various concentrations. The mixtures were poured into their corresponding moulds and allow to cure at ambient temperature (no application of heat) as

can be seen in figure 2. Releasing agent was applied on the moulds before casting for easy removal of the composites when cured. The cured samples were cut to appropriate sizes for various test analyses.

Fig. 2: Cast samples

Characterization

The characterization of the BFS flakes and PKS particles was done using, SEM. The SEM analyses were carried out at the University of Witwatersrand**,** Johannesburg, South Africa.

Testing of Fabricated Samples

The following tests were carried out on these samples: breakdown voltage, dielectric constant, dielectric loss, water absorption capacity and moisture content.

Determination of Dielectric Strength: The samples which are about2 mm tick were placed in between electrodes. The DC voltage was applied and the reading was observed from the control desk till break down occur and the values were recorded.

Determination of Dielectric Loss: The loss of power in a dielectric is caused by the loss of energy in the form of heat generated by an electric field.

Determination of Dielectric Constant: To determine the dielectric constant, an air gap was created between two parallel plate capacitors with same thickness as the composite sample. The parallel plate capacitors were connected to the battery and the voltage across was measured (Vo). The samples were then used separately to fill the air gap between the capacitor plates that are connected to a battery and the voltage across was also measured differently for each of the composite samples.

Equation 1.0 gives the relationship between Vo (voltage across the capacitors with an air gap between them) and V (voltage across the capacitors with the composite sample between them). Thus, the dielectric constant $\boldsymbol{\varepsilon_r}$ is expressed as follows:

$$\varepsilon_r = \frac{V_o}{V} \quad \textbf{1.0}$$

Results and Discussion

General Effect of Increased Weight Percent of Flakes on the Developed Composites.

Breakdown Voltage

The composition with best breakdown voltage in figure 3 was that of 70wt% of BFS flakes. Between 50 and 70wt% loading of flakes, there was fair interfacial bonding between the fillers and the matrix, which enhanced the materials breakdown voltage. Higher loading of flakes may have resulted to poor interfacial bonding between the particles and the polymer. Thus, the values of the breakdown voltage increased as the percentage of BFS flakes loading was increased (between 50wt% and 70wt%) but started to decrease after exceeding 70wt% flakes composition. This was because smaller wt% of BFS flakes dispersed evenly with the PKS particulates in the matrix thereby enhancing better wettability between the reinforcements and the matrix, thus better property; but interfacial bonding between the particulate and the resin got weaker after exceeding the 70wt% reinforcement of flakes. With increased number of flakes, the number of particles that were present decreased due to surface area; thus, poor bonding between the reinforcements and the resin. This is in agreement with the work of other researchers [17].

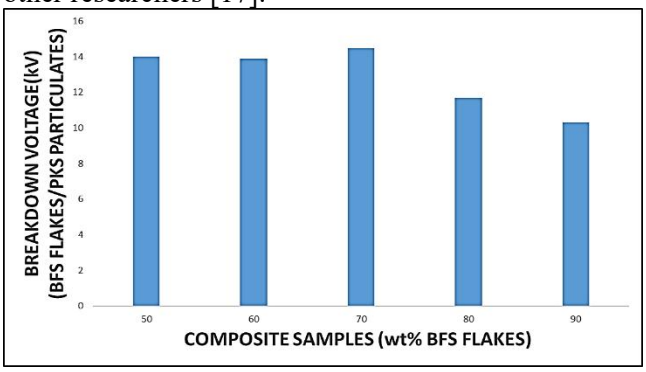

Fig.3 Breakdown Voltage of BFS and PKS Hybrid Composite

Dielectric Constant

From the graph of figure 4, the dielectric constant of the samples increased with the proportion of flakes added from 50wt% composition of BFS flakes to 70wt% flakes composition. This implies that the sample with 70wt% BFS flakes and 30wt% PKS particulates has the highest value for dielectric constant, while sample with 50wt% BFS flakes and 50wt% PKS particulates has the lowest value for the dielectric constant. There was however, a gradual decrease in the dielectric constant after the optimal value at 70 wt.% composition of flakes. This is because, increased flakes composition led to weak filler compaction (unlike the case of particles) which induced the presence of more pores due to insufficient resin for strong bond formation. The presence of free volume in the form of pores results in a decrease in dielectric constant as the relative permittivity of air is about one [18]. Thus, the result showed that the dielectric constant of the samples slightly reduced at higher flakes composition ((i.e. 80 – 90 wt%).) with increased porosity. This is in agreement with the work done by Jie*et al*[19] and Chi*et al* [20].

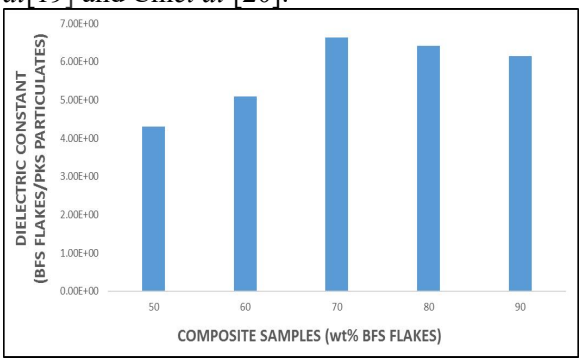

Fig. 4 Dielectric Constant of BFS and PKS Hybrid Composite

Dielectric Loss

The dielectric loss was found to increase as the percentage of flakes loading increased. See figure 5. This is because dipole friction is more at higher flakes wt.% due to the presence of more dipoles
for polarization process. However, the dielectric loss for all the compositions are reasonably low, thus, better dielectric property.

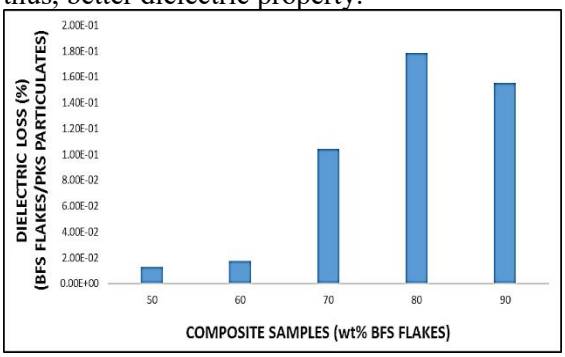

Figure 5 Dielectric Loss of BFS and PKS Hybrid Composite

MICROSTRUCTURAL ANALYSISON BFS/PKS COMPOSITE

SEM was used to study the morphology of the BFS flakes and PKS particulates hybrid composites. The SEM/EDS of the composites were shown in figures 6 – 10, A strong flakes-particle-matrix interfacial bond was critical for good dielectric properties of composites.

Morphological study of the composites under study was heavily dependent on the flakes-particle-matrix interaction i.e. interfacial bonding. It was observed that flakes which have smooth spherical surfaces had more surface area for interaction, thus better property. There was a good dispersion of flakes and particles in the polymer matrix. This led to good interfacial bonding between the polymer and the reinforcing materials, which can be seen clearly from the SEM at different composites compositions. There was no particle pull-out observed in the SEM which could lead to pores thus, poor dielectric properties. The SEM micrographs showed that there was great dispersal of reinforcement and appreciable homogeneity in all directions at different wt.% composition.

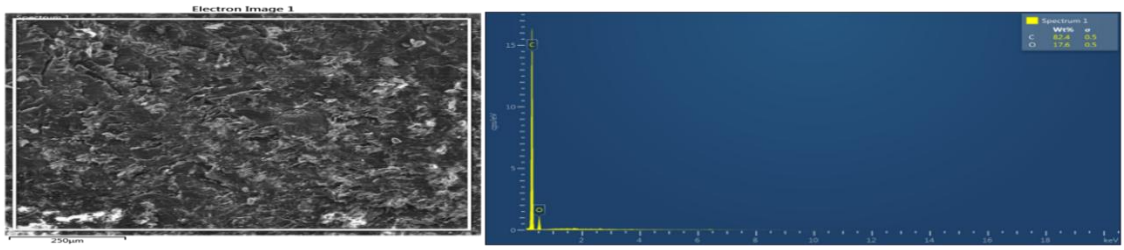

Figure 6:SEM/EDS of 50:50 wt.% BFS Flakes/PKS Particulates Composite.

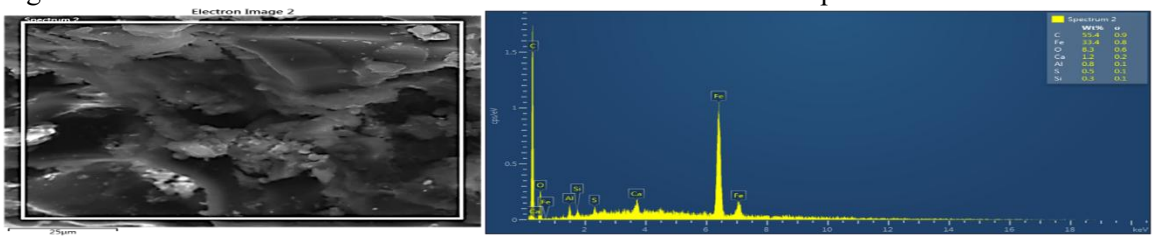

Figure 7:SEM/EDS of 60:40 wt.% BFS Flakes/PKS Particulates Composite.

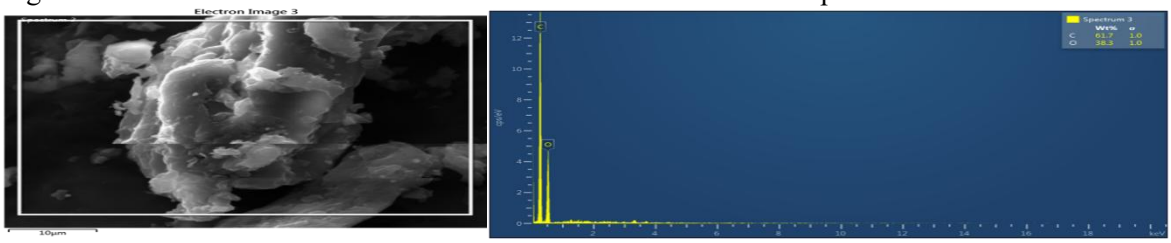

Figure 8:SEM/EDS of 70:30 wt% BFS Flakes/PKS Particulates Composite.

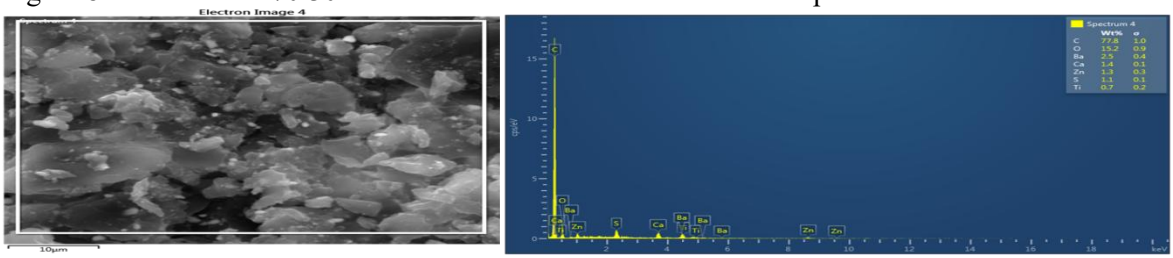

Figure 9:SEM/EDS of 80:20 wt% BFS Flakes/PKS Particulates Composite.

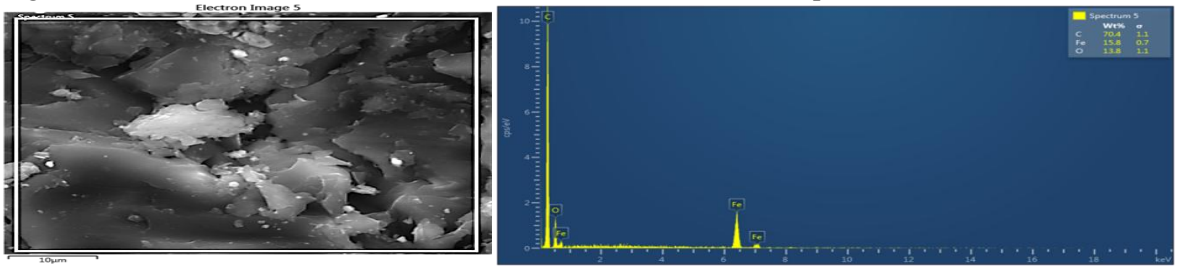

Figure 10:SEM/EDS of 90:10 wt% BFS Flakes/PKS Particulates Composite.

Conclusion:

1. Composite hybridization improved the dielectric properties of the agro waste composites.
2. Increased flakes enhanced the dielectric properties of the developed composites.
3. Dielectric Strength and Dielectric Constant have their optimal values at 70 wt% while Dielectric Loss has its best value at 50 wt%.
4. They have also proved to be better insulator than glass, paper etc.
5. The studied agro-waste materials (BFS/PKS) are better substitutes for the reinforcement of Polymer Matrix Composites than other agro-

waste materials (ground nut shell, rice husk, bean shell, etc.).

Acknowledgement

The authors hereby appreciate and acknowledge the Africa Centre of Excellence for Sustainable Power and Energy Development, ACE-SPED, University of Nigeria, Nsukka for their support.

References:

1. H. Peng, X. Sun, W. Weng, and X. Fang, Energy storage devices based on polymers, 1st ed. (Polymer Materials for Energy and Electronic Applications). Elsevier, 2017, p. 373.
2. R. Safipour, "Optimal planning of energy storage systems in microgrids for improvement of operation indices," Int. Journal of Renewable Energy Research (IJRER), vol. 8, no. 3, pp. 1483-1498, 2018.
3. A. Harrouz, M. Abbes, I. Colak, and K. Kayisli, "Smart grid and renewable energy in Algeria," in Renewable Energy Research and Applications (ICRERA), 2017 IEEE 6th International Conference on, 2017: IEEE, pp. 1166-1171.
4. A. Lemma, I. Massa, A. Scott, and D. Te Velde, "What are the links between power, economic growth and job creation," Development Impact Evaluation, Evidence Review, Overseas Development Institute, 2016.
5. J. Song, Y. Yu, G. Zhao, J. Qiu, and Q. Ding, "Comparative study of tribological properties of insulated and conductive polyimide composites," Friction, pp. 1-10, 2019.
6. A. Obeidat and M. A. Gharaibeh, "Electrochemical Performance of MnO2 for Energy Storage Supercapacitors in Solid-State Design," International Journal of Renewable Energy Research (IJRER), vol. 8, no. 3, pp. 1229-1235, 2018.
7. V. Ogbonna, A. Popoola, O. Popoola, and S. Adeosun, "A review on polyimide reinforced nanocomposites for mechanical, thermal, and electrical insulation application: challenges and recommendations for future improvement," Polymer Bulletin, pp. 1-33, 2020.
8. U. Uyor, A. Popoola, O. Popoola, and V. Aigbodion, "Advancement on suppression of energy dissipation of percolative polymer nanocomposites: a review on graphene based," Journal of Materials Science: Materials in Electronics, vol. 30, pp. 16966–16982, 2019.
9. M. El-Wazery, M. El-Elamy, and S. Zoalfakar, "Mechanical properties of glass fiber reinforced polyester composites," Int. journal of applied science and engineering, vol. 14, no. 3, pp. 121-131, 2017.
10. R. Lal, B. S. Rathore, and M. Gaur, "Structural and polarization properties of polyimide/TiO 2 nanocomposites," Ionics, vol. 18, no. 6, pp. 565-572, 2012].
11. [R. H. Martin and M. S. H. Bhuiyan, "Degradation of polymer matrix composites," 2018.
12. J. Zheng, L. Xie, X. Tan, W. Fang, and X. Qiao, "Failure Analysis and Suggestions of Composite Insulators," in IOP Conference Series: Earth and Environmental Science, 2019, vol. 300, no. 4: IOP Publishing, p. 042040
13. K. Jain, S. Shit, and S. Jain, "Evaluation of mechanical & thermal properties of polypropylene—palm kernel nut shell powder composites for green roof technology," Journal of Information, Knowledge and Research in Mechanical Engineering, vol. 2, no. 2, pp. 456-459, 2013.
14. A. J. Olumuyiwa, T. S. Isaac, O. A. Adewunmi, and A. I. Ololade, "Effects of palm kernel shell on the microstructure and mechanical properties of recycled polyethylene/palm kernel shell particulate composites," J. of Minerals & Materials Characterization and Engineering, vol. 11, no. 08, p. 825, 2012.
15. O. P. Oti, K. N. Nwaigwe, and N. A. Okereke, "Assesment Of Palm Kernel Shell As A Composite Aggregate In Concrete," Agricultural Engineering International: CIGR Journal, vol. 19, no. 2, pp. 34-41, 2017.
16. U. O. Uyor, A. P. Popoola, O. Popoola, and V. S. Aigbodion, "Energy storage and loss capacity of graphene-reinforced poly (vinylidene fluoride) nanocomposites from electrical and dielectric properties perspective: A review," Advances in Polymer Technology, vol. 37, no. 8, pp. 2838-2858, 2018.
17. Saira T. “Preparation and Characterization of Agro-wastes Based Polymer Composites for Commercial Use” Ph.D. Thesis, Department of

Chemistry, University of the PUNJAB, Lahore Pakistan, 2011, pp.1– 38.
18. Simpson, J.O. and St.Clair, A.K. "Fundamental insight on developing low dielectric constant polyimides, Thin Solid Films", https://books.google.com/books 1997, pp.308-309, 480-485.
19. [Jie, X. Dongmei, Z. Fa, L. Wancheng, Z. and Peng, L. "Dielectric Properties of Porous Reaction-boned Si3N4 Ceramics with Controlled Porosity and Pore Size" Journal Material Science of Technology, Vol.24, Number 2, 2008, pp. 207-210.
20. Chi, Q.G. Dong, J.F.Liu, G.Y. Chen, Y. Wang, X. Lei, Q.Q. "Effect of particle size on the dielectric properties of $0.5Ba(Zr_{0.2}Ti_{0.8})O_3$–$0.5(Ba_{0.7}Ca_{0.8})TiO_3$/polyvinylidene fluoride Hybrid films", International Journal of Hybrid Information Technology Vol.8, No.4 2015, pp.49-54.

NMS-TP015

INVESTIGATION OF THE MECHANICAL BEHAVIOUR OF Al-Si COMPOSITE PRODUCED USING STIR CASTING TECHNIQUE

Lasisi Shaibu.[1], Tukur Shehu.,[1] Olagunju Suraj Jare[2], Sanni Habeeb Muhammed[2], AlozieUchenna Henry [2], Okpara Ikenna Oko[3], IbearugbulemChristain Nwokeorie[3], Idris Isah Tanko[4]

[1] Department of Metallurgical Engineering, Waziri Umaru Federal Polytechnic, Brinin Kebbi, Nigeria

[2]Department of Mechanical Engineering, Federal Polytechnic, Nekede, Imo Nigeria

[3]Department of Metallurgical and Materials Engineering, Federal Polytechnic, Nekede, Imo Nigeria

[4]Department of Electrical and Electronics Engineering, Federal Polytechnic, Nekede, Imo Nigeria

Corresponding Author Email:mallamyobe@gmail.com

ABSTRACT

Aluminum based matrix composites remain the most explored metal matrix materials for the production of metal matrix composites. This work deals with the fabrication of aluminum metal matrix composites (AMMCs) reinforced with silica sand. The specimens were prepared in six different weight fraction of silica sand containing 2.5g, 5g,7.5g,10g, 12.5gand 15g via stir casting method. The mechanical properties of the composite were investigated and the results obtained shows significant increase in tensile strength between 2.5g and 5g (63.63N/mm^2, 76.36N/mm^2) while the highest tensile value was obtained at 7.5g and 10g (89.1N/mm^2). It was also observed that the tensile value dropped at 12.5g and 15g composition (50.91N/mm^2, 63.63N/mm^2) under the same load (1000N/mm). The Vickers hardness values obtained shows appreciable increase in hardness properties as composition increases while the highest value was also obtained at 7.5g (10.6) composition. There was significant drop in hardness value as composition increases to 10g and 12.5g (10.3, 8.2). The XRF analysis showed that the sand contains mostly silica (SiO_2) which serves as hardener in the AMMCs

Key Words: Stir Casting, Aluminium Metal Matrix Composites, Hardener, Weight Fraction

1.0 INTRODUCTION

Aluminum alloys are widely used in automobile industries and aerospace application due to their great mechanical properties; low density, low coefficient of thermal expansion, better corrosion resistance and wear as compared with conventional metals and alloys. The low production cost and better mechanical properties of composites makes them very useful for various applications in many areas from technological point of view. Alumina (Al_2O_3) and Silicon carbide (SiC) when used as reinforcements to form composites enhance the density of the base alloy. Furthermore Miyajima*et.al* (2003) reported that the density of Al_20_{24}-SiC particles possesses higher density. Among the various reinforcements, the low aspect ratio particle reinforcement is of much significant in imparting the hardness of the material when they are dispersed (the hardness of the fiber reinforced MMC < Whisker reinforced MMC < particle dispersed MMC). The particulate reinforcement such as SiC, Al_2O_3 and aluminide are generally referred to impart higher hardness. TiC when dispersed in Al matrix, increase the hardness to weight

ratio. Moreover, it imparts thermodynamic stability to the composites.

Discontinuously reinforced aluminum composites are being recognized as an important class of engineering materials that are making significant progress. The reasons for their success are related to their desirable properties including low density, high hardness, high compressive strength, wear resistance, etc.

(Aigbodion and Hassan, 2007). The high cost of current MMCs compared to aluminum alloys has inhibited production on a large industrial scale, for example, in the automotive industry. In the attempt to overcome this limitation, several research and development (R&D) programs (Aigbodion, 2010) were focused on the refinement of aluminum-based MMCs using low cost industrial waste by-products as the reinforcement particulate. Reinforcing an aluminum alloy with particles of a second phase can improve the physical, mechanical and tribological properties of the material, or it may result in material savings at little detriment to the properties desired. This could reduce the cost and the weight of energy intensive metals for potential applications in engineering components for a new generation of vehicles (Arun Kumar and Swamy, 2011). The ever-increasing demand for low cost reinforcements stimulated the interest towards production and utilization of by-products from industries as reinforcements since they are readily available or are naturally renewable at affordable cost. Aigbodion (2007) has used Kankara clay (alumino-silicate) in reinforcing Al–Si alloy, Naresh (2006) worked on the development and characterization of metal matrix composite using red mud, an industrial waste for wear resistant applications. Bienia et al. (2003) used fly ash in reinforcement of aluminum matrix. They all reported good dispersion and recovery of the particles in the composite castings. Fly ashes from coal combustion have been successfully combined with aluminum alloys using the foundry process to produce a class of MMCs called Ash alloys. It was demonstrated by Rohatgi et al. (2007) that Ash alloys offer the advantages of reducing the disposal volumes of electric utility industries, providing a high value-added use of fly ash, and at the same time introduced a class of new materials

with improved properties at reduced cost. It is in the light of the foregoing researches that investigation into the possibility of using maize stalk ash in metal matrix particulate composite for engineering applications was motivated. Research has showed that Al–Si–Mg alloys were reinforced with ceramic materials such as SiC, Al_2O_3, and Ti3. But recent research has showed that biodegradable agricultural wastes can be used to reinforce the alloy. Locust bean shell waste particulates were used as reinforcement on Al–Si–Mg alloy and it was observed that the tensile strength and hardness values increase as the reinforcement increases (Sidi, 2011). Moreover, orange peel ash particulates were used to reinforce Al–Si–Mg alloy and the results showed that there is a slight decrease in the mechanical properties due to poor adhesion of the reinforcement to that of the alloy (Shehu, 2011). Carbonized maize stalk particulates have been used to reinforce polyester and the results showed an enhancement in the mechanical properties of the developed composites (Hassan et al., 2012).(Howell *et.al1995)*reasoned the improvement of the hardness of the composites to the increase particle volume fraction. He attributed this increase in the hardness to the decreased particle size and increase specific surface of the reinforcement for a given fraction.

(Devis*et.al* 2001) concluded that the increase in the hardness of the composites containing hard ceramic particles not only depends on the size of reinforcement but also on the structure of the composite and good interface bonding. The micro-hardness is a direct, simple and easy method of measuring the interfacial bonding strength between the matrix and reinforcement.

2.0 MATERIALS AND METHODS

2.1 Materials and Equipment

The materials used in this research include: Aluminum electric wire, Silica powder, Silica sand, Carbide papers and Diamond paste while the equipment used in this project includes Stirring road, Tube rod pattern, rammer, sieve shaker, hack saw, file, compaction machine sieve of 6.0mm,4.75mm,3.00mm,1.80mm,0.90mm and 0.75, Crucible furnace and Digital weighing balance.

2.2 Research Procedures

The specimens were prepared in six different weight fraction of silica sand containing 2.5g, 5g,7.5g,10g, 12.5g and 15g via stir casting method. The moulding sand was sieved to particle sizes of 6.00, 4.75, 3.00, 1.80 0.90 and 0.75µm respectively. The prepared Al MMCs was charged in to open hearth furnace for melting operation at the temperature of 700℃ + 30℃ above the liquidus temperature of aluminum while the reinforcement was preheated and added to the molten aluminum and stirred mechanically. The molten composites poured into mould and allowed to solidify.

2.3 Tensile test

Tensile test was carried out using universal tensile testing machine. The samples were mounted and a load of 20KN was applied. The specimen undergoes a uniaxial strength which causes elongation and fracture at different forces. The breaking points were recorded and analyzed.

Figure 1: images of the specimen before and after tensile test

2.4 Hardness Test

The hardness test was carried out via Vickers hardness testing machine. The samples were loaded, the indenter was forced on the test samples under a preliminary load of a 10kgf. Equilibrium point was achieved following the movement of the penetration of the indenter. An additional major load was measured on the digital scales. The hardness values were taken. This process was carried out at three different points for each sample for accuracy

3.0 RESULTS AND DISCUSSION

3.1 Results of silica sand sieve.

Sieve analysis of silica sand was done using American Standard Test Sieve (ASTMs) the results of the sieved of different aperture were recorded after 15minutes.

Table 1: silica sand sieve analysis

S/N	Sieve size(mm)	Weight retained(kg)	%weight retained(kg)	Cumulative retained	Total % passing
1.	6.00	1.200	10.730	10.730	89.27
2.	4.75	1.848	16.530	27.260	72.74
3.	3.00	1.750	15.653	42.913	57.087
4.	1.80	2.240	20.036	62.949	37.05
5.	0.90	2.722	24.347	87.296	12.704
6.	0.75	1.300	11.628	98.924	1.076
	pan	0.008	0.0716	98.996	1.004
	Fineness modulus	0.109	0.975	100	0

3.2 Results of tensile test

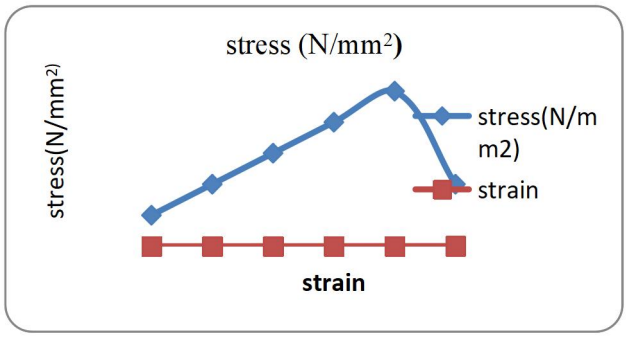

Figure 2:Results of stress vs strain of as-received sample

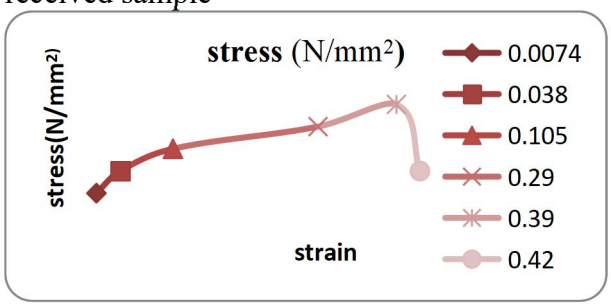

Figure 3: Results of stress vs strain of 2.5g composition

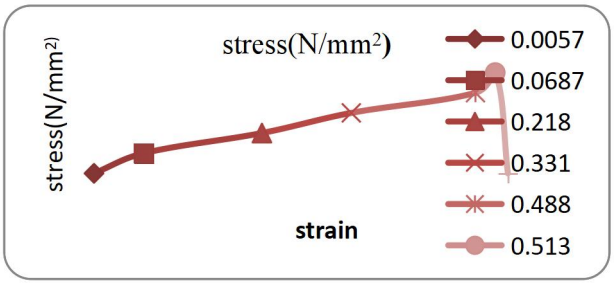

Figure 4: Results of stress vs strain of 5g composition

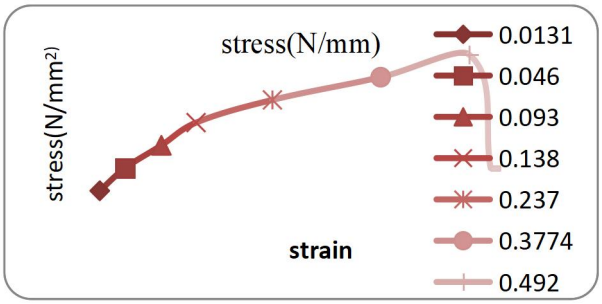

Figure 5: Result of stress vs strain of composition of 7.5gram

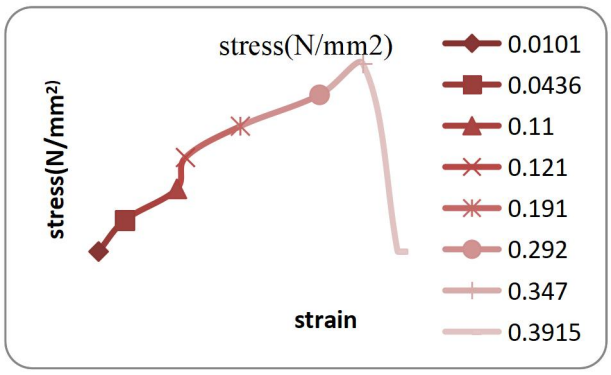

Figure 6: Graph of stress vs strain of composition 10 gram

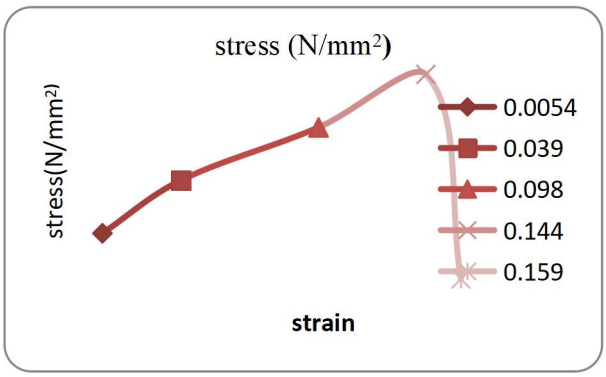

Figure 7: Graph of stress vs strain of composition12.5 gram

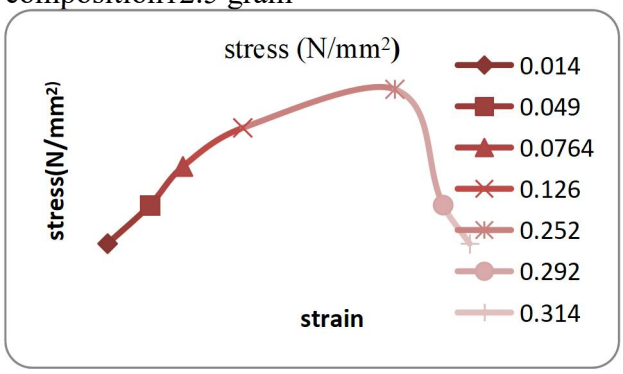

Figure 8: Graph of stress vs strain of composition of 15 gram

Figure 2-9 shows the tensile behaviuor of Al-Si composite and different compositions of silica sand. The results shows drastic increase in the tensile strength as composition increases up to 10g

3.3 Results of Hardness Test

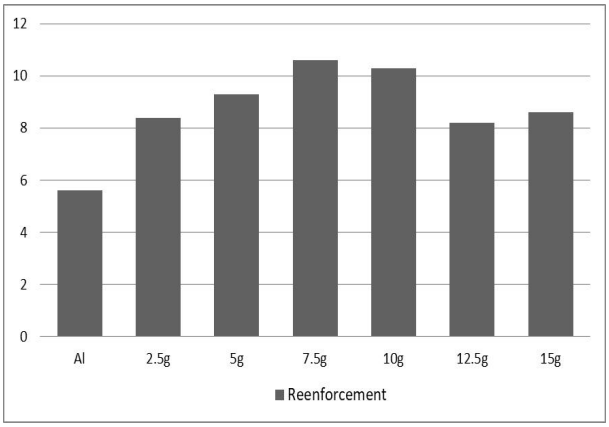

Figure 9: Graphical representation Hardness values
at different compositions of Al-Si composite

Figure 9 represent the hardness values of the composite; the indentation values shows an improvement on the mechanical property of the composite under study

4.0 CONCLUSIONS

From the research carried on the mechanical behaviour of Al-Si composite produced using stir casting technique. it can be concluded that:

1. the tensile strength of the specimen increases by increase in silica sand composition while the highest tensile value was obtained at 7.5g and 10g respectively while the strength reduces as composition increases above 10g.
2. the hardness test of the Al-silica matrix composites results shows an appreciable increase in hardness values with increase in composition while the hardness values reduce as composition increases above 7.5g

3. the as-received sample exhibit lowest hardness value across the investigation while that containing 7.5g reinforcement recorded the highest value.

REFERENCES

Aigbodion, V. S., & Hassan, S. B. (2007). Effects of silicon carbide reinforcement on microstructure and properties of cast Al-Si-Fe/SiC particulate composites. *Materials Science and Engineering A*, *447*(1–2), 355–360. https://doi.org/10.1016/j.msea.2006.11.030

Aigbodion, V. S., Hassan, S. B., & Oghenevweta, J. E. (2010). Microstructural analysis and properties of Al-Cu-Mg/bagasse ash particulate composites. *Journal of Alloys and Compounds*, *497*(1–2), 188–194. https://doi.org/10.1016/j.jallcom.2010.02.190

Alam, M. A., Haider, K., Alam, M. A., Redhewal, A., & Saxena, V. (2015). Investigation of Mechanical Properties of Aluminium Based Metal Matrix Composites Reinforced With Sic & Al 2 O 3. *Article in International Journal of Engineering Research and Applications*, *5*(2), 63–69. www.ijera.com

Alaneme, K. K., Bodunrin, M. O., & Awe, A. A. (2018). Microstructure, mechanical and fracture properties of groundnut shell ash and silicon carbide dispersion strengthened aluminium matrix composites. *Journal of King Saud University - Engineering Sciences*, *30*(1), 96–103. https://doi.org/10.1016/j.jksues.2016.01.001

Alaneme, K. K., Eze, H. I., & Bodunrin, M. O. (2015). Corrosion behaviour of groundnut shell ash and silicon carbide hybrid reinforced Al-Mg-Si alloy matrix composites in 3.5% NaCl and 0.3M H 2SO4 solutions. *Leonardo Electronic Journal of Practices and Technologies*, *14*(26), 141–158.

Effects of reinforcements on sliding wear behavior of aluminum matrix composites - ScienceDirect. (n.d.). Retrieved February 19, 2022, from ttps://www.sciencedirect.com/science/article/abs/pii/S0043164803000668

Hassan, S. B., Oghenevweta, E. J., & Aigbodion, V. S. (2012). Potentials of Maize Stalk Ash as Reinforcement in Polyster Composites. *Journal of Minerals and Materials Characterization and Engineering*, *11*(04), 445–459. https://doi.org/10.4236/jmmce.2012.114032

Krauklis, A. E. (2021). Predicting Environmental Ageing of Composites: Modular Approach and Multiscale Modelling. *Materials Proceedings*, *6*(1), 11. https://doi.org/10.3390/cmdwc2021-09890

Krauklis, A. E., Karl, C. W., Gagani, A. I., & Jørgensen, J. K. (2021). Composite material recycling technology—state-of-the-art and sustainable development for the 2020s. *Journal of Composites Science*, *5*(1). https://doi.org/10.3390/jcs5010028

Krauklis, A.E., Karl, C.W., Gagani, A.I., Jørgensen, J.K. (2021) Composite material recycling technology-state-of-the-art and sustainable development for the 2020s. *Journal of Composites Science*, 5(1): 28-28 YucelBirol,

Miyajima, T., & Iwai, Y. (2003). Effects of reinforcements on sliding wear behavior of aluminum matrix composites. *Wear*, *255*(1–6), 606–616. https ://doi.org/10.1016/S0043-1648(03)00066-8

Oghenevweta, J. E., Aigbodion, V. S., Nyior, G. B., & Asuke, F. (2016). Mechanical properties and microstructural analysis of Al–Si–Mg/carbonized maize stalk waste particulate composites. *Journal of King Saud University - Engineering Sciences*, *28*(2), 222–229. https://doi.org/10.1016/J.JKSUES.2014.03.009

Sood, P. K., Sehgal, R., & Dwivedi, D. K. (2017). Machinability of hypereutectic cast Al–Si alloys processed by SSM processing technique. *Sadhana - Academy Proceedings in Engineering Sciences*, *42*(3), 365–378. https://doi.org/10.1007/s12046-017-0609-9

Stack, M. M., & Mathew, M. (2003). Micro-abrasion transitions of metallic materials. *Wear*, *255*(1–6), 14–22. https://doi.org/10.1016/S0043-1648(03)00204-7

Vidyapeetham, V., & Campus, B. (2015). *Evaluation of Mechanical Properties of Al6061 Reinforced with Hematite*. *2*(1).

NMS-TP016

Phytochemical Evaluation and Corrosion Behaviour of *MagniferaIndica*extracts (bark and leaf) on mild steel in hydrochloric acid solution

Ayotunde O. ALUKO[1*]; Gbenga, J. ADEYEMI[2]; Patrick A. UKACHI[1]
[1*]*Mineral and Petroleum Resources Engineering Department,*
The Federal Polytechnic Ado Ekiti, Nigeria
[2]*Mechanical Engineering Department,*
Ekiti State University Ado Ekiti, Nigeria
[1]*Mechanical Engineering Department,*
The Federal Polytechnic Ado Ekiti, Nigeria
E-mail(s): aluko_ao@fedpolyado.edu.ng; gbenga.adeyemi@eksu.edu.ng;
patrickukachi@gmail.com
* Corresponding author: +234 803 248 0613

***Abstract*:**
This work investigates the inhibitive effect of *MagniferaIndica* extracts (bark and leaf) as corrosion inhibitors for mild steel in 1.5M HCl solution at room temperature using gravimetric method and phytochemical analysis. It is observed that the corrosion rate, C_R of the blank compared to the mild steel coupon inhibited with the MI extracts (bark and leaf) are higher, and further increases with the period of immersion. However, the inhibition efficiency, %IE of the MI extract (leaf) inhibited coupon indicated a decrease as the period of immersion progresses, particularly between the 3rd and 5th day unlike the MI extract (bark) which shows a stable trend. The concentration of the corrosive medium (1.5M HCl) may be attributed for this trend, in which the inhibitor, MI extract (leaf), could not sustain its inhibitive efficiency for such a long period of time. However, the MI extract (bark), significantly, showed a peak value (91.63%), at 0.5g/L on the 4th day, compared to the MI (leaf) with a value of 60.10% at 0.5g/L on the same 4th day in 1.5M HCl solution respectively, which is in tandem with the result of the phytochemical screening.
Keywords: phytochemical profile, *MagniferaIndica*, mild steel, hydrochloric acid, weight loss

1.0 INTRODUCTION

The subject of corrosion and material degradation has been an issue of concern in the metallic and engineering industry. This global menace has necessitated increasing research interest on controlling the deteriorating effects of corrosion on metals and their metallic alloys (Singh et al., 2019; Akinbulumo et al., 2020; Aluko and Oke, 2022). Corrosion is a phenomenon resulting in materials deterioration through chemical or electrochemical interaction with the environment (Chen et al., 2022).It is known to cause a very significant loss, both to human lives and to the economy; and moreover, it leads to loss of products, waste of resources, higher maintenance needs and overall cost of design (Fouda et al., 2021; Rbaa et al., 2020). Mild steel is found to be the most widely metallic material in the oil and gas, food, energy, chemical, and construction industries owing to its excellent mechanical properties, durability and toughness among others, as well as due to its relative low cost and high availability (Prabhu et al., 2020).Hydrochloric acid, HCl, among the acid solutions is commonly

utilized in chemical treatment processes such as acid cleaning, oil-well acidizing, acid descaling, and pickling. It is a highly aggressive medium for corrosion of mild steel, and, hence, such treatment with an acid and particularly, in high concentration, brings about undesirable consequences, especially when used in direct contact on mild steel.

The corrosion of metals and alloys, particularly, mild steel, is an important and well-studied industrial problem which has found a fertile research field in green chemistry in the last decade. Green corrosion inhibitorsare attracting great interest in the corrosion field considering the factor of health, safety, biodegradability, ecologically acceptability and renewability. These include for examples amino acids, alkaloids, polyphenols and often extracts of plants largely distributed and of low economic value, including byproducts of agro-industrial processes and agricultural-wastes (Dehghani et al., 2020; Marsoul et al., 2020; Marzorati et al., 2019). The volume of publications around the topic of green corrosion inhibitors for mild steel surfaces in the last decade has made it imperative for ongoing concerted efforts and continuous research (Chen et al., 2022; Obot et al., 2022; Zakari, et al., 2022; Abolanle et al., 2021; Yousfi et al., 2019).

The selection of efficient corrosion inhibitors requires detailed knowledge regarding the interaction mechanism which is predicated on the type of molecular structure, the amount of functional groups within the inhibitor molecule and the number of functional groups per molecule (Ryl et al., 2019). It is noteworthy to point out that the size ratio of the molecular structure depends on the geometry of the organic inhibitor. Therefore, an organic inhibitor with planar geometry will provide higher surface coverage, thereby exhibiting higher strength as a corrosion inhibitor (Chen et al., 2022).El Hamdani et al. (2015)demonstrated that alkaloids in Retama monosperma (L.) Boiss.seeds extract was responsible for the mitigation of carbon steel corrosion in 1.0 M HCl medium. Inhibition of aluminium corrosion in HCl environment by Cashew nut testa extract was linked by Nnaji et al. (2014) to the presence of tannins. Raja et al. (2013)also showed that the alkaloids isolated from Alstoniaangustifolia var. latifolia leaves were good inhibitor for mild steel in 1.0 M HCl. The alkaloids exhibited inhibition efficiency higher than 80% at concentrations between 3 and 5 mg/L.

Corrosion inhibitor selection is based on the metal substrate and the surrounding medium (solvent nature, temperature, pH of the solution and velocity, among others), while at the same time, the economy, efficacy and environmental factors should be considered. Furthermore, the inhibition mechanisms aredistinct, and for the organic compounds, they are adsorbed physically or chemically or both interact with metal surfaces, and limit the cathodic, anodic or both reaction rates by blocking the active sites. In this case, the physical adsorption takes place through van der Waals forces between them, while the chemical interaction means that the S, N, O, P, Se and conjugated groups (heteroatoms,functional groups, multiple bonds) contained within organic inhibitors act as adsorption centers that link the inhibitor (donating electron) to the metal surface (accepting electron) (Chen et al., 2022; Fouda et al., 2021; Marzorati et al., 2019; Popoola, 2019; Fdil, et al., 2019). Both the surface adsorption of molecule and the bonding between them consequently, play a major role in inhibiting corrosion. It is on this premise that this study addresses the evaluation of phytochemical characterization and gravimetric analysis of *MagniferaIndica*

(bark and leaf) for the corrosion inhibition of mild steel in 1.5M HCl acid medium in order to determine the corrosion mechanism. It is pertinent to state that there is little or no work in literature carried out on *MagniferaIndica* extracts (bark and leaf) in 1.5M HClat room temperature at a prolonged immersion time of 120days.

2.0 Experimental Procedure

2.1 Mild Steel Coupon Preparation

Mild steel was obtained from OlusegunObasanjo Engineering Innovation Centre, Federal Polytechnic Ado Ekiti, Ekiti State. The composition (wt. %) of mild steel samples used for all the experiment was as follows: C=0.128; P=0.010; S=0.030; Cr=0.820; Mn=0.292. Ni=11.500; Ar=1.420; Pb=0.096; Cu=0.074; Fe=78.300; N=0.066. The specimens were cut into dimensions of 1.8 cm x 1.4 cm and thickness 1.5 mm. The alloy specimen were polished mechanically using emery papers of grade numbers 220, 320, 400 and 600, 800, 1000 and then, washed thoroughly with distilled water and degreased with ethanol and acetone, air dried before being immersed in the acid solution.

2.2 Electrolytic Solution

The corrosive solution, 200ml of 1.5M HCl was prepared by dilution of analytical grade Hydrochloric acid (HCl) of pre-determined normality with distilled water. The concentration range of the extract used was 0.1 - 0.5g/L and volume of the electrolyte used was 200ml in each experiment.

2.3 Preparation of Extract

MangiferaIndica extract is the inhibitor used. The MI extract (bark and leaf) were sourced from the campus of the Federal Polytechnic, Ado Ekiti, Nigeria. The leaves sample were washed, oven dried at 90^0C for four hours and pulverized using an electrically powered blender. About 50gram of pulverized leave was weighed and soaked in 250ml of ethanol for 48hours. The mixture was then filtered to obtain the extract. The filtrates was furthered subjected to evaporation at 352k to leave the sample free of the ethanol MI extract (bark and leaf)was prepared in volumetric concentration of 0.1, 0.2, 0.3, 0.4, 0.5 g/L^{-1} per 200ml of the acid solution respectively.

2.4 Phytochemical Screening:

The phytochemical constitution of the *MagniferaIndica*extract (bark and leaf) was evaluated following standard procedures (in accordance to Trease and Evans, 1991). Specifically, the tannin, cardiac glycosides, saponnin, terpenoids, phenols, alkaloids, sterols and flavonoids were determined as follows:

Test for Alkaloids

A portion of extract was treated with 3-5 drops of Wagners reagent and observed for the formation of reddish brown precipitate.

Test for Cardiac Glycosides

5ml of extract was treated with 2ml of glacial acetic-acid in a test tube and a drop of Ferric-chloride solution was added to it. This was carefully underplayed with 1mlConcentrated sulphuric acid. A brown ring at the interface indicated the presence of Deoxysugar characteristic of cardenolides. A violet ring may appear below the ring while in the acetic acid layer, a greenish ring may form.

Test for Flavonoid

2ml of extract was treated with few drops of 20% sodium hydroxide solution. Formation of intense yellow colour, which becomes colourless on addition of dilute hydrochloric acid indicate the presence of flavonoid.

Test for Phenols

A portion of the extract was treated with aqueous 5% ferric and observed for formation of deep blue or black colour.

Test for Saponins

To 2mlf extract was added to 6ml of water in a test tube. The mixture was shaken vigorously and observed for the formation of

persistent foam that confirms the presence of saponins.

Test for Sterols

1ml of extract was treated with drops of chloroform, acetic an hydride and conc.H_2SO_4
and observed for the formation of dark pink or red colour.

Test for Tannins

2ml of extract was treated with 10% alcoholic ferric chloride solution and observed for formation of blue or greenish colour solution.

Test for Terpernoids

1ml of chloroform was added to 2ml of each extract followed by a few drops of conc.
sulphuric acid. A reddish brown precipitate produce immediately indicate the presence ofterpenoids.

2.5 Gravimetric measurement

The weight loss measurements were carried out by weighing the specimen in triplicate before and after immersion in 200ml for 24hrs in 1.5M of HCl in the absence and presence of 0.1, 0.2, 0.3, 0.4, 0.5 g/lMI extract (bark and leaf) at 30^0C.Each of the test specimen was taken out every 24hrs, was washed thoroughly with liquid soap rinsed with distilled water, cleansed with acetone, dried and re-weighed. The test was also carried out progressively for 120hrs (5days). The corrosion rate (C_R), inhibition efficiency (%IE), and surface coverage (ø), were calculated from the following equation in accordance with ASTM G31 standard (9) (ASTM, 2012).

$$CR\ (mmpy) = \frac{87.6w}{DAT} \quad 1$$

$$\%IE = 1 - \frac{CRinh}{CRblank} \text{x } 100 \quad 2$$

$$\emptyset = 1 - \frac{CRinh}{CRblank} \quad 3$$

Where W is the weight loss in grammes, D is density in g/cm^3, A is the surface area in cm^2, T is the immersion time inhrs, CR_{inh} and CR_{blank} are corrosion rate of mild steel with and without inhibitor respectively. The procedure was utilized for all the 120hrs (5days) using thermostat to study the inhibition efficiency of inhibitor.

3.0Results and Discussion

3.1 Results

Table 3.1: Phytochemical constituents of the MagniferaIndica extract (bark and leaf)

Constituents	Bioassays	Bioassays
Tannin	++	++
Terpenoids	++	+
Saponins	-	+
Phenols	++	++
Flavonoids	++	++
Alkaloids	++	++
Cardiac glycoside	++	-
Sterols	++	++

Table 3.2: Corrosion parameters obtained from gravimetric measurement of mild steel in 1.5MHCl in the presence of different concentration of MI extract (bark) at 30^{o}C

TIME (hrs)	Concentration(g/l)	Weight loss (g)	C.R (mm/yr)	%I E	Ø
24	Blank	0.08	0.0186	-	
	0.1	0.05	0.01161	37.58	0.3758
	0.3	0.01	0.0023	87.63	0.8763
	0.5	0.01	0.0023	87.63	0.8763
48	Blank	0.18	0.0209	-	
	0.1	0.06	0.00697	66.65	0.6665
	0.3	0.02	0.0023	88.99	0.8899
	0.5	0.02	0.0023	88.99	0.8899
72	Blank	0.28	0.0217	-	
	0.1	0.09	0.00697	67.88	0.6788
	0.3	0.03	0.0023	89.40	0.8940
	0.5	0.03	0.0023	89.40	0.8940
96	Blank	0.35	0.0203	-	
	0.1	0.10	0.0058	71.43	0.7143
	0.3	0.03	0.0017	91.63	0.9163
	0.5	0.03	0.0017	91.63	0.9163

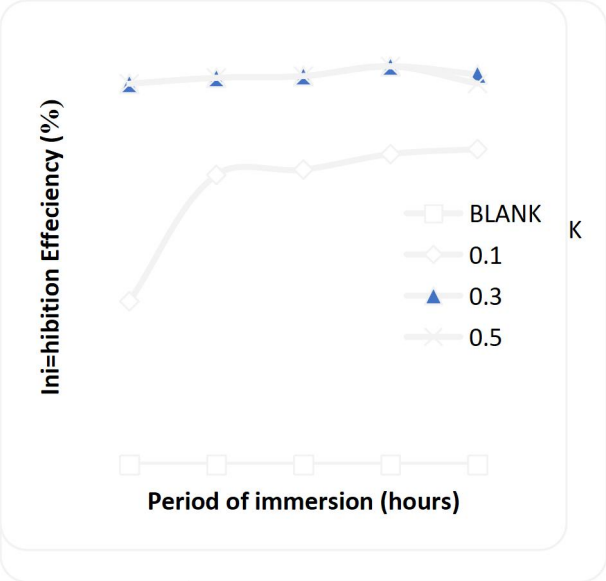

120	Blank	0.40	0.00186	-	
	0.1	0.11	0.0051	72.58	0.7258
	0.3	0.04	0.0019	89.78	0.8678
	0.5	0.05	0.0023	87.68	0.8763

Fig.3.1:Corrosion rate, C_R as a function of time for mild steel in 1.5M HCl in the absence/presence of MI extracts (bark)

Fig.3.2:Inhibition efficiency, %IE, as a function of time for mild steel in 1.5M HCl in the absence/presence of MI extracts (bark).

Table 3.5: Corrosion parameters obtained from gravimetric measurement of mild steel in 1.5M HCl in the presence of different concentration of MI extract (leaf) at 30°C.

Time (hrs)	Concentration (g/l)	Weight loss (g)	C.R mm/yr	% IE	Ø
24	Blank	0.080	0.0186	-	
	0.1	0.030	0.00697	62.53	0.6253
	0.3	0.011	0.0026	86.03	0.8603
	0.5	0.010	0.0023	87.63	0.8763
48	Blank	0.18	0.0209	-	
	0.1	0.07	0.0081	61.24	0.06124
	0.3	0.01	0.0012	94.26	0.9426
	0.5	0.11	0.0128	38.76	0.3876
72	Blank	0.28	0.0217	-	
	0.1	0.13	0.0101	53.46	0.5346
	0.3	0.05	0.0039	82.03	0.8203
	0.5	0.13	0.0101	53.46	0.5346
96	Blank	0.35	0.0203	-	
	0.1	0.18	0.0104	48.77	0.4877
	0.3	0.05	0.0029	85.71	0.8571
	0.5	0.14	0.0081	60.10	0.601
120	Blank	0.40	0.0186	-	
	0.1	0.19	0.0088	52.69	0.5267
	0.3	0.06	0.0028	84.95	0.8495
	0.5	0.15	0.0069	62.53	0.6253

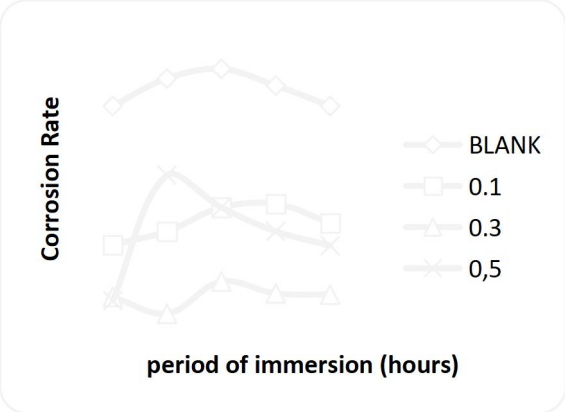

Fig. 3.3: Corrosion rate, C_R as a function of time for mild steel in 1.5M HCl in the absence/presence of MI extracts (leaf)

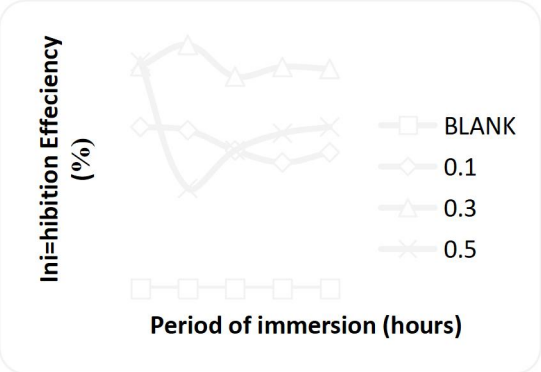

Fig. 3.4**:** Inhibition efficiency, **%**IE, as a function of time for mild steel in 1.5M HCl in the absence/presence of MI extracts (leaf)

4.2 Discussion

4.2.1 Phytochemical screening

The phytochemical screening of *MagniferaIndica* extracts (back and leaf) are presented in the Table 4.1. It showed that active constituents of tannins, terpenoids, flavonoids, phenols, cardiac glycosides, sterols, and alkaloids are found to be present in high quantities in theMI extracts (although more in the bark than in the leaf) (Okwu and Ezenagu, 2008). However, terpenoids and cardiac glycosides are revealed to be more in the bark than in the leaf. The presence of these compounds has been reported to promote the inhibition of mild steel in aggressive acidic media (Nnanna et al., 2016).

These compounds are also bioactive which contains functional groups and possess molecular structures of inhibitory potentials of plant extracts.

4.2.2 Gravimetric measurements

The gravimetric monitoring of corrosion rate (C_R) and inhibitors efficiency (I.E %) is a versatile tool and this has been employed by several researchers (Anyiam et al., 2020; Nnanna et al., 2016; Alaneme et al., 2016a and 2016b). The data of the variation in weight loss of the mild steel substrates in the absence and presence of varying concentrations of MI extracts (bark and leaf) as a function of exposure time at 30^{o}C and different extract concentrations is given in Table 4.2. The values of C_R and I.E % obtained from the weight loss experiment at varying concentration of MI (bark and leaf) in 1.5M HCl solution are also shown in Table 4.5 and Figs 1-4. The results showed that the corrosion rate, C_R, increased with increase in exposure time in the blank solution. However, the addition of the extracts in 1.5M HCl solution resulted in a significant reduction in the corrosion rates of mild steel substrate in comparison with the blank solution. The reduction can be attributed to the increase in the inhibitor concentration, which is more prominent in 0.3g/L and 0.5g/L extracts concentration on mild steel coupons. Moreover, it is also due to the adsorption of the extract active constituents (inhibitor compounds) on the mild steel substrate as revealed by the phytochemical screening. The adsorption of such compounds on the metal surfaces result in the formation of a surface layer barrier for charge and mass transfer between the base metals and the corrosive environments (Alaneme et al., 2015a; Alaneme et al., 2015b). It is noteworthy to mention that, as indicated in Table 2, the C_R decreases noticeably with increase in inhibitor concentration, that is, the inhibition efficiency (%IE) increases with increase in the inhibitor concentration in the MI extracts. It is also noticed that, at 24 hour immersion, the %IE of the extract (bark) and extract (leaf) in the test solution gave the same highest value of 87.63% at 0.5g/l at room temperature. However, further increase in the period of immersion in the 1.5M HCl acidic solution shows decrease in the inhibition efficiency of the MI extract (leaf) compared to extract (bark), which is in tandem with the results of the phytochemical screening obtained (Okwu and Ezenagu, 2008). This could be may due to fact that the inhibitor, MI extract (leaf), could not sustain its efficiency for such a long period of time with the aggressive nature of the 1.5M HCl solution (Akinbulumo et al., 2020). The stable trend observed in the extract (bark) maybe attributed to the presence ofterpenoids and cardiac glycosides which are lacking in the leaf extract. Thus, the MI extracts can be recommended as an efficient organic inhibitor of corrosion for mild steel in 1.5M HCl solution at room temperature with the MI extract (bark) showing higher stability than the MI extract (leaf) as the immersion time progresses.

5.0 Conclusion and Recommendation

5.1 Conclusion

This work shows that *MagniferaIndica* extract (bark and leaf) can be used as corrosion inhibitor for mild steel in an acid environment. The gravimetric (weight loss) test and phytochemical analysis were evaluated. As the concentration of the inhibitor increased, the corrosion rate decreased with the MI extract (bark) obtaining a maximum inhibition efficiency of 91.63% at 0.5g/L concentration on the 4th day compared to the MI (leaf) with a value of 60.10% at 0.5g/l concentration on 4th day respectively.

The reduction of the corrosion rate, C_R by the MI extracts (bark and leaf) is found to be responsible for the decrease in the corrosion of the mild steel, and the effect is more significant in the MI extract (bark).

5.2 RECOMMENDATIONS

Further investigations to assess the corrosion morphology, and to isolate and confirm the active phytochemicals in MI extracts (bark and leaf) responsible for the inhibition of mild steel corrosion in acidic media (1.5M HCl solution) through the use of Gas chromatography-Mass spectrometry (GC-MS), and electrochemical measurements (PP and EIS) should be carried out. Moreover, theoretical studies via density functional theory, DFT are required to gain insight into the active centers of the inhibitors investigated.

REFERENCE

Yousfi F., El Azzouzi M, Ramdani M, Elmsellem H, Aouniti A, and Saidi N, (2019), Zingiber Officinal Roscoe Extract Using as Green Corrosion inhibitor for Mild Steel.

Oguzie, E.E., Enenebeaku, C.K., Akalezi, C.O., Okoro, S.C.,Ayuk,A.A., Ejike, E.N., (2010). Adsorption and corrosion-inhibiting effect of Dacryodisedulis extract on low-carbon- Steelcorrosion in acidic media. *J. Colloid Interf. Sci*. 349, 283-292.

Okwu D. E. and Ezenagu V.(2008): Evaluation of the phytochemical composition of mango(mangiferaindicalinn) stem bark and leaves , *Int. J. Chem. Sci*.: 6(2), 705-716

Alaneme, K. K.;Osasona, B.;Okotete, E.; Olusegun, S. J.and Donatus, U. (2016a). Corrosion Inhibitionbehaviour of biden pilosa extract on aluminium matrix composites in 1M HCl solution. *The Journal of the Association of Professional Engineers of Trinidad and Tobago* , 35-42; Vol. 44; No. 2.

Alaneme, K. K.; Olusegun S. J. and Alo, A.(2016b): Corrosion inhibitory properties of elephant Grass(Pennisetum purpureum) extract on mild steel corrosion in 1M HCl solution. *Alexandria Engineering Journal*, 1-8.Nnanna, I.;Nnanna, G.; Nnakaife, J.;EkekweN. and Eti, P.(2016): Aqueous extracts of PentaclethraMacrophylla Bentham Roots as Eco-friendly Corrosion Inhibition of mild steel in 0.5M KOH medium, *International Journal of Materials Chemistry*, 6 (1), 12-18.

Alaneme, K. K.; Olusegun, S. J. and Adelowo, O. (2015a): Corrosion inhibition and adsorption mechanism studies of Hunteria umbellata seed husk extracts on mild steel immersed in acidic solutions. *Alexandria Engineering Journal* , 1-9.

Alaneme, K. K.; Daramola, Y.;Olusegun, S. J. and Afolabi, A.(2015b): Corrosion inhibiton and absorption characteristics of rice husk extracts on mild steel immersed in 1M H2SO4 and HCl solutions. *International Journal of Electrochemical Science* , 3553-3567.

Aluko, A. O. and Oke, G. O.(2022): Adsorption and thermodynamics studies of *carica papaya* leaves extract (yellow) as corrosion inhibitor for mild steel in acidic medium, *Journal of Materials Science Research and Reviews,* 9(1): 1-12, Article No. JMSRR. 73435.

Ikeuba, A. I. and P. C. Okafor, P. C. (2018); Green corrosion protection for mild steel in acidic media:Saponins and crude extracts of *Gongronemalatifolium,Pigm.Resin Technol*., vol. 48, pp. 57–64, 2018. https://doi.org/10.1108/PRT-03-2018-0020

Rbaa, M. *et al.* (2020): Synthetic, spectroscopic characterization, empirical and theoretical investigations on the corrosion inhibition characteristics of mild steel inmolar hydrochloric acid by three novel 8-hydroxyquinoline derivatives. *Ionics,* **26**, 503–522.

Fouda, A. S.; El- Askalany, A. H.; Molouk,A. F. S.; Elsheikh, N. S. and Abousalem, A. S.(2021): Experimental and computational chemical studies on the corrosion inhibitive properties of carbonitrile compounds of carbon steel in aqueous solutions, *Scientific Reports*, 11:21672 https://doi.org/10.1038/s41598-021-00701-z

Marzoratti S.; Verotta, L. and Trazatti, S. P.(2019): Green corrosion inhibitors from natural sources and biomass wastes. *Molecules.* 19, 48, 1-24. doi:10.3390/molecules24010048

El Hamdani, N.; Fdil, R.; Tourabi, M.; Jama, C.; Bentiss, F.(2015): Alkaloids extract of *Retama monosperma* (L.) Boiss.seeds used as novel eco-friendly inhibitor for carbon steel corrosion in 1 M HCl solution: electrochemical and surface studies *Appl. Surf. Sci.,* 357 (2015), pp. 1294-1305

Raja, P. B.;Qureshi, A. K.; Rahim, A. A.; Awang, K.; Mukhtar, M. R. Osman, H.(2013): Indole alkaloids of Alstoniaangustifolia var. latifolia as green inhibitor for mild steel corrosion in 1 M HCl media *J. Mater. Eng. Perform.*, 22 (2013), pp. 1072-1078 701-z

Zakeri, A.; Bahmani, E; Aghdam, A. S. R. (2022): plant extracts as sustainable and green corrosion inhibitors for protection of ferrous metals in corrosive media: a mini review; *Corrosion Communications* 5; 25-38. ttps://doi.org/10.0016/j.cor.com.2022.03.002

Abolanle, S. A.; Lukman, O. O.; Solomon, S. D.; John, A. O. O. and Temitope, O. O. (2021): Investigation on corrosion inhibitor of mild steel by extract of *Dracaenaarborea* leaves in Acidic medium, *Chemistry Africa*; 1-12. https://doi.org/10.1007/s42250-021-00246-8

Akinbulumo, O. A.; Odejobi, O. J. andOdekanle, E. L. (2020): Thermodynamics and Adsorption study of the corrosion inhibition of mild steel by *Euphorbia heterophylla*L. extract in 1.5M HCl. *Results in Materials*. 5 (2020).100074. https://doi.org/10.1016/j.rinma.2020.100074

Chen, L.; Lu, D.; and Zhang, Y.(2022): Organic compounds as corrosion inhibitors for carbon steel in HCl solution: A comprehensive Review. *Materials,* 2022. 15, 2023.https://doi.org/10.3390/ma15062023

Ryl, J.; Brodowski, M; Kowalski, M.; Lipinska, W.; Niedzialkowski, P. and Wysocka, J. (2019): Corrosion inhibition mechanism and efficiency differentiation of DihydroxybenzeneIsomers towards Aluminium alloy 5754 in Alkaline media, *Materials,* 12, 3067, 1-12. https://doi.org/10.3390/ma12193067

Popoola, L. T. (2019): Organic green corrosion inhibitors (OGCIs): A critical review.*Corro Rev*. 37 (2): 71-102.

Marsoul A, Ijjaali M, Elhajjaji F, Taleb M, Salim R, Boukir A. (2020): Phytochemical screening, total phenolic and flavonoid methanolic extract of *pomegranate* bark (*Punicagranatum*L): Evaluation of the inhibitory effect in acidic medium 1M HCl. *Mater. Today Proc*. S2214785320328170.

Anyiam CK, Ogbobe O, Oguzie EE, Madufor IC, Nwanonenyi, SC, Onuegbu, GC, Obasi HC, andChidiebere,MA. (2020): Corrosion inhibition of galvanized steel in hydrochloric acid medium by a physically modified starch. SN *Appli. Sci.*2: 520.

Dehghani, A.;Bahlakeh, G.; Ramezanzaeh, M.(2020): Potential Role of a novel green eco -friendly inhibitor in corrosion inhibition of mild steel in HCl solution: Detailed macro/micro-scale experimental and computational explorations. *Constr. Build. Mater.* 2020; 245:1164-84

Prabhu D, Prabhu PR, and Rao R. (2020): Thermodynamics, adsorption and response surface methodology investigation of the corrosion inhibition of aluminium by *Terminaliachebula Ritz*. Extract in H3PO4, *Chemical Papers*. Available: https://doi.org/10.1007/s11696-020-01318-8

Fdil, R.; Tourabi, M.; Derhali, S.; Mouzdahir, A.; Sraidi, K.; Jama, C.; Zarrouk, A.; and Bentiss, F. (2018): Evaluation of alkaloids extract of Retama monosperma (L.) Boiss.stems as a green corrosion inhibitor for carbon steel in pickling acidic medium by means of gravimetric, AC impedance and

surface studies. *J. Mater. Environ. Sci*. 9, 358–369.

Obot, A. S.; Boekom, E. J.; Ita, B. N. and Utam, E. C. (2022): Kinetics consideration of ethanol leaves extract of *CostusLucanusianus* as green corrosion inhibitor for mild steel and aluminium in HCl solution; *International Journal of Research-Granthaalayah* 10(1), 106-118.doi.10.29121/granathaalayah.v10.i1.2022.4461.

NMS-TP017

ROLE OF NIGERIAN COAL IN ENERGY SUSTAINABILITY AND ECONOMIC DEVELOPMENT

[1]Felix B. Fatoye and [2]Olusegun T. Joshua

[1]Department of Mineral and Petroleum Resources Engineering, Kogi State Polytechnic, Lokoja.
[2]Department of Metallurgical and Materials Engineering, Kogi State Polytechnic, Lokoja..
E-mail: feliztoye@yahoo.com; segetin80@yahoo.com

ABSTRACT

Coal is one of the fossil fuels found in abundance in Nigeria that if well managed, will sustain the energy and improve the economy of the nation. In countries like USA, China, India, Germany and South Africa coal is their primary source of electricity and it has sustained their economy. Apart from sparsely reported occurrences of lignites and minor sub-bituminous coals in the Sokoto Basin, in the Mid-Niger (Bida) Basin and in the Dahomey Embayment, all the coal deposits of Nigeria occur in the Benue Trough and the Anambra Basin. However, Anambra Basin appears to contain the largest and most economically viable coal resources in the country. Nigerian coal is suitable for electricity generation and coke making blends for metallurgical processes such as iron and steel manufacture. It is also appropriate in heating boilers and ovens in industrial process heating. The cement, glass, ceramic, paper and brick industries can use it for this purpose. The coal is also a good source of raw material for manufacturing products such as drugs, dyes, plastics, synthetic rubbers, insecticides, antiseptics, paint products, solvents, synthetic fibres, flavourings, perfumes, varnishes, adhesives and numerous other organic chemicals. It can as well be used for the production of gas and automotive fuel. Discussed in this paper are the geological setting, occurrences, reserves, production and uses of Nigerian coal. This paper is generally a review and an assemblage of separate works on Nigerian coal with some minor new information generated in the course of carrying out this work.

Keywords: Nigerian Coal, Occurrences, Reserves, Production, Electricity.

INTRODUCTION

Coal is a combustible organic sedimentary rock that is composed principally of consolidated carbonaceous material derived from vegetation. In other words it is a carbon-rich, combustible, stratified organic sedimentary rock composed of altered and/or decomposed plant remains of non-marine origin, combined with varying minor amounts of inorganic material. What is now coal was originally formed as peat millions of years ago by the prolonged accumulation of plant material in a swampy environment. The peat was subsequently altered to coal through chemical and physical processes.

Nigeria is endowed with large coal deposits. Apart from sparsely reported occurrences of lignites and minor sub-bituminous coals in the Sokoto Basin (Kogbe, 1989), in the Mid-Niger (Bida) Basin (Adeleye, 1989) and in the Dahomey Embayment (Reyment, 1965), all the coal deposits of Nigeria occur in the Benue Trough and the Anambra Basin (Fatoye, *et al*., 2020).

The Anambra Basin is a major coal producing basin in Nigeria where intensive exploration and exploitation activities have been on since 1916 owing to the discovery of commercial coal in Udi near Enugu in 1909 by the Mineral Survey of Sothern Nigeria (Famuboni, 1996).

Coal mining commenced in Nigeria in 1916 at Ogbete drift mine near Enugu. Coal production was initially concentrated in Enugu where four mines (Iva Valley, Onyeama, Okpara and Ribadu) were worked by the Nigerian Coal Corporation (Orajaka *et al*., 1990). Two other mines were later opened at Okaba in Kogi State and Orukpa in Benue State. Production started from a modest beginning (24,903 tonnes in 1916) and gradually rose to an annual output of about

700,000 tonnes in 1966 just before the outbreak of the Nigerian civil war (NCC, 1982).

Coal production in Nigeria has however ceased since 1990s due to the national policy of total dependence on oil and oil-derived foreign exchange in planning the nation's economy. Attempts by the Federal Government in large scale carbonization of Nigerian coal especially Enugu coal remained unsuccessful.

Coal is one of the cheapest and most important sources of energy, responsible for 41% of electricity production worldwide. In many countries like India, China, Germany, USA, coal is the primary source of electricity and energy. Other smaller countries also heavily rely on coal, for example Poland 94%, South Africa 92%, China 77% and Australia 76% of electricity (Shah, 2011).

The Nigerian coal industry must be seen as a long neglected economic frontier that needs urgent resuscitation. It is one major area that can change the economic fortune of this great country. Its potential for growth is on the upward swing.

This article therefore, discussed the role of Nigerian coal in energy sustainability and economic develoment.

Geological Setting

The coal resources discovered so far in Nigeria occur within geological units known as the Coal Measures, represented by the Early to Late Maastrichtian Mamu Formation (Lower Coal Measures) and the Late Maastrichtian to Danian Nsukka Formation (Upper Coal Measures). The structural setting and general geology of the Anambra Basin have been widely reported (Nwajide and Reijers, 1996; Obaje *et al*., 1999; Umeji, 2005). Stratigraphically, the coal bearing sequence lies within the Mamu Formation (Early to Late Maastrichtian) which consists of paralic sandstones, mudstones and coals. The Formation is underlain by the Nkporo Formation (Campanian to Maastrichtian), which is predominantly marine and paralic shales, and is overlain by the Ajali Formation (Middle to Late Maastrichtian) which consists of fluviodeltaic sandstones (Fig. 1). And the Nsukka Formation (Late Maastrichtian to Danian), also a paralic coaly sequence, completes the succession (Umeji, 2005).

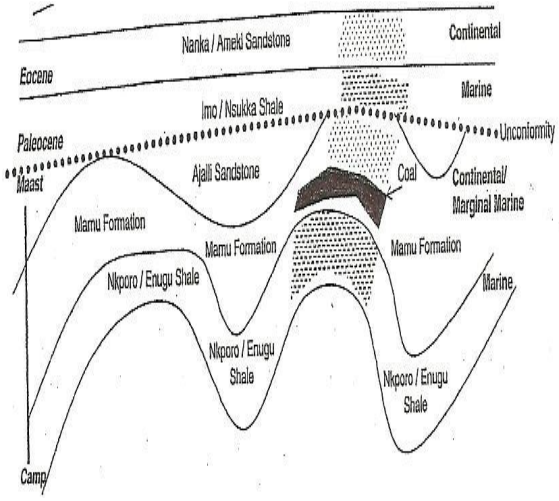

Fig. 1. Stratigraphic succession in the Anambra Basin (after Obaje, 2009).

Coal Occurrences in Nigeria

The Nigerian coals are sub-bituminous (black coals) of Campanian–Maastrichtian age, and lignites (brown coals) of Tertiary age. However, the Obi-Lafia coal deposit is geologically, the oldest coal deposit in Nigeria so far discovered. This deposit is believed to be Turonian–Coniacian in age (Obaje and Hamza, 2000). The Obi-Lafia coal deposit in Nasarawa State has been described as coking coal by the Nigerian Steel Development Authority (NSDA) now National Steel Raw Materials Exploration Agency (NSRMEA) which carried out detailed investigation of the deposit some decades after it had been reported by the Geological Survey. It is the only coking coal so far discovered in this country with estimated reserves of 22.4 million tonnes and the greater part of the deposit is yet to be fully explored (Obaje, 1994). The coal occurs within the Awgu Formation, which is dominantly shales, limestones, and sandstones.

Mineable coal deposits in Nigeria occur at Enugu, Ezimo and Inyi in Enugu State; Orukpa in Benue State; Okaba, Okobo, Ogboyaga and Odokpono in Kogi State; Obi-Lafia in Nasarawa State; and Chikila in Adamawa State (Obaje, 2009).

Other areas where coal outcrops in Nigeria include: Jamata in Kogi State, occurring as thin seams in Patti Formation of Maastrichtian–Campanian age. Coal seams were also discovered near Doho in Gombe area of Gombe State. They occur in Kerri-Kerri Formation of Paleocene age. Several coal outcrops have been reported from Garin Maiganga, south of Gombe. National Steel Raw Materials Exploration Agency (NSRMEA) has been exploring for coal in that area. This coal belongs to the Gombe sandstone Formation of Cretaceous age.

Coal seams are exposed at Igaliwo, Olokwu and Ogbagebe around Ankpa and at Ibobo, Effin-Okai, Emewe-Effopa, Okatakpokpo, Udane-Biomi and Edimogo/Ikpabacha around Dekina, all in Kogi State. The coal seams which occur near Afikpo, Ebonyi State, in sediments older than the Lower Coal Measures have been examined, but proved to be patchy and unworkable. Coal seams have been discovered at Afuze, near Auchi in Edo State, and at Ute near Owo in Ondo State, but they are very thin and it is unlikely that economic deposits will be found further to the west. Thin, unworkable seams of poor quality are also known to occur around Lamja in Adamawa State.

A large coal reserve probably in excess of 1,000 million tonnes is also believed to occur within the Mamu Formation at depth of over 600 m in Amansiodo area of Enugu State (Famuboni, 1996). Thin coal seams have also been discovered at Gindi-Akunti, Plateau State and at Janata-Koji area of Kwara State

.

Table 1: Locations of some coal deposits in Nigeria.

Mineral	Location	State
Coal	Chikila and Lamja	Adamawa
	Orukpa	Benue
	Afikpo	Ebonyi
	Afuze	Edo
	Enugu, Ezimo, Inyi and Amansiodo	Enugu
	Doho (Gombe) and Garin Maiganga	Gombe
	Okaba, Okobo, Ogboyaga, Odokpono, Igaliwo, Olokwu, Ogbagebe, Ibobo, Effin-Okai, Emewe-Effopa, Okatakpokpo, Udane-Biomi, Edimogo/Ikpabacha and Achokpa	Kogi
	Janata-Koji	Kwara
	Obi-Lafia	Nasarawa
	Ute	Ondo
	Gindi-Akunti	Plateau

Coal Reserves

The Nigerian type of coals is generally classified as sub-bituminous and lignitic coals and are geologically young (about 70 million years). Some lignite exposures have been found around Afuze in Edo State, Ogwashi/Asaba in Delta State and Nnewi Oba areas of Anambra State. The total reserves of the lignite is estimated at over 250 million tonnes, while the nation is known to have an estimated 2.5 billion tonnes of coal reserves, of which only 43% are proven (MSMD, 2008).

Coal Production – Historical Perspective

In 1909, coal was discovered in Udi near Enugu, Nigeria. The Ogbete drift mine opened six years later. Coal production took off in 1916 with a modest initial figure of 24,903 tonnes consequent upon the completion in the same year of the Eastern Rail-line from Port Harcourt to Enugu (NCC, 1974; 1982). The Ogbete mine's operations and others in the country were merged into a new corporation in 1950: The Nigerian Coal Corporation (NCC). The NCC was tasked with exploiting coal resources, and held a monopoly on coal mining, production, and sales until 1999.

Coal production in Nigeria took an exponential leap over the years to 1929 when about 350,000 tonnes were produced. The world economic crisis and the famed depression in the 1930's registered its mark and caused a drop in coal output. Production picked up again with the second world war of 1939 to 1945, as extra fuel was required for the numerous boiler stations and steam boats used to prosecute the war.

The period 1955 to 1959 could be said to be the years of glory for the industry. This rise is explained in the fact that the Nigerian Cement Company (NIGERCEM), Nkalagu in 1955 became yet another major consumer of coal in addition to the traditional users, the Nigerian Railway Corporation (NRC) and Electricity Corporation of Nigeria (ECN). Coal was also exported to Ghana and Egypt within the period. Coal was the only energy resource available to the country. It therefore single-handedly pioneered Nigeria's industrial growth in the pre-oil era.

Nigeria's coal industry suffered after 1956, when oil was discovered. Up until this point, the NRC was the largest consumer of coal in the country. However, after the discovery of oil, the Railway Corporation began to replace its coal burning trains with diesel-powered engines thereby abandoning coal. An additional negative impact came when the ECN began converting its power generation equipment from coal to diesel and gas as well.

Shortly after, the Nigerian civil war set in and climaxed the decline. With Enugu as the main theatre of the Nigerian civil war, the coal industry was grounded, a fortuitous combination of circumstances indeed for the industry. Given the situation, a number of other industrial set-ups at the point of considering coal as fuel source found a ready excuse and went for alternative energy sources.

At the end of the civil war in 1970, the abandoned coal mines at Enugu had become the source of formidable rivers with all the underground and surface installations completely inundated and damaged. The period 1970 to 1975 witnessed a picking up situation until the military administration in 1976 decided to mechanize the mines. The contract went to a Polish Company, Kopex. Unfortunately for the industry, the mechanization bid was a colossal failure. Production even went below pre-mechanization levels.

In the over ninety years of coal mining in Nigeria, about twenty-five million tonnes of coal have been mined, largely from the Enugu coal field in the Anambra Basin. Coal production figures from Nigeria coal fields between 1916 and 1981 are as shown in Table 2.

Table 2: Coal production in Nigeria between 1916 and 1981 (after NCC, 1974; 1982)

Year	Production (Tonnes)	Year	Production (Tonnes)	Year	Production (Tonnes)
1916	24,903	1937/38	397,418	1958/59	919,883
1917	34,739	1938/39	328,438	1959/60	695,757
1918	147,733	1939/40	304,891	1960/61	565,473
1919	140,050	1940/41	323,692	1961/62	606,046
1920	183,004	1941/42	409,082	1962/63	625,532
1921/22	197,178	1942/43	471,402	1963/64	609,833
1922/23	114,623	1943/44	536,875	1964/65	709,678
1923/24	117,939	1944/45	678,849	1965/66	742,922
1924/25	233,684	1945/46	513,654	1966/67	544,485
1925/26	246,463	1946/47	643,993	**Total**	**22,870,192**
1926/27	358,926	1947/48	560,533	1970/71	24,794
1927/28	350,828	1948/49	620,048	1971/72	179,351
1928/29	369,563	1949/50	534,429	1972/73	323,001
1929/30	352,669	1950/51	592,768	1973/74	314,457

1930/31	332,924	1951/52	575,455	1974/75	250,769
1931/32	267,763	1952/53	623,188	1975/76	257,832
1932/33	264,018	1953/54	690,308	1976/77	249,446
1933/34	238,045	1954/55	686,734	1977/78	246,192
1934/35	263,035	1955/56	762,059	1978/79	188,806
1935/36	261,406	1956/57	802,670	1979/80	153,005
1936/37	315,273	1957/58	860,070	1980/81	114,875

Uses of Coal

The uses of coal include the following;

Electricity Generation: Coal is used for electricity generation. When burned, coal generates energy in the form of heat. In a power plant that uses coal as fuel, this heat converts water into steam, which is pressurized to spin the shaft of a turbine. This spinning shaft drives a generator that converts the mechanical energy of the rotation into electric power.

Their characteristics properties (low sulphur and ash content and low thermoplastic properties) (MSMD, 2008), make Nigerian coals ideal for coal-fired electric power plants.

Coke Manufacture: Coal is used by the steel industry, mostly for the manufacture of coke (coking coal) for metallurgical processes such as iron and steel manufacture. The steel industry uses coal by first heating it and converting it into coke, the primary source of carbon used in steel making. The coke is combined with iron ore and limestone. Then the mixture is heated to produce iron. The high-volatile bituminous coal in Obi-Lafia, Middle Benue Trough is most suitable raw material for coke making in steel manufacture. Enugu coal however, blended with Obi-Lafia coal and imported high grade coals could be useful in this respect.

Domestic Fuel: The calorific value of an air dried sample of Nigerian coal is usually between 7,000 and 8,000 kca/kg (Orajaka *et al*,. 1990), and as its combustibility is good, it can be used as a domestic fuel. It gives a gas of high calorific value and produces exceptional yields during low-temperature carbonization processes.

Gas Fuel: Fuel companies convert coal into easily transportable gas or liquid fuels. Coal-based vapour fuels are produced through the process of gasification. Gasification may be accomplished either at the site of the coalmine or in processing plants. In processing plants, the coal is heated in the presence of steam and oxygen to produce synthesis gas, a mixture of carbon monoxide, hydrogen, and methane used directly as fuel or refined into cleaner-burning gas.

Industrial Uses: Coal is a source of a vast number of chemical products, most of them by-products of the carbonization or dry distillation of coal. In this process of carbonization, coal is heated to about $1{,}100^0$ C ($2{,}012^0$ F) in a carbonizing chamber, driving off the volatile constituents and leaving metallurgical coke. In the process of making coke from coal, a large number of volatile matters are produced as by-products such as coal tar, light oils, chemicals, sulphur, ammonia and gas.

Products made from coal tar include nylon and other artificial fibres, dyes, antiseptics, flavourings, perfumes, drugs such as aspirin and the sulfa drugs, pitch, materials for paints and varnishes synthetic rubbers and plastics, and a large number of organic chemicals.

The light oils are used to make solvents, detergents, synthetic fibres, and insecticides. Ammonia, as ammonium sulphate, is used as fertilizer, and sulphur is an ingredient in plant insecticides.

CONCLUSION

Their characteristics properties of low sulphur and ash content and low thermoplastic properties make the Nigerian coal ideal for coal-fired electric power plants. Nigerian coal is found suitable for boiler fuel, production of high calorific gas, domestic heating, briquette, formed coke and the manufacture of a wide range of chemicals including waxes, resins, adhesives, and dyes. Bituminous coal at Obi-Lafia can be used to produce formed-coke of metallurgical quality.

The proficient management of the Nigerian coal industry to ensure maximum coal exploration and utilization, coupled with well articulated government policies will have a considerable impact not only on the energy sustainability but also on the economic development of the country. Good management of the industry will enhance coal development leading to additional income per capital earnings and improved balance-of-payments position for Nigeria.

Also the development and utilization of coal will create job opportunities for many unemployed Nigerians. Furthermore, utilization of Nigerian coal will have a multiplier effect on other industries.

REFERENCES

Adeleye, D. R. (1989). The Geology of the Mid-Niger Basin. In: Kogbe C. A. (Ed) Geology of Nigeria, 2nd Edn. Elizabethan Publishing Co., Lagos, pp. 283 – 287.

Famuboni, A. D. (1996). Maximizing Exploration of Nigeria's Coal Reserves. In: Nigerian Coals: A Resource for Energy and Investments, Famuboni, A. D. (ed.). Raw Materials Research and Development Council (RMRDC), Abuja, Nigeria, pp. 39 – 62.

Fatoye F. B., Gideon,Y. B. and Omada J. I. (2020). Maceral Characterization of the Cretaceous Effin–Okai Coal Deposit in Northern Anambra Basin, Nigeria. *Communication in Physical Sciences,* 5, 3, pp. 223 – 232.

Kogbe, C. A. (1989): Geology of Nigeria, 2nd edition. Rockview Nigeria Ltd, Jos, 538 pp.

Ministry of Solid Minerals Development, (2008). Coal – Exploration Opportunities in Nigeria. Ministry of Solid Minerals Development in Conjunction with Nigerian *Geological Survey Agency*, pp. 4 – 7.

Nigerian Coal Corporation, NCC (1974). Analysis and Calorific Values of Nigerian Coal, Enugu, 3.Nigerian Coal Corporation, NCC (1982). Information on the Nigerian Coal, Enugu. pp. 7.

Nwajide, C. S. and Reijers, T. J. A. (1996). Sequence Architecture in Outcrops: Examples from the Anambra Basin, Nigeria. *NAPE Bulletin* 11, pp. 23–33.

Obaje, N. G. (1994). Coal Petrography, Microfossils and Palaeo-environments of Cretaceous Coal Measures in the Middle Benue Trough of Nigeria. Tubinger Mikropalaotonlogische Mitteilungen, 11:1 – 165.

Obaje, N. G., Ulu, O. K. & Petters, S. W. (1999). Biostratigraphic and Geochemical Controls of Hydrocarbon Prospects in the Benue Trough and Anambra Basin, Nigeria. *NAPE Bulletin*, 14, pp. 18–54.

Obaje, N. G. and Hamza, H. (2000). Liquid Hydrocarbon Source-rock Potential of Mid-Cretaceous Coals and Coal. Measures in the Middle Benue Trough of Nigeria. *International Journal of Earth Science*, 89:130 – 139.

Obaje, N. G. (2009). Geology and Mineral Resources of Nigeria. Springer Dordrecht Heidelberg London New York, 60:140 – 141.

Orajaka, I. P., Onwuemesi, G., Egboka, B. C. E. and Nwanfor, G. I. (1990). *Nigerian Coal Mining Magazine*. pp. 446 – 451.

Shah, A. (2011). Uses of Coal – Electricity, Steel and Cement Biggest Users of Coal. Green World Investor. www.greenworldinvestor.com

Reyment, R. A. (1965): Aspects of the Geology of Nigeria. University Press, Ibadan. 145 pp.

Umeji, O. P. (2005). Palynological Study of the Okaba Coal Mine Section in the Anambra Basin, Southern Nigeria. *Journal of Mining and Geology*. 41(2), pp. 194.

NMS-TP018

DEVELOPMENT OFA COMPREHENSIVE MECHANISTIC MODEL FORPREDICTION OF EROSIVE WEAR IN PIPELINES DUE TO SOLIDPARTICLES IMPACT

Martins Obaseki*[1], Paul T. Elijah[1], Peter B. Alfred[2]
[1] Department of Mechanical Engineering, Faculty of Engineering, Nigeria Maritime University, Okerenkoko, Nigeria
[2] Department of Mechanical Engineering, Faculty of Engineering, University of Port Harcourt, Port Harcourt, Nigeria
Corresponding author email: martins.obaseki@nmu.edu.ng; paul.elijah@nmu.edu.ng; peteralfred.b@gmail.com

Abstract
Inner-wall erosive wearis a key problem in particles-liquid slurry pipeline and petroleum pipeline carrying raw crude or gas in mixture of particles from wells. To overcome the challenges of erosion in slurry pipeline, a predictive model is required to always monitor the conditions of flow and to determine when maintenance and/or replacement of parts will be required. The intent of this study is to develop aninner-wall erosive wear rate mechanistic model that can predict erosion of pipeline due to the presence of solid particles. A mechanistic inner-wall erosive wear rate model was developed based on Hertzian contact model and Du and Wang elastoplastic impact model taken the deformation of the erodent particles and the effective impact angle into consideration. The developed model was compared with three different models, namely the Erosion and Corrosion Research Center(E/CRC) erosion model, Det Norske Veritas (DNV) erosion model and the Oka's erosion model. The mechanisticmodel of this study shows a perfect agreement with all the models but more perfect agreement was observed with the E/CRC and the DNV model. The trend of variation of erosive wear rate with impact angle, particle velocity, and mass flow rate was the same for all the tested models and the developed model. On the occasion of particle diameter, the developed model shows that particle erosion rate is independent of particle diameter for any given constant particle mass flow rate. This observation is consistent with the E/CRC and DNV models but not Oka's model. The developed mechanistic modelpresented in this study will be useful for accurate prediction of inner-wall erosion wear of pipelines conveying slurries of solid particles in fluid thereby reducing associated danger.
Keywords: Mechanistic erosive wear rate model, impact angle, impact velocity, eroded crater.

1. Introduction

Slurry flow in pipeline is one of the common ways of transporting coal from the point of mining to where it is utilized. Slurry flow is a combination of liquid and solid in a single flow in pipeline. Slurry flow is mostly turbulent so as to prevent particles settling in the pipeline bed as they were carried along the career fluid in the pipeline. Slurry pipelines are not only for transporting coal but for long distance transportation other mining and chemical products such as iron, copper, phosphate concentrates oil-sand mixture and other mineral ores [1, 2]. In the Petroleum industries, oil and gas taken from well through pipelines can be described as a form ofslurry flow consisting of fluid (oil or gas), sand and several other solid particles components [3, 4].

One of the problems of slurry pipeline is erosive wear of the pipeline inner-walls.Pipeline carrying mixture of solid particles and fluid such as air, water,

petroleum etc. are subject to erosion rate of the internal surfaces, pipe bents and fittings. The erosion rate of the pipeline surface is as a result of repeated particle impact causing several indentations, cuttings, gradual removal and wearing away of the surface [5]. All slurry pipelines are more susceptible to erosive wear. Erosive wear in pipeline causes reduction in the pipe thickness thereby reducing the integrity of the pipe and the ability to withstand higher pressure. Also, erosive wear in pipeline creates spots where pitting corrosion may likely emanate especially when the pipeline is temporarily out of service. If erosion is not properly monitored, it can be hazardous and can lead to complete damage and shut down of pipelines and the entire production facility leading to economic losses [2, 4].

An in-depth understanding of the mechanism and processes of erosive wear and methods of controlling or monitoring it is necessary especially for oil and gas industries and chemical transporting products through pipelines. Estimating erosion rate of pipeline is a tedious one; however, researchers in the field of Computational Fluid Dynamics (CFD) are doing more work aimed at simplifying the analysis of erosion rate. One of the ways to do this is mathematical modeling and simulations. A Simplemathematical model is developed, then written in CFD codes and run in a software such as ANSYS which produces the result in a graphical user interface (GUI) for better understanding. There are many existing erosion models, some of which will be look at here.

The erosive wear model of particles flowing in fluid and impinging in a surface was first proposed by Finnie [6]. Finnie developed an erosion model in which the volume of material remove per impact is proportional to the square of the particle impact velocity and depends on other factor such the impact angle and the particle mass. Bitter [7] and Bitter [8] proposed another model for erosion due to impact. He explained that impact by particle can either cause indentation or scratching of the surface, all depending on the particle impact angle. Bitter's erosion volume rate is the sum of the eroded volume due to indentation and that due to scratching or cutting processes. Bitter's model was later modified for ductile materials by Nelson and Gilchrist [9]. Nelson and Gilchrist [9] erosion model were based on their experimental data and it is a two-part equation model, one part accounting for deformation and the other part for cutting mechanism. Hashish [10] presented a modified model of Finnie erosive wear model. In the modified model, the impact velocity exponent of Finnie which was originally 2 was changed to 2.5. The impact angle function was also modified. Hashish also introduces the particle shape function in the modified model. Huang et al. [11] developed a model which includes both indentation and cutting of the target material and also account for property of both the erodent and the target that aid erosion. The model was compared with experimental data of Bitters and Finnie and good agreement was reported. Huang et al. [11] noted that particle impingement on straight pipe wall is due to gravitational settling and turbulence fluctuation and as such the impact angle is much smaller, however there are much larger impact angle at bents and fittings leading to much erosion in them.

Many empirical correlation models for erosive wear were formulated by researchers most of which are based on experimental data. Most of these correlations are preferable in industrial application and are included in Codes and Standards. Some of these correlation models will be discussed briefly here; The Erosion and Corrosion

Research Center (E/CRC) of the University of Tulsa developed an empirical erosive wear model for carbon steel based on direct McLaury'sexperimental data [12]. In this model, some key parameters such as the erodent sharpness factor and the target hardness were considered. Oka et al. [13] developed an empirical model for erosion of material surface due to particle impingement. Many influencing factors which include target material hardness and mechanical properties of the erodent. Oka and Yoshida [14] modified the model in part 2 of their article by including the reference erodent particle velocity and diameter. Oka's model is also applicable for predicting erosive wear in ductile materials. The model was one of the preferable models for predicting erosion. Det Norske Veritas [15] developed an empirical erosive wear model popularly known as the DNV model for predicting erosion in straight, bent pipes and pipe fittings. Large number of experimental data and numerical results were gathered to formulate the model. The DNV erosion model was found to predict erosion rate at much accuracy when compared with experiment data from a different source other than that of the developer Peng and Cao [16].

Other erosive wear models were also reported by Ahlert, [17], Meng and Ludema, [18], Hutchings, [19], Chen et al. [20] etc. Most of these models are empirical correlation and are material specific, that is, they are developed based on the experimental data obtained from experiment performed on a particular target material and erodent. One major problem with empirical models is that they may fail if use to predict erosion of materials with different properties from the one used in developing it. For instance, Oka's model was more realistic, but it was reported by Peng and Cao, [16] to have deviated in the prediction of erosion rate of steel pipe elbow when compared with experimental data of Eyler, [21]. Again, to the best of our knowledge, few specific empirical correlation modelshave been reported for coal slurry pipeline.

To study the erosion of particles slurry in carbon steel pipeline, this study will attempt to developed a more general and mechanistic model to ascertain inner-wall erosion wear rate. The model will first be tested against some preferable existing erosive wear models for carbon steel in this study. Finally, the verification of the developed mechanistic model by using a large rang experimental database is draw at the end of the study in order to showcase the accuracy and universal applicability of the developed model.

2 METHODS

The aim of this study is to develop an inner-wall erosive wear rate mechanistic model that can predict erosion of pipeline due to the presence of solid particles.A mechanistic inner-wall erosive wear rate model was developed based on Hertzian contact model and Du and Wang elastoplastic impact model taken the deformation of the erodent particles and the effective impact angle into consideration. The developed model was compared with three different models, namely the Erosion and Corrosion Research Center (E/CRC) erosion model, Det Norske Veritas (DNV) erosion model and the Oka's erosion model. Ultimately, the verification of the developed mechanistic model by using a large rang experimental database is draw at the end of the study in order to showcase the accuracy and universal applicability of the developed model.

2.1 Model implementation

There are several erosion models; however, most of the models are empirical correlations. Most of the existing empirical models are CFD-based erosion models, some of which are already built-in in

ANSYS FLUENT. The study will look at different predictive equations model'swhich include Finnie model, Oka's model, DNV model and the E/CRC erosion model.

The Finnie erosion model was developed by Finnie et al. [22] and is given as Brown, [23];

$$E_v = CV_p^n g(\alpha) \quad (1a)$$

$$g(\alpha) = \begin{cases} \frac{1}{3}cos^2\alpha & for\ 18.5^0 \le \alpha \le 90^0 \\ \sin(2\alpha) - 3sin^2\alpha & for\ \alpha \le 18.5^0 \end{cases} \quad (1b)$$

Where; E_v is the erosion rate, C is the target material constant n is the velocity exponent.$\alpha$is the impact angle.The Oka's model was proposed from experimental results of Oka and Yoshida, [14] and Oka et al. [13]. The Oka's model is given as;

$$E_v = \left[10^{-9} m_p k (H_v)^{k_1} \left(\frac{V_p}{V'}\right)^{k_2} \left(\frac{d}{d'}\right)^{k_3}\right] g(\alpha) \quad (2a)$$

$$g(\alpha) = (\sin\alpha)^{n_1}[1 + H_v(1 - sin\alpha)]^{n_2} \quad (2b)$$

Where; E_v is the erosion rate $(m^3/impact)$,H_v is the Vickers hardness of the target materials, m_p is the mass of the particle, V' and d' are the reference velocity and diameter of particle. $k, k_1, k_2, k_3, n_1, n_2$ are constants depending on the particle type.Det Norske Veritas formulated an erosion model in 2007 known as the DNV model [15]. The erosion model was developed based on experimental data. The model predictive equation is given as;

$$E_v = KV_p^n g(\alpha) \quad (3a)$$

$$g(\alpha) = \sum_{i=1}^{8} (-1)^{i+1} A_i \alpha^i \quad (3b)$$

Where; E_v is the erosion rate, K is the target material constant (K =2 x10^{-9} for steel), n is the velocity exponent (n = 2.6 for steel), $A_1\ to\ A_8$ are given in order as; 9.37, 42.295, 110.864, 175.804, 170.137, 98.398, 31.211, and 4.17.E/CRC Erosion Model, this model was proposed by the Erosion /Corrosion Research Center (E/CRC) of the University of Tulsa McLaury, [12]. The erosion model was developed based on experimental data obtained by direct impact of particles of different shapes on carbon steel. The model is given as reported in Zhang et al. [24] as;

$$E_v = Kf(BH)^{-0.59} V_p^n g(\alpha) \quad (4a)$$

$$g(\alpha) = \sum_{i=1}^{5} A_i \alpha^i \quad (4b)$$

Where; E_v is the erosion rate, K is the target material constant (K =2.17 x10^{-7} for carbon steel), n is the velocity exponent (n = 2.41 for carbon steel), BH is the Brinell hardness of target material, f is the particle sharpness factor ($f = 1$ for sharp angular shape, $f = 0.53$ for semi-round, $f = 0.2$ for fully round shape. $A_1\ to\ A_5$ are given in order as; 5.3983, -10.1068, 10.9327, -6.3283, and 1.4234.

2.2Erosion Wear Model Development Process

Erosion of coal slurry pipeline is due to particles impact on the wall of the pipe. The impacting particles cause elastic-plastic deformation of the surface of the pipeline creating temporary asperity-like-protrusions which are washed away by the combine effect of fine particles and high-pressured flowing fluid.

2.2.1. Impact Velocity and Impact Angle.
Particles in a slurry flow always impact on the walls and bent of the pipeline conveying the slurries. Most times, the particles impact on the pipeline at angle called the impact angle. The impact angle depends on the particle trajectory, and as such impact angle varies depending on the turbulence of the slurry flow.

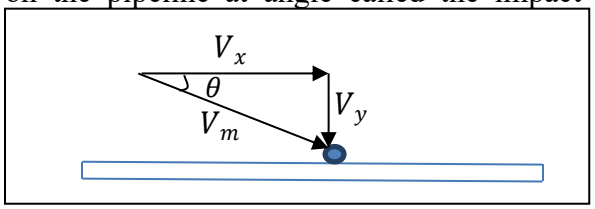

Fig. 1: Impact velocity and impact angle

The particle velocity is in the direction of flow, but may swill due to turbulence and hit the adjacent surface at angle. From Fig 1, the vertical component of the velocity V_y is directed. Where; V_x is the horizontal component of the velocity of impact, θ is the impact angle and V_m is the impact velocity. From Fig 1, the impact angle and the impact velocity can be calculated as;

$$\theta = \tan^{-1}\left(\frac{V_y}{V_x}\right) \quad (5)$$

The vertical and the horizontal component of the impact velocity is given in terms of α as;

$$V_x = V_m \cos\alpha \quad (6a)$$

$$V_y = V_m \sin\alpha \quad (6b)$$

Where; α is a function of θ. For ductile material, the effective value of the impact angle has been modeled by many researchers. In this study, carefully studying the E/CRC model and the DNV model, the impact angle function is proposed as;

$$\alpha = \sum_{i=1}^{5} A_i \theta^i \quad (7a)$$

Where; A_1 to A_5 are given in order as; 4.15, -9.62, 11.02, -6.26, and 1.368.Expanding (7a) and inserting the numerical values of A_i gives;

$$\alpha = 4.15\,\theta - 9.62\,\theta^2 + 11.02\,\theta^3 - 6.26\,\theta^4 + 1.368\,\theta^5 \quad (7b)$$

θ is in Radian, therefore, α in this study is computed in Radian and the final result converted to degrees. Fig 2 shows the variation of impact angle function α with θ for DNV, E/CRC and this study.

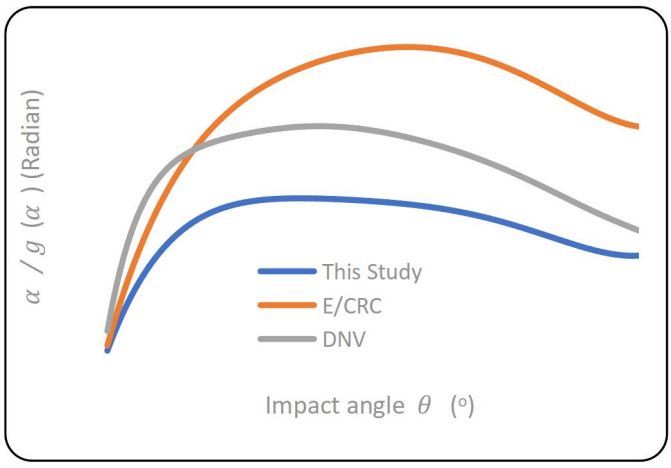

Fig 2: Variation of α and g(α) with θ

2.2.2. Impact Erosion Damage

According to impact theory, when two bodies collide, they deform. The depth of deformation is a function of yield strength (or Hardness of the bodies). For the case of slurry flow in pipeline, the indenters are the suspended slurry particles and the target is the pipeline. According to Du and Wang [25], the interaction of two bodies during impact can be divided into elastic and elastoplastic region. The impact model is given as;

$$m\ddot{\delta} + F = 0 \tag{8}$$

Where; δ is relative indentation of the impacting bodies (m), F is the impact force (N), $m = m_1 m_2/(m_1 + m_2)$ and m_1, m_2 are the masses of the two impacting bodies. The elastic deformation is model due to Hertz theory and the impact force is given as;

$$F_e = \frac{4}{3} E R^{1/2} \delta^{3/2} \qquad for \quad 0 \le \delta \le \delta_e \tag{9}$$

Where; δ_e is maximum elastic indentation, E and R are the equivalent elastic modulus and radius given as;

$$E = \left[\frac{1 - v_1^2}{E_1} + \frac{1 - v_2^2}{E_2}\right]^{-1} \tag{10}$$

$$R = \left[\frac{1}{r_1} + \frac{1}{r_2}\right]^{-1} \tag{11}$$

Where; E_1 and E_2 are the elastic modulus of the indenter and the target respectively, v_1 and v_2 are the poison ratio for indenter and target respectively and r_1 and r_2 are the radius of indenter and target respectively, for spherical indenter impact on a flat surface target $R = r_1$. The maximum elastic indentation has been derived for spherical object punch-impact on a flat surface as Du and Wang [25];

$$\delta_e = R\left(\frac{\pi P_0}{2E}\right)^2 \tag{12}$$

Where; P_0 is Maximum impact pressure (Pa). The maximum impact pressure for spherical impactor on a flat surface of the target material at the onset of elastoplastic

deformation has been determined to have a value of $P_0 = 2.57\sigma_y$, σ_y is the yield strength of the target material Du and Wang, [25].

The elastic deformation is not permanent, rather it restores to original shape after impact. If the energy of the impactor is enough to go beyond the elastic limit, permanent indentation occurs. For wear to ccur in the pipeline, particles impact must cause permanent indentation. Beyond the elastic limit of the target material, plastic indentation occurs in the inner core layers while elastic deformation occurs on the outer layer in contact with the impactor. This is known as elastoplastic deformation.

$$\delta_p = \delta_m - \left[\frac{3R^{1/2}\pi P_0 \delta_m}{4E} - \frac{1}{16}\left(\frac{R^{1/2}\pi P_0}{E}\right)^3\right]^{2/3}$$

Equation (13) and (14) was originally developed for impact analysis of two deformable spheres but will be applied here to analyze the deformation of a pipe wall due to spherical particle impact. To apply this model, we assumed that both the impactor and the target are indented, that is;

$$\delta_w = \delta_p\left(1 + \frac{H_w}{H_p}\right)^{-1}$$

2.2.3. Erosion Crater Depth

To get the erosion volume per impact, the permanent indentation depth and the crater length are required. From Fig 1, the normal

The impact force for elastoplastic deformation has been modeled by Du and Wang [25] for impact of two deformable spheres as;

$$F_{ep} = R\pi P_0 \delta - \frac{R^2(\pi P_0)^3}{12E^2} \qquad for \quad \delta_e \leq \delta \leq \delta_m \qquad (13)$$

Where; δ_m is maximum indentation (m). At the end of the impact, the elastic deformation is restituted but the plastic deformation is permanent leaving a crater on the target surface. The relative maximum permanent indentation, δ_p , on the surface due to normal load was derived as Du and Wang, [25];

the sum of the indentations of the wall (target), δ_w, and the particle (indenter), δ_s, equals the relative indentation, i.e., $\delta_p = \delta_s + \delta_w$. Also, that the indentation is inversely proportional to Vickers hardness of the materials, i.e, $\delta_s/\delta_w = H_w/H_p$. Where H_p and H_w are the Vickers hardness (GPa) of the solid impacting particles and the pipe wall target respectively. Vickers Hardness, H , in GPa is obtained as, $H\,(GPa) = 0.009807H_V$ where H_V is Vickers Hardness Number. Therefore, the non-reversible permanent indentation depth on the pipe wall is given as;

(15)

impact velocity, V_y , of particles is due to settling and the tangential impact velocity, V_x, is particle axial velocity.

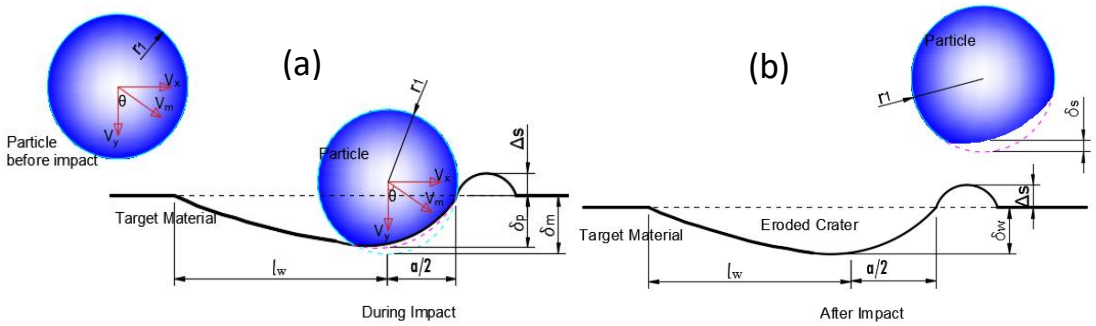

Fig 3: Eroded Crater due to impact (a) Before Impact (b) After Impact

The study also assumed that the kinetic energy (KE) of particles is completely converted to total work done (W_T) during impact as the indenter decelerates to zero at maximum indentation, thus,

at maximum indentation, the final velocity is zero and the total normal kinetic energy is $KE = \frac{1}{2}mV_m^2Sin^2\alpha$. Where; $m =$ mass of particle.

$$KE = W_T \tag{16}$$

The total Work done, W_T, is the sum of the work done in the elastic, W_e, and elastoplastic, W_{ep}, region during impact.

$$W_T = \int_0^{\delta_e} F_e\, d\delta + \int_{\delta_e}^{\delta_m} F_{ep} d\delta \tag{17}$$

Substituting (9) and (13) into (17) gives the total work done as;

$$W_T = \frac{2}{5}K\delta_e^{5/2} + \frac{1}{2}R\pi P_0\delta_{me}^2 - \frac{R^2(\pi P_0)^3}{12E^2}\delta_{me} \tag{18}$$

Where; $K = \frac{4}{3}ER^{0.5}$ = Hertz constant and $\delta_{me} = \delta_m - \delta_e$

Substituting equation (18) in equation (16) and simplifying gives equation (19) as;

$$\frac{1}{2}R\pi P_0\delta_{me}^2 - \frac{R^2(\pi P_0)^3}{12E^2}\delta_{me} + \frac{2}{5}K\delta_e^{\frac{5}{2}} - \frac{1}{2}mV_m^2Sin^2\alpha = 0 \tag{19}$$

Let;

$$\eta = \frac{R}{6}\left(\frac{\pi P_0}{E}\right)^2 \tag{20a}$$

and

$$\lambda = \frac{4K\delta_e^{5/2}}{5R\pi P_0} - \frac{mV_m^2Sin^2\alpha}{R\pi P_0} \tag{20b}$$

Then, δ_{me} is calculated from equation (19) and (20) as;

$$\delta_{me} = \frac{1}{2}\left(\eta + \sqrt{\eta^2 - 4\lambda}\right) \tag{21}$$

From which the maximum relative indentation δ_m is determined as;

$$\delta_m = \delta_{me} + \delta_e \tag{22}$$

Equation (14) and (15) are then used to calculate relative permanent normal depth of indentation, δ_p and permanent normal depth of indentation on the pipe wall δ_w.

2.2.4. Erosion Crater Length

To determine the crater length, δ_l , the average work done to deform a sectional area of depth, $\frac{\delta_m}{2}$, through a length, δ_l, along the target surface was equated to the total tangential kinetic energy of the impacting particle. Assuming no rolling and sliding of particle, the effective eroded crater length is due to the impact force on a smaller average contact area with contact radius $\frac{\delta_m}{4} \leq a$, where a is the maximum contact radius given as $a = \sqrt{R\delta_m}$. Therefore, going by the equation from Hertz contact model given as $a = \frac{\pi R P_0}{2E}$ and substituting $a = \frac{\delta_m}{4}$, P_0 is updated as P_t given as;

$$P_t = \frac{\delta_m}{4a} P_0 = 0.25 P_0 \left(\frac{\delta_m}{R}\right)^{1/2} \quad (23)$$

Thus, equation (19) -(22) are updated as;

$$\frac{1}{2} R\pi P_t \delta_{ml}^2 - \frac{R^2(\pi P_t)^3}{12E^2}\delta_{ml} + \frac{2}{5} K\delta_e^{\frac{5}{2}} - \frac{1}{2} m V_m^2 cos^2\alpha = 0 \quad (24)$$

Where; $V_m^2 cos^2\alpha = V_x^2$, $\delta_{ml} = \delta_l - \delta_{el}$, and $\delta_{el} = R\left(\frac{\pi P_t}{2E}\right)^2$

Let;

$$\eta_1 = \frac{R}{6}\left(\frac{\pi P_t}{E}\right)^2 \quad (25a)$$

and

$$\lambda_1 = \frac{4K\delta_e^{\frac{5}{2}}}{5R\pi P_t} - \frac{m V_m^2 cos^2\alpha}{R\pi P_t} \quad (25b)$$

Then, δ_{ml} is calculated from equation (24) and (25) as;

$$\delta_{ml} = \frac{1}{2}\left(\eta_1 + \sqrt{\eta_1{}^2 - 4\lambda_1}\right) \quad (26)$$

From which the maximum relative indentation δ_l is determined as;

$$\delta_l = \delta_{ml} + \delta_{el} \quad (27)$$

Equation (14) and (15) are updated as (28) and (29) and used to calculate relative permanent eroded crater length, l_p and permanent crater length on the pipe wall, l_w.

$$l_p = \delta_l - \left[\frac{3R^{1/2}\pi P_t \delta_l}{4E} - \frac{1}{16}\left(\frac{R^{1/2}\pi P_t}{E}\right)^3\right]^{2/3} \quad (28)$$

$$l_w = l_p\left(1 + \frac{H_w}{H_p}\right)^{-1} \quad (29)$$

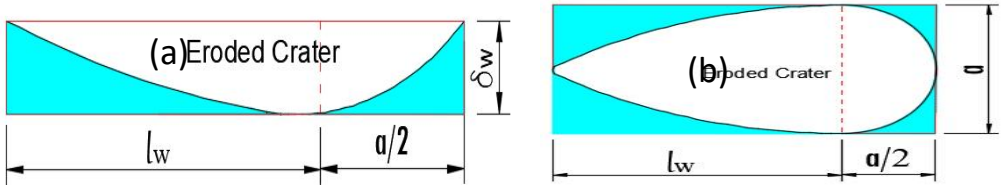

Fig 4: Eroded Crater due to impact (a) Side View (b) Top View

2.2.5 Erosion per Impact

The Erosion volume, E_v, per impact is calculated from the geometry of the indentation in Fig 4 as;

$$E_v = \frac{1}{3}a\delta_w\left(l_w + \frac{1}{2}a\right) \quad (30)$$

Substituting $a = \sqrt{R\delta_w} = \sqrt{r_1\delta_w}$ and simplifying gives;

$$E_v = \frac{1}{3}\left(l_w r_1^{1/2}\delta_w^{3/2} + \frac{1}{2}r_1\delta_w^2\right) \quad (31)$$

Equation (31) was developed assuming the particles is spherical and that erosion is due to indentation only. To account for cutting effect, the sharpness factor, f, of the particle is incorporated into the equation. Some particles may just slide and roll over the surface of the target causing no indentation, i.e., $E_v = 0$. While others cause a maximum indentation, i.e., $E_v = E_{v(Max)}$, the erosion of the surface varies from 0, to maximum, so, the average value is taken. $E_v = \frac{0 + E_{v(Max)}}{2}$, Also, a material constant, k, is added to account for target types. k can be calibrated using experimental data. Fig 5 shows the effect of k on the performance of the model. However, for carbon steel material target, we assumed $k = 1$. Therefore, the final erosion volume ($m^3/impact$) is given as;

$$E_v = k\frac{f}{6}\left(l_w r_1^{1/2}\delta_w^{3/2} + \frac{1}{2}r_1\delta_w^2\right) \quad (32)$$

Where; f is the sharpness factor ($f = 1$ for sharp angular shape, $f = 0.53$ for semi-round, $f = 0.2$ for fully round shape. The erosion volume in (32) can be converted to erosion volume rate, $\dot{E}_v(m^3/s)$, by multiplying it by η, where; $\eta = \frac{\dot{m}}{m}$ is the number of impacting particles per unit time interval, $\dot{m}$ is the mass flow rate of particles and m is the mass of one particle calculated from density and diameter as $m = \frac{\rho\pi d^3}{6}$. $\dot{E}_v$ can also be converted to erosion mass loss rate $\dot{E}_m(Kg/s)$ by multiplying by the target material density, ρ_w. Erosion density, $\dot{E}_d(Kg/m^2s)$, is calculated by dividing $\dot{E}_m$ by the target area, A_t. For $A_t = 1.0\,m^2$, $\dot{E}_d(Kg/m^2s) = \dot{E}_m(Kg/s)$. $\dot{E}_v(m^3/s)$, $\dot{E}_m(Kg/s)$ and $\dot{E}_d(Kg/m^2s)$ are given in equation (33a-c).

$$\dot{E}_v = \eta E_v \quad (33a)$$

$$\dot{E}_m = \eta\rho_w E_v \quad (33b)$$

$$\dot{E}_d = \frac{\eta\rho_w}{A_t}E_v \quad (33c)$$

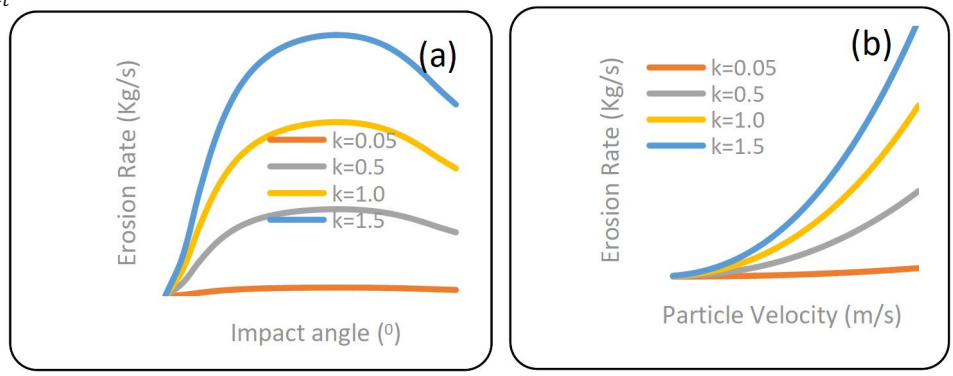

Fig 5: Effect of material constant on the develop model (a) Variation with impact angle (b) Variation with velocity

3. RESULTS AND DISCUSSION

3.1. ResultsVerification and Validations of Model

The Oka's model, DNV model and the E/CRC erosion model is employed to validate the mechanistic model developed in

this study. The erosion rate is calculated in Kg/m^2s . The constants for each of the model as applied to carbon steel target and spherical sand particles (S_iO_2) as erodent are given in Table 1. The mechanical properties of steel required in the developed model are given in Table 2. The material constant for the developed model was taken as unity for carbon steel material (*k=1*).

Table 1: Model constants sand particles erodent and steel target

S/N	Oka's Model		DNV Model		E/CRC Model	
	Constant	Value	Constant	Value	Constant	Value
1	k	65	K	2 x10^{-9}	K	2.17 x10^{-7}
2	k_1	-0.12	n	2.6	n	2.41
3	k_2	$2.3H_w^{0.038}$	A_1	9.37	f	0.2
4	k_3	0.19	A_2	42.295	A_1	5.3983
5	n_1	$0.71H_w^{0.14}$	A_3	110.864	A_2	-10.1068
6	n_2	$2.4H_w^{-0.19}$	A_4	175.804	A_3	10.9327
7	V'	104 m/s	A_5	170.137	A_4	-6.3283
8	D'	$326\mu m$	A_6	98.398	A_5	1.4234
			A_7	31.211		
			A_8	4.17		

Table 2: Mechanical Properties of Erodent and Target material

S/N	**Target (Steel)**		**Erodent (S_iO_2)**	
	Property	Value	Property	Value
1	H_w	1.34	H_p	20
2	BH	120	d	$100\ \mu m$
3	E_2	$209\ GPa$	E_1	74.8GPa
4	v_2	0.3	v_1	0.17
5	σ_y	$470MPa$	V	10-104m/s
6	ρ_2	$7800\ Kg/m^3$	ρ_1	$2600Kg/m^3$

3.2. Variation with Impact Angle

The developed mechanistic model in this study was compared to three existing models, which are, Oka's model, DNV model and E/CRC model. The developed model varies with impact angle just like the rest of the models. The developed model agrees more with the DNV and E/CRC model. Fig 6 shows the variation of the mechanistic model with the impact angle for a range of 1-90^0. The developed model in this study however returns a complex number 0^0 impact angle which we take as zero erosion. The model will return a complex number for a condition in which erosion due to impact is impracticable, for instance, velocity of 0.5m/s at impact angle of 1.0^0 or velocity of 2m/s at impact angle of 0.5^0 in such condition where the model returns complex number it means no erosion has taken place. Fig 6 (A) shows a perfect agreement between the proposed model and E/CRC model between 0^0 to 20^0 and with DNV model between 60^0 to 90^0 for impact velocity of 104m/s and particles mass flow rate of 0.05Kg/s. For a very low impact

velocity, there is general perfect agreement between the DNV, E/CRC and the developed model of this study for instance; Fig 6 (C) to (F) confirmed it.

Fig 6 also shows that Oka's models tend to be predicting values higher than the rest. The behaviour is more pronounced at lower velocities as shown in Fig 6 (C) to (F).

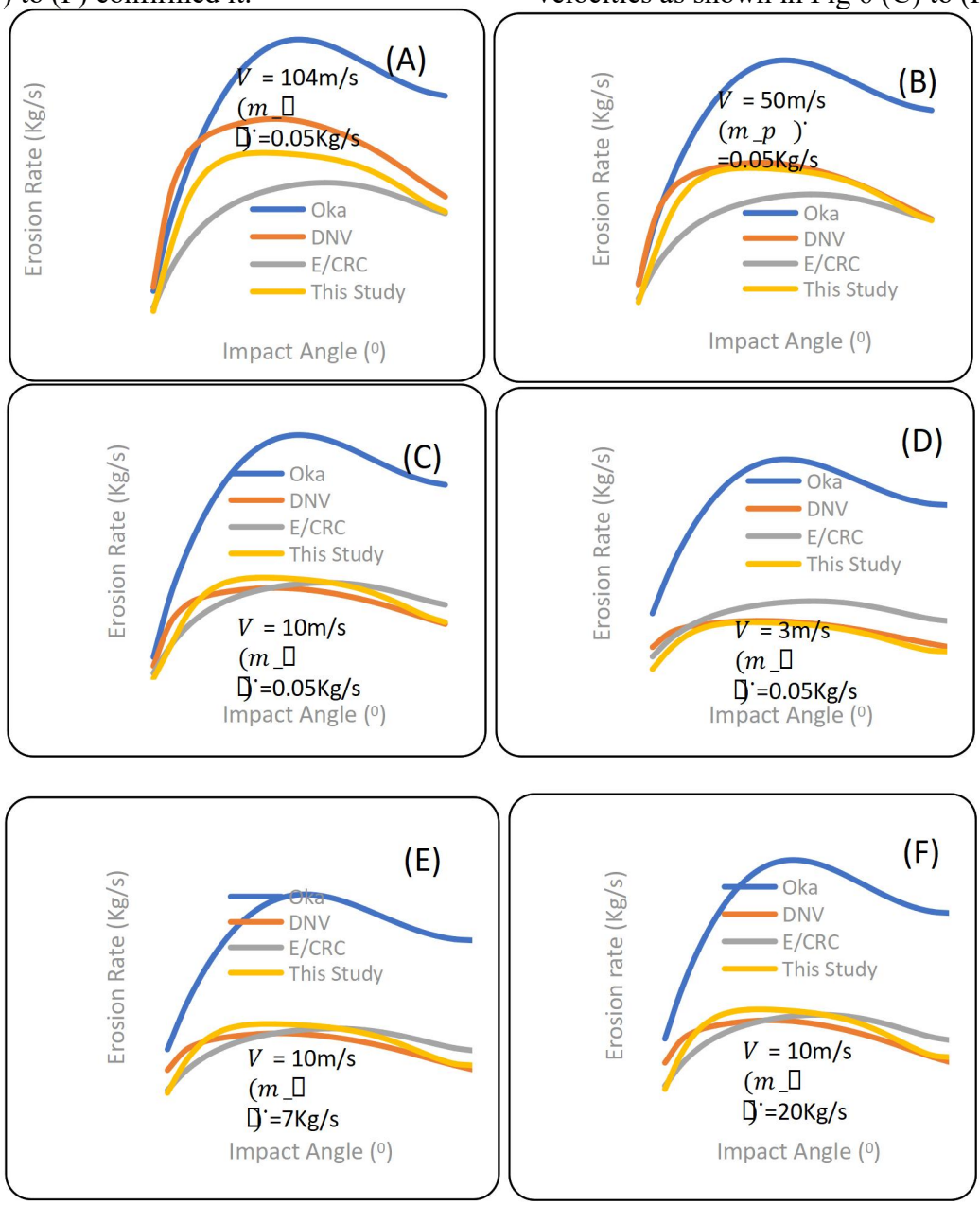

Fig 6: Effect of Impact angle for particle diameter d = 100µm

3.3. Variation with Impact Velocity

The effect of impact velocity on the developed model was also investigated in comparison with the selected three models. Fig 7 shows that all the four models follow the same trend. The developed mechanistic model competes favorably with the DNV and E/CRC model. Fig 7 (F) shows that at normal impact, 90^0, the developed model and DNV and E/CRC model perfect agree at particle mass flow rate of 0.05kg/s.Increase in velocity increase the erosive wear rate

because the particle has more kinetic energy which is converted to do more work on the target material causing more wear damage on the material. Higher velocity also means higher turbulence which causes the particle to impact at different angle causing a combine effect of indentation, crack and abrasion, all leading to higher erosive wear. Fig 7 (A) and (B) shows the effect of particle velocity at higher particle mass flow rate. The model developed in this study show good agreement with the rest of the model especially at particle velocity between 1.0m/s and 50m/s. Generally, the developed model is responsive probably because of the inclusion of many materials' mechanical properties in the model. Fig 7 also shows that Oka's model predicts values that are higher than the rest of the model

.

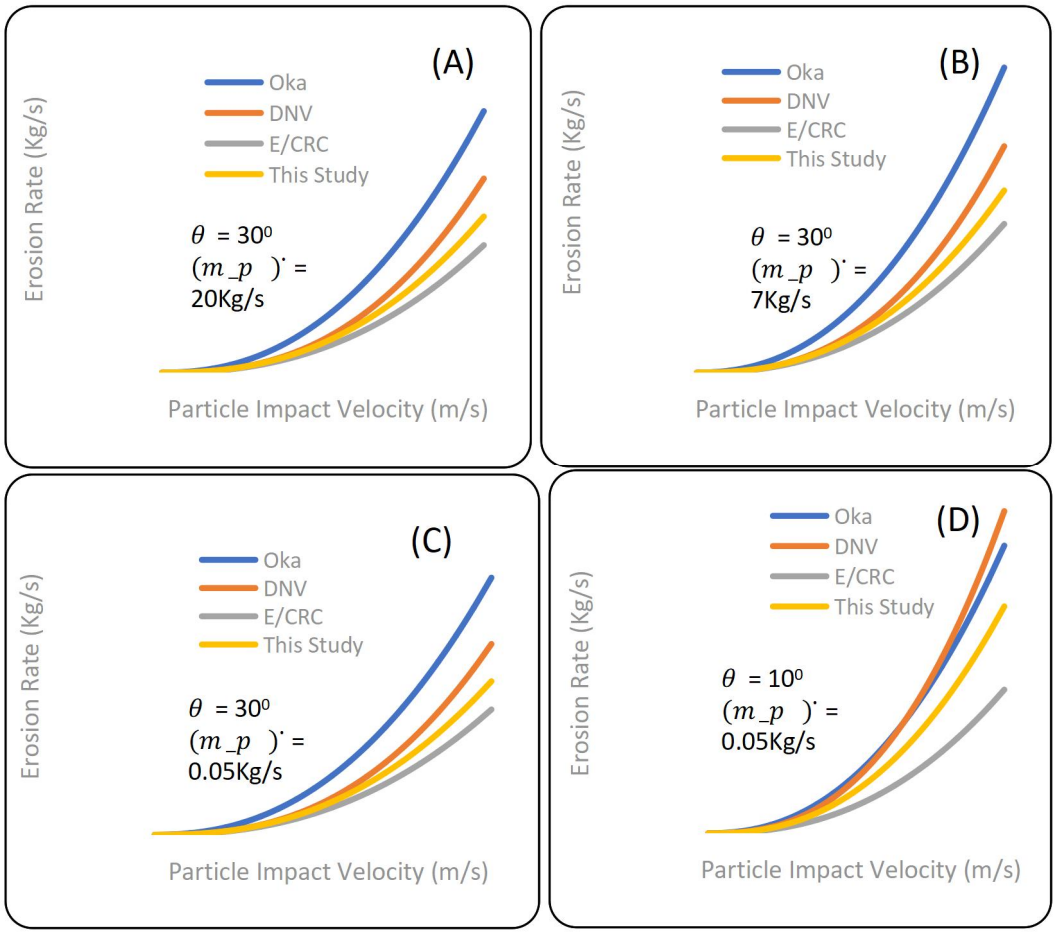

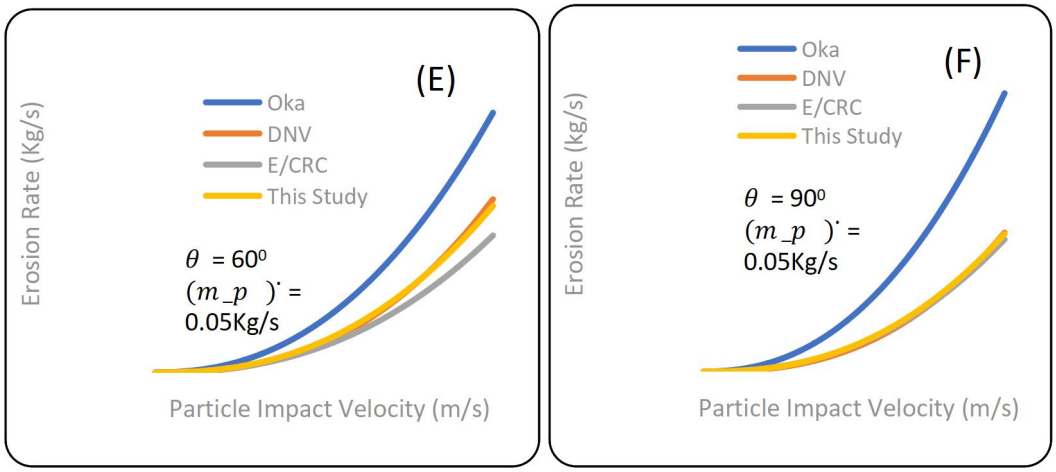

Fig 7: Effect of Impact Velocity for particle diameter d = 100µm

3.4Effect of Particle Mass Flow rate

The effect of mass flow rate of particles on the erosive wear of steel surface and the response of the model developed in this work was also investigated. Fig 8 shows similar trend for all the models. Increase in mass flow rate of particles has a linear effect on the erosive wear rate of the target material. However, the effect of particle mass flow rate is more on the Oka's model than the rest of the models. The developed model of this study shows much lower response to particle mass flow rate at lower impact angle less than 15^0. However, a much higher agreement is observed between the developed model, DNV and E/CRC models for impact angles between 20^0 and 90^0 as captured in Fig 8 (B) to (F). Little agreement between Oka's model and the rest of the models were observed at higher velocity and it can be observed in Fig 8 (E).

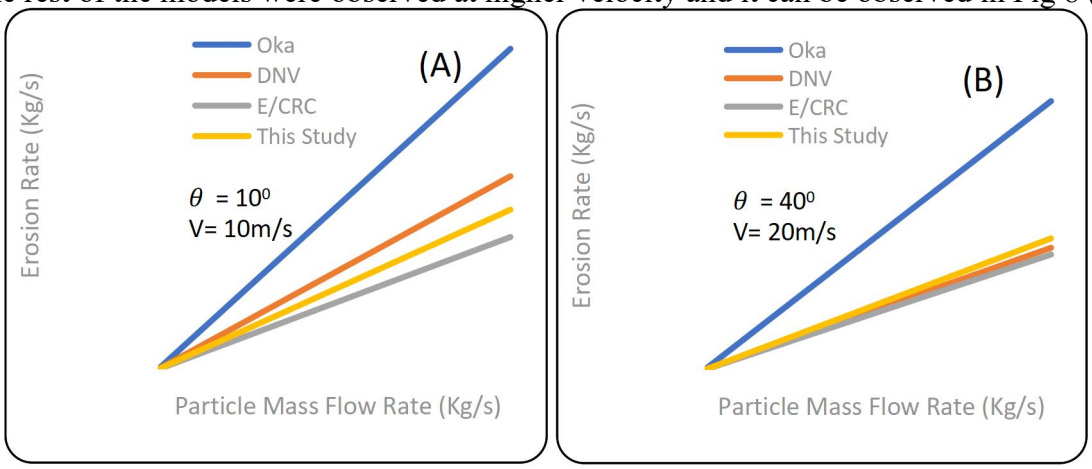

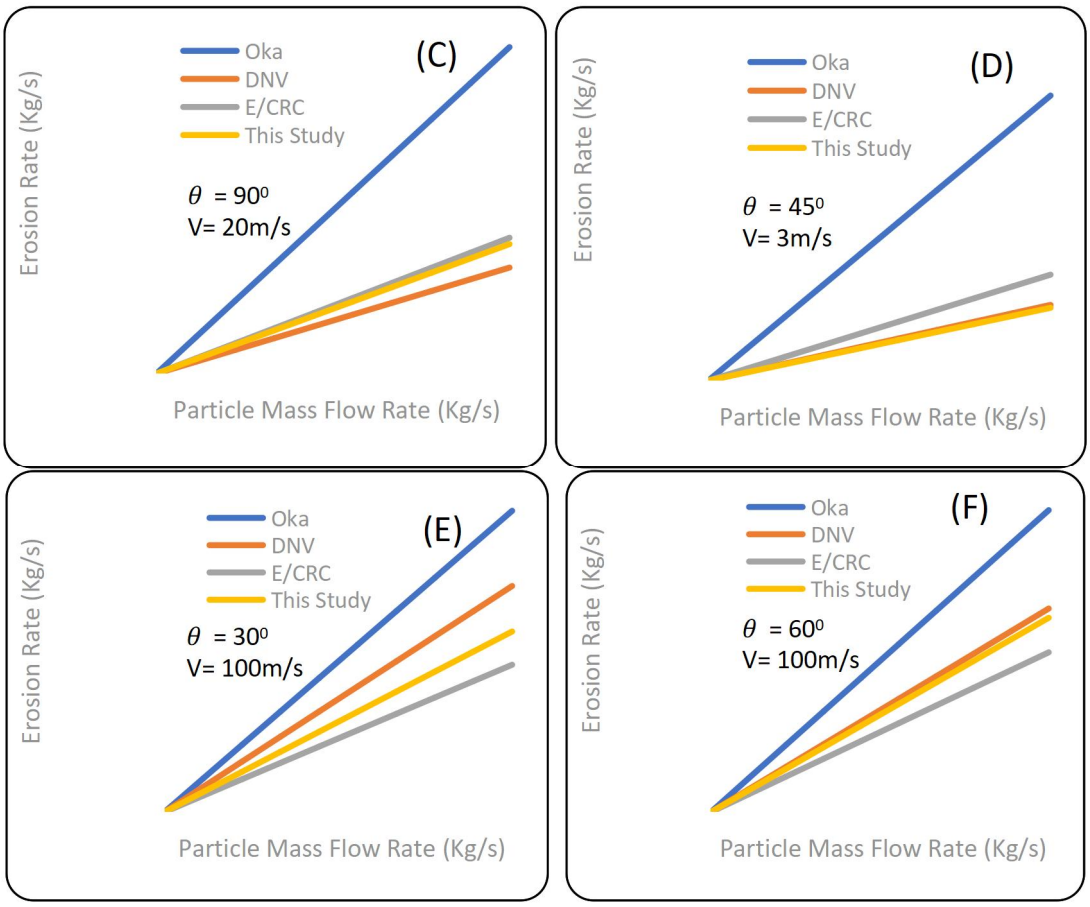

Fig 8: Effect of particle mass flow rate for particle diameter d = 100µm

3.5 Effect of Particle Diameter

The effect of particle diameter is not captured in the empirical correlation of DNV and E/CRC models, probably because of its insignificant contribution to erosive wear phenomenon, However, Oka's correlation model include the particles average diameter. The developedmodel, being mechanistic, combines all the material parameters including the particle mean diameter. Fig 9 shows the variation of erosion rate with particle diameter. Oka's model shows that particle diameter affects the erosion rate for a given mass flow rate. The developed model however shows that the particle diameter has no significant effect on the erosion rate at any given fix mass flow rate.

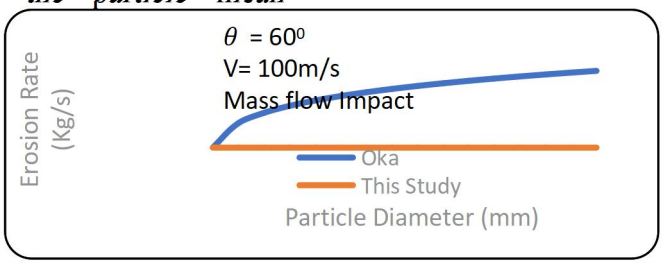

Fig 9: Effect of particle diameter at constant particle mass flow rate of 0.05Kg/s

This study undertakes extra steps to analyzed the effect of particle diameter on the erosion rate by plotting eroded mass (Kg/Impact) against particle diameter as shown in Fig 10. The result shows that increase in particles size (diameter) leads to increase indentation or erosive damage for both Oka's and the developed model. The response of the developed model in Fig 9 can be explained by analyzing the relation $\eta = \frac{\dot{m}}{m}$, where; $\eta =$ number of particles impacting on the target surface per second, $\dot{m} =$ the mass flow rate of particles flowing on to the target surface and $m =$ average mass of single particle. The average mass of the particle is a function of particle diameter given as $= \frac{\rho \pi d^3}{6}$. If the mass flow rate of the particles is constant, the diameter increase will imply particle mass increase and reduction in number of particles in the flow stream consequently result in insignificant change in the erosion rate. Simply put, the few larger particles produced the same effect as the many smaller particles. By this analysis, the DNV and E/CRC erosion model is more accurate in not including the particle mean size or diameter in the model. The developed mechanistic model of this study shows perfect agreement with the DNV and the E/CRC in terms of particle diameter effect on erosion rate

.

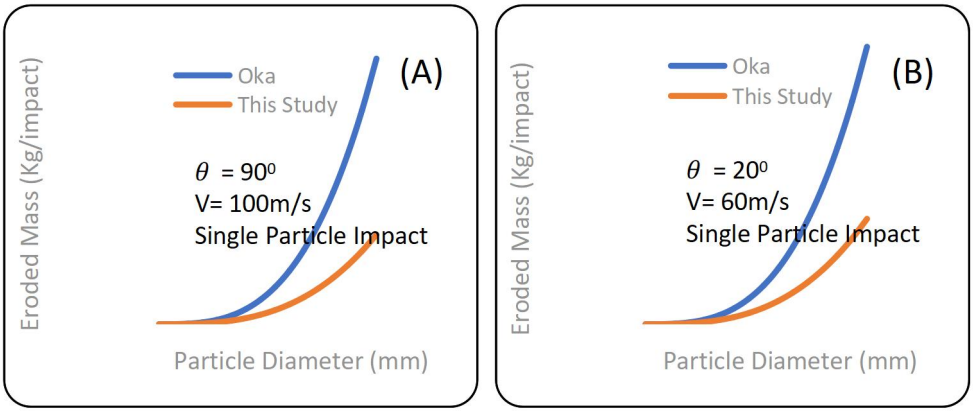

Fig 10: Effect of particle diameter for a single particle impact

3.6 Effect of Elastic Modulus and Yield Strength

The developed model incorporates many mechanical properties of both the target material and the erodent. The effect of the modulus of elasticity and the yield strength of the target material was investigated using the developedmodel; the results are displayed in Fig 11a and Fig 11b. Fig 11 (A) and (B) show that erosion rate increase with increase in the modulus of elasticity of the target material. The same trend is observed in the equivalent elastic modulus as shown in Fig 11 (B).Fig 12 shows that the erosion rate decreases with increase in the value of the target material yield strength. For Carbon steel, the yield strength is proportional to hardness; therefore, similar trend is expected for material hardness.

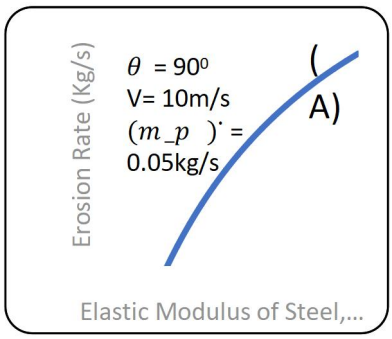

Fig 11: Effect of Elastic Modulus

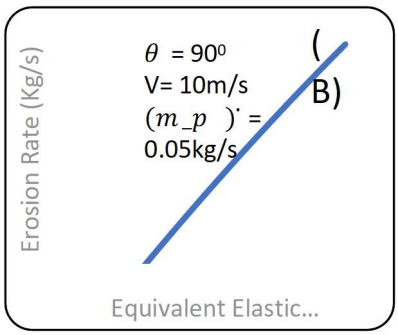

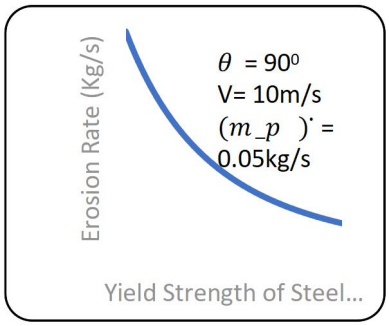

Fig 12: Effect of Yield Strength and Hardness

4.CONCLUSIONS

A mechanistic inner-wall erosive wear model has been developed in this study by applying the Hertzian impact model and the impact model of Du and Wang. The model development involves determining the impact crater depth and length and computing the volume of created crater due to impact by single particle. The inner-wall mass loss rate of the target surface is determined by simple dimensional manipulation which involves the inclusion of the target material density and particles mass flow rate. The developed mechanistic model has been compared to three erosion model and found to have a very high level of agreement.

The model developed in this study has the following advantages:

1. It is general though validated for carbon steel in this study. Simple variation of the material constant, k, in the model will make it suitable for variety of target materials.
2. The Mechanistic model can include several parameters which are core mechanical properties of the materials that determine the level of response of it surface to erosive wear.
3. The model is responsive to material property change since many of the mechanical properties are included in it.
4. The developed model can be easily combined with other applications such as computational fluid dynamics (CFD) codes.
5. This study undertakes extra steps to analyzed the effect of particle diameter on the erosion rate by plotting eroded mass (Kg/Impact) against particle diameter as shown in Fig 10. The result shows that increase in particles size (diameter) leads to increase indentation or erosive damage.
6. The developed model incorporates many mechanical properties of both the target material and the erodent. The effect of the modulus of elasticity and the yield strength of the target material was investigated using the developed model.

The model, though developed in an attempt to find a suitable model for prediction of erosion rate of coal slurry carbon steel pipeline, can be apply in many other areas of surface erosion due to particle flow. The developed mechanistic model presented in this study will be useful for accurate prediction of inner-wall erosion wear rate of pipelines conveying coal slurries particles in fluid thereby reducing associated danger.

Availability of data and materials

The datasets applied and analyzed during the current research are available from the corresponding author on reasonable request.

Abbreviations

CFD = computational fluid dynamics;**GUI** = graphical user interface; **E/CRC**= Erosion and Corrosion Research Center; **DNV**=Det Norske Veritas; E_v= the erosion rate, C= the target material constant; n = the velocity exponent. α= the impact angle; η = number of particles impacting on the target surface

per second, $\dot{m}$ = the mass flow rate of particles flowing on to the target surface and m =average mass of single particle.

Competing interest

The authors said to the best of their knowledge there was no conflict of interest at the time of this study.

Authors' contributions

MO: Supervision, Conceptualization, Methodology, Funding acquisition, Project administration, Writing - review & editing. PBA: Data curation, Writing-original draft, Formal analysis, Validation. PTE: Writing - review & editing, Supervision, Validation. All authors read and approved the final manuscript.

Acknowledgements

The authors acknowledge the financial support provided for this research by the Tertiary Education Trust Fund (TETFund) as well as the year 2022 TETFund Conference Attendance Intervention.

References

[1] Capecelatro J. & Desjardins O. (2013). Eulerian–Lagrangian modeling of turbulent liquid–solid slurries in horizontal pipes. *International Journal of Multiphase Flow* 55 (2013) 64–79.

[2] Obaseki, M., Elijah, P.T and Alfred, P.B. (2020). Development of model to eliminate sand trapping in horizontal fluid pipelines. *Journal of King Saud University-Engineering Sciences*. https://doi.org/10.1016/j.jksues.2020.11.006.

[3] Obaseki, M., and Elijah, P., T., 2020. Dynamic modeling and prediction of wax deposition

thickness in crude oil pipelines. J. King Saud Univ. Engr-Sci. https://doi.org/10.1016/j.jksues.2020.05.003.

[4] Obaseki, M., Nwankwojike, B.N., & Abam, F.I., (2021). Diagnostic and Prognostics Development of a Mechanistic Model for Multiphase Flow in Oil-Gas Pipelines. J. King Saud Univ. Engr-Sci. https:// doi.org/10.1016/j.jksues.2020.12.010.

[5] Oka Y.I., Olmogi H., Hosokawa T. & Matsumura (1997), The impact angle dependence of erosion damage cause by solid particle impact. *Wear*, Vol. 203-204, pp573-579.

[6] Finnie I. (1958), The mechanism of erosion of ductile materials. *Proceedings of 3rd US National Congress of Applied Mechanics*. pp527-532.

[7] Bitter J.P.A. (1963a), A study of erosion phenomenon part I. *Wear*, Vol. 6, pp5-21.

[8] Bitter J.P.A. (1963b), A study of erosion phenomenon part II. *Wear,* Vol. 6, pp169-190.

[9] Neilson, J.H. & Gilchrist, A. (1968), Erosion by a stream of solid particles. *Wear* 11 (2), pp111-122.

[10] Hashish, M.1.(987), An improved model of erosion by solid particle impact. *Proceedings of the 7th International Conference on Erosion by Liquid and Solid Particle*, Cambridge, pp. 66/1- 66/9.

[11] Huang, C., Chiovelli, S., Minev, P., Luo, J. & Nandakumar, K. (2008). A comprehensive phenomenological model for erosion of materials in jet flow. *Powder Technology*. 187 (3), 273e279.

[12] McLaury, B.S. (1996). Predicting Solid Particle Erosion Resulting from Turbulent Fluctuations in Oilfield Geometries.

[13] Oka, Y.I., Okamura, K. & Yoshida, T. (2005). Practical estimation of erosion damage caused by solid particle impact: part 1: effects of impact parameters on a predictive equation. *Wear* 259 (1), 95-101

[14] Oka, Y.I. & Yoshida, T. (2005). Practical estimation of erosion damage caused by solid particle impact: part 2: mechanical properties of materials directly associated with erosion damage. *Wear* 259 (1), 102-109.

[15] Det N. V. (2007), Recommended Practice RP 0501: Erosive Wear in Piping Systems.

[16] Peng W. & Cao X. (2016), Numerical prediction of erosion distributions and solid particle trajectories in elbows for gas-solid flow. *Journal of Natural Gas Science and Engineering* 30 (2016) 455-470.

[17] Ahlert, K.R. (1994). Effects of Particle Impingement Angle and Surface Wetting on Solid Particle Erosion of AISI 1018 Steel. *Ph.D. thesis. Department of Mechanical Engineering, The University of Tulsa*.

[18] Meng H.S. & Ludema K.C. (1995), Wear model and predictive equations: their form and content. *Wear*, Vol 181-183, pp443-457.

[19] Hutchings I.M. (1981), A model for erosion of metals by spherical particles at normal incidence. *Wear*, Vol. 70, pp256.

[20] Chen, X., McLaury, B.S. & Shirazi, S.A. (2004), Numerical and experimental investigation of the relative erosion severity between plugged tee and elbow in diluted gas/solid two-phase flow. *Wear*, Vol. 261, pp715-729.

[21] Eyler, R.L. (1987), Design and Analysis of a Pneumatic Flow Loop. *M.S. thesis. West Virginia University, Morgantown, WV.*

[22] Finnie I. (1960), "Erosion of surfaces by solid particles", *Wear*, 3, 87-103.

[23] Brown G. (2006), Use of CFD to predict and reduce erosion in an industrial slurry piping system. *Fifth International Conference on CFD in the Process Industries CSIRO, Melbourne*, Australia 13-15

[24] Zhang, Y., Reuterfors, E.P., McLaury, B.S., Shirazi, S.A. & Rybicki, E.F. (2007). Comparison of computed and measured particle velocities and erosion in water and air flows. *Wea*r 263 (1), 330-338.

[25] Du, Y. and Wang, S. (2009): Energy dissipation in normal elastoplastic impact between two spheres, Transactions of ASME: *Journal of Applied Mechanics*, 76, 061010-1 - 061010-8.

NMS-TP019

Fault Tree Analysis for Failure Checks on Rotodynamic Systems: A case study of a Refinery.

Paul Tamaragaibi ELIJAH*,Martins OBASEKI and Chukwuekum ORUMGBE
Applied Mechanics and Design/Production Research Group, Department of Mechanical Engineering, Nigeria Maritime University, Okerenkoko, Delta State, Nigeria.
Corresponding Author Email: paul.elijah@nmu.edu.ng
Co-author Email: martins.obaseki@nmu.edu.ng

Abstract

Rotodynamic system maintenance is key for safe and efficient refinery operations. In trying to minimize unexpected breakdowns, decrease in productivity and high maintenance cost, associated with gas compressing system failures, this paper presents a maintenance model developed to integrates fault tree analysis (FTA) derived from Weibull's exponential distribution, in determining the probability of failure and reliability of the gas compressing systems.This study is aimed at applying the FTA to check the failures of a selected rotodynamic system (gas compressing system) of a refinery. The FTA was applied as a root cause of failure analysis (RCFA) technique in determining the probability of failure and the system's reliability based on previous failure data of the components of the gas compressing system (rotodynamic system). Results obtained showed that the gas compressing system's failure probability and reliability were 34.5% and 65.5% respectively. Comparison with existing model at case study indicates a significant improvement.

Keywords: Fault tree analysis; Gas compressing system; Reliability; Weibull's exponential distribution

1. Introduction

The petroleum industry still plays a major role in the economic development of most countries around the world and refineries are critical in meeting the needs of manufacturing, transportation, agricultural and other sectors of the economy [1]. In an industry of such strategic importance, the reliability of its processes and functional units are of paramount importance.

Addressing the needs of the market and the increasingly critical economic competition amongst manufacturers, has resulted in the expansion and automation of industrial systems [2-4]. This has increased their complexity and cost, hence, reducing their unavailability. As a result of this, maintenance is needed to guarantee performance of these production equipment. To reduce unnecessary risks and ensure safe practices, several methods such as monitoring, diagnoses, supervision and regular maintenance are common in high risk environments such as oil and gas refineries, chemical industries, and so on. Reliability analysis is important for the study of operating safety in these industrial systems of which the gas compressing system is one.

In recent times, reliability has become a major parameter of quality and decision support, housing many aspects such as operational functions, predictive capabilities and failure analysis systems. Researchers have continued to break bounds in the development of suitable reliability models that would meet organizational objectives (profit making and customer satisfaction). According to Nathalie [5]a reliability model is usually proposed to verify the impact ofnew maintenance method, and to make better informed decisions in the maintenance management process.

Proper modelling of reliability maintenance systems requires adequate and quality data [6, 7]. Rahmoune et al. [8] proposed solutions to a real-time reliability model, applied to an industrial pump. Their proposed model was to assist in developing satisfactory maintenance plans, increase equipment life span and assign a probability to operating systems examined to choose the best pump technology. They showed that their model takes fault analysis into consideration by providing a better understanding of the costs and causes of failures, as this will help increase the profitability of the pumping station. Also, the real-time methodology provides guidelines for maintenance and availability. They concluded that, to improve the

reliability of an industrial pump, real time systems are better tools [9].

Liang et al. [10] tried to minimize work safety, system failures and uncertainties associated with maintenance by employing reliability centered maintenance (RCM) on the major parts of a reciprocating compressor. Failure mode and effect analysis carried out, maintenance plan for high-risk faults were obtained using logical method, and a risk matrix to assess the importance of failure modes. They concluded that, employing reliability centered maintenance (RCM) onkey parts of a reciprocating compressor, as a preventive maintenance plan, will not only minimize maintenance cost and total work-load, but put to anend major accidentsand reduce the likelihood of general accidents. They further predicted that in future, reliability centered maintenance approaches will work in conjunction with network information technology, thereby making dynamic maintenance of compressors a reality.

In cases where a researcher is faced with the issue of inadequate and quality data, even if his model is correct, the outcome of such modelling would be non-optimal. Hussin and Hashim[6] proposed an alternative approach for addressing such situations by employing expert opinion inputs. They employed preventive maintenance on an offshore gas compression system using expert opinion. The correct set of questionnaires, downtime distribution and fractile technique, were successfully obtained from expert. A comparison was made between downtime distribution obtained from raw gas compressor maintenance data and that derived from expert opinion. Results obtained showed that the expert opinion approach was a good option for estimating the downtime measures of maintenance tasks.

A new model for reliability centered maintenance (RCM) in petroleum refineries, was proposed by Deepak and Jagathy[11]. They capitalized on the fact that refiners and process plants find it difficult to adoptstandardized methodology of RCM, mainly due to the complexity and the large amount of analysis that needs to be done, resulting in a long drawn out implementation, requiring the services of a number of skilled people. They proposed a standard reliability centered maintenance that integrated the existing model into its design.Based on the simulated results obtained, their RCM model and process provides refineries with a comprehensive tool for accelerated improvement in reliability when compared to existing maintenance models.

In the works of Hussin et al. [12], a practical approachto carrying out maintainability analysis of an offshore system was performed. Their approach systematically analyzed maintenance data, identified critical performance factors affecting the system and developed satisfactory downtime distribution model with applications of statistical analysis techniques and expert opinion. Their result showed that the improvement actions in spare-parts logistic and equipment change-outscheduling are crucial factors in reducing the duration of downtime and should be incorporated in newer industrial systems.

Baig et al. [13] presented the general procedure for fault tree analysis (FTA), its application in various fields and the modifications that have been made through the time to overcome the inadequacies of the method. An analysis on the disadvantages of FTA was made, and possible changes made to counter these problems. It was observed that for FTA, the presence of reliability data is very important but its unavailability is a major problem for risk assessment.

Nesekati et al. [14] carried out reliability analysis of a k-out-of-n:F system under linear degradation by considering both soft and hard failures associated with system's components through various internal and external factors. They developed a linear model for degradation path of each component, thereby obtaining the system's reliability function. Their result showed that the reliability function was sensitive to varying parameters. They further investigated the effect of calibration on the system's reliability and degradation, with achieved results showing that an increase in the number of calibrations, results in a corresponding increase in the system's reliability.

As the complexities in newer compressors increase, in order to meet the needs of the market, researchers are also devising newer reliability maintenance approaches to account for unsafe practices and costs associated with breakdown or compressor failure. Zhou et al. [15] proposed a new maintenance approach, dynamic reliability centered maintenance (DRCM) for industrial system management. The dynamic centered reliability maintenance (DCRM) focused at enlarging the application of reliability centered maintenance plan to include preventive maintenance decision making online, and was suitable for maintaining gas compression stations according to them. They developed a maintenance model and decision diagram for their maintenance plan. In validating their model, they applied dynamic centered reliability maintenance to three different gas compressing systems. From the results obtained, they concluded that their method was better for complex systems such as compressors, since it is an add-on to existing reliability centered maintenance (RCM) plans, and can also give corrective and quantitative suggestions with the help of its diagnostic and prognostic technology.

Vishnu and Regikumar[16] proposed a general methodology to implement reliability centered maintenance (RCM) in process plants. The RCM strategy was framed up for the process plant by following Analytical Hierarchy Process (AHP) based methodology. A comparison between their reliability centered maintenance (RCM) strategy and the schedule and breakdown maintenance strategy currently employed by the firm was initiated. Maintenance simulations showed that the current maintenance approach used in the process plant had a lower availability and performance index.

In the works of Chen et al. [17], a hybrid kriging-based reliability method for small failure probabilities was produced. Their work employed a modified algorithm based on krigingmetamodel (AK-MCS) and Monte Carlo simulation, with the aim of determining the failure probability of a structure by considering the randomness of the input. They revealed that the problem associated with existing methodology (AK-MCS), particularly, constraints when evaluating small failure probabilities due to the large populations that are required to make an accurate assessment, was overcame by their proposed methodology, through the replacement of a large population with two or more populations.

Wen et al. [18] employed universal generating function (UGF), a reliability estimation method which has shown significant result in multi-state systems, to an actual industrial system – a gas compressing system. The compressing system which is a series-parallel multi-state system, has its compressor units in each compressor station working in parallel and the pressure boosting stations connected in series. Based on gas pipeline attributes, they

developed two universal generating functions (UGFs) to analyze the compressing systems' reliability. Model 1 established a system model from each compressor unit while model 2 considered the entire system as a function of multi-state components. The various weight parameters used in the model, were acquired from engineering thermal hydraulic model and probabilities obtained from Monte Carlo simulation. Results obtained indicates that system reliability calculated by various universal generating functions (UGFs) are approximately identical.

Akuno et al. [19] proposed a classical parametric regression approach for estimation of shape (α) and slope (β) parameters, failure rate function λ(t), and the mean time between failures (MTBF) for a software reliability model. Their classical approach was stemmed from the fact that the logarithm of the failure rate function of the Goel-Okumoto software reliability model is a linear function of the software failure times. They concluded that the model can be taken as a simple linear regression. Results obtained were validated using root means squared error (RMSE) and the mean absolute value difference (MAVD), which are the common error measurement criteria. Upon comparison with maximum likelihood estimation (MLE) and a simple regression without assuming Goel-Okumoto model, their classical regression approach outperformed both methods.

Hameed et al. [20] proposed a decision support tool for risk-based maintenance plan for a large heavily equipped gas sweetening unit in a Liquefied Natural Gas plant. Their maintenance approach was based on two issues - reliability of the plant and total maintenance cost. They developed a bi-objective schedule optimization using risk-based maintenance framework. In finding the optimal maintenance schedules, the model integrated genetic algorithm and simulation-based optimization. Their results showed that the risk-based maintenance approach, helped in minimizing production loss by generating a standard maintenance strategy for inspection, repair, overhaul or replacement schedule of the unit without initiating the shutdown. However, they recommended state-dependent models for various failure modes as this will result in obtaining a better representation of the model, in case of future work.

Several reliability maintenances models have been developed and/or employed by various researchers in order to determine the optimal inspection, repair intervals and maintenance cost minimization for gas compressing systems. The intent of this study is therefore to develop a statistical maintenance model for gas compressing systems and validate with plant data obtained from the case study.

2.0 Materials and Methods

This section presents models and maintenance plan for the detection of failure in a gas compressing system at its earliest point, so as to minimize the risks associated with working with this complex system, and to reduce maintenance cost associated with unexpected breakdowns.

System Description

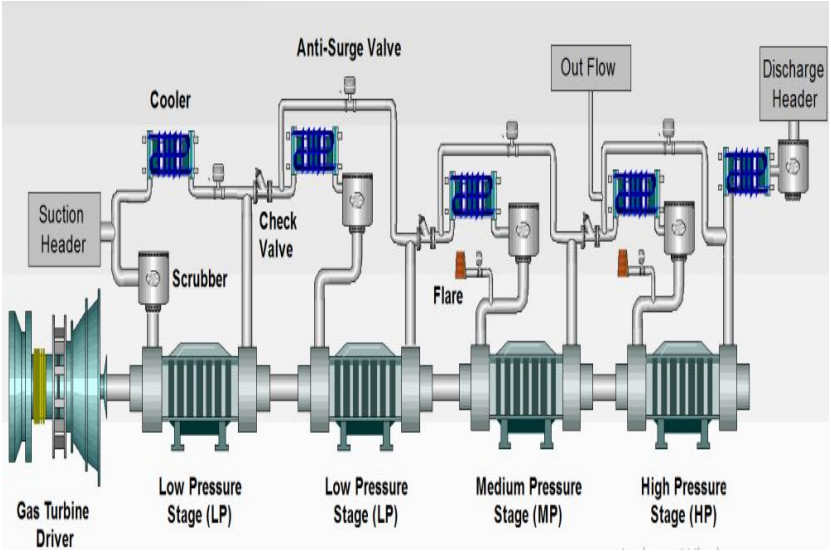

Figure 1: Gas Compressing System (Source: Integrated Publishing, 2019).

A standard gas compressing system is composed of a high, medium and low-pressure compression train, with different stages. A typical stage has a heat exchanger, a scrubber and a compressor. The heat exchanger is used to cool the gas, as a lower temperature in the gas requires less energy to compress this gas. The scrubber is used to remove small fractions of liquid from the gas (either water or hydrocarbon), as liquid droplets entering the compressor will contribute to the corrosion of the compressor's blades (arising from reactions with acid gases in the stream and more importantly is prevention of hydrates formation). The division in several trains is aimed at improving the maintainability and availability of the system, as well as improving the capacity of the system. The gas compressing system investigated in this work comprises of three sections; high pressure section, high compression section and a low-pressure booster section. Each high-pressure compression train consists of four compressor stages with inter-stage cooling and vapor/liquid separation, with condensate liquids returning to the previous compression stage.

Gas from the high-pressure compressor suction manifold (at 30°C) is separated within the first stage high-pressure compressor suction scrubber, with liquids returned to the closed drain system. This separated gas is then compressed in two parallel throws of a reciprocating compressor, from 11.3 bar to 30.6 bar. The vapor discharge, along with the condensate return from the third stage high-pressure compressor suction scrubber is cooled in the second stage compressor suction cooler to a temperature of 30°C. The gas/liquid from the second stage high-pressure compressor suction cooler is separated within the second stage high pressure suction scrubber, with liquids returned to the high-pressure compressor common suction scrubber. The separated gas is then compressed in two parallel throws of the reciprocating compressor, from 29.9 bar to 79.2 bar. The vapor discharge along with the condensate returned from the fourth stage high pressure compressor suction scrubber to a temperature of 35°C.

The higher temperature is to avoid hydrates in the liquid recycle line from the third stage high pressure compressor suction scrubber.

The gas from the third stage high pressure compressor suction cooler is separated within the third stage high pressure suction scrubber, with condensate/water returned to the second stage high pressure compressor suction cooler. The separated gas is then compressed in a single throw of the reciprocating compressor, from 78.5 bar to 170.9 bar. The vapor discharge is cooled in the fourth stage high pressure compressor suction cooler to a temperature of 30°C. The gas from the fourth stage high pressure compressor suction cooler is separated within the fourth stage high pressure compressor suction scrubber, with water (low flow rates) returned to the third stage high pressure compressor suction cooler. The separated gas is then compressed in a single throw of the reciprocating compressor, from 169.9 bar to either 352 bar, or the back pressure exerted by the gas reinjection reservoir (typically 300 bar). The vapor discharge is then routed to the high-pressure fuel gas system or the gas reinjection pipeline, depending upon which supply is required. The final discharge temperature is kept below 65°C in accordance with the Design Basis.

The compression trains have four stages; each first stage is composed of a reciprocating compressor and a scrubber while the second to fourth stages are composed of a cooler, a reciprocating compressor and a scrubber. To control the process, there are level, temperature and pressure transmitters, as well as control valves.

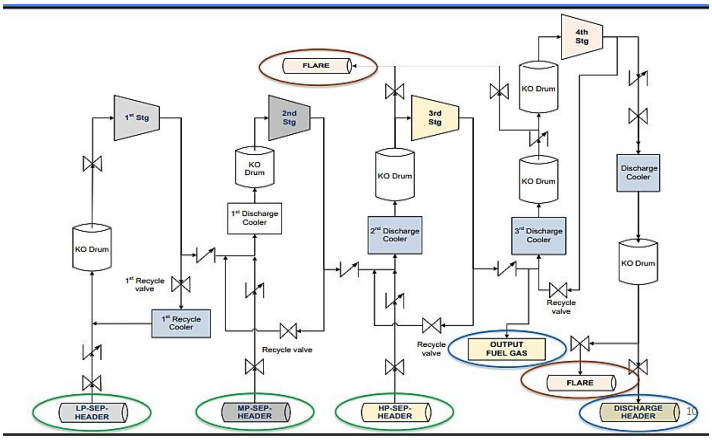

Figure 2: Detailed Gas Compressing System (Source: Integrated Publishing, 2019).

Reliability Centered Maintenance (RCM)

Reliability centered maintenance (RCM) is a unique tool used by reliability, safety, and/or maintenance engineers for developing optimum maintenance plans which define requirements and tasks to be performed in achieving, restoring, or maintaining the operational capability of a system or equipment. RCM is employed in this study to create a cost-effective maintenance strategy to address dominant causes of equipment failure. It is a systematic approach to defining a routine maintenance program composed of cost-effective tasks that preserve important functions.

Smith and Hinchcliffe[21]characterized reliability centered maintenance methodology into four:

Preserve Functions: One of the primary tenets of the Reliability Centered Maintenance approach is that maintenance activities should be focused toward

preserving equipment functionality. Therefore, it follows that the first step in analyzing a particular piece of equipment is to identify the function(s) it is intended to perform. Many RCM references recommend including specific performance requirements in function descriptions, which will help to specifically identify functional failures.

ii. **Identify Failure Modes That Can Defeat the Functions:** Functional failures describe ways that the equipment may fail to perform its intended functions. This may include failure to perform a function, poor performance of a function, over-performance of a function, performing an unintended function, etc. As mentioned above, the performance limits that have been identified for the function may provide a guide to the functional failure description.

iii. **Prioritize Function Need:** Identifying and evaluating the effects of failure will help the team to prioritize and choose the appropriate maintenance strategy to address a potential failure. Many Reliability centered maintenance (RCM) references contain logic diagrams that can be used to evaluate and categorize the effects of failure. These logic structures often differentiate evident versus hidden effects and whether the issue has safety, environmental, operational and/or economic consequences.

iv. **Select Only Applicable and Effective Preventive Maintenance Task:** Once the function equipment is intended to perform is identified as well as the ways that it might fail to perform those intended functions and the consequences of failures evaluated, the next step is to define the appropriate maintenance strategy for the equipment. The decision of which reliability centered maintenance approach(s) to employ for each potential failure may be based on judgment/experience, a pre-defined logic diagram (connected to the failure effect categorization), cost comparisons or some combination of factors.

These four features can also be presented as the answer to seven questions[22]. These questions set out the minimum criteria any process should meet before it can be called reliability centered maintenance. They are:

What are the functions and associated performance standards of the asset in its present operating context?

In what way does it fail to fulfill its functions? What causes each functional failure? What happens when each failure occurs? In what way does each failure matter? What can be done to predict or prevent each failure?

What should be done if a suitable proactive task cannot be found?

The ‘preserve functions’ features answers the first two questions, identifying failure modes that can defeat these functions, provides answers to question iii and iv. Feature three answers questions v, while feature four provides answers to vi and vii. Reliability centered maintenance (RCM) emphasizes the use of predictive maintenance (PM) techniques in addition to traditional preventive measures.

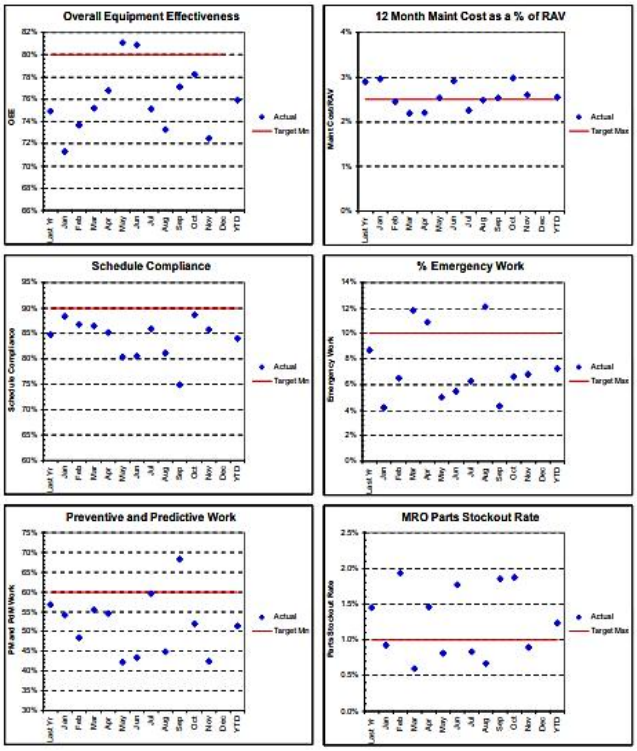

Figure 3: Reliability Centered Maintenance Metric Charts (Source: Integrated Publishing, 2019).

The reliability centered maintenance metric chart is a chart that shows record of a company's preventive and predictive maintenance action on equipment, cost associated with equipment maintenance, scheduled maintenance action, and so on. The reliability metrics help companies make improved decision based on historic data.

The existing maintenance response for preventing failures has always been to have a predictive maintenance (PdM) program that has both condition-based tasks and time-driven tasks. Condition-based tasks are derived mainly from vibration analysis while time-driven tasks typically arise out of equipment manufacturer recommendations and are conventionally referred to as preventive maintenance (PM) Plans. In addition to the PM and PdM plans, firms that employ this maintenance model like that of the refinery used in the case study, also employ Root Cause Failure Analysis program (RCFA) in the case of compressing system breakdown, so as to determine the actual cause of failure. The whole process ensures that a preliminary level of reliability assurance is achieved in these systems.

As shown in Figure 3, the gas compressing system undergoes preventive maintenance regularly, to reduce the likelihood of component failure, which would have adverse effect on the system. Predictive maintenance is also carried, to predict future failure of the system's components so that they can be replaced before it fails. Criticality analysis implies that key components are rated based on their potential risk, giving rise to predictive maintenance. And in the case of system failure, a root cause analysis (RCFA) is carried out to determine the actual cause of failure in the system and corrective maintenance employed.

Gas Compressing System Failure Mode and Effect Analysis (FMEA)

It is usually important to understand the failure modes of a maintainable system, so as to device suitable maintenance plan for that system. Failure mode and effect analysis (FMEA), recommended when complex or critical systems such as gas compressing systems are being used, is a methodology used to identify and analyze all significant failure modes and effects associated with the system under consideration. FMEA is one of

the many tools used to discover failure at its earliest possible point in product or process design. Discovering a failure earlier, provides the benefits of multiple choices for mitigating risks associated with the system and lower cost solutions.

For optimum result, a failure mode and effect analysis (FMEA) is usually performed when there is a quality improvement goal for a particular process, when there is a need to understand and improve the failures of a process or when designing a new product, process or service. In this work, a failure mode and effect analysis (FMEA) is carried out on the gas compressing systems located at case study. As seen from Table 1, the failure mode and effect analysis (FMEA) is made of the following fields:

i. **Failure Mode:** The failure mode is manner in which the gas compressing system fails to perform its required function. A failure may have one or more failure mechanism.
ii. **Failure Mechanism:** It is a physical, chemical or other process which may lead to failure. Examples of failure mechanisms are corrosion, fatigue, wear, etc.
iii. **Effect of Failure:** It is the immediate consequence of a failure. That is, what happens to the system or process if the failure mode takes effect?

Failure Cause: It is the circumstance during specification, design, manufacturing, installation, use or maintenance that results in failure. That is, the underlying reason that caused a failure to occur.

Maintenance Model Fault Tree Analysis (FTA)

The reliability maintenance model developed is based on Fault Tree Analysis (FTA) and a linear regression model for estimating the availability of the gas compressing system.

The Fault tree analysis (FTA) is a top-down, deductive failure analysis, in which an undesired state of a system is analyzed using Boolean logic to combine a series of lower-level events. It is mainly used in the fields of safety and reliability engineering to understand how systems can fail, to identify the best ways to reduce risk or to determine event rates of a safety accident or a particular system's functional failure.

Figure 4 shows the fault tree employed in this work, to determine the reliability and safety of the gas compressing system by analyzing the probability of failure of its components. This analysis is aided by historical data of basic event failures in the past, obtained from case study.

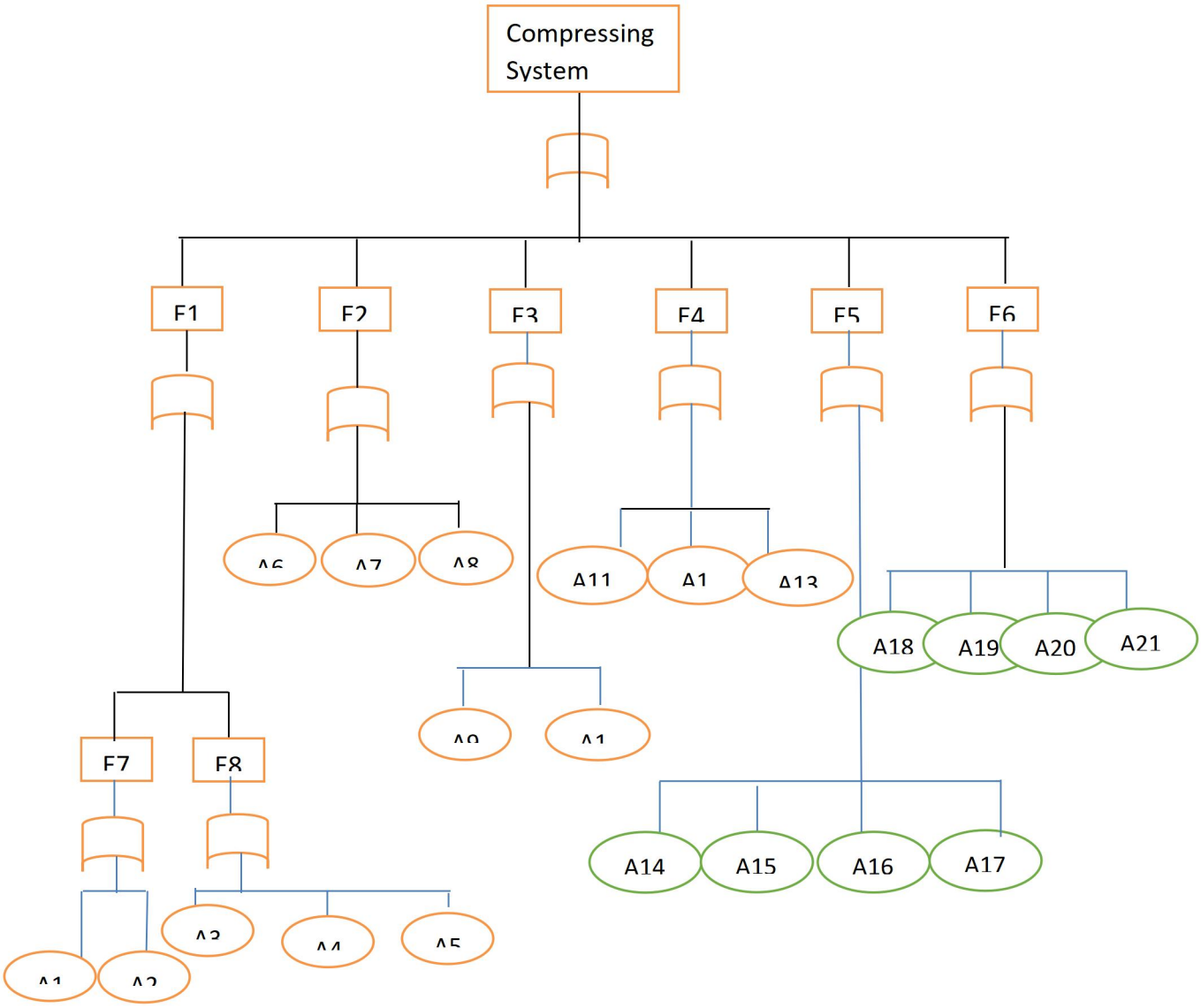

Figure 4: Compressor Fault Tree.

From the fault tree; the probability of event E1 occurring:

$$P(E1) = P(E7) + P(E8) - P(E7)(E8) \quad (1)$$

The probability of event E2 occurring is obtained as:

$$P(E2) = P(A5) + P(A6) + P(A7) - P(A5)(A6) - P(A5)(A7) - P(A6)(A7) + P(A5)(A6)(A7) \quad (2)$$

The probability of event E3 occurring is:

$$P(E3) = P(A9) + P(A10) - P(A9)(A10) \quad (3)$$

The probability of event E4 occurring is:

$$P(E4) = P(A11) + P(A12) + P(A13) \quad (4)$$

The probability of event E5 occurring is:

$$P(E5) = P(A14) + P(A15) + P(A16) + P(A17) - P(A14)(A15) - P(A14)(A16) - P(A14)(A17) - P(A15)(A16) - P(A15)(A17) - P(A16)(A17) - P(A14)(A15)(A16) - P(A14)(A16)(A17) - P(A15)(A16)(A17) + P(A14)(A15)(A16)(A17) \quad (5)$$

The probability of event E6 occurring is:

$$P(E6) = P(A18) + P(A19) + P(A20) + P(A21) - P(A18)(A19) - P(A18)(A20) - P(A18)(A21) - P(A19)(A20) - P(A19)(A21) - P(A20)(A21) - P(A18)(A19)(A20) - P(A18)(A20)(A21) - P(A19)(A20)(A21) + P(A18)(A19)(A20)(A21) \quad (6)$$

The probability of event E7 occurring is:

$$P(E7) = P(A1) + P(A2) - P(A1)(A2) \quad (7)$$

The probability of event E8 occurring obtained as:

$$P(E8) = P(A3) + P(A4) + P(A5) - P(A3)(A4) - P(A4)(A5) - P(A4)(A5) + P(A3)(A4)(A5) \quad (8)$$

Hence, the gas compressing system failure, F(t) is obtained thus:

$$F(t) = P(E_1) + P(E_2) + P(E_3) + P(E_4) + P(E_5) + P(E_6) + P(E_7) + P(E_8) \quad (9)$$

where: E1 is failure due to faulty valve, E2 is pressure packing ring fault, E3 is faulty piston ring, E4 is failure due to piston and piston rod cylinder, E5 vibration fault, E6 wear, E7 is material failure, E8 corrosion, A1 valve plate surface debris, A2 the valve fracture, A3 inner surface crack, A4 improper selection of spring, A5 spring , A6 wear, A7 filler rod and the piston rod seal failure, A8 packing box temperature increased, A9 piston ring gap too small, A10 piston ring tension too large, A11 piston and piston rod of the mechanical properties and smoothness does not meet the requirements, A12 the piston rod and the piston are not firmly connected, A13 piston rod positioning terminal and the central line of the piston verticality does not meet the requirements, A14 cooling water system in short supply, A15 lubrication system oil supply shortage, A16 suction valve cavity leakage, A17 Exhaust valve jammed or broken, A18 oil wiper wear, A19 scraping the oil ring incorrectly installed, A20 piston rod worn or scratched, A21 ring side clearance abnormalities.

3. Results and Discussion

3.1. Results verification and model validation

The model developed in this work, Equation(9) is a model to determine theprobability of system failure (the gas compressing system failure). **MATLAB** scripts based on the equation was used to plot the gas compressing system reliability profile in Tables 1 and 2. The results are shown in Figures 5, and 6.

To validate this model, experimental results of the case studywere used. The performance of the model was also compared with that of other models reported in this work. Table 1 shows the probability of failure of the gas compressing system components obtained using fault tree analysis (FTA).

Table 1: Probability of Failure of Basic Events.

S/N	Fault	Probability of failure (%)
1	Valve	4
2	Pressure packing ring	1.5
3	Piston ring	2
4	Piston rod cylinder	2
5	Vibration	15
6	Wear	5
7	Material failure	3
8	Corrosion	2

Table 2 present two additional performance indicators (probability of failure and the system's reliability).

Table 2: Gas Compressing System Indicators.

Parameter	Value
Probability of failure, F(t)	34.5%
Reliability, R(t)	65.5%

The probability of system failure F(t) which is the sum of failure of crucial components presented in Table 1 was obtained as 34.5%. Probability of failure below 50% indicates system effectiveness. The reliability R(t) of the system which is the probability that the system will operate for a specified period of time without failure, was obtained as 65.5%. This implies that system will operate effectively without failure for 7200 hours, which is average operational time for a year. Reliability above 50% implies that the system is effective and would carry out its intended purpose without failing, for the specified period of time. The reliability of the gas compressing system, which is the probability that the gas compressing system will operate for a number of times without failure, is shown in Figure 5. As the number of operating hours' increases, the reliability of the system decreases. This implies that the system's reliability is dependent on the number of operating hours. Also, the average number of operating hours of the gas compressing system at case study is 7200 hours, which is equivalent to 65.5% as seen in the Figure 5. Since the reliability of the system is above 50%, it means that system will function continue to function properly for its 7200 hours.

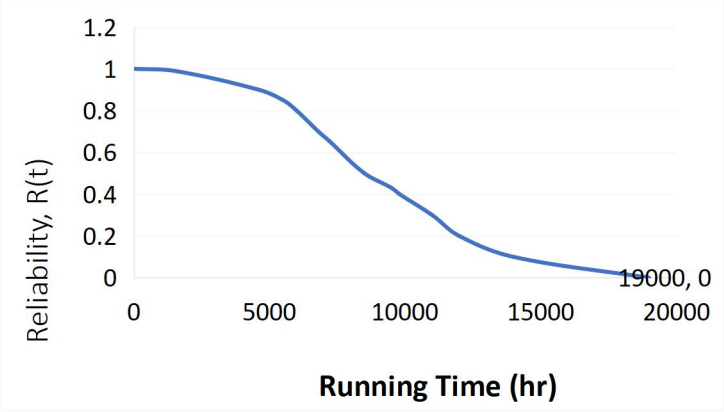

Figure 5: Compressing System Reliability.

Comparison of Existing and Proposed Models

Comparison of the reliability on the existing maintenance model at case study and the proposed reliability maintenance model is shown in Figure 6. The reliability of the system decreases in both models as the number of hours the system is in use increases, although the reliability of both models decreases with increased operation time. This indicates that the proposed model is more reliable, as it has greater values at same operating times. Also, at 7200 hours, which is the average number of hours the system is operated yearly at case study, the reliability of the system was 65.6% and 51.3% in the proposed and existing models respectively. This also confirms the fact that the proposed model has significant improvement compared to the existing model. Proposed and existing model operating hour's increases with the probability that the system will fail at any time also increases. Although, the failure rate of existing model is greater than that of the proposed reliability maintenance model at same operating time.

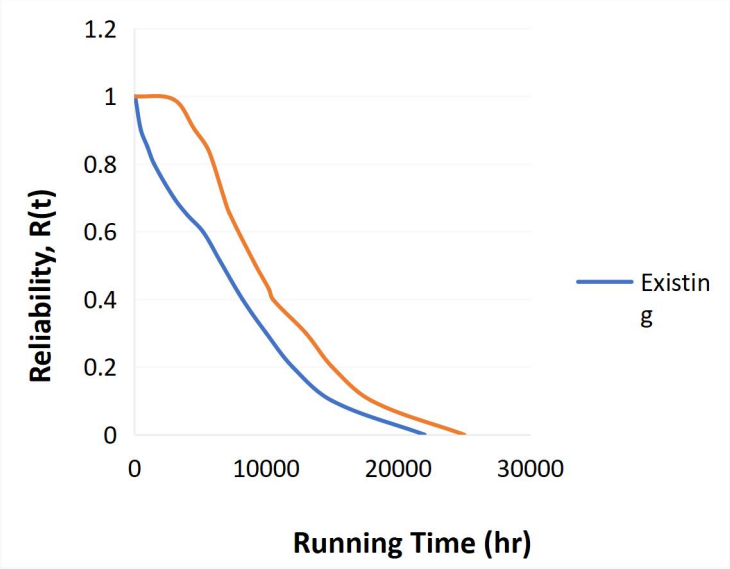

Figure 6: Existing Versus Proposed Gas Compressing System Reliability.

4. Conclusion

The proposed reliability maintenance model showed significant improvement in terms of the system's reliability compared to the existing model used in the case study, which means lower maintenance cost and higher availability. The work also showed that the application of fault tree analysis (FTA) derived from Weibull's distribution, for gas compressing systems, results in appreciable effect when compared to the existing model at case study.

5. Recommendation

Maintenance and reliability practitioners or researchers can also apply this methodology to other complex industrial/non-industrial systems for optimal result. Future work should focus on cost indicators, in order to measure improvements on the gas compressing system, brought by the application of the proposed reliability centered maintenance approach. Classical fault tree analysis (FTA) depends on the complexity of the system, maybe prone to errors from the failure probability of basic events during the root cause of failure analysis (RCFA). Fuzzy fault tree (FFT), an advanced technique is recommended for better failure probability estimation of basic events.

Abbreviation/Nomenclature

Symbol	Meaning	Unite
RCM	Reliability Centered Maintenance	%
UCF	Universal Generating Function	-
LP	Low Pressure	bar
HP	High Pressure	bar
MP	Medium Pressure	bar
PdM	Predictive Maintenance	-
PM	Preventive Maintenance	-
FMEA	Failure Mode and Effect Analysis	-
RCFA	Root Cause of Failure Analysis	-
F(t)	Probability for an item to Fail	%
R(t)	Reliability Function	%
A_i	Fault of items	-
E_i	Event of i	-
FFT	Fuzzy Fault Tree	%
DRCM	Dynamic Reliability Centered Maintenance	%

Declaration of Interests

The authors declare that to the best of their knowledge there was no conflict of interest at the time of this study.

Acknowledgments

The authors acknowledge the Department Petroleum Resources under Ministry of Petroleum Resources(Port Harcourt zonal office) for granting approval for access to data and other relevant information. The authors also wish to acknowledge theTertiary Education Trust Fund (TETFund) for the year 2022 TETFund Conference Attendance Intervention.

References

Obaseki, M. & Elijah P.T., (2020). Dynamic modeling and prediction of wax deposition thickness in crude oil pipelines. *Journal of King Saud University Engineering- Sciences*, https://doi.org/10.1016/j.jksues.2020.05.003, Elsevier.

*Elijah, P.T. and Ezeife, N.C., (2020).*Challenges of the Automobile Industry and Performance Analysis of an Assembly Plant in

Nigeria. *Saudi Journal of Engineering and Technology,* 5(9), 337-342. DOI: 10.36348/sjet.2020.v05i09.003

[3] Elijah, P.T. and Etebu, O.M.O., (2021). Towards Modern Manufacturing Technology and Practice for National Economic growth. *Journal of the Nigerian Institution of Mechanical Engineers,* 10(1), 26-36.

[4] Elijah, P. T. and Obaseki, M. *(2021).* Application of Linear Regression Maintenance Models on Rotodynamic Systems. *Nigerian Research Journal of Engineering and Environmental Sciences,* 6(2), 695-705.

[5] Nathalie, O., (2015). Risk Based Maintenance for Compressor Systems. A Masters Thesis,

Department of Marine Technology, Norwegian University of Science and Technology.

[6] Hussin, H. andHashim, F., (2011). Modeling of Maintenance Downtime Distribution using

Expert Opinion. *Journal of Applied Sciences*, 11(9), 1573 – 1579.

[7] Cheng, K. and Lu, Z.,(2019). Time-variant reliability analysis based on high dimensional

modelrepresentation. *Reliability Engineering & System Safety*, 188: 310-319.

[8] Rahmoune, B.M. Hafaifa, A. andMouloud, G., (2017). Reliability Modelling Using

WeibullDistribution on Real-time System in Oil Drilling Installations, The International Conference on Advanced Engineering in Refinery Industry (ICAEPI'17), Skikda, Algeria.

[9] Wang, W., (2010). Reliability Centered Maintenance for Promoting Compressor Operational

Level. Compressor Technology, 4(2), 61-63.

[10] Liang, W., Pang, L., Zhang, L.and Hu, J., (2012). Reliability-Centered Maintenance Study

onKey Parts of Reciprocating Compressor. International Conference on Quality, Reliability, Risk, Maintenance and Safety Engineering, Chengdu, China.

[11] Deepak, P.P. and Jagathy, V.P., (2013). A New Model for Reliability Centered

Maintenance in Petroleum Refineries. *International Journal for Scientific and Technology Research*, 2(5), 56-64.

[12] Hussin, H., Hashim, F., Ramli, H.O. andGhazali, S., (2013). Maintainability Analysis of an

Offshore Gas Compression Train System: A Case Study. *International Journal of Quality and Reliability Management*, 30(5), 495 – 510.

[13] Baig, A. A.,Ruzli, R. andBuang, A.B., (2013). Reliability Analysis using Fault Tree Analysis:A Review. *International Journal of Chemical Engineering and Applications*, 4(3), 169-173.

[14] Nezakati, E.,Razmkhah, M. andHaghighi, F., (2018). Reliability Analysis of a k-out-of-n:f

System under a Linear Degradation Model with Calibrations. Annals of the Institute of Statistical Mathematics, 71(3), 537-552.

[15] Zhou, D., Zhang, H., Li, G. andWeng, S., (2015). A Dynamic RCM Analysis Method for

Natural Gas Compressor Station Based on Diagnostic and Prognostic Technology. *Journal of Engineering Gas Turbines and Power*, 138(6), 06-09.

[16] Vishnu, C.R. andRegikumar, V., (2016). Reliability Based Maintenance Strategy Selection

inProcess Plants: A Case Study. Procedia Technology, 25(16), 1080-1087.

[17] Chen, W., Xu, C., Shi, Y., Ma, J.andLu, S., (2019). A hybrid Kriging-based Reliability

Method for Small Failure Probabilities. *Journal Reliability Engineering & System Safety*.http:///doi:10.1016/j.ress.2019.04.00.

[18] Wen, K., Li, Y., Yang, Y. and Gong, J., (2018). Reliability Evaluation of Compressor
Systems Based on Universal Generating Function Method. *Journal of Shanghai Jiaotong University*, 23(2), 291-296.

[19] Akuno, A.O., Ndonye, T.M., Nthiwa, M.J. andOrawo, L.A., (2016). Regression Approach
toParameter Estimation of an Exponential Software Reliability Model. *American Journal of Theoretical and Applied Statistics*, 5(3), 80-86.

[20] Hameed, A., Raza, S. A., Ahmed, Q., Khan, F. and Ahmed, S.,(2019). A Decision Support
Tool for Bi-objective Risk-based Maintenance Scheduling of an LNG Gas Sweetening Unit. *Journal of Quality in Maintenance Engineering*, 25(1), 65-89.

[21] Smith, A.M. and Hinchcliffe, G.R., (2004). Reliability-Centered Maintenance. Elsevier
Butterworth Heinemann, Amsterdam.

[22] Moubray, J. (1997). Reliability-Centered Maintenance. Butterworth-Heinemann, Oxford, Uk.

NMS-TP020

INTERVENTION OF NANOTECHNOLOGY AND NANOSTRUCTURED MATERIALS IN THE ENERGY SECTOR

N.I. Amalu[1], B.A. Okorie[2], P.O. Offor[3] and C. Ocheri[3]

1. Projects Development Institute, Enugu

2. Faculty of Engineering and Technology, Madonna University, Nigeria

3. Dept. of Metallurgical and Materials Engineering, University of Nigeria, Nsukka.

ABSTRACT

The exciting behaviour of nanostructured materials has inspired tremendous efforts in various scientific fields to identify possible areas of application of the materials. So far, several new application areas have been identified in various fields, such as in medicine, agriculture, communications, manufacture of consumer products, and energy. Our human society is beset with many serious problems, especially problems of poverty and food insufficiency, population growth, insecurity, climate change, disease, crimes, political instability, and inadequacy of energy. A cursory survey shows that the shortage of energy to meet the needs of the growing population, is at the root of most of the other problems. This paper has evaluated the role that nanotechnology and nanostructured materials have been playing in the areas of energy production and energy storage. It shows that the potential of nanotechnology in this regard is tremendous.

Key words: *Nanotechnology, Diode, Quantum dots, Carbon Nanotubes, Fuel cells, capacitors.*

1.0 INTRODUCTION

Nanomaterials or nanostructured materials are materials possessing extremely small grain sizes, in the range of a few billionths of a metre (10 to 100 nanometres in diameter, where one nanometre is 10^{-9} metre). When a material is reduced to particulate matter in this size range, it exhibits fascinating properties very different from the properties of the same material of bulk size. The surge of interest in nanotechnology within the global scientific community is a result of the multiple intriguing properties exhibited by nano-scale materials which make them useful in a wide-range of new applications. As a result, nanotechnology has now emerged as a favourite multidisciplinary scientific field that is of interest to professionals in engineering, medicine, pure and applied sciences, pharmacy, agriculture and food production, and the military, just to mention a few. Research and development activities in nanotechnology have led to several innovations such as fabrication of materials at the molecular scale giving rise to self-repairing structures, new types of computers, high sensitivity nano-sensors, high-energy density batteries, nano-biosensors, nanogenetic manipulation of agricultural crops, agricultural diagnostics, and much more. In the medical field, nanotechnology has facilitated medical diagnostics, drug delivery to specific target cells (bioavailability), cancer therapy, and development and use of lab-on-a-chip, among several other developments.

In the energy field, nanotechnology has already demonstrated its impact in many areas, and there is clear evidence of its potential impact in several others such as better efficiency in the use of transportation fuels, as well as lighter but stronger materials for vehicles, aircraft and wind turbines. The energy-related areas in which nanotechnology

is playing (or has the potential to play) beneficent roles include:

Lighting	Renewable energy
Heating	Energy storage
Transportation	Fuel cells
Electrical energy transmission	Hydrogen generation and storage
Batteries and capacitors	

At the present time, there are already available in the market nano-scale materials synthesized from carbon, metals and alloys, ceramics, polymers, glass, semiconductors, and composite materials. In this paper, effort has been made to highlight some of the main nanostructured materials involved in selected areas of the energy sector.

2.0 LIGHTING

In the area of light energy supply, we need to focus on the role of light emitting diodes (LEDs) and quantum dots.

2.1 Light Emitting Diodes (LEDs)

A very high percentage of available electrical energy (over 25%) in most countries has traditionally been used for provision of incandescent and fluorescent lighting. Much of the energy used for incandescent and fluorescent light is wasted in the form of heat energy.

Light emitting diodes (LEDs) are semiconductor materials that convert electrical energy into light [1]. Aluminium gallium arsenide (AlGaAs) is one of the most commonly used materials for LEDs. The material can be doped with impurities to produce a p-n junction, with free electrons (negatively charged particles) in the n-layer and holes (with positive charges) in the p-layer. Electrodes are located at the ends of the two layers, and may be connected through an external circuit. This arrangement allows electricity to flow in one direction only, with electrons moving from the n-type layer to the p-type layer. When there is no voltage on the diode, the electrons in the n-type material occupy the holes in the p-type material along the junction between the two layers forming what is called a depletion zone. Thereafter, there can be no further flow of charge across the diode unless the electrode at the n-type layer is connected to the negative end of the power source, and the p-type layer is connected to the positive end. With this, free electrons will be rejected by the negative electrode and drawn through the depletion layer to the p-type layer and the positive electrode, while the holes move in the opposite direction. When the voltage between the electrodes is high enough, the electrons in the depletion zone will be pushed out of their holes and will begin to move freely again. The depletion zone disappears, charges move freely in the diode, and the interaction between the holes and the electrons produces light. The photons released as the electrons move to the holes from their conduction bands will produce colours of light depending on the energy gap of the semiconductor used for the diode.

LEDs have tremendous advantages over conventional light bulbs. They do not release heat, and therefore convert the electrical energy they consume entirely into light. Furthermore, they use only about 10% of the total energy used by ordinary light bulbs. Currently, nanotechnology has been involved in the development and manufacture of various types of LEDs. An important example is the use of quantum dots in LEDs.

2.2 Quantum Dots

A quantum dot is a semiconductor nanocrystal that exhibits quantum behaviour in optical and electrical processes. The electrons in a quantum dot show discrete energy levels, much like an atom. Quantum dots may be viewed as zero-dimensional structures, with diameters in the range of 1 to 10 nanometres. Colour emissions from quantum dots depend on particle size, being red for the bigger particles (diameter ≈ 10nm), and blue or

violet for the small ones (diameter ≈ 1 or 2nm). Quantum dots can be produced from lead sulphide (PbS), cadmium sulphide (CdS), copper sulphide (CuS), ferrous sulphide (FeS), and zinc sulphide (ZnS). The structure may comprise a semiconductor core made of heavy metals such as cadmium selenide (CdSe), lead selenide (PbSe), or indium arsenide (InAs), and an outer shell [zinc sulphide (ZnS), cadmium sulphide (CdS)] to prevent toxicity. Quantum dots can be manufactured by several processes, from colloidal synthesis to chemical vapour deposition (CVD). They are very useful for medical imaging and for energy efficient light bulbs.

Quantum dots (QDs) can be made to produce light of almost any colour in the visible region of the electromagnetic spectrum. Quantum dot LEDs have more choices than the colour of white LEDs. A lot of research efforts focused on LED-based quantum dots [2, 3], and on a new generation of LED equipment consisting of very thin polymer films or organic molecules [4, 5] have been reported in the literature.

3.0 CARBON NANOTUBES (CNTS) IN THE ENERGY SECTOR

A carbon nanotube is a graphite sheet rolled up into a tube, with the tube diameter in the range of about 1 – 2 nanometres. The CNT is generally extremely light (with density about one quarter that of steel), strong and resilient. The armchair CNT is 30-100 times stronger than steel. It conducts heat better than diamond, and conducts electricity much better than copper, silver, or any other material discovered to date. The extremely high

It has already been highlighted above that carbon nanotubes possess great thermal and electrical conductivities. There are three strength of carbon nanotubes can be ascribed to two reasons – the interlocking carbon-to-carbon covalent bonds, and the fact that each nanotube is one large molecule. It therefore does not have weak spots or grain boundaries such as we have in crystalline grains. Because of their special properties, CNTs are extremely useful as composite reinforcement, conductive wire, fuel cells, and high resolution displays.

3.1 CNTs as Reinforcement Materials for Strong Composites

Because of the very high strength of CNTs, they can be used as reinforcement material for steel and other metallic alloys. There is therefore the prospect for high-strength, light-weight materials which will be of benefit to the transportation industry (automobiles, aircraft, etc). The wind energy sector will benefit from the use of strong and light nanocomposites for stronger rotor blades, wear and corrosion resistant nanocoatings, and excellent materials for bearings and power trains.

3.2 CNTs for Heating

Energy-efficient central heating systems can be developed for temperate countries by the efforts in nanotechnology. CNTs disperse to form a nanofluid when added to water. Researchers have developed nanofluids with forced convection heat transfer rates four times better than the norm. When added to the commercial water boiler in a home, such nanofluids will be able to make the central heating device much more efficient [6].

3.3 CNTs for Transmission of Electrical Energy

different kinds of nanotubes as shown in Figure 1.

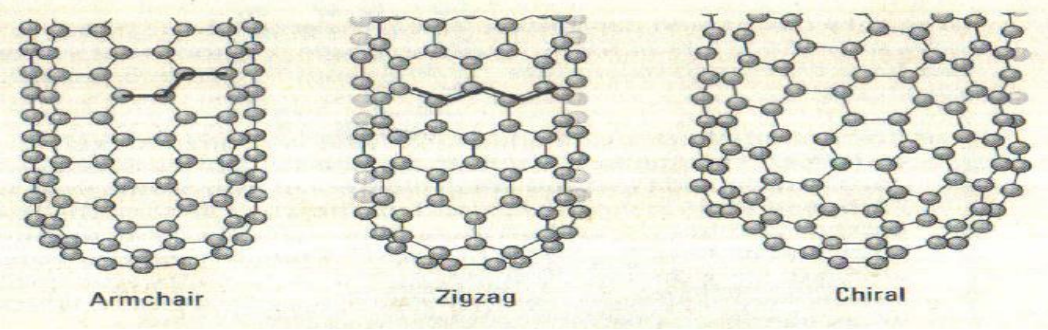

Figure 1: Armchair, Zig-Zag and Chiral Nanotubes

The electrical conductivity of the CNT depends on the type. The armchair nanotube is fully conductive (or metallic in behaviour) because there is no energy gap between their valence and conduction bands. In about 70% of the zig-zag and chiral nanotubes, an energy gap exists between the valence and conduction bands, and this makes them semi-conducting. To obtain a preponderance of a particular type of nanotube, short lengths of the type desired are attached to a nanocatalyst at one end and then placed in a reaction chamber where they act as seeds for production of long lengths of the desired type. The unusually high potential of armchair nanotubes for electrical energy transmission has been described by Richard Smalley [7].

4.0 NANOTECHNOLOGY IN ENERGY STORAGE AND GENERATION DEVICES: BATTERIES, CAPACITORS, AND FUEL CELLS

Nanotechnology is currently in use for significantly upgrading the performance of energy storage devices (batteries and capacitors) as well as energy generation facilities such as fuel cells.

- **Batteries**

  Traditionally, lithium-ion batteries with carbon anodes have been used only for such devices as watches and lap-tops that do not need a lot of power. Now Altair Nanotechnologies, Inc., has developed improved lithium-ion batteries by replacing the carbon anode with lithium titanate nanocrystals which provide 30 times greater surface area than carbon anodes. Therefore, electrons from the chemical reaction in the battery can come out faster, which means more current and therefore more power for running our gadgets.

  Carbon nanotubes, with their extraordinarily high surface area and excellent electrical conductivity are now used for batteries with CNT-based electrodes for the generation and storage of increased electricity.

- **Capacitors**

  Capacitors, unlike batteries, store electricity between a pair of metal electrodes. To increase the storage capacity requires increase of the surface area of the electrodes. Researchers have now solved the problem by covering the capacitor electrodes with millions of nanotubes [8].

- **Fuel Cells**

  Fuel cells are composed of electrodes that convert the energy of a chemical reaction directly to electrical energy, heat and water. Unlike a battery, it does not require recharging because it is designed for continuous replenishment of the reactants that become consumed in the chemical reaction. Basically they change hydrogen and oxygen into water, producing electricity and heat in the process, but no other products.

Currently, there are efforts to use nano-engineered polymer membranes as the structure through which the hydrogen passes and on which the catalysis occurs. This may increase the volume of hydrogen conversion and therefore result in more energy [9]

Precious metal nanoparticles of various compositions have been optimized to act as effective electro-catalysts in polymer electrolyte fuel cells and direct methanol fuel cells at both the anode and the cathode sides [10].

5.0 OTHER KEY INTERVENTIONS OF NANOTECHNOLOGY IN THE ENERGY SECTOR

In addition to the areas so far discussed, nanotechnology researchers have addressed and solved problems in several other areas of the Energy Sector. Some of these are:

- Development of nanosensors to meet the requirements of precision farming in agriculture.
- Quantum Dot Solar Cells: In this, quantum dot nanoparticles, or other semiconductor nanoparticles, are sandwiched between two sheets of transparent and conductive plastic.
- Gratzel Cell (Dye Sensitized Solar Cells, DSSC) Here, nanoparticles of TiO_2 are soaked in vegetable dyes, and this, together with a triiodide electrolyte, is placed between two conductive glass plates.
- Hydrogen Generation and Storage. In a photoelectrochemcial cell, hydrogen can be produced by the splitting of water molecules in a reaction with solar-energy activated nanoparticles deposited on a conductive glass substrate.
- Development of nanocatalysts for reduction of energy usage in industries.

6.0 CONCLUSION

Energy is one of the most critical requirements of mankind. With the rapid growth of human population, the need for Research and Development in the energy sector cannot be overstressed. This paper has shown that efforts have been made to use nanotechnology to help address the problems of energy generation, energy storage, and energy conservation. There is hope that with the pace of work in this area, it will be possible to harness and store energy to meet the needs of the growing population of the world.

REFERENCES

1.Haisen (2011), “LED Working Principles”, 2011-11-18, http//www.hs-lighting.com/FAQ/7html.

2. Bowers M.J. 2nd, McBride J.R., Rosenthal S.J. (2005), “White light emission from magic-sized cadmium selenide nanocrystals”, *Journal of the American Chemical Society*, 2005, 127(44), 15378-15379.

3. Plasma Chem GmbH (2012), ‘Quantenpunkten “Feht” grunes und sonne-nahnliches licht aus LEDs. Nanotechnologie Actuell. 2012-11-20, http//www.plasmachem.com/led-true-green_de.html

4. ScienceDaily, (2011), “Nanotechnology being used in new-generation LED lights”, 2011-11-20, http//www.sciencedaily.com/release/2007/03070319175617 htm.

5. Auvray A., Pigeon S., Izquierdo R., Desjardins P., and Martel R. (2006), “Carbon nanotube sheets as electrodes in organic light emitting diodes”, Applied Physics Letters, 2006, 88(18), 183104-183106.

6. Pollitt M. (2006), “Tiny Tubes Could Bring Big Savings on Fuel Bills”, The Guardian, April 13, 2006. Available at http//technology.guardian.co.uk weekly story: 0.1752275.00html. Accessed June 27, 2006.

7. Smalley R. (2003), Testimony before the US House of Representatives, Committee on Science, Energy Subcommittee, heating, “Review of Non-Oil and Gas Research Activities in the Houston-

Galveston Gulf Coast Area", Dec. 4, 2006. Available at http://commdocs_house_gov/committees/science/hsy90674000/hsy90674_0HTM. Accessed February 19, 2007.
8 Limjoco V. (2006), "Super Battery" Scien Central News. Available at http://www.sciencentral.com/articles/viewphp3?type_articles&articles_id=218392803.
9. McGahn, D.P. (2006), "Nanotechnology and its impact on industry". Available at http://www.mtpe.org/institute/research/nano_report_04/energy_pdf./ Accessed July 12, 2006.
10. Strem (Strem Chemicals, Inc.) 2006. Supplier data from Strem Chemicals on Azonano.com. Available at http.//www.azonano.com/details asp? Article ID = 1339. Accessed June 27, 2006.

NMS-TP021

A STUDY OF THE EFFECT OF ANNEALING TEMPERATURES OF 0.17% C OF HSLA STEELS USING IMAGEJ ANALYSIS

[1].Ngozi Grace Emordi, .[2]Iweriolor Sunday
[1,2]Department of Metallurgical Engineering, Delta State Polytechnic, Ogwashi-Uku, Nigeria
Correspondence- hisministersng@gmail.com

Abstract:

Annealing is a heat treatment method in which the mechanical properties of a material are changed, resulting in changes in attributes such as strength and hardness; it is typically used to increase ductility and toughness, reduce hardness, and remove carbides. The structures of six annealed samples of 0.17 percent High Strength Low Alloy (HSLA) Steels (840^{o}C-990^{o}C) were measured with a 30^{o} C interval and a 90-minute soaking duration. Using the Image software, several metrics such as area computation, pixel value statistics, distances and angles measurements, edge identification, such as circularity, ferret angle, solidity and perimeter, average area, and percentage area were investigated using optical microscope images. The 900 ^{o}C annealed sample had the greatest grain count of 515, a perimeter of 35.403, a standard deviation of 5.960, and a mean of 26.881, indicating that annealing considerably increased the steel's fatigue life. The annealed sample at 840oC had the highest hardness value of 99.28 BHN and the lowest impact value of 62.79 J, according to the mechanical analysis results. The hardness value of the steel in this study decreased significantly as the annealing temperature increased, indicating that the annealing temperature improved the fatigue property and tensile strength (wear strength) of the steel in this study. We looked at circularity, ferret angle, solidity and perimeter, average area, and % area.

Keywords: High Strength Low Alloy Steel, Microstructure and ImageJ

1. INTRODUCTION

An important feature of any Engineering component is its fatigue life and it's measured by the number of cycles it can with stand before fatigue failure takes place. Fatigue is a problem that can affect any type of component that moves [Sreeteja, 2017]. Heat treatment is an operation or combination of operations which involve heating at a specific rate. The aim is to obtain a desired microstructure to achieve certain predetermined properties (mechanical, physical, electrical or magnetic). Heat treatment and alloying are two methods which are considerably used for controlling material properties. In heat treatment, the microstructures of the materials are altered; which influences mechanical properties such as strength, ductility, toughness, hardness and wear [Sreeteja, 2017] Annealing in metallurgy and materials science is a heat treatment that alters the physical and sometimes the chemical properties of a material to increase its ductility and reduce its hardness, making it more workable. It involves heating the material to above its recrystallization

temperature, maintaining a suitable temperature, and then cooling [Seeteja et al, 2017]. Hu,et al (2010) and Zhao (2017) described Annealing process as a thermal system applied to a material to transform or modify its internal structure from cold worked propagation; Metallurgically, the effect of these changes in properties impact on the performance characteristics and the expected application. According to Vervynckts, et al (2012) Annealing is the as strength and hardness. In this process, a material is heated to an elevated temperature for a specific period of time and then slowly cooled in the furnace. This kind of process is usually carried out to relieve stresses and improve ductility. It often enables the design of desired microstructure by altering the annealing parameters such as annealing temperature and soaking time.

New materials that impart excellent structural performance; while reducing weight and being cost-effectively manufactured is on the increasing demand [Vervynckts, 2012]. Due to this fact, for the past 30 years now, an exceptional type of steel which has low amount of carbon (0.05-0.25) which also combines with other alloying elements like Cr, Ni, Mo, Cu, N, V, Nb, Ti, W, and Zr, in little proportions and in diverse concentrations has evolved often known as high strength low alloy HSLA steels [Honeycombe, 2006]. Manricino,2019 in his work on fatigue failure analysis of High Strength Low Alloy steel sheet described High strength low alloy steels (HSLA) as steels that are made up of microstructures formed by hard martensite particles distributed in the ductile ferrite matrix [Erdogan, 2003]. They are compared to dual-phase steels due to their high hardening ability during deformation, high malleability and good surface quality "[Dzupon et al, 2006]". It also contributes to the stiffness and weight reduction being type of heat treatment most frequently applied in order to soften iron or steel materials and refines its grain due to ferrite-pearlite microstructure; it is used where elongations and appreciable level of tensile strength are required in engineering materials. Jia, et al 2003 ; Yu, C.Y et al 2005 described Annealing as a heat treatment procedure in which a material is altered such alteration causes changes in its properties such

preferred in automobile industry. This is attributed to its good formability characteristics. These groups of steels play an effective role in the production of parts in vehicles such as suspension systems, support elements, longitudinal beams, transverse components and chassis "[Kadkhodpour et al, 2011]". When these materials are exposed to high temperatures, there is a recrystallization of the microstructure in the heat affected zone which directly influences the resistance limit of the material [Costa, 2010] Utilization of HSLA steels are found in many engineering fields which include oil and gas pipelines, constructions and farm machinery, heavy- duty highway and off road vehicles, industrial equipment storage tanks, mine and rail road car, barges and dredges snow mobiles, power transmission towers light poles, lawn mowers, and passengers car components. Bridges, offshore structures, and building beams and panels are additional uses of these steels (ASM international, 2001).

Image analysis deals generally with acquisition of quantitative information about various parameters of microstructure of a material such as determination of percentage fraction of phases, particular size, circularity etc. Circularity can be calculated as a shape parameter index in the ImageJ software. The definition of circularity (C I) in the ImageJ software is as follows:

$C_1=4\pi\frac{A^1}{P_1^2}$

Where, A1 and P1 are the area and the perimeter using imageJ.

There are numerous commercial software such as Amira, Comsolmultiphysics, etc., for analysis features

(Schneider et al., 2012). However, this paper describes an investigation of six different annealed samples from 840°C-990 °C with 30 °C interval of 0.17%C HSLA steels structure analyzing from OM image using imageJ program software (Katarina and Gejza, 2009). Several researchers [Zhuang Li, 2015; Offor et al 2010, Sherman, 2016] have investigated DP steels to find out the effect of heat treatment, soaking times on its properties. Miroslaw, 2020 observed that annealing process reduces the true stress and effectively decreases the hardness of 42 $CrMO_4$ Steel and also improves microstructural Spherodization. Senthil (2016) reported that improved fatigue strength was attainable by the combined heat treatment process of Nitriding followed by induction hardening. Sreeteja, (2017) investigated the quantitative measurement of the influence of Annealing on the fatigue life of SAE202 and 440° C steels from his results, he concluded that there is a definite improvement in the fatigue life due to annealing in both steels; however, the extent of improvement was more in 440°C steel when compared to SAE202. Gaurav, 2018 reported that to improve fatigue life, effect of heat treatment on fatigue life and strength need to be studied for better designing and mechanical system. Also, little or no work has been done to set out the fatigue life of HSLA steel at different annealing temperature; hence this work investigated on the use of ImageJ to analyze the effect of annealing temperatures on the fatigue properties of 0.17% C HSLA steels.

1. Materials and Method

Samples of HSLA steel containing about 0.17% Carbon were provided and used for this experiment. The samples were grouped into 10 having 5 samples in each of the group. They were then heat treated at different pre-determined temperature as follows: 840^0C, 870^0C, 900^0C, 930^0C, 960^0C and 990^0C respectively and the control which served as the austenizing temperature. Furthermore each of these group of five were held at 30 minutes interval and were then left to cool in the furnace (annealing) before various test were carried out on them..

2.1. HEAT TREATMENT

This section is aimed at producing microstructures from the as-received steel through different annealing temperatures. The focus here is to develop different microstructure at different temperatures for each of the samples, with a view to determining the effect of the new microstructures on the mechanical properties of the investigated steel.

Normalizing

This was done to remove the effect of past mechanical, thermo- mechanical or thermal treatment the steel has been subjected to. This was done by heating the sample to 890°C, soaking for one hour (1hr) in the furnace (muffle) and then allowing it to cool in air.

2.2 ANNEALING

Before the annealing was done the Carbon equivalent was calculated to tell the starting temperature from the Iron Carbon phase diagram.

$CE= C+\frac{Cr+Mo+V}{5}+\frac{Mn+Si}{6}+\frac{Ni+Cu}{15}$ ----------3.

From the chemical composition in table 3.1 above we have

Cr =0.2559; Mo=0.0100; V=0.0100 ;Mn=1.2089; Si=0.3016 Ni=0.1218 and Cu=0.2560 and C=0.17

Substituting these figures in fig 3.1 above, we have

$$CE = 0.17 + \frac{0.2559+0.0100+0.0100}{5} + \frac{1.2089+0.3016}{6} + \frac{0.1218+0.2560}{15}$$

CE=0.17+0.05518+0.25175+0.02513=0.502 06 hence CE is 0.5 .

2.3 Metallographic Examination

2.3.1. Grinding

This operation aims at producing a perfectly flat and smooth surface Silicon carbide papers of different grades placed on the grinding machine was used in the order of 220,320,400 and 600 grits paper i.e. from coarse grade to finer grade. The grinding process was done under running water to wash away the grits and also to avoid overheating. The samples was turned through 90^0 while changing from one grit size to another in the materials laboratory at Obafemi Awolowo University, Ile-Ife. Osun State ,Nigeria.

2.3.2. Polishing

A universal polishing machine was employed. A polishing cloth (selvt cloth) was placed on the polisher for the initial polishing swamped with solution of one micron of silicon carbide solution, then, followed by the final polishing stage with selvt cloth swamped with solution of 0.5 µm Silicon carbide until a mirror-like surface is attainable. It is then washed and dried

2.3.3. Etching

This is done to reveal the microstructure of the polished surface. Etching is the selective attack on the grain boundaries being a region of high energy and dislocation density. The mirror-like surface was etched in 2 % NITAL. The sample was again washed, dried and later viewed under the metallurgical microscope.

4.Optical Microscopy

The samples were etched in 2 % NITAL (2% Nitric Acid and 98% Ethyl Alcohol), they were put in a desiccator and viewed with metallurgical optical microscope.

3.0. Results and Discussion

Figure 1 showed the flowchart of the ImageJ process of HSLA Steel. In Fig.2a Steels taken with metallurgical Optical microscope. The images were uploaded and analyzed with imageJ software. *After the capturing of the micrographs. The Image J analysis was then used to analyse for the following parameters, standard deviation, perimeter, angle, circularity, percentage area, ferret angle, roundness, solidity, histogram, 3D dimensioned and results are presented in plate1:0* .Images in Fig. 2a were thresholded by using Image-Adjust and Threshold tool. The thresholded colour images of Fig. 2b were masked to give the outlines in Fig. 2d while Fig. 2f showed the 3D interactive surface plot drawn by intensity of any colour offers a basic vision of observed surface morphology of the steel such as the grid size, the smoothing and the perspective of the minimum and maximum percentage in relation to the z-scale. This was also attested to by the work of Dang et al. (2014). The circularity (shape descriptors) parameter allows for evaluating the shape of grains. Fig. 2e showed the bins which is the number used for the particle size distribution histogram while Table 3 showed the microstructural parameters of the six annealed samples of HSLA steels using **ImageJ analysis**

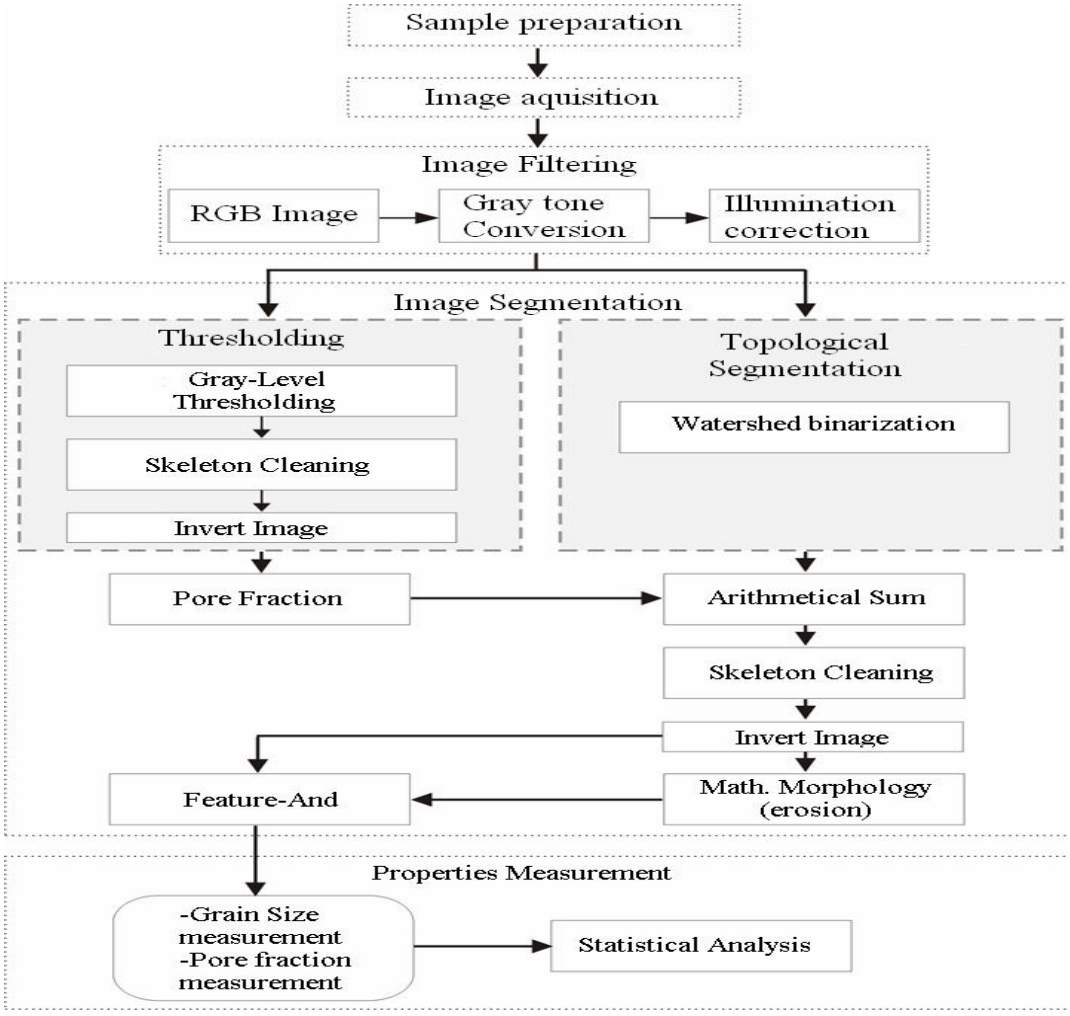
Sample preparation
Image aquisition
Image Filtering
RGB Image
Gray tone Conversion
Illumination correction
Image Segmentation
Thresholding
Gray-Level Thresholding
Skeleton Cleaning
Invert Image
Topological Segmentation
Watershed binarization
Pore Fraction
Arithmetical Sum
Skeleton Cleaning
Invert Image
Feature-And
Math. Morphology (erosion)
Properties Measurement
-Grain Size measurement
-Pore fraction measurement
Statistical Analysis

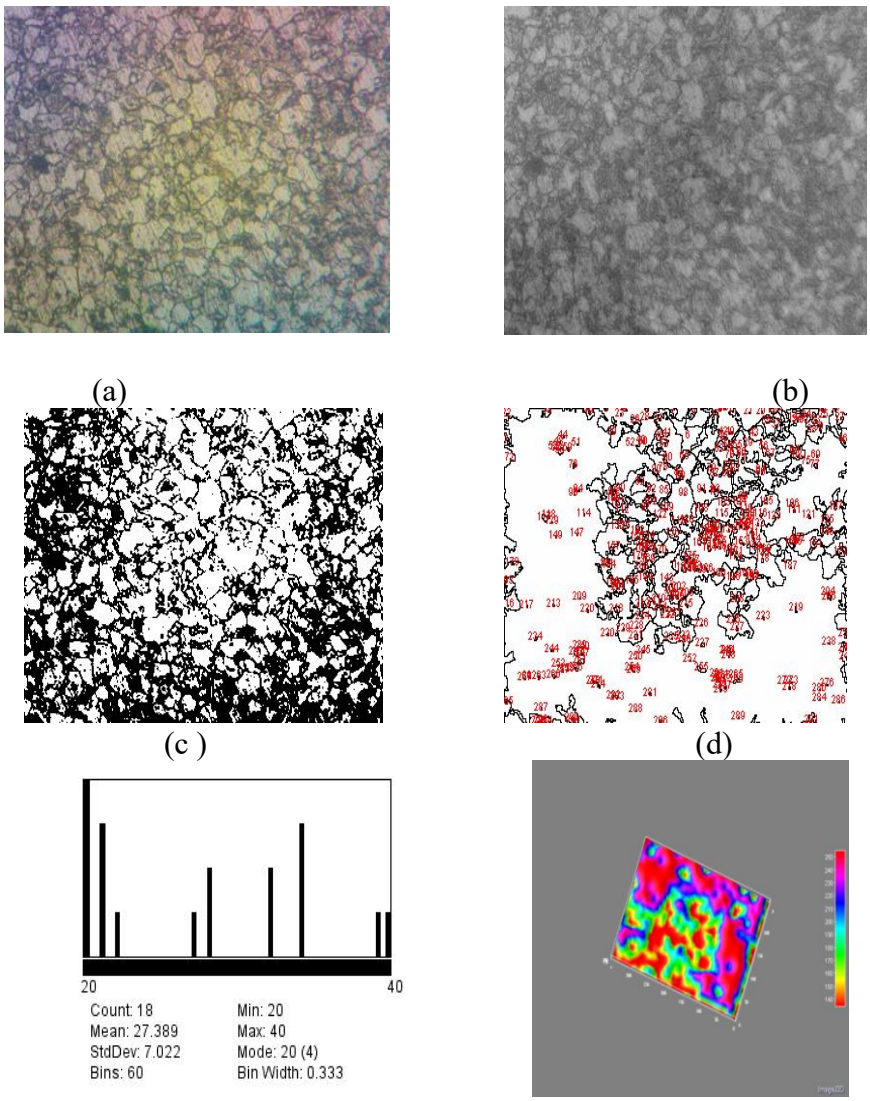

Fig. 2.0. Processed image of 840°C annealed steel by image analysis (using) ImageJ. (a) Original image – Optical Microscope (b) processing and threshold (blue). (c) thresholded (black and white) (d) result of particle distribution(using analysis tool in ImageJ) (e) Area distribution of the grains (f) Interactive 3D surface plot

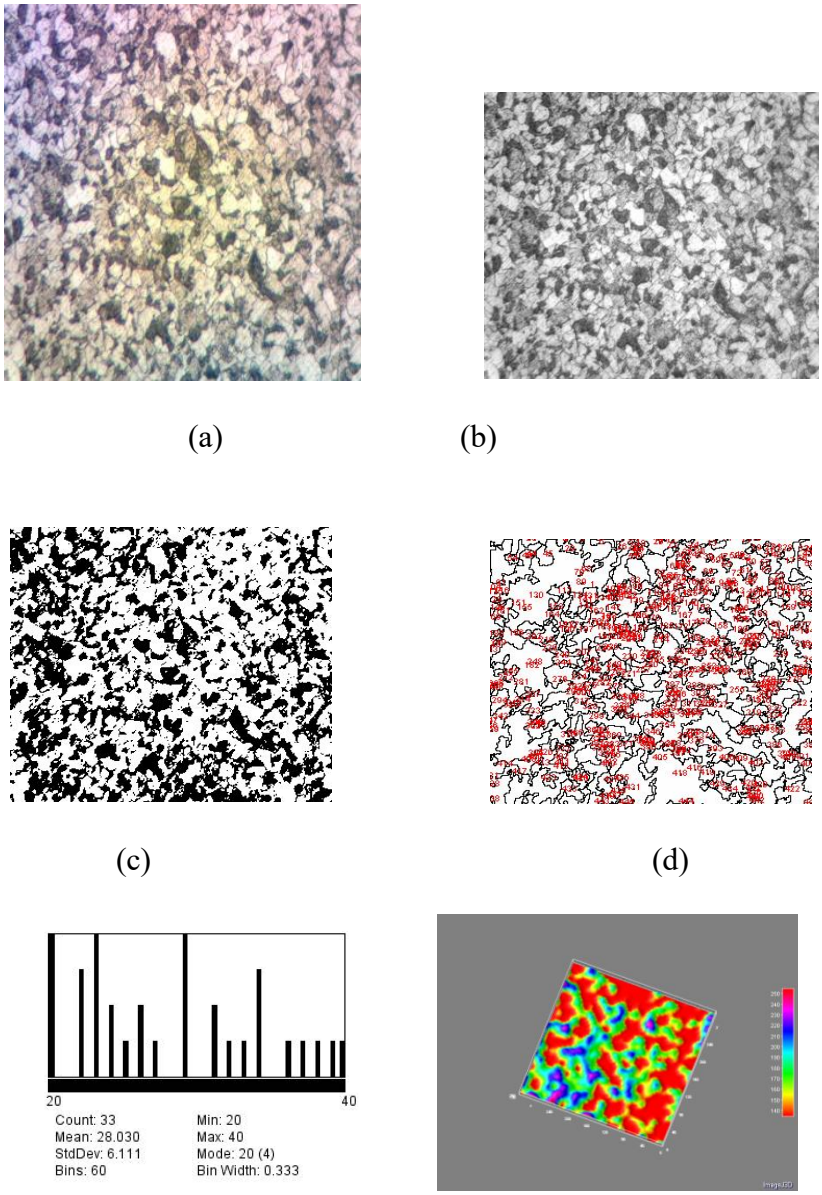

Fig. 3.0. Processed image of 870°C annealed steel by image analysis (using) ImageJ. (a) Original image – Optical Microscope (b) processing and threshold (blue). (c) thresholded (black and white) (d) result of particle distribution(using analysis tool in ImageJ) (e) Area distribution of the grains (f) Interactive 3D surface plot

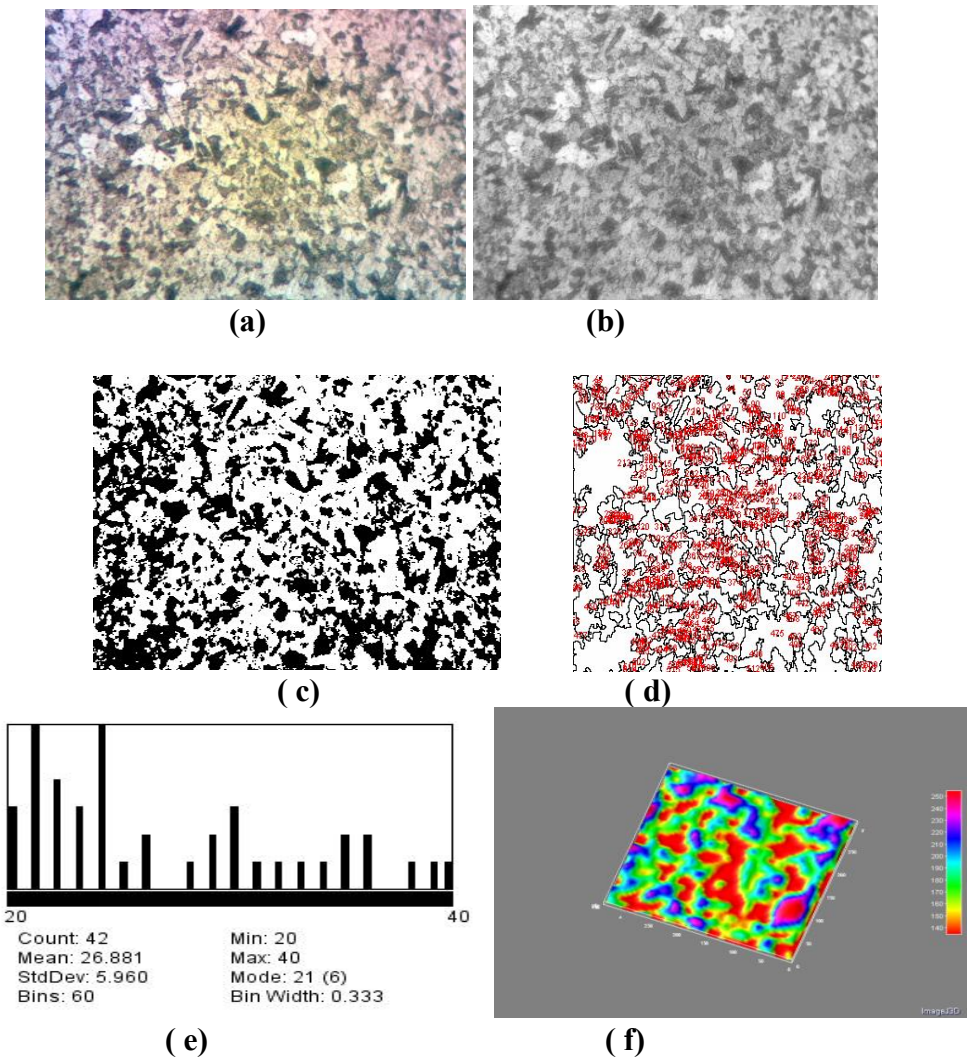

Fig. 4.0. Processed image of 900°C annealed steel by image analysis (using) ImageJ. (a) Original image – Optical Microscope (b) processing and threshold (blue). (c) thresholded (black and white) (d) result of particle distribution(using analysis tool in ImageJ) (e) Area distribution of the grains (f) Interactive 3D surface plot

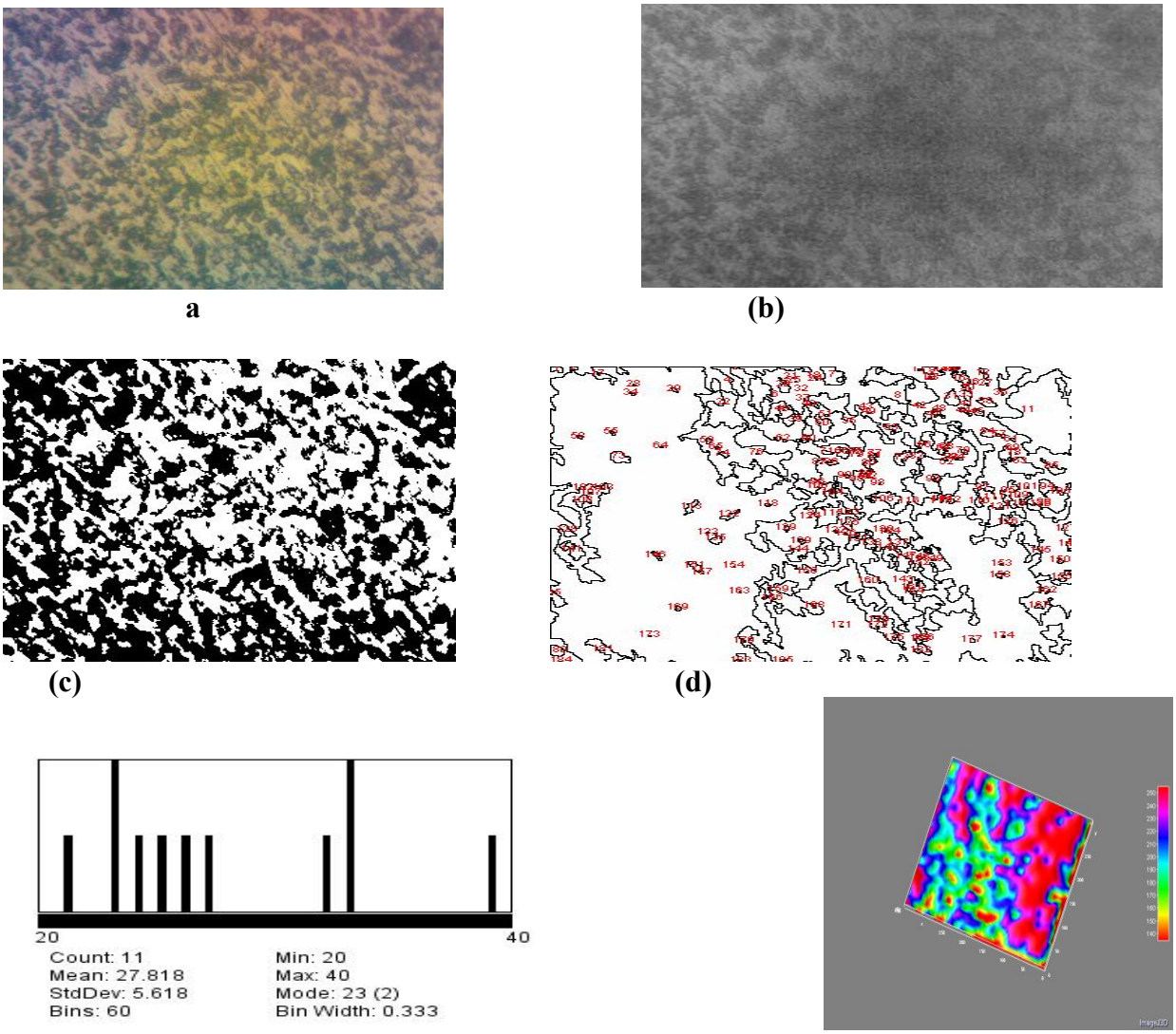

Fig. 5.0. Processed image of 930°C annealed steel by image analysis (using) ImageJ. (a) Original image – Optical Microscope (b) processing and threshold (blue). (c) thresholded (black and white) (d) result of particle distribution(using analysis tool in ImageJ) (e) Area distribution of the grains (f) Interactive 3D surface plot

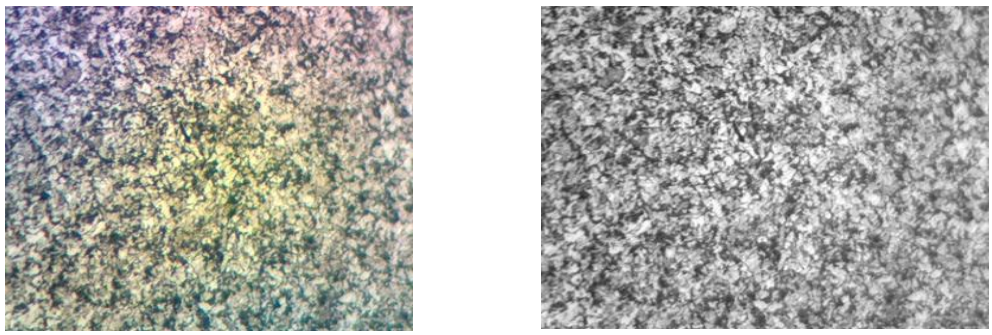

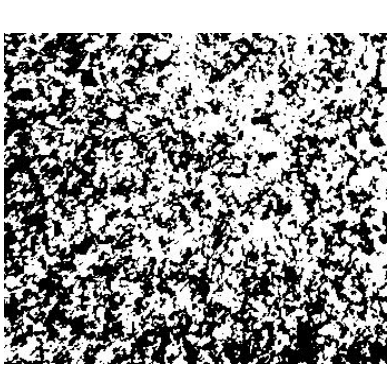

(c)

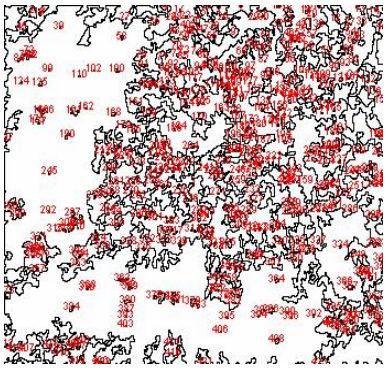

(d)

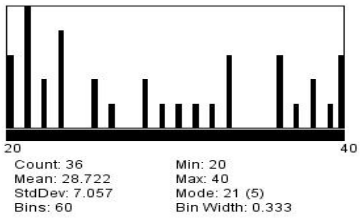

(e)

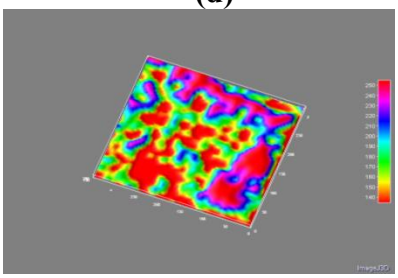

(f)

Fig. 6.0. Processed image of 960°C annealed steel by image analysis (using) ImageJ. (a) Original image – Optical Microscope (b) processing and threshold (blue). (c) thresholded (black and white) (d) result of particle distribution(using analysis tool in ImageJ) (e) Area distribution of the grains (f) Interactive 3D surface plot

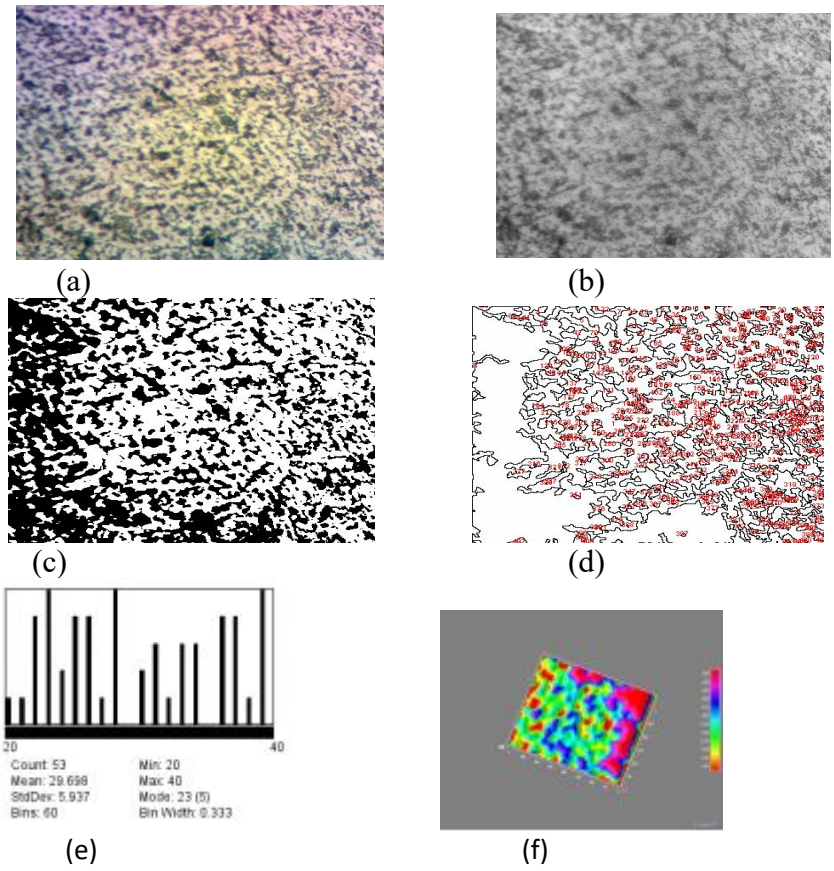

Fig. 7.0. Processed image of 990°C annealed steel by image analysis (using) ImageJ. (a) Original image – Optical Microscope (b) processing and threshold (blue). (c) thresholded (black and white) (d) result of particle distribution(using analysis tool in ImageJ) (e) Area distribution of the grains (f) Interactive 3D surface plot

Table 1: Microstructural properties of six annealed samples of 0.17% HSLA steels by ImageJ analysis

TEMP °C	COUNT	TOTAL AREA	AV. SIZE	% AREA	CIRC	perimeter	FERET	FERET X	FERET Y	FERET ANG	ERET
840	296	44059	148.848	48.11	375.67	38.83	7.064	186.06	112.45	122.24	3.975
870	446	38570	86.48	41.33	336.16	38.00	8.965	162.97	133.44	100.48	4.874
900	515	42280	82.097	41.90	423.65	35.40	8.916	165.50	130.09	110.26	4.954
930	185	54641	295.357	50.49	161.89	65.10	12.92	200.15	124.135	119.14	7.542
960	423	48151	115.251	45.42	353.62	41.36	8.146	193.96	133.32	103.55	4.726
990	405	62097	153.326.	43.86	317.52	49.56	13.524	267.61	149.08	115.26	7.406

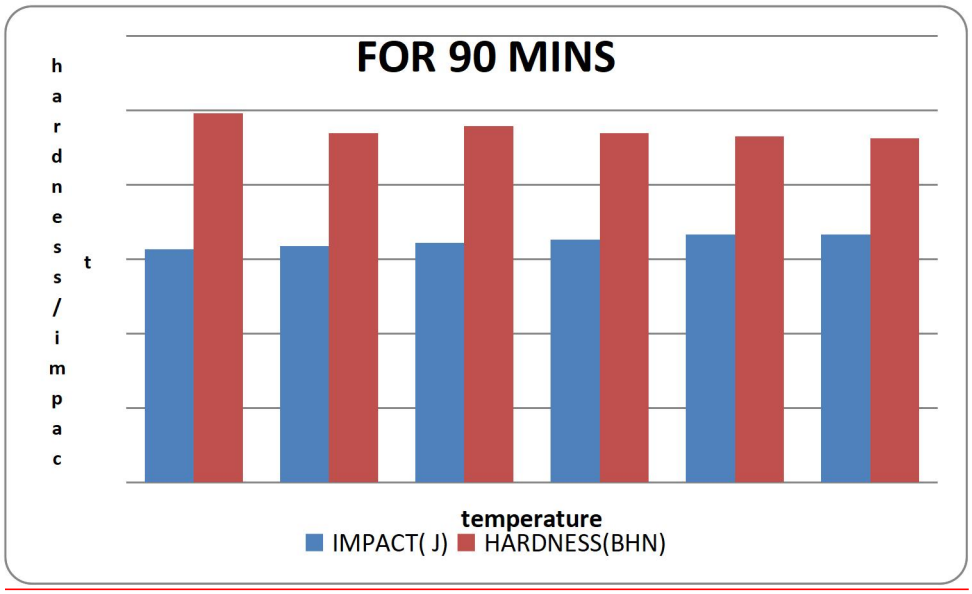

Fig. 8 IMPACT AND HARDNESS TEST FOR 90 MINS SOAKING TIME OF 0.17% C HSLA STEELS

In Fig. 8, the Impact and Hardness were conducted using the ASTM E23 for notched bar impact testing, from the figure, it will be observed that the highest hardness point in the series was at 99.28 BHN at 840° C the hardness decreased gradually to point 92.96BHN which is at 990 °C . It is worthy of note that 840°C also had the lowest impact value at 62.79 J and this value was seen to increase significantly to 66.63 J at 990°. However, it was observed that as the annealing temperature increased, the hardness decreased while the impact increased. This may be due to annealing; because annealing helps to relieve internal stress and improve ductility. (Zhoo, et al., 2018; Seeteja, et al , 2017;Jia et al.,; Al-Qaabah. et al,2003; yu, et al, 2005).

Conclusion

In this study, we have successfully analyzed some basic parameters of 0.17%C of HSLA Steels such as the circularity, ferret angle, solidity and perimeter, average area and the percentage area using imageJ. It also showed the differences in the images of the six annealed samples. The method is automated and very reliable, and accurate, very fast and can be used for some sundry analysis. From the mechanical analysis result, From the mechanical analysis result, the annealed sample at 840°C has a highest hardness value of 99.28 BHN and an impact value of 62.79 J. it was observed that at 870°C annealing temperature, the hardness value decreased to 93.84 BHN while the impact value increased to 63,62 J; 900°C gave an hardness value of 95.88 BHN and impact value of 93.84J; 930°C has a hardness value of 93.84 BHN and impact value of 65.38 J; At 960°C the hardness value is 93.02 BHN while the impact value increased to 66.66J. At 990°C we had the least value of hardness value of 92.96BHN and an impact value of 66.63 J. from the above , we can conclude that annealing

enhanced the fatigue property and tensile strength (wear strength) of the steel in study.

References

[1] Al-QawabahS.M.A., NabeelAlshabatat, U.F. Al-Qawabeha / International Journal of Engineering Research and Applications (IJERA) ISSN: 2248-9622 www.ijera.com Vol. 2, Issue 3, May-Jun 2012, pp.1550-1553 1550 | P a g e " Effect of Annealing Temperature on the Microstructure, Microhardness, Mechanical Behavior and Impact Toughness of Low Carbon Steel Grade 45"

[2] American society for metas(ASM)international, materials park, Ohio USAwww.asminternational.org,2001,.Alloying: understanding the basics.

[3] Arasu, T.P. Dhansekaram**, R., Kumar, S.P. and Srinivasan, N. (2013)."** Effect of Hardness and Microstructure on En 353 Steel by Heat Treatment ".International Journal of Engineering and Science, Vol 2 pp 01-05

[4] Bhadesia, H.K.D.H and Honeycombe (2006)."Steel: Microstructure and Properties."3rd edition, Pub. Butterworth-Heinemann.

[5] Hu J., S.Wang, X.Zhoa, B.Yu. " Structure and Performance of Welding Structure and Performance of Welding Joint of Q235 Steel Welded by SHS Welding" Mechanical Engineering in China, 2010, Vol 5, issue 2 pp 189-193.

[6] Jia D., K.T. Ramesh and E, Ma, " Effect of Monocrystalline and Ultrafine Grain Sizes on Constructive Behaviour and Shear Bands in Iron". ActaMaterialia, Vol. 51, No.12, 2003,pp. 3495-3509. Doi:10.1016/51359-6454(03)00169-1

[7] Katarina, B. and R. Gejza, 2009. Qualification of microstructural parameter, ferrite-martensitedualphase steel by ImageJ analysis. MEAL.

[8] Liang, J.; Zhao, Z.; Wu, H.; Peng, C.; Sun, B.; Guo, B.; Liang, J.; Tang, D. Mechanical Behavior of Two Ferrite–Martensite Dual-Phase Steels over a Broad Range of Strain Rates. Metals **2018**, 8, 236.

[9] Schneider, C.A., W.S. Rasband and K.W. Eliceiri, 2012. NIH image to imageJ: 25 years of image analysis. Nat. Methods, 9: 671-675. DOI: 10.1038/nmeth.2089

[10] Sreeteja M., S. Pranavadithya, V. Nitish and GundaSowmya. (2017): Experimental Investigation on the Effect of Annealing on Fatigue Life of SAE 202 and 440C Steels. International Journal of Current Engineering and Technology.Vol.7,No. 3 p 857-861.

[11] Wang K.F. ,Wang S. , Chandraseker. Yang H.T.Y. "Experimental and Computational Study of the Quenching of Carbon Steel Product s" Material Science Technology 1997; 257-265

NMS-TP022

CHARACTERIZATIONAND GRAVITY CONCENTRATION OF AZARA-NASSARAWA BARITE MINERAL ORE FOR OIL AND GAS INDUSTRIAL APPLICATIONS

NNAEMEKA STANISLAUS NZEH[1,*], PATRICIA A. I. POPOOLA[1], SAMSON O. ADEOSUN[2], GODSON N. NZENWATA[2,3]

1) Department of Chemical, Metallurgical and Materials Engineering, Tshwane University of Technology, Pretoria, 0183, South Africa

2) Department of Metallurgical and Materials Engineering, University of Lagos, Akoka, 100213, Lagos, Nigeria

3) Projects Department, Dangote Industry Limited, 100282, Ikeja, Lagos state, Nigeria

* Corresponding Author: nstannzeh@gmail.com

ABSTRACT

The comparative study for the recovery of Azara barite mineral ore found in Nassarawa State, Nigeria using jigging and tabling gravity separations was investigated. The microstructural, chemical compositionand physical properties of the as-mined sample of Azara barite mineral ore were analysed. The sample was concentrated using the gravity separation processes. The microstructural and chemical composition analyses of the products of concentration were carried out to establish the effectiveness and efficiency of the methods for the recovery of Azara barite mineral ore. Xray Diffraction (XRD), Xray Fluorescence (XRF), Scanning Electron Microscope (SEM) and Energy Dispersive Spectrometry (EDS) tests; were used to carry out the morphology and chemical analysis of the Azara barite ore. From the results, the Azara barite ore contains approximately 36.2% barium (Ba) based on XRF and 50.5% barium (Ba) based on EDS tests with a specific gravity of 3.85. A random sieve size of -355+250µm was selected for jigging and tabling of the Azara barite ore. The EDS result of the products of jiggling and tabling shows that jigging had a recovery of 69.8% Barium with an average specific gravity of 4.28 while tabling had a recovery of 69.5% Barium with an average specific gravity of 4.18. Therefore, the results of this research work have established that the Azara barite ore found in Nassarawa state, Nigeria is suitable for oil and gas applications.

Keywords: Barite, Non-metallicmineral, Gravity separation/beneficiation, Jigging, Tabling, Underflow, Concentrate, Specific gravity.

1. INTRODUCTION

The mineral, barite is one of the most common mineral of barium; composed of barium sulphate ($BaSO_4$). It is a dense non-metallic mineral with an average specific gravity of 4.5 and a hardness of 3.0 [**1**]. Barite is one of the major sources and principal ore of barium and its compounds whose many uses are nearly hidden among the technical complexities of modern industrial processes and products. It receives its name from the Greek word "barus" which means "heavy [**2**]. This name is in response to its high specific gravity of 4.5, which is exceptional for a non-metallic mineral. The high specific gravity of barite makes it suitable for a wide range of industrial, medical and manufacturing uses. It is extremely important in the petroleum industry where, 80% of the world's production of 44 million tons in 1973 was consumed by that industry in the form of a heavy fluid (weighting agent) which is circulated in rotary drilling. The remaining 20% went chiefly to the production of barium chemicals [**2**]. Barite is generally easy to identify. It is one of just a few non-metallic minerals with a specific gravity of four or higher. Combine that with its low

hardness (2.5 to 3.5) and its three characteristic directions of right angle cleavage and crystals, the mineral can usually be reliably identified with just these observations: Chemical classification: sulfate mineral; Chemical composition and formula: barium sulfate, $BaSO_4$; Cleavage: very good cleavage, basal, prismatic; Colour: colourless, white, light shades of blue, yellow, red, green, grey and brown; Streak: white; Crystal system: orthorhombic; Fracture: irregular/uneven; Fusibility: yellowish green barium flame; Luster: vitreous to pearly; Melting point temperature: 1580^oC; Hardness: 2.5 to 3.5; Optical properties: biaxial positive; Refractive: n_α = 1.634-1.636, n_β = 1.636-1.638, n_γ = 1.646-1.648; Solubility: low; Tenacity: brittle; Density: 4.48g/cm^3; Specific gravity: 4.5; Uses: drilling mud; high density filler for paper, rubber/plastics,etc. [**2**].

Barite is of common occurrence and is available from three major geologic types of ore deposits that is: vein, cavity filling and residual or bedded deposits. It belongs to the colloidal mineral like silica. Barite occurs in tabular crystal-granular form or in compact masses resembling marble. China and India are the leading producers of barite and they also have the largest reserves [**2-3**]. Although, other than China and India, barite has also been largely found at some locations in Nigeria, Brazil, Canada, Chile, Pakistan, Greece, Guatemala, Iran, Ireland (where it was mined on Benbulben), Liberia, Mexico, Morocco, Peru, Romania (Baia-Sprie), Turkey, South Africa (Barberton Mountain Land), Thailand, UK (Cornwall, Cumbria, Derbyshire, Durham, Perthshire, Argyllshire and Surrey) and in the US from Cheshire, Connecticut, De Kalb, New York and Fort Wallace, New Mexico. It is mined in Arkansas, Connecticut, Virginia, North Carolina, Georgia, Tennessee, Kentucky, Nevada and Missouri [**3**]. Barite is a hydrothermal deposit which originated from hot aqueous solution in joint fault, permeable rock formation and fractures within the middle Benue trough of Nigeria, notably in Benue, Taraba, Adamawa, Gombe, Plateau, Nassarawa, Ebonyi and Cross-river states [**4, 5**].Barite occurrence in part of Benue and Nassarawa state, Nigeria; was first discovered by R. B. Tale. The initial reconnaissance work covering Azara/WuseAkiri district across the River Wuse in Azara local government area of Nassarawa state which lead to the discovery of 18 veins of barite out of which Azara revealed and indicated reserve of about 730,000 million tonnes of barite within average specific gravity of 4.2 [**6**].Azara falls within the cretaceous sedimentary series in the middle Benue basin and it is a district in Awe Local government council of Nassarawa state which is about 97.6km south of Lafia and 150km from Lafia to Jos. Azara is accessible from Lafia by road whereby 60km of the road is tarred from Lafia and the remaining 37km is untarred. The deposit is located at a distance from Lafia interior, it is found in former Awe local government in Plateau state which is now Azara local government area in Nassarawa state, Nigeria [**7**].

FIG. 1

FIG. 2

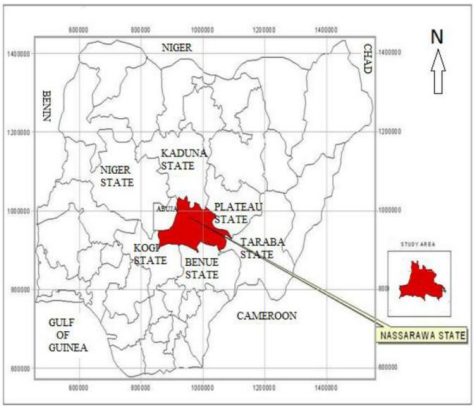

FIG. 3

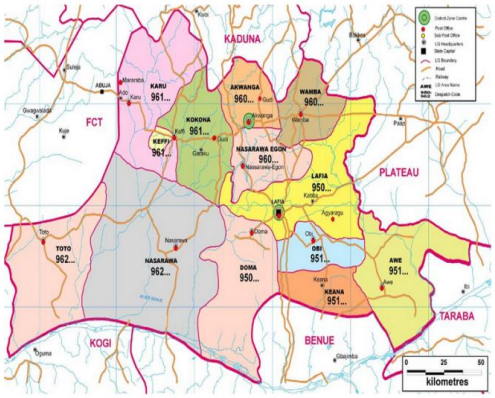

FIG. 4

FIG. 1/2 and **FIG. 3/4: The Geographical Map of Nigeria and Nassarawa state respectively [8]**

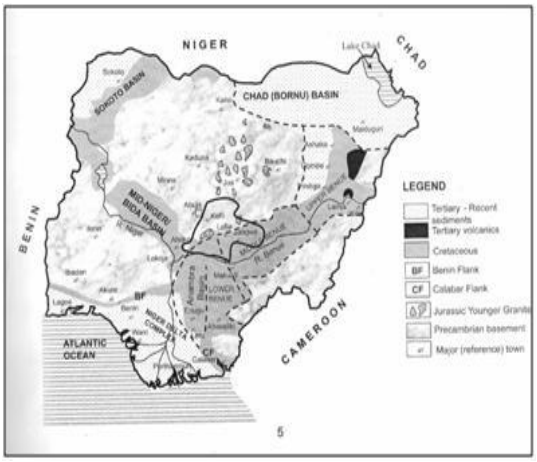

FIG. 5: The Geological Map of Nigeria showing the Study Area (Azara, Nassarawa state) [9]

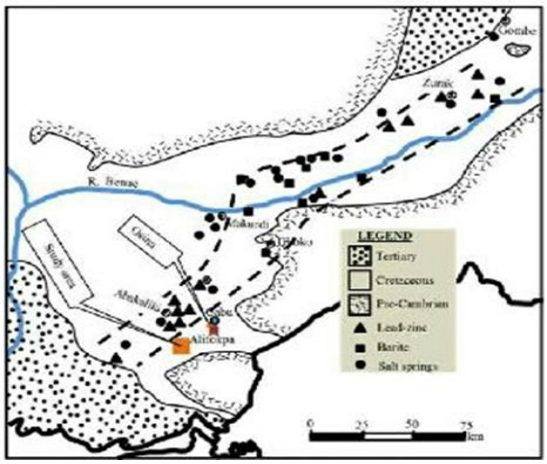

FIG. 6: The Map of the Benue Trough showing Barite Deposits [8]

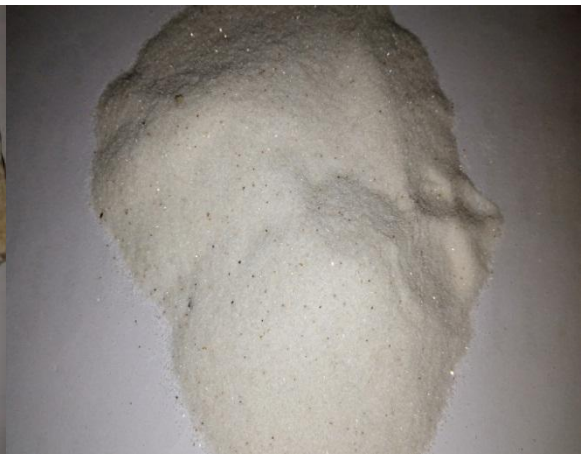

FIG. 7:As-mined Azara-Nassarawa Barite oreFIG. 8:Pulverized Azara-Nassarawa Barite mineral

In crude oil producing countries like Nigeria, barite is basically usedas weighting agents for drilling fluids/muds by the petroleum oil and gas industrial exploration to suppress high formation pressures and prevent blowouts. An additional benefit of barite is that it is non-magnetic and thus does not interfere with magnetic measurements taken in the borehole, either during logging-while-drilling or in separate drill hole logging [**10**]. However, other uses of barite are in added-value applications which include filler in paint and plastics, sound reduction in engine compartments, coat of automobile finishes for smoothness and corrosion resistance, friction products for automobiles and trucks, radiation-shielding cement, glass ceramics and medical applications.Barite is also used by chemical industries to produce barium chemicals (such as chloride, nitrate, carbonate and hydrate compounds); notably barium carbonate which is used for the manufacture of LED glass for television and computer screens (historically in cathode ray tubes); and for dielectrics. Historically, barite is used for the production of barium hydroxide for sugar refining, as white pigments for textile, paper, plastic, paintand glass production and by the metallurgical industries for brass melting. Although barite contains a "heavy" metal (barium), it is not a toxic chemical because of its extreme insolubility [**10**].

According to Nzeh and Hassan [**11**], the demand for barite by the manufacturing/oil and gas industries is practically more than the demand for water by human beings because of its numerous applications but the supply is very low because only a very few individuals are aware of this business opportunity. The most significant barite application is its usage by the oil and gas companies when drilling for crude oil or petroleum. Barite is also used for both its physical attributes, such as its potential relatively high specific gravity and/or chemical inertness (drilling mud additive, construction and functional filler), and for its chemical properties (sourceof BaO and chemical feedstock).The principle worldwide application of barite is estimated as 88% for additive to drilling fluids and 6% for chemicals[**11-12**].

Despite intense extraction of barite ore in Azara, Nassarawa state, Nigeria over the years; production has remained low. The need for the most efficient method of processing the barite mineral, to boost the local supply due to its enormous applications is the reason for theresearch study since there is steady and increasing demand for the product because of the numerous industrial applications of the mineral. The quality of the Nigerian barites is moderate to high. It is often

associated with fluorite, calcite, dolomite, quartz, etc. The major impurities are quartz, iron oxide (goethite), and carbonates of iron, calcium and magnesium. These impurities tend to increase the ore volume, suppress and reduce the specific gravity of the unprocessed barites to about 2.0–4.0. The cost of processing is increased and the oil mills wear out rapidly. The goethite and silica impurities can be removed by magnetic and gravity separation. Once processed the specific gravity of the Nigerian barite increases and meets the 4.2–4.5 specified standard value [**13**].

2. EXPERIMENTAL PROCEDURE

Mineral processing also called ore dressing or mineral dressing prepares for the extraction of valuable metals [**14**]. It commenced by liberating the desired mineral (barite) by comminution which entails crushing and grinding to suit the desired particle size. The products were mixtures of relatively clean particles of minerals and gauges, which were then followed by the gravity separation beneficiation/concentration process.Gravity separation is the beneficiation of two or more minerals of different specific gravity by their relative movement in response to the force of gravity and one or more other forces (such as centrifugal forces, magnetic forces, buoyant forces), one of which is resistance to motion (drag force) by a viscous medium such as heavy media, water or, less commonly, air.There are four (4) methods of gravity concentration: Panning, Sluicing, Jigging and Tabling [**14-15**]. The gravity separation beneficiation/concentrationof the sample of barite collected from Azara in Awe Local Government Area of Nassarawa state, Nigeria; was carried out using two (2) different processes: Jigging and Tabling processes with Jigs and Shake tables respectively.

2.1 Sample Collection and Preparation:

The bariteore sample was randomly procured from the above location, clean with distilled water to remove dirt and placed to dry. This was mixed and reduced using a sledge hammer. The mixture was further crushed with Schutte Buffalo Hammer Mill and ground using a ShambhaviImpex Ball Mill; (both are equipment of Kaduna Polytechnic, Tudun Wada in Kaduna state, Nigeria).

2.2 Sample Characterisation:

To establish the microstructural, chemical composition and physical properties of Azara barite ore before and after the mineral separation processes; specific gravity test, XRD, XRF, SEM and EDS investigations were carried out accordingly.In the course of sample preparation for XRF test, the samples were pulverized to fine homogenous size and then pelletized, packed and labelled. The prepared sample was weighed each with a sensitive weighing beam balance into a sample cup. The cup and the content were carefully placed in their respective measuring position on the sample changer of the machine. The machine was calibrated after which samples were measured by clicking the respective position of the sample changer and the voltage used was 45kv X-ray tube. The XRF analysis was carried out with a SKYRAY INSTRUMENT: EDX3600B X-ray fluorescence spectrometer; a facility of the Nigerian Geological Survey Agency, Kaduna state.

The XRD test of the barite sample was carried out at the Engineering Materials Development Institute, Akure, in Ondo State, Nigeria. The barite sample was prepared by pulverising to fine homogenous size and loaded to the XRD sample holder. The XRD analysis was carried out with a GBC Enhance material analyser which employs the X-ray Diffraction technology to conduct material analysisand characterisation (a facility of EMDI, Akure, in Ondo state, Nigeria).The SEM/EDS analysis of the barite sample after surface preparation was carried out with a PhenomProx Scanning Electron

Microscope (SEM) and Energy Dispersive Spectrometer (EDS); at the Mechanical Engineering Department, Covenant University, Ota, in Ogun state, Nigeria.

2.3Gravity Separation:

The gravity separation of the sample of Azara barite was carried out using Jigging with a Reliance Jig machine and subsequently Tabling with a Denver Shake Table; both are facilities of the Mineral and Petroleum Resources Engineering Department, Kaduna Polytechnic, Tudun Wada, in Kaduna state, Nigeria. The samples were sieved to a particle size of -355+250µm and two (2) test samples with different weights were measured out: sample A weighing 500g and sample B weighing 600g. Both samples were subjected to two (2) different Gravity separation processes in order to separate barite from the impurities: sample A was subjected to Jigging while sample B subjected to Tabling. After the separation processes, sample A had Underflows (Concentrates) and Overflows (Tailings) while sample B yielded Concentrates, Middlings and Tailings. All the samples were simultaneously placed in a Gen Lab Drying Oven to dry and Specific gravity (after gravity separation) was got for all the samples: concentrates,middlings and tailings; which were compared with the required standard. The microstructure and elemental/chemical composition analysis were carried out on the concentrate samples to check for the composition of the barite and any possible impurity that may still be present in the concentrates after the gravity separation processes using Scanning Electron Microscope (SEM) and Energy Dispersive X-ray Spectrometry (EDS) tests.

2.3.1 Jigging:

The sample was poured into a container to form the slurry feed. The jigging machine (jig) was rinsed of dirt to avoid contamination. The spigot hutch compartment was placed properly with the rubber cork and filled with water to cover the raging in the feed compartment. The sample (slurry) was fed into the jig and the jigging operation commenced while the operation was going on, overflow materials in the feeding compartment was washed out as overflow and at the end of the operation, the spigot of the compartment was opened and the product was collected as underflow. The underflow and overflow products were dried in an oven and were then weighed and recorded. According to Lymma (1992) [**16**], the aim of the jigging operation is to dilute the bed of material being treated and to control the diluted so that the heavier, smaller particles penetrate the interstices of the bed and the larger high specific gravity particles fall under a condition probably similar to hindered settling.

2.3.2 Tabling:

The shake table was rinsed of dirt to avoid contamination. The sample (slurry) was fed onto the shake table forming a fluidized bed and the tabling operation commenced while the operation was going on, the lighter particles were separated from the denser particles as a result of the shaking / vibrations of the table. The lighter particles went into a chamber as the tailings while the denser particles went into the middlings and concentrates chambers respectively. The concentrates, middlings and tailings were dried in an oven and were then weighed and recorded. In order to establish the most efficient method for the recovery of Azara barite ore, the result of the concentration processes were examined for (percentage) recovery using the following relationships:

$$\mathrm{R} = \frac{C}{F} \times 100 \quad and \quad R = \frac{T}{F} \times 100$$

Where: R = Percentage Recovery;C = Weight of Concentrates

T = Weight of Tailings;F = Weight of Feed

2.4 Chemical and Specific Gravity Analysis:

The different products obtained from the Jigging and Tabling gravity separation

methodswere taken for chemical analysis and their specific gravities obtained. The amount of barite in the sample of the underflows of the particle size from jigging operation and that in the concentrates of the same particle size from tabling operation were analysed by determining the percentage of Barium, Sulphur and other elements in the samples. The Specific gravity was got with the mathematically relationship:

$$S.G = \frac{W1}{W2 - W3}$$

Where: S.G = Specific Gravity

W1 = Weight of Barite Sample in Air

W2 = Weight of Water

W3 = Weight of Water Displaced by Barite Sample

3. RESULTS AND DISCUSSION

The XRF elemental composition of the as-mined Azara barite ore with a specific gravity of 3.85 shows that the ore contains 36.2% Barium, 34.4% Sulphur, 14.7% Titanium, 5.5% Vanadium, 1.8% Aluminium, and 1.5% Silicon, amidst others. This shows that the specific gravity value obtained confirms that the barite ore in Azara-Nassarawa, Nigeria has a specific gravity between 3.0 to 4.0 and has low percentage contents of barium and sulphur elements in the presence of other elements (impurities).After the separation processes, jigging had Underflows (Concentrates) and Overflows (Tailings) while tabling yielded Concentrates, Middlings and Tailings. All the samples were simultaneously dried in an oven with a temperature of about 120°C and an average time of 2 hours. Specific gravity (after gravity separation) was got for all the samples: concentrates,middlings and tailings; which were compared with the required standard. The microstructure and elemental/chemical composition analysis was carried out on the concentrate samples to check for the composition of the barite and any possible impurity that may still be present in the concentrates after the gravity separation processes using Scanning Electron Microscope (SEM) and Energy Dispersive X-ray Spectrometry (EDS) tests. Finally, the results of the samples were analysed as their final specific gravity were compared.

The XRD pattern in **FIG. 9** confirms the Barite ($BaSO_4$) phase pattern which is similar to that of a typical Nigerian barite mineral ore from Bukkuyum Local Government Area, Zamfara state [**17**], and therefore indicates that the Azara-Nassarawa barite mineral can be used industrially, especially in the oil and gas sections.

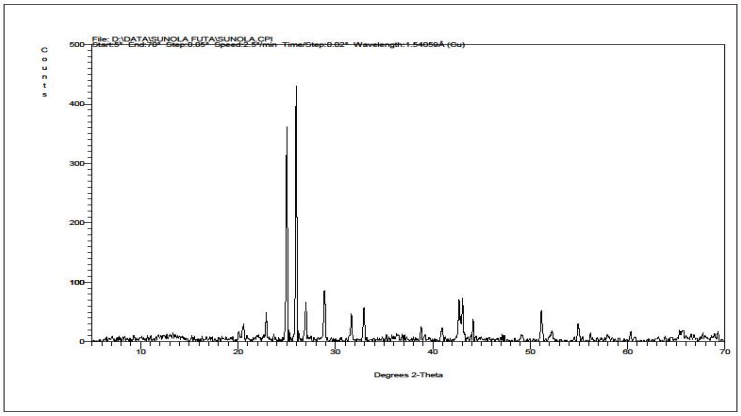

FIG. 9: Xray Diffraction (XRD) Phase Pattern of Azara-NassarawaBarite

Similar to the report by Mgbemere, et al [**18**]; the scan electron photomicrograph reveals the morphology/fracture surface of barite crude that is representative of a (typical) barite ore deposit in Azara LGA of Nassarawa State, Nigeria (as in **FIG. 10**).

FIG. 11 represents the Energy Dispersive Spectroscopy (EDS) peak intensities of elemental composition of the as-mined,

showing the different peaks with barium element (metal) at the highest peak which gave the distribution of elements and their compositions, thus: 50.5% Barium, 12.6% Sulphur, 22.7% Oxygen, 5.0% Gold, 2.4% Molybdenum, 2.3% Lead, 1.6% Tungsten, 0.7% Sodium, 0.6% Zinc, 0.4% Niobium, 0.3% Copper and Silicon respectively, 0.2% Alminium, Potassium and Rubidium respectively, amidst others; which confirms the XRF results of the as-mined Azara barite. Also, this corresponds with the report by Mgbemere, et al [**18**].

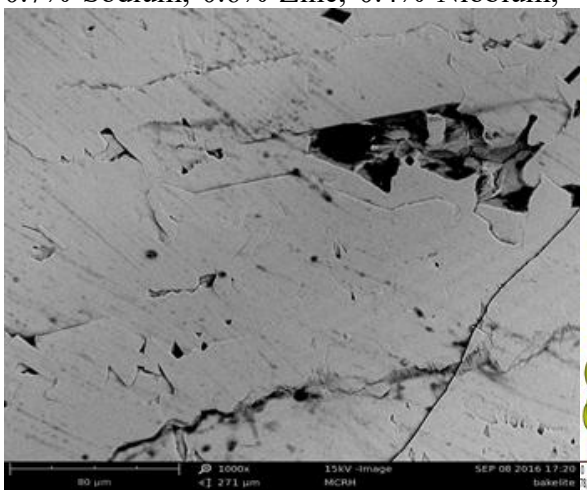

FIG. 10

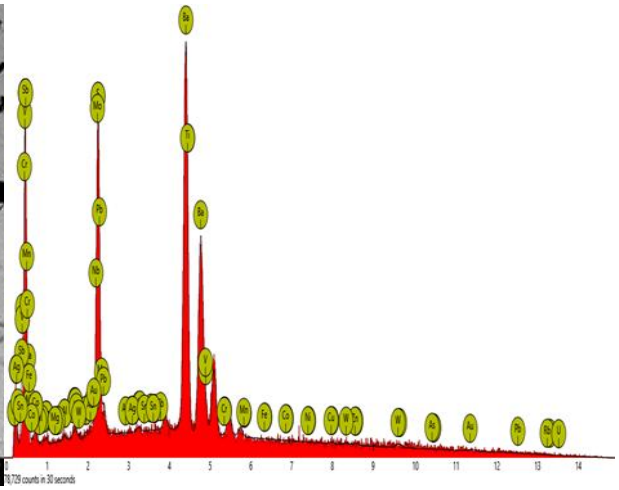

FIG. 11

FIG. 10 and FIG. 11:SEM Microstructure and EDS Analysis ofAzara-Nassarawa Barite,respectively

TABLE 1shows the result of gravity separation recovery using jigging operation. -350+250µm particle size of the feed material was used for the jigging operation. 76% of the feed was recovered as underflow (concentrates) and 8.4% of the feed was recovered as overflow (tailings) with 15.6% loss during the jigging operation process

.

TABLE 1: Result of Concentration of Azara-Nassarawa barite using Jigging method

SIEVE SIZE	FEED	UNDER FLOW	OVER FLOW	LOSS	UNDER FLOW	OVER FLOW	LOSS
-350 + 250µm	500g	380g	42g	78g	76%	8.4%	15.6 %

TABLE 2shows the result of gravity separation recovery using tabling operation. -350+250µm particle size of the feed material was used for the tabling method. 52.3% of the feed was recovered as concentrates, 40.3% as middlings, and 0.3 as tailings with 7.0% loss during the tabling operation process.

TABLE 2: Result of Concentration of Azara-Nassarawa barite using Tabling method

FEED	CONC.	MIDDLING	TAILING	LOSS	CONC.	MIDDLING	TAILING	LOSS
600g	314g	242g	2g	42g	52.30 %	40.30%	0.30%	7.00 %

FIG. 12 and **FIG. 13** represent the scan electron photomicrograph of the concentrates after jigging and tabling respectively. This shows a clearer SEM microstructure than that of the as-mined ore and also similar to the microstructure

of a typical standard Azara-Nassarawa barite mineral ore. Similarly, in **TABLE 3**, the Energy Dispersive Spectroscopy (EDS) elemental compositions of both jigging underflows and tabling concentrates were compared to that of the as-mined azara barite ore. This result confirms a higher percentage content of barium with 69.8% and 69.5% for jigging and tabling concentrates respectively, compared to the initial 50.5% barium by SEM and 36.2% by XRF of the as-mined barite ore and therefore indicates that both gravity separation methods can be successfully used to eliminate the impurities found in azara barite mineral, which confirmsprevious research work/literature [**11, 18, 19**].

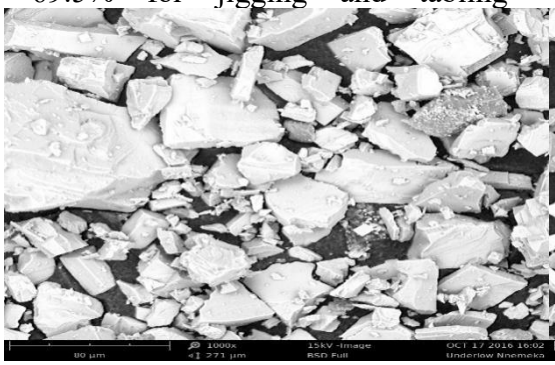

FIG. 12

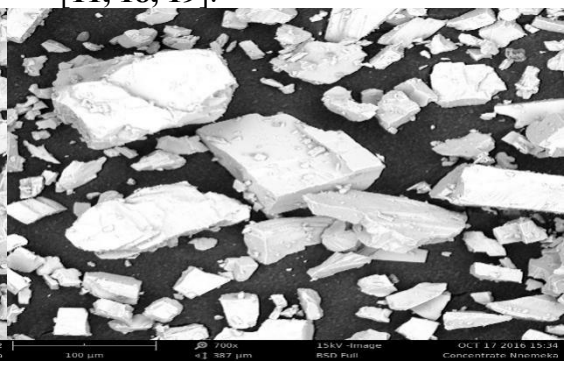

FIG. 13

FIG. 12 and 13: SEM Microstructure of the Underflows after Jigging andTabling, respectively

TABLE 3: EDS Elemental Composition of the As-mined, Jigging Underflows and Tabling Concentrates

Element %	Ba	S	Ti	Nb	V	W	P	Si	Fe	Al	Cu	Sn	Rb	Mo	Na	Zn	Pb	K
Atomic No., Z	56	16	22	41	23	74	15	14	26	13	29	50	37	42	11	30	82	19
As-mine XRF	36.2	34.4	14.7	-	5.5	0.1	0.4	1.5	0.2	1.8	-	0.3	-	0.1	-	0.1	-	0.1
As-mine EDS	50.5	12.6	-	0.4	-	1.6	-	0.3	-	0.2	0.3	-	0.2	2.4	0.7	0.6	2.3	0.2
Jigging EDS	69.8	7.4	-	0.2	-	0.3	-	0.2	-	0.1	0.2	-	0.1	0.2	0.4	0.3	1.1	0.1
Tabling EDS	69.5	8.0	-	0.2	-	0.0	-	0.3	-	0.1	0.2	-	0.0	0.0	0.6	0.3	0.0	0.2

TABLE 4and **FIG. 14**shows the comparison of the specific gravity (S.G) results of the as-mined barite ore of 3.85 specific gravity and the concentrates from jigging and tabling gravity separation methods. Jigging gave an underflow with specific gravity of 4.28 while the concentrates from tabling gave a specific gravity of 4.18. This shows that jigging and tabling underflows/concentrates obviously have better specific gravities than as-mined.

TABLE 4: Specific Gravity of the Industrial Standard and the Azara-Nassarawa Baritesamples

SAMPLES	SPECIFIC GRAVITY
STANDARD	*4.20 – 4.50*
AV. STANDARD	*4.35*
A	3.85
B	**4.28**
C	2.30
D	**4.18**
E	3.88
F	Negligible

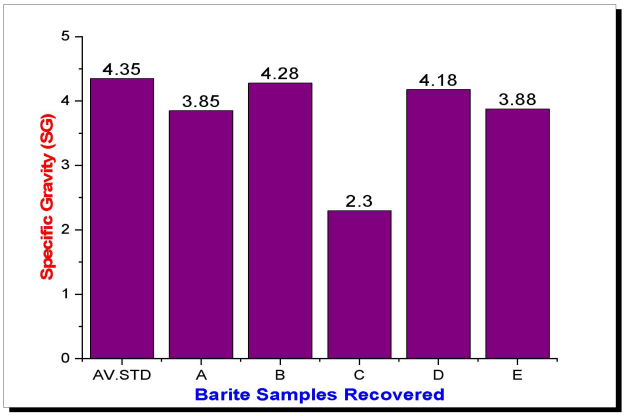

FIG. 14: Graphical Representation of the Specific Gravities results of the Azara- Nassarawa Barite samples in comparison with the (Oil and Gas) Industrial Standard

Where: Sample A = As-minedAzara-Nassarawa Barite
Sample B = Underflows after Jigging process
Sample C = Overflows after Jigging process
Sample D = Concentrates after Tabling process
Sample E = Middlings after Tabling process
Sample F = Tailings after Tabling process

4. CONCLUSIONS

Azara barite contains about 36.2% to 50.5% barium metal, 12.6% to 34.4% sulphur and about 22.7% oxygen. The jigging and tabling methods of gravity separation (Samples B and D) were used to improve the specific gravity of Azara barite as-mined ore (Sample A) as compared to the standard of 4.20 to 4.50 specific gravity required by the oil and gas industries. Jigging method of gravity separation on Azara barite ore is more efficient and effective giving a specific gravity of 4.28 than tabling, with a specific gravity of 4.18 especially at a sieve size of -355+250µm. Therefore,the specific gravity of Azara barite ore found in Nassarawa State, Nigeria has been upgraded to a range of 4.18 to 4.28 from the 3.85 specific gravity of the as-mined ore. The results of this research work have established that the Azara barite ore found in Nassarawa state, Nigeria is suitable for oil and gas applications. This confirmsthe conclusion by Nwoko and Onyemaobi, (1996) [**20**] in their research study.

ACKNOWLEDGEMENTS

The authors would like to thank the following institutions and personalities for their support towards the success of this paper:

1. Chemical, Metallurgical and Materials Engineering Department, Faculty of Engineering and the Built Environment, Tshwane University of Technology, Pretoria, Republic of South Africa.

2. Metallurgical and Materials Engineering Department, University of Lagos, Akoka, Lagos state, Nigeria.
3. Mineral and Petroleum Resources Department, Kaduna Polytechnic, Tudun Wada, Kaduna state, Nigeria.
4. Mechanical Engineering Department, Covenant University, Ota, Ogun state, Nigeria.
6. Engineering Materials Development Institute (EMDI), Akure, Ondo state, Nigeria.

Special appreciation goes to Mrs Cecilia N. Nzeh, Dr Swithin N. Nzeh, Mrs Chiamaka A. Nzeh, Esther S. Stan-Nzeh, Mrs Constance A. Nwahiri, Arch Goziemnna C. Akah and Mr. Godson N. Nzenwata; who were of tremendous assistance in the course of this research work.

REFERENCES

[1] P.W. Thrush, A dictionary of mining, mineral, and related terms: U.S. Bureau of mines, ed.1968, p. 1049.
[2] T. Edward, (http://geology.com/minerals/barite.shtml, 2022).
[3] S. J. Lefond, Industrial minerals and rocks, 4th edition, Baltimore Maryland, port city press, USA, 1975,426
[4] T. Agboola,Nigeria loses N6.2billion annually to imported barite, The Nation Newspaper, 2009.
[5] Ministry of Mines and Steel Development (MMSD), Barites Exploration Opportunities in Nigeria, Abuja, Nigeria, 2010.
[6] A. D. Bida,Mitigating the environmental effect of Artisinal Mining, Case study of Azara barite deposits in Nassarawa state, 2011.
[7] B. O. Adetoroye, Preliminary returns on Barite occurrence in Nassarawa state, 1998, pp. 2-5.
[8] M. I. Oden, Barite veins in the Benue Trough: Field characteristics, quality issue and some tectonic implications, Environmental and natural resources research, Dept of Geology, University of Calabar, Cross River state, Nigeria. Vol. 2, No. 2, 2012, pp. 21-31.
[9] I. Y. Tanko, M. Adam and B. Shettima, Petrology and Geochemistry of Barite MineralisationAroundAzara, North Central, Nigeria. IJSTRV, Vol. 4, 05, 2015, pp. 44-49.
[10] M. M. Miller, Barite Minerals Yearbook, Uses of Barite from Wikipedia, 2009.
[11] N. S. Nzeh and S. B. Hassan,Gravity Separation and Leaching Beneficiation Study of AzaraNassarawa Barite Mineral Ore, Global Journal of Researches in Engineering: J. General Engineering, Vol. 17, Issue 5, Version 1.0, 2017, pp. 40-46.
[12] I. Hauwa, Chemical oxides analysis from Azara Barite, African Journal of pure and applied chemistry, Zaira, Nigeria, Vol. 1 (2), 2007, pp. 15-17.
[13] F. M. Ayim and E. Enoch, Petroleum Technology Development Journal ISSN 1595-9104,An International Journal; Vol. 2-3, 2009, pp. 2-5.
[14] B. A. Wills, Mineral Processing Technology, 7th Elsevier Ltd, New York, United States of America, 2006.
[15] M. Mill, TheWilfley Table, Copper Country Explorer, 2010.
[16] G. J. Lyman, Review of jigging principle control, coal preparation, 11 (3-4), 1992, p. 145.
[17] G. S. Abubakar, B. A. Yagana and M. Zarah, Environmental and health hazards associated with exploration of barite from Bukkuyum (Zamfara State), Nigeria. ISABB – Journal of Health and Environmental Sciences, Kaduna, Nigeria, Vol. 2(3). 2015, pp. 11-15.
[18] H. E. Mgbemere,S. B. Hassan&J. A. Sunmola, Beneficiation of Barite Ore from Azara in Nassarawa State, Nigeria, using

Froth Flotation, Nigerian Journal of Technological Development, Vol. 16(1), 2019, 43-48.

[19] H. E.Mgbemere, E. O. Obidiegwu and E. Obareki, Beneficiation of Azara Barite Ore using a Combination of Jigging, Froth Flotation and Leaching, NIJOTECH, Vol. 37, No. 4, 2018, pp. 957-962.

[20] V. O. Nwokoand O. O. Onyemaobi,Benefication study on a Nigerian baryte ore for industrial use. Journal of Material Science Technology, Volume 13, 1997, pp 76-78.

NMS-TP023

THE HARDNESS AND TRIBOLOGICAL BEHAVIOUR OF SPARK PLASMA SINTERED W-Cu And Mo-Cu COMPOSITES

N.I. Amalu[1], B.A. Okorie[2,3], C.S. Obayi[3], and C. Ocheri[3]
1. Projects Development Institute, Enugu
2. Department of Metallurgical and Materials Engineering, Enugu State University of Science and Technology, Enugu, Nigeria
3. Department of Metallurgical and Materials Engineering, University of Nigeria, Nsukka, Nigeria.
Email: ninablaise5050@gmail.com

ABSTRACT

The hardness and tribological properties of Spark – Plasma Sintered W-Cu and Mo-Cu composites with weight percent copper in the range 20-40%, have been investigated. The results show that the hardness levels of the SPS – processed composites are substantially superior to those of composites produced by the conventional processes of infiltration and liquid phase sintering. The high hardness levels are attributed to the relatively low-temperature, short-time characteristic of the SPS process. The SPS – produced composites also have excellent wear resistance. Wear volume losses of only 32.6,29.3 and 24.0mm^3 were, for example, obtained after a 4500–meter-sliding distance (with load of 10N) wear test on W-20Cu, W- 30Cu and W-40Cu specimens respectively. Wear surface topographies showed excellent sliding properties, and dynamic friction coefficients of approximately 0.21 were found between the composite specimens and the steel ring used for the wear tests.

Key Words: *Hardness, Wear, Friction, Topography, Asperity*

1.0 INTRODUCTION

Composites of refractory metals such as tungsten and molybdenum with metals like copper and silver are generally desirable for electrical contact applications, where superior and robust mechanical properties and resistance to electrical arc erosion and welding are required. Such composite materials are not produced by regular solidification processing techniques because of the high melting points of tungsten(3410^{0}C) and molybdenum (2610^{0}C), but by powder metallurgy (PM) processing techniques. The general commercial PM techniques used are liquid phase sintering (LPS), and contact Infiltration processes, and other specialized variant processes associated with them. More recently, since its advent in the late 1970s [1, 2, 3], the relatively new technique of Spark Plasma Sintering (SPS) has been attracting a lot of attention among scientists, engineers, and industrial manufacturers.

The Spark Plasma Sintering (SPS) process, also called the Pulsed Electric Current Sintering (PECS) process, is a field-assisted sintering technique. Contrary to the conventional processing techniques where the starting powders are pre-pressed prior to sintering, in the SPS process, the starting powders are simultaneously pressed and sintered under the application of temperature and pressure. The powder blend is placed in a graphite die which is then placed in the furnace, where two pistons operating as electrodes apply pressure from the top and bottom surfaces. Simultaneously, a pulsed DC power supply connected to the upper and lower punches (electrodes) sends current

pulses at relatively low voltages through the powder mass. Micro-plasma electrical discharges form uniformly between powder particles throughout the sample volume causing localized and momentary heating of the particle surfaces up to several thousands ^{0}C. The overall heating rate can then be as high as 1000^{0}C/ minute. The combination of compressive pressure and high heating rate yields dense compacts, often with nano-sizedgrains, under a relatively lower sintering temperature (generally about 200^{0}C to 250^{0}C lower than the temperatures used in conventional sintering). Currently SPS is applied extensively in the dielectric, piezoelectric and thermoelectric fields, among other areas [4, 5, 6, 7, 8]. The SPS technique has also been found very useful for the processing of transparent ceramics [9, 10, 11, 12].

The interest in SPS processed materials is due mainly to the virtually full densification (relative densities often in the range of 98.5-100%) achieved by the process, and its ability to produce compacts with grain size in the nanometer range Interest in the present work is on the properties of pore-free W-Cu and Mo-Cu compacts produced by the SPS technique. This paper focuses attention on the hardness and tribological properties of these materials.

2.0 MATERIALS AND METHODS

2.1 Materials and Equipment

The materials used for this work include powder specimens of tungsten, molybdenum, copper and cobalt obtained from manufacturers in the United Kingdom and the United States of America, and paraffin wax and stearic acid procured from Conraws Nigeria, Ltd, Enugu, Nigeria.

The equipment used include a pneumatic single action press, steel dies, graphite dies, a digital microbalance, a turbular mixer for powder specimens, controlled atmosphere furnace, a spark plasma sintering (SPS) machine, a Vickers hardness testing machine, a tribometer, a scanning electron microscope/energy dispersive spectrometer (SEM/EDS), and an X-ray diffractometer (XRD).

2.2 Methods

2.2.1 Production of Sintered Compacts of Composites

Powder blends of composition W-20% Cu, W-30% Cu, W-40% Cu, and Mo-20% Cu, Mo-30% Cu, and Mo-40% Cu were prepared and each blend was thoroughly tumbled for ten (10) hours in a tubular mixer. To evaluate the behavior of a W-Cu composite obtained by cobalt-activated sintering, a W-0.50% Co – 30% Cu blend was also prepared and similarly tumbled in the turbular mixer for 10 hours. Graphite dies of diameter 15mm were put in place and each powder mixture was placed in the dies between matching graphite punches, and then placed in the spark plasma sintering (SPS) machine. The selected SPS parameters were Heating Rate = 100^{0}C/min.; Sintering Temperature = 1000^{0}C; Dwell time = 10 minutes; pressure = 40MPa; Cooling rate after the dwell period = 100^{0}C/minute.

For purposes of comparative analysis of hardness properties, W-Cu and Mo-Cu specimens of identical composition were also produced using the conventional techniques of Liquid Phase Sintering (LPS) and infiltration. For this, the rigid metal dies were used for compaction (with a compaction pressure of 300MPa), and the controlled atmosphere (nitrogen atmosphere) furnace was used for sintering at 1200^{0}C. Infiltration was also done at 1200^{0}C.

2.2.2 Characterization of Specimens

The digital microbalance, with an accuracy of 0.001gm/cm^3, was used to obtain the weight of the specimens, and the volumes were obtained by use of Archimedes principle and also by taking physical dimensions of

each specimen. From the results, the relative densities of the specimens were obtained.

The specimens were further characterized by SEM/EDS, XRD, hardness tests, wear tests, and SEM images of wear surface topography.

2.2.2.1 Hardness Test

The hardness test was carried out using a Vickers hardness tester (Matsizuwa Seiki Vickers hardness tester) at a constant load of 100gm and dwelling time of 15 seconds. Five measurements were obtained from each specimen and the average value was recorded. The tester calculates the hardness value using the formula:

$$HV = 1.854 \, P/d^2 \qquad (1)$$

where HV = Vickers Hardness, P = Load, and d = diagonal of the indentation(cm).

2.2.2.2 Wear Tests

The tribological properties of the specimens were investigated using a CETR UMT-2 tribometer (serial No. 1000031520; Tribometer/version 7.3.13). During the test, a ball of radius 3mm and a load of 10N were used to maintain contact between the mating surfaces throughout the test duration.

The number of cycles was 968 per sample and test duration was 2702 seconds (approx. 45 minutes), for each sample. The linear speed was 6.28cm/sec, and the sliding distance was 4500 metres (4.5km). The wear volume V was then calculated by the following equation [13]:

$$V = B.\left[\frac{\pi R^2}{180}.\arcsin\left(\frac{b}{2R}\right) - \frac{b}{2}\sqrt{R^2 - \frac{b^2}{4}}\right] \qquad (2)$$

where V = wear volume loss (mm^3)

B = width of the block sample (mm)

R = radius of the steel ring (mm), and

b = width of the worn track on the block specimen (mm).

The specific wear rate K (mm^3/N.m) was calculated using the equation:

$$k = \frac{V}{d.L} \qquad (3)$$

where d = sliding distance (m)

L = load (N)

During the test, the coefficient of friction, μ, was continuously recorded by the equipment.

3.0 RESULTS AND DISCUSSION

3.1 Structural Features

Figure 1 ((a) and (b)) below presents scanning electron micrographs of W-30wt.%Cu and Mo-30wt.%Cu sintered compacts respectively, produced by Spark Plasma sintering.

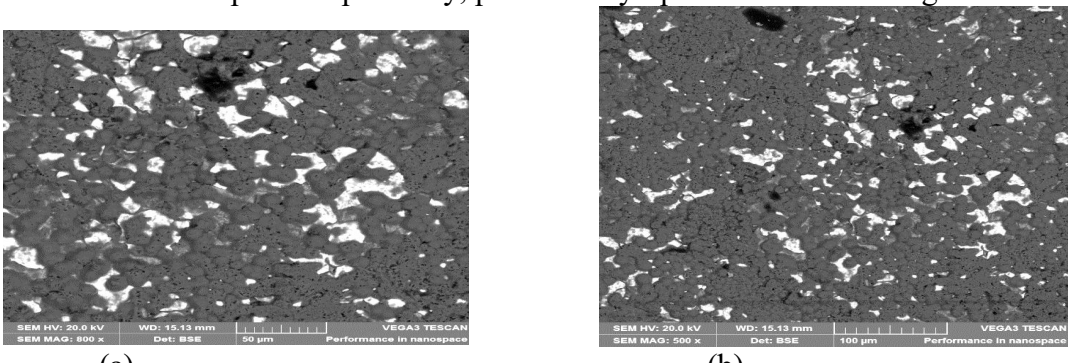

(a) (b)

Fig.1: Scanning Electron Micrographs of (a) W-30wt.%Cu, and (b) Mo-30wt.%Cu specimens produced by Spark Plasma Sintering.

The Micrographs show a very even distribution of the copper powder particles in the matrices of tungsten and molybdenum. The micrographs of the other specimens have identical appearance. The even distribution is a result of the prolonged tumbling and the fact that only thin surface films of the powder particles get molten during the SPS process. With the application of pressure during the process, strong particle bonding is obtained by a combination of plastic deformation and atomic diffusion, leading to a very high level of densification.

The Scanning Electron Micrographs (SEMs) and Energy Dispersive Spectra (EDS) reveal the presence of oxygen, carbon, and a number of trace elements such as Zn, La, Fe, Si, Al, Ca and K. The oxygen (from the residual gas in the vacuum environment) and carbon (probably picked up from the graphite die and punches), are in the form of small quantities of oxides and carbides of tungsten and molybderum, and oxides of copper developed during the sintering process. The SEM image and EDS analysis of W-20wt.%Cu compact developed by SPS are presented in Figure 2.

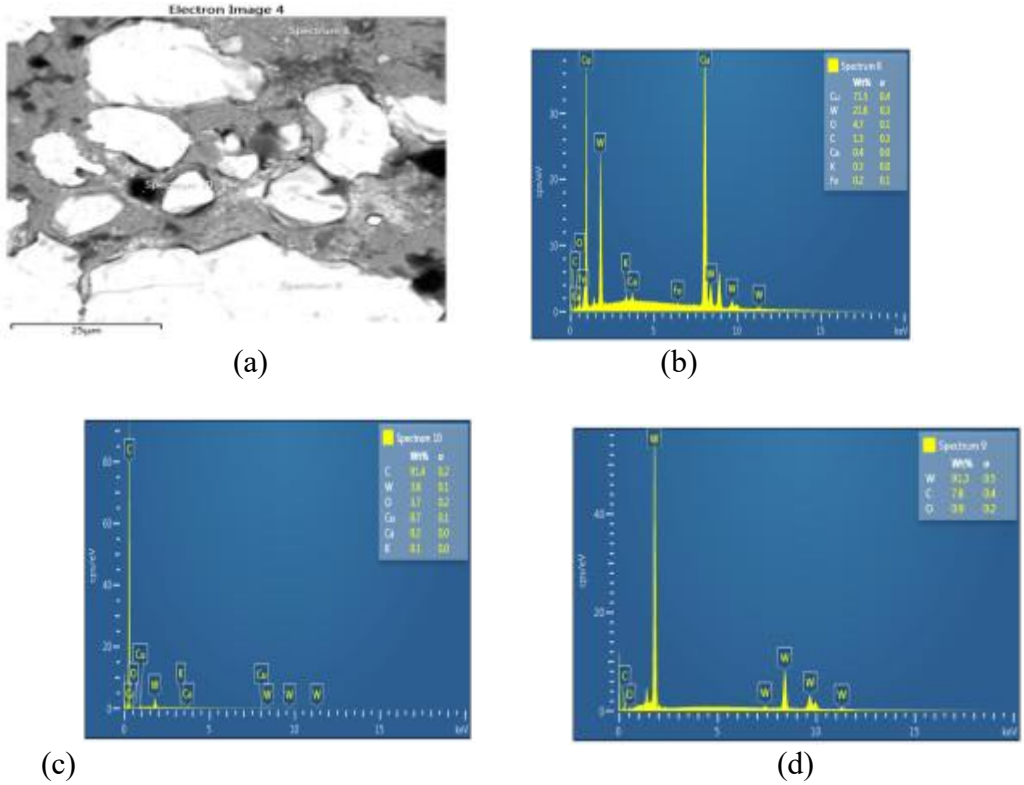

Fig 2 SEM image (a), and EDS analysis (b), (c), and (d) of W-20wt.%Cu spark plasma sintered specimen.

The X-ray diffraction (XRD) patterns of the W-Cu specimens generally reveal the presence of tungsten, copper and small amounts of compounds such as cuprospinel $(CuFe_2O_4)$, cuprite (Cu_2O) and tungsten carbide (WC). The diffractograms of the Mo-Cu composites showed the presence of Mo, Cu, cuprite (Cu_2O), molybdenum iron oxide, and tugarinovite (Mo_4O_8). Figure 3 presents the X-ray diffraction pattern of W-20%Cu specimen and Table 1 presents the identified pattern list from the XRD analysis.

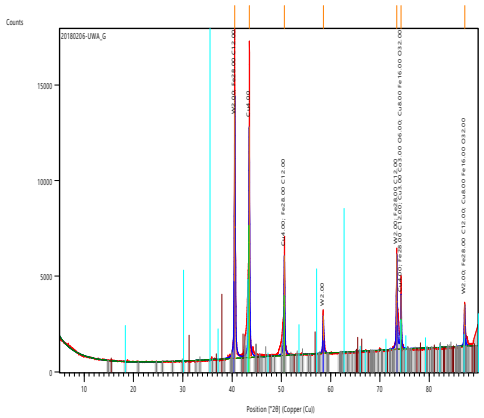

Fig. 3: X-ray Diffraction (XRD) pattern of W-20%Cu composite specime

Table 1: Identified Pattern list from the XRD Analysis of W-20Cu specimen.

Peak position $(2\theta)^0$	Peak Height (cts)	d-spacing (A^0)	Relative Intensity (%)	Compound Name	Compound Formula
40.557	13747.68	2.223	100	Tungsten	W_2
43.481	12074.05	2.0796	87.83	Copper	Cu_4
50.606	5225.26	1.8023	38.01	Iron Carbide	$Fe_{28}C_{12}$
74.285	2832.10	1.2758	20.60	Cobalt(III)Copper(I)Oxide	$Cu_3Co_3O_6$
87.217	2178.71	1.1168	15.85	Cuprospinel	$Cu_8Fe_{16}O_{32}$

3.2 Hardness Test Results

The hardness test results are presented in Figure 4 for the W-Cu and Mo-Cu specimens produced by Spark Plasma Sintering, Infiltration, and Liquid Phase Sintering.

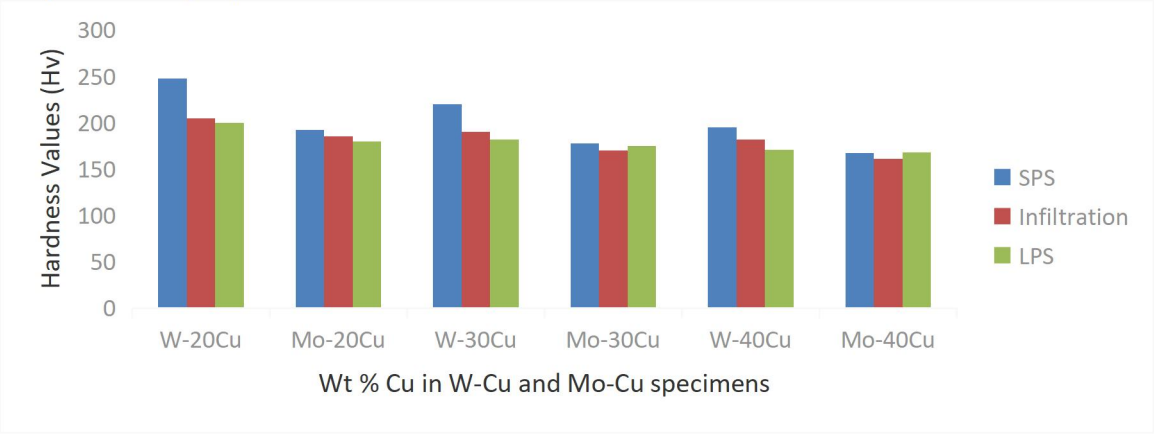

Fig 4: Hardness of W-Cu and Mo-Cu specimens, (HV), produced by SPS, infiltration, and LPS.

The Figure shows that the hardness values of the W-Cu specimens produced by the SPS technique were in the range of 248HV,

220HV and 195HV for the W-20Cu, W-30Cu, and W-40Cu specimens respectively. For the Mo-Cu specimens, the hardness values were 192HV, 178HV and 167HV for the Mo-20Cu, Mo-30Cu and Mo-40Cu specimens respectively. From the figure, it is clear that these values are substantially higher than the values obtained for corresponding specimens obtained by the conventional sintering techniques of infiltration and
liquid phase sintering. It is observed that the specimens obtained by the infiltration process are only marginally harder than those produced by LPS for the W-Cu compacts, while for the Mo-Cu compacts, the reverse is the case for the Mo-30Cu and Mo-40Cu compacts.
The superior hardness of the specimens produced by the SPS process may be attributed to enhanced inter-particle bonding achieved during the relatively low-temperature, short-time sintering process. These conditions are not favourable to microstructural phenomena such as grain growth which result in depreciation of mechanical properties. The specimens produced by LPS and infiltration at much higher temperatures and longer processing times are bound to lose some mechanical properties as a result of grain coarsening and microstructural inhomogeneity. The high levels of hardness obtained in this work are in agreement with reports in the literature on SPS – processed W-30Cu specimens [14, 15].

.

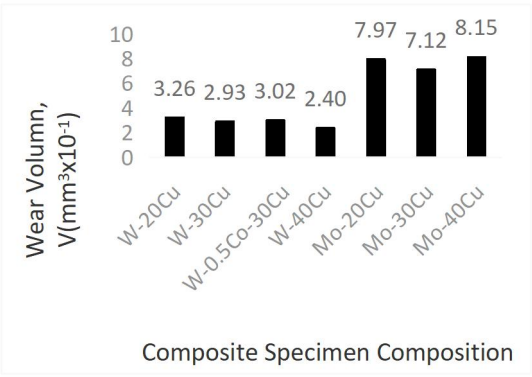

Fig. 5: Wear volume loss by specimens of various compositions after 4500m. sliding distance.

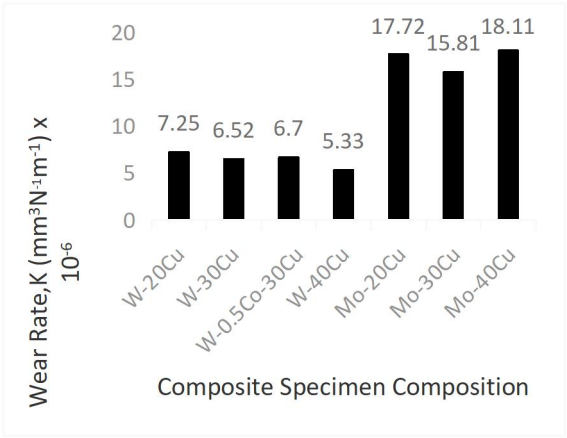

Fig. 6: Wear rate of the specimens of various compositions

3.3 Wear Test Results

The wear test results are presented in Figures 5 and 6 below. The wear volume and specific wear rate have been determined using equations (2) and (3), respectively, and are presented in the bar charts of Figures 5 and 6 respectively

The results show that the compositions of the composites significantly affect their wear behaviour.

The W-Cu composites are significantly more wear – resistant than the Mo-Cu composites of equivalent wt.% Cu content. It is noteworthy that, for the W-Cu composites, there is a trend towards a slightly increasing wear resistance (or decreasing wear volume loss and wear rate) with increase in copper content. Ordinarily, a decrease in wear resistance would have been expected from an increase in wt.%Cu in a W-Cu composite. The present result suggests that the copper provides quasi-lubrication effects and better sliding properties in W-Cu

composites. The results also suggest that use of small amounts of cobalt for activated sintering of W-Cu composites may lead to small decrements in wear resistance (see, for example, the wear volume losses of 29.3mm^3 and 30.2mm^3 presented in Figure 5 for W-30Cu and W-0.50 Co-30Cu composites, respectively).

Figures 7 and 8 respectively present the wear track geometry and wear surface topographies after the wear test for selected specimens. The surface topographies do not show any signs of digging or ploughing by particulate matter as would have happened if hard particles of W or Mo had been dug out of the surface. This is a further evidence to show that very strong inter-particle bonding was achieved during the production of the specimens by the SPS technique.

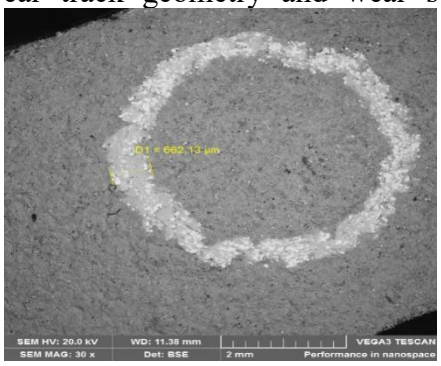

(a)

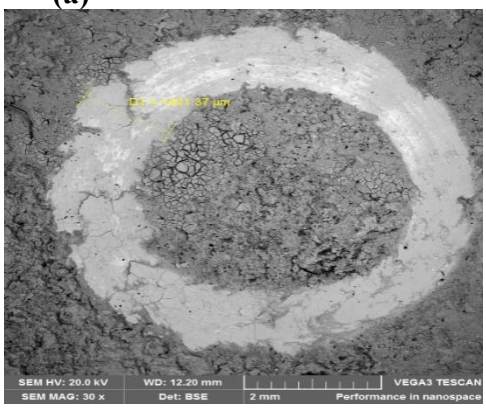

(c)

Fig. 7: Wear track profile after the wear test on (a) W=40wt.%Cu, and (b) Mo-40wt%Cu.

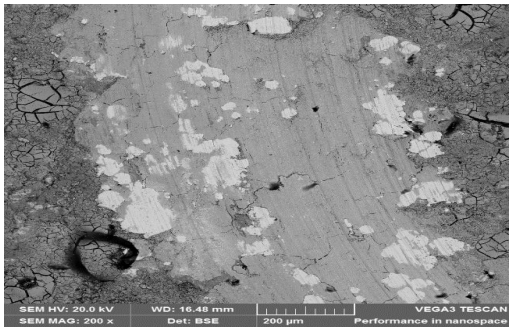

(b)

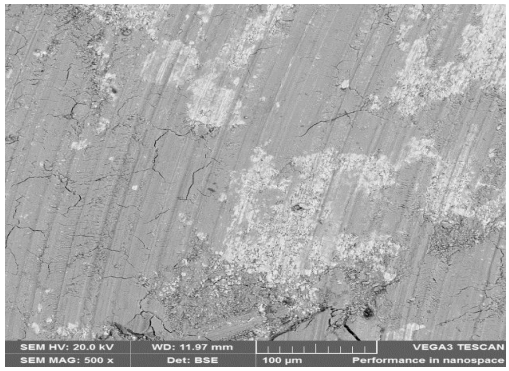

(d)

Fig. 8: Surface topographies of worn surfaces after the wear test on (a) W-20wt.%Cu, and (b) Mo-40wt.%Cu.

The surface topographies of Figure 8 show smooth flow lines which indicate good sliding properties and relatively low frictional forces between the contacting surfaces during the wear test.

The variation of coefficient of friction (dynamic friction), μ, during the wear tests, was recorded throughout the tests. Figure 9 shows the variation of $\mu$with time for selected specimens, while Figure 10 is a bar chart representation showing the variation of the coefficient of dynamic friction for the various specimens at 600 second intervals of time, from the start of the test up to 2400 seconds test time

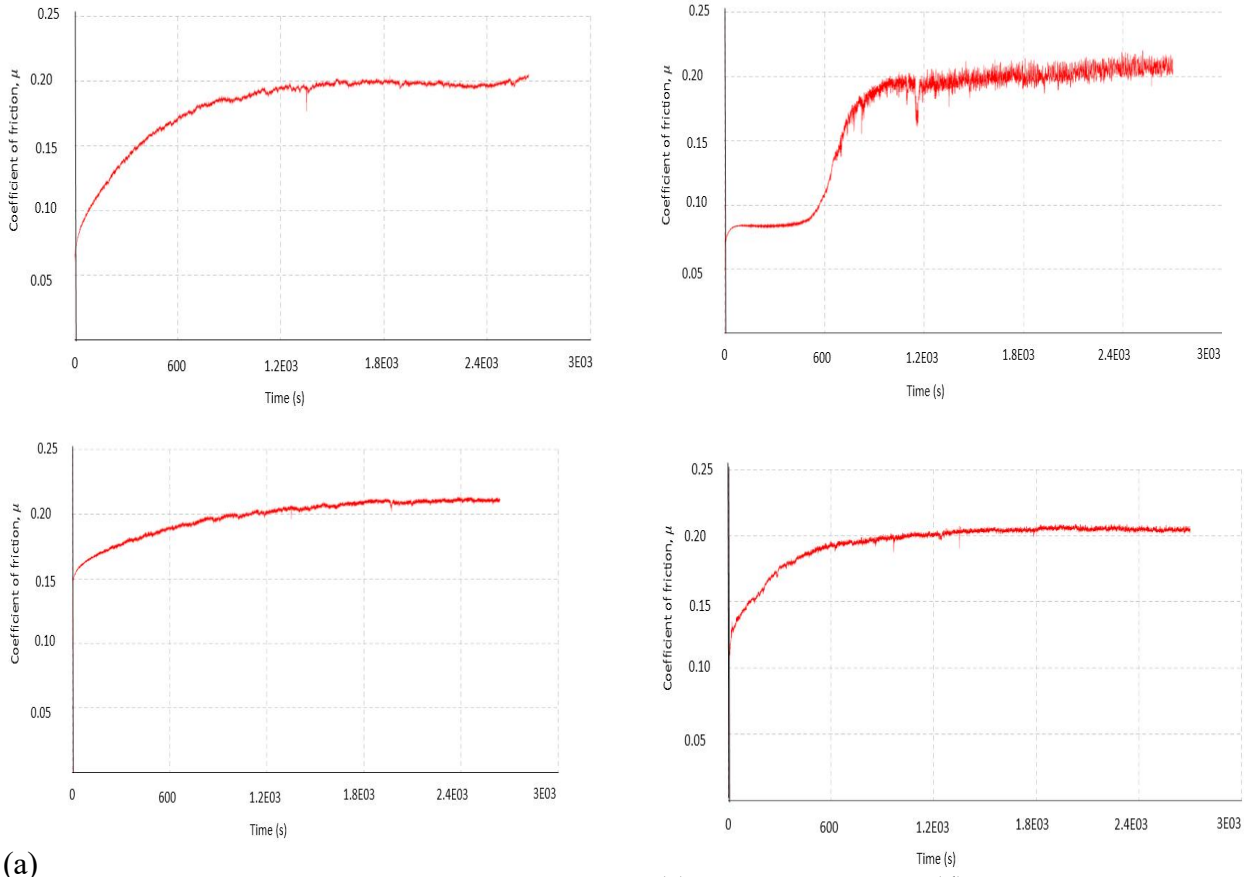

(a) (c) (d)
(b)

Fig. 9: Variation of Coefficient of friction, μ, against time during wear test on: (a) W-20Cu; (b) W-30Cu; (c) Mo-30Cu; (d) Mo-40Cu specimens

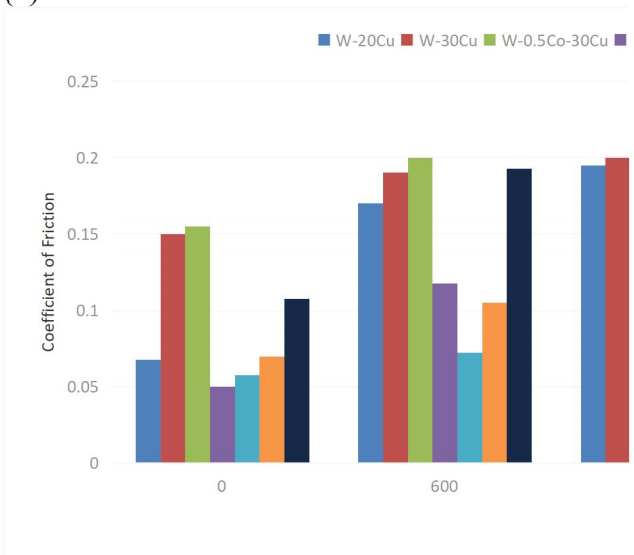

Fig. 10:Variation of coefficient of friction (μ,) against time during wear test on (a) W-20Cu; (b) W-30Cu (c) W-0.50Cu – 30Cu, (d) W-40Cu; (e) Mo-20Cu; (f) Mo-30Cu; (g) Mo-50Cu specimens.

It may be observed from the Figures that there was variation of coefficient of friction, exhibited by some of the specimens, from the start of the test up to 1200 seconds. After this time, the values of μ, stabilized at a level of approximately 0.21 for almost all the specimens. The most significant variations were exhibited by the specimens W-40Cu Mo-20Cu and Mo-30Cu which showed fairly low values of μ, (0.05 – 0.12) up to 1200

seconds. The coefficient of dynamic friction should ideally be a constant, being dependent only on the properties of the materials involved and the roughness and texture of the surfaces in contact. The initial variations in μ observed here may be attributed to minor non-uniformity of surface asperity at the start of the test, and to thermal stresses owing to temperature build-up.

4.0 CONCLUSIONS

The following conclusions may be drawn from the results of this work.

(i) Using the spark plasma sintering process, refractory-metal based composites such as W-Cu and Mo-Cu of superior hardness levels can be produced.

The high hardness of the SPS – processed composites may be attributed to the relatively low-temperature, short – duration character of the process which yields strong inter-particle bonding while disallowing the grain coarsening and microstructural inhomogeneities that occur with conventional processing techniques where higher temperatures and longer sintering times are required.

The SPS – processed composites have excellent tribological properties – with low wear volume losses, low wear rates, and good frictional characteristics.

(iv) The W-Cu composites are more wear-resistant than the Mo-Cu composites.

The wear resistance of the W-Cu composites increases with wt.% copper content within the 20-40 wt.% Cu range investigated.

REFERENCES

[1] Hulbert, D.M.; Anders, A.; Andersson, J.; Lavernia, E.J.; Mukherjee, A.K.(2009), "A discussion on the absence of plasma in Spark Plasma Sintering". Scr. Mater. 2009, 60, 835-838.

[2] Orru, R.; Licheri, R.; Locci, A.M.; Cimcotti, A.; Cao, G.(2009), "Consolidation/synthesis of materials by electric current activated/assisted sintering". Mater. Sci. Eng., R-Rpt. 2009, 63, 127-287.

[3] Hulbert, D.M.; Anders, A.; Dudina, D.V.; Andersson, J; Jiang, D.; Unuvar, C., Anselmi-Tamburuni, U.; Lavernia. E.J.; Mukherjec, A.K.(2008), "The absence of plasma in "Spark plasma sintering" J. Appl. Phys.2008, 104, 033305.

[4] Munir, Z.A.; Anselmi – Tamburini, U.; Ohyanagi, M.(2006), "The effect of electric field and pressure on the synthesis and consolidation of materials: A review of the Spark plasma sintering method". J. Mater Sci. 2006, 41, 763-777.

[5] Zhou, M.; Li, J.F.; Kita, T.(2008), "Nanostructured $AgPb_mSbTe_{m+2}$ system bulk materials with enhanced thermoelectric performance", J. Am. Chem. Soc. 2008, 130, 4527-4532.

[6] Biswas, K; He, J.; Blum, I.D.; Wu, C.I.; Hogan, T.P; Seidman, D.N.; Dravid, V.P.; Kanatzidis, M.G.(2012), "High – performance bulk thermoelectric with all-scale hierarchical architectures," Nature 2012, 489, 414 – 418.

[7] Zhang, B. P.; Li, J.F.; Wang, K.; Zhang. H.(2006), "Compositional dependence of piezoelectric properties in $Na_xK_{1-x}NbO_3$ Lead –free ceramics prepared by Spark Plasma Sintering", J. Amer. Ceram. Soc., 2006, 89. 1605-1609.

[8] Yanagiya, S.; Van Nong, N.; Xu, J.; Pryds, N.(2010), "The effect of (Ag, Ni, Zn) – addition on the thermoelectric properties of copper aluminate", Materials 2010, 3,318-328.

[9] Wang, S.F.; Zhang, J.; Luo, D.W.; Gu, F.; Tang, D.Y.; Dong, Z.I.; Tan, G.E.B.; Que, W.X; Zhang, T.S.; Li, S, et. al.(2013), "Transparent Ceramics: Processing, Materials, and Applications," Prog. Solid State Chem. 2013, 41, 20-54.

[10] Kim, B.N.; Hiraga, K; Morita, K.; Yoshida, H.(2007), "Spark Plasma sintering of transparent alumina", Scr. Mater. 2007, 57, 607-610.

[11] Deng, X; Wang, X.; Wen, H.; Kang. A.; Gui, Z.; Li, L.(2006), "Phase transitions in nanocrystalline barium titanate ceramics prepared by spark plasma sintering", J. Amer. Ceram. Soc. 2006, 89, 1059-1064

[12] Alaniz, J.E.; Perez-Gutierrez, F.G.; Aguilar, G.; Garay, J.E.(2009); "Optical properties of transparent nanocrystalline yttria – stabilized zirconia", Opt. Mater, 2009, 32, 62-68.

[13] Hung Liu, Yuqi Li, Tingmai Wang, and Qihua Wang,(2012), "In – situ Synthesis and Thermal, Tribological properties of Thermosetting Polyimide/Graphene Oxide Nanocomposites", J. Materials Science (2012), 47: 1867 – 1874: DOI 10.1007/s10853 – 011 – 5975-9.

[14] Eagle Alloys Corp. (2000) "Copper Tungsten Alloys "http://www.eaglealloys.com/t-tungs_alloys copper.aspx. Accessed 24 January, 2020.

[15] Ceta Tech. Inc. (2020) "Tungsten – copper Alloy" http://www.cetatach .com/english/sub_03 /index.php?a_page=3& b_page = 3. Accessed 24 January2020

NMS-TP024

PLASTIC DEFORMATION OF 0.857%FE COMMERCIAL ALUMINIUM ALLOY 8011

*YakubuO.H., Sam Obu V. S., Woli T. O. and Makun B. A.
Department of Mechanical Engineering, Federal Polytechnic, Offa, Nigeria
Email Addresses:
*yhassan27@yahoo.com,samobu.chijioke78@gmail.com,taiyewoli@gmail.comandmakun.tade@gmail.com
*Corresponding author:yhassan27@yahoo.com

ABSTRACT

The effect of plastic deformation on commercial aluminium alloy (AA8011) has been investigated. As-received commercial aluminium alloy 8011 of 0.857%Fe cast by continuous twin roll casting was cut into seven samples of each of dimension 240mm x 140mm x 7mm. The alloy was cold rolled in thickness at various degrees of deformation (30% to 80%), followed by testing of mechanical properties and qualitative metallographic analysis. From the results obtained, it was observed that aluminium alloy 8011 generally exhibited softening characteristics as shown by its maximum ultimate tensile strength of 176.45MPa at 60% reduction in thickness and decrease in hardness value for given levels of percent reduction in thicknessafter reaching the peak hardness values. The ductility decrease at the initial deformation of 30% cold reduction in thickness but shows a little increasement at 40% deformation and subsequently decrease for further plastic deformations.

Keywords: aluminium, deformation, microstructure, strength, ductility, hardness

1.0 INTRODUCTION

Aluminium alloy 8xxx series have found wider application in construction industries and automobile as a result of their good physical and chemical properties such as formability, corrosion, light weight and also because it is possible to control the micro structural composition of the alloy by means of specific thermal and mechanical treatments (Xing, Kang and Kim, 2001).

The iron composition of 8011 aluminium alloy ranges from 0.6-1% has greatly influenced the mechanical properties of the alloy. During metalworking, the optimum level of the iron that will not impact any negative effect to the ductility of the alloy is highly required in order to avoid some defects such as cracking due to the low level of material ductility. The processing capabilities of the aluminium alloy and/or the strength of the final wrought product are greatly influenced by the level of iron content (John, 2009). In aluminium alloy, a large number of iron-containing intermetallic phases have been identified in the microstructures, depending on the solidification conditions and alloy composition. Although iron is highly soluble in liquid aluminium and its alloys, it has very little solubility in the α-Al solid (0.05wt %), and so it tends to combine with other elements to form intermetallic phase particles of various types (John, 2009).

Investigation on the effect of cold rolling on bending and tensile behaviour of 7075 aluminium alloy by Tajally, Huda and Masjuki(2009) observed that after 58% cold working, there was a rapid increase in yield strength of 119.25% due to high density of dislocations. In addition, increases in the tensile strength and hardness value with decrease in percentage elongation of the rolled material were observed. The effect of hot cumulative roll bonding process on the mechanical properties of AA 5058 by Hassan and Ebrahim, 2011 revealed that the strength of the sheet increased considerably by the first two ARB cycles which is attributed to work hardening caused by an increase in dislocation density and sub-grains. The aim of this present study is to investigate the effect of plastic deformation on the mechanical property of the AA 8011 in order to ascertain the optimum percentage deformation that will give the best mechanical property of the rolled products.

2.0 EXPERIMENTAL PROCEDURE

The as-received commercial aluminium alloy 8011 of 0.857%Fe (from Tower Aluminium Rolling Mills) was cut into seven pieces of dimension 240mm x 140mm x 7mm. The chemical compositions of the alloys are shown in Table 2.1.

Table 2.1: Chemical composition of as-received commercial aluminium alloy 8011.

Elements	Al	Fe	Si	Mn	Cu	Mg	Ti	Zn	Cr	Pb
Composition (%)	98.183	0.857	0.551	0.117	0.072	0.020	0.015	0.120	0.050	0.015

2.1 Cold Rolling Experiment

The rolling operation was carried out using four-high commercial rolling mill consisting of a pair of work rolls and backup rolls was used to carry out cold rolling experiment. The work roll and backup roll were 240mm and 520mm in diameters respectively. The upper rolls were vertically adjustable; such that the roll gap could be set to any desired gap. The two sides of the mill were designated; drive side (DS) and operator side (OP). Two motors on the drive side powered the rolls, which ran at a constant speed of 43rpm.

A total of 7 samples were used for the experiment. Each plate was fed directly between the work rolls, which imposed no forward or back tension loads on the plate. The sample were cold-rolled from 7mm-1.4mm i.e. 30%-80% reductions in thickness.

2.2 Tensile Strength Test

Tensile strength measurement was conducted on a Hounsfield Tensometer Machine. The tensile test samples with gauge dimension 100mm x 40mm x 10mm were machined from the as-received samples oriented along the rolling direction according to ASTM E8M standard.

2.3 Impact Strength Test

The impact test was done on Charpy Impact Testing Machine of capacity 25J. A V-notch was machined into a 10mm wide and 100mm long test specimen and the depth of the notch is 4mm.

3.4 Hardness Test

The hardness of the samples was carried out with Micro-vicker Hardness Tester of capacity 5kgf using a load of 0.3kgf to indent the samples for about 15 seconds.

2.5 Metallographic Examination

Two samples were prepared from the batches of samples (as-received and 80% cold-rolled reduction in thickness) for microstructural examination. The specimens were prepared for optical examination by cutting, successive grinding using silicon carbide grit paper of 240, 320, 400 and 600 microns following a standard guide for preparation of metallographic specimens.

Polishing was carried out on a rotating cloth to ensure mirror-like surface. A solution containing 5ml nitric acid, 2ml hydrofluoric acid and 100ml of distilled water was used to etch the specimens for about 10 seconds. The specimens were observed under Digital Metallurgical Microscope with an in-built camera; micrograph of each specimen was recorded at a magnification of 100X.

3.0 RESULTS AND DISCUSSIONS

3.1 Evaluated Mechanical Properties

The ultimate tensile strength, percentage elongation, hardness value and impact strength of as-received samples cold-rolled to various reductions in thickness are presented in Tables 3.1.

Table 3.1: Mechanical properties of aluminium alloy 8011

Reduction in thickness (%)	Ultimate tensile strength (MPa)	Elongation (%)	Microvicker hardness (HV)	Impact strength (J)
0	125.80	25.50	10.40	24.32
30	138.89	15.50	10.90	19.35
40	142.53	17.50	11.40	10.70
50	162.23	13.50	11.80	7.80
60	176.45	12.25	12.10	4.50
70	149.48	11.75	11.80	3.90
80	130.00	10.20	10.70	1.35

3.2 Effect of Plastic Deformation on Tensile Property of Cold-rolled AA8011

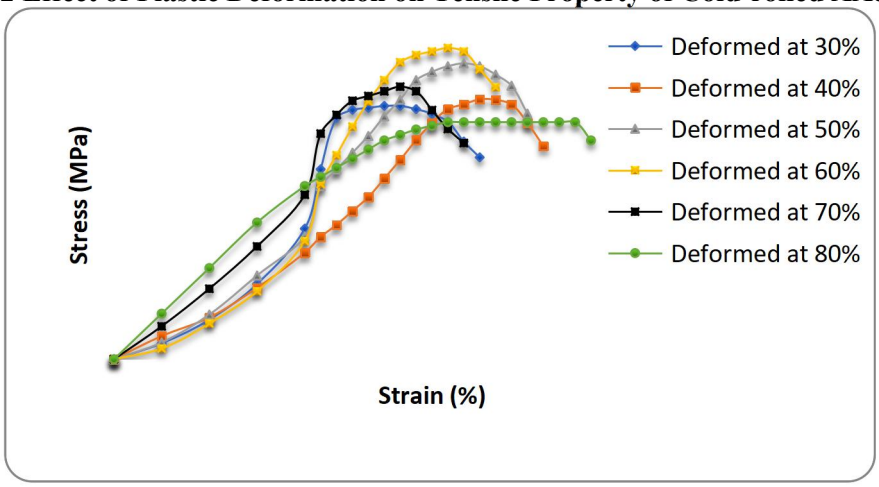

Figure 3.1: Stress-strain curves of AA 8011 with 0.857%Fe

It can be deduced from Figure 3.1 that sample deformed at 80% has the highest tensile property at the initial strain of about 13% and this was overtake by sample deformed at 70% and at highest strain of about 17% and above the material deformed at 60% take the lead.

3.3 Effect of Plastic Deformation on Ultimate Tensile Strength of Cold-rolled AA 8011

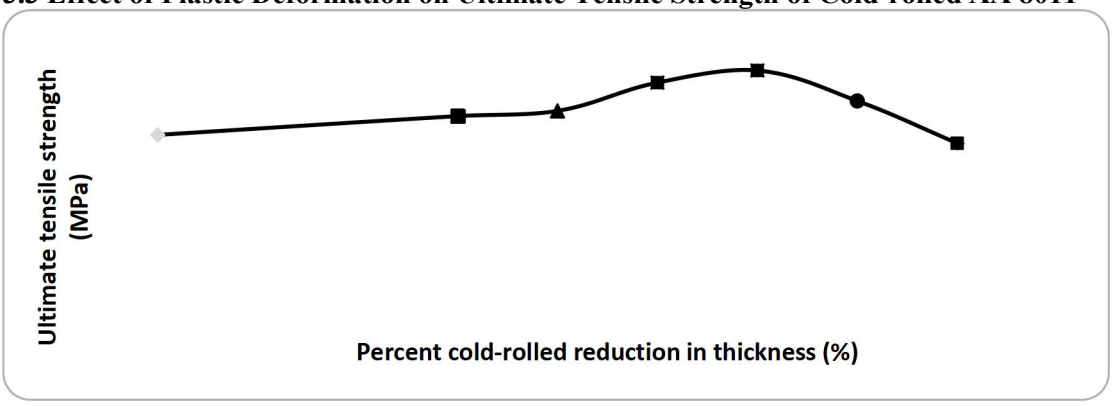

Figure 3.2: Graph of ultimate tensile strength against percent cold-rolled reduction in thickness

Plastic deformation of metals is one of the most important parameters in increasing the mechanical properties of the metals and its alloys. The rapid increase of the values of the ultimate tensile strength of as-received sample cold-rolled up to 60% reduction in thickness

could be attributed to the complicated array of defects such as high density of dislocations produced in the alloys during deformation. As previously claimed by Tajally*et al.* (2009), the level of dislocation density is often responsible for variation in mechanical properties such as ultimate tensile strength, ductility and hardness. Dislocations density increases with increasing cold deformation; new dislocations which are created by cold deformation interact with existing one in the material thereby promoting an increase in strength value (Zainul, 2009).

The negative effect of the intermetallic particles becomes less when the size of the intermetallic impurity becomes small (Haga, Sakaguchi, Watariand Kumai, 2008). During cold rolling of the alloys, dislocation density increases as the degree of deformation increases; the fragmentation of interdendritic particles also occur. Due to the interaction of dislocations with each other and with impurities, there is increase in work hardening rate, resulting in an increase in both the strength and hardness values. It is expected therefore that the ultimate tensile strength will increase with increasing percent reduction in thickness since the intermetallic particles have been broken down by rolling operation.

At 70% reduction in thickness, the ultimate tensile strengths of all the alloys decreased. This might be due to release of stress carried by the second phase particles. When crack occurs in these particles, it affects the overall load bearing capacity of the alloys and hence, it limits its work hardening behaviour since the flow stress increase in the matrix leads to a higher level of load transfer to the second phase intermetallic particles as have been previously reported by Salem, (2007).

3.4 Effect of Plastic Deformation on Ductility of Cold-rolled AA 8011

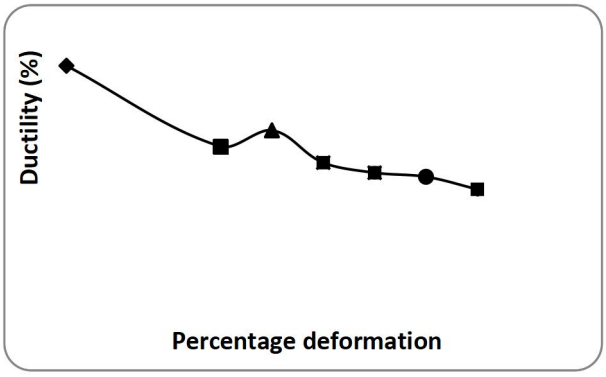

Figure 3.3: Graph of ductility against percent cold-rolled reductions in thickness

The quantitative ductility measure of as-received sample subjected to 30% reduction in thickness shows rapid decrease in ductility of 39.22% (Figure 3.3). The rapid decrease in ductility is as a result of large immobile dislocation created by the complicated network of interlocking dislocations leading to strength increment and large loss in ductility.

At 40% reduction in sample thickness, rapid increases in ductility was observed. The increase in ductility could be attributed to the microstructural changes occurring during deformation process. As reported by Valiev (2003), the main deformation mechanisms were dislocation movements and twining for coarse grains materials. In ultrafine grained materials, the grains with high grain boundaries impeded the motion of dislocations and hence improved the strength of the materials and at the same time, the ultrafine grains formed during deformation might facilitate an increase in grain boundary sliding and hence grain rotation which could improve ductility (Akshay and Ibrahim, 2008). The increase in ductility therefore should have been linked to grain boundaries sliding as observed in the research finding of Akshay and Ibrahim, (2008).

Above 40% reduction in sample thickness, the ductility levels of the samples decreased drastically with the increasing percent reduction in thickness. The general decrease in ductility might be due to dislocations generation which interacted and impeded each other and hindering their motion, thereby decreasing the ductility of the alloys.

3.5 Effect of Plastic Deformation on Hardness of Cold-rolled AA 8011

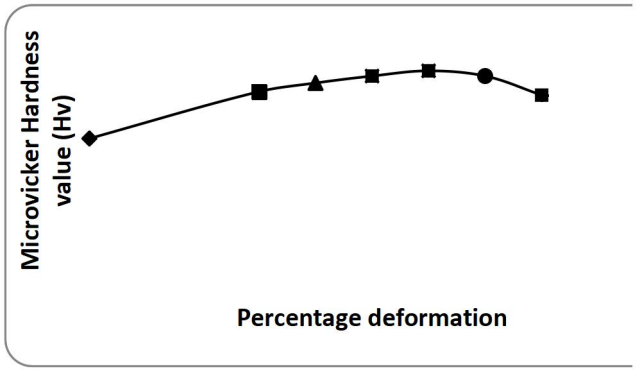

Figure 3.4: Graph of hardness values against cold-rolled reduction in thickness

The microvicker hardness values plotted against percent cold-rolled reduction in thickness (Figure 3.4) of as-received alloy sample increased steadily up to 60% reductions in thickness. This could be attributed to strain hardening tendency of the alloy samples under investigation caused by cold rolling operation.

The hardness values of the investigated alloy samples 60% reductions in thickness and after the attainment of these peak levels of hardness value, the samples displayed decrease in hardness with increasing percent reduction in thickness. This observation is in agreement with Chang and Shan (2003) who reported that dislocation density in the interiors of the grain decrease with increase in strain leading to a situation in most interiors to become eventually free of dislocation after a large deformation resulting to a reduced hardness value. Conclusively, the decrease in hardness of the alloys after large deformation is as a result of decrease in dislocation density in the interior of subgrains while the obtained lower hardness values with higher iron content can be linked to a high dislocation density originating from high iron intermetallic particles.

3.6 Effect of Plastic Deformation on Impact Strength of Cold-rolled AA 8011

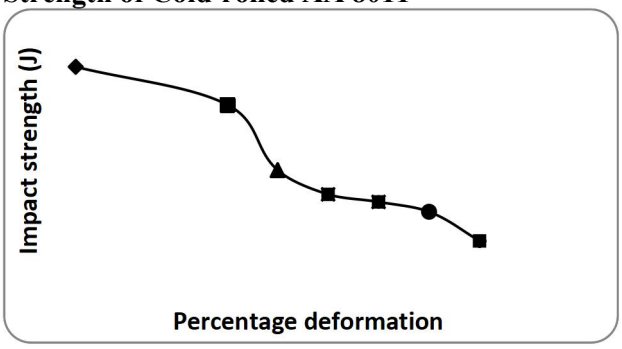

Figure 3.5: Graph of impact strength against cold-rolled percent reduction in thickness

The toughness values of the samples decreased progressively with increasing percent cold-rolled reduction in thickness (Figure 3.5). This trend could be due to thermomechanical process (rapid solidification and hot rolling in a single operation) which accompanied the twin-roll casting method employed in the casting of the test samples as previously observed by Sanguinetti, Riberio and Rocha, (2000). As highlighted, the specific thermal and mechanical treatments usually improve the mechanical properties of the alloy in general.

This could also be due to high concentration of iron-rich intermetallic phase particles, suggesting a higher potential for fracture by the mechanism of coalescence when subjected to impact load and this is in agreement with the work of Salem, (2007).

3.7 Effect of Plastic Deformation on Microstructures of Cold-rolled Samples of AA 8011

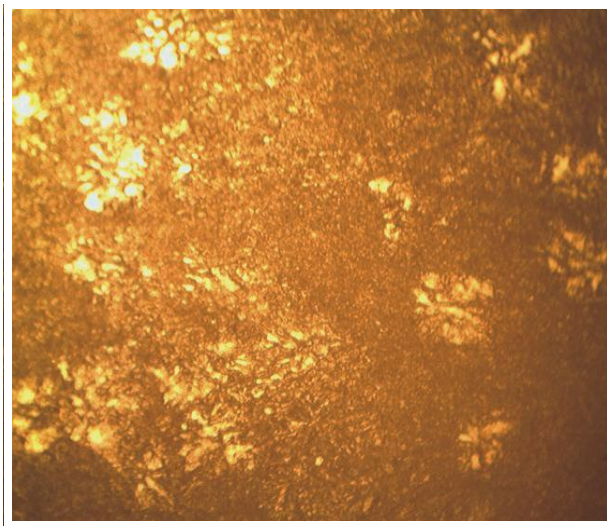

Plate 3.1

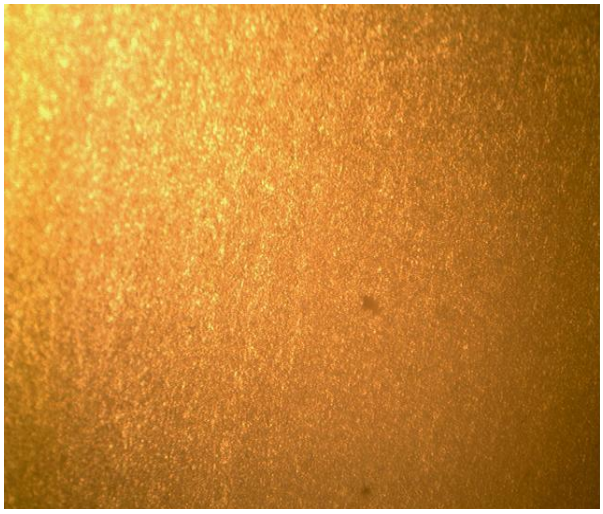

Plate 3.2

Plate 3.1: Optical micrographs of as-received AA 8011. White spots are interdendritic of intermetallic particles distributed in aluminium matrix (yellow back-ground). X100. Plate 3.2: Optical micrographs of samples AA 8011 cold-rolled to 80% reduction in thickness. White spots are fragmentation of interdendritic particles elongated along rolling direction in aluminium matrix (yellow back-ground). X100.

From the micrographs of as-received in Plates 3.1, the aluminium matrix contained volume fractions of intermetallic phases predominately $FeAl_3$ and AlFeSi crystals. These crystals are finely dispersed within the matrix phase. In agreement with the finding of Sanders, Hollinshead and Simielli,(2004), the grains of as-received alloy cast by twin-roll casting method are fine because of the segregation of alloying elements in the as-cast condition at approximately the center of the strip thickness due to the shearing action of the rolls on the formed dendrites.

The ensuring squeezing of the interdendritic liquid towards the center enriched its concentration, giving rise to a region that contained higher amount of AlFeSi intermetallic phases. This observed phenomenon is a justification of the good mechanical properties obtained in the as-received samples.

The micrographs of cold-rolled samples shown in Plate 3.2 revealed a segregation of $FeAl_3$ and AlFeSi intermetallic phases in aluminium matrix. With an increase in percent reduction in thickness up to 80%, the fragmented grains become denser being elongated in the rolling direction. The redistribution of impurities that occurred during the rolling process resulted in segregation reduction observed in the samples at 80% reduction in thickness.

CONCLUSION

Based on the experimental finding, aluminium alloy 8011 generally exhibits softening characteristics as it was displayed by its maximum ultimate tensile strength of 176.45MPa at 60% reduction in thickness. On reaching the peak hardness values, all samples displayed decreasing in hardness property for a given levels of percent reductions in thickness- a behaviour which is in general agreement with the work of Xing *et al.* (2001). Due to its softening behaviour when subjected to mechanical working operations, AA 8011 generally exhibits excellent ductility.

REFERENCES

Akshay G. P. and Ibrahim M. (2008). Mechanical properties of Zn-9%Al-3%Cu alloy after equal channel angular extrusion. *Proceedings of the XIth International Congress and Exposition,* Society for Experimental Mechanics Inc. Orlando, Florida USA, pp 1-7.

Chang J. Y. and Shan A. (2003). Microstructure and mechanical properties of AlMgSi alloys after equal channel angular pressing at room temperature. *Materials Science and Engineering Journal,* A327, 165-170.

Haga T., Sakaguchi H., Watari H. and Kumai S. (2008). High speed twin roll casting of 6061 alloy strip. *Archives of Materials Science and Engineering Journal,* 31, 49-52.

Hassan S. and Ebrahim P.: "Effect of hot cumulative roll bonding on the mechanical properties of AA 5058", Open Journal of Metal, 1, 2011, pp 12 – 15.

John A. T. (2009). The effect of iron in Al-Si casting alloy. *Cooperative Research Centre for Cast Metals Manufacturing (CAST),* the University of Queensland, Brisbane, Australia, pp 1-10.

Salem S. (2007). The influence of iron on the microstructure and mechanical properties of cast Al-Si alloys. Unpublished Ph.D Thesis, Jonkoping University, The School of Engineering Component Technology, Sweden.

Sanders R. E., Hollinshead P. A. and Simielli (2004). Industrial development of non-heat treatable aluminium alloy. *Materials Forum,* Institute of Materials Engineering, Austral/Asia, 28, pp 53-64.

Sanguinetti F., Riberio F. G. and Rocha L. (2000). Study of development in AA 8023; kinetics and morphological aspect. *Scripta Mater,* 43, pp 929-934.

Sansome D. H. (1975). Factors affecting the shape of strip emerging from a rolling mill. *Metal Technology,*pp 522-530.

Tajally M., Huda Z. and Masjuki H. H. (2009). Effect of cold rolling on bending and tensile behaviour of 7075 aluminum alloy. *Journal of Applied Sciences,* 9, 3888-3893.

Valiev R. Z. (2003). Recent developments of SPD processing for fabrication of bulk nanostructured materials. *Materials Science Forum,* 426-432, pp 237-244.

Xing Z. P., Kang S. B. and Kim H. W. (2001). Softening behavior of 8011 alloy produced by accumulative roll bonding process. *Scripta Material* 45, ActaMateria Inc. Published by Elsevier Science Ltd, pp 597-604.

Zainul H. (2009). Effect of degree of cold working and recrystallization on the microstructure and hardness of commercial purity aluminium. *European Journal of Scientific Research,* 26(4), 549-557.

NMS-TP025

EFFECT OF CALCINATION TEMPERATURE ON EVOLUTION OF HYDROXYAPATITE FROM CATTLE BONE WASTE FOR BIOMEDICAL APPLICATIONS

[1]Eze H.E.,[1]Okolo C.S., [1,2]Obayi C.S., [1,2]Nnamchi P.S., [1]Daniel-Mkpume C.C.
harrison.eze.200158@unn.edu.ng, chukwuemerie.okolo.200164@unn.edu.ng,
camillus.obayi@unn.edu.ng, paul.nnamchi@unn.edu.ng, cynthia.daniel@unn.edu.ng
1 Department of Metallurgical and Materials Engineering, University of Nigeria, Nsukka
2 Department of Biomedical Engineering, University of Nigeria, Nsukka
Corresponding Author: Dr. Camillus S. Obayi, camillus.obayi@unn.edu.ng

Abstract

Hydroxyapatite (HAP)is extensively used in supporting bone-healing processes in orthopedics and dentistry and other biomedical applications. There is increased interest in the synthesis of hydroxyapatite from natural bone wastes. This is because unlike synthetic HAP, natural HAP hasthe ability to mimic apatite of human bones and contains essential trace elements beneficial for bone growth and supporting biological functions. This work investigated the effect of calcination temperature on the evolution of hydroxyapatite from cattle bone (CB) waste for biomedical applications. CB wastewas obtained from an abattoir; washed; dried; pulverized and sieved to obtain CB powder of 75 µmthat was calcined at 600°C, 750°C and 900°C using constant holding time of 3 hrs. The functional groups present in uncalcined and calcined powders were identified using Fourier Transform Infra-Red Spectroscopy (FTIR).The colour changes that accompanied the calcination process indicated that hydroxyapatite was successfully extracted from the cattle bone waste at 750°C and 900°C. The FTIR result confirmed the presence of associated functional groups in the synthesized HAP consisting of phosphate ions ($PO4^{3-}$), hydroxyl ions (OH^{-}) and carbonate ions ($CO3^{2-}$) and proved the evolution of HAP from CB waste and hence, adding value to it.

Keywords: *calcination temperature, holding time, hydroxyapatite, cattle bone, biomedical applications*

1.0 Introduction

In recent years there has been increased interest in the synthesis of hydroxyapatite from natural bone wastes for biomedical applications.Hydroxyapatite (HAP) is a bio-ceramic and a type of calcium phosphatewidely studied because of its physico-chemical similarity with the mineral component of bone tissue [1-3]. HAPhas achemical formular of $Ca_{10}(PO_4)_6(OH)_2$ [4] and iteasily forms chemical bonds with hard tissues of the bone and teeth. Besides having similar composition to human bones, HAP has been found to be the most stable phase of Calcium phosphates (CAPs) and it exhibits excellent biocompatibility, bioactivity, and stability [5, 6, 7, 8]. As a result, it is used extensively in supporting bone-healing processesin orthopedics and dentistry [6, 7, 8]and other biomedical applications such asdrug delivery and coating of medical implants [9, 10]. HAP has a complex crystalline structure consisting of phosphate ions ($PO4^{3-}$), hydroxyl ions (OH^{-}) and calcium ions (Ca^{2+})[11]. The amounts of calcium, phosphate and hydroxyl ions in HAP are 39.84, 56.77 and 3.39 wt.%, respectively [4].

HAP has a standard Ca/P atomic ratio of 1.67; a stable phase and is highly crystalline [12].

Although, synthetic HAP has been studied earlier than now for bone implantation and dental reconstruction [1], but it has some shortcomings leading to the current interest in synthesizing HAP from natural sources. One of such draw backs of synthetic HAP is that it does not mimic apatite of human bones due to absence of essential trace elements found in the bones such as Sodium, Magnesium, Aluminium, Iron and minerals like carbonates that are beneficial for bone growth and supporting biological functions [1, 13, 14]. A good number of researchers has worked and are still working on synthesizing HAP from waste natural sources such as cattle (bovine) bones, goat (caprine), chicken (galline) bones, fish bones, pig (porcine) bones, eggshellsand seashells, using several methods.

One popular and cheap technique used in obtaining HAP from natural sources is calcination and sintering [15, 16, 17, 18, 19, 20]. Since calcination involves heating natural bone powders to high temperatures for certain time durations, calcination temperature and holding time are important parameters on evolution of HAP from natural bone powders and these variables affect the realization of medical grade HAP [20]. As a result, researchers working on synthesizing HAP from natural sources have been either varying the two parameters (temperature and holding time) at the same time or holding one parameter constant while varying the other.

Jojor et al [21] studied the effect of calcination temperature on hydroxyapatite synthesized from bovine bone by keeping the temperature constant at 850°Cwhile varying holding time from 2-10 hrs. and medical grade hydroxyapatite with Ca/P ratio of 1.679 was obtained at a holding time of 5 hrs.MOHD PU'AD et al [22], used different calcination temperatures of 700°C, 900°C and 1100C at a fixed holding time of 3 hrs. to extract HAP from bovine bone powders. The results indicated that bovine powders calcined at 700°C and 900°C showed the presence of HAP, but the best result was got at 900°C (Ca/P ratio = 1.70). However, increasing the temperature to 1100°C led to phase change (formation of beta-tricalcium phosphate) which influenced the ratio of Ca/P.Ramesh, et al [5] studied HAP evolution from cattle, goat and chicken (galline) bones through calcination at 600-1000°C at a fixed holding time of 2 hrs. and compared the characteristics of the evolved HAP.Odusote et al [23] synthesized and characterized hydroxyapatite from bovine bone by heating the powder to 650°C for 3 hrs. and 750°C for 6 hrs. The results showed that calcinating at 650°C for 3 hrs. produced semi-decomposed powder, while heating at 750°C for 6 hrs.produced hydroxyapatite from the raw bovine bone powder. W. Khoo et al [24] prepared and characterized natural hydroxyapatite from bovine femur bone powder calcined at700°C, 900°C, and 1100°C for 3 hrs. The results indicate that calcination temperature above 700°C can produce organic free and natural crystalline HAP.

It was observed by Kerim Emre Öksüz, et al [25] that purer form of HAP with higher degree of crystallinity, larger crystallite size, and a less porous structure was obtained at higher temperatures following calcination of cattle, goat and chicken bones at 600-1000°C for a fixed holding time of 2 hrs.Figueiredo et al [26] also observed progressive increase in crystallinity and crystallite size, but there was a phase change (formation of CaO) and strong degree in porosity at elevated temperatures (1200°C) after calcining bovine samples at 600°C,

900°C and 1200°C for a constant holding time of 18 hrs.

It is obvious from the literatures that extreme temperatures and long holding times affect the properties of extracted HAP negatively and could lead to increase in the cost of producing HAP from natural wastes. Taking into consideration the effects of low, extreme calcination temperature and long holding times, this work attempted to evaluate the effect of moderate calcination temperatures (600°C, 750°C and 900°C) and constant holding time of 3 hrs. on the evolution of HAP from cattle bone waste. The results of this work will contribute data for the optimization of calcination temperature and holding time that have determining effects on the evolution of HAP by calcination process. Moreso, cattle bone wasteis highly available in Nigeria and synthesizing HAP from it amounts to recycling and adding value to it.

2.0 Experimental procedure

2.1 Materials

The materials used for the preparation of hydroxyapatite are cattle bone (femur), which was sourced from an abattoir at Ogige market, Nsukka, Nigeria; distilled water for washing and cleaning the bones and acetone for de-fatting the cleaned bones. Other materials were pestle and mortar for crushing the cattle bone into small pieces; grinding machine for pulverizing the bones into smaller particles; a sieve for separating the particles into particle sizes $\leq 75\ \mu m$ and a muffle furnace for heat treatment of the bone powder.

2.2 Preparation of cattle bone powder

The obtained cattle bone was cleaned and sun dried for two weeks to reduce the moisture content and the organic matter therein. The bone was subsequently dried in the heat treatment furnace at 200°C for 2½ hours to further reduce the moisture and organic matter content. The bone was allowed to stay in the oven for another 1 hour before its removal. The dried cow bone was crushed to smaller pieces in a crusher followed by pulverization using a grinding machine. The pulverized cattle bone was then sieved to obtain fine powder sizes ≤ 75 μm and stored in a sealed plastic container for later use.

The pulverized CB powder was placed in air-tight ceramic cups and calcined separately at 600°C, 750°C and 900°C using a muffle furnace. The temperature was limited to < 1000°C to avoid phase transformation into Tricalcium Phosphate (TCP) [C] or Calcium oxide (CaO) [B]. The holding time at these temperatures was 3 hours each. Calcination was necessary for the final removal of organic matter such as collagen and protein as well as to enable the production of HAP. The colour changes that occurred at different calcination temperatures were monitored. The functional groups in the uncalcined and calcined CB were determined using Fourier-Transform Infrared Spectroscopy (FTIR).

3.0 Results and discussion

3.1 Colour changes at different calcination temperatures

The colour changes that occurred at different calcination temperatures showing the evolution of HAP are shown in Figure 3.1. Hydroxyapatiteis known for its white colour [23, 27].It can be seen from Figure 3.1 that HAP present in the powder calcined at 600°C is not fully developed as it has not acquired white colour of HAP. HAP is more evolved in the CB powders calcined at 750°C and 900°C as they are whiter than in the one calcined at 600°C.

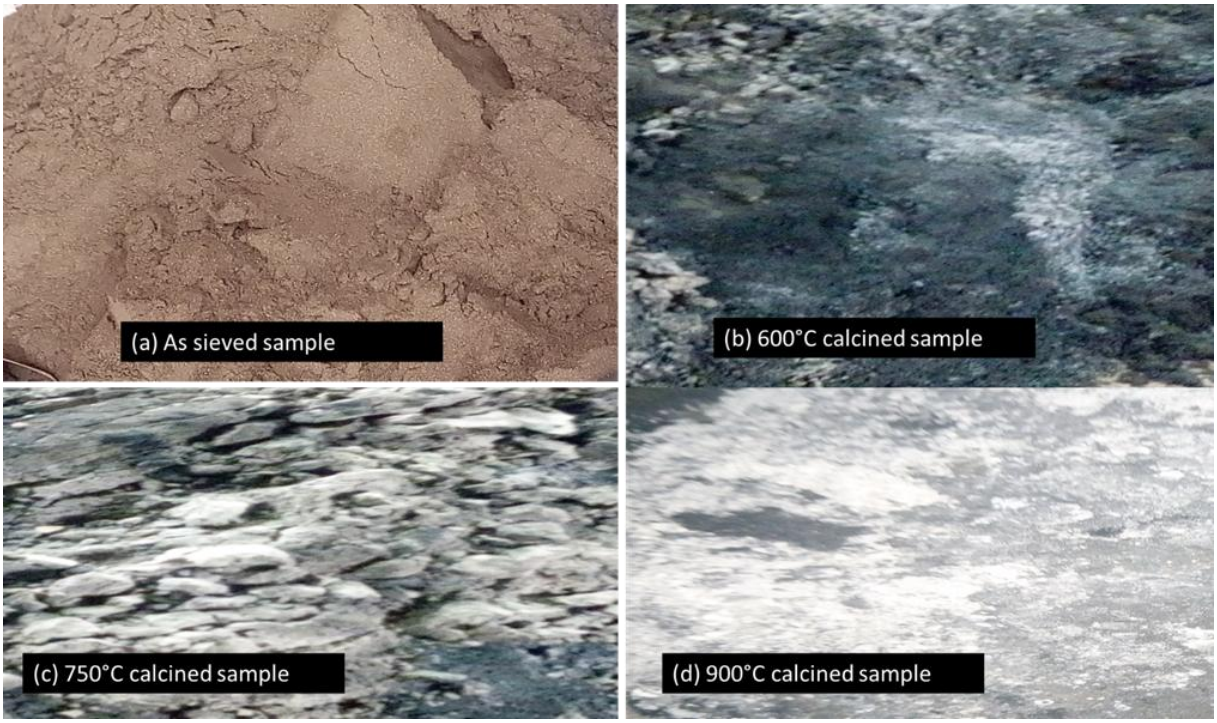

Figure 3.1: Colour changes that accompanied the calcining of CB powder at 600°C, 750°C and 900°C

3.2 Fourier Transform Infra-Red Spectroscopy (FTIR)

Fourier Transform Infra-Red Spectroscopy (FTIR)was performed to identify the functional groups present in the as-sieved CB sample and CB powders calcined at 600°C, 750°C and 900°C. Figures 3.2 to 3.4 show the spectra absorption ranges of the calcined powders compared to the uncalcined one while the extracted wavenumbers and peak intensities are shown in Table 3.1.

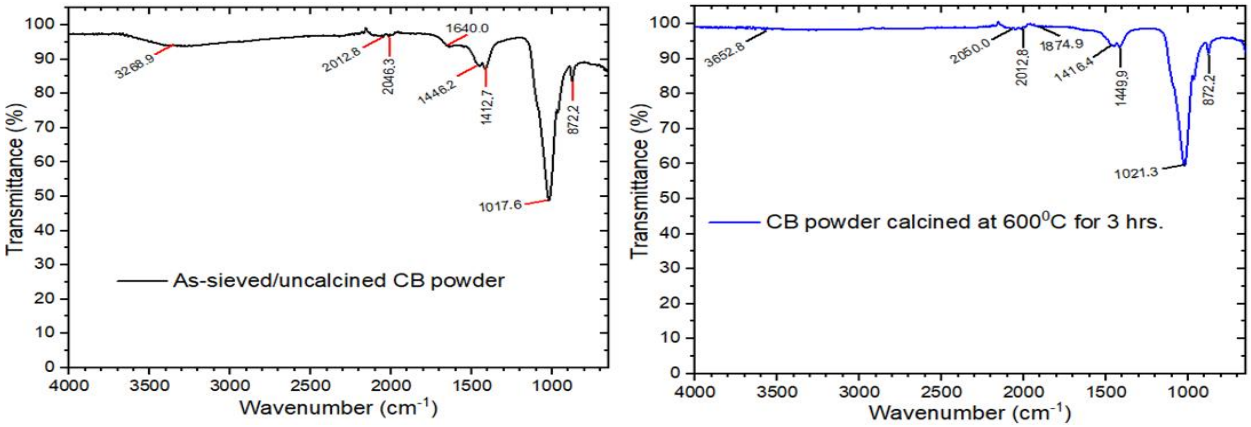

Figure 3.2: FTIR spectra of uncalcined CB and CB calcined at 900°C for 3 hrs.

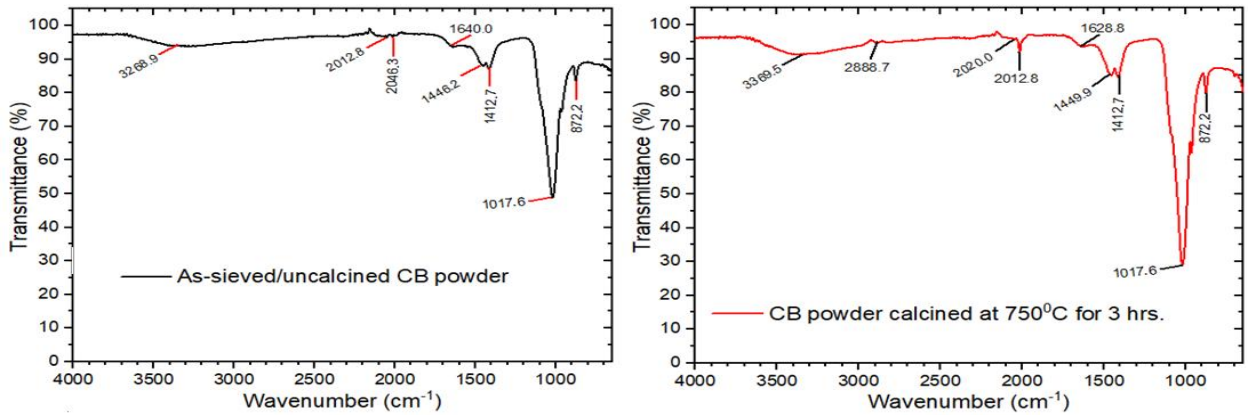

Figure 3.3: FTIR spectra of uncalcined CB and CB calcined at 750°C for 3 hrs.

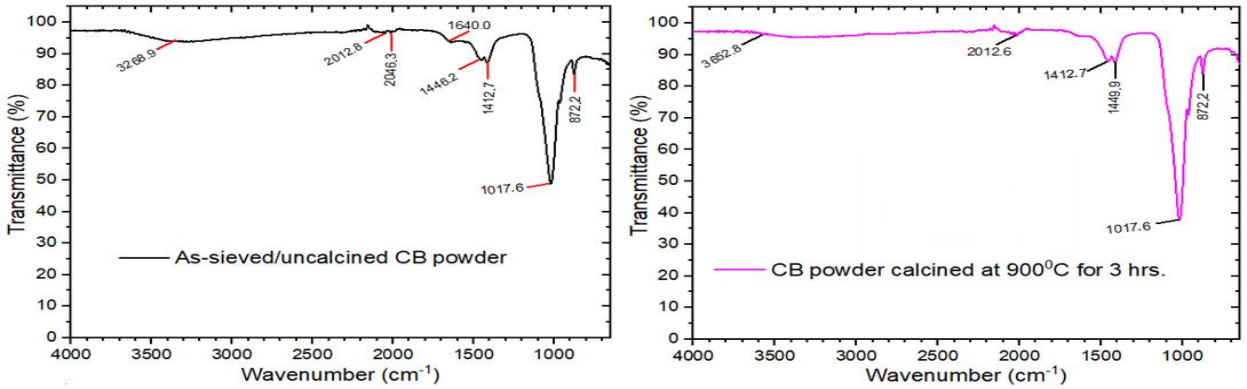

Figure 3.4: FTIR spectra of uncalcined CB and CB calcined at 900°C for 3 hrs.

The FT-IR spectra show many bands corresponding to different stretching-vibrational modes that identify similar or different functional groups. The spectra absorbent range was within the wave number of 4000 cm^{-1} to 650 cm^{-1}. There is presence of phosphate (PO_4^{3-}), carbonate (CO_3^{2-}) and hydroxyl (OH^-) groups in the bone powders. However, the peak intensities are higher in the carbonate and hydroxylgroups than in phosphate group. Since high peak intensities meant higher amount (per unit volume) of the functional group associated with the molecular bond among these groups, carbonate and hydroxylgroups are predominant in the samples.

It can also be observed that the peak intensities of the phosphate group for the uncalcined sample and the sample calcined at *600°C* are higher than the samples calcined at 750°C and 900°C. It has been observed elsewhere that the bands associated with phosphate vibrations of hydroxyapatite decrease in intensity significantly after calcination [28, 29]

Table 3.1: Functional groups identified in uncalcined and calcined CB powder samples

Functional group	Wave-number (cm^{-1})/absorbent intensity			
	Uncalcined CB powder	CB powder calcined at 600°C	CB powder calcined at 750°C	CB powder calcined at 900°C
Hydroxyl (OH^-)	3268.9/93.8	3652.8/98.5	3369.5/91.2	3652.8/96.9
Carbonate (CO_3^{2-})	2046.3/96.7 2012.8/96.5 1640.0/93.7(stretching) 1446.2/87.9 1412.7/87.2 872.2/83.5	2050.0/98.3 2012.8/98.4 1874.9/99.4 (stretching) 1416.4/93.4 1449.9/93.5 872.9/91.5 (asymmetric bending)	2888.7/94.7 (stretching) 2050.0/95.5 2012.8/91.8 1628.8/93.4 (stretching) 1449.9/84.9 1412.7/84.5 872.2/79.7	2012.8/96.1 (stretching) 1412.7/87.7 1449.9/87.9 872.2/84.2
Phosphate (PO_4^{3-})	1017.6/48.8	1021.3/59.3	1017.6/29.0	1017.6/37.6

The wide band within the region of 3652-3268 cm–1) in FTIR spectra corresponds to the stretching mode of vibrations of the OH^- group and depicts the presence of hydroxyapatite. Similar wide band was obtained by Khoo et al [TC] at 3572 cm^{-1} after calcining cattle bone between 700°C and 1100°C for 3 hrs., which proved the presence of HAP phase. However, the HAP present in the powder calcined at 600°C is not fully developed as can be seen from Figure 3.1 as it has not acquired white colour of HAP [8F]. The band at frequency number from 1628 to 1412 cm^{-1} shows the asymmetric stretching vibration for the carbonate group (CO_3^{2-}) while the band around 872 cm^{-1} shows the asymmetric bending mode of vibrations for CO_3^{2-}. The wavenumber around 1017 or 1021 cm^{-1} indicates the asymmetric stretching mode of vibrations in the phosphate group (PO_4^{3-}). Similar results were observed by Khoo et al [TC] at wavenumbers of 962 cm^{-1}, 1022 and 1087 cm^{-1}, which were associated with the phosphate group.

4.0 Conclusion

The effect of calcination temperature on the evolution of hydroxyapatite from cattle bone waste for biomedical applications was investigated in this work, and the following conclusions can be made:

1. The colour changes that accompanied the calcination process indicated that hydroxyapatite was successfully extracted from the cattle bone waste.
2. The colour changes also showed that HAP was more evolved in the CB powders calcined at 750°C and 900°C as they were whiter than the one calcined at 600°C, confirming the fact that HAP was more developed at temperatures above 700°C. However, the HAP produced at 900°C was whiter than those produced at lower temperatures.
3. The FTIR result confirmed the presence of associated functional groups in the extracted HAP consisting of phosphate ions ($PO4^{3-}$), hydroxyl ions (OH^-) and carbonate ions ($CO3^{2-}$).However, carbonate and hydroxylgroups were predominant in the samples as the phosphate group decreased with increase in calcination temperature.

4. This work has succeeded in adding value to cattle bone waste

References

[1]S.A. ISMAIL H.Z. ABDULLAH (2020). Extraction and Characterization of Natural Hydroxyapatite from Goat Bone for Biomedical Applications, Materials Science Forum, Vol. 1010, pp 573-578 doi:10.4028/www.scientific.net/MSF.1010.573.

[2] Fiume E., Magnaterra G., Rahdar, A., Verné E., Baino, F. (2021). Hydroxyapatite for Biomedical Applications: A Short Overview. Ceramics, 4, 542–563. https:// doi.org/10.3390/ceramics4040039

[3] Aleksandra Szcześ, LucynaHołysz, Emil Chibowski (2017). Synthesis of hydroxyapatite for biomedical applications, Advances in Colloid and Interface Science, doi: 10.1016/j.cis.2017.04.007].

[4] Fiume, E.; Magnaterra, G.; Rahdar, A.; Verné, E.; Baino, F. Hydroxyapatite for Biomedical Applications: A Short Overview. Ceramics 2021, 4, 542–563. doi.org/10.3390/ceramics40400

[5] S. Ramesh, Z.Z. Loo, C.Y. Tan, W.J. Kelvin Chew, Y.C. Ching, F. Tarlochan, Hari Chandran, S. Krishnasamy, L.T. Bang, Ahmed A.D. Sarhan (2018). Characterization of biogenic hydroxyapatite derived from animal bones for biomedical applications, Ceramics International, https://doi.org/10.1016/j.ceramint.2018.03.072

[6] F Afriani, Siswoyo , R Amelia , M Hudatwi , Zaitun, Y Tiandho (2020). Hydroxyapatite from natural sources: methods and its characteristics. IOP Conf. Series: Earth and Environmental Science 599, 012055. doi:10.1088/1755-1315/599/1/012055

[7] Feng C, Zhang K, He R, Ding G, Xia M, Jin X,Xie C (2020).Additive manufacturing of hydroxyapatite bioceramic scaffolds: Dispersion, digital light processing, sintering, mechanical properties, and biocompatibility. Journal of Advanced Ceramics 9, 360-373. https://doi.org/10.1007/s40145-020-0375-8

[8] C. Piccirillo, R. C. Pullar, E. Costa, A. Santos-Silva, M. M. E. Pintado, and P. M. L. Castro (2015). "Hydroxyapatite-based materials of marine origin: A bioactivity and sintering study," Mater. Sci. Eng. C, 51,309–315.

[9] S. Mazumder, A. K. Nayak, T. J. Ara, and M. S. Hasnain, Hydroxyapatite composites for dentistry. Elsevier Inc., 2018

[10] Akhlis Rahman Sari Nurhidayat, A.P. Bayuseno, Rifky Ismail, RiloBerdinTaqriban (2021). Review of the temperature and holding time effects on hydroxyapatite fabrication from the natural sources. Journal of Biomedical Science and Bioengineering. 1 (1) 2021: 27-3. https://doi.org/10.14710/jbiomes.2021.v1i1.27-31

[11] Wopenka, B.; Pasteris, J.D. A mineralogical perspective on the apatite in bone (2005). Mater. Sci. Eng. C, 25, 131–143. https://doi.org/10.1016/j.msec.2005.01.008

[12] Levingstone T J, Herbaj S and Dunne N J (2019). Calcium Phosphate Nanoparticles for Therapeutic Applications in Bone Regeneration. Nanomaterials 9, 1570 http://dx.doi.org/10.3390/nano9111570

[13] A. F. A. Yazdi, A. Yazdani T. T. Khozani and M. Kalantar (2013). Extraction and viability checking of various carbonated hydroxyapatite by Wharton's jelly mesenchymal stem cell, Sci. Int. 132–138. https://scialert.net/abstract/?doi=sciintl.2013.132.138

[14] M. Akram, R. Ahmed, I. Shakir, W. A. W. Ibrahim, R. Hussain (2014). Extracting hydroxyapatite and its precursors from natural resources, J. Mater. Sci. 49, 1461–1475.https://doi.org/10.1007/s10853-013-7864-x

[15] C. Piccirillo, R. C. Pullar, E. Costa, A. Santos-Silva, M. M. E. Pintado, and P. M. L. Castro (2015). Hydroxyapatite-based materials of marine origin: A bioactivity and sintering study. Mater. Sci. Eng. C, 51,309–315.

[16] S. Pramanik, A. K. Agarwal, K. N. Rai, A. Garg (2007). Development of high strength hydroxyapatite by solid-state-sintering process. Ceram. Int., 33 (3), 419–426,

[17] C.F. Ramirez-Gutierrez, S.M. Londoño-Restrepo, A. del Real, M.A. Mondragón, M.E. Rodriguez-García (2017). Effect of the temperature and sintering time on the thermal, structural, morphological, and vibrational properties of hydroxyapatite derived from pig bone, Ceram. Int. 43, 7552-7559

[18] N.A.S. MohdPu'ad, J. Alipal, H.Z. Abdullah et al. (2020). Synthesis of eggshell derived hydroxyapatite via chemical precipitation and calcination method, Materials Today: Proceedings, https://doi.org/10.1016/j.matpr.2020.11.276

[19] A. Niakan, S. Ramesh, P. Ganesan, C.Y. Tan, J. Purbolaksono, H. Chandran, S. Ramesh, W.D. Teng (2015). Sintering behaviour of natural porous hydroxyapatite derived from bovine bone, Ceram. Int. 41, 3024-3029.

[20] Akhlis Rahman Sari Nurhidayat, A.P. Bayuseno, Rifky Ismail, RiloBerdinTaqriban (2021). Review of the temperature and holding time effects on hydroxyapatite fabrication from the natural sources. Journal of Biomedical Science and Bioengineering. 1 (1). 27-31

[21] JojorLamsiharManalu, Francisca Tjhay, Theodora Kristoforus (2020). Effect of Calcination Time on Bovine-Derived Hydroxyapatite as Bone Implant Material: An In Vitro Study. Asian Journal of Applied Sciences, 8(5), 275-282.

[22] N.A.S. MOHD PU'AD, A.F.A. LATIF, N.D. RAMLI, M.S MUHAMAD, H.Z ABDULLAH, M.I. IDRIS, T.C. LEE (2020). Extraction of Biological Hydroxyapatite from Bovine Bone for Biomedical Applications.Materials Science Forum,1010, 579-583 doi :10. 4028/ www.scientific.net/MSF.1010.579

[23] Jamiu K Odusote, Y Danyuo, Abdulazeez D Baruwa, Akeem A Azeez (2019). Synthesis and characterization of hydroxyapatite from bovine bone for production of dental implants. Journal of `Applied Biomaterials & Functional Materials, 1–7. https: //doi.org /10.1 1 77 /2280800019836829

[24] W. Khoo,F. M. Nor, H. Ardhyananta and D. Kurniawan (2015). Preparation of Natural Hydroxyapatite from Bovine Femur Bones Using Calcination at Various Temperatures. Procedia Manufacturing 2, 196 – 201.

[25] Kerim Emre Öksüz, Seyran Kilinç, Ali Özer (2019). Effect of Calcination on Microstructure Development and Properties of Hydroxyapatite Powders Extracted from Human and Bovine Bones. Trans. Ind. Ceram. Soc., 78 (1), 41-45.

[26] M. Figueiredo, A. Fernando, G. Martins, J. Freitas, F. Judas, H. Figueiredo (2010). Effect of the calcination temperature on the composition and microstructure of hydroxyapatite derived from human and animal bone. Ceramics International 36, 2383–2393.

[27] Bahrololoom M, Javidi M, Javadpour S, J. Ma (2009). Characterization of natural hydroxyapatite extracted from bovine cortical bone ash. J Ceram Process Res, 10(2), 129- 138

[28] Ooi, C.Y., Hamdi, M. and Ramesh, S. (2007). Properties of Hydroxyapatite Produced by Annealing of Bovine Bone. Ceramics International, 33, 1171-1177.https://doi.org/10.1016/j.ceramint.2006.04.001

[29] V. K. Mishra, B. N. Bhattacharjee, O. Parkash, D. Kumar and S. B. Rai (2014). Mg-doped hydroxyapatite nanoplates for biomedical applications: A surfactant assisted microwave synthesis and spectroscopic investigations. J. Alloy. Compd., 25, 283-288. http://dx.doi.org/10.1016/j.jallcom.2014.06.082

NMS-TP026

HYDROPHOBIC PARAMETER INVESTIGATIONOF FIBRE AND PARTICULATE REINFORCED POLYMER (FPRP) COMPOSITE-BASED ELECTRICAL INSULATOR

By

S.C Madu[#Θ1], V.S Aigbodion[#Θ*2], A.B Udochukwu[β]

[#]*Department of Metallurgical and Materials Engineering, Faculty of Engineering,*

[Θ]*Africa Centre of Excellence for Sustainable Power and Energy Development (ACE-SPED), University of Nigeria, 410001 Nsukka, Nigeria.*

[β]*Department of Electrical Engineering, Faculty of Engineering and Built Environment, Tshwane University of Technology, Pretoria, South Africa.*

[*]*Faculty of Engineering and Built Environment, University of Johannesburg, P. O. Box 534 Auckland Park, South Africa.*

[1] solomon.madu@unn.edu.ng

[2]victor.aigbodion@unn.edu.ng

[3]AkuruUB@tut.ac.za

Abstract:

Hydrophobicity is a decisive factor in evaluating one of the most essential parameters of fibre and particulate reinforced polymer (FPRP) composite needed for the electrical insulation. In this study, glass fibre, oyseter shell, and gel coat were added at various percentages using Tanguchi array methods to find the optimal composition combination in the investigation of the hydrophobicity parameters of a composite. The parameters are true density, bulk density, and true porosity of FPRP composite-based electrical insulator. Optimal hydrophobic parameter were obtained at the true density and bulk density of the composite composition variation of 82% vinyl ester, 4% glass fibre, 6% gel coat, and 8% oyster shell which had a value of 1.2724 g/cm^3, which indicated highest density composite with no porosity.

Key words: Hydrophobicity, density, polymer, composite, electrical insulation.

1.INTRODUCTION

Continued advances in polymer science have been an advantage in vital fields of engineering and electrical insulation applications and have attracted a lot of attention from researchers in recent years [1]. Polymer materials like Vinyl ester, epoxy, polystyrene, polypropylene, polylactic acid (PLA), unsaturated polyester resins (UP), etc are practically unique and essential in our society especially at homes, hospitals, schools and industries. Most of the household products, textile industry products, flooring materials, flexible polyvinyl chloride (PVC) coated fire retardants, PVC hoses, automobile parts, and structural building materials are made from polymer products [2]–[6] Some polymeric materials can either be thermoplastic, thermoset, or amorphous polymer and they are widely used in electrical engineering applications due to their excellent characteristics and essential properties such as transparent in nature, easy to process, dimensional property, corrosion resistance, flame retardant property, elevated thermal stability, and low density which make them ideal [1]–[3].

Developmental advances in the field of electrical insulators are been developed in recent years due to the need in manufacturing processability that has targeted towards efficiency, durability, superiority, and reliability [1]. These advances in the development of electrical insulators has breeded more manufacturing of polymer composite-based electrical insulator over glass and ceramic-based electrical insulator [2].Glass or ceramic based electrical insulators are associated with the disadvantages of micro cracks, flashover mechanism, and brittleness [3][4]. High electric voltage is safely and effectively transmitted through the transmission grid when there is a better insulation system. The desire for better electrical insulation performance, electric resistivity, availability, and energy and time savings, low cost of production have greatly propelled the development and use of epoxy composite material for insulation of electric voltage [5]–[7]. Plesa I., et al pictorially showed different areas polymer-based

electrical insulators can be applied in the electrical sectors as shown in figure 1

Fig. 1. 1: Different electrical applications of polymer-based insulation material (Plesa I., et al) [8].

However, epoxy-based electrical insulators are made from organic constituents slowly deteriorate in a given period of time as a result of their salvage value and exposures to different environmental factors such as: ultra-violent radiative rays, thermal exposure, hydrophobicity moisture, environmental pollutants, ozone, and wind [9]–[11].

The structure and hydrophobic properties of polymer can be physically modified and enhanced by introducing different kinds of fillers such as inorganic or organic fillers, with inclusion of waste materials to suit different applications [4][5]. Synthetic and natural polymer products are essentially unique because of its ubiquitous application [14]. Beyer [9] noted that synthetic polymer nanocomposites can be manufactured in three different ways which include in-situ polymerization method, melt interaction method, and solvent method. Interestingly, polymers can be fibre reinforced naturally or synthetically [7]. However, Hamid et al., [8] reported that natural fibre has greater advantage than synthetic fibre due to its availability, environmental friendliness, and cost effectiveness. Epoxy polymer is estimated to rank the second biggest produced resin around the globe. This is because of its ease in manufacturing, low production cost, and its excellent mechanical properties which make them to be used extensively in construction and automotive industries, toys, packaging of foods, tubes, bags, credit cards, sealing papers, cable wires, and water bottles [15]. More so,Beyer et al., [9] noted that polymer composites like glass fibre/polyester used in commercial and domestic products, fibre epoxy systems applied in the military equipment and other polymer composite products have found application in structure, construction, aviation, and automotive industries as a result of their low-weight and high specific stiffness and strength. Typical structure of polymer composite is showcased in Figure 2.2.

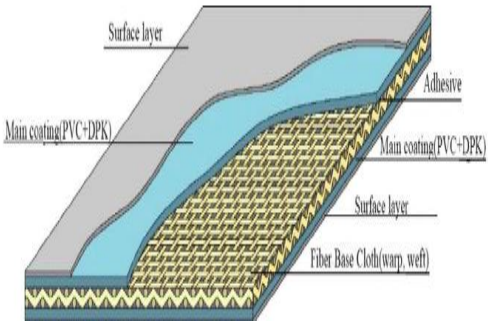

Fig. 1.2: Structure of Typical Polymer Composite, [5], [9].

Meanwhile, polymer is an organic compound that is made up of chains of carbon that is covalently bonded and shares a pair of electrons to stay together with other elements like oxygen, hydrogen, or nitrogen. Polymers have excellent mechanical, thermal and anti-corrosion properties. Take for instance, epoxies which are thermosetting polymers possess tensile strength of 40 MPa, heat conductivity of 0.2 W/mK and good corrosion resistance [10][11]. An epoxy resin is a monomer that contains at least two epoxide groups. Polymer can be cross-linked or homopolymerised. Polymer resins are cured by using curing or hardening agents like polyfunctional acids, amines, phenols, thiols, alcohols and anhydride. Curing of polymer is a chemical process in which it hardens after exposure to air, heat, or chemical additives that serves as a catalyst. This curing is an exothermic reaction that creates a cross-linkage in the polymer, which is responsible for the rigidity and strength of polymer composite materials. Polymer resins are widely used in array of consumer and industrial applications because of its high mechanical toughness, strong adhesive property, and resistance to chemical attack [11]. Some adhesives, plastics, paints, coatings, primers and sealers are manufactured with epoxy resins. Adhesives that are made of Solvent-free epoxy provide water

resistance, durability, chemical resistance and thermal resistance which are majorly found useful in the automotive and aerospace industries [12]. Epoxies are used in floor of buildings and other structural applications. Epoxy coatings are used on metal substrates and surfaces to control corrosion and provide tough, hard and protective coating. Epoxy resins can serve as sealers for concrete floors, and are used industrially to coat and protect other materials from corrosion.

Catastrophic failure of high voltage electrical insulators is a major concern in electric transmission grid. Some electrical insulators will inevitably and conditionally become polluted when exposed in the atmosphere after several duration of time in operational service [12]. It has been observed and tested that fatigue, tensile stress, radial cracking, brittleness, dew, fog, bulk dielectric damage, spontaneous shattering of the glass shell, partial damage to discs or housings, UV radiation, and pin corrosion are intrinsic and external factors that causes catastrophic failure of the electrical insulators [11], [13], [14]. Observations of electric transmission grid has shown that surface discharge, flashover voltage or leakage current occurs in almost every grid in wet conditions due to high level of contaminations on the electrical insulators [11], [15], [16].

2.0 Challenges of Electrical Insulation Materials

2.1 Pin deterioration mode of electrical-based insulator

The complications of pin corrosion can occur in surface areas of porcelain or glass with severe contaminated pollution which are basically dielectric bulk material independent [17]. In some cases, the polymeric stretched rod between both ends of different potential restricts current discharge to an infinitesimal amount that hardware deterioration is not a serious risk on the composite-based electrical insulators [18]. The use of newer designs with sacrificial zinc sleeves for corrosion protection is a proven way to avoid onset of this problem but of course has no impact on ageing of the existing population of discs from earlier generations.

2.2 External flashover failure mode of electrical insulator

External flashover of current occurs in an electrical insulator as a result of the initiation and emission of electrons from the cathode triple junction region of the insulator in vacuum [19]. This mode of failure can externally occur on the electrical insulator which can lead to a temporary loss of dielectric strength. The occurrence of flashover on the electrical insulator depends mainly on the activities of lightening, snow, accumulation of salt, wind, dust, propagation of discharge across wetted polluted area, and condition of contamination as related to key parameters of design of the string (for example; current leakage, shed profile, and distances of dry arc) as well as the electrical insulation coordination of the system [20]–[22]. For any given distance of current leakage, external flashover of electrical insulator is a more common problem for porcelain-based electrical insulator and glass-based electrical insulator due to their relatively easy wettability when it is relatively compared to polymer composite-based electrical insulator that utilizes low surface energy housing that resists filming of water on its surface and prevents external flashover that leads to catastrophic failure of the insulator [13], [15], [20].

Fig. 1. 3: Damaged glaze on porcelain insulator due to power arc from lightning.

2.3Internal Puncture failure mode

This mode of failure is seen in porcelain-based electrical insulators and relates primarily to problems with processing of raw materials and production procedures. Some insulator manufacturers may have inferior methods of the control of quality and this does not only have impact on the macroscopic property such as color but also microstructure of the ceramic body itself. The presence of pores (voids) and many grain boundaries between crystals are common to all porcelain, but sometimes micro-cracks can exist [23]. These can grow under the multiple stresses generated by service conditions and eventually lead to electrical breakdown through the bulk dielectric.

Such internal punctures of porcelain insulators are detectable only with a close-up inspection of the line using measuring instruments. Reliable statistics for this type of failure are therefore not available on a global basis. But experience at many power supply companies shows that this problem, while generally rare in new insulators, is more common on older lines, especially if the porcelain insulators were not of the highest quality to begin with. A past report from Canada, for example, revealed large numbers of punctured porcelain insulators on 230

kV and 500 kV transmission lines that have been in service for over 20 years.

Brittle fracture of composite insulators leads to mechanical separation of the fiberglass rod, also causing the conductor to drop [22].

3.0 MATERIALS AND METHODS:

3.1 Materials preparation

Vinyl ester resin, Oyster Shell (OS), Glass fibre (GF), and gel coatwere used for this study. Oyster shells werecollected from the River line area and washed with clean water so as to remove the dirty particles that might have been stuck to it, after which it wassun dried for 4 weeks. The dried oyster shells were subsequently crushed with hammer and finally milled. The particles from the process were reduced to 45micronsized particles by sol-gel method.

3.2Mould preparation

Cylindrical moulds of 4.8 g/cm^3 were prepared for the evaluation of the hydrophobic parameters.

3.3 Production of the composites.

To develop the composites, each of catalyst and accelerator was added to a specific weight % of vinyl ester resin and as well as a specific weights % of fibreglass, gel coat and particulates which were varied in a predetermined proportion as stated in the table below. After proper stirring, the homogenous slurry was poured into the mould and allowed to be cured at room temperature before it was removed.

4.0 RESULTS:

Sixteen samples were produced from each of the weight% proportion composition and the true density and as well as bulk densities were determined with the GasPycnometer and Archimedes Principle respectively. The true porosity of the samples werecalculated with use of the formula in equation (i):

$$T_p = \frac{\rho - \beta}{\rho} x\, 100 \qquad \text{(i)}$$

In which:

T_p = True porosity.

ρ = True density.

β = Bulk density.

Table 1 shows the Tanguishi weight % variation proportion of vinyl ester resin, glass fibre, oyster shell, and gel coat, the true and bulk densities, and true porosity of individual composition of the composite- based electrical insulator.

Table 1: Variation of composite materials with respect to Water absorption property

S/N	Poly (wt. %)	GF (wt. %)	GC (wt. %)	OS (wt. %)	Water Absorption		
					ρ (g/cm^3)	β(g/cm^3)	T_p (%)
P_{GOGC1}	94	2	2	2	1.2129	1.21230	0.06
P_{GOGC2}	90	2	4	4	1.2360	1.23550	0.05
P_{GOGC3}	86	2	6	6	1.2229	1.22250	0.04
P_{GOGC4}	82	2	8	8	1.2565	1.25650	0.00
P_{GOGC5}	90	4	2	4	1.2422	1.18009	0.05
P_{GOGC6}	90	4	4	2	1.2339	1.17221	0.05
P_{GOGC7}	82	4	6	8	1.2724	1.27240	0.00
P_{GOGC8}	82	4	8	6	1.2628	1.26280	0.00
P_{GOGC9}	86	6	2	6	1.2343	1.13556	0.08
P_{GOGC10}	82	6	4	8	1.2541	1.16631	0.07
P_{GOGC11}	86	6	6	2	1.2548	1.16696	0.07
P_{GOGC12}	82	6	8	4	1.2558	1.18045	0.06
P_{GOGC13}	82	8	2	8	1.2178	1.09602	0.10
P_{GOGC14}	82	8	4	6	1.2491	1.13668	0.09
P_{GOGC15}	82	8	6	4	1.2612	1.16030	0.08
P_{GOGC16}	82	8	8	2	1.2722	1.2468	0.02

5.0 Discussion and Conclusion:

The results show that both true density and bulk density of the composite composition variation of82% vinyl ester, 4% glass fibre, 6% gel coat, and 8% oyster shell is 1.2724 g/cm^3, which indicated highest density composite with no porosity. The result shows that optimal hydrophobic parameter is obtained at such combination composition.

In conclusion, the hydrophobic property of polymer composite-based insulator can be evaluated using tanguichi array. The parameter helps in determining the true porosity of the material using gas pycnometer.

6.0 Acknowledgement:

The authors also wish to appreciate the support and the facilitating environment provided by the African Centre of Excellence for Sustainable Power and Energy Development (ACE-SPED), University of Nigeria, Nsukka that enhanced the completion of this review.

SPONSORED BY THE Federal Ministry of Education and Research

AGNES African-German Network of Excellence in Science

Madu, Solomon C. wishes to thank the African-German Network of E (AGNES) for granting a Mobility Grant in 2021; the Grant was gene German Federal Ministry of Education and Research and supported b Humboldt Foundation.

7.0 REFERENCES:

[1]"Ceramics : Materials and Processes Ceramic Compounds : Ceramic Materials."

[2]A. Aman, A. R. Abdullah, and M. M. Yaacob, "Dielectric property of Waste Tire Dust-Polypropylene (WTD-PP) composite for high voltage outdoor insulation application," *2012 IEEE Int. Power Eng. Optim. Conf. PEOCO 2012 - Conf. Proc.*, no. June, pp. 124–128, 2012.

[3]B. F. Hampton, "Flashover mechanism of polluted insulation," *Electron. Power*, vol. 10, no. 4, p. 113, 1964.

[4] S. Kumar and V. Dave, "Impact of Pollution on High Voltage Insulators: Research Status and Recommendations," vol. 9, no. 2, pp. 722–730, 2018.

[5]L. S. Nasrat, A. F. Hamed, M. A. Hamid, and S. H. Mansour, "Study the flashover voltage for outdoor polymer insulators under desert climatic conditions," *Egypt. J. Pet.*, vol. 22, no. 1, pp. 1–8, 2013.

[6] L. Desmars, J. Galy, D. Bachellerie, A. Cristiano-Tassi, S. Haller, and S. Pruvost, "High Voltage Electrical Properties of Epoxy / h-BN Microcomposites," *2018 IEEE 2nd Int. Conf. Dielectr. ICD 2018*, no. 1, 2018.

[7] A. Said, A. Gamal Nawar, E. Alaa Eldesoky, S. Kamel, and M. Awdallah Abd-Allah, "Enhancing the High Voltage XLPE Cable Insulation Characteristics Using Functionalized TiO₂ Nanoparticles," *Am. J. Polym. Sci. Technol.*, vol. 6, no. 3, p. 21, 2020.

[8] I. Pleşa, P. V. Noţingher, S. Schlögl, C. Sumereder, and M. Muhr, "Properties of polymer composites used in high-voltage applications," *Polymers (Basel).*, vol. 8, no. 5, 2016.

[9] A. Jaya, H. Berahim, T. Tumiran, and R. Rochmadi, "The Performance of High Voltage Insulator Based on Epoxy-Polysiloxane and Rice Husk Ash Compound in Tropical Climate Area," *Electr. Electron. Eng.*, vol. 2, no. 4, pp. 208–216, 2012.

[10]A. Khattak *et al.*, "Investigation of dielectric properties and methylene intactness under multiple environmental stresses for high voltage epoxy composites," *Mater. Res. Express*, vol. 7, no. 7, 2020.

[11]T. Tanahashi *et al.*, "Effect of insulator configuration on ageing deterioration of polymer insulators," *2011 Electr. Insul. Conf. EIC 2011*, no. June, pp. 102–105, 2011.

[12]C. Sitompul, Z. Nawawi, and I. Jambak, "Detection of Polymer Insulator Surface Based on the Effects of Tropical Climate Using Partial Discharge Signals Measurement," *J. Phys. Conf. Ser.*, vol. 1500, no. 1, 2020.

[13]H. Rosli, N. A. Othman, N. A. Mohd Jamail, and M. N. Ismail, "Effects of external shed damage on voltage and electric field profile for overhead insulators," *World J. Eng.*, vol. 16, no. 4, pp. 468–476, 2019.

[14]N. K. Kar, Y. Hu, E. Barjasteh, and S. R. Nutt, "Tension-tension fatigue of hybrid composite rods," *Compos. Part B Eng.*, vol. 43, no. 5, pp. 2115–2124, 2012.

[15]Darwison *et al.*, "Estimated leakage current based on the thermal image of the polymer insulator using the color detection method," *J. Phys. Conf. Ser.*, vol. 1317, no. 1, 2019.

[16]V. J. Narayanan and S. C. A. Vanitha, "Analysis of Surface Condition of Polymeric Insulators for High Voltage Power Transmission Line Applications Using Partial Discharge Analysis," *Res. Inven. Int. J. Eng. Sci.*, vol. 4, no. 7, pp. 31–40, 2014.

[17] O. Mardianaliza, M. Amirruddin, F. S. Abdullah, and N. Anida, "Investigation on the Characteristics of Cap and Pin Glass Insulator due to Effect of Contamination," *Appl. Mech. Mater.*, vol. 793, pp. 95–99, 2015.

[18] E. Jayaprakash and S. Vaideki, "Analysis of Electric Field on Insulator for Different Pollution Condition," vol. 1, no. 3, pp. 125–129, 2017.

[19]S. Y. Teo, H. A. Illias, N. Mokhtar, H. Mokhlis, and A. H. A. Bakar, "Flashover voltage of insulator string under various conditions," *Conf. Proceeding - 2014 IEEE Int. Conf. Power Energy, PECon 2014*, pp. 119–122, 2014.

[20]D. Filipović-Grčić, B. Filipović-Grčić, and I. Uglešić, "Lightning critical flashover voltage of high voltage insulators: Laboratory measurements and calculations," *Int. Rev. Electr. Eng.*, vol. 7, no. 2, pp. 4321–4328, 2012.

[21] J. M. Rodríguez-Serna and R. Albarracín-Sánchez, "A study on the life estimation and cavity surface degradation due to partial discharges in spherical cavities within solid polymeric dielectrics using a simulation based approach," *Polymers (Basel).*, vol. 13, no. 3, pp. 1–25, 2021.

[22]I. H. Choi, T. K. Kim, Y. B. Yoon, T. Kim, H. T. T. Nguyen, and J. Yi, "A Study on the Life-Time Assessment Ways and Various Failure Types of 154 kV Porcelain Insulators Installed in South Korea," *Trans. Electr. Electron. Mater.*, vol. 19, no. 3, pp. 188–194, 2018.

[23]S. Anjum, "A Study of the Detection of Defects in Ceramic Insulators Based on Radio Frequency," p. 97, 2014.

NMS-TP027

ROLE OF METALLURGICAL FORENSIC ENGINEERING IN FORESTALLING STEEL STRUCTURE COLLAPSE

Prof. B. O Adewuyi[1], Olaniran O[1], Daramola O.O. [1], Ocheri C.[2]
([1]Federal University of Technology, Akure; [2]University of Nigeria, Nsukka)
Corresponding Author:
Prof. B.O. Adewuyi
Email: tayo_adewuyi@yahoo.com
Phone No: +234 347 00715

ABSTRACT

After routine or severe use, many materials can deteriorate, crack, or rust. The time may be right to conduct an in-depth failure analysis to determine the nature and cause of the failure, though, when such occurrences happen prematurely or repeatedly. Professional engineers, metallurgists, and other related professionals should be consulted to identify the nature and cause of the failure as well as who is responsible for the loss whenever such failure is suspected to be caused by the premature or abnormal deterioration of a component due to a manufacturing defect, an installation problem, or abusive usage. The role of metallurgical forensic engineering in preventing steel structure collapse was thus investigated in this research to determine the causes of failures on some important structures such as church buildings, aircrafts, cranes, bridges, hip prothesis, truck trailer frame corrosion, pitting and cracking SS weld, buildings pedestrian bridges. The study also covered some of the most common types of failure, common metallurgical causes of failure, and the impact of metallurgical parameters.

Keywords: Metallurgical Forensic, Engineering Forestalling, Steel, Structure, Collapse

1. INTRODUCTION

Most engineering failures at service involve damage to the material comprising the failed component(s). Metallurgy focuses on physical and chemical aspects of metallic elements, inter-metallic compounds and alloys. Ferrous metallurgy covers the study of iron and iron-based alloys, while non-ferrous metallurgy encompasses all other metals. Structural failure refers to defects in which a load bearing component of the structure is unable to support and transfer loads to another element. When failures happen and are analyzed, the root causes are to be identified and steps should be taken to change the conditions that allowed such an event to happen. Metallurgy-based study of failures involves proper understanding of the details of metallic components of structures which constitute in most cases the life-wire of structures. Forensic material is a material obtained from the accident site to determine the probable causes of structural failures. Metallurgy-based study of failures will reveal the history of the metal i.e. the production processes (melting, casting, heat treatment etc.), composition, microstructure and the properties. Therefore, Metallurgical Forensic analysis provides understanding of intrinsic structural failures and also provides possible solutions to mitigate or eliminate the conditions that led to the failures. A detailed process of analysis involves carrying out various tests including mechanical,

microstructural, corrosion and other physical property tests. The aims of such tests are to detect the reason(s), course(s), and consequences of any security incident or breach of integrity of materials used in construction. In recent times, collapse of buildings and other structures are common. The aim of this paper therefore is to highlight the aspect of structural failure analysis which is very crucial but often neglected. The paper recommends inclusion of Metallurgical Forensic Engineering as highly essential to determine cause(s) of failure and how to prevent future occurrences.

2.0 THE MAIN TYPES OF FAILURE

- Failure by fracture due to static overload, the fracture being either brittle or ductile.
- Buckling in columns due to compressive overloading.
- Yield under static loading which leads to misalignment or overloading on other components.
- Failure due to impact loading or thermal shock.
- Failure by fatigue fracture. Creep failure.
- Failure due to the combined effects of stress and corrosion.
- Failure due to excessive wear

2.1 COMMON METALLURGICAL CAUSES OF FAILURE

Structural failure develops due to breakdown in the performance of the materials in a structural component may be caused by improper metallurgical considerations. The typical root cause of failure mechanisms include: Fatigue failures, Corrosion failures, Stress corrosion cracking, Ductile and brittle fractures, Hydrogen embrittlement, Liquid metal entrapment , Creep and stress rupture. It is possible for fracture to be a result of multiple failure mechanisms or root causes. A failure analysis can provide the information to identify the appropriate root cause of the failure.

If a part does not fulfill its intended function satisfactorily, it "fails" by: (*a*) excessive deformation, (*b*) fracture, (*c*) surface disintegration, and (*d*) deterioration of properties.

- **Manufacturing Defects:** Microstructure is key to engineering properties. The ability to tune properties is central to materials processing and design:
  Composition + Processing = Microstructure + Properties.
- **Unstable Properties**:
- Thermal, electrical, optical and magnetic behaviors are most directly influenced by the atomic scale of microstructure.
- Strength, toughness and fatigue depend on structure at a slightly larger scale.
- All steels tend to lose strength with increasing temperature.
- At 600^{o}C, most structural steels are likely to have lost more than half their strength.
- At intermediate temperatures the strength is independent of time, but above 500^{o}C, creep, or time-dependent deformation, further reduces the load-carrying capability.
- **Improper Material Selection**: Poor material selection for welding, reinforcement etc. can lead to progressive collapse of steel structures. For instance due to inadequate mechanical strength - or loss of integrity due to corrosion

products. If correct materials for construction are chosen from the beginning, damage deriving from corrosion, wear and mechanical impact can be prevented.

4. **Consideration for Environment:** Environment imposes very high demands on materials: If the environment is sufficiently aggressive, constant mechanical impact will often increase the risk of corrosion failure. Corrosion can be avoided by choosing a corrosion resistant material for the environment

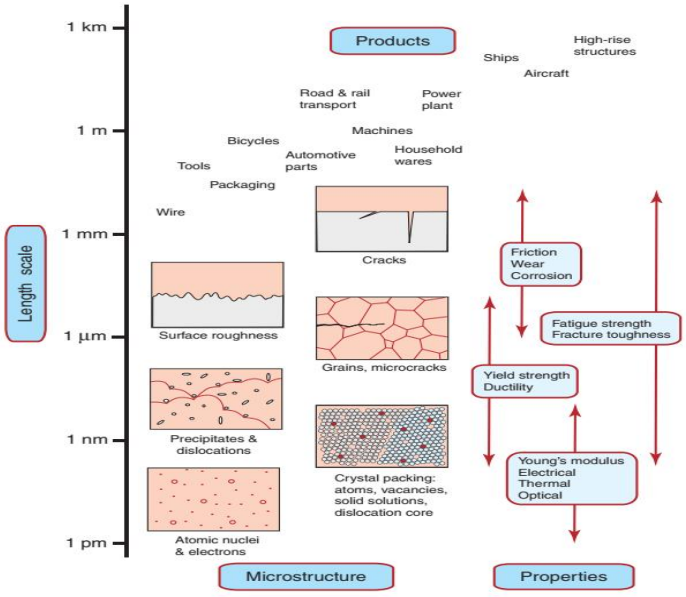

Fig 1 Comparative analysis of Microstructure and Properties

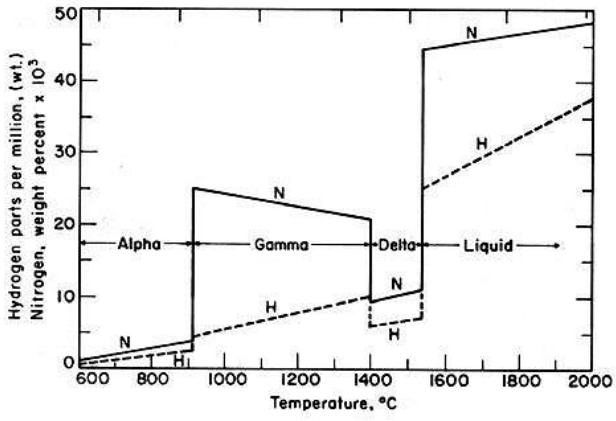

Fig 2 Solubility of Nitrogen and Hydrogen in Steel

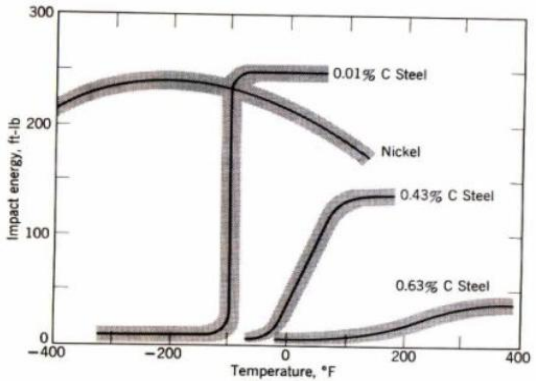

Fig 3 Response different composition to impact test

3.0 INFLUENCE OF METALLURGICAL FACTORS

Metallurgical forensic engineering uses basic engineering principles and practices, a metallurgical forensic engineer analyzes the collected specimen from accident site and carried out assessment of the probable causes of structural failure

Factor	Influence	Result
Quality of Rebar (Poor mechanical e.g. low plasticity, etc.)	Rebar acts as the tension member to protect structure from sudden impacts	Rebar with less yield stress capacity breaks after a small amount of load/seismic stress, Resulting in the collapse of the structure.
Unbalanced Carbon content	Carbon added during production to impart toughness to steel	Adding more than the required amount in the greed of more strength renders steel brittle, jeopardizing the life of the structure
Chemical Composition is compromised (Alloying elements)	Compromised integrity not meeting standard	Steel fails to sustain the enormous strength and energy, when there is unexpectedly high (seismic) forces
Aluminum	Ferrite hardener;	Graphite former; Deoxidizer
Chromium	Mild ferrite hardener;	Moderate effect on hardenability Graphite former; Resists corrosion; Resists abrasion
Cobalt	High effect on ferrite as a hardener;	High red hardness (hot-hardness), resistance to tempering
Molybdenum	Strong carbide former;	High red hardness; Increases abrasion resistance
Manganese	Strong ferrite hardener	Form manganese sulfide (MnS) which prevents hot-shortness.
Nickel	Ferrite strengthener; Graphite former	Increases toughness of the hypoeutectoid steel; With chromium, retains austenite;
Copper	Austenite stabilizer;	Improves resistance to corrosion
Silicon	Ferrite hardener;	Increases magnetic properties in steel
Phosphorus	Ferrite hardener;	Improves machinability; Increases hardenability P- (>0.12%P) reduces the ductility, increasing the tendency to crack when cold worked. Brittle when $T<T_{rec}$ (cold-shortness)
Sulfur		Form iron sulfide (FeS) at grain boundaries; low melting point destroys cohesion between the grains. High temperatures brittleness (hot-shortness)
Gaseous impurities (Hydrogen, Nitrogen)	High concentration	H and N in steel affects the plasticity, formability, embrittlement (heat affected zone in weld)
Nonmetallic Inclusions : (sulphides, Phosphides, oxides, oxyphosphides etc.)	Retained Inclusions retained in steel during production	Porosity (blow holes, pinholes etc); Cold Cracking; Hot Cracking; Cold Shuts; Surface irregularities; Distortion.

4.0 CASE STUDY: CHURCH BUILDING COLLAPSE

Structural failure as reported by three government agencies, (the Nigeria Building and Road Research Institute (NBBRI), the

Council for the Regulation of Engineering in Nigeria (COREN) and the Building Collapse Prevention Guild (BCPG))

- **Inadequate beams** of 750mm by 225mm (should have been 900mm by 300mm)
- **Inadequately reinforced columns** (should have been reinforced with 12 x Y25 bars or 20 x Y20mm bars. Instead they used 10 x Y20 bars
- **Inadequate bearing pressure**: central column due to the 2m x 2m x 0.9m foundations.
- **Failure to introduce rigid zones** for bracing the structure and did not design the frames as an unbraced structure.
- **Failure to provide movement joints** that could have absorbed any movement due to creep, contraction, expansion and differential settlement etc.
- 8 out of the 12 main beams of the structure failed because they were undersized, under-reinforced (both in tension and shear), the tension bars were poorly anchored to the column supports and 8 x Y20 was used instead of 14 x Y20.

The ground floor columns were slender and readily gave in to buckling

5.0 EXAMPLES OF STRUCTURE COLLAPSE:

Forensic engineering include material failures that can be considered to be minor, severe or severely critical. Common ones include oil refinery pipeline rupture, collapse of buildings; Aircraft fuel line fracture, collapse of cranes, natural gas line failure, etc. Figs 4-11 show various examples of structure collapse while fig 12 shows Diagram of the Pedestrian Bridge

Fig 4 Aircraft Collapse

Fig 5 Crane Collapse

Fig 6 Bidge Collapse

Fig 7 Hip Prothesis

Fig 8 Truck Trailler Frame Corrosion

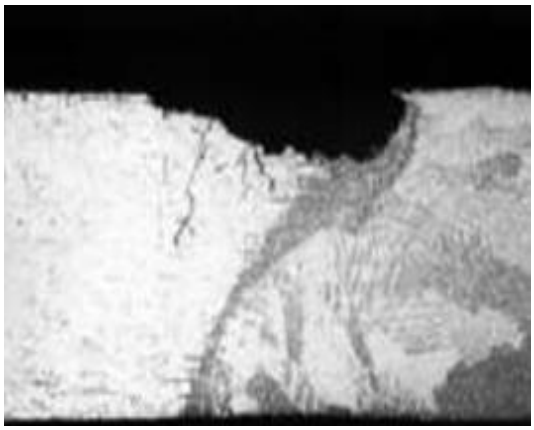

Fig 9 Pitting and Cracking in SS weld

Fig 10 Building Collapse

Fig 11 Pedestrian Bridge Collapse

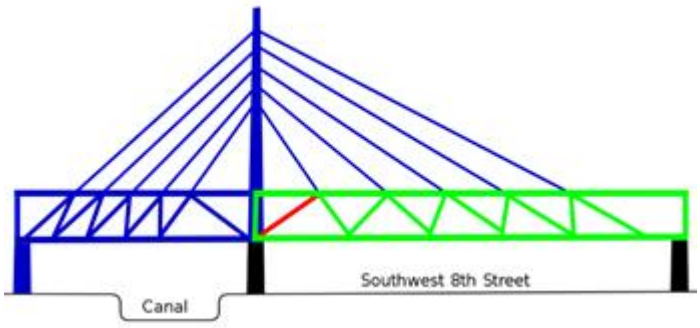

Fig 12 Diagram of the Pedestrian Bridge

CONCLUSION

1. Failure analysis requires careful sorting of a wide variety of information to determine how and why a metal part failed in service, evaluation of material behavior is carried out using standard failure analysis to identify failure mechanisms, formation and characteristics.
. In most cases, collapse of bridges and buildings after years of construction may be due to the poor quality of steel with embedded impurities from improper manufacturing procedure.
. At every stage of construction, qualified professionals should be involved in design, procurement and supervision.

NMS-TP028

DEVELOPMENT OF INTELLIGENT MEDICAL MOBILE ROBOT FOR TRANSPORTATION OF HOSPITAL EQUIPMENT USING Q-LEARNING TECHNIQUE.

Solomon Chibuzo Nwafor[1], Timothy Oluwaseun Araoye[2], Sochima Vincent Egoigwe[3],Oluchi Christiana Ugbe[4]
[1,2,3]Department of Mechatronic Engineering, University of Nigeria, Nsukka, Nigeria
[4]Department of Electrical Engineering, University of Nigeria, Nsukka, Nigeria
[5]Department of industrial Technical Education.

ABSTRACT

Nowadays, autonomous mobile robots are being deployed in hospitals and clinics to replace time-consuming repetitive transportation tasks performed by doctors and hospital professionals. These robots are used to deliver hospital equipment, meals, and medications to patients in order to improve communication between hospital staff and patients and thus improve health care quality. However, a highly advanced and cost-effective indoor navigation system is required to improve the navigational capability of these robots. To improve the performance of these mobile robots, some researchers created a navigation system based on sensor fusion location and trajectory tracking. Other researchers used intelligent controllers such as the A* search algorithm, simultaneous localization and mapping (SLAM) navigation, and 3-path planning algorithms for autonomous mobile robot navigation. In this research, a Q-learning-based reinforcement learning is proposed for autonomous mobile robot navigation. This technique has the ability to navigate an unknown environment and learn from previous experience, giving it an advantage over other intelligent controllers. The working principle of this technique is based on Bellman concepts such as state action reward and new state (SARS). Q-learning uses samples to optimize its performance by receiving a reward (both negative and positive), and it also employs function approximation to deal with large unknown environments via an action-reward policy. The mobile robot mathematical model is created by taking into account the kinematics and dynamics of the system as the agent. This model is being trained and tested in a stochastic environment using Python simulation to validate its performance.

Keywords: autonomous mobile robots, intelligent controllers, Q-learning, Hospital, Python

1. Introduction

Currently, with the development of Industry 4.0, there is an increasing demand for intelligent equipment upgrades in various industries. Mobile robots, as an integral part of the intelligent industry, have been applied to serve indispensable roles in different fields [1]. Path planning is the central crux in the research field of mobile robots such that they know how to move from source to target and how to execute the desired task. The mobile robots not only need to complete tasks but also have to be able to avoid various obstacles, which will adversely affect their performance. Therefore, path planning is important for mobile robots. Since path planning problems were proposed, many scholars have proposed many representative algorithms, such as Dijkstra [2]. In addition, there are also popular methods based on optimal control

theory, such as co-evolutionary multi-population genetic algorithm (CMGA) [3], CMGA takes a time-optimal path planning approach to complete the cooperation between vehicles, and Xiaoshan Bai [4] utilized the accessible area analysis and optimal control theory to generated the time optimal path. With the deepening of research and technological progress, the speed and accuracy of path planning have been enhanced. However, in the complex environments, the above algorithms have shortcomings such as low planning efficiency and easily fall into locally optimal solutions [5]. Therefore, in order to overcome these shortcomings, machine learning techniques endow new solutions in the field of path planning. With the development of artificial intelligence, many scholars used machine learning (ML) methods to solve the above problem.

The Q-Learning (QL) algorithm adopts a time series differential method of off-policy [6]. Off-policy means that agents explore diversified data through behavior policy in the process of interacting with the environment, so as to continuously optimize the target policy and finally obtain a global optimal value.

2.Hardware system

The hospital autonomous omni-directional mobile transfer robot system is shown in Fig. 1. The robot has an omni-drive system with four roller wheels, shown in Figure 1. A transportation method pulling a wagon truck, which can correspond to various transportation capabilities, in addition to transportation with the robot itself, is shown in Figure2.The four-wheel omni-drive system is utilized to increase the freedom of the moving direction and to improve the stability of the robot while it is moving. It has a Laser Range Finder (LRF), sixteen ultrasonic sensors, and a stereo vision system as external sensors. In order to recognize the environment, the robot has external sensors, such as a stereo camera, laser range finder and ultrasonic sensors. However, in this research the robot recognizes the environment making use only of the laser range finder. The velocity limit of the robot is 0.5 m/s and the acceleration limit is 1.0 m/s^2. Moreover, the performance was determine through the path tracking and collision avoidance in the hospital.

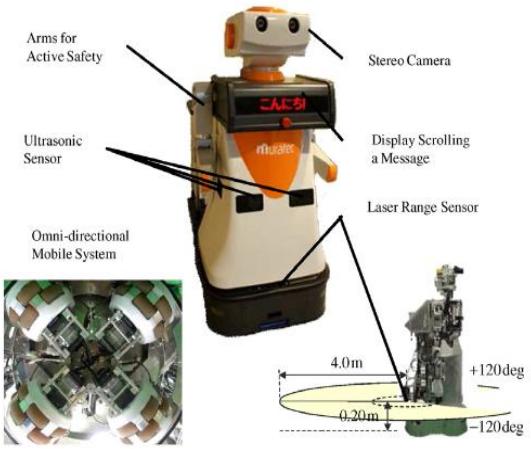

Fig. 1. Robot and sensor

Fig. 2. Traction type autonomous omni-directional mobile robots.

3.Result and Discussions

We carried out several experiments to verify the performance of the path tracking and collision avoidance in the hospital. Figure3 shows the map based on the LRF data which are collected when manually joy-sticking the robot in the first floor of the hospital, and the path produced by the path planning method. In this map, a black area shows the area in which there is no obstacle and a white line shows the path produced by path planning. In the result, point 1 is the start point and point 2 is the goal point.

Figure3: Map of the floor in the hospital and path produced by the path planning method

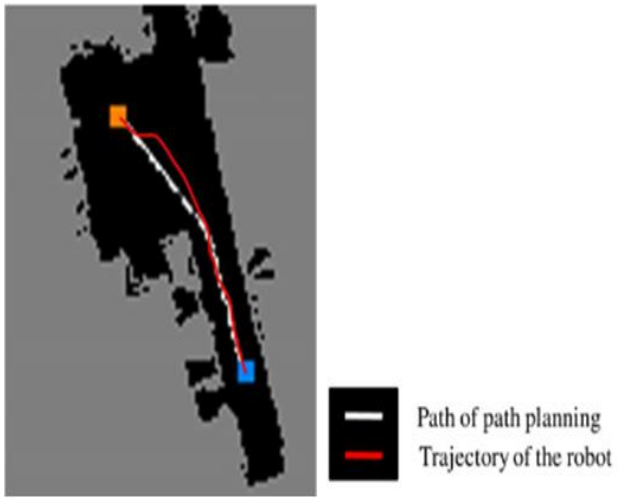

Figure4: Trajectories of the robot in the hospital special ward.

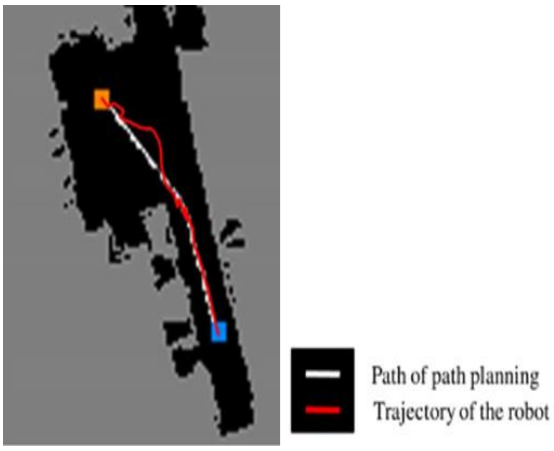

Figure5: Trajectories of the robot in the hospital General Ward.

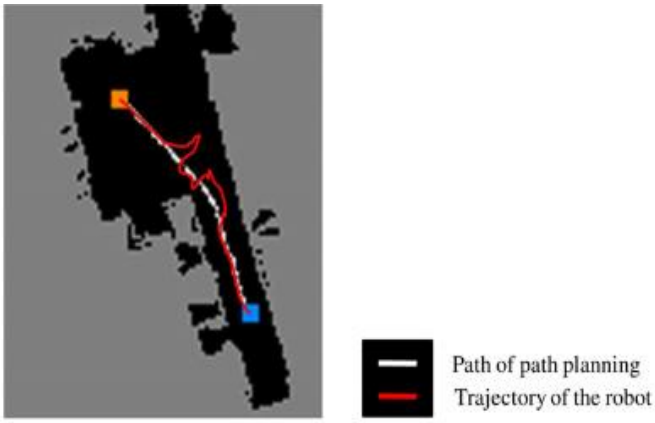

Figure6: Trajectories of the robot in the hospital Children Ward.

The length between the start and goal points is 12 m. The velocity of the robot is 0.5 m/s. In the Simulation, some people obstruct the progress of the robot at random in the space in front of an elevator and in the narrow aisle. From the Simulation results in Fig. 4-6, it was confirmed that the robot recognizes the human, does the collision avoidance, recovers the path tracking, and can reach the goal point (point 2) in all the ward.

Conclusions

This study proposed an obstacle collision avoidance technique for a wagon truck pulling robot which uses an omni-directional wheel

system as a safe movement technology. Moreover, this paper proposed a method to reach the goal along a global path produced by path planning without colliding with static and dynamic obstacles. The method is based on virtual potential fields. In the method, several modules with different prediction times are processed in parallel to change the robot response according to its relative velocity and position to the obstacle. The virtual force calculated from each potential field is used to generate the velocity command for the robot. Some experiments were carried out to verify the performance of the proposed method. The robot can deal with emergency situations adequately by acting on several modules simultaneously according to the situation. Moreover, from the Simulation results in the hospital it was confirmed that the robot can move along its planned path, and reach the goal without colliding with static and moving obstacles.

References

[1] S. Thrun, M. Bennewitz, W. Burgard, A.B. Cremers, F. Dellaert, D. Fox, D. Hahnel, C. Rosenberg, N. Roy, J. Schulte, D. Schulz, MINERVA: a second-generation museum tour-guide robot, in: IEEE International Conference on Robotics and Automation, vol. 3, 1999, pp. 1999–2005.

[2] H. Asoh, Y. Motomura, F. Asano, I. Hara, S. Hayamizu, K. Itou, T. Kurita, T. Matsui, N. Vlassis, R. Bunschoten, B. Kroese, Jijo-2: an office robot that communicates and learns, IEEE Intelligent Systems 16 (5) (2001) 46–55.

[3] Bai, X.; Yan,W.; Ge, S.S.; Cao, M. An integrated multi-population genetic algorithm for multi-vehicle task assignment in a drift field. Inf. Sci. **2018**, 453, 227–238.

[4] Bai, X.; Yan, W.; Cao, M. Clustering-based algorithms for multivehicle task assignment in a time-invariant drift field. IEEE Robot. Autom. Lett. **2017**, 2, 2166–2173.

[5]Hentout, A.; Maoudj, A.; Guir, D.; Saighi, S.; Harkat, M.A.; Hammouche, M.Z.; Bakdi, A. Collision-free path planning for indoor mobile robots based on rapidly-exploring random trees and piecewise cubic hermite interpolating polynomial. Int. J. Imaging Robot. **2019**, 19, 74–97.

[6]Kober, J.; Bagnell, J.A.; Peters, J. Reinforcement learning in robotics: A survey. Int. J. Robot. Res. **2013**, 32, 1238–1274.

NMS-TP029

Energy Mix in Nigeria: A Myth or Reality

Omitayo S. A., Bawa F. S., Kudu M. M., Abdulrahman A. S.

Department of Mechanical engineering, Federal University of Technology, Minna.
234-703-8676-774 omisam2009@yahoo.co.uk
234-813-1979-797 felixbawa2016@gmail.com
234-807-5899-696 kudumuhammadm@gmail.com
Department of Materials and Metallurgical Engineering, Federal University of Technology, Minna
asipita.salawu@futminna.edu.ng

Abstract

No single energy resource can sustainably meet the energy demands of any country. Integrating all exploitable energy sources is a viable way of achieving stability in energy supply for Nigeria. Hence, the paper focuses on the role of energy mix in sustainable development of Nigeria. Secondary data was analyzed using linear regression (Ordinary Least Square) estimation procedure to measure the impact of existing energy mix (crude oil, coal and electricity) on sustainable development of Nigeria. Granger causality test was also used to ascertain whether growth in per capita energy consumption influenced growth in per capita carbon emissions in Nigeria. Empirical results indicate that existing energy mix has not significantly influenced sustainable development given that electricity generation is inadequate and coal is no longer in use. Results also show that per capita increase in oil consumption resulted in per capita increase in carbon emission and global warming. Exploitable energy sources were however identified in anticipation that an integrated energy plan with emphasis on renewable energy sources for off-grid areas would promote stability in energy

INTRODUCTION

Nigeria is endowed with large oil gas, hydro and solar resource it has the potential to generate 12,522mw of electricity from the existing plant on most days however It is only able to dispatch around 4000megawatt which is insufficient for a country of over 195, million.

Electricity generation in Nigeria started in Lagos in 1886 with the use of generator that provide 60kilowat. In 1923 tin miner installed a 2mw plant on the Kwali river 6years later the Nigeria electricity supply company a private form was establish near Jos to manage an electric power plant at Kura to power the mining industry another private enterprise was establish in sapele by united Africa company to power the activities of Africa timber and plywood company between 1886 and 1945 Electric power Generation was rather low with power provider largely to Lagos and commercial Centre.

1n 1950 The legislative council of Nigeria began move to integrate the electricity industry which is it Enacted a law to establish Electricity corporation of Nigeria (ECN) with the duties of suppling and Developed Electricity.

ECN take over the electricity sector activities with PWD and Generating Set of native Authority in 1951 the form manages 46mw of electricity between 1952 and 1960 the form establishes coal power turbine at Oji and Ijora Lagos state and began making preliminary plan for transmission network to link the power generating site with another

commercial center. In 1962 ECN completed a 132kva line transmission linking Lagos, Ibadan to Sagamu and extended to Oshogbo etc. Furthermore, the statutory organization the Niger dam authority NDA was form to build and maintain dam along river Niger and river Kaduna NDA went on to commission a 320mw hydropower plant at Kaniji dam and was sold to ECN in 1969

In 1972 NDA and ECN merge to form NEPA that was the only power sector Nigeria and the name was change to PHCN after the reformed.

Electricity is generating in Nigeria through the following means Thermal and hydro power source the major source of electricity generated in Nigeria is through fossil fuel especially gas which is very costly. About 86%of the power come I through the major source. And the remaining percentage from hydropower plant. The Electricity sector in Nigeria is classify under the following generation, Distribution, and trasnsmision.in 2012 the industry labor to distribute 5000 megawatts very much less than 40000 megawatts needed to sustain the basic population. This deficit is also exacerbated by clamoring load shedding partial and total system collapse and power failure to meet the demand many house hold and business resort to purchase generating set to power their properties.

SOME ENERGY SOURCES IN NIGERIA

Source of Electric power energy we use in Nigeria

- Hydropower plant: Energy through water
- Solar power (sun)
- Wind power plant (wind)
- Nuclear power plant
- Renewable Energy
- Biomass Energy etc.

STRUCTURE

Nigeria Energy sector has in recent years undergone a concerted shift toward increased private sector involvement by targeting policy that govern the Electricity market and its regulatory even non-governmental stake holder are encouraged to participate in the policy making process reform and the action that underpin it. Are squarely aimed at addressing the structured challenges of poor services low availability and intermitted reliability.

Key component of the country process is to create an investor friendly environment to reduce political interferences and establish strong central regulation

Asset belonging to NEPA the former energy activity has been split into 18 separate successor company the result was 11 distribution, and 6 generation company that were privatized while the remaining wholly owned by the Government management of the transmission company was however outsource. Nigeria boasts of the second largest involvement in IPPS in sub-Sahara Africa after south Africa.

GENERATION COMPANY includes:

- Afam generation company
- Sapele generation company
- Egbin power generation
- Ughelli power generation
- Kainji power generation
- Jebba power generation
- Shiroro power generation station etc.

All this mention is connected to national grid that was send to transmission companies and later send to different distribution companies for sales to the customers

TRANSMISSION STATION

The transmission company of Nigeria (TCN) operate the grid of Nigeria. The average capacity evacuated to distribution companies DISCOs distribute for the first quarter of the year 2019 was 2868mw, transmission losses from generation to DISCO Amounted to 22%

DISTRIBUTION COMPANIES

DISCO operate regional distribution grid in Nigeria during the first quarter of the year 2019

The total loss across the DISCO amounted to 40% Some of the elven distribution companies are.

- ABUJA Distribution company,
- IBADAN Distribution company,
- IKEJA Distribution company,
- KADUNA Distribution company,
- KANO Distribution company,
- BENIN Electricity Distribution company, etc.

ENERGY MIX IN NIGERIA A THING OF REALITY

There are currently Two major source of electrical energy in Nigeria hydropower plant and thermal or fossil fuel power plant within a total installed capacity of 8457.6mw 81% of the early 2014 thermal plant (gas fired plant dominate the Nigeria power supply mix

The hydropower plant production was reported to be 17.59% in that same 2014. According to the work bank collection of development indicator compiled from officially recognized source. There have been two main types of fossil thermal plant in the country coal fired plant and natural gas fired plant. As of December 2013, the total installed capacity was 6953mw and the available capacity was 4549mw actual average capacity generated was 3800mw.

As of December 2014, the total installed capacity of the power plant was7445mw the available capacity was 4949mw and the actual power plant generated was not less than 3900mw. Till today both thermal and hydropower plant generation.

Problems faced BY GENERATION SYSTEM

- Shortage of both water and gas for both hydropower and thermal plant
- High level of unpaid Electricity bill
- Poor maintenance system to power generation
- Lack or inadequate overhauling to generating system
- Problem of technical know how

PRIVATIZATION OF POWER SECTOR IN NIGERIA.

Since 1972 until the early part of 1998; electricity generation transmission and distribution in Nigeria had been a monopoly of the federal government-owned electric utility body known as National Electric Authority (NEPA). However, a combination of factor as earlier stated such as inadequate funding, institutional corruption and excessive political interference along with poor managerial and operational strategies implied that electricity supply during the era of NEPA was abysmal (Adoche et Ali, 2009. Consequently, the Electric power sector return (EPSR) act was essential to by the Nigeria federal Government in 2005. The essence of the reform was the

- Liberalization: deregulation and privatization of the nation's power sector in order to engender stable uninterrupted power sector supply in the country.

- The problem facing power sector can be traced to the facts that it is government owned and this is why there is political interference; the management are not given a free hand to manage privatization will remove political interface and an administrative red tape from public inter price.
- Privatization will abolish unproductive use of the sector; eliminate fraud and embezzlement and infuse financial discipline into the organization. Government all over the world are not suited to run certain enterprises efficiently. As stated in the business concord editorial of June 17,1985, "the history of public utilities in Nigeria has been such that continue maintenance of their corporations will only amount to general economic myopia" (Ojobo 2005).
- Government can still control the power sector without necessary owned them.
- Privatization will improve the efficiency of the sector.
- Provision of opportunity to introduce competitions.
- Attraction of foreign investment into the sector.
- Reduction of government interference in the economy and promoting market force in the economic equity.

The further provides for establishment of the Nigeria Electricity Regulatory Commission (N. E. R. C) which is charged with the following

- Regulate tariffs and quality service
- Institutional and enforcement of the regulation regime.
- Oversee the activities of the industry efficiency.
- Licensing of Generation, Transmission, Distribution and Trading Companies that result from unbundling of N. E. P. A.
- Provision relating to public policy interest in relation to fuel supply, environmental laws, energy conservation, management of scale resources, promotion of efficient energy, promotion of renewable energy and publications of reports and statistics.
- Providing a legal basis with necessary enabling provisions for establishing, changing, enforcing and regulating technical rules, market rules and standards.

Nigeria Electricity Regulation Commission was inaugurated to take full responsibility in November 2005. Other aspect of reforms provided for the management of the Rural Electrification Agency (REA), The National Electric Liability Management Company (NEJMCO) when is a special purpose entity created to manage the residential assets and liability of the defund NEPA after privatization of the unbounded companies the acts also provided for the establishment of the power consumers Assistance found (POLAF) to subsidize under privileged electricity consumers (Balogun 2010).

However, despite these efforts, the problem of the power sector continues until November 2013 when PHCN was formerly handed over to the new investors. Most Gas and steam plants were 100% sold while Kanji hydro power plant, Jebba Hydro power plant and Shiroro Hydro power plant were given out on long term concession.

THE IMPACT OF PRIVATIZATION OF POWER SECTOR IN NIGERIA

Since privatization policy is based on capitalist ideology and orientation an in its drive for profit, it has led to the following:

a) Continuous increase in tariff without Commensurate electricity supply the ordinary consuming masses are at the receiving end as their electricity bills go up multiple folds. Today scores are incurring huge electricity bills as the new Distribution Companies (DIS COS) tariffs have continue to go up and leaving huge dent in the pocket of toiling masses. Increment in tariffs and outright deregulation are part of the consequences of the privatization of PHCN the argument of the government according to Ayode (2012) is that the price increment and total deregulation of electricity tariff would attract the "Foreign investors" however, the privatization program has already entered into major crises as anticipated there has not been in flow of the so-called foreign investors who supported to come in with huge foreign exchange to save the power sector in Nigeria.
b) Another concern is that the companies are owned by the few political elites and their fronts (past presidents; Governors, Ministers to government contractors etc.). The same elements that was responsible for the crisis in the first instance. Most of these companies have no experience in the power sector and little or no capacity to manage the power sector.
c) The companies have not enough financial resources to meet the massive capital requirement; Nigeria's electricity sector requires huge capital to reagitate the transmission and distribution network on order to be robust enough to meet the national electricity demand.
d) There is no effective and fair regulation of the prevised power sector. Since privatization take place in 2013 there have been numerous infractions; non - compliance with extend rules and regulations, arbitrariness and impurity persist in the Nigeria electricity industry.eg. unwillingness of the DIS COS to provide prepaid maters to ensure appropriate pricing of electricity, instead still relies on estimated billing, which is not justifiable, despite their overt malpractices. NERC has been unwilling to enforce its authority as a regulator by applying appropriate penalties and sanctions.
e) There has a conflict between TCN and DIS COS over local rejection allocated to the DIS COS while NERC have refused to penalize the DIS COS for their mal practices.
f) Transmission company of Nigeria TCN which is still owned by federal Government have no willing capacity to transmit the total generation capacity present. The operational capacity has dropped by 33 percent.
g) The lay-off of staff in the sector after privatization had led to under staff in the sector thereby over laboring the which does not commensurate with their wages.

RECOMMENDATIONS

Having identified examined the power sector reform programme and the challenges facing the nations privatized electricity industry in it is evident that the power sector has delivered below expectation of Nigerians. In view of

these, privatization cannot be seen to be a one-off concluded programme. The following recommendations would suffice:

- The electric power reform act 2005 should be amended to prevent the ruling elites, their business affiliates and fronts from hijacking subsequent tender and bidding process to their advantage.
- Government should encourage the states at their level to initiate off- grid mini power generation from renewable energy e.g., solar power and wind power serve rural areas since their load demands are little.
- The electricity industry should be made attractive to foreign investors and lenders who can meet the massive capital requirement of the industry.
- The present power grid system in Nigeria is very weak; there is critical need for the TCN equipment to brought to an optimum operating condition so as to accommodate the present generation capacity; this will strengthen the grid system thereby reducing power outages (i.e., frequent system collapse).
- The Nigerian Electricity Commission (NERC) in conjunction with Distribution companies (Discos) should agree on deadline after which most if not all electricity consumers in the country will not be billed if not provided with pre-paid meters. This will mitigate the present incidence of estimated/outrageous billing.
- The Nigerian Electricity Commission (NERC) should not hesitate to enforce its authority as a regulator by applying appropriate penalties and sanctions to those who violate the rules, regulations and guide lines of the electricity market. This will reduce, stop load rejection, level of impunity and arbitrariness in the sector.

CONCLUSION

Integrating energy sources is a viable way to address the energy problems of Nigeria, which include irregular power supply and rising costs / scarcity of conventional or traditional energy sources. The paper discussed Energy generation in Nigeria is a thing of reality the energy sources is from different generation either hydro or thermal. Utilization of the country's abundant renewable energy resources combined with efficient use of fossil fuels facilitated by technological innovations can improve their environmental impact and economic conditions. Moreover, efficient management of energy resources is imperative for economic growth, environmental protection and energy systems sustainability.

REFERENCES

Amina, Isa Peterside, Zainab Brown. Vol 5, No 26 Nov 2014, The Impact of Privatization of Power Sector in Nigeria: Apolitical Economy Approach. Mediterranean Journal of Social Sciences.

Ojobo J. A. (2005), The Impact of Privatization; Policy on Labour in Africa: A Political Approach, The Nigerian Journal of Administration Studies. Vol 3, No1

Okoro, O. I. Govender, P Chikuni, E 2007 "Power Sector Reforms in Nigeria Opportunities and Challenges Proceeding for 10th International Conference on The Domestic Use of Energy, Cape Town, South Africa

Enojo Audu; Salisu Ojonemi Paul; Abraham Ameh: Privatization of Power Sector and Poverty of Power Supply in Nigeria; A Policy Analysis: International Journal of Development and Sustainability Volume 6 No 10 (2017): Pages 1218-1231

Engr Samson Ubogu (Aug 2015); Country Report on Nigeria Energy System

Nnemeka Vincent Emodi, Samson D. Yusuf Vol 5 No 1, 2015 Pg. 335-351: "Improving Electricity Access in Nigeria: Obstacles and The Way Forward"; International Journal of Energy Economic and Policy.

Babatunde; M A. & shuaibu M I (2008) "the demand for residential electricity in Nigeria: abound testing approach"

Privatization in the power sector. Navigating the transition. http://www.pwc.com/ng

Transmission company of Nigeria, 2017. Existing transmission network. http://www.tcnorg.com/#

Ayodeji A (2012) "oppose the fraud called privatization of PHCN

Sunday Olayinka Oyedepo (2015): "energy and sustainability development in Nigeria": way forward

Nextier/power (April 13, 2020): "five reasons for unstable power supply in Nigeria"

Okechukwu Marcellus, 2021; Nigeria's post-privatization energy sector is a mess: here are some solutions

CBN (2007). Statistical bulletin. Doi: HTTP://www.cenbank.org/documents/Statbulletin.asp. CBN (2008).

Statistical bulletin. Doi: HTTP://www.cenbank.org/documents/Statbulletin.asp.

Chukwudi, M. (2008). Nigeria's energy mix and climate change. In: Alexander's Gas & Oil Connections: Company News Africa.

Doi: HTTP://www.thetidenews.com. Climate Institute (2010).

Doi: HTTP://www.climate.org/climatelab/Wind_Energy_opportunities_in_Nigeria.

Dickey, D. A. & Wayne A. F. (1979). Distribution of the estimators for Dickey, D. & Wayne, A. F. (1981). "Likelihood ratio statistics for autoregressive timeseries with a unit root."

Econometrica, (49), pp.1057-1072. autoregressive time series with a unit root, cited in Journal of, American Statistical Association, No. 74, pp. 427-431. 28

Uzoma, C.C.: Continental J. Social Sciences 5 (1): 21 - 29, 2012

Droege, P. (2004). Energy conscious architecture: our post-fossil habitat cited in Words into Ac

VISION

To position Nigeria as one of the leading automotive manufacturing nations in the world.

Mission Statement

To create an enabling environment for the manufacture of Nigerian made vehicles of international standards at competitive prices using local, human and material resources.

The Council pursues this aspiration through the creation of an enabling environment achieved by an appropriate mix of protective measures, incentives, regulatory activities, and local content programmes.

The incremental results of this effort potentially generate large employment, transfer technology, boost transportation capacities, save foreign exchange and even bring about export. The Council's policy activities essentially complement the industrial policy of Nigeria.

Corporate Headquarters:
No. 13 David Ejoor Street
Opp. Anglican Girls Grammar School
Gudu District, P. M. B. 320 Garki,
Abuja, Nigeria.
E-mail:contact@naddc.gov.ng
Website: www.naddc.gov.ngachivefm@yahoo.com

Zaria Office:
Industrial Development Centre
P. O. Box 491
A.B.U. Post Office
Samaru, Zaria, Kaduna State.
+2348037021155

NIGERIANINSTITUTE OF MINING AND GEOSCIENCES (NIMG), JOS, PLATEAU STATE, NIGERIA

ADMISSION INTO POSTGRADUATE DIPLOMA PROGRAMMES

Background:
The NIMG Jos, **an Affiliate of University Jos** was established by the Ministry of Mines and Steel Development in 2007 to become an international Centre of Excellence for mining skills acquisition and specialist training in all aspects of mineral resources development.
The objectives of NIMG are to:

i. Provide skills and knowledge to the artisanal and small-scale miners;
ii. Train the middle and senior cadre of staff for the Industry, including the provision of in-house training for the Ministry of Mines and Steel Development and Agencies related with Mining Industry;
iii. Conduct research in exploration, extraction and value addition including the development of simple equipment and tools for the industry; and
iv. Constantly conduct short courses, workshops, conferences and seminars to train all stakeholders and advance informed knowledge on the "realities and best practices in Mining".

The NIMG hereby invites applications for admission into full residential Postgraduate Diploma Programme (PGD) for **2021/2022 Session**. The programmes are designed to upgrade students' skills to meet the peculiar manpower needs of the modern day mining sector.

Available Postgraduate Diploma (PGD) programmes:

i. Mining Engineering;
ii. Minerals Engineering; and
iii. Mineral Exploration

Entry Qualifications for all Postgraduate Diploma Programmes (PGD):

a) Basic Requirements:

Candidates must possess at least five (5) 0' Level credits from WAEC, NECO, GCE, or NABTEB as the basic University/Polytechnic entry requirements. This must include: Mathematics, Physics and Chemistry

b) Additional Requirements:

Candidates who possess B.Sc. or its equivalent and above from accredited programmes in recognized Institutions, in science-based disciplines such as: Mining Engineering, Minerals Engineering, Metallurgical Engineering, Metallurgical and Materials Engineering, Mineral Processing, Geology, Applied Geology, Mineral Sciences, Geophysics, Applied Geophysics, Mineral Exploration, Geography, Chemistry, Civil Engineering, Mechanical Engineering, Chemical Engineering, Science Laboratory Technology, Applied Science, Physics, allied or related disciplines to Mining or Geosciences may apply.

Duration and Programme Content:

Each PGD programme is for **eighteen (18) months** duration. The NIMG is oriented towards practical skills acquisition in all aspects of mineral resources development. The Institute focuses on producing ready entrepreneurs and manpower for the contemporary mining industry.

Mode of Application:

Application forms may be downloaded from the websites www.mmsd.gov.ng. Also, hard copies are obtainable from NIMG, Tudun Wada Campus, Jos or our Liaison office at Abuja, Nigeria upon payment of N10,000 or USD100.00 only into NIMG Account through REMITA platform.

Closing Date:

Completed Applications must reach the office of the Director General/CE, not later than four (4) weeks from the date of publication.

Contact Address:

For further information, please contact:
The Head of Training and Research,
Nigerian Institute of Mining and Geosciences,
No 1 Metropolitan Avenue, Tudun-Wada.
P.M.B. 2183, Jos, Plateau State, Nigeria.
Email: nimg.jos.plateau@gmail.com.
Tel +234(0)7089686552, +234(0)8092777914

NATIONAL METALLURGICAL DEVELOPMENT CENTRE (NMDC) PMB 2116, OPPOSITE NEW STADIUM, ZARIA ROAD, JOS PLATEAU STATE

Website: https://www.nmdc.gov.ng

VISION

To be a global Centre of Excellence in Minerals and Metals sector Innovation

MISSION

To Add Value to Minerals and Metals through Research and Development

NMDC'S SERVICES IN THE MINERAL, METALS AND ALLIED INDUSTRIES

	SECTOR	SERVICES OFFERED
1.	**CONSTRUCTION INDUSTRY**	• Tensile, Hardness, Impact, Fatigue Tests and Analysis of Construction Rods and Bars • Failure Analysis of Construction Rods in Building Collapses • Corrosion Monitoring and Control • Chemical and Physical Tests on Construction Bricks
2.	**OIL AND GAS INDUSTRY**	• Tensile, Hardness, Impact, Fatigue and Metallographic Tests and Elemental Tests on Machine Components and Structures • Failure Analysis • Weld Inspection and Certification • Corrosion Monitoring and Control • Chemical and Physical test on Bulk and Insulating Bricks • Environmental Impact Assessment (EIA) • Environmental Audit • Determination of Calorific Value of Materials • Carbon Sulphur Determination
3.	**MANUFACTURING INDUSTRY** • Automobile Industry • Iron and Steel Industry • Cement Industry • Refractories and Ceramics Industry (Testing)	• Monitoring of Input Materials, Production Processes and Products (TQM) • Test on Industrial Castings (Steel, Cast Iron and Non-Ferrous Metals) • Determination of Molding Materials Properties • Metallurgical Tests and Analysis of Iron and Steel Products • Metallographic Analysis of Metallic Components • Tests on Raw Materials for Cement Production • Chemical and Physical Tests on Refractory Bricks, Ceramics and Raw Materials • Analysis of Iron and Steel Raw Materials and Finished Products

4.	**MINERAL SECTOR**	• Characterization and Chemical Analysis of Minerals • Determination of Calorific Value of Coals • Environmental impact assessment (EIA) • Mining and Mineral Processing Waste Analysis and Management • Carbon Sulphur Determination • Determination of Work Index in Mineral Comminution
5.	**WATER RESOURCES**	• Chemical and Microbiological Analysis of Raw and Treated Water
7.	**DEFENCE INDUSTRY**	• Mechanical Tests and Failure Analysis of Components and Structures • Weld Inspection and Certification • Chemical Analysis of materials • Determination of Calorific Value of Materials • Carbon Sulphur Determination • Manufacturing of materials for ammunition production
8.	**CONSULTANCY**	• Design of Mineral Processing and Metal Extraction Flowsheets • Monitoring of Production Input Materials, Processes and Product Tests (TQM) • Human Capacity Development (Metallurgy, Mineral Processing, etc) • Failure Analysis of Steel/Metal Components and Structures • Corrosion Monitoring and Control • Environmental Impact Assessment (EIA)

Journal of Metallurgy and Materials Engineering (JMME)

OBJECTIVES AND SCOPE

The Journal of Metallurgy and Materials Engineering is an international journal published under the auspices of the Nigerian Metallurgical Society with the primary objective of documenting previously unpublished research findings in the broad field of Metallurgy and Materials Science and Engineering. Subject areas covered by the journal include Metallurgy, Ceramic Engineering, Polymer Science and Technology, Semiconductor materials, and Corrosion Science and Engineering.

Types of Papers published:

Papers for submission to JMME must be clearly written and may take any of the following forms:
a) Original research papers: These will constitute the main thrust of the journal. These papers must present important advances beyond present knowledge.
b) Review articles: These papers must present a critical assessment of a specified area of literature, emphasizing strengths and weaknesses of existing data and interpretations.
c) Technical Notes: These should be abbreviated forms of (a) and (b), and are in general intended to announce a significant new finding or to beef up information already given out in a previous paper.
d) Technical-Reviews: The purpose of these is to present the state-of-the-art in the field, or to review important industrial problems. However, articles under this category must be very well written in a scholarly manner and must emphasize important technical innovations. Properly documented new designs may also be considered under this category.
e) Discussions/Communications: Issues pertaining to the contents of an earlier paper by another author may be raised under this category. The reaction of the author to such issues (comments or questions) may also be presented.
f) Special Papers: Papers of a special nature, such as policy papers highlighting important advances in the field and furnishing relevant data, will occasionally be considered for publication.

Length of Paper:

Authors are advised to limit the length of Research papers and Review articles to 20 typewritten pages, Technical notes to 5 pages, and Discussions to 3 pages; (Prints should be limited to 15, 3 and 2 pages respectively).

SUBMISSION OF MANUSCRIPTS

Manuscripts should be submitted to the Editor-in-Chief through the form on our website or CD/DVDs to the address on the next page. All manuscripts submitted for publication must not have been sent elsewhere for publication. An author whose article is accepted for publication after review may be formally required to agree not to publish it elsewhere.

FREQUENCY OF PUBLICATION: Twice yearly (Biannually).

Authors of accepted papers will be required to pay modest page costs at a rate that may vary from time to time according to the journal editorial policy. Currently applicable rates are as follows:

Nigerian Authors – ₦30, 000.00 per publication, Other Authors Based elsewhere in Africa - US$200

All correspondence should be addressed to:

Engr. Prof. B.A. Okorie
Editor-in-Chief, JMME,
bonokorie@yahoo.com

Engr Prof. V.S.Aigbodion
Production JMME
aigbodionv@gmail.com


THE NIGERIAN METALLURGICAL SOCIETY
IN COLLABORATION WITH
UNIVERSITY OF ABUJA, ENERGY COMMISSION OF NIGERIA,
KAM HOLDING INDUSTRIES, AFRICAN INDUSTRIES GROUP LIMITED, TOP METALLURGICAL, MINERALS,
MATERIALS & MINING INDUSTRIES AND OTHER RELATED ESTABLISHMENTS/ORGANIZATIONS IN NIGERIA
Certificate of Participation
This is to certify that:
PROMOTING METALLURGICAL , MATERIALS ENGINEERING & OTHER ALLIED PROFESSIONS
was a participant at the 37th Annual Conference & General Meeting tagged Abuja Hybrid 2022 on the ROLE OF MATERIALS INDUSTRY IN ENERGY MIX TRANSITION AND ENVIRONMENTAL SUSTAINABILITY
DATE: 26–29 OCTOBER 2022
VENUE: CONFERENCE HALL, ASUU RESEARCHERS' CHALETS, UNIVERSITY OF ABUJA, ABUJA, FCT
ENGR. PROF. O.B. OLOCHE, FNMS
PRESIDENT, NMS
ENGR. M. K. OLASUPO, FNMS
CHAIRMAN, COC
african industries
HOLDING